

BULGARIAN CHEMICAL COMMUNICATIONS

2014 Volume 46 / Special Issue A

Commemorative Issue in Honor of Acad. Dimiter Ivanov on the occasion
of his 120th birth anniversary

*Journal of the Chemical Institutes
of the Bulgarian Academy of Sciences
and of the Union of Chemists in Bulgaria*

ACADEMICIAN DIMITER IVANOV

120 Years of His Birth



13.10.1894 – 25.10.1975

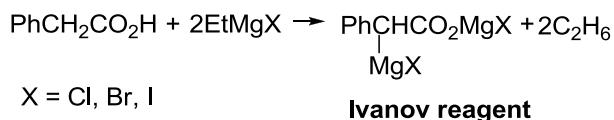
In the annals of Bulgarian science the name of Dimiter Ivanov holds a special place. In his fifty years of work he left ineffaceable and lasting traces in organic chemistry. His personal qualities and scientific achievements were on such a high international level that in him Bulgarian chemistry has one of its most outstanding representatives. The 120th anniversary of his birth is in October 2014.

Dimiter Ivanov Popov was born in the family of a clergyman on October 13 (27), 1894 in the village of Makotzevo in the district of Sofia. He graduated from the First High School for Boys in Sofia. He won a competition for a grant awarded by Stefan Beron from Kotel and in 1914 and 1915 he was studying chemical engineering in Lyon, France. On the declaration of mobilization in 1915, he returned to Bulgaria and took part in the First World War in Dobrudzha and Macedonia near Chervenata Stena. During the defeat of the Bulgarian army at Dobro Pole he was captured along with a Bulgarian army division near Thessaloniki and kept there up to the end of 1918.

He graduated in chemistry from Sofia University in 1920 and was immediately appointed as an assistant of Professor Zachary Karaoglanov in inorganic and analytical chemistry. Soon after that he obtained a grant to study in France again. He graduated as a chemical engineer in Nancy in 1922 with a Ph.D. degree and stayed for a year in the same university as a postdoc with G. Vavon, one of the outstanding stereochemists at that time. His first scientific paper on steric hindrance in catalytic hydrogenation dating from that time (1923) was published in *Comptes rendus de l'Académie des Sciences de Paris*.

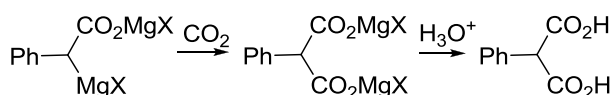
In 1926 Dimiter Ivanov became an Assistant Professor at the Chair of Organic Chemistry headed by Professor Pencho Raykov. The same year he obtained a Rockefeller Scholarship and went to work with Victor Grignard, a Nobel Prize winner who discovered the organomagnesium compounds. This was, to a great degree, the decisive factor in determining his further scientific career. Years afterwards Academician Ivanov would never forget and would emphasize to his students what he owed to this great man and scientist. Grignard welcomed his young Bulgarian colleague by handing over his own laboratory bench with the words "Here were discovered the magnesium reagents (known today as the Grignard reagents, author's remark) and I wish you with all my heart to move forward".

In 1931 Dimiter Ivanov, already an associate professor of organic chemistry in Sofia University, published a paper entitled "On a Method of Preparing Phenylmalonic Acid" in the *Bulletin de la Société Chimique de France*. Co-author of this work was his young Ph.D. student, later one of Bulgaria's great synthetic chemists Professor Alexander Spassov. Dimiter Ivanov had already published a dozen or more scientific communications abroad, but the above-mentioned paper laid the foundations of what is named today "*Ivanov reagents*" or "*Ivanov reaction*". Ivanov and Spassov reported that phenylacetic acid reacts with lower aliphatic Grignard reagents by liberating *ca.* two equivalents of hydrocarbon, for example:



Ivanov reagent

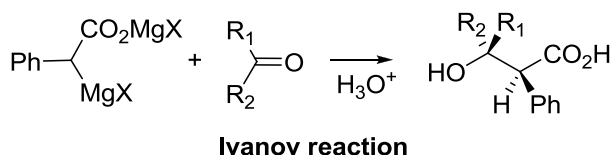
Phenylacetic acid thus behaves simultaneously as a carboxylic and as a C-H acid, i.e. a hydrogen atom of the methylene group can be replaced by metal. The organomagnesium compound so-obtained has a more complex structure than that of Grignard reagents but, to a considerable degree, possesses the reactivity of the latter. Different kinds of compounds give with the Ivanov reagent products which are either very hard or impossible to synthesize by other means. The first reaction of the newly obtained Ivanov reagent was carried out by the authors with carbon dioxide to yield phenylmalonic acid:



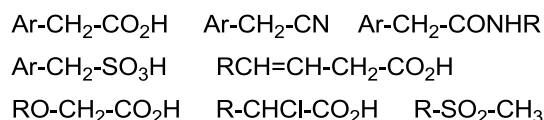
Thus a general method of preparing Ivanov reagents was set: metallation by means of Grignard reagents of compounds containing labile hydrogen atoms, called today C-H acids.

The same year D. Ivanov and A. Spassov discovered the reaction which would later be named the *Ivanov reaction*. It involves the interaction of the Ivanov reagents with aldehydes or ketones leading to β -hydroxy acids.

As recognition of this achievement next year, 1932, Dimiter Ivanov was awarded the honorary title of "Laureate of the French Academy of Sciences".



In the course of more than forty years Academician Ivanov worked steadfastly and systematically to develop the chemistry of organometallic compounds obtained by metalating C-H acids. After 1950, both in Bulgaria and abroad, there was a very intensive development of research along the perspectives outlined by Ivanov. Apart from magnesium, alkaline metals, zinc and calcium came into use and, in the case of each one, new features and fresh possibilities for application were found. The number of parent compounds which could be metalated was greatly expanded. The following are only a few examples:

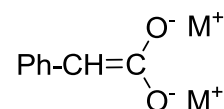


Dimiter Ivanov called the metal derivatives so-obtained "*polyfunctional organometallic reagents*". Already in the 'fifties outstanding scientists in USA, France, the USSR and other countries were introducing, using and substantiating the terms "*Ivanov reagents*", "*Ivanov-like reagents*", "*Ivanov reaction*".

Nowadays the concept of Ivanov reagents implies deprotonated derivatives of C-H acids, whose organic moiety, independently of the metal, may be considered as a two-charged anion capable to interact with one equivalent electrophile.



These reagents provide great synthetic opportunities because they are readily oxidized, alkylated, acylated and silylated, added to carbonyl and azomethine groups and conjugated double bonds. It was established that the formulas shown in the figure above, although easy to visualize, do not correspond to the real structure of Ivanov reagents. In some cases they are for example enediolates, as for the phenylacetic acid:



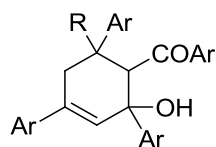
The reaction with carbonyl compounds named after Dimiter Ivanov belongs to the class of the so-called aldol reactions which are among the most important ones in organic chemistry. Many studies at home and abroad have clarified its similarities and differences with other aldol type reactions, such as Perkin, Reformatsky, Claisen. The kinetic stereoselectivity shows moderate degrees, *threo* diastereoisomer prevails, and depends on the metal and the solvent used. A mechanism of the reaction proposed by American scientists Zimmerman and Traxler, based on a six-membered transition state, explains the majority of the experimental data.

In experiments to react the Ivanov reagents with the unsaturated ketone dypnone an unexpected course occurred. It turned out that the product (no matter which organometallic reagent was used) was *dypnopinacone*, a class of *ca.* 60 compounds prepared and systematically studied by the great

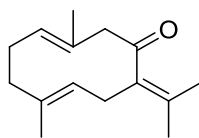
Belgian chemist Maurice Delacre. This was the beginning of another remarkable line of D. Ivanov's research. His first publications on this problem at the end of the 'thirties initiated a revision of the structure of dypnopinacones. Delacre himself, greatly impressed by the results obtained by his Bulgarian colleague with whom he had not been till then acquainted, sent Dimiter Ivanov his complete laboratory files. He wished Ivanov to bring to a successful conclusion the problem which had been his lifework. An extraordinary example of high moral behavior in the world of science!

In the 'forties, after having made use of a remarkable research strategy, Dimiter Ivanov and his then assistant Professor Tchavdar Ivanov disproved the structures suggested by Delacre and unequivocally determined the structure and mechanism of formation of dypnopinacones - a class of unsaturated cyclic hydroxy ketones. The brilliant solution to the dypnopinacone problem was the reason why dypnopinacone synthesis has been named "*Reaction of Delacre-Ivanov*".

The above examples are only a brief illustration of the impulse given to science by Academician Ivanov's research in the field of synthetic organic chemistry. This great scientist was not only a witness to its further useful development but also an active participant even in the last years of his life.



Dypnopinacone



Germacrone

In 1947 D. Ivanov took charge of a team of scientists who systematically investigated the composition of Bulgarian essential oils, above all rose oil, but also lavender, mint, sweet basil, zdravets (wild geranium) and the oil of other plants. The papers published became very widely known and contributed towards raising the international prestige of the products of the Bulgarian essential oil industry and the confidence in them. Academician Ivanov was welcomed everywhere as the "scientific ambassador" of the Kazanluk Oleaginous Rose.

The studies on zdravets oil, which is produced only in Bulgaria, deserve special attention. The crystal component of the oil, named *germacrone*, has a sesquiterpene carbon skeleton unknown in other natural compounds. In 1957 and 1958 a joint team of Bulgarian and Czech scientists, headed by

D. Ivanov and Fr. Šorm, proved germacrone to be a ten-membered ring ketone. This was the starting point for intensive research on various transformations on this structure, which contributed significantly to the prestige of the Bulgarian School of natural products chemistry.

Dimiter Ivanov published over 180 original scientific papers, some of them in Bulgarian journals but the greater part in foreign ones. In 1948 he was elected Corresponding Member of the Bulgarian Academy of Sciences and in 1961 Academician. Up to 1972 he was head of the "Organic Chemistry" section of the Chemical Institute of the Bulgarian Academy of Sciences, from the time of its foundation in 1951 (later this became "Laboratory of Organic Synthesis" to the Institute of Organic Chemistry).

The services rendered by Professor Dimiter Ivanov as a teacher and instructor were exceptional and indisputable. On the death of Professor Assen Zlatarov he was appointed (1937) to the Chair of Organic Chemistry at Sofia University, which he held up to 1962. His text-book on organic chemistry, which was excellent for that time, went through seven editions in the course of twenty five years. It has been the corner-stone in preparing many generations of chemists and chemical engineers. This text-book is now of great bibliographical value and today is still often used as a source of reference. Professor Ivanov had a profound feeling of responsibility and devotion in fulfilling his teaching duties. Having a marvelous memory he remembered everyone who had passed during decades through "his organic chemistry" and he always called them "our alumni". His lectures were unforgettable for many generations of students. Already in 1933 he was the initiator in introducing diploma works (master theses) which later became a well-established form for the instruction of students in most fields of study.

Academician Dimiter Ivanov stood out with his vivid and unique individuality. People's attitude towards his personality never was, and never could be, indifferent or indefinite. But everyone was, and is, unanimous in respect to his uncompromising attitude towards mediocre, opportunistic, lazy people, towards those who instead of serving science live on its back (these, to some extent, succeeded in avenging themselves on him when they provoked and caused his removal from the university in 1945 for one year, because of his "anti-people's behavior"). Nothing except personal qualities mattered to him in his estimation of people and his attitude towards them in general and towards his colleagues in particular. Maybe in this

lay the secret of his enviable insight in choosing his assistants and coworkers (never very many in numbers) and his approach in working with them. By creating a school in organic chemistry from which many of Bulgarian chemists started their career, Dimiter Ivanov raised a monument to himself already during his own lifetime.

He had a remarkable gift for getting in touch with people who were on most various professional and social levels. His inherent interest and curiosity about ordinary everyday problems made him a good listener and always good company. He would talk with equal satisfaction about his experiences with Nobel Prize winners or with some old neighbor in his native village of Makotzevo. It is easy to imagine him in lively conversation with students, or with the postman, or as the centre of attention at some scientific congress. This feature of his personality combined with his scientific and language culture made Academician Ivanov a desirable participant or guest at different international scientific meetings. The last event which he attended, still showing his youthful emotion, was the celebration of the centenary of the birth of Grignard in 1971. The Bulgarian scientist was invited to take part in it and was given the honor of delivering the speech on behalf of the

grateful former Grignard students, then scattered around many countries, whose indisputable doyen he was.

Academician Ivanov described his long career, illuminated by the rays of his sunset in his short "Memoirs", completed several weeks before he departed from us forever. The publication of these "Memoirs", unfortunately concealed by ill-wishers, would have provided not only an interesting, but also instructive reading matter. He passed away on October 25, 1975.

The absence of the personality of Dimiter Ivanov is very strongly felt at a time when the future of Bulgarian science is at stake! One always imagines that he would appear at the end of the corridor with his easy step and lively look, ready to tell us the next of his stories, to give us hope and faith in eternal values.

Blagoy Blagoev

Institute of Organic Chemistry with Centre of Phytochemistry, Bulgarian Academy of Sciences, Acad. G. Bonchev str., bl. 9, 1113 Sofia, Bulgaria; E-mail: ib_blagoev@yahoo.com

Interaction between charged groups. pK-values and conformations of the diastereomers of 3-amino-2,3-diphenylpropanoic acids and their ester and N-acetyl derivatives

P. M. Ivanov¹, I. G. Pojarlieff^{1*}, S. D. Simova¹, G. D. Velinov²

¹*Institute of Organic Chemistry with Centre of Phytochemistry, Bulgarian Academy of Sciences, Acad. G. Bonchev str., bl. 9, 1113 Sofia, Bulgaria*

²*Faculty of Pharmacy, Medical University of Sofia, 2 Dunav str., 1000 Sofia, Bulgaria*

Received July 03, 2014; Revised July 22, 2014

Dedicated to Acad. Dimiter Ivanov on the occasion of his 120th birth anniversary

The system of 1,2-disubstituted-1,2-diphenylethanes is characterized by the strong preference of the conformation with *antiperiplanar* phenyl groups in both diastereomers which positions the other substituents *ap* in the *erythro* and (+)-*sc* in the *threo* isomer. This proved true for the isomers of 3-amino-2,3-diphenylpropanoic acid and its N-acetyl and ester derivatives as evidenced by J_{2H3H} -couplings above 10 Hz found in formamide. Only the zwitterion of *erythro* amino acid **1a** showed a smaller value of 9 Hz indicating charge attraction overcoming partly the steric interactions. Molecular mechanics calculations by means of the Scheraga force field corroborated the interpretation. An IR-study of the equilibrium zwitterion – neutral amino acid showed the latter to be preferred in aprotic solvents $\approx 100\%$ in pure DMSO for **1a** but decreased in the presence of water, until only the zwitterion was detected in 80% DMSO. The J_{2H3H} -couplings of **1a** (10.3 Hz in D₂O and 7.7 Hz in pure DMSO) indicated that solvation by water increases steric hindrance and suggested a strong hydrogen bond CO₂H...NH₂ in aprotic media. The pK-values of all compounds were determined potentiometrically in 80% methylcellosolve and in 90% DMSO. The pK₁'s of *threo* zwitterion **1a** for COOH were 0.8 pK units larger than those of the *erythro* isomer as predicted for *anti* vs. *gauche* charged groups. The pK₂-values of the isomers do not differ significantly, the electrostatic effects are apparently offset by steric hindrance from solvation of NH₃⁺. The pK's of the ester and N-acetylated derivatives differ from those of the zwitterion by ca. 2 pK units evidencing strong effects of charge interaction. In organic solvents the acidities of COOH and NH₃⁺ change strongly in opposite directions leading to appearance of neutral amino acid bands proven by the IR data.

Key words: intramolecular electrostatic interactions, vicinal charged groups in *sc* and *ap* conformations, *erythro-threo* isomers, pK-values in 80% methylcellosolve and 90% DMSO, zwitterion vs. free amino acid, conformations, molecular mechanics

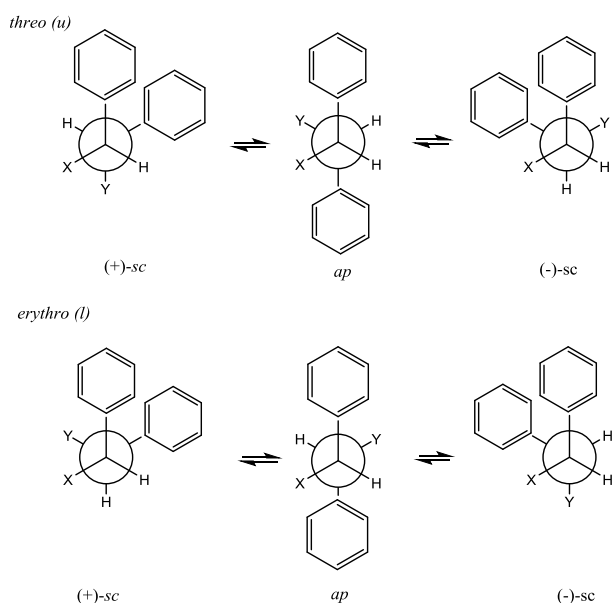
INTRODUCTION

D. Ivanov and A. Spassov in 1931 [1,2] discovered the Ivanov reaction by reacting benzaldehyde with the dimagnesium salt of phenylacetic acid (known as the Ivanov reagent) opening the road to a wide range of 1,2-disubstituted-1,2-diphenyl compounds. The two chiral centres give rise to two diastereomers, the *threo* isomer being preferred. In general terms the Ivanov reaction is a base catalysed aldol reaction. Alternately, B. Kurtev and N. Mollov [3] discovered an acid catalysed version e.g. in the presence of AlCl₃ esters of phenylacetic acid add to hydrobenzamide yielding the esters of the title amino acids. The opposite *erythro* selectivity was observed [4]. Early studies on the conformations of 1,2-disubstituted-1,2-diphenyl compo-

unds revealed from optical rotation studies [5] and from ¹H NMR vicinal coupling constants [6,7] an intriguing feature: the *threo* isomer existed mainly as the conformer with *gauche* Ph groups ((+)-*sc*, Scheme 1) contrary to qualitative conformational analysis. As shown on the conformational formulae below when X and Y are medium sized groups then the preferred conformers with both diastereomers should be with the large phenyl groups *anti*. Actually appreciation of “large” applied to a phenyl group stems from Eliel's A-values derived from *equatorial/axial* equilibria in cyclohexane systems; 3 kcal for Ph versus 1.8 kcal for Me. In open-chain systems there emerged from numerous studies reviewed in reference [8] that the *syn/anti* equilibrium in 1,2-diphenylethane is very similar of the methyl groups with a ΔG of ca. 0.8 kcal/mol. In 1,2-diphenylethane some attraction between *syn* phenyl groups is outweighed by the greater librational entropy

* To whom all correspondence should be sent:
E-mail: ipjarli@orgchm.bas.bg

in the *anti* position. These preferences have been confirmed by advanced computational methods [9]. The case of 1,2-disubstituted-1,2-diphenyl compounds has also drawn a great amount of attention and has been also reviewed in [8] both with respect to experimental determination of preferred conformations and their theoretical interpretation. Molecular mechanics permitted conformational preferences to be discussed in terms of separate contributions: steric strain (torsional, angle and bond deformations), electrostatic interactions, hydrogen bonding. Among the huge mass of accumulated data on the diphenylethane system the absence of examples where X and Y are charged groups is conspicuous.

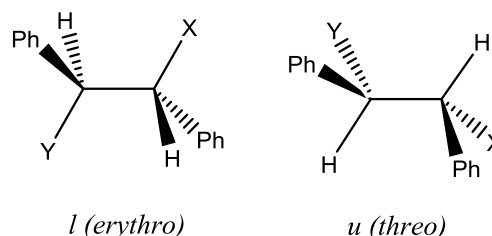


Scheme 1. Designation of conformations for rotation around the C-C bond bearing the neighbouring phenyl groups (the *like* or *unlike* from the R/S nomenclature coincide with *erythro/threo* designations when X and Y are more senior than the phenyl groups).

We now report the pK-values of the diastereomers of the 3-amino-2,3-diphenyl-propanoic acid and its N-acetyl and methyl and ethyl ester derivatives, their ^1H NMR vicinal coupling constants as a measure of the conformational preferences and the results of molecular mechanics study by means of the Sherraga force field. The dimethyl analogue, 3-amino-2-methylbutanoic acid, studied previously [10], exhibited evenly distributed populations of conformers and similar pK with both diastereomers. The general tendency observed in the case of compounds with vicinal phenyl groups shown on Scheme 1 for preferred *ap* conformation of the phenyl groups with the *erythro* isomer and (+)-*sc* conformation for the *threo* isomer meant that the

expected disposition of the amino and carboxy groups in the amino acids will be *anti* in *erythro* but *syn* in *threo*. Thus the interactions of the two charged groups of the amino acid zwitterion in the two positions *anti* in *erythro* and *syn* in *threo* could hopefully be examined.

Table 1 Compounds studied.



Compound	Configuration	X	Y
1a ¹	<i>erythro</i>	CO ₂ ⁻	NH ₃ ⁺
1b ²	<i>erythro</i>	CO ₂ H	NH ₃ ⁺
1c ³	<i>erythro</i>	CO ₂ ⁻	NH ₂
2a ¹	<i>threo</i>	CO ₂ ⁻	NH ₃ ⁺
2b ²	<i>threo</i>	CO ₂ H	NH ₃ ⁺
2c ³	<i>threo</i>	CO ₂ ⁻	NH ₂
3a	<i>erythro</i>	CO ₂ Me	NH ₂
3b ²	<i>erythro</i>	CO ₂ Me	NH ₃ ⁺
4a	<i>threo</i>	CO ₂ Me	NH ₂
4b ²	<i>threo</i>	CO ₂ Me	NH ₃ ⁺
5a	<i>erythro</i>	CO ₂ Et	NH ₂
5b ²	<i>erythro</i>	CO ₂ Et	NH ₃ ⁺
6a	<i>threo</i>	CO ₂ Et	NH ₂
6b ²	<i>threo</i>	CO ₂ Et	NH ₃ ⁺
7a	<i>erythro</i>	CO ₂ H	NHCOMe
7c ³	<i>erythro</i>	CO ₂ ⁻	NHCOMe
8a	<i>threo</i>	CO ₂ H	NHCOMe
8c ³	<i>threo</i>	CO ₂ ⁻	NHCOMe

¹The amino acids exist as zwitterions, see however text. ²Hydrochloride. ³Potassium salt.

EXPERIMENTAL

Uncorrected melting points were measured in capillaries. IR spectra on a Specord IR 75 or Bruker IFS 113v instrument in a 0.1 mm CaF₂ cell. ^1H NMR spectra in formamide on a Tesla 80 MHz or Jeol 100 MHz instruments. ^1H -NMR signals were referenced DMSO or DSS and coupling constants are given in Hz and without sign.

Materials

Inorganic materials and buffer components were of analytical grade and were used without further purification. Potassium hydroxide solutions were prepared with CO₂-free distilled water. Formamide used for NMR as solvent was purified by freezing and subsequent distillation. Dimethylsulfoxide for

pK determinations was dried over CaH₂ and then distilled *in vacuo*, Bp₁₀ 73°C. Compounds **1a**, **1b**, **2a**, **2b**, **3a**, **3b**, **4a**, **4b**, **5a**, **5b**, **6a**, **6b** were obtained according to [4].

All potassium salts were obtained treating a weighed amount of the substrate with the exact equivalent volume of a KOH solution of known molarity. The solution obtained was evaporated to dryness on a rotatory evaporator.

*3-acetylamino-2,3-diphenylpropanoic acids
erythro 7a and threo 8a*

3-Amino-2,3-diphenylpropanoic acids **1a** and **2a** (0.033 mmol) and NaOH (0.08 mmol) were dissolved in 10 ml of water. 0.1 mmol of (CH₃CO)₂O were added under stirring. The precipitate formed is filtered and dissolved in aqueous KOH. The solution obtained is filtered and made acid with HCl. The precipitates obtained were recrystallized: **7a** from acetic acid, **8a** from ethyl acetate-benzene. **7a** m.p. 244°C. Calcd for C₁₇H₁₇NO₂: C, 72.08; H, 6.01; N, 4.95. Found: C, 71.87; H, 6.26; N, 5.08. IR cm⁻¹ γ_{COOH} 1718; γ_{CONH} 1638. **8a**, m.p. 184-185°C. γ_{COOH} 1705; γ_{CONH} 1640. Calcd for C₁₇H₁₇NO₂: C, 72.08; H, 6.01; N, 4.95. Found: C, 71.58; H, 6.08; N, 4.66.

*Determination of pK-values in
methylcellosolve(2-methoxyethanol)-water 80:20*

The pK-values were determined by the procedure developed by Simon [11] adapted as follows:

Samples of a volume of 5 ml and a substrate concentration of 4.6 x 10⁻³ M were used. The galvanic cell comprised a vessel temperature controlled at 25.0 ± 0.1°C provided with a glass electrode Typ G 2222c, a calomel electrode, an electromagnetic stirrer and a flow of nitrogen. The titrating solution is added manually by means of an automatic burette (ABU13) with a total volume of 0.25 ml and accuracy of ± 0.001 at a rate of 40x in ten equal portions sufficient for the complete titration of the weighed sample. The pH was measured after each portion titrant on a Radiometer Typ PHM 26c pH-meter. The pK-values were obtained from the equation:

$$pK = pH - \log \frac{[A^-]}{[AH]}$$

The deviations from the average is maximally 0.05 pK units within a single titration. Two titrations were carried out for each compound and the average value was taken. The reability of the proce-

cedure was checked by determining the pK-value of benzoic acid. We obtained 6.63 which agrees well with the value of 6.57 given by Simon [11].

*Determination of pK-values in
DMSO(dimethylsulfoxide)-water 90:10*

The procedure followed has been described previously [12]. The solvent mixture was prepared by weight from purified DMSO and bidistilled water free of carbonates. NMe₄Br (Schuchard, pure) was used without further purification. HCl solution was prepared from analytical grade reagent, NBu₄OH was from Fluka, a 40% water solution purified by passing through ion exchange resin Dowex 21K to remove CO₃²⁻. DMSO was added to these water solutions as needed.

The potentiometric titrations were carried out in a temperature controlled cell (25 ± 0.2°C) with a diffusional potential comprising a glass electrode Radiometer Typ G 2222c and a reference electrode silver nitrate.



The contact between the sample and the reference electrode was J-shaped. The ionic strength of the samples was maintained constant at I = 0.1 M by means of NMe₄Br. The cell potential was measured with a Radiometer PHM-52 instrument (accuracy 0.2 mV). The galvanic cell was calibrated by determining the specific constant of the cell E_a^{o'} in the acid region. E_a^{o'} comprises the standard potential of the glass electrode, the potential of the reference electrode, the diffusion potential and the activity coefficients. The determination of E_a^{o'} is based [12] on the full dissociation of HCl in 90% DMSO. With an available E_a^{o'} pH in the cell can be found by the well known formula:

$$pH \equiv pC_H = \frac{E_{ao'} - E_{meas}}{59.16}$$

where pC_H is the exponent of 10 of the proton concentration. Thus the pK-values are obtained from

$$pK = pC_H - \lg \frac{[A^-]}{[AH]}$$

The equivalent volume, needed to perform the calculation, is determined by Gran's method [13].

The listed pK-values present the averages of two determinations.

pK-Value of benzoic acid in 90% DMSO was determined as 8.52.

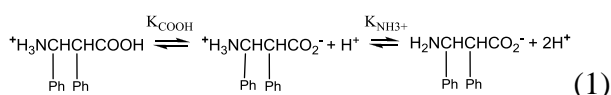
IR-spectra in DMSO

In order to assess the tautomeric forms of the amino acid: zwitterion – uncharged amino acid IR spectra were taken in 85-100% DMSO in CaF₂ 0.1 mm cells.

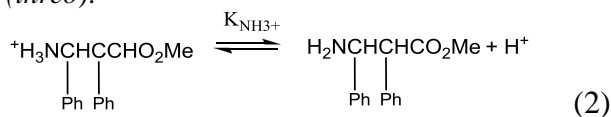
RESULTS AND DISCUSSION

The pK-values obtained concern the following equilibria:

Amino acids, **1a** (*erythro*) and **2a** (*threo*):



Esters of amino acids (only Me ester shown), Me **3a** (*erythro*), **4a** (*threo*); Et **5a** (*erythro*), **6a** (*threo*):



N-Acetylamino acids, **7a** (*erythro*) and **8a** (*threo*):

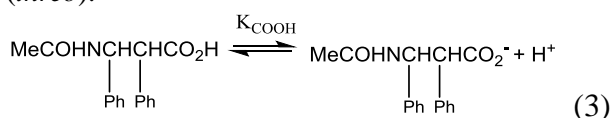


Table 2. pK-values of the diastereomeric amino acid and their N-acetyl and ester derivatives.

Compd	80% methylcellosolve		90% dimethylsulfoxide	
	K _{COOH}	K _{NH₃⁺}	K _{COOH}	K _{NH₃⁺}
1a	4.96	8.86	6.81	9.54
2a	4.18	8.98	6.08	9.25
3a		6.49		7.29
4a		6.57		7.28
5a		6.56		7.31
6a		≈6.6		7.28
7a	6.82		8.46	
8a	6.38		8.03	

In the zwitterion of the parent amino acids, **1a** and **2a**, Coulomb interactions are expected to increase K_{COOH} (decrease pK_{COOH}) because the attraction between the positively and negatively charged groups will shift the first equilibrium of Eqn. 1 to the right. Alternately the second equilibrium will be shifted to the left making the conjugated acid of the amino group a weaker acid i.e. increase pK_{NH₃⁺}. This effect is nicely demonstrated by the roughly 2 pK units larger pK_{COOH}-values in the N-acetyl derivatives **7a** and **8a** compared to **1a** and **2a** in 80% methylcellosolve. The same difference

persists with the data obtained in 90% DMSO only the ΔpK_{COOH}-values are slightly smaller (see below). Comparison of the pK_{NH₃⁺}-values of the free acids with those of the esters in both solvents exhibits the expected effect which noteworthy is very similar to the one with pK_{COOH} in magnitude but opposite in sign. The similarity of the results obtained on the pK in the two solvents systems suggests that the measurements are reliable.

The main reason for carrying out the present investigation is to establish the importance of the electrostatic interaction in the *syn* versus the *anti* position of the charged groups in zwitterions of β-amino acids making use of the unique conformational preferences in the system with neighbouring phenyl groups: the *erythro* isomer providing *anti* charged groups and the *threo* isomer – *syn* charged groups (Scheme 1). The closer distance in the *threo* isomer **2a** than in the *erythro* isomer **1a** predicts the former to be a stronger carboxylic acid which is confirmed by pK_{COOH} of **2a** found to be smaller by 0.8 pK units than that of **1a** in 80% methylcellosolve. In 90% DMSO ΔpK_{COOH} is slightly smaller 0.7 which fits the finding by means of IR-spectra that in 90% an appreciable amount of the neutral form of the amino acid is present (≈20%).

However, no significant difference was found for pK_{NH₃⁺}-values of the two diastereomeric amino acids. We shall return to this point later.

The gap between pK_{COOH} and pK_{NH₃⁺} in 90% DMSO is smaller *ca.* 2.5 - 3 pK units compared to 4-5 units in 80% methylcellosolve. This is readily explained by the well known phenomenon that aprotic dipolar solvents strongly destabilize anions and stabilize cations because the negative pole of the S=O bond is on the surface of the DMSO molecule. On the other hand, a disturbing fact concerning the assignment of the two pK-values, which one is due to COOH and which to NH₃, is that pK_{COOH} of the N-acetylamino acids and pK_{NH₃⁺} of the amino esters become the same in values in 80% methylcellosolve, while in 90% DMSO the order is even reversed - the amino group becomes a weaker base than the carboxy anion: pK_{NH₃⁺} of the esters in 90% DMSO are close in value to pK_{COOH} of the amino acids and similarly to pK_{COOH} of the N-acetylamino acids are close to pK_{NH₃⁺} of the amino esters. This casts doubt on the assignment of first and second ionization constants of the amino acid. Another consequence is that if the order of the ionization constants of monocharged derivatives holds in amino acids then the neutral amino acid should be the prevailing tautomer.

This problem was solved by measuring the tautomeric equilibria utilizing the fact that IR-bands

of COO⁻ and COOH appear at different frequencies. As reference, the bands in the N-acetylamino derivative **7a** and its potassium salt **7c** were taken. The intensities or absorbances, respectively, of these bands were utilised for a quantitative estimation of the concentration of the species in the tautomeric equilibria.

The data on the vicinal coupling constants summarised in Table 4 were collected in order to gain insight on the preferred conformations of the diastereoisomers **1a** and **2a** of the amino acids, their esters and N-acetyl derivatives as well as their salts.

The solubility of the parent amino acids is low in both water and organic solvents of low polarity, particularly of the *threo* isomer whose spectrum could only be recorded in 1:1 DMSO/H₂O. The spectra of all the remaining compounds were taken in formamide, a polar solvent with proton donor capacity. The protons of HCONH₂ resonate at low fields which permits spectra to be taken up to δ 5 ppm with the non deuterated solvent.

Table 3. Data on the tautomeric constants K_T of *erythro* amino acid **1a** for equilibria in DMSO/ H₂O solutions.

$$\text{H}_2\text{NCH}(\text{Ph})\text{CH}(\text{Ph})\text{CH}_2\text{OOH} \xrightleftharpoons{K_T} \text{}^+\text{H}_3\text{NCH}(\text{Ph})\text{CH}(\text{Ph})\text{COO}^-$$

Solvent	K _T =[Zw]/[Neut]	Note
pure DMSO	≈0	Only the neutral form observed
95% DMSO	1.26	
90% DMSO	3.5	
80% DMSO	≈∞	Only the zwitterionic form observed

With the exception of **1a**, the *erythro* free amino acid, all vicinal couplings 2H:3H of the remaining compounds are greater than 10 Hz as expected because steric energy is known to determine the preference of *erythro anti* and *threo (+)-sc* conformations of Scheme 1. The lower J-constant of **1a** of

Table 4. Coupling constants, J_{2H,3H} Hz, of amino acids, methyl and ethyl esters and N-acetylamino acids and their salts in HCONH₂.¹

<i>erythro</i>			<i>threo</i>		
Compd	Form	J _{2H,3H} Hz	Compd	Form	J _{2H,3H} Hz
1a ²	Free amino acid	9.0 (7.7 ^{3a} , 10.3 ^{3b})	2a ⁶	Free amino acid	10.9
1b ⁴	HCl salt	10.0	2b ⁷	HCl salt	10.9
1c ⁵	Potassium salt	10.3	2c ⁸	Potassium salt	10.5
3a ⁹	Free methyl ester	10.1	4a ¹¹	Free methyl ester	10.8
3b ¹⁰	HCl salt	11.0	4b ¹²	HCl salt	11.2
5a ¹³	Free ethyl ester	10.5	6a ¹⁵	Free ethyl ester	10.5
5b ¹⁴	HCl salt	11.2	6b ¹⁶	HCl salt	≈11
7a ¹⁷	Free acetylamino acid	11.8	8a ¹⁹	Free acetylamino acid	10.3
7c ¹⁸	Potassium salt	11.5	8c ²⁰	Potassium salt	9.6

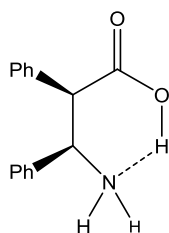
¹Concentration of samples 0.04 g in 0.5 ml HCONH₂. Chemical shifts in δ (ppm) are listed in the corresponding footnotes; ²4.04 (d 1H), >5.25; ^{3a}In DMSO_{d6}; ^{3b}In D₂O 4.10 (d 1H), 4.95 (d 1H), 7.32 (s 10H); ⁴4.27 (d 1H), 4.98 (d 1H); ⁵3.72 (d 1H), 4.45 (d 1H); ⁶In DMSO_{d6}/ D₂O 1:1; 3.80 (d 1H), 4.60 (d 1H), 7.04 (s 4H), 7.18 (s 6H); ⁷4.24 (d 1H), 4.90 (d 1H); ⁸3.62 (d 1H), 4.39 (d 1H); ⁹3.20 (s 3H), 3.81 (d 1H), 4.40 (d 1H); ¹⁰3.30 (s 3H), ≈4.37 (d 1H), 5.50 (d 1H); ¹¹3.57 (s 3H), ≈3.85 (d 1H), 4.40 (d 1H); ¹²3.57 (s 3H), ≈4.35 (d 1H), 4.96 (d 1H); ¹³0.70 (t 3H), 3.3 (q 2H), 3.67 (d 1H), 4.39 (d 1H); ¹⁴0.71 (t 3H), 3.72 (q 2H), 4.34 (d 1H), 4.96 (d 1H); ¹⁵1.01 (t 3H), 3.8 (d 1 H), ≈ 4 (4H, CH₂ + NH₂), 4.32 (d 1H); ¹⁶1.02 (t 3H), 4.2 (q 2H), ≈4.0 (d 1H), 4.92 (d 1H); ¹⁷1.57 (s 3H), 3.96 (d 1H), >5.25; ¹⁸1.46 (s 3H), 3.93 (d 1H), >5.25; ²⁰1.83 (s 3H), 3.84 (d 1H), >5.25.

Table 5. Local minima of the conformational energy of the zwitterions of the 3-amino-2,3-diphenylpropanoic acid in kcal/mol and statistical weight at 300°K.

	ΔE = E _o - (E _o)g	Nonbonded	Electrostatical	Hydrogen bonding	Normalized stat. weight
<i>threo</i> global minimum (E _o)g = -15.7					
(+)- <i>sc</i>	0.0	-3.6	-11.3	-1.0	1.0
<i>ap</i>	11.0	5.0	-11.9	-1.1	0.0
(-)- <i>sc</i>	8.5	1.0	-6.6	0.0	0.0
<i>erythro</i> global minimum (E _o)g = -10.7					
(+)- <i>sc</i>	5.3	6.9	-11.9	-1.0	0.0
<i>ap</i>	0.0	-4.5	-6.5	0.0	1.0
(-)- <i>sc</i>	2.2	3.8	-11.8	-1.1	0.0

9 Hz in formamide is also not surprising because *gauche* charged groups of opposite sign will lower the energy of the *sc* conformations in the *erythro* isomer and thus decrease the population of *erythro anti*. The same interaction of course stabilizes the (+)-*sc*-conformation in the *threo* isomer **2b**.

The still lower value of J_{2H3H} of 7.7 Hz observed with **1a** in pure $DMSO_{d6}$ shows that an attractive interaction arises in the neutral amino acid stronger than that in the zwitterion, where according to the IR data the neutral form of the amino acid entirely prevails in practice. This apparently is due to a hydrogen bond.



In D_2O on the contrary a larger J_{2H3H} of 10.3 Hz is observed. Although the obvious reason appears the higher dielectric coefficient of water, this is hardly the whole reason because intramolecular Coulomb interactions take place mainly through the hydrocarbon skeleton of low dielectric coefficient. Actually $\epsilon = 2.0$ is most commonly used in molecular mechanics. More likely of importance is the solvation of the groups: water solvates both cations and anions thus increasing their steric demands and thus overriding the attraction of the charged groups. The better solvation of $-NH_3^+$ than of $-NH_2$ explains the systematically higher J_{2H3H} -couplings found in the hydrochlorides of the amino esters compared to the free amino esters (Table 4).

MM deals with empirical force fields which agree quantitatively with experiments when they are well calibrated for a class of compounds. The preferred conformations are properly predicted. The closer local minima over the global one in the *erythro* case correspond to the greater mobility of the conformational equilibrium. The computed difference in the electrostatic interactions between the *sc* and *ap* positions of the charged groups amounts to ca. 4.5 kcal/mol. Only a small part of it is expressed to change pK_1 by 0.8 pK units indicating the complexity of factors determining experimental pK-values. Noteworthy is that in the case of the amino acid studied the *threo* isomer is more stable which is not common. On Table 5 are listed the local minima for the conformational energy of the conformations of the zwitterions of the *threo* and

erythro isomers of 3-amino-2,3-diphenylpropanoic acid (Scheme 1), calculated by means of the Sheraga force field [14].

CONCLUSION

The 1H NMR J_{2H3H} -couplings above 10 Hz found in formamide for the diastereomers of 3-amino-2,3-diphenylpropanoic acid, its salts and ester and N-acetyl derivatives confirmed the expectation of *anti* amino and carboxy groups in the *erythro* isomers and *syn* in the *threo* ones according to general preferences found in 1,2-disubstituted-1,2-diphenylethane systems. Coulomb attraction in the zwitterion only slightly enhances the *gauche* conformation in the *erythro* isomer ($J = 9.0$ Hz). This conformation is disfavored in water (10.3 Hz) apparently because of increasing steric demands due to solvation. An entirely different phenomenon was observed in DMSO – the low $J = 7.7$ Hz is actually the result of a strong hydrogen bond between the NH_2 and $COOH$ groups in the neutral form of amino acid with an abundance of ca. 100% in pure DMSO according to IR spectral data. The presence of water rapidly decreases the percentage of the neutral form: around 20% in 90% DMSO and ca 0% in 80% DMSO. The traditional measure of electrostatic effects is $\Delta pK = pK_2 - pK_1$ for ionizations of the two charged groups. When the groups are different, as in the case of amino acid, the effect of charge is exhibited by ΔpK between the pK's in the zwitterion and the N-acetyl or ester derivatives where one of the charges is removed. These ΔpK -values amounted to ca. 2 pK units according to our pK-measurements in two solvents: 80% methyl cellosolve and 90% DMSO. The effect of proximity of the charged groups, *syn* versus *anti* disposition in the zwitterion, is measured by $\Delta\Delta pK$ between ΔpK of the diastereomers. An early study of Gentschew and Toleva [15] showed a small $\Delta\Delta pK$ of 0.3 between **1a** and **2a** in water (0.1M KCl). This was interpreted by means of Tanford's model [16] that closer proximity in *threo* (*syn*) is compensated by a lower effective dielectric constant, D , in *erythro* (*anti*) because less interaction is realized through the solvent of large D [10]. As expected, in solvents with smaller D , 80% methyl cellosolve and 90% DMSO, larger $\Delta\Delta pK$ of 0.9 and 0.5 were found, respectively. Molecular mechanics calculations gave an electrostatic energy difference of 4.5 kcal/mol between the diastereomeric zwitterions corresponding to 3.2 $\Delta\Delta pK$ at 300 K.

REFERENCES

1. D. Ivanoff, A. Spassoff, *Bull. Soc. Chim. France*, **49**, 19 (1931).
2. D. Ivanoff, A. Spassoff, *Bull. Soc. Chim. France*, **49**, 375 (1931).
3. B. Kurtev, N. M. Mollov, *Acta Chim. Acad. Sci. Hungar.*, **18**, 430 (1959).
4. B. J. Kurtev, N. M. Mollov, M. J. Ljapova, A. S. Orahovats, *Monatsh. Chem.*, **94**, 904 (1963).
5. G. Fodor, J. Stefanovsky, B. Kurtev, *Chem. Ber.*, **98**, 705 (1965).
6. G. Fodor, R. F. Reavill, J. Stefanovsky, B. Kurtev, H. J. Bernstein, *Tetrahedron*, **22**, 235 (1966).
7. S. L. Spassov, *Tetrahedron*, **25**, 3638 (1969).
8. P. M. Ivanov, I. G. Pojarlieff, *J. Mol. Struct. (Theochem)*, **170**, 257 (1988).
9. N. Kurita, P. M. Ivanov, *J. Mol. Struct.*, **554**, 183 (2000).
10. M. Gentshev, A. Toleva, I. G. Pojarlieff, *Compt. r. Acad. Bulg. Sci.*, **23**, 799 (1970).
11. W. Simon, *Helvetica Chim. Acta*, **41**, 1835 (1958).
12. J. Tencheva, G. Velinov, O. Budevsky, *J. Electroanal. Chem. Interfacial Electrochem.*, **68**, 65 (1976).
13. F. J. C. Rossotti, H. Rossotti, *J. Chem. Educ.*, **42**, 375 (1965).
14. F. A. Momany, R. F. McGuire, A. W. Burgess, H. A. Scheraga, *J. Phys. Chem.*, **79**, 2361 (1975).
15. M. Gentschew, A. Toleva, *Nauchni trud. Ped. I-tut, Plovdiv*, **5**, 78 (1967).
16. C. Tanford, *J. Am. Chem. Soc.*, **79**, 5348 (1957).

ВЗАИМОДЕЙСТВИЕ НА ЗАРЕДЕНИ ГРУПИ. РК И КОНФОРМАЦИИ НА ДИАСТЕРЕОМЕРИТЕ НА 3-АМИНО-2,3-ДИФЕНИЛПРОПАНОВАТА КИСЕЛИНА, МЕТИЛОВИТЕ И ЕТИЛОВИТЕ Й ЕСТЕРИ И N-АЦЕТИЛНИ ПРОИЗВОДНИ

П. М. Иванов¹, И. Г. Пожарлиев^{1*}, С. Д. Симова¹, Г. Д. Велинов²

¹Институт по Органична химия с Център по Фитохимия, Българска Академия на Науките, ул. Акад. Г. Бончев, бл. 9, 1113 София, България

²Фармацевтичен Факултет, Медицински Университет - София, ул. Дунав 2, 1000 София, България

Постъпила на 03 юли 2014 г.; Коригирана на 22 юли 2014 г.

(Резюме)

Характерно за системата на 1,2-дизаместени-1,2-дифенилетани е силното предпочитание на конформацията с *антиперипланарни* фенилни групи, поради което другите заместители застават *ар* в *еритро* и (+)-*sc* в *трео* изомера. Същото явление бе установено за изомерите на 3-амино-2,3-дифенилпропановата киселина и нейните N-ацетилни и естерни производни съгласно J_{2H3H} -константите > 10 Хц, измерени в формамид. Само цвитерийонът на *еритро* аминокиселината **1a** даде по-ниска стойност 9.0 Хц, указание, че привличането на зарядите е преодоляло частично стеричните взаимодействия. Пресмятания с молекулярна механика със силовото поле на Шерага подкрепиха тази интерпретация. ИЧ-спектроскопски изследвания на равновесието цвитерийон - неутрална аминокиселина показаха, че неутралната форма е предпочетена в апротни разтворители, при **1a** $\approx 100\%$ в чист DMSO, но намалява при добавяне на вода като при 80% DMSO вече се наблюдава само цвитерийонът. рК-константите бяха определени потенциометрично в 80% метилцелосолв и в 90% DMSO. рК₁-константите за *трео* цвитерийона **1a** са с 0.8 рК единици по-големи от тези на *еритро* изомера, очаквано съотношение между *анти* и *гош* заредени групи. рК₂-константите на изомерите не се различават съществено; видимо електростатичното взаимодействие частично се компенсира поради стерично пречене породено от солватиране на NH_3^+ . рК на естерите и на N-ацетилираните производни се различават с около 2 рК единици от тези на цвитерийона, отразяващо силното влияние на взаимодействието на заредените групи. В органичните разтворители силно се променят киселинностите на $COOH$ и NH_3^+ в обратни посоки, което води до поява на неутралната форма, доказана с ИЧ изследванията.

Catalytic method for synthesis of Grignard compounds with magnesium attached to tertiary bridge head C-atom

V. Dimitrov

Institute of Organic Chemistry with Centre of Phytochemistry, Bulgarian Academy of Sciences, Acad. G. Bonchev str., bl. 9, 1113 Sofia, Bulgaria

Received June 30, 2014; Revised July 13, 2014

Dedicated to Acad. Dimiter Ivanov on the occasion of his 120th birth anniversary

The reaction of 1-norbornyl chloride, 1-bicyclooctyl chloride and 1-adamantyl bromide with magnesium was realized through the catalytic influence of anthracene. The formation of anthracene magnesium species, the so called “organic dissolved” magnesium, is the highly active form of the metal, responsible for the formation of the corresponding Grignard compounds in very pure form.

Key words: 1-norbornyl, 1-bicyclooctyl, 1-adamantyl, magnesium

INTRODUCTION

The organomagnesium compounds discovered by Victor Grignard over 100 years ago are indispensable for the organic synthetic chemistry [1,2]. The interest to the synthesis of Grignard-reagents is steadily growing since the development of new approaches to obtain functionalized organomagnesium compounds [3-5] expand the application area significantly in particularly for the preparation of pharmaceutically relevant structures. For the synthesis of Grignard compounds in some cases it is not easy to bring organic halides into reaction with metallic magnesium and therefore several methods for the activation of magnesium have been developed [6]. Among them the preparation of highly active magnesium is one of the very useful tools for synthesis of organomagnesium compounds. Highly active magnesium, the so called “Riecke-magnesium” could be obtained by reduction of anhydrous $MgCl_2$ with alkali metals [7-9]. Alternatively, highly active magnesium is produced during the decomposition of anthracene magnesium [10]. In the first case the active magnesium is a component of a highly heterogeneous mixture containing also metallic potassium and in the second, organic by-products are contained. Therefore the Grignard reagents prepared by using magnesium obtained through these methods may contain impurities or disturbing components for further applications.

In this work we were interested to prepare

Grignard reagents with the bridgehead substituted organic halides 1-norbornyl chloride (**1**), 1-bicyclooctyl chloride (**2**) and 1-adamantyl bromide (**3**).

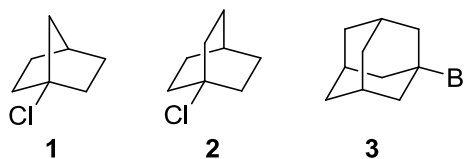


Fig. 1. Bridgehead substituted organic halides.

The chloride **1** forms 1-norbornyl-magnesium chloride after reaction with “Riecke-magnesium” [11] and 1-adamantyl-magnesium bromide has been prepared in the course of prolonged reaction after activation of magnesium with 1,2-dibromoethane [12,13]. The synthesis of 1-bicyclooctyl-magnesium has been realized *in situ* by means of “Riecke-magnesium” in order to obtain ^{13}C -labeled compound for NMR studies [14,15]. In general there is difficult to prepare Grignard reagents from organic halides with quaternary substituted C-atom. Generation of the Grignard reagents with these bridgehead substituted halides is very useful alternative to the corresponding organolithium compounds. The synthesis of organolithium or organomagnesium compounds with metal attached to the same organo-group offers excellent opportunity to use different conditions and to vary the reactivity within further transformations. Herein we are presenting very convenient catalytic method for the synthesis of bridgehead-substituted organomagnesium compounds.

* To whom all correspondence should be sent:
E-mail: vdim@orgchm.bas.bg

EXPERIMENTAL

General

All reactions were carried out in flame-dried *Schlenk*-flasks under argon atmosphere. Hexane and deuterated solvents were distilled over Na[Et₄Al]. Etheral solvents were distilled from sodium/benzophenone. Thin layer chromatography (TLC) was performed on aluminum sheets pre-coated with silica gel 60 F₂₅₄ (Merck). Flash column chromatography was carried out using silica gel 60 (230-400 mesh, Merck). The NMR spectra were recorded in THF-d₈ or CDCl₃ on a Bruker AM200 (200 MHz for ¹H NMR, 50.3 MHz for ¹³C NMR) and DRX 250 (250.13 MHz for ¹H NMR, 62.9 MHz for ¹³C NMR) spectrometer with TMS as the internal standard for chemical shifts (δ , ppm). ¹H and ¹³C NMR data are reported as follows: chemical shift, multiplicity (s = singlet, d = doublet, t = triplet, q = quartet, br = broad, m = multiplet), coupling constants (Hz), integration, and identification. Mass-spectra were recorded on a Finnigan MAT 8200 and Finnigan MAT SSQ 7000.

Reaction of 1-norbornyl lithium (**4**) with tetrahydrofuran (**5**) - synthesis of vinyloxy-lithium **7** and norbornane **8**

1-Norbornyl lithium (**4**) (1.09 g, 10.69 mmol) was placed in a *Schlenk*-flask and cooled to -50°C. Tetrahydrofuran (**5**) (50 ml) precooled to -50°C was added and the mixture was slowly warmed up by stirring it constantly. The gas evolution started slowly between -10 and 0°C and was intensive between 5°C and room temperature. The gas was collected and analyzed by mass-spectrometry as mixture of ethylene (**6**) and argon. The estimated quantity of ethylene corresponded to the expected value (there was deviation because of the argon content). The tetrahydrofuran (**5**) was evaporated in vacuum and the solid residue was treated with 70 ml of *n*-pentane. After filtration 0.41 g (77%) of **7** was isolated as colorless crystalline substance. The pentane filtrate was evaporated to dryness and the residue chromatographed (150 g silica gel; pentane/diethyl ether = 10:1) to give 0.91 g (88%) of **8**.

Data of **7**: ¹H NMR (THF-d₈, 200 MHz) δ 6.91 (dd, $J_{1-H, 2-H(Z)} = 13.3$ Hz, $J_{1-H, 2-H(E)} = 5.1$ Hz, 1H, 1-H), 3.54 (dd, $J_{2-H(Z), 2-H(E)} = 1.6$ Hz, 1H, 2-H(Z)), 3.15 (dd, 1H, 2-H(E)) ppm. ¹³C NMR (THF-d₈, 50.3 MHz) δ 158.98 (2-C), 81.74 (1-C), 68.22 and 26.30 coordinated THF.

General procedure (GP) for synthesis of 1-norbornyl-magnesium chloride (**9**), 1-bicyclooctyl-magnesium chloride (**10**) and 1-adamantyl-magnesium bromide (**11**)

Magnesium turnings (fivefold excess related to the quantity of the corresponding alkyl halide) were placed in a *Schlenk* flask and were dried in vacuum by heating over 100°C. After cooling to rt the solvent THF was introduced under argon atmosphere in such quantity to cover the magnesium turnings. For activation of magnesium ethyl bromide (5 mol % of the quantity of the corresponding alkyl halide) was introduced and the mixture was allowed to stand over the night. Anthracene (2 mol %) was introduced and after several seconds green color appeared on the surface of magnesium, which turned after several minutes in blue color indicating the good activation. The blue mixture was stirred for 0.5 h and the corresponding alkyl halide was introduced drop wise as THF-solution (approximately 90 ml THF for 10 mmol of alkyl halide). The reaction mixture was stirred for the necessary time (see below), filtered and the volume of the solution was measured. The content of the corresponding Grignard compound in the obtained solution was determined, as follows: Aliquot of the RMgX-solution was quenched in 0.1N HCl-solution and the reacted HCl was determined by titration with 0.1N NaOH-solution. Magnesium content was determined by complexometric titration.

Synthesis of 1-norbornyl-magnesium chloride (**9**)

According to GP, after stirring the reaction mixture at rt for 5 h and standing for 15 days, 250 ml THF-solution of **9** in 85% yield was prepared from 3.94 g (162.00 mmol) magnesium, activated with 0.176 g (1.62 mmol) ethyl bromide and 0.115 g (0.65 mmol) anthracene, and 4.23 (32.38 mmol) of **1**. ¹³C NMR (THF-d₈, 50.3 MHz) δ 47.27 (7-C), 39.09 (2-C, 6-C), 35.66 (4-C), 31.44 (3-C, 5-C), 13.75 (1-C), 68.20 and 26.19 coordinated THF.

Synthesis of 1-bicyclooctyl-magnesium chloride (**10**)

According to GP, after stirring the reaction mixture at rt for 5 h and standing for 15 days, 120 ml THF-solution of **10** in 78% yield was prepared from 2.02 g (83.09 mmol) magnesium, activated with 0.090 g (0.83 mmol) ethyl bromide and 0.059 g (0.33 mmol) anthracene, and 2.40 (16.59 mmol)

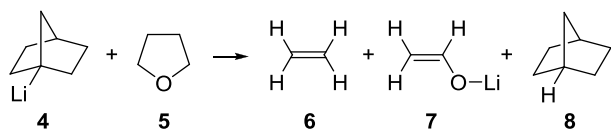
of **2**. ^{13}C NMR (THF- d_8 , 50.3 MHz) δ 33.21 (β), 29.00 (δ), 28.89 (γ), 25.13 (α), 68.06 and 25.77 coordinated THF.

Synthesis of 1-adamantyl-magnesium bromide (**11**)

According to GP, after stirring the reaction mixture at rt for 5 h and standing for 4 days, 250 ml THF-solution of **11** in 80% yield was prepared from 1.70 g (69.93 mmol) magnesium, activated with 0.076 g (0.70 mmol) ethyl bromide and 0.050 g (0.28 mmol) anthracene, and 3.00 (13.95 mmol) of **3**. ^{13}C NMR (THF- d_8 , 50.3 MHz) δ 38.38 (β), 36.05 (δ), 30.13 (γ), 26.36 (α); no coordinated THF could be observed.

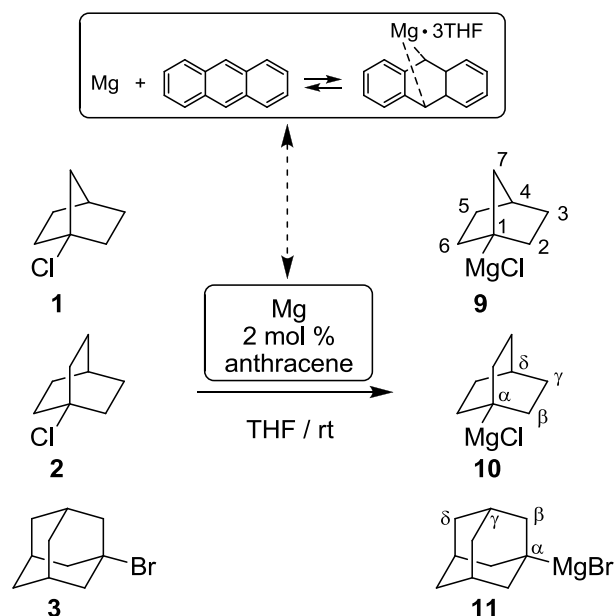
RESULTS AND DISCUSSION

We have long standing interest in the synthesis of 1-norbornyl transition metal compounds [16-18] in which 1-norLi **4** is the reagent of choice. Some of the reactions have to be performed in ethereal solvents and therefore, it is advantageous to avoid the possibility of side reactions caused by ether-cleavage of 1-norLi. Consequently our initial interest to prepare bridgehead substituted organo-magnesium compounds arose from the fact that 1-norbornyl lithium (1-norLi, **4**) undergoes rapid ether-cleavage with ethereal solvents (Scheme 1). The reaction of 1-norLi (**4**) with tetrahydrofuran (THF, **5**) occurs even at low temperature with formation of ethen (**6**). Between -10 and 0°C the ether-cleavage reaction is relatively slow; from 5°C up to room temperature there is intensive gas evolution. The generated gas was collected and proved by mass-spectrometry to be ethen (**6**). After evaporation of the solvent **5** and treatment the residue with pentane colorless solid was precipitated, which was identified as vinyloxy-lithium (**7**) (see Experimental). This compound was in fact the lithium enolate of acetaldehyde and this was proved through the identification of acetaldehyde formation generated by hydrolysis of **7**. In the pentane filtrate was identified norbornane **8** (by GC-MS experiments). The reaction observed is supported by published data [19,20].



Scheme 1. Reaction between 1-norbornyl lithium and tetrahydrofuran.

On these grounds we were interested to develop valuable pathway to generate 1-norbornyl-magnesium chloride in ethereal solvent (preferably THF). The use of the organometallic reagent anthracene magnesium in stoichiometric reactions with alkyl halides has been described previously as method providing in some cases excellent results [10]. The formation of anthracene in the course of the corresponding Grignard reagent generation is disadvantageous if further transformations are aimed. Catalytic variants of the anthracene magnesium promoted Grignard reagents formation have also been tested [21]. The present work has been inspired by published reports [22,23] describing that the addition of catalytic quantities of anthracene to magnesium in tetrahydrofuran results in the formation of the so called “organic dissolved” magnesium.



Scheme 2. Synthesis of bridgehead substituted organo-magnesium compounds **9-11**.

The optimization was performed first in the reaction of 1-norbornyl chloride (**1**) with magnesium in THF catalyzed by anthracene (Scheme 2). The generation of magnesium anthracene is the decisive step. However, the reaction of magnesium with anthracene is very sensitive and can be initiated only if very dry THF and properly activated magnesium are used. For this purpose it is important to dry Mg in vacuum by heating it above 100°C and to use THF freshly distilled from sodium/benzophenone. To the mixture of Mg and THF prepared in *Schlenk*-flask under argon atmosphere is introduced ethyl

bromide (5% related to the organic halide to be used for the formation of RMgX) and then the mixture is kept at room temperature for several hours (better over night; see Experimental). The ethyl bromide used forms Grignard reagent activating thus the Mg-surface. Besides, the EtMgBr formed contributes on prolonged standing to additional activation of the metal surface. The magnesium activated in this manner reacts with anthracene (2 mol %) rapidly forming yellow-green mixture turning into blue after stirring for several minutes. After stirring for 0.5 h 1-norbornyl chloride (**1**) was introduced drop wise. The reaction of the organic halide and the “organic dissolved” magnesium starts immediately indicated by the disappearance of the blue color. If no further 1-norbornyl chloride is introduced the species causing the blue color are formed within several minutes. These species are most probably anthracene magnesium radical anion complexes which nature has been extensively discussed elsewhere [24]. The formation of the anthracene magnesium species is reversible with two consequences, formation of quasi atomic magnesium in solution and additional activation of the metal surface [22].

The reaction of 1-norbornyl chloride (**1**) to form the Grignard reagent was slow. For the formation of the reagent in 48% yield reaction time of 24 h was necessary and acceptable yield (85%) was achieved only after 14 days (see Table 1). For comparison the related bridgehead substituted bicyclooctyl chloride (**2**) and adamantyl bromide (**3**) were applied in the reaction with magnesium. Compound **2** has been synthesized according own published procedure [25] whereas **3** is commercially available. The formation of the Grignard reagent with **2** was slow and good yields could be realized after 14 days although acceptable conversion has been observed in the first 24 h. In the case of **3** the formation of the corresponding magnesium reagent proceeded in 4 h in good yield (70%). The yield could be improved slightly up to 80% if the reaction time is prolonged to 4 days. It should be pointed out that apart from the prolonged time for the formation of the reagents the method described is definitely synthetically valuable. The obtained Grignard reagents are very pure and could be stored under argon atmosphere for months.

The structure of the synthesized compounds **9-11** was confirmed by ^{13}C NMR spectroscopy (see Experimental). The samples were prepared by evaporating the THF to dryness and dissolution of the remaining solid residue in THF- d_8 . As expected the persistent coordinated THF could be observed in the ^{13}C spectra, however only for compounds **9**

and **10**. It was surprising the absence of coordinated THF in the case of **11** which is probably a result of the very crowded structure of the adamantyl-Mg-compound. The ^1H NMR spectra do not provide useful structural information due to the overlapping multiplets. Compounds **9-11** react with water to form the corresponding hydrocarbons proved by mass-spectra. The 1-norbornyl magnesium reagent was used successfully for reactions with nickelocene [16,18] to prepare CpNi(1-nor)-olefin complexes. These results will be reported elsewhere [26].

Table 1. Reaction time for the formation and yields of Grignard compounds **9-11**.

Compound	Reaction time	Yield [%]
1-nor-MgCl (9)	24 h	48
	4 days	60
	14 days	85
1-boc-MgCl (10)	24 h	58
	4 days	65
	14 days	78
1-ad-MgBr (11)	24 h	70
	4 days	80

CONCLUSION

Convenient method for anthracene magnesium catalyzed preparation of Grignard compounds has been demonstrated in which the magnesium is attached to the bridgehead carbon atom of the norbornyl, bicyclooctyl and adamantyl organic groups. The magnesium compounds are stable in form of THF solutions under argon atmosphere and can be easily stored for further applications.

Acknowledgements: Financial support of Alexander von Humboldt Foundation is gratefully acknowledged.

REFERENCES

- G. S. Silverman, P. E. Rakita, Eds., Handbook of Grignard Reagents, Marcel Dekker, New York, 1996.
- B. J. Wakefield, Organomagnesium Methods in Organic Synthesis, Academic Press, London, 1995.
- T. Klatt, J. T. Markiewicz, C. Saemann, P. Knochel, *J. Org. Chem.*, **79**, 4253 (2014).
- P. Knochel, M. A. Schade, S. Bernhardt, G. Manolikakes, A. Metzger, F. M. Piller, C. J. Rohbogner, M. Mosrin, *Beilstein J. Org. Chem.*, **7**, 1261 (2011).
- P. Knochel, W. Dohle, N. Gommermann, F. F. Kneisel, F. Kopp, T. Korn, I. Sapountzis, V. A. Vu, *Angew. Chem. Int. Ed.*, **42**, 4302 (2003).

6. U. Tilstam, H. Weinmann, *Org. Proc. Res. Dev.*, **6**, 906 (2002).
7. R. D. Rieke, P. M. Hudnall, *J. Am. Chem. Soc.*, **94**, 7178 (1972).
8. R. D. Rieke, S. E. Bales, *J. Chem. Soc., Chem. Commun.*, 879 (1973).
9. R. D. Rieke, S. E. Bales, *J. Am. Chem. Soc.*, **96**, 1775 (1974).
10. B. Bogdanovic, N. Janke, H.-G. Kinzelmann, *Chem. Ber.*, **123**, 1507 (1990).
11. R. D. Rieke, S. E. Bales, P. M. Hudnall, T. P. Burns, G. S. Poindexter, *Org. Synth.*, **59**, 85 (1979); Coll. Vol. **6**, 845 (1988).
12. G. Molle, P. Bauer, J. E. Dubois, *J. Org. Chem.*, **47**, 4120 (1982).
13. G. Schäfer, C. Matthey, J. W. Bode, *Angew. Chem. Int. Ed.*, **51**, 9173 (2012).
14. M. Barfield, S. E. Brown, E. D. Canada, Jr., N. D. Ledford, J. L. Marshall, S. R. Walter, E. Yakali, *J. Am. Chem. Soc.*, **102**, 3355 (1980).
15. E. W. Delia, H. Gangodawila, P. E. Pigou, *J. Org. Chem.*, **53**, 592 (1988).
16. H. Lehmkuhl, V. Dimitrov, *J. Organomet. Chem.*, **519**, 69 (1996).
17. H. Lehmkuhl, V. Dimitrov, *J. Organomet. Chem.*, **519**, 83 (1996).
18. V. Dimitrov, A. Linden, *Angew. Chem. Int. Ed.*, **42**, 2631 (2003).
19. P. Stanetty, H. Roller, M. Mihovilovic, *J. Org. Chem.*, **57**, 6833 (1992).
20. A. Maercker, *Angew. Chem. Int. Ed.*, **26**, 972 (1987).
21. S. Harvey, P. C. Junk, C. L. Raston, G. Salem, *J. Org. Chem.*, **53**, 3134 (1988).
22. H. Bönemann, B. Bogdanovic, R. Brinkmann, D.-W. He, B. Spliethoff, *Angew. Chem., Int. Ed.*, **22**, 728 (1983).
23. B. Bogdanovic, S.-T. Liao, R. Mynott, K. Schlichte, U. Westeppe, *Chem. Ber.*, **117**, 1378 (1884).
24. B. Bogdanovic, *Acc. Chem. Res.*, **21**, 261 (1988).
25. K. Kostova, V. Dimitrov, *Synth. Commun.*, **25**, 1575 (1995).
26. V. Dimitrov, Synthesis of CpNi(1-nor)-olefin complexes, in preparation for publication.

КАТАЛИТИЧЕН МЕТОД ЗА СИНТЕЗ НА ГРИНЯРОВИ СЪЕДИНЕНИЯ С МАГНЕЗИЙ СВЪРЗАН С ТРЕТИЧЕН МОСТОВИ ВЪГЛЕРОДЕН АТОМ

В. Димитров

Институт по Органична химия с Център по Фитохимия, Българска Академия на Науките, ул. Акад. Г. Бончев, бл. 9, 1113 София, България

Постъпила на 30 юни 2014 г.; Коригирана на 13 юли 2014 г.

(Резюме)

Реакцията на 1-норборнил хлорид, 1-бициклооктил хлорид и 1-адамантил бромид с магнезий е осъществена чрез каталитичното влияние на антрацен. Формирането на антрацен магнезиеви интермедиати, така наречения „органично разтворен“ магнезий, е високо активната форма на метала, отговорна за формирането на съответните гринярови реагенти в чист вид.

Phosphino-carboxamide hybrid ligands with a camphane scaffold for Pd-catalyzed asymmetric allylic alkylation

I. Philipova¹, G. Stavrakov², V. Dimitrov^{1*}

¹Institute of Organic Chemistry with Centre of Phytochemistry, Bulgarian Academy of Sciences, Acad. G. Bonchev str., bl. 9, 1113 Sofia, Bulgaria

²Faculty of Pharmacy, Medical University of Sofia, 2 Dunav str., 1000 Sofia, Bulgaria

Received April 03, 2014; Revised April 29, 2014

Dedicated to Acad. Dimiter Ivanov on the occasion of his 120th birth anniversary

Condensation of *ortho*-diphenylphosphino benzoic acid with 3-*exo*-aminoisoborneol, isobornylamine and bornylamine afforded three new ligands, which were evaluated in the palladium-catalyzed allylic alkylation of (*E*)-1,3-diphenyl-2-propen-1-yl acetate. The catalytic performance strongly depended on the system used to generate the dimethyl malonate anion. The best enantioselectivity was achieved with the 3-*exo*-aminoisoborneol derived ligand when Cs₂CO₃ was used as a base. The isobornylamine and bornylamine derived ligands gave generally low enantioselectivities.

Key words: (+)-camphor, phosphino-carboxamides, P,O-ligands, allylic substitution

INTRODUCTION

Palladium-catalyzed asymmetric allylic alkylation has proven to be a powerful method for the preparation of a wide variety of chiral compounds and the rapid assembly of complex molecular architecture from simple starting materials [1]. While many types of catalyst systems have been successfully employed with certain systems, diphenylphosphino benzoic acid (DPPBA) based ligands have found use over a broad range of substrate classes [2].

Over the years, there has been a steady interest in the synthesis and application of simple, hybrid, hemilabile, P,O-type ligands [3]. Among the latter compounds, phosphino-carboxamides evolved into a specific class of structurally diverse molecules, bearing the combination of weak and strong donor heteroatom pairs, which enables them to bind to almost any metal, generating electronic asymmetry [4]. Another privilege is their stability and the ease with which they could be accessed. The advantages presented above and the unambiguous proof that P,O-mode of coordination with palladium center is giving catalytically active complex (Fig. 1, I) [5-7] justify the efforts to the development and application of amido-phosphine ligands in asymmetric allylic alkylation (AAA) [8-17].

A number of simple phosphino-carboxamides

have been studied. For example, Marinho *et al.* [18, 19] have prepared a series of phosphino-amide ligands bearing a free hydroxyl function (Fig. 1, II).

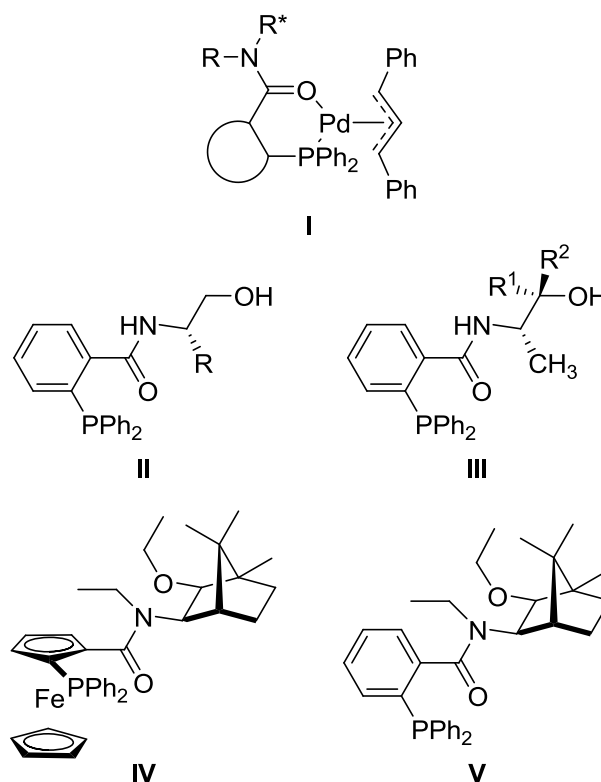


Fig. 1. Phosphino-carboxamides as hybrid, hemilabile, P,O-type ligands.

* To whom all correspondence should be sent:

E-mail: vdim@orgchm.bas.bg

The application of the ligands in AAA resulted in moderate enantioselectivities (up to 62% ee) and the authors hypothesized that the free-OH group was also coordinating with Pd, resulting in a deactivation of the latter. Mahadik *et al.* [20-22] reported the synthesis and application of nor-ephedrine and pseudonorephedrine analogues (Fig. 1, **III**) that furnished slightly better enantioselectivities (up to 75% ee). Noteworthy is that in both cases the ligands are secondary amides.

Recently, we have accomplished practical synthesis of camphane based planar chiral diphenylphosphino-ferrocenecarboxamide (Fig. 1, **IV**) and diphenylphosphino-benzenecarboxamide ligands (Fig. 1, **V**) [23-25]. Application of these ligands in the Pd-catalyzed AAA as P,O-chelates proceeded with promising degree of enantio-selectivity (up to 92%) [25]. The use of camphane based chiral auxiliary proved to be the major contributor to the asymmetric induction in the catalytic process.

Encouraged by these results, we dedicated our efforts toward the synthesis of secondary benzenecarboxamides. A switch of tertiary to secondary amides gave us the opportunity to investigate the influence of the amide hydrogen in the catalytic process. Furthermore, examination of the effect of the OH-function on the ligand structure/activity study, made us interested in the synthesis of secondary amide analogue of **V** (Fig 1.), bearing a free hydroxyl group. Herein, we report a practical synthesis of new camphor derived phosphino-benzenecarboxamide ligands and their application in Pd-catalyzed asymmetric allylic alkylation.

EXPERIMENTAL

Reagents were commercial grade and used without further purification. CH₂Cl₂ was distilled from CaH₂. THF and Et₂O were distilled over sodium/benzophenone. Thin layer chromatography (TLC) was performed on aluminum sheets pre-coated with Merck Kieselgel 60 F₂₅₄ 0.25 mm (Merck). Flash column chromatography was carried out using Silica Gel 60 230-400 mesh (Fluka). Melting points of the compounds were determined using "Electrothermal" MEL-TEMP apparatus (uncorrected). Optical rotations ($[\alpha]_D^{20}$) were measured on Perkin-Elmer 241 polarimeter. The NMR spectra were recorded on a Bruker Avance II+ 600 (600.13 for ¹H NMR, 150.92 MHz for ¹³C NMR and 242.92 MHz for ³¹P NMR) spectrometer with TMS (85% H₃PO₄ for ³¹P) as internal standard for chemical shifts (δ , ppm). ¹H and ¹³C NMR data are reported as follows: chemical shift, multiplicity (s = singlet, d = doublet, t = triplet, q = quartet, br =

broad, m = multiplet), coupling constants (Hz), integration and identification. The assignment of the ¹H and ¹³C NMR spectra was made on the basis of DEPT, COSY, HSQC, HMBC and NOESY experiments. Mass spectra (MS) were recorded on a Thermo Scientific DFS (High Resolution Double Focusing Magnetic Sector) mass spectrometer (Bremen, Germany) and are reported as fragmentation in m/z with relative intensities (%) in parentheses. The high performance liquid chromatography (HPLC) separations were performed with an Agilent 1100 System fitted with diode array detector and manual injector with a 20 μ l injection loop Chiralpak IA, 250x4.6mm particle size 5 μ m, and Chiralpak IC 250x4.6mm, particle size 5 μ m stainless-steel columns from Chiral Technologies Europe LTD were used. The analyses were performed at 25°C. Elemental analyses were performed by Microanalytical Service Laboratory of Faculty of Chemistry, University of Sofia, using Vario EL3 CHNS(O) and Microanalytical service Laboratory of the Institute of Organic Chemistry, Bulgarian Academy of Science.

General Procedure for the preparation of the amides 2, 4 and 6 (GP)

1-Hydroxybenzotriazole (HOBt) (1.1 equiv) and 2-diphenylphosphinobenzoic acid (1 equiv) were suspended in dichloromethane, and the mixture was stirred for 5 min. Then, *N*-[3-(dimethylamino)propyl]-*N*-ethylcarbodiimide (EDC) (1.1 equiv) was added, followed by the appropriate amine, diluted with a small amount of dichloromethane (1.1 equiv). Stirring was continued for 24 h at room temperature until the starting material was completely consumed (TLC). Then the mixture was directly subjected to flash column chromatography.

*Synthesis of 2-(diphenylphosphino)-*N*-((1*S*,2*R*,3*S*,4*R*)-3-hydroxy-4,7,7-trimethylbicyclo[2.2.1]heptan-2-yl)benzamide 2*

According to GP, a mixture of 2-diphenylphosphinobenzoic acid (0.100 g, 0.326 mmol), HOBt (0.049 g, 0.359 mmol), EDC (0.069 g, 0.359 mmol) and (1*R*,2*S*,3*R*,4*S*)-3-amino-1,7,7-trimethyl-bicyclo[2.2.1]heptan-2-ol [26] (0.061 g, 0.359 mmol) afforded after column chromatography (silica gel, CH₂Cl₂/Et₂O, 100:1) 0.127 g (85% yield) of **2** as a white solid; mp >89°C decomp. $[\alpha]_D^{20}$ +16.0 (c 0.53, CHCl₃). ¹H NMR (CDCl₃, 600 MHz) δ 0.76 (s, 3H, 9-H), 0.91 (s, 3H, 10-H), 0.97 (s, 3H, 8-H), 1.01-1.07 (m, 1H, 6-H_{endo}), 1.12-1.16 (m, 1H, 5-H_{endo}), 1.44-1.49 (m, 1H, 6-H_{exo}), 1.65-1.70 (m, 1H, 5-H_{exo}), 1.68 (d, *J* 2.3 Hz, 1H, 4-H), 2.23 (d, *J* 2.6 Hz, 1H, OH), 3.78 (dd, *J* 7.2, 3.4 Hz, 1H, 2-H),

3.80-3.83 (m, 1H, 3-H), 6.40 (d, J 5.9 Hz, 1H, NH), 6.98 (ddd, J 7.6, 4.0, 1.0 Hz, 1H, arom.), 7.27-7.31 (m, 5H, arom.), 7.32-7.34 (m, 6H, arom.), 7.37 (dt, J 7.5, 1.3 Hz, 1H, arom.), 7.55 (ddd, J 7.5, 3.8, 1.2 Hz, 1H, arom.) ppm. ^{13}C NMR (CDCl_3 , 150.9 MHz) δ 11.32 (10-C), 20.94 (8-C), 21.37 (9-C), 26.23 (5-C), 33.23 (6-C), 46.93 (7-C), 49.10 (1-C), 50.03 (4-C), 58.41 (3-C), 80.09 (2-C), 127.35 (d, $J_{\text{P,C}}$ 5.3 Hz, 1 arom. CH), 128.48 (d, $J_{\text{P,C}}$ 7.1 Hz, 2 arom. CH), 128.57 (d, $J_{\text{P,C}}$ 7.1 Hz, 2 arom. CH), 128.73 (2 arom. CH), 128.83 (1 arom. CH), 130.00 (1 arom. CH), 133.71 (d, $J_{\text{P,C}}$ 19.8 Hz, 2 arom. CH), 133.95 (d, $J_{\text{P,C}}$ 20.1 Hz, 2 arom. CH), 134.27 (1 arom. CH), 135.84 (d, $J_{\text{P,C}}$ 19.4 Hz, 2 arom. C), 136.92 (d, $J_{\text{P,C}}$ 9.8 Hz, 2 arom. C), 137.21 (d, $J_{\text{P,C}}$ 11.0 Hz, 2 arom. C), 141.95 (d, $J_{\text{P,C}}$ 26.7 Hz, 2 arom. C), 169.14 (CO) ppm. ^{31}P NMR (CDCl_3 , 242.92 MHz): δ -10.44 (s) ppm. MS (ESI): m/z 458 (100, $[\text{M}+1]^+$). $\text{C}_{29}\text{H}_{32}\text{NO}_2\text{P}$ (457.54): calcd. C 76.13, H 7.05, N 3.06, found C 76.24, H 7.13, N 3.10.

Synthesis of 2-(diphenylphosphino)-N-((1R,2R,4R)-1,7,7-trimethylbicyclo[2.2.1]heptan-2-yl)benzamide 4

According to GP, a mixture of 2-diphenylphosphinobenzoic acid (0.100 g, 0.326 mmol), HOBt (0.049 g, 0.359 mmol), EDC (0.069 g, 0.359 mmol) and (1R,2R,4R)-1,7,7-trimethyl bicyclo[2.2.1]heptan-2-amine [27] (0.055 g, 0.359 mmol) afforded after column chromatography (silica gel, $\text{CH}_2\text{Cl}_2/\text{Et}_2\text{O}$, 100:1) 0.142 g (99% yield) of **4** as a white solid; mp 73-75 °C. $[\alpha]_{\text{D}}^{20}$ -58.1 (c 0.74, CHCl_3). ^1H NMR (CDCl_3 , 600 MHz) δ 0.67 (s, 3H, 9-H), 0.78 (s, 3H, 8-H), 0.82 (s, 3H, 10-H), 1.09-1.14 (m, 1H, 5- H_{endo}), 1.27-1.31 (m, 1H, 6- H_{endo}), 1.39-1.43 (m, 1H, 3- H_{exo}), 1.50-1.55 (m, 1H, 6- H_{exo}), 1.64-1.66 (m, 1H, 5- H_{exo}), 1.66 (d, J 4.2 Hz, 1H, 4-H), 1.77 (dd, J 13.3, 9.1 Hz, 1H, 3- H_{endo}), 4.00 (dt, J 9.0, 5.1 Hz, 1H, 2- H_{endo}), 5.89 (d, J 8.3 Hz, 1H, NH), 6.94 (dd, J 7.0, 4.0 Hz, 1H, arom.), 7.22-7.29 (m, 4H, arom.), 7.31-7.34 (m, 7H, arom.), 7.38 (dt, J 7.5, 1.0 Hz, 1H, arom.), 7.57 (ddd, J 6.6, 3.8, 0.9 Hz, 1H, arom.) ppm. ^{13}C NMR (CDCl_3 , 150.9 MHz) δ 11.76 (10-C), 20.05 (9-C), 20.19 (8-C), 26.94 (5-C), 35.82 (6-C), 38.46 (3-C), 44.77 (4-C), 47.01 (7-C), 48.63 (1-C), 57.14 (2-C), 127.81 (d, $J_{\text{P,C}}$ 5.2 Hz, 1 arom. CH), 128.50 (d, $J_{\text{P,C}}$ 7.0 Hz, 2 arom. CH), 128.65 (d, $J_{\text{P,C}}$ 7.0 Hz, 2 arom. CH), 128.70 (1 arom. CH), 128.82 (1 arom. CH), 128.86 (1 arom. CH), 129.91 (1 arom. CH), 133.76 (d, $J_{\text{P,C}}$ 20.0 Hz, 2 arom. CH), 133.85 (d, $J_{\text{P,C}}$ 20.0 Hz, 2 arom. CH), 134.21 (1 arom. CH), 135.15 (d, $J_{\text{P,C}}$ 20.0 Hz, 1 arom. C), 136.87 (d, $J_{\text{P,C}}$ 11.3 Hz, 1 arom. C), 137.11 (d, $J_{\text{P,C}}$ 11.5 Hz, 1 arom. C), 142.31 (d, $J_{\text{P,C}}$ 27.0 Hz, 1 arom. C), 168.38 (CO)

ppm. ^{31}P NMR (CDCl_3 , 242.92 MHz): δ -11.37 (s) ppm. MS (ESI): m/z 442 (100, $[\text{M}+1]^+$). $\text{C}_{29}\text{H}_{32}\text{NOP}$ (441.54): calcd. C 78.88, H 7.30, N 3.17, found C 78.99, H 7.42, N 3.19.

Synthesis of 2-(diphenylphosphino)-N-((1R,2S,4R)-1,7,7-trimethylbicyclo[2.2.1]heptan-2-yl)benzamide 6

According to GP, a mixture of 2-diphenylphosphinobenzoic acid (0.100 g, 0.326 mmol), HOBt (0.049 g, 0.359 mmol), EDC (0.069 g, 0.359 mmol) and (1R,2S,4R)-1,7,7-trimethyl bicyclo[2.2.1]heptan-2-amine [28] (0.055 g, 0.359 mmol) afforded after column chromatography (silica gel, $\text{CH}_2\text{Cl}_2/\text{Et}_2\text{O}$ 100:1) 0.140 g (97% yield) of **6** as a white solid; mp 71-72 °C. $[\alpha]_{\text{D}}^{20}$ +10.2 (c 0.47, CHCl_3). ^1H NMR (CDCl_3 , 600 MHz) δ 0.63 (dd, $J_{\text{H,H}}$ = 13.4, 4.6 Hz, 1H, 3- H_{endo}), 0.77 (s, 3H, 10-H), 0.82 (s, 3H, 9-H), 0.85-0.89 (m, 1H, 5- H_{endo}), 0.91 (s, 3H, 8-H), 1.19-1.24 (m, 2H, 6- H_{endo} , 6- H_{exo}), 1.57 (d, J 4.5 Hz, 1H, 4-H), 1.60-1.66 (m, 1H, 5- H_{exo}), 2.24-2.29 (m, 1H, 3- H_{exo}), 4.30-4.34 (m, 1H, 2- H_{exo}), 6.02 (d, J 7.3 Hz, 1H, NH), 6.92 (ddd, J 7.7, 4.1, 1.0 Hz, 1H, arom.), 7.23-7.29 (m, 4H, arom.), 7.30-7.35 (m, 7H, arom.), 7.40 (dt, J 7.5, 1.2 Hz, 1H, arom.), 7.65 (ddd, J 7.6, 3.8, 1.2 Hz, 1H, arom.) ppm. ^{13}C NMR (CDCl_3 , 150.9 MHz) δ 13.61 (10-C), 18.66 (8-C), 19.74 (9-C), 28.06 (6-C), 28.12 (5-C), 37.00 (3-C), 44.71 (4-C), 47.99 (7-C), 49.36 (1-C), 54.51 (2-C), 127.30 (d, $J_{\text{P,C}}$ 5.3 Hz, 1 arom. CH), 128.60 (d, $J_{\text{P,C}}$ 6.9 Hz, 2 arom. CH), 128.82 (1 arom. CH), 128.90 (1 arom. CH), 128.92 (1 arom. CH), 129.97 (1 arom. CH), 133.79 (d, $J_{\text{P,C}}$ 18.6 Hz, 4 arom. CH), 134.10 (1 arom. CH), 134.43 (d, $J_{\text{P,C}}$ 19.6 Hz, 1 arom. C), 136.64 (d, $J_{\text{P,C}}$ 11.0 Hz, 1 arom. C), 136.93 (d, $J_{\text{P,C}}$ 11.4 Hz, 1 arom. C), 142.52 (d, $J_{\text{P,C}}$ 27.3 Hz, 1 arom. C), 169.10 (CO) ppm. ^{31}P NMR (CDCl_3 , 242.92 MHz): δ -11.17 (s) ppm. MS (ESI): m/z 442 (100, $[\text{M}+1]^+$). $\text{C}_{29}\text{H}_{32}\text{NOP}$ (441.54): calcd. C 78.88, H 7.30, N 3.17, found C 78.96, H 7.25, N 3.21.

General procedure for the palladium-catalyzed allylic alkylation

A: A mixture of chiral ligand (0.03 mmol), $[\text{Pd}(\eta^3\text{-C}_3\text{H}_5\text{Cl})_2]$ (6.0 mg, 0.016 mmol), and LiOAc (0.05 mmol) in a dry solvent (3 mL) was stirred at rt in a Schlenk tube for 30 min. Then, rac-(*E*)-1,3-diphenylprop-2-en-1-yl acetate (126 mg, 0.5 mmol) was introduced followed, after stirring for another 5 min, by N,O-bis-(trimethylsilyl)acetamide (BSA; 0.37 mL, 1.5 mmol) and dimethyl malonate (0.17 mL, 1.5 mmol). The mixture was stirred at rt for 24 h, then the reaction mixture was diluted with

diethyl ether (10 mL) and washed consecutively with sat. aq. NH_4Cl and water. The organic phase was dried over anhydrous Na_2SO_4 , filtered and concentrated in vacuo. The residue was purified by flash column chromatography (silica gel, hexane:ethyl acetate, 9:1).

B: A mixture of chiral ligand (0.03 mmol), $[\text{Pd}(\eta^3\text{-C}_3\text{H}_5)\text{Cl}]_2$ (6.0 mg, 0.016 mmol), in a dry solvent (3 mL) was stirred at rt in a Schlenk tube for 30 min. Then, rac-1,3-diphenylprop-2-en-1-yl acetate (126 mg, 0.5 mmol) was introduced followed, after stirring for another 5 min, by Cs_2CO_3 (0.326 g, 1.0 mmol) and dimethyl malonate (0.11 mL, 1.0 mmol). The mixture was stirred at rt for 24 h. The reaction was quenched with sat. aq. NH_4Cl , extracted with EtOAc (3×20 mL). The organic phase was washed with saturated aqueous NaHCO_3 , water, and brine, dried over Na_2SO_4 , and concentrated under reduced pressure. The residue was purified by flash column chromatography (silica gel, hexane:ethyl acetate, 9:1).

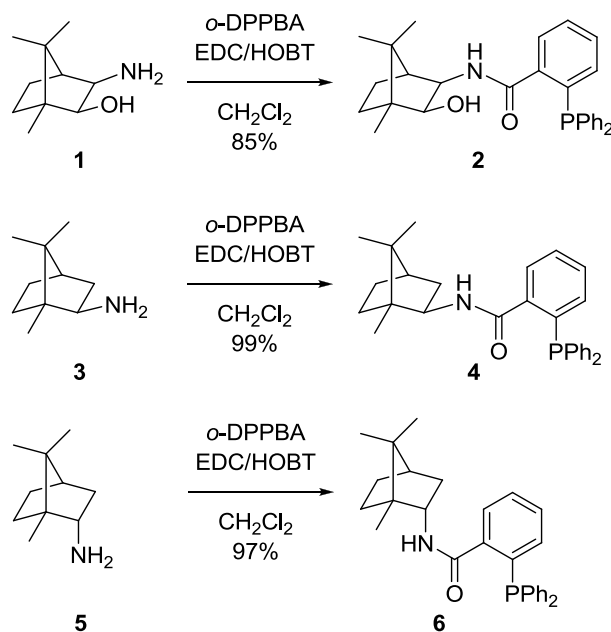
The enantioselectivity was determined by HPLC analysis with a chiral column (Chiralpak IA; hexane/*i*-PrOH, 95:5; flow rate, 0.7 mL/min; t_{R} , 14.321; t_{S} , 17.871 min). The absolute configurations of the enantiomers were determined by comparison of the retention times with that of an authentic sample and by measurement of the optical rotation of the product.

RESULTS AND DISCUSSION

For the planned condensation reactions, readily available, 3-*exo*-aminoisoborneol [26], iso-bornylamine [27] and bornylamine [28] were selected as key (+)-camphor-derived starting compounds.

First, we synthesized the secondary amide analogue of **V** (Fig 1.), bearing a hydroxyl group on the camphane scaffold. Thus, we had the chance to exploit whether the presence of the free OH-group might serve as a third coordination site in the formation of more rigid chelates of the palladium catalyst, resulting in enhanced enantioselectivity, or will lead to a problem of deactivation of the palladium in the catalytic process [18-22]. One more aspect of our investigation was modification of the electronic properties of the amide carbonyl group as a coordination center. The desired diphenylphosphino-benzenecarboxamide ligand **2** was easily obtained by condensation of *o*-DPPBA with (2*S*)-(-)-3-*exo*-aminoisoborneol **1** in dry CH_2Cl_2 in the presence of *N*-[3-(dimethyl amino)propyl]-*N'*-ethylcarbodiimide (EDC) and 1-hydroxybenzotriazole (HOBT) (Scheme 1). The amide **2** was isolated by column chromatography as air

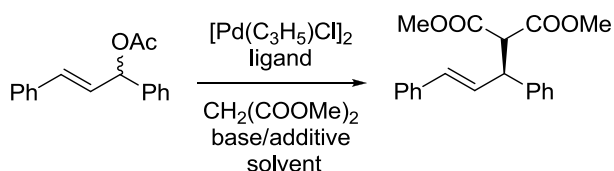
stable white solid in 85% yield. The influence of the camphane chiral source was further investigated by the synthesis of diphenylphosphino-benzenecarboxamide ligands **4** and **6**, starting from isobornylamine or bornylamine, respectively. Thereby, we had the possibility to investigate how the difference in the camphor derived fragment influences the reactivity of the transition metal complexes and the asymmetric induction in the catalytic process. Moreover, the ligand structures lacking a hydroxyl function afforded an opportunity to examine additionally the effect of the latter. Formation of the amide linkage was accomplished by applying the EDC/HOBT/*o*-DPPBA coupling procedure to *exo*-bornylamine **3** and *endo*-bornylamine **5**. The desired products **4** and **6** were isolated in quantitative yields after purification (Scheme 1).



Scheme 1. Synthesis of diphenylphosphino-benzenecarboxamide ligands **2**, **4** and **6**.

In all cases the oxidation of the phosphines to the corresponding phosphine oxides was minimized by using a non-aqueous work-up procedure, subjecting the reaction mixtures directly to flash column chromatography on silica gel. The structures of the newly synthesized compounds were confirmed by 1D and 2D NMR spectra, MS data and elemental analysis.

The chiral diphenylphosphino-benzene carboxamide ligands **2**, **4** and **6** were evaluated in the palladium-catalyzed asymmetric allylic alkylation of (*E*)-1,3-diphenyl-2-propen-1-yl acetate with dimethyl malonate using $[\text{Pd}(\eta^3\text{-C}_3\text{H}_5)\text{Cl}]_2$ as a palladium source (Scheme 2).



Scheme 2. Pd-catalyzed asymmetric allylic alkylation of (*E*)-1,3-diphenyl-2-propen-1-yl acetate.

Initially, the reaction was performed with ligand **2** under our previously reported conditions [25]. The nucleophile was generated in situ by Trost's procedure [29] using *N,O*-bis(trimethylsilyl) acetamide (BSA) and a catalytic amount of LiOAc as a base additive (Table 1). The reaction carried out in Et₂O proceeded with excellent conversion but no asymmetric induction was observed (Table 1, entry 1). Performing the alkylation in THF instead of Et₂O led to enantioselectivity of 16% ee in favor of (*R*)-enantiomer (Table 1, entry 2). The best enantioselectivity of 52% ee was achieved when 2 equivalents of anhydrous cesium carbonate were employed as the base, instead of BSA/LiOAc, in CH₂Cl₂ (Table 1, entry 3). An interesting comparison can be made with the *N,O*-disubstituted analogue of ligand **2**. Both the reactions in Et₂O and in THF with ligand **V** (Fig. 1) proceeded with excellent enantioselectivity of 91% ee, favoring the same (*R*)-enantiomer [25]. Obviously, the presence of free-OH group greatly influences the catalytic performance, leading to substantial drop of enantioselectivity.

Applying the optimized for ligand **2** reaction conditions to the isobornylamine derived ligand **4** resulted in excellent conversion but lack of asymmetric induction (Table 1, entry 4). When a mixture of BSA and a catalytic amount of LiOAc in THF was used as the base instead of Cs₂CO₃, the enantioselectivity raised to 12% ee, favoring (*R*)-configuration of the substitution product (Table 1, entry 5). Performing the alkylation in Et₂O instead of THF did not influence the catalytic performance (13% ee, entry 6). In comparison, the *N*-ethylated analogue of ligand **4** afforded enantioselectivity of 30% favoring the same (*R*)-enantiomer [25]. Evidently, the secondary amide performs no better than the tertiary.

Ligand **6**, the *endo*-diastereoisomer of **4**, also afforded low level of enantioselectivity favoring the same (*R*)-enantiomer (12% ee, entry 7). Surprisingly, a change of the configuration at the carbon atom bonded to the amide nitrogen did not influence the enantioselectivity and the configuration of the products obtained.

Table 1. Palladium-catalyzed AAA of racemic (*E*)-1,3-diphenyl-2-propen-1-yl acetate with dimethyl malonate^a.

Entry	L*	Solvent	Base/Additive	Yield (%) ^b	ee (%), conf ^c
1	2	Et ₂ O	BSA/LiOAc	99	1, <i>R</i>
2	2	THF	BSA/LiOAc	99	16, <i>R</i>
3	2	CH ₂ Cl ₂	Cs ₂ CO ₃	99	52, <i>R</i>
4	4	CH ₂ Cl ₂	Cs ₂ CO ₃	99	1, <i>S</i>
5	4	THF	BSA/LiOAc	99	12, <i>R</i>
6	4	Et ₂ O	BSA/LiOAc	99	13, <i>R</i>
7	6	Et ₂ O	BSA/LiOAc	99	12, <i>R</i>

^aReaction conditions: **A** 1 equiv. substrate, 0.03 equiv [Pd(η³-C₃H₅)Cl]₂, 0.06 equiv. ligand, 3 equiv. *N,O*-bis(trimethylsilyl) acetamide (BSA), 3 equiv. dimethylmalonate, catalytic amount of additive salts, 24 h. **B** 1 equiv. substrate, 0.03 equiv [Pd(η³-C₃H₅)Cl]₂, 0.06 equiv. ligand, 2 equiv. Cs₂CO₃, 2 equiv. dimethylmalonate, 24 h; ^bIsolated pure products after column chromatography; ^cEnantiomeric excess determined by HPLC analysis (Chiralpak IA chiral column). The absolute configuration was determined by comparison of the specific rotation to the literature value, see Ref [30].

The low enantio-selectivity made us forsake further optimizations. Quite controversial was also the result obtained with its *N*-ethylated analogue. No asymmetric induction was detected when employing the latter in the AAA, under the same reaction conditions [25]. Obviously, in the case of the bornylamine derived ligands the secondary amide is more potential than the tertiary. The opposite result was observed for the isobornylamine derived ligands.

CONCLUSION

New ligands were synthesized by condensation reactions of 3-*exo*-aminoisoborneol, isobornyl amine and bornylamine with *ortho*-diphenyl phosphino benzoic acid and evaluated in the palladium-catalyzed asymmetric allylic alkylation. The system used to generate the dimethyl malonate anion strongly determined the catalytic performance of 3-*exo*-aminoisoborneol derived ligand **2**. The best enantioselectivity of 52% ee was achieved when Cs₂CO₃ was used as a base. The combination of secondary amide with a free-OH group led to a drop of enantioselectivity compared to tertiary amide alkoxy analogues. The isobornylamine and bornylamine derived ligands gave generally low enantioselectivities of 13% ee and 12% ee, respectively. A comparison with their tertiary amide analogues revealed that the electronic properties of the amide carbonyl group greatly influenced the asymmetric induction.

Acknowledgements: Financial support of National Science Fund, Bulgaria (DID02/33/2009 and DRNF-02/13/2009) is gratefully acknowledged.

REFERENCES

1. B. M. Trost, C. Lee, *Catalytic Asymmetric Synthesis*, In: I. Ojima, editor, 2nd ed, New York: Wiley-VCH, 2000.
2. B. M. Trost, M. R. Machacek, A. Aponick, *Acc. Chem. Res.*, **39**, 747 (2006).
3. P. Braunstein, N. Frederic, *Angew. Chem. Int. Ed.*, **40**, 680 (2001).
4. P. Stepnicka, *Chem. Soc. Rev.*, **41**, 4273 (2012).
5. C. P. Butts, E. Filali, G. C. Lloyd-Jones, P.-O. Norrby, D. A. Sale, Y. Schramm, *J. Am. Chem. Soc.*, **131**, 9945 (2009).
6. C. Amatore, A. Jutand, L. Mansah, L. Ricard, *J. Organomet. Chem.*, **692**, 1457 (2007).
7. C. P. Butts, J. Crosby, G. C. Lloyd-Jones, S. Stephen, *Chem. Commun.*, 1707 (1999).
8. J. Clayden, P. Johnson, J. H. Pink, M. Helliwell, *J. Org. Chem.*, **65**, 7033 (2000).
9. T. Mino, K. Kashihara, M. Yamashita, *Tetrahedron: Asymmetry*, **12**, 287 (2001).
10. J. Clayden, L. W. Lai, M. Helliwell, *Tetrahedron: Asymmetry*, **12**, 695 (2001).
11. W.-M. Dai, K. K. Y. Yeung, J.-T. Liu, Y. Zhang, I. D. Williams, *Org. Lett.*, **4**, 1615 (2002).
12. M. Tollabi, E. Framery, C. Goux-Henry, D. Sinou, *Tetrahedron: Asymmetry*, **14**, 3329 (2003).
13. Y.-H. Lee, Y. K. Kim, J.-H. Son, K. H. Ahn, *Bull. Korean Chem. Soc.*, **24**, 225 (2003).
14. N. W. Boaz, J. A. Ponasik, Jr., S. E. Large, S. D. Debenham, *Tetrahedron: Asymmetry*, **15**, 2151 (2004).
15. M. Lamac, J. Tauchman, I. Cisarova, P. Stepnicka, *Organometallics*, **26**, 5042 (2007).
16. K. Glegoła, E. Framery, C. Goux-Henry, K. M. Pietrusiewicz, D. Sinou, *Tetrahedron*, **63**, 7133 (2003).
17. V. Benessere, F. Ruffo, *Tetrahedron: Asymmetry*, **21**, 171 (2010).
18. V. R. Marinho, A. I. Rodrigues, A. J. Burke, *Tetrahedron: Asymmetry*, **19**, 454 (2008).
19. V. R. D. Marinho, J. P. P. Ramalho, A. I. Rodrigues, A. J. Burke, *Chirality*, **23**, 383 (2011).
20. G. S. Mahadik, S. A. Knott, L. F. Szczepura, S. R. Hitchcock, *Tetrahedron: Asymmetry*, **20**, 1132 (2009).
21. G. S. Mahadik, S. A. Knott, L. F. Szczepura, S. J. Peters, J. M. Standard, S. R. Hitchcock, *J. Org. Chem.*, **74**, 8164 (2009).
22. G. S. Mahadik, S. R. Hitchcock, *Tetrahedron: Asymmetry*, **21**, 33 (2010).
23. G. Stavrakov, I. Philipova, B. Ivanova, V. Dimitrov, *Tetrahedron: Asymmetry*, **21**, 1845 (2010).
24. I. Philipova, G. Stavrakov, A. Chimov, R. Nikolova, B. Shivachev, V. Dimitrov, *Tetrahedron: Asymmetry*, **22**, 970 (2011).
25. I. Philipova, G. Stavrakov, V. Dimitrov, *Tetrahedron: Asymmetry*, **23**, 927 (2012).
26. Y. K. Chen, S. Jeon, P. J. Walsh, W. A. Nugent, *Org. Synth.*, **82**, 87 (2005).
27. J. Ipaktschi, *Chem. Ber.*, **117**, 856 (1984).
28. R. M. Carman, K. L. Greenfield, *Aust. J. Chem.*, **37**, 1785 (1984).
29. B. M. Trost, D. J. Murphy, *Organometallics*, **4**, 1143 (1985).
30. T. Hayashi, A. Yamamoto, T. Hagihara, Y. Ito, *Tetrahedron Lett.*, **27**, 191 (1986).

ФОСФИН-КАРБОКСАМИДИ С КАМФАНОВ СКЕЛЕТ КАТО ЛИГАНДИ ЗА Pd-КАТАЛИЗИРАНО АСИМЕТРИЧНО АЛКИЛИРАНЕ

И. Филипова¹, Г. Ставраков², В. Димитров^{1*}

¹Институт по Органична химия с Център по Фитохимия, Българска Академия на Науките, ул. Акад. Г. Бончев, бл. 9, 1113 София, България

²Фармацевтичен Факултет, Медицински Университет – София, ул. Дунав 2, 1000 София, България

Постъпила на 03 април 2014 г.; Коригирана на 29 април 2014 г.

(Резюме)

Чрез кондензация на *орто*-дифенилфосфино бензоена киселина с 3-*екзо*-аминоизоборнеол, изоборниламин и борниламин са получени три нови фосфин-карбоксамиди, които са изследвани като лиганди в Pd-катализирано асиметрично алилово алкилиране на (*E*)-1,3-дифенил-2-пропен-1-ил ацетат. Каталитичното действие силно зависи от условията използвани за получаване на диметил малонатния анион. Най-висока енантиселективност е постигната с лиганд произведен на 3-*екзо*-аминоизоборнеол и използването на Cs₂CO₃ като база. Лигандите, производни на изоборниламин и борниламин, индуцират по-ниска енантиселективност.

Synthesis and antimycobacterial activity of bornylamine derived amido-alcohols

G. Stavrakov^{1*}, I. Philipova², V. Valcheva³, G. Momekov¹

¹Faculty of Pharmacy, Medical University of Sofia, 2 Dunav str., 1000 Sofia, Bulgaria

²Institute of Organic Chemistry with Centre of Phytochemistry, Bulgarian Academy of Sciences, Acad. G. Bonchev str., bl. 9, 1113 Sofia, Bulgaria

³Institute of Microbiology, Bulgarian Academy of Sciences, Acad. Bonchev str., bl. 26, 1113 Sofia, Bulgaria

Received April 16, 2014; Revised May 30, 2014

Dedicated to Acad. Dimiter Ivanov on the occasion of his 120th birth anniversary

Three novel amido-alcohols were synthesized on the base of the camphane scaffold. Natural amino acids were transformed into their α -hydroxy analogues with retention of configuration, and attached to bornylamine. The compounds were evaluated for their in vitro activity against *Mycobacterium tuberculosis* H37Rv. The activity shifts from micromolar to nanomolar inhibitory concentrations depending on the α -hydroxy acid moiety. The valine derived compound demonstrates activity 25 times higher than the referent ethambutol. The amido-alcohols with camphane scaffolds emerge as promising new class of antimycobacterial agents.

Key words: camphane, α -hydroxy acids, *M. tuberculosis* H37Rv, cytotoxicity

INTRODUCTION

Tuberculosis (TB) still remains a growing problem in the context of diagnosis and treatment of multidrug-resistant TB [1]. The unacceptable large number of TB deaths necessitates the search for new antimycobacterial agents with novel structures and mode of action. SQ 109 (Fig. 1. **I**), emerged as capable second line drug with promising antimycobacterial potencies and pharmacokinetic properties [2]. It is very likely that its highly lipophilic adamantane structure helps the penetration into the bacterial wall and thus is decisive for the activity [3].

Inspired by the analogy of the camphane scaffold as compact lipophilic moiety to the adamantyl fragment in SQ 109, we have previously studied camphor derived structures as novel antimycobacterial agents [4,5]. A practical synthesis of a small number of new amido-alcohols and amido-diols was accomplished on the base of 3-*exo*-aminoisoborneol (Fig. 1. **II**) [4]. These were screened for antimycobacterial activity against two MTB strains (H37Rv and MDR strain 43) and some of the compounds show activity much higher than the referent ethambutol. Additionally, we expanded the study towards amido-alcohols derived from isobornylamine and α -hydroxy acids (Fig. 1. **III**) [5]. Thereby, we had the opportunity to investigate

how the difference in the camphor derived fragment influences the activity. The latter shifted from micromolar to nanomolar inhibitory concentrations depending on the α -hydroxy acid moiety. Noteworthy, two of the structures possess very high activity in combination with low levels of cytotoxicity.

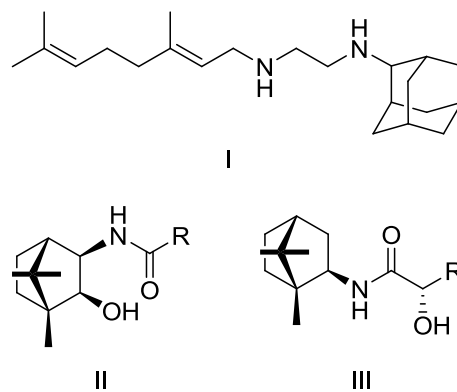


Fig. 1. Structures of SQ109 (**I**), 3-*exo*-aminoisoborneol (**II**) and isobornylamine (**III**) based amido-alcohols.

Encouraged by these observations, we expanded the approach to the synthesis of bornylamine analogues where the asymmetric center neighboring the nitrogen in the targeted structures is with the opposite (*S*)-configuration compared to the isobornylamine and 3-*exo*-aminoisoborneol structures. This afforded the chance to investigate the role of chirality on the structure-activity relationship.

* To whom all correspondence should be sent:
E-mail: gstavrakov@pharmfac.net

Thus, we pursue the exploration of the camphane based structures as novel class of anti-TB compounds.

EXPERIMENTAL

General

Reagents were commercial grade and used without further purification. Thin layer chromatography (TLC) was performed on aluminum sheets pre-coated with Merck Kieselgel 60 F₂₅₄ 0.25 mm (Merck). Flash column chromatography was carried out using Silica Gel 60 230-400 mesh (Fluka). Commercially available solvents for reactions, TLC and column chromatography were used after distillation (and were dried when needed). Melting points of the compounds were determined using "Electrothermal" MEL-TEMP apparatus (uncorrected). Optical rotations ($[\alpha]_D^{20}$) were measured on Perkin-Elmer 241 polarimeter. The NMR spectra were recorded on a Bruker Avance II+ 600 spectrometer (600.13 MHz for ¹H, 150.92 MHz for ¹³C NMR) in CDCl₃ with TMS as internal standards for chemical shifts (δ , ppm). ¹H and ¹³C NMR data are reported as follows: chemical shift, multiplicity (s = singlet, d = doublet, t = triplet, q = quartet, br = broad, m = multiplet), coupling constants (Hz), integration, identification. The assignment of the ¹H and ¹³C NMR spectra was made on the basis of DEPT, COSY, HSQC, HMBC and NOESY experiments. Elemental analyses were performed by Microanalytical Service Laboratory of Faculty of Pharmacy, Medical University of Sofia, using Vario EL3 CHNS(O). Dimethyl sulfoxide (DMSO) for testing of bioactivities was commercial (spectroscopic grade) and was used without distillation.

General Procedure for the Preparation of the Amides (**4a-c**).

1-Hydroxybenzotriazole (HOBt) (1.1 equiv) and the respective α -hydroxy acid (1 equiv) were suspended in dichloromethane, and the mixture was stirred for 5 min. Then, *N*-[3-(dimethylamino)propyl]-*N*-ethylcarbodiimide (EDC) (1.1 equiv) was added, followed by bornylamine (1 equiv). Stirring was continued at room temperature until the starting material was completely consumed (TLC). The mixture was quenched with water, extracted with CH₂Cl₂, washed with 2M HCl, sat. aq. NaHCO₃ and brine. The organic phase was dried over Na₂SO₄, and concentrated under

vacuum. The residue was purified by flash column chromatography on silica gel.

(*S*)-2-Hydroxy-2-phenyl-*N*-((1*R*,2*S*,4*R*)-1,7,7-trimethylbicyclo[2.2.1]heptan-2-yl)acetamide **4a**. Yield: 54%; waxy solid. $[\alpha]_D^{20} = +41.3$ (c 0.492, CHCl₃). ¹H NMR 7.41-7.38 (m, 4H, arom.), 7.35-7.33 (m, 1H, arom.), 5.99 (d, $J_{H,H} = 8.8$ Hz, 1H, NH), 5.01 (d, $J_{H,H} = 2.6$ Hz, 1H, CHOH), 4.23-4.18 (m, 1H, 2-*H*_{exo}), 3.90 (d, $J_{H,H} = 3.2$ Hz, 1H, OH), 2.33-2.28 (m, 1H, 3-*H*_{exo}), 1.73-1.68 (m, 1H, 5-*H*_{exo}), 1.64 (t, $J_{H,H} = 4.5$ Hz, 1H, 4-H), 1.27-1.21 (m, 1H, 5-*H*_{endo}), 1.10-1.05 (m, 2H, 6-*H*_{exo}, 6-*H*_{endo}), 0.91 (s, 3H, 8-H), 0.83 (s, 3H, 9-H), 0.76 (dd, $J_{H,H} = 13.4, 4.5$ Hz, 1H, 3-*H*_{endo}), 0.69 (s, 3H, 10-H) ppm. ¹³C NMR 172.16 (CO), 139.83 (1 arom. C), 128.87 (2 arom. CH), 128.62 (1 arom. CH), 126.73 (2 arom. CH), 73.98 (CHOH), 53.92 (2-C), 49.64 (1-C), 48.09 (7-C), 44.77 (4-C), 37.33 (3-C), 28.21 (6-C), 27.48 (5-C), 19.68 (9-C), 18.55 (8-C), 13.48 (10-C) ppm. C₁₈H₂₂NO₂ (287.40): calcd. C 75.22, H 8.77, N 4.87, found C 75.18, H 8.56, N 5.12.

(2*S*,3*S*)-2-Hydroxy-3-methyl-*N*-((1*R*,2*S*,4*R*)-1,7,7-trimethylbicyclo[2.2.1]heptan-2-yl)pentanamide **4b**. Yield: 60%; white crystals; m.p. 97-101°C. $[\alpha]_D^{20} = -20.5$ (c 0.538, CHCl₃). ¹H NMR 6.44 (d, $J_{H,H} = 8.8$ Hz, 1H, NH), 4.28-4.23 (m, 1H, 2-*H*_{exo}), 4.02 (dd, $J_{H,H} = 5.2, 3.3$ Hz, 1H, CHOH), 2.96 (d, $J_{H,H} = 5.3$ Hz, 1H, OH), 2.39-2.33 (m, 1H, 3-*H*_{exo}), 1.90-1.83 (m, 1H, CH₃CH), 1.81-1.75 (m, 1H, 5-*H*_{exo}), 1.68 (t, $J_{H,H} = 4.5$ Hz, 1H, 4-H), 1.46-1.51 (m, 1H, 6-*H*_{exo}), 1.44-1.37 (m, 2H, 6-*H*_{endo}, CH₃CH₂), 1.24-1.17 (m, 2H, 5-*H*_{endo}, CH₃CH₂), 1.01 (d, $J_{H,H} = 7.0$ Hz, 3H, CH₃CH), 0.96 (s, 3H, 8-H), 0.90 (t, $J_{H,H} = 7.5$ Hz, 3H, CH₃CH₂), 0.88 (s, 3H, 9-H), 0.82 (s, 3H, 10-H), 0.81 (dd, $J_{H,H} = 13.3, 4.5$ Hz, 1H, 3-*H*_{endo}) ppm. ¹³C NMR 173.08 (CO), 76.20 (CHOH), 53.42 (2-C), 49.44 (1-C), 48.13 (7-C), 44.85 (4-C), 39.06 (CH₃CH), 37.57 (3-C), 28.32 (5-C), 27.94 (6-C), 23.08 (CH₃CH₂), 19.78 (9-C), 18.61 (8-C), 15.63 (CH₃CH), 13.67 (10-C), 11.91 (CH₃CH₂) ppm. C₁₆H₂₉NO₂ (267.41): calcd. C 71.86, H 10.93, N 5.24, found C 71.93, H 10.64, N 5.58.

(*S*)-2-Hydroxy-3-methyl-*N*-((1*R*,2*S*,4*R*)-1,7,7-trimethylbicyclo[2.2.1]heptan-2-yl)butanamide **4c**. Yield: 48%; white crystals; m.p. 88-91°C. $[\alpha]_D^{20} = -25.2$ (c 0.445, CHCl₃) ¹H NMR 6.44 (d, $J_{H,H} = 6.4$ Hz, 1H, NH), 4.26-4.22 (m, 1H, 2-*H*_{exo}), 3.97 (dd, $J_{H,H} = 5.2, 3.1$ Hz, 1H, CHOH), 3.05 (brs, 1H, OH), 2.38-2.35 (m, 1H, 3-*H*_{endo}), 2.15-2.10 (m, 1H, (CH₃)₂CH), 1.80-1.74 (m, 1H, 5-*H*_{exo}), 1.67 (t, $J_{H,H} = 4.6$ Hz, 1H, 4-H), 1.46-1.50 (m, 1H, 6-*H*_{endo}), 1.41-1.36 (m, 1H, 6-*H*_{exo}), 1.20-1.16 (m, 1H, 5-*H*_{endo}), 1.03 (d, $J_{H,H} = 6.9$ Hz, 3H, (CH₃)₂CH), 0.94 (s, 3H, 8-H), 0.87 (s, 3H, 9-H), 0.86 (d, $J_{H,H} = 6.9$ Hz, 3H,

(CH_3)₂CH), 0.81 (s, 3H, 10-H), 0.80 (dd, $J_{\text{H,H}} = 13.4, 4.6$ Hz, 1H, 3- H_{endo}) ppm. ¹³C NMR 173.22 (CO), 76.13 (CHOH), 53.46 (2-C), 49.47 (1-C), 48.18 (7-C), 44.89 (4-C), 37.63 (3-C), 32.18 ((CH_3)₂CH), 28.36 (5-C), 28.00 (6-C), 19.82 (9-C), 19.23 ((CH_3)₂CH), 18.66 (8-C), 15.44 ((CH_3)₂CH), 13.72 (10-C) ppm. C₁₅H₂₇NO₂ (253.38): calcd. C 71.10, H 10.74, N 5.53, found C 71.44, H 10.97, N 5.63.

Antimycobacterial activity

The antimycobacterial activity was determined through the proportional method of Canetti towards reference strain *M. Tuberculosis* H37Rv and multi-drug resistant strain 43 (resistant to Rifampin and Isoniazid), recovered from Bulgarian adult HIV-negative pulmonary TB patient, who was permanent resident of the country. This method, recommended by the WHO, is the most commonly used one worldwide for exploration of sensitivity/resistance of tuberculosis strains towards chemotherapeutics [6-10]. It allows precise determination of the proportion of resistant mutants to a certain drug.

A sterile suspension/solution of each tested compound was added to Löwenstein-Jensen egg based medium before its coagulation (30 min at 85°C). Each compound was tested at five concentrations – 5 mg/ml, 2 mg/ml, 0.2 mg/ml, 0.1 mg/ml and 0.05 mg/ml in DMSO. Tubes with Löwenstein-Jensen medium (5 ml) containing tested compounds and those without them (controls) were inoculated with 0.2 ml suspension of *M. tuberculosis* H37Rv (10⁵ cells/ml) and incubated for 45 days at 37°C. The ratio between the number of colonies of *M. tuberculosis* grown in medium containing compounds and the number of colonies in control medium were calculated and expressed as percentage of inhibition. The MIC is defined as the minimum concentration of compound required to inhibit bacterial growth completely (0% growth). The MIC values are calculated and given as µM.

Cytotoxicity

The human embryonal kidney cell line 293T cells were obtained from the German Collection of Microorganisms and Cell Cultures. Cells were kept in controlled environment e RPMI-1640 medium, supplemented with 10% heat-inactivated fetal calf serum and 2mM L-glutamine, at 37°C in a 'Heraeus' incubator with 5% CO₂ humidified atmosphere.

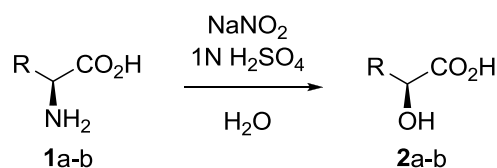
The cytotoxicity of the newly synthesized compounds was assessed using the MTT [3-(4,5-dimethylthiazol-2-yl)-2,5-diphenyltetrazolium bromide]-dye reduction assay as described by Mossman with some modifications [11,12]. In brief, exponentially growing cells were seeded in 96-well microplates (100 µl/well) at a density of 3.5 - 105 cell/ml and allowed to grow for 24 h prior the exposure to the studied compounds. Stock solutions of the tested compounds were freshly prepared in DMSO and thereafter were subset to serial dilutions with growth medium in order to obtain the desired final concentrations. At the final dilutions the solvent concentration never exceeded 0.5%. Cells were exposed to the tested agents for 72 h, whereby for each concentration a set of at least 8 separate wells was used. After the exposure period MTT solution (10 mg/ml in phosphate-buffered saline) aliquots (100 µl/well) were added to each well. The plates were further incubated for 4 h at 37°C and the MTT-formazan crystals formed were dissolved through addition of 110 µl of 5% HCOOH in 2-propanol. The MTT-formazan absorption of the samples was measured by a multimode microplate reader DTX 880 (Beckman Coulter) at 580 nm. Cell survival fractions were calculated as percentage of the untreated control. The experimental data were fitted to sigmoidal concentration-response curves and the corresponding IC₅₀ values (concentrations causing 50% reduction of cellular survival vs the untreated control) via non-linear regression (GraphPad Prism software for PC).

RESULTS AND DISCUSSION

Chemistry

Since peptides and peptide-related structures have a wide variety of physiological and pharmacological actions, the concept of peptidomimetics was aimed by the design of α-amino acids derived amido-alcohols. A series of chiral α-hydroxy acids as starting building blocks was prepared from their corresponding natural amino acid analogues. Ingold first developed the transformation of L-phenylalanine to its α-hydroxy acid analogue with retention of configuration [13]. The reaction proceeded via initial deamination followed by nucleophilic attack of the neighbouring carboxyl group to heterocyclic intermediate and final nucleophilic attack of water. The product had the same configuration due to two consecutive Walden inversions. Applying the procedure to isoleucine **1a**

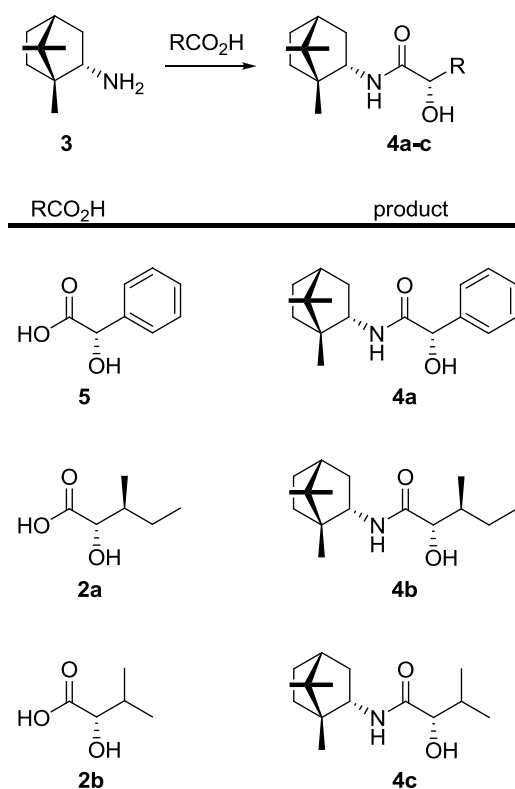
and valine **1b** afforded the corresponding α -hydroxy analogues **2a** and **2b** (Scheme 1).



- (a) Isoleucine, R = sBu-; 43%
 (b) Valine, R = iPr-; 35%

Scheme 1. Synthesis of α -hydroxy acids.

Readily available bornylamine **3** was selected as the camphane starting compound [14]. The targeted structures were aimed by simple and effective synthetic transformations (Scheme 2).



Scheme 2. Synthesis of bornylamine based amido-alcohols.

The amide linkage between the α -hydroxy acids and bornylamine **3** was accomplished by procedures developed for peptide synthesis. The reaction was optimized for the commercially available mandelic acid **5** in the presence of *N*-(3-dimethylaminopropyl)-*N'*-ethylcarbodiimide hydrochloride (EDCI) and 1-hydroxybenzotriazole hydrate (HOBT) as coupling reagents to yield **4a**. Following the same protocol for α -hydroxy acids

2a-b we synthesized the corresponding amido-alcohols **4b-c** (Scheme 2). The products were obtained in good yields and excellent purity after flash column chromatography.

All compounds were identified by elementary analysis, ^1H NMR and ^{13}C NMR. The spectral analyses were in accordance with the assigned structures.

Antimycobacterial activity

The synthesized compounds were evaluated for their in vitro activity against *M. tuberculosis* H37Rv using the method of Canetti (Table 1). The mandelic acid derived amido-alcohol **4a** exhibited activity against *M. tuberculosis* H37Rv with MIC of 6.96 μM , which is comparable with the one of the reference compound ethambutol. In the case of the isoleucine derived amido-alcohol **4b** the activity dropped to MIC of 18.70 μM . The best result was observed with the valine derived amido-alcohol **4c**, which exhibited MIC of 0.20 μM (Table 1). Interestingly, a slight variation of the alkyl side chain, a switch of the isobutyl group to isopropyl, greatly increased the activity.

No correlation could be assigned between the configuration of the stereogenic center at the nitrogen and the activity. In both cases: compounds with (*R*)-configuration derived from 3-*exo*-aminoisoborneol [4] and isobornylamine [5], and compounds with (*S*)-configuration derived from bornylamine; we detected either nanomolar or micromolar activities. Therefore, SAR dependence on the chirality in camphane based structures should be handled with care.

Cytotoxicity

The cytotoxicity of the presented compounds was assessed against the human embryonal kidney cell line 293T in order to examine the selectivity of the antiproliferative effects. Evident from the IC_{50} values (Table 1), the compounds were characterized with low **4a** to moderate **4b**, **4c** cytotoxicity against the human cells. The results are in favour of structure **4c**. The latter exhibits high antimycobacterial activity and moderate cytotoxicity, which is represented by its excellent selectivity index: 217.15. Considering that compounds **4b** and **4c** are practically equi-toxic against human cells while displaying prominent selective inhibition of H37RV it could be concluded that they modulate a distinct target peculiar for mycobacteria.

Table 1. In vitro screening data for antimycobacterial activity and cytotoxicity of the synthesized compounds.

Compound	Anti-MTB ^a	Cytotoxicity ^b	SI ^c
	MIC (μM)	IC ₅₀ (μM)	IC ₅₀ /MIC
4a	6.96	124.40	17.87
4b	18.70	43.86	2.34
4c	0.20	43.43	217.15
ETM.2HCl ^d	7.20	-	-

^aAntimycobacterial activity towards reference strain of *Mycobacterium tuberculosis* H37Rv; ^bIn vitro cytotoxicity towards human embryonal kidney cell line 293T; ^cSelectivity index; ^dEMB.2HCl – ethambutol dihydrochloride (reference compound).

The analogy between the bulky lipophilic camphane fragment and the adamantyl fragment in the molecule of SQ109, a drug currently in clinical trials for the treatment of tuberculosis, made us speculate that they share the same target [3]. Further docking studies are due in a short time.

CONCLUSION

In summary, three new amido-alcohols were synthesized by condensation of bornylamine with α -hydroxy acids. The compounds were screened for their antimycobacterial activity against *M. tuberculosis* H37Rv. The activity shifts from micromolar to nanomolar inhibitory concentrations depending on the α -hydroxy acid moiety. The valine derived compound shows 25 times higher activity than the classical anti-TB drug ethambutol and moderate level of cytotoxic activity against a human embryonal kidney cell line 293T. The mandelic acid derived amido-alcohol demonstrates activity comparable with ethambutol and low level of cytotoxicity. Further evaluation of camphane based structures as potential anti-TB agents is in progress and will be reported in due lines.

Acknowledgements: Financial support of National Science Fund, Bulgaria (DMU 02/3 – 2009) is gratefully acknowledged.

REFERENCES

1. World Health Organization, Global tuberculosis report 2013, http://www.who.int/tb/publications/global_report/en/
2. L. Jia, J. E. Tomaszewski, C. Hanrahan, L. Coward, P. Noker, G. Gorman, B. Nikonenko, M. Protopopova, *Br. J. Pharmacol.*, **144**, 80 (2005).
3. K. Tahlan, R. Wilson, D. B. Kastrinsky, K. Arora, V. Nair, E. Fischer, S. W. Barnes, J. R. Walker, D. Alland, C. E. Barry 3rd, H.I. Boshoff, *Antimicrob. Agents Chemother.*, **56**, 1797 (2012).
4. G. Stavrakov, V. Valcheva, I. Philipova, I. Doytchinova, *Eur. J. Med. Chem.*, **70**, 372 (2013).
5. G. Stavrakov, I. Philipova, V. Valcheva, G. Momekov, *Bioorg. Med. Chem. Lett.*, **24**, 165 (2014).
6. G. Canetti, N. Rist, J. Grosset, *Rev. Tuberc. Pneumol.*, **27**, 217 (1963).
7. G. Canetti, S. Froman, J. Grosset, P. Hauduroy, M. Langerova, H. T. Mahler, G. Meissner, D. A. Mitchison, L. Sula, *Bull. WHO*, **29**, 565 (1963).
8. G. Canetti, W. Fox, A. Khomenko, H. T. Mahler, N. K. Menon, D. A. Mitchinson, N. Rist, N. A. Smelev, *Bull. Org. Mond. Sante*, **41**, 21 (1969).
9. L. Heifets, Conventional methods for antimicrobial susceptibility testing of *Mycobacterium tuberculosis*, in: I. Bastian, F. Portaels (Eds.), *Multidrug-Resistant Tuberculosis*, Kluwer Academic Publishers, Dordrecht, The Netherlands, 2000.
10. CellTiter 96 Non-Radioactive Cell Proliferation Assay, Technical Bulletin #TB112, Promega Corporation USA, Revised 12/99.
11. T. J. Mosmann, *Immunol. Meth.*, **65**, 55 (1983).
12. S. M. Konstantinov, H. Eibl, M. R. Berger, *Br. J. Haematol.*, **107**, 365 (1999).
13. P. Brewster, F. Hiron, E. D. Hughes, C. K. Ingold, P. A. D. S. Rao, *Nature*, **166**, 179 (1950).
14. R. M. Carman, K. L. Greenfield, *Aust. J. Chem.*, **37**, 1785 (1984).

СИНТЕЗ И АНТИМИКОБАКТЕРИАЛНА АКТИВНОСТ НА АМИДОАЛКОХОЛИ ПРОИЗВОДНИ НА БОРНИЛАМИН

Г. Ставраков^{1*}, И. Филипова², В. Вълчева³, Г. Момеков¹

¹Фармацевтичен Факултет, Медицински Университет – София, ул. Дунав 2, 1000 София, България

²Институт по Органична химия с Център по Фитохимия, Българска Академия на Науките, ул. Акад. Г. Бончев, бл. 9, 1113 София, България

³Институт по Микробиология Стефан Ангелов, ул. Акад. Г. Бончев, бл.26, 1113 София, България

Постъпила на 16 април 2014 г.; Коригирана на 30 май 2014 г.

(Резюме)

Синтезирани са три нови амидо-алкохоли с камфанов скелет. Природни аминокиселини бяха трансформирани в техните α -хидрокси аналози със запазване на конфигурацията и в последствие кондензирани с борниламин. Веществата бяха изследвани за тяхната *in vitro* активност срещу щама *Mycobacterium tuberculosis* H37Rv. Активността варира от микромолярни до наномолярни инхибиращи концентрации в зависимост от α -хидрокси киселинния остатък. Валиновото производно показва активност 25 пъти по-висока от референта етамбутол. Амидоалкохолите с камфанов скелет се проявяват като обещаващ нов клас антимикобактериални агенти.

Enantioselective addition of diethylzinc to ferrocene carbaldehyde - reaction outcome by using natural compound based catalysts

K. Dikova, M. Kamenova-Nacheva, K. Kostova, V. Dimitrov*

Institute of Organic Chemistry with Centre of Phytochemistry, Bulgarian Academy of Sciences, Acad. G. Bonchev str., bl. 9, 1113 Sofia, Bulgaria

Received June 19, 2014; Revised July 15, 2014

Dedicated to Acad. Dimiter Ivanov on the occasion of his 120th birth anniversary

The efficiency of the alkaloids quinine, cinchonine, cinchonidine and ephedrine, the aminoalcohols prolinol, and alaninol, as well as the aminoacids proline, and phenylalanine as catalysts for the enantioselective addition of diethylzinc to ferrocene carbaldehyde and benzaldehyde has been studied. The addition reactions proceeded with acceptable yields and low to moderate enantioselectivities. The side products ferrocenyl methanol and 1-ferrocenyl-1-propanone, observed during the additions to ferrocene carbaldehyde were isolated and characterized.

Key words: diethylzinc, addition to aldehydes, natural products

INTRODUCTION

The synthesis of chiral aminoalcohols, first reported by Oguni and Omi [1-3], to catalyze enantioselectively the addition of diorganozinc compounds to aldehydes, still attracts considerable interest due to the utility of the secondary alcohols formed by this reaction [1-7]. Over the past decades a large number of aminoalcohols has been synthesized and tested as ligands [1-9]. One of the most potent aminoalcohols used as a catalyst is the dimethylamino-isoborneol investigated by Noyori [10-16]. For the synthesis of aminoalcohols natural sources of chirality (e.g. terpenoids, aminoacids, alkaloids) are generally used. In many cases catalysts based on naturally occurring aminoalcohols have been applied as such or aminoalcohols have been obtained after minor modifications. The cinchona alkaloids quinine, quinidine, cinchonine and cinchonidine have been used directly [17,18] or after simple chemical transformations [19,20] as efficient catalyst for enantioselective addition of diethylzinc to aldehydes. In similar manner ephedrine and norephedrine derivatives have been obtained and used in catalytic diethylzinc addition reactions [21-25]. On the other hand various strategies have been developed for the synthesis of structurally diverse aminoalcohols which are suitable ligands for different catalytic applications [4-9]. Among them are the 1,2-substituted ferrocenyl aminoalcohols of type C

(Fig. 1; E = -CH(R¹)OH) and other derivatives that possess chirality plane and have proven to be very useful for asymmetric catalysis [26-29].

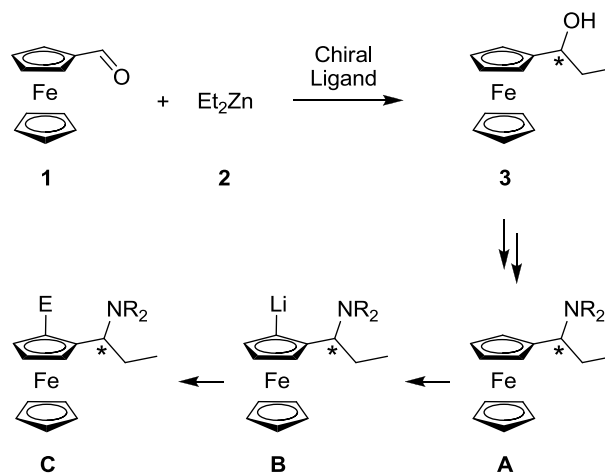


Fig. 1. Synthesis of chiral ferrocene derivatives by using the enantioselective addition of diethylzinc to ferrocene carbaldehyde as key transformation step.

Key compounds for synthesis of planar chiral 1,2-disubstituted ferrocenes are the chiral alkyl- (or aryl-) ferrocenyl methanols obtained either by asymmetric reduction of alkyl- (or aryl-) ferrocenyl ketones [26-29] or through enantioselective addition of dialkylzinc compounds to ferrocene carbaldehyde (Fig. 1). After the enantioselective addition of e.g. diethylzinc to ferrocene carbaldehyde (1), catalyzed by suitable chiral ligand, the resulting 1-ferrocenyl-1-propanol (3) can be easily trans-

* To whom all correspondence should be sent:
E-mail: vdim@orgchm.bas.bg

formed to dialkylamino derivative **A** with retention of the configuration. Compounds of type **A** undergo highly diastereoselective *ortho*-lithiation (up to 96% de) with butyllithium reagents due to the directed *ortho*-metallation caused by the dialkylamino group attached to the stereogenic center. The reaction of the lithiated ferrocene **B** with suitable electrophiles (e.g. aldehydes, ketones) leads to the formation of planar chiral amino-alcohols or other aminoalkylferrocenyl derivatives of type **C** bearing various functionalities [26-29].

The aim of the present work is to evaluate the ability of some alkaloids (quinine, cinchonine, cinchonidine, ephedrine), aminoalcohols obtained from aminoacids (prolinol, alaninol) and aminoacids (proline, phenylalanine), (see Fig. 2), to catalyze enantioselectively the addition of diethylzinc to ferrocene carbaldehyde.

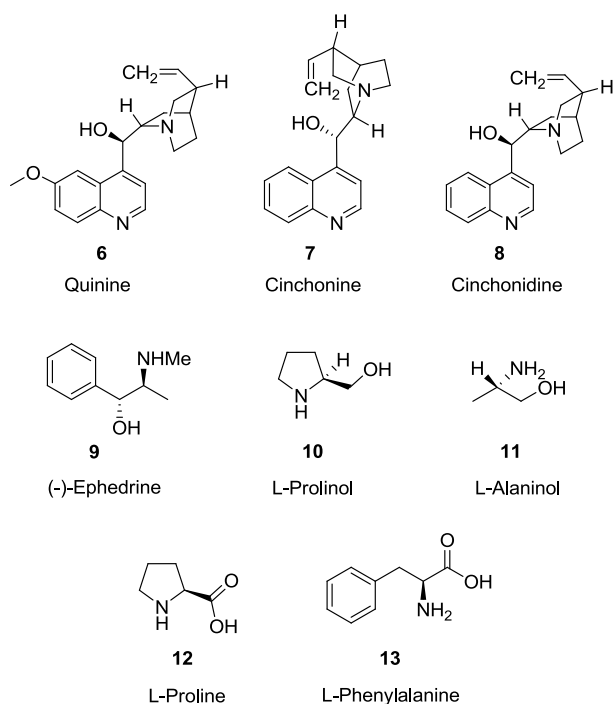


Fig. 2. Chiral natural compounds and derivatives applied as catalysts for enantioselective addition of diethylzinc to ferrocene carbaldehyde.

EXPERIMENTAL

General

All reactions were carried out in flame-dried *Schlenk* flasks under argon atmosphere. Hexane was distilled over Na[Et₄Al]. Thin layer chromatography (TLC) was performed on aluminum sheets pre-coated with silica gel 60 F₂₅₄ (Merck). Flash column chromatography was carried out using silica gel 60 (230-400 mesh, Merck). Optical rota-

tions ($[\alpha]_D^{20}$) were measured on a Perkin Elmer 241 polarimeter. The NMR spectra were recorded in CDCl₃ on a Bruker DRX 250 (250.13 MHz for ¹H NMR, 62.9 MHz for ¹³C NMR) spectrometer with TMS as the internal standard for chemical shifts (δ , ppm). ¹H and ¹³C NMR data are reported as follows: chemical shift, multiplicity (s = singlet, d = doublet, t = triplet, q = quartet, br = broad, m = multiplet), coupling constants (Hz), integration, and identification. EI-MS (70eV) were recorded on a Hewlett Packard 6890/5973 and reported as fragmentation in *m/z* with relative intensities (%) in parentheses.

General procedure for enantioselective addition of diethylzinc to carbaldehydes

To a solution of the corresponding ligand **6-13** (3 mol %) in hexane or toluene (20 ml) Et₂Zn (2.1 mmol, 1M solution in hexane) was added dropwise at 0°C under Ar atmosphere. The mixture was stirred for 30 min at 0°C and then the corresponding aldehyde (1.40 mmol) was added at -20°C. The reaction mixture was stirred at 20°C (in 2 cases at 60°C) and monitored by TLC (petroleum ether/Et₂O = 1:1) until the aldehyde was consumed or no further consumption was observed. The mixture was quenched (aq. NH₄Cl), extracted with Et₂O, and dried (Na₂SO₄). After evaporation of the solvent, the crude product was purified by column chromatography (petroleum ether/Et₂O = 5:1).

General procedure for enantioselective addition of diethylzinc to carbaldehydes in the presence of Ti(O-*i*Pr)₄

To a suspension of the ligands **6**, **10** and **12** (0.57 mmol, 20 mol %) in toluene (8 ml), Ti(O-*i*Pr)₄ (0.58 mmol) was added at 20°C under Ar atmosphere. The reaction mixture was stirred at 20°C for 1.5 h and then benzaldehyde (**14**) (2.83 mmol) and Ti(O-*i*Pr)₄ (3.40 mmol) were added. After 1 h the mixture was cooled to -20°C and Et₂Zn (5.66 mmol, 1M solution in hexane) was added. It was stirred at -20°C until completion of the reaction (monitored by TLC). The mixture was quenched (aq. NH₄Cl), filtered through a pad of Celite, extracted with Et₂O, and dried (Na₂SO₄). After evaporation of the solvent, the crude product was purified by column chromatography (petroleum ether/Et₂O = 10:1).

Data of 1-ferrocenylpropan-1-ol (3): ¹H NMR: 4.27-4.14 (m, 10H, C₅H₅, C₅H₄, CH), 1.99 (br. s, 1H, OH), 1.76-1.61 (m, 2H, CH₂), 0.95 (t, *J* = 7.5

Hz, 3H, CH₃). ¹³C NMR: 94.20 (s, C₅H₄), 71.00 (d, C₅H₄), 68.18 (5d, C₅H₅), 67.78 (d, C₅H₄), 67.63 (d, C₅H₄), 67.22 (d, C₅H₄), 65.12 (d, CH-OH), 30.95 (t, CH₂), 10.33 (q, CH₃). (Data obtained correspond to the literature [30]).

Data of ferrocenyl methanol (4): ¹H NMR: 4.32 (s, 2H, CH₂), 4.23 (s, 2H, C₅H₄), 4.17 (s, 7H, C₅H₄, C₅H₅), 1.74 (br. s, 1H, OH). ¹³C NMR: 88.25 (s, C₅H₄), 68.22 (7d, C₅H₄, C₅H₅), 67.85 (2d, C₅H₄), 60.69 (t, CH₂-OH). MS (EI) *m/z* (rel. int.) = 216 (74, M⁺), 138 (100), 121 (10), 73 (19). (Data obtained correspond to the literature [31-35]).

Data of 1-ferrocenyl-1-propanone (5): ¹H NMR: 4.79 (s, 2H, C₅H₄), 4.49 (s, 2H, C₅H₄), 4.19 (s, 5H, C₅H₅), 2.74 (q, *J* = 7.4 Hz, 2H, CH₂), 1.20 (t, *J* = 7.4 Hz, 3H, CH₃). ¹³C NMR: 205.09 (s, C=O), 78.90 (s, C₅H₄), 72.05 (2d, C₅H₄), 69.69 (5d, C₅H₅), 69.24 (2d, C₅H₄), 32.73 (t, CH₂), 8.50 (q, CH₃). MS (EI) *m/z* (rel. int.) = 242 (23, M⁺), 213 (100, [M-CH₂CH₃]⁺), 185 (62), 149 (35), 129 (81), 121 (47), 69 (62), 57 (88), 43 (97). (Data obtained correspond to the literature [36-40]).

Data of 1-phenylpropan-1-ol (15): ¹H NMR: 7.33 (m, 5H, C₆H₅), 4.57 (t, *J* = 6.6, 1H, CH), 2.22 (br. s, 1H, OH), 1.78 (m, 2H, CH₂), 0.91 (t, *J* = 7.5 Hz, 3H, CH₃).

RESULTS AND DISCUSSION

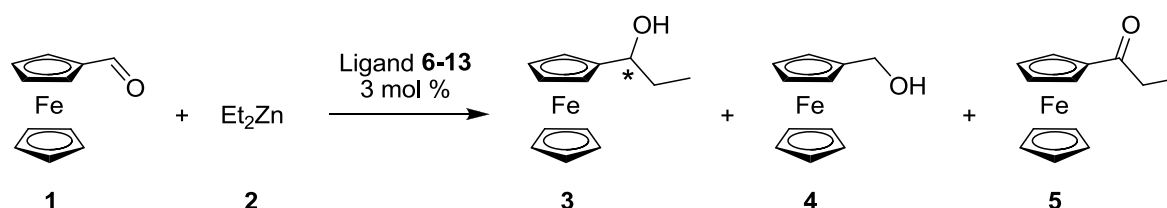
The addition of diethylzinc (**2**) to ferrocene carbaldehyde (**1**) was performed in most cases in hexane according standard conditions [2,4,10,41-46] by using 3 mol % of the corresponding chiral compounds **6-13** as ligands (Scheme 1). In general prolonged reaction times (up to 190 h) were necessary for the formation of the desired product and the conversion of the aldehyde **1** was not complete in several cases. It was, however, remarkable to observe the formation of significant amounts of ferrocenyl methanol (**4**) and 1-ferrocenyl-1-propanone (**5**) as side products. The formation of **4** and **5** could be explained with the assumption [47] that redox Cannizzaro like reaction between **1** and **3** occurs leading to oxidation of **3** to the keton **5** and reduction of **1** to the alcohol **4**. It is

noteworthy to mention that in a paper of Noyori [11] the formation of 1-phenyl-1-propanone has been described beside the 1-phenyl-1-propanol formation in the course of the addition of diethyl zinc to benzaldehyde, however without any discussion. The primary alcohol **4** could also be a result of reduction of the aldehyde **1** through β-hydrogen transfer from the ethyl-group of the diethylzinc reagent.

The addition reactions catalyzed by ligands **6-13** provided acceptable yields of 1-ferrocenylpropan-1-ol (**3**). The ratios of unreacted **1**, product **3** and side-products **4**, and **5**, determined by NMR experiments and the quantities of isolated products are introduced in Table 1. Considering the composition of the compounds observed after performing the reactions it can be concluded that the conversion of the starting aldehyde **1** is very good despite of the prolonged reaction time. Enhancement of the reaction temperature to 60°C shortened significantly the reaction time (Table. 1, entry 1 vs 2 and 7 vs 8), however the enantioselectivity was lowered.

The best enantioselectivities were observed with quinine (**6**) and prolinol (**10**), however the values were significantly lower in comparison with some literature data [19,20,48,49]. The insufficient degree of enantioselectivity in case of ligands **7**, **8**, **9** and **11** was also surprising if compared with reported results [17,18,50,51]. The enantioselectivity realized with proline (entry 10) was low and it could not be enhanced attempting to block the carboxy group through reaction with n-BuLi (entry 11) prior to performing the catalytic addition of diethylzinc. In the case of phenylalanine (entry 12) there is no enantioselectivity at all.

For the purpose of comparison ligands **6**, **10** and **12** furnishing promising enantioselectivities were tested in the addition reaction of diethylzinc to benzaldehyde (Table 2). The reaction catalyzed by ligand **6** provided very good yields whereas in all other cases the yields were moderate. The observed prolonged reaction times could be shortened by applying titanium tetraisopropoxid (Ti(O-*i*Pr)₄)



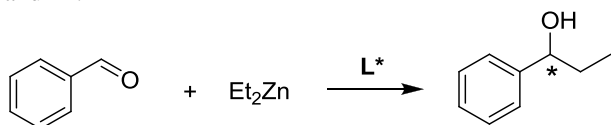
Scheme 1. Enantioselective addition of diethylzinc to ferrocene carbaldehyde.

Table 1. Enantioselective addition of Et₂Zn to ferrocene carbaldehyde (**1**) catalyzed by chiral ligands (L*) **6-13**.

Entry	L*	Reaction Temp.	Reaction Time [h]	Composition [%]				ee [%] ^a
				1	3	4	5	
1	6	20°C	101	28	61	7	1	27 (S)
2	6	60°C ^b	7	-	72	9	9	19 (R)
3	7	20°C	164	16	50	7	4	0
4	8	20°C	183	4	72	7	8	9 (S)
5	9	20°C	67	6	66	7	4	1 (R)
6	10	20°C	191	2	53	9	2	34 (R)
7	10	20°C ^b	168	8	52	7	traces	50 (R)
8	10	60°C ^b	24	7	51	17	7	42 (R)
9	11	20°C	138	14	27	10	5	5 (S)
10	12	20°C	193	10	60	7	2	18 (S)
11	12/n-BuLi ^c	20°C	193	4	67	10	6	11 (S)
12	13	20°C	191	5	8	10	10	0

^aDetermined by polarimetry based on the maximum values for the specific rotations of R(-)-**3**; $[\alpha]_D^{20} = -57.5$ (c 1.0, benzene) for >96% ee [30]; ^bThe reaction is carried out in toluene; ^cButyllithium was added aiming to block the carboxylate function of ligand **12**.

as promoter, however without affecting the enantioselectivity (Table 2, entry 1 vs. 2). Ligand **10** provided comparable results compared with those obtained with aldehyde **1**.

Table 2. Enantioselective addition of Et₂Zn to benzaldehyde (**14**) catalyzed by chiral ligands (L*) **6**, **10** and **12**.

Entry	L*	Reaction Time [h]	Yield of 15 [%]	ee [%] ^a
1	6	193	71	40 (R)
2	6 /Ti(O- <i>i</i> Pr) ₄	4	77	34 (R)
3	10	193	24	38 (R)
4	10 /Ti(O- <i>i</i> Pr) ₄	193	47	0
5	12 /Ti(O- <i>i</i> Pr) ₄	114	51	0

^aDetermined by polarimetry based on the maximum values for the specific rotations of (S)-(-)-**15** ($[\alpha]_D^{20} = -47$ (c 2.2, hexane) for 98% ee [52]).

CONCLUSION

Comparative study has been performed to evaluate the efficiency of the alkaloids quinine, cinchonine, cinchonidine, ephedrine, the amino-alcohols prolinol, and alaninol, and the aminoacids proline, and phenylalanine as catalysts for the enantioselective addition of diethylzinc to ferrocene carbaldehyde. The important intermediate 1-ferrocenyl-1-propanol has been obtained in moderate enantioselectivity besides ferrocenyl methanol and 1-ferrocenyl-1-propanone as side products. The

efficiency of the natural products studied as enantioselective catalysts was not sufficient for additions of diethylzinc to ferrocene carbaldehyde and also to benzaldehyde.

Acknowledgements: Financial support of National Science Fund, Bulgaria (DID02/33/2009 and DRNF-02/13/2009) is gratefully acknowledged.

REFERENCES

1. N. Oguni, T. Omi, *Tetrahedron Lett.*, **25**, 2823 (1984).
2. R. Noyori, *Angew. Chem., Int. Ed.*, **30**, 49 (1991).
3. K. Soai, S. Niwa, *Chem. Rev.*, **92**, 833 (1992).
4. L. Pu, H. H. L. Yu, *Chem. Rev.*, **101**, 757 (2001).
5. R. Noyori, in: *Asymmetric Catalysis in Organic Chemistry*; John Wiley and Sons: New York, 1994.
6. *Catalytic Asymmetric Synthesis*, I. Ojima (Ed.), Wiley-VCH: New York, 2000.
7. *New Frontiers in Asymmetric Catalysis*, K. Mikami, M. Lautens (Eds.), Wiley-Interscience: Hoboken, 2007.
8. R. G. Arrays, J. Adrio, J. C. Carretero, *Angew. Chem., Int. Ed.*, **45**, 7674 (2006).
9. V. Dimitrov, K. Kostova, *Lett. Org. Chem.*, **3**, 176 (2006).
10. M. Kitamura, S. Suga, K. Kawai, R. Noyori, *J. Am. Chem. Soc.*, **108**, 6071 (1986).
11. M. Kitamura, S. Okada, S. Suga, R. Noyori, *J. Am. Chem. Soc.*, **111**, 4028 (1989).
12. R. Noyori, S. Suga, K. Kawai, S. Okada, M. Kitamura, N. Oguni, M. Hayashi, T. Kaneko, Y. Matsuda, *J. Organomet. Chem.*, **382**, 19 (1990).
13. M. Kitamura, S. Suga, M. Niwa, R. Noyori, *J. Am. Chem. Soc.*, **117**, 4832 (1995).
14. M. Yamakawa, R. Noyori, *J. Am. Chem. Soc.*, **117**, 6327 (1995).

15. M. Yamakawa, R. Noyori, *Organometallics*, **18**, 128 (1999).
16. R. Noyori, *Angew. Chem., Int. Ed.*, **41**, 2008 (2002).
17. A. Smaardijk, H. Wynberg, *J. Org. Chem.*, **52**, 135 (1987).
18. R. R. Deshmukh, D. H. Ryu, C. E. Song, in: *Cinchona Alkaloids in Synthesis and Catalysis*, John Wiley and Sons, 2009, pp. 73-104.
19. B. Shen, H. Huang, G. Bian, H. Zong, L. Song, *Chirality*, **25**, 561 (2013).
20. V. Casarotto, Z. Li, J. Boucau, Y. M. Lin, *Tetrahedron Lett.*, **48**, 5561 (2007).
21. S. Bräse, F. Lauterwasser, R. E. Ziegert, *Adv. Synth. Catal.*, **345**, 869 (2003).
22. M. W. Paixao, M. de Godoi, C. R. B. Rhoden, B. Westermann, L. A. Wessjohann, D. S. Lüdtkke, A. L. Braga, *J. Mol. Catal. A - Chem.*, **261**, 120 (2007).
23. A. Mastalir, Z. Király, *Catal. Commun.*, **9**, 1404 (2008).
24. S. Abramson, M. Laspéras, D. Brunel, *Tetrahedron: Asymmetry*, **13**, 357 (2002).
25. M. P. Sibi, L. M. Stanley, *Tetrahedron: Asymmetry*, **15**, 3353 (2004).
26. H.-U. Blaser, W. Chen, F. Camponovo, A. Togni, in: *Ferrocenes*, P. Štěpnička (Ed.), John Wiley & Sons Ltd, UK, 2008, Chapter 6, p. 205.
27. T. Hayashi, in: *Ferrocenes*, A. Togni, T. Hayashi (Eds.), VCH, Weinheim, Germany, 1995, p. 105.
28. A. Togni, in: *Metallocenes*, A. Togni, R. L. Halterman (Eds.), Wiley-VCH GmbH, Weinheim, Germany, 1998, p. 685.
29. M. Perseghini, A. Togni, in: *Science of Synthesis (Houben-Weyl)*, Vol. 1, M. Lautens (Ed.), Thieme, Stuttgart, Germany, 2001, p. 889.
30. Y. Matsumoto, A. Ohno, S. Lu, T. Hayashi, N. Oguni, M. Hayashi, *Tetrahedron: Asymmetry*, **4**, 1763 (1993).
31. C. Imrie, L. Cook, D. C. Levensis, *J. Organomet. Chem.*, **637-639**, 266 (2001).
32. W. L. Davis, R. F. Shago, E. H. G. Langner, J. C. Swarts, *Polyhedron*, **24**, 1611 (2005).
33. D. Kalita, M. Morisue, Y. Kobuke, *New J. Chem.*, **30**, 77 (2006).
34. M. Merabet-Khellasi, L. Aribi-Zouioueche, O. Riant, *Tetrahedron: Asymmetry*, **20**, 1371 (2009).
35. M. I. Ikhile, M. D. Bala, V. O. Nyamoria, J. C. Ngila, *Appl. Organomet. Chem.*, **27**, 98 (2013).
36. V. A. Darin, A. F. Neto, J. Miller, M. M. de Freitas Afonso, H. C. Fonsatti, Á. D. L. Borges, *J. Prakt. Chem.*, **341**, 588 (1999).
37. W. G. Jary, A.-K. Mahler, T. Purkathofer, J. Baumgartner, *J. Organomet. Chem.*, **629**, 208 (2001).
38. K. Tappe, P. Knochel, *Tetrahedron: Asymmetry*, **15**, 91 (2004).
39. D. Plazuk and J. Zakrzewski, *Synth. Commun.*, **34**, 99 (2004).
40. V. H. Purecha, N. S. Nandurkar, B. M. Bhanage, J. M. Nagarkar, *J. Chem. Res.*, 426 (2007).
41. M. Genov, V. Dimitrov, V. Ivanova, *Tetrahedron: Asymmetry*, **8**, 3703 (1997).
42. W. A. Nugent, *Chem. Commun.*, 1369 (1999).
43. I. Philipova, V. Dimitrov, S. Simova, *Tetrahedron: Asymmetry*, **10**, 1381 (1999).
44. S. Panev, A. Linden, V. Dimitrov, *Tetrahedron: Asymmetry*, **12**, 1313 (2001).
45. N. Garcia-Delgado, M. Fontes, M. A. Pericas, A. Riera, X. Verdager, *Tetrahedron: Asymmetry*, **15**, 2085 (2004).
46. V. Dimitrov, M. Kamenova-Nacheva, *J. Univ. Chem. Technol. Metall.*, **44**, 317 (2009).
47. L. Bonetto, R. Fornasier, U. Tonellato, *Gazz. Chim. Ital.*, **125**, 63 (1995).
48. P. Hodge, R. J. Kell, J. Ma, H. Morris, *Aust. J. Chem.*, **52**, 1041 (1999).
49. C. L. Gibson, *Tetrahedron: Asymmetry*, **10**, 1551 (1999).
50. E. J. Corey, F. J. Hannon, *Tetrahedron Lett.*, **28**, 5233 (1987).
51. P. A. Chaloner, S. A. R. Perera, *Tetrahedron Lett.*, **28**, 3013 (1987).
52. www.sigma-aldrich.com

ЕНАНТИОСЕЛЕКТИВНО ПРИСЪЕДИНЯВАНЕ НА ДИЕТИЛЦИНК КЪМ
ФЕРОЦЕНКАРБАЛДЕХИД – РЕЗУЛТАТИ ОТ ИЗПОЛЗВАНЕ НА ПРИРОДНИ
СЪЕДИНЕНИЯ КАТО КАТАЛИЗАТОРИ

К. Дикова, М. Каменова-Начева, К. Костова, В. Димитров*

*Институт по Органична химия с Център по Фитохимия, Българска Академия на Науките, ул. Акад. Г. Бончев,
бл. 9, 1113 София, България*

Постъпила на 19 юни 2014 г.; Коригирана на 15 юли 2014 г.

(Резюме)

Изучена е ефективността на алкалоидите хинин, цинхонин, цинхонидин и ефедрин, на аминокиселините пролин и фенилаланин за енантиселективно присъединяване на диетилцинк към фероценкарбалдехид и бензалдехид. Присъединителните реакции протичат с приемливи добиви и ниски до умерени енантиселективности. При присъединителните реакции към фероценкарбалдехид се наблюдават страничните продукти фероценил метанол и 1-фероценил-1-пропанон, които са изолирани и охарактеризирани.

Bifunctionalized allenes. Part XIV. A convenient and efficient regioselective synthesis of phosphorylated β -hydroxyallenes with protected and unprotected hydroxy group

I. E. Ismailov, I. K. Ivanov, V. C. Christov*

Department of Organic Chemistry & Technology, Faculty of Natural Sciences, Konstantin Preslavsky University of Shumen, 115 Universitetska str., 9712 Shumen, Bulgaria

Received May 09, 2014; Revised June 24, 2014

Dedicated to Acad. Dimiter Ivanov on the occasion of his 120th birth anniversary

A convenient and efficient regioselective synthesis of phosphorylated β -hydroxyallenes by an atom economical [2,3]-sigmatropic rearrangement of the mediated propargyl phosphite or phosphinite which can be readily prepared *via* reaction of protected 5-methyl-dec-6-yn-5-ol with dimethyl chlorophosphite or chlorodiphenyl phosphine respectively in the presence of a base is described.

Key words: synthesis, protection of hydroxy group, [2,3]-sigmatropic rearrangement, phosphorylated β -hydroxyallenes

INTRODUCTION

In the past three decades, synthesis and use of allene derivatives have been expanded in preparative organic chemistry. The presence of two π electron clouds separated by a single sp hybridized carbon atom is the identifying structural characteristic of allenes, and it is this unique structural and electronic arrangement that is responsible for the extraordinary reactivity profile displayed by allenic compounds [1-8].

Functionalized allenes have attracted a growing attention because of their versatility as key building blocks for organic synthesis. The synthetic potential of functionalized allenes has been explored extensively in recent years, and this has led to the development of novel methods for the construction of a variety of functionalized heterocyclic and carbocyclic systems [9-13].

A plethora of methods exists for the construction of hydroxyallenes, including prototropic rearrangement of propargylic alcohols [14,15], metal-catalyzed nucleophilic addition of propargylic derivatives to aldehydes [16-22], Cu(I)-catalyzed reaction of propargylic chlorides with Grignard reagents [23,24], metal-catalyzed reaction of propargylic oxiranes with organometallic compounds [25-29] and ketones [30,31], reduction of alcohols, ethers, oxiranes etc. with aluminium reagents [32-34], Pd(0)-catalyzed reaction of cyclic carbonates with

acetylenic compounds [35,36], S_N2' [37,38] and A_N [39-41] reactions of metallated alkoxy-allenes with oxiranes and ketones [5], and by other methods [42].

There are methods [43-46] for the synthesis of phosphorus-containing allenes (phosphonates [47-50], phosphinates [51,52], and phosphine oxides [53-58]) including reactions of α -alkynols with chloride-containing derivatives of phosphorus acids followed by [2,3]-sigmatropic rearrangement. Several diethylphosphono-substituted α -allenic alcohols were prepared by Brel [59,60] directly from alcohols by Horner-Mark rearrangement of unstable propargylic phosphites.

Since its discovery five decades ago [51,52], the reversible interconversion of propargylic phosphites, phosphonites and phosphinites to allenyl phosphonates, phosphinates and phosphine oxides has become one of the most studied and synthetically useful [2,3]-sigmatropic rearrangement. Numerous synthetic applications of the rearrangement have been reported, including its use in the synthesis of allenic steroids as substrate-induced inactivation of aromatase [61], in the efficient synthesis of (2*R*)-2-amino-5-phosphonopentanoic acid (AP5) as a powerful and selective N-methyl-D-aspartate (NMDA) antagonist [62], in the preparation of the phosphonate analogues of phosphatidyl derivatives [63,64], and in the synthesis of new acyclic analogues of nucleotides containing a purine or pyrimidine moiety and an allenic skeleton [65,66].

* To whom all correspondence should be sent:
E-mail: vchristo@shu-bg.net

As a part of our research program on the chemistry of the bifunctionalized allenes, we required a convenient method to introduce a phosphorus-containing group such as phosphonate or phosphine oxide group as well as a β -hydroxy-alkyl group in the first position to the allenic system of double bonds. The above mentioned groups attract increasing attention as useful functionalities in organic synthesis. Of particular interest are the applications of these groups as temporary transformers of chemical reactivity of the allenic system in the synthesis of eventually heterocyclic compounds.

In a continuation to our previous reports on the synthesis [67] and electrophilic cyclization reactions [68] of bifunctionalized allenes, we have found a convenient and efficient method for regioselective synthesis of phosphorylated β -hydroxyallenes by an atom economical [2,3]-sigmatropic rearrangement of the mediated 4-(tetrahydro-2H-pyran-2-yloxy)-propargyl phosphite or phosphinite.

EXPERIMENTAL

General information

All new synthesized compounds were purified by column chromatography and characterized on the basis of NMR, IR, and microanalytical data. NMR spectra were recorded on DRX Bruker Avance-250 (Bruker BioSpin, Karlsruhe, Germany) (^1H at 250.1 MHz, ^{13}C at 62.9 MHz, ^{31}P at 101.2 MHz) and Bruker Avance II+600 (Bruker BioSpin GmbH, Karlsruhe, Germany) (^1H at 600.1 MHz, ^{13}C at 150.9 MHz, ^{31}P at 242.9 MHz) spectrometers for solutions in CDCl_3 . All ^1H and ^{13}C NMR experiments were measured referring to the signal of internal TMS and ^{31}P NMR experiments were measured referring to the signal of external 85% H_3PO_4 . J values are given in hertz. IR spectra were recorded with an FT-IRAffinity-1 Shimadzu spectrophotometer (Shimadzu, Tokyo, Japan). Elemental analyses were carried out by the Microanalytical Service Laboratory of Faculty of Chemistry and Pharmacy, University of Sofia, Bulgaria, using Vario EL3 CHNS(O) (Elementar Analysensysteme, Hanau, Germany). Column chromatography was performed on Kieselgel F₂₅₄60 (70-230 mesh ASTM, 0.063-0.200 mm, Merck). Et_2O and THF were distilled from Na wire/benzophenone, CH_2Cl_2 was distilled over CaH_2 , other commercially available chemicals were used without additional purification unless otherwise noted. Reactions were carried out in oven dried glassware under an argon atmosphere and exclusion of moisture. All compo-

unds were checked for purity on TLC plates Kieselgel F₂₅₄ 60 (Merck).

Procedure [21] for synthesis of 2-(1-methyl-but-3-yn-1-yloxy)-tetrahydro-2H-pyran 2

A solution of the pent-4-yn-2-ol **1** (60 mmol) and DHP (3,4-dihydro-2H-pyran) (7.57 g, 90 mmol) in dry methylene chloride (50 ml) containing PPTS (pyridinium *p*-toluenesulfonate) (1.50 g, 6 mmol) is stirred for 4 h at room temperature. Then the reaction was quenched with saturated NaHCO_3 and extracted with methylene chloride. The organic layer was dried over anhydrous sodium sulfate. After evaporation of the solvent, the residue was chromatographed on a column (silica gel, Kieselgel Merck 60 F₂₅₄) with a mixture of ethyl acetate and hexane (3:1) as an eluent. The pure product **2** had the following properties:

2-(1-Methyl-but-3-yn-1-yloxy)-tetrahydro-2H-pyran (2). Colourless oil, yield: 87%. R_f 0.55. IR (neat, cm^{-1}): 1125 (C-O-C), 2106 (C \equiv C), 3292 (\equiv C-H). $^1\text{H-NMR}$ (250.1 MHz): δ = 1.09-1.25, 3.65-3.77, 4.74-4.81 (mmm, 9H, OTHP), 1.27 (d, J = 7.2 Hz, 3H, Me-CHO), 2.02 (m, 1H, H-C \equiv), 2.38, 2.59 (mm, 2H, CH-C \equiv), 3.80-3.89 (m, 1H, Me-CHO). $^{13}\text{C-NMR}$ (62.9 MHz) δ = 20.1 (CH_2), 22.7 (CH_3), 25.8 (CH_2), 26.4 (CH_2), 31.9 (CH_2), 63.8 (CH_2), 67.0 (CH), 75.2 (CH), 81.2 (C), 95.9 (CH). Anal. Calcd. for $\text{C}_{10}\text{H}_{16}\text{O}_2$ (168.23): C 71.39; H 9.59; found: C 71.32; H 9.65.

Synthesis of the 5-methyl-9-(tetrahydro-2H-pyran-2-yloxy)-dec-6-yn-5-ol 5

Ethylmagnesium bromide [prepared from magnesium (1.22 g, 50 mmol) and ethyl bromide (5.50 g, 50 mmol) in dry THF (50 ml)] is added dropwise under stirring to substituted alkynyloxy-tetrahydro-2H-pyran **2** (50 mmol) and then the mixture is refluxed for 2 h. The solution of the prepared pentynyl magnesium bromide **3** is added dropwise under stirring to the hexan-2-one **4** (100 mmol). The mixture is refluxed for 24 h and after cooling is hydrolyzed with a saturated aqueous solution of ammonium chloride. The organic layer is separated, washed with water, and dried over anhydrous sodium sulfate. Solvent and the excess of ketone are removed by distillation. Purification of the residue is achieved by column chromatography (silica gel, Kieselgel Merck 60 F₂₅₄) with ethyl acetate and hexane (5:1). The pure product **5** had the following properties:

5-Methyl-9-(tetrahydro-2H-pyran-2-yloxy)-dec-6-yn-5-ol (5). Colourless oil, yield: 55%. R_f 0.51.

IR (neat, cm^{-1}): 1122 (C-O-C), 3408 (OH). $^1\text{H-NMR}$ (250.1 MHz): δ = 0.88 (t, J = 6.5 Hz, 3H, Me-(CH_2)₃), 1.15-1.37, 3.60-3.81, 4.73-4.81 (mmm, 9H, OTHP), 1.28 (d, J = 7.1 Hz, 3H, Me-CHO), 1.30-1.58 (m, 2H, Me-(CH_2)₂), 1.37 (s, 3H, Me-C), 2.54 (s, 1H, OH), 2.57-2.64 (m, 2H, O-CH- CH_2 -C \equiv), 3.83-3.88 (m, 1H, Me-CHO). $^{13}\text{C-NMR}$ (62.9 MHz) δ = 14.7 (CH_3), 20.1 (CH_2), 22.7 (CH_3), 24.3 (CH_2), 24.7 (CH_2), 25.1 (CH_2), 25.6 (CH_2), 30.0 (CH_3), 31.8 (CH_2), 45.3 (CH_2), 63.9 (CH_2), 68.1 (C), 75.7 (CH), 78.4 (C), 82.3 (C), 96.1 (CH). Anal. Calcd. for $\text{C}_{16}\text{H}_{28}\text{O}_3$ (268.39): C 71.60; H 10.52; found: C 71.66; H 10.44.

Synthesis of dimethyl 3-methyl-1-[2-(tetrahydro-2H-pyran-2-yloxy)-propyl]-hepta-1,2-diene-phosphonate 7

To a solution of phosphorus trichloride (2.75 g, 20 mmol) and triethylamine (2.23 g, 22 mmol) in dry diethyl ether (60 ml) at -70°C was added dropwise with stirring a solution of the 5-methyl-9-(tetrahydro-2H-pyran-2-yloxy)-dec-6-yn-5-ol **5** (20 mmol) in the same solvent (20 ml). After 30 min stirring at the same conditions a solution of pyridine (3.16 g, 44 mmol) and of methanol (1.28 g, 40 mmol) in dry diethyl ether (50 mL) were added. The reaction mixture was stirred for an hour at the same temperature and for 10 hours at room temperature. The mixture was then washed with water, 2N HCl, extracted with ether, washed with saturated NaCl, and dried over anhydrous sodium sulfate. After evaporation of the solvent, the residue was chromatographed on a column (silica gel, Kieselgel Merck 60 F₂₅₄) with a mixture of ethyl acetate and hexane (10:1) as an eluent to give the pure product **7** as an oil, which had the following properties:

Dimethyl 3-methyl-1-[2-(tetrahydro-2H-pyran-2-yloxy)-propyl]-hepta-1,2-dienephosphonate (7). Orange oil, yield: 71%. R_f 0.45. IR (neat, cm^{-1}): 1118 (C-O-C), 1258 (P=O), 1955 (C=C=C). $^1\text{H-NMR}$ (600.1 MHz): δ = 0.90 (t, J = 7.3 Hz, 3H, Me-(CH_2)₃), 1.17 (d, J = 6.0 Hz, 3H, Me-CHO), 1.20-1.23, 1.24-1.29, 1.42-1.47, 3.84-3.95, 4.90-4.94 (mmmm, 9H, OTHP), 1.32-1.38 (m, 2H, Me- CH_2 (CH_2)₂), 1.51-1.57 (m, 2H, Me- CH_2 CH_2 CH_2), 1.76 (d, J = 7.0 Hz, 3H, Me-C=), 2.14-2.42 (m, 2H, O-CH- CH_2 -C=), 2.35-2.42 (m, 2H, Me-(CH_2)₂ CH_2), 3.73 (d, J = 11.1 Hz, 3H, MeO), 4.67-4.71 (m, 1H, Me-CHO). $^{13}\text{C-NMR}$ (150.9 MHz) δ = 13.9 (CH_3), 18.8 (J = 5.3 Hz, CH_3), 19.7 (CH_2), 20.0 (J = 7.8 Hz, CH_3), 20.4 (CH_2), 25.3 (CH_2), 29.4 (CH_2), 32.0 (CH_2), 36.1 (J = 6.7 Hz, CH_2), 36.9 (J = 8.9 Hz, CH_2), 52.8 (J = 6.4 Hz, CH_3), 62.9 (J = 12.1 Hz, CH), 63.7 (CH_2),

88.4 (J = 191.8 Hz, C), 96.2 (CH), 102.4 (J = 13.2 Hz, C), 208.3 (J = 5.1 Hz, C). $^{31}\text{P-NMR}$ (242.9 MHz): δ 21.9. Anal. Calcd. for $\text{C}_{18}\text{H}_{33}\text{O}_5\text{P}$ (360.43): C 59.98; H 9.23. Found: C 59.93; H 9.16.

Synthesis of 2-(3-diphenyl-phosphinoyl-1,5-dimethyl-nona-3,4-dienyloxy)-tetrahydro-2H-pyran 9

To a solution of the 5-methyl-9-(tetrahydro-2H-pyran-2-yloxy)-dec-6-yn-5-ol **5** (20 mmol) and triethylamine (2.23 g, 22 mmol) in dry diethyl ether (60 ml) at -70°C , a solution of freshly distilled diphenylchlorophosphine (4.41 g, 20 mmol) in the same solvent (20 ml) was added dropwise with stirring. The reaction mixture was stirred for an hour at the same temperature and for 8 h at room temperature and then washed with water, 2N HCl, extracted with diethyl ether, and the extract was washed with saturated NaCl, and dried over anhydrous sodium sulfate. The solvent was removed using a rotary evaporator, and the residue was purified by column chromatography on a silica gel (Kieselgel Merck 60 F₂₅₄) with ethyl acetate-hexane (10:1) to give the pure product **9** as an oil, which had the following properties:

2-(3-Diphenylphosphinoyl-1,5-dimethyl-nona-3,4-dienyloxy)-tetrahydro-2H-pyran (9). Yellow oil, yield: 79%. R_f 0.43. IR (neat, cm^{-1}): 1122 (C-O-C), 1156 (P=O), 1436, 1490 (Ph), 1951 (C=C=C). $^1\text{H-NMR}$ (600.1 MHz): δ = 0.81 (t, J = 7.3 Hz, 3H, Me-(CH_2)₃), 1.11-1.16, 1.23-1.28, 1.44-1.49, 3.86-3.94, 4.88-4.93 (mmmm, 9H, OTHP), 1.17 (d, J = 6.1 Hz, 3H, Me-CHO), 1.35-1.39 (m, 2H, Me- CH_2 (CH_2)₂), 1.49-1.55 (m, 2H, Me- CH_2 CH_2 CH_2), 1.79 (d, J = 7.1 Hz, 3H, Me-C=), 2.04-2.16 (m, 2H, O-CH- CH_2 -C=), 2.29-2.36 (m, 2H, Me-(CH_2)₂ CH_2), 4.66-4.70 (m, 1H, Me-CHO), 7.37-7.88 (m, 10H, 2Ph). $^{13}\text{C-NMR}$ (150.9 MHz) δ = 13.9 (CH_3), 19.1 (J = 5.4 Hz, CH_3), 19.8 (J = 8.0 Hz, CH_3), 21.1 (CH_2), 21.3 (CH_2), 25.4 (CH_2), 29.3 (CH_2), 32.1 (CH_2), 35.1 (J = 6.2 Hz, CH_2), 35.6 (J = 8.7 Hz, CH_2), 62.7 (J = 12.2 Hz, CH), 62.9 (CH_2), 93.8 (J = 103.6 Hz, C), 96.2 (CH), 102.9 (J = 13.2 Hz, C), 127.7-133.2 (2Ph), 207.9 (J = 6.6 Hz, C). $^{31}\text{P-NMR}$ (242.9 MHz): δ 32.6. Anal. Calcd. for $\text{C}_{28}\text{H}_{37}\text{O}_3\text{P}$ (452.57): C 74.31; H 8.24; found: C 74.39; H 8.20.

Synthesis of dimethyl [1-(2-hydroxypropyl)-3-methyl-hepta-1,2-dienyl]-phosphonate 10 and 4-diphenylphosphinoyl-6-methyl-deca-4,5-dien-2-ol 11

A solution of the dimethyl 3-methyl-1-[2-(tetrahydro-2H-pyran-2-yloxy)-propyl]-hepta-1,2-dienephosphonate **7** or the 2-(3-diphenyl-phosphinoyl-

1,5-dimethyl-nona-3,4-dienyloxy)-tetrahydro-2H-pyran **9** (5 mmol) and PPTS (0.5 mmol) in ethanol (10 ml) was stirred at room temperature for 6 h. The mixture was then washed with water, extracted with methylene chloride and dried over anhydrous sodium sulfate. After evaporation of the solvent, the residue was chromatographed on a column (silica gel, Kieselgel Merck 60 F₂₅₄) with a mixture of ethyl acetate and hexane (10:1) as an eluent to give the pure products **10** or **11** as oils, which had the following properties:

Dimethyl 1-(2-hydroxypropyl)-3-methyl-hepta-1,2-dienephosphonate (10). Yellow oil, yield: 83%. R_f 0.59. IR (neat, cm⁻¹): 1259 (P=O), 1951 (C=C=C), 3420 (OH). ¹H-NMR (600.1 MHz): δ = 0.91 (t, *J* = 7.3 Hz, 3H, Me-(CH₂)₃), 1.22 (d, *J* = 6.4 Hz, 3H, Me-CHO), 1.33-1.38 (m, 2H, Me-CH₂(CH₂)₂), 1.41-1.47 (m, 2H, Me-CH₂CH₂CH₂), 1.78 (d, *J* = 6.9 Hz, 3H, Me-C=), 2.03-2.06 (m, 2H, O-CH-CH₂-C=), 2.27-2.33 (m, 2H, Me-(CH₂)₂CH₂), 2.88 (s, 1H, OH), 3.74 (d, *J* = 11.1 Hz, 3H, MeO), 4.59-4.62 (m, 1H, Me-CHO). ¹³C-NMR (150.9 MHz) δ = 13.8 (CH₃), 18.0 (*J* = 5.8 Hz, CH₃), 22.2 (CH₂), 22.7 (*J* = 7.9 Hz, CH₃), 29.3 (CH₂), 33.0 (*J* = 6.6 Hz, CH₂), 39.4 (*J* = 12.1 Hz, CH₂), 52.9 (*J* = 6.3 Hz, CH₃), 66.9 (*J* = 9.7 Hz, CH), 88.6 (*J* = 190.3 Hz, C), 102.3 (*J* = 15.9 Hz, C), 208.1 (*J* = 5.2 Hz, C). ³¹P-NMR (242.9 MHz): δ 22.6. Anal. Calcd. for C₁₃H₂₅O₄P (276.31): C 56.51; H 9.12; found: C 56.43; H 9.19.

4-Diphenylphosphinoyl-6-methyl-deca-4,5-dien-2-ol (11). Orange oil, yield: 88%. R_f 0.58. IR (neat, cm⁻¹): 1167 (P=O), 1436, 1491 (Ph), 1949 (C=C=C), 3401 (OH). ¹H-NMR (600.1 MHz): δ = 0.82 (t, *J* = 7.2 Hz, 3H, Me-(CH₂)₃), 1.20 (d, *J* = 6.4 Hz, 3H, Me-CHO), 1.40-1.44 (m, 2H, Me-CH₂(CH₂)₂), 1.46-1.51 (m, 2H, Me-CH₂CH₂CH₂), 1.80 (d, *J* = 7.1 Hz, 3H, Me-C=), 2.04-2.10 (m, 2H, O-CH-CH₂-C=), 2.30-2.36 (m, 2H, Me-(CH₂)₂CH₂), 2.90 (s, 1H, OH), 4.58-4.61 (m, 1H, Me-CHO), 7.35-7.89 (m, 10H, 2Ph). ¹³C-NMR (150.9 MHz) δ = 13.9 (CH₃), 18.7 (*J* = 5.9 Hz, CH₃), 21.1 (CH₂), 22.9 (*J* = 8.0 Hz, CH₃), 29.2 (CH₂), 32.9 (*J* = 6.4 Hz, CH₂), 39.5 (*J* = 12.4 Hz, CH₂), 67.3 (*J* = 9.8 Hz, CH), 94.6 (*J* = 102.4 Hz, C), 102.2 (*J* = 15.7 Hz, C), 128.0-132.5 (2Ph), 209.0 (*J* = 5.4 Hz, C). ³¹P-NMR (242.9 MHz): δ 34.5. Anal. Calcd. for C₂₃H₂₉O₂P (368.45): C 74.98; H 7.93; found: C 75.04; H 7.88.

RESULTS AND DISCUSSION

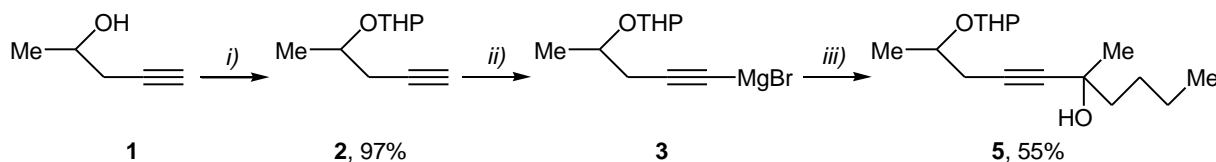
Our strategy for the synthesis of the phosphorylated α-hydroxyallenes, using our experience on the preparation of the 4-heteroatom-functiona-

lized allenecarboxylates [67], relies on the well-precedented [2,3]-sigmatropic shift of propargylic phosphites to allenephosphonates [47-50] and propargylic phosphinites to allenyl phosphine oxides [53-58]. Precedent exists for such an approach to the synthesis of the diethylphosphono-substituted α-allenic alcohols [59,60] only. However, to the best of our knowledge, synthesis of phosphorylated (phosphonates and phosphine oxides) β-hydroxyallenes with protected or unprotected hydroxy group has not been reported.

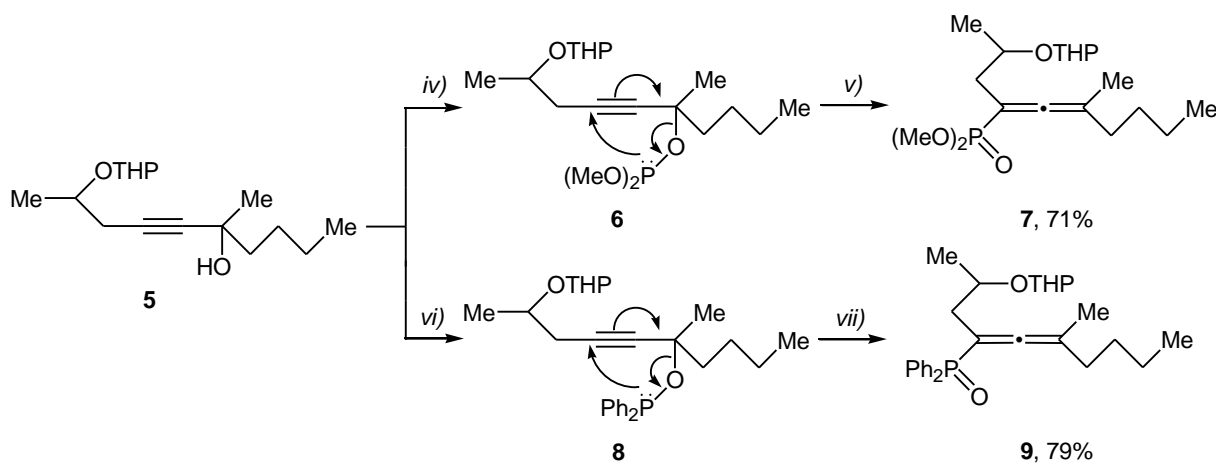
In order to assess this approach towards the target 1,1-bifunctionalized allenes, a range of the phosphorylated β-hydroxyallenes **7**, **9**, **10**, and **11**, was prepared by the following four-step procedure including i) protection of hydroxy group in the pent-4-yn-2-ol **1**; ii) subsequent reaction with Grignard reagent and butylmethyl ketone to give the 6-methyl-dec-4-yne-2,6-diol **5** with protected hydroxy group at 2 position; iii) interaction with chloride of phosphorus acid in the presence of a base; and finally iv) [2,3]-sigmatropic rearrangement of the mediated protected propargyl phosphite or phosphinite.

As a starting point for our investigation, we first examined the protection of hydroxy group in the pent-4-yn-2-ol **1** with DHP in the presence of PPTS [69-72] (Scheme 1). Thus, the formed 2-(1-methylbut-3-ynyloxy)-tetrahydro-2H-pyran **2** was isolated by column chromatography with excellent yield (87%). Reaction of the protected pent-4-yn-2-ol **2** with ethyl magnesium bromide and subsequent dropwise addition of *in situ* the generated pentynyl magnesium bromide **3** to the hexan-2-one **4** and reflux for 24 hours gave the 5-methyl-9-(tetrahydro-2H-pyran-2-yloxy)-dec-6-yn-5-ol **5**, which was stable and was isolated by column chromatography in 55% yield.

With the required dec-4-yne-2,6-diol **5** with protected hydroxy group at 2 position in hand, we were then able to investigate the proposed reactions with the corresponding chlorocontaining phosphorus reagents such as dimethyl chlorophosphite and chlorodiphenyl phosphine in the presence of a base and subsequent [2,3]-sigmatropic rearrangement of the mediated 4-(tetrahydro-2H-pyran-2-yloxy)-propargyl phosphite **6** or phosphinite **8**. In the first instance, the dimethyl 1-(tetrahydro-2H-pyran-2-yloxy)-alka-1,2-dienephosphonates **7** can be readily prepared *via* an atom economical 2,3-sigmatropic rearrangement of the 4-(tetrahydro-2H-pyran-2-yloxy)-propargyl phosphite **6**, intermediate formed by reaction of the (tetrahydro-2H-pyran-2-yloxy)-alkynol **5** with dimethyl chlorophosphite, prepared *in situ* from phosphorus trichloride and 2 equiv of



Scheme 1. Synthesis of the 5-methyl-9-(tetrahydro-2*H*-pyran-2-yloxy)-dec-6-yn-5-ol **5**. Reagents and Conditions: i) DHP (1.5 eq), PPTS (0.1 eq), CH₂Cl₂, rt, 4 h, distillation; ii) EtMgBr (1 eq), THF, reflux, 2 h; iii) dropwise addition of **3** to MeC(O)Bu **4** (2 eq), reflux, 24 h, column chromatography.



Scheme 2. Synthesis of the dimethyl-3-methyl-1-[2-(tetrahydro-2*H*-pyran-2-yloxy)-propyl]-hepta-1,2-dienephosphonate **7** and 2-(3-diphenylphosphinoyl-1,5-dimethyl-nona-3,4-dienyloxy)-tetrahydro-2*H*-pyran **9**. Reagents and Conditions: iv) PCl₃ (1 eq), Et₃N (1.1 eq), Et₂O, -70°C, 30 min stirring, pyridine (2.2 eq), MeOH (2 eq), Et₂O, -70°C; v) [2,3-σ]-rearrangement, -70°C, 1 h, rt, 10 h; vi) Ph₂PCl (1 eq), Et₃N (1.1 eq), Et₂O, -70°C, 1 h, rt, 10 h, column chromatography; vii) [2,3-σ]-rearrangement, -70°C, 1 h, rt, 8 h, column chromatography.

pyridine, according to Scheme 2.

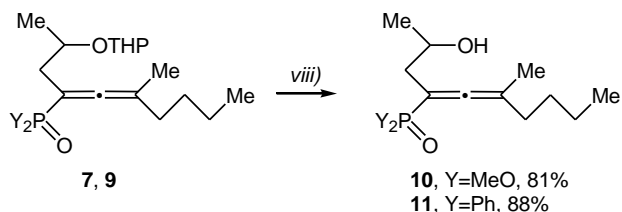
Pleasingly, the reaction of the (tetrahydro-2*H*-pyran-2-yloxy)-alkynol **5** with chlorodiphenyl phosphine in the presence of triethylamine at -70°C gave the expected 2-(2-(diphenylphosphinoyl-alka-2,3-dienyloxy)-tetrahydro-2*H*-pyrans **9** in very good yield (79%) as a result of [2,3]-sigmatropic rearrangement of the 4-(tetrahydro-2*H*-pyran-2-yloxy)-propargyl phosphinite **8** for 8 hours at room temperature, according to the reaction sequence outlined in Scheme 2.

A new family of phosphorylated β-hydroxyallenes with protected hydroxyl group **7** and **9** was synthesized *via* an atom economical and regioselective [2,3]-sigmatropic rearrangement of the intermediate formed propargyl phosphite **6** or phosphinite **8** in the reaction of protected alkynol **5** with dimethylchloro phosphite or chlorodiphenyl phosphine in the presence of triethylamine.

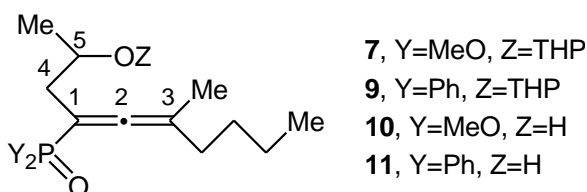
Compounds **7** and **9** were stable enough to be handled at ambient temperature. The hydroxy group was deprotected by stirring the ethanol solution of the protected hydroxypropyl-allenephosphonate **7** and hydroxypropyl-allenyl phosphine oxide **9** in the

presence of 0.1 *equiv* PPTS at room temperature for 6 hours, according to Scheme 3.

After a conventional work-up, all allenic products **7**, **9**, **10**, and **11** were isolated as stable yellow or orange oils by column chromatography and identified by ¹H, ¹³C, and ³¹P NMR and IR spectra as well as by elemental analysis. Some characteristic chemical shifts and coupling constants in the ¹³C and ³¹P NMR spectra of the prepared phosphorylated β-hydroxyallenes **7**, **9**, **10**, and **11** are summarized in Table 1.



Scheme 3. Synthesis of the dimethyl [1-(2-hydroxypropyl)-3-methyl-hepta-1,2-dienyl]-phosphonate **10** and the 4-(diphenylphosphinoyl)-6-methyl-deca-4,5-dien-2-ol **11**. Reagents and Conditions: viii) PPTS (0.1 eq), EtOH, rt, 6h, stirring, column chromatography.

Table 1. Some characteristic ^{13}C and ^{31}P NMR spectral data of the prepared phosphorylated β -hydroxyallenes **7**, **9**, **10**, and **11**.

Allene	$\delta_{\text{C-1}}$ ($^1J_{\text{P-C-1}}$)	$\delta_{\text{C-2}}$ ($^2J_{\text{P-C-2}}$)	$\delta_{\text{C-3}}$ ($^2J_{\text{P-C-4}}$)	$\delta_{\text{C-4}}$ ($^3J_{\text{P-C-3}}$)	$\delta_{\text{C-5}}$ ($^3J_{\text{P-C-5}}$)	$\delta^{31}\text{P}$
7	88.4 (191.8)	208.3 (5.1)	102.4 (13.2)	36.9 (8.9)	62.9 (12.1)	21.9
9	93.8 (103.6)	207.9 (6.6)	102.9 (13.2)	35.6 (8.7)	62.7 (12.2)	32.6
10	88.6 (190.3)	208.1 (5.2)	102.3 (15.9)	39.4 (12.1)	66.9 (9.7)	22.6
11	94.6 (102.4)	209.0 (5.4)	102.2 (15.7)	39.5 (12.4)	67.3 (9.8)	34.5

A series of new phosphorylated β -hydroxyallenes with protected **7** and **9** and unprotected hydroxy group **10** and **11** were synthesized by a convenient, efficient, atom economical and regioselective method.

CONCLUSION

In conclusion, a convenient and efficient method for regioselective synthesis of a new family of 1,1-bifunctionalized allenes has been explored. Phosphorylated α -hydroxyallenes prepared were derived from [2,3]-sigmatropic rearrangement of the intermediate propargyl phosphites or phosphinites formed in the reaction of protected alkynols with dimethylchloro phosphite or chlorodiphenyl phosphine in the presence of a base.

Further investigations on this potentially important synthetic methodology are currently in progress. At the same time, the synthetic application of the prepared phosphorylated β -hydroxyallenes with protected or unprotected hydroxy group for synthesis of different heterocyclic compounds is now under investigation in our laboratory as a part of our general synthetic strategy for investigation of the scope and limitations of the electrophilic cyclization and cycloisomerization reactions of bifunctionalized allenes. Results of these investigations will be reported in due course.

Acknowledgements: Support from the Research Fund of the Konstantin Preslavsky University of Shumen (Project No. RD-08-208 / 2014), National

Research Fund of Bulgaria (Project No. DRNF-02-13/2009) and Human Resources Development Operational Programme of the European Union (BG051PO001-3.3.06-0003/2012) is gratefully acknowledged.

REFERENCES

- S. Patai (Ed.), *The Chemistry of Ketenes, Allenes and Related Compounds*, John Wiley & Sons, New York, 1980.
- S. R. Landor (Ed.), *The Chemistry of the Allenes*, Academic Press, London, 1982, Vol. 1-3.
- D. J. Pasto, *Tetrahedron*, **40**, 2805 (1984).
- H. F. Schuster, G. M. Coppola, *Allenenes in Organic Synthesis*, John Wiley & Sons, New York, 1988.
- R. Zimmer, *Synthesis*, 165 (1993).
- C. J. Elsevier, *Methods of Organic Chemistry (Houben-Weyl)*, R. W. Helmchen, J. Mulzer, E., Schaumann (Eds.), Vol. E21a, Thieme, Stuttgart, 1995, pp. 537-566.
- N. Krause, A. S. K. Hashmi (Eds.), *Modern Allene Chemistry*, Wiley-VCH, Weinheim, 2004, Vol. 1,2.
- K. M. Brummond, J. E. DeForrest, *Synthesis*, 795 (2007).
- R. W. Bates, V. Satcharoen, *Chem. Soc. Rev.*, **31**, 12 (2002).
- S. Ma, *Aldrichimica Acta*, **40**, 91 (2007).
- H. H. A. M. Hassan, *Curr. Org. Synth.*, **4**, 413 (2007).
- T. M. V. D. Pinho e Melo, *Curr. Org. Chem.*, **13**, 1406 (2009).
- T. G. Back, K. N. Clary, D. Gao, *Chem. Rev.*, **110**, 4498 (2010).
- M. Enomoto, T. Katsuki, M. Yamaguchi, *Tetrahedron Lett.*, **27**, 4599 (1986).
- S. Phadtare, J. Zemlicka, *J. Am. Chem. Soc.*, **111**, 5925 (1989).
- S. Ma, H. Hou, S. Zhao, G. Wang, *Synthesis*, 1643 (2002).
- J. Ye, S. Li, B. Chen, W. Fan, J. Kuang, J. Liu, Y. Liu, B. Miao, B. Wan, Y. Wang, X. Xie, Q. Yu, W. Yuan, S. Ma, *Org. Lett.*, **14**, 1346 (2012).
- G. P. Boldrini, L. Lodi, E. Tagliavini, C. Tarasco, C. Trombini, A. Umanl-Ronchi, *J. Org. Chem.*, **52**, 5447 (1987).
- R. W. Hoffman, U. Weldmann, *Chem. Ber.*, **118**, 3966 (1985).
- E. J. Corey, R. Imwinkelried, S. Pikul, Y. B. Xiang, *J. Am. Chem. Soc.*, **111**, 5493 (1989).
- E. J. Corey, C.-M. Yu, D.-H. Lee, *J. Am. Chem. Soc.*, **112**, 878 (1990).
- E. J. Corey, G. B. Jones, *Tetrahedron Lett.*, **32**, 5713 (1991).
- J. Li, W. Kong, C. Fu, S. Ma, *J. Org. Chem.*, **74**, 5104 (2009).
- J. Li, C. Zhou, C. Fu, S. Ma, *Tetrahedron*, **65**, 3695 (2009).

25. A. Alexakis, I. Marek, P. Mangeney, J. F. Normant, *Tetrahedron Lett.*, **30**, 2387 (1989).
26. A. Alexakis, I. Marek, P. Mangeney, J. F. Normant, *Tetrahedron*, **47**, 1677 (1991).
27. J. A. Marshall, K. G. Pinney, *J. Org. Chem.*, **58**, 7180 (1993).
28. N. Krause, A. Hoffmann-Röder, J. Canisius, *Synthesis*, **12**, 1759 (2002).
29. N. Krause, A. Hoffmann-Röder, *Tetrahedron*, **60**, 11671 (2004).
30. J. M. Aurrecochea, M. Solay, *Tetrahedron Lett.*, **36**, 2501 (1995).
31. J. M. Aurrecochea, E. Alonso, M. Solay, *Tetrahedron*, **54**, 3833 (1998).
32. J. S. Cowie, P. D. Landor, S. R. Landor, *J. Chem. Soc., Chem. Commun.*, 541 (1969).
33. J. S. Cowie, P. D. Landor, S. R. Landor, *J. Chem. Soc., Perkin Trans. 1*, 720 (1973).
34. M. Nakano, N. Furuichi, H. Mori, S. Katsumura, *Tetrahedron Lett.*, **42**, 7307 (2001).
35. C. Darcel, C. Bruneau, P. H. Dixneuf, *J. Chem. Soc., Chem. Commun.*, 1845 (1994).
36. C. Darcel, S. Bartsch, C. Bruneau, P. H. Dixneuf, *Synlett*, 457 (1994).
37. S. Hoff, L. Brandsma, J. F. Arens, *Rec. Trav. Chim. Pays-Bas*, **87**, 916 (1968).
38. S. Hoff, L. Brandsma, J. F. Arens, *Trav. Chim. Pays-Bas*, **87**, 1179 (1968).
39. S. Hormuth, H.-U. Reissig, *Synlett*, 179 (1991).
40. S. Hormuth, H.-U. Reissig, D. Dorsch, *Liebigs Ann. Chem.*, 121 (1994).
41. S. Hormuth, H.-U. Reissig, *J. Org. Chem.*, **59**, 67 (1994).
42. J. Marshall, Y. Tang, *J. Org. Chem.*, **58**, 3233 (1993).
43. V. Mark, The Uncatalyzed Rearrangements of Tervalent Phosphorus Esters, in: *Selective Organic Transformations*, B. S. Thyagarajan (Ed.), John Wiley & Sons, New York, 1970, pp. 319-437.
44. P. D. Landor, in: *The Chemistry of the Allenes*, Vol. 1, S. R. Landor (Ed.), Academic Press, New York, 1982, pp. 174-178.
45. R. W. Saalfrank, C.-J. Lurz, in: *Methoden der Organischen Chemie (Houben Weyl)*, H. Kropf, E. Scheumann (Eds.), Thieme, Stuttgart, 1993, pp. 2959-3102.
46. A. S. K. Hashmi, *Synthesis of Allenes*, in: *Modern Allene Chemistry*, Vol. 1, N. Krause, A. S. K. Hashmi (Eds.), Wiley-VCH, Weinheim, 2004, pp. 3-50.
47. R. S. Macomber, *J. Am. Chem. Soc.*, **99**, 3072 (1977).
48. S. E. Denmark, J. E. Marlin, *J. Org. Chem.*, **56**, 1003 (1991).
49. B. Cai, G. M. Blackburn, *Synth. Commun.*, **27**, 3943 (1997).
50. R. W. Saalfrank, M. Haubner, C. Deutscher, U. Bauer, *Eur. J. Org. Chem.*, 2367 (1999).
51. A. P. Boiselle, N. A. Meinhardt, *J. Org. Chem.*, **27**, 1828 (1962).
52. V. Mark, *Tetrahedron Lett.*, **3**, 281 (1962).
53. K. C. Nicolaou, P. Maligres, J. Shin, E. de Leon, D. Rideout, *J. Am. Chem. Soc.*, **112**, 7825 (1990).
54. M. L. Curfin, W. H. Okamura, *J. Org. Chem.*, **55**, 5278 (1990).
55. J. W. Grissom, D. Huang, *Angew. Chem. Int. Ed.*, **34**, 2037 (1995).
56. C. Darcel, C. Bruneau, P. H. Dixneuf, *Synthesis*, 711 (1996).
57. O. de Frutos, A. M. Echavarren, *Tetrahedron Lett.*, **38**, 7941 (1997).
58. M. Schmittel, J.-P. Steffen, M. Maywald, B. Engels, H. Helten, P. Musch, *J. Chem. Soc., Perkin Trans. 2*, 1331 (2001).
59. V. K. Brel, *Synthesis*, 463 (1999).
60. V. K. Brel, E. V. Abramkin, *Mendeleev Commun.*, **12**, 64 (2002).
61. B. W. Metcalf, C. L. Wright, J. P. Burkhart, J. O. Johnston, *J. Am. Chem. Soc.*, **103**, 3221 (1981).
62. M. Muller, A. Mann, M. Taddei, *Tetrahedron Lett.*, **34**, 3289 (1993).
63. V. K. Brel, P. J. Stang, *Eur. J. Org. Chem.*, 224 (2003).
64. V. K. Brel, *Synthesis*, 1539 (2001).
65. V. K. Brel, V. K. Belsky, A. I. Stash, V. E. Zvodnik, P. J. Stang, *Org. Biomol. Chem.*, **1**, 4220 (2003).
66. V. K. Brel, V. K. Belsky, A. I. Stash, V. E. Zvodnik, P. J. Stang, *Eur. J. Org. Chem.*, 512 (2005).
67. I. K. Ivanov, I. D. Parushev, V. C. Christov, *Heteroatom Chem.*, **24**, 322 (2013).
68. I. K. Ivanov, I. D. Parushev, V. C. Christov, *Heteroatom Chem.*, **25**, 60 (2014).
69. D. N. Robertson, *J. Org. Chem.*, **25**, 931 (1960).
70. M. Miyashita, A. Yoshikoshi, P. A. Griecolb, *J. Org. Chem.*, **42**, 3772 (1977).
71. M. C. Joshi, P. Joshi, D. S. Rawat, *ARKIVOC*, (xvi), 65 (2006).
72. B. Partha, I. Pimkov, *US Patent 8378123 B2* (2011).

**БИФУНКЦИОНАЛИЗИРАНИ АЛЕНИ. ЧАСТ XIV. УДОБЕН И ЕФИКАСЕН
РЕГИОСЕЛЕКТИВЕН СИНТЕЗ НА ФОСФОРИЛИРАНИ β -ХИДРОКСИАЛЕНИ СЪС
ЗАЩИТЕНА И НЕЗАЩИТЕНА ХИДРОКСИ ГРУПА**

И. Е. Исмаилов, И. К. Иванов, В. Х. Христов*

*Катедра по органична химия и технология, Факултет по природни науки, Шуменски университет „Епископ
Константин Преславски“, ул. Университетска 115, 9712 Шумен, България*

Постъпила на 09 май 2014 г.; Коригирана на 24 юни 2014 г.

(Резюме)

Описан е удобен и ефикасен региоселективен синтез на фосфорилирани β -хидроксиалени чрез атом-икономична [2,3]-сигматропна прегрупировка на междинно образуваните пропаргилови фосфити или фосфонити, които лесно се получават чрез реакция на защитения 5-метил-дец-6-ин-5-ол с диметил хлорофосфит или хлородифенил фосфин съответно в присъствие на база.

2,3-Disubstituted imidazo[1,2-a]pyridines from 2-aminopyridines and acetophenones. Catalyst's efficiency and solid state NMR study.

V. B. Kurteva*, L. A. Lubenov, S. D. Simova[†]

Institute of Organic Chemistry with Centre of Phytochemistry, Bulgarian Academy of Sciences, Acad. G. Bonchev str., bl. 9, 1113 Sofia, Bulgaria

Received June 16, 2014; Revised June 30, 2014

Dedicated to Acad. Dimiter Ivanov on the occasion of his 120th birth anniversary

Various sulfonic and carboxylic acids were tested as catalyst in a direct acid catalyzed conversion of 2-aminopyridines and acetophenones into 2,3-disubstituted imidazo[1,2-a]pyridines in order to improve the reaction yield. The most effective catalyst, isoquinoline-5-sulfonic acid, was applied in the reaction between substituted aminopyridines and acetophenones. The efficiency of the catalysts and their influence on the products distribution is discussed. Several chiral acids were also used but no stereoselectivity was induced. NMR study shows existence of two different species in the solid state, differentiation between them was not possible based on the available experimental and theoretical considerations.

Key words: imidazo[1,2-a]pyridines, 2-aryl-3-(1-arylethyl) substituted, 2-aryl-3-(1-arylethenyl) substituted, catalysts, solid state NMR

INTRODUCTION

Imidazo[1,2-a]pyridines are fused nitrogen-bridged heterocyclic compounds exhibiting a broad spectrum of biological activities [1-5]; antimicrobial, anti-inflammatory, antiviral, cytotoxicity, sedative, and many others. These properties are critically dependent on the presence and nature of substituents at positions 2 and 3 of the imidazole ring [6-8], which is demonstrated by the immense efficiency of some formulations on the market like zolpidem, necopidem, saripidem, alpidem, zolimidine, olprinone [9].

The observed pharmacological activities stimulated the development of numerous methods for the preparation of compounds possessing imidazo[1,2-a]pyridine scaffold [10-14]. 2,3-Disubstituted products are most commonly obtained by multicomponent reactions of 2-aminopyridines with aldehydes and alkynes, nitriles, isocyanides, thiocyanates [15-21], including catalytic variants. In the latter, Lewis acids like Zn(II) [22], Cu(II) [23,24], Cu(II)/Fe(III) [25], Fe(III) [26], In(III) [27] salts are found to be highly efficient catalysts. Contrary to aldehydes, ketones are poorly examined, mainly in direct reaction with 2-aminopyridine in a bromine

containing ionic liquid [28] or in iodine [29,30] or iodobenzene [31] catalysed conversions.

Recently, we reported on the direct acid catalyzed conversion of 2-aminopyridines and acetophenones into 2,3-disubstituted imidazo[1,2-a]pyridines [32,33]. Two products were obtained as easy separable mixtures, 2-aryl-3-(1-arylethyl) and 2-aryl-3-(1-arylethenyl)imidazo[1,2-a]pyridines. However, the reaction was not complete; the products were isolated in moderate to high total yields. The aim of the current work is to improve the conversion by finding out more efficient catalysts. Additionally, since the main product is obtained as a racemic mixture, attempts to conduct the reaction stereoselectively have been undertaken. Moreover, solid state NMR spectra of racemic 2-phenyl-3-(1-phenylethyl)imidazo[1,2-a]pyridine reveal two different forms, pointing out to a possible alternative explicit method for enantiomeric purity estimation.

EXPERIMENTAL

Materials, Methods and Apparatus

All reagents were purchased from Aldrich, Merck and Fluka and were used without any further purification. Merck Silica gel 60 (0.040-0.063 mm) was used for flash chromatography purification of the products. The high performance liquid chroma-

* To whom all correspondence should be sent:

E-mail: vkurteva@orgchm.bas.bg

[†] For NMR study:

E-mail: sds@orgchm.bas.bg

tography (HPLC) enantioseparations were performed on an Agilent 1100 System fitted with diode array detector and manual injector with a 20 μ l injection loop. A stainless-steel Nucleosil Chiral-2 column (Macherey-Nagel GmbH & Co. KG, Düren, Germany) was used; 250x4 mm, particle size 5 μ m, pore size 100 Å, chiral selector *N*-(3,5-dinitro-benzoyl)-*D*-phenylglycine. The HPLC grade solvents were purchased from Sigma-Aldrich and LabScan.

Synthetic Procedure

All reactions were carried out in constant conditions by following a published protocol [32,33]. Shortly, a mixture of 2-aminopyridine (1 mmol), acetophenone (5 mmol), and catalyst (10 mol %) was refluxed for 1 h; acetophenone 202°C, 4-methylacetophenone 226°C, 4-chloroacetophenone 232°C. The products were purified by flash chromatography on silica gel by using mobile phase with a gradient of polarity from CH₂Cl₂ to acetone:CH₂Cl₂ 5:95. The results are summarized on Tables 1 and 2. The characterization of the compounds is published in ref. 32 and 33.

HPLC Analyses

Resolution of **3a** enantiomers by HPLC was performed at 25°C by using hexane/*i*-PrOH 80:20 as eluent: the flow rate was varied and similar separations were achieved: flow rate 0.7 ml/min, retention times: t_{R-1} 12.18 min, t_{R-2} 12.84 min; flow rate 1 ml/min, retention times: t_{R-1} 10.75 min, t_{R-2} 11.38 min.

NMR Spectra

The NMR spectra were recorded on a Bruker Avance II+ SB 600 spectrometer (Rheinstetten, Germany) at room temperature using standard Bruker library pulse programs [34]. ¹³C and ¹⁵N NMR spectra were recorded at 150.91 and 60.81 MHz. The liquid state ¹⁵N chemical shifts were extracted from the heteronuclear multiple bond (long range) correlation and quoted as δ -values in ppm using the unified Ξ scale [35]. For the spectra in solid state α -glycine (43.5 ppm for ¹³C and 33.4 ppm for ¹⁵N) has been employed as external reference [36].

Solid state ¹³C and ¹⁵N NMR spectra were recorded on a 4 mm double resonance CPMAS probehead. The sample was ground softly with a mortar and pestle and then packed tightly in a 4-mm zirconium oxide rotor. The magic angle was adjusted using the ⁷⁹Br resonance of KBr. Samples were spun at 6.0 kHz for all experiments. Typical radio-frequency (RF) field strengths were 30-65 kHz for

¹³C and ¹⁵N. The Hartmann–Hahn polarization transfer was optimized to a contact time of 2 ms for ¹³C and 4 ms for ¹⁵N with a linear ramp starting at 50%. ¹³C NMR spectra were obtained using a combination of CP/MAS and total sideband suppression (TOSS) methods (CP/MAS/TOSS) with SPINAL64 proton decoupling. Non Quaternary Suppression (NQS) technique was applied to distinguish unambiguously the quaternary carbons. 128 transients for ¹³C and 3072 for ¹⁵N were accumulated with a 5 s relaxation delay.

Computational Method

Calculations were done on Spartan 08 program package v. 1.2.0 [37]. The structures were first optimized using the MMFF94 field. The geometry optimization was performed with DFT calculations using B3LYP/6-31G(d) basis set. Energies and NMR chemical shifts were calculated from the DFT derived structures, using the SM8 routine for solvation with chloroform [38]. ¹³C NMR chemical shifts are corrected from an empirical relationship in Spartan for the effects of local chemical environment. Referencing to TMS (0 ppm) and CH₃NO₂ (381.7) is done internally in the Spartan package.

RESULTS AND DISCUSSION

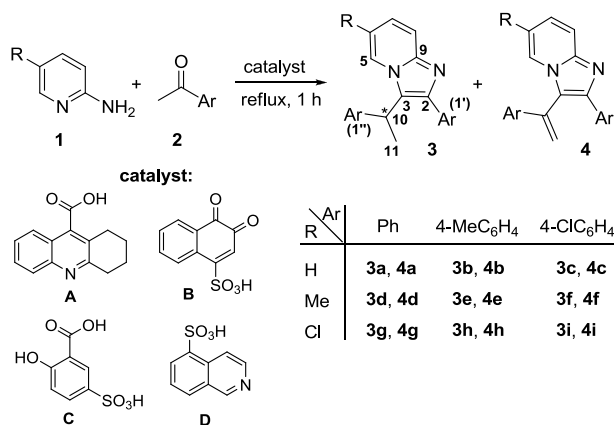
Catalyst's efficiency

In our previous study [32,33], we achieved a direct acid catalyzed conversion of 2-aminopyridines and acetophenones into an easy separable mixtures of 2-aryl-3-(1-arylethyl) (**3**) and 2-aryl-3-(1-arylethenyl)imidazo[1,2-a]pyridines (**4**), shown on Scheme 1. It was found that acetic and trifluoroacetic acid did not catalyze the transformation significantly, while *p*-toluenesulfonic and sulfuric acid led to considerable conversion of 2-aminopyridines. The products were isolated in 42-91% total yields depending on the 2-aminopyridine and acetophenone substituents [33].

A possible way to improve the reaction yield is to find more effective catalysts. Various acids were checked, which can be divided in two general groups: sulfonic acids and carboxylic acids. Their efficiency was first studied on a model reaction, the formation of imidazopyridines **3a** and **4a** by refluxing (202°C) a mixture of 2-aminopyridine and 5-fold excess acetophenone in solventless conditions for 1 h in the presence of 10 mol % catalyst.

As expected, sulfonic acids led to better conversions than carboxylic. Among the latter, the aromatic acids 1-naphthoic acid, 5-methylthiophe-

ne-3-carboxylic acid, and pyridine-3-carboxylic acid catalyzed poorly the transformation, 5-12% total yields, while aliphatic mono- and polycarboxylic acids were not efficient in general. The best conversion was achieved with 1,2,3,4-tetrahydro-9-acridinecarboxylic acid (**A**, Scheme 1, Table 1). Contrary, the sulfonic acids tested, 3,4-dioxo-3,4-dihydronaphthalene-1-sulfonic acid (**B**), 2-hydroxy-5-sulfobenzoic acid (**C**), and isoquinoline-5-sulfonic acid (**D**), showed moderate to excellent efficiency. As seen on Table 1, the polyfunctionalized catalyst **C** showed commensurable efficacy with *p*-toluenesulfonic acid, while isoquinoline sulfonic acid **D** led to almost complete conversion with significant superior of 2-aryl-3-(1-arylethyl) substituted product **3a**.



Scheme 1. Synthesis of imidazo[1,2-a]pyridines **3** and **4**.

Table 1. Formation of imidazo[1,2-a]pyridines **3a** and **4a** in the presence of various catalysts.

Entry	Catalyst	Reaction yield, %*			3a:4a ratio
		Total	3a	4a	
1	<i>p</i> -TSA [33]	76	72	4	95:5
2	H ₂ SO ₄ [33]	61	50	11	82:18
3	A	34	33	1	97:3
4	B	54	47	7	87:13
5	C	77	73	4	95:5
6	D	94	86	8	92:8

*Isolated yields by flash chromatography.

The most effective catalyst, isoquinoline-5-sulfonic acid **D**, was further applied in the formation of imidazopyridines **3b-3i** and **4b-4i**. The results are summarized on Table 2. As seen, significant improvement of the reaction yield was achieved in all cases compared to *p*-TSA and sulfuric acid [33]. This effect is most clearly demonstrated on the example of **3c/4c** mixture formation (Entry 3), where the products were isolated in 99% total yield when catalyst **D** was used, while *p*-TSA and sulfuric acid led only to

83% and 81% yield, respectively. Similarly to the previous results, the lowest yields were obtained from 5-chloro-2-aminopyridine and 4-methylacetophenone; 71% with **D** (Entry 8), 66% with *p*-TSA and 68% with H₂SO₄.

Table 2. Formation of imidazo[1,2-a]pyridines **3** and **4** in the presence of catalyst **D**.

Entry	Total yield*	Compound 3		Compound 4		3:4 ratio
		Prod	Yield	Prod	Yield	
1	94	3a	86	4a	8	92:8
2	96	3b	80	4b	16	82:18
3	99	3c	87	4c	12	87:13
4	93	3d	83	4d	10	89:11
5	96	3e	80	4e	16	83:17
6	92	3f	79	4f	13	86:14
7	94	3g	71	4g	23	76:24
8	71	3h	41	4h	30	58:42
9	87	3i	65	4i	22	75:25

*Isolated yields by flash chromatography.

From the other side, isoquinoline sulfonic acid **D** accelerated the Ortoleva-King type intermediated transformation better than *p*-toluenesulfonic acid [33], i.e. more like sulfuric acid in terms of **3:4** ratio. The latter was most significant when 4-methylacetophenone was used. The reaction output was similar from 2-aminopyridine and 5-methyl-2-aminopyridine, 94% of 82:18 **3a:4a** and 96% of 83:17 **3e:4e** catalyzed by **D** vs 76% of 95:5 **3a:4a** and 86% of 90:10 **3e:4e** catalyzed by *p*-TSA vs 61% of 82:18 **3a:4a** and 80% of 86:14 **3e:4e** catalyzed by sulfuric acid, while lower yields with significant percentage of vinylated product were observed from 5-chloro-2-aminopyridine, 71% of 58:42 **3h:4h** with **D** vs 66% of 70:30 **3h:4h** with *p*-TSA vs 68% of 62:38 **3h:4h** with H₂SO₄.

Enantioseparation

The main reaction products, 2-aryl-3-(1-arylethyl)imidazo[1,2-a]pyridines (**3**), are racemic compounds due to the presence of a chiral center in the substituent at position 3. We were interested to achieve the transformation enantioselectively despite the relative low prospects because the chiral center is not sufficiently close to any nitrogen. Several chiral acids were examined in the formation of **3a**. The carboxylic acids (L)-mandelic, (L)-malic, N-Z-(D)-norleucine, N-Boc-(L)-glutamic acid 5-benzyl ester, O,O'-dibenzoyl-(L)-tartaric acid led to insignificant conversion (up to 17%), while **3a/4a** were obtained in 85% total yield in 94:6 ratio with (+)-camphor-10-sulfonic acid. Surprisingly, (R)-1,1'-binaphthyl-2,2'-diyl hydrogen phosphate efficiently catalyzed the reaction; the products were isolated in 89% total yield in 96:4 ratio.

The products were analyzed by HPLC on chiral stationary phase. Sufficient separation of the enantiomers was achieved, as illustrated on Fig. 1, but no enantioselectivity was induced with all acids tested. All attempts to separate the enantiomers by salts formation were also unsuccessful.

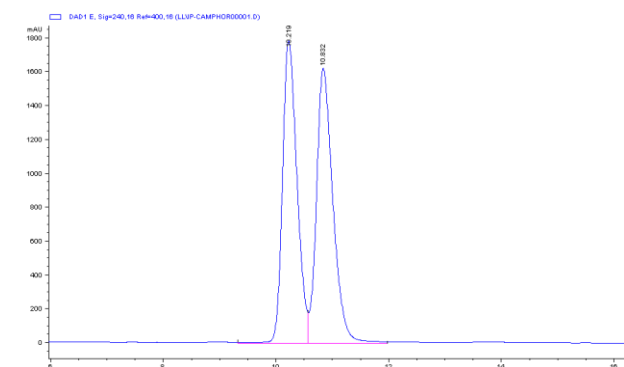


Fig. 1. Resolution of **3a** enantiomers by HPLC; eluent: hexane/*i*-PrOH 80:20; flow rate 1 ml/min; retention times: t_{R-1} 10.22 min, t_{R-2} 10.83 min.

Solid State NMR Study

Contrary to the liquid state spectra ^{15}N solid state NMR experiments of 2-phenyl-3-(1-phenylethyl)imidazo[1,2-a]pyridine (**3a**) reveal doubling of the signals for both nitrogen atoms, indicating the presence of two species with different structure (Fig. 2).

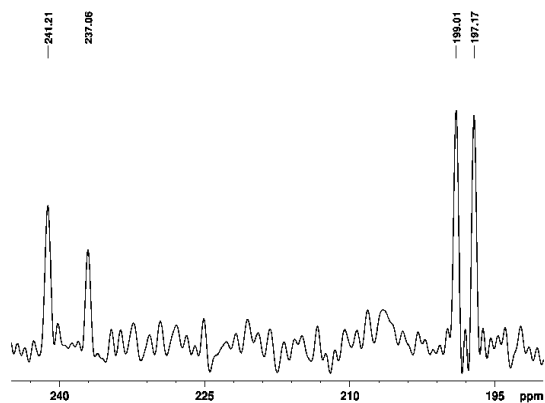


Fig. 2. ^{15}N CPMAS spectrum of **3a**.

^{13}C CPMAS spectra for **3a** are also compatible with two different species since most of the carbon atoms are doubled as revealed in Fig. 3. Using the unambiguous assignment of the liquid state spectra [32] and the technique of nonquaternary atom suppression the quaternary atoms could be unambiguously recognized, along with some rest signals for the methyl groups. The small difference

between the experimental NMR chemical shifts of the two species precludes differentiation of the two species.

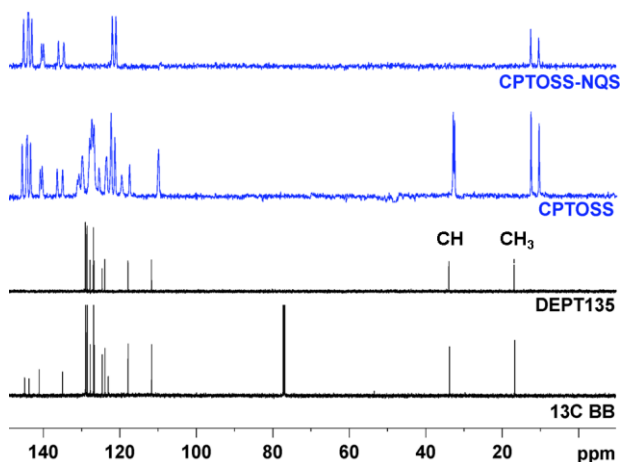


Fig. 3. Comparison of liquid state (^{13}C BB and DEPT135) with ^{13}C CPMAS (CPTOSS and CPTOSS-NQS) spectra of **3a**.

Two main alternatives are possible: polymorphic structures or different chemical shifts for two enantiomers in the solid state. Two conformational isomers in the solid state could also not be excluded. The energy difference between the major and minor isomers of **3a** in chloroform amounts only 2.4 kcal/mol (Fig. 4), making the minor isomer also a possible alternative for the solid state. The major conformer corresponds to the atom arrangement in the solid X-ray structure [32]. Theoretical NMR chemical shifts were calculated for both isomers.

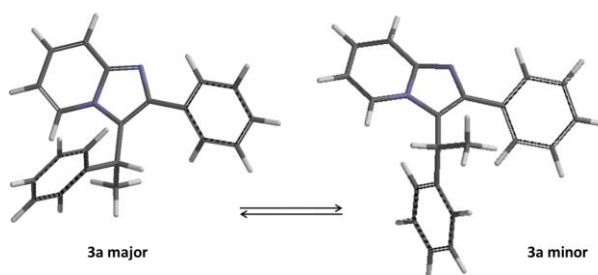
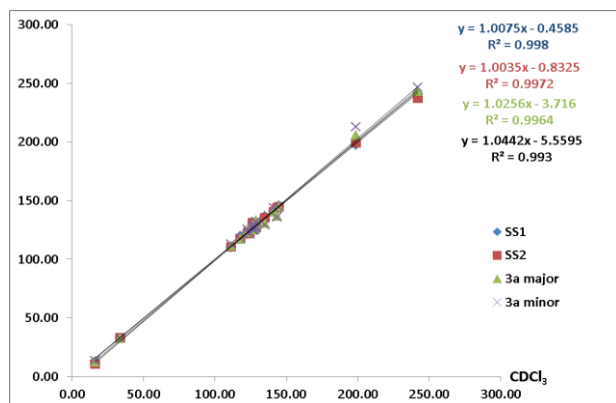


Fig. 4. Theoretical structures of the major and minor conformers of **3a**.

Table 3 and Fig. 5 reveal the close resemblance of the experimentally determined in the liquid and the solid state and the theoretically predicted NMR chemical shifts. This precludes unambiguous determination of the differences between the two species in the solids state based on the so far available data. Further experiments are in progress.

Table 3. Experimentally determined ^{13}C and ^{15}N NMR chemical shifts in CDCl_3 and the two solid state forms (SS1 and SS2), along with theoretically calculated values.

No.	Experimental			Theoretical	
	CDCl_3	SS1	SS2	3a major	3a minor
1	-	241.20	237.06	243.14	246.62
2	143.76	144.50	143.67	136.91	136.02
3	122.96	122.61	121.63	124.98	125.31
4	198.66	197.17	199.01	205.74	212.99
5	124.53	125.72	122.61	125.42	121.53
6	111.56	110.15	110.35	111.43	112.80
7	123.74	123.99	123.75	122.54	122.51
8	117.78	119.81	117.76	117.21	117.59
9	144.86	145.85	144.70	144.78	144.33
10	33.78	32.77	33.14	32.42	32.72
11	16.17	12.78	10.68	12.40	13.51
1'	135.02	136.69	135.27	130.49	129.30
2'	128.92	130.18	130.18	133.20	132.13
6'	128.92	129.87	128.18	129.15	131.53
3'	128.42	127.61	127.08	127.67	126.70
5'	128.42	127.61	127.08	127.08	126.70
4'	127.68	131.37	130.95	125.39	125.22
1''	141.11	141.10	140.61	141.23	144.00
2''	126.80	130.18	130.18	129.43	128.07
6''	126.80	129.87	128.18	124.88	124.58
3''	128.81	127.61	127.08	128.14	127.98
5''	128.81	127.61	127.08	127.26	127.85
4''	126.61	131.37	130.95	125.07	127.97

**Fig. 5.** Comparison of experimental data in CDCl_3 with experimental solid state ^{13}C NMR shifts and theoretically predicted shifts for the two possible conformers of **3a**.

CONCLUSION

The catalytic efficiency of various sulfonic and carboxylic acids in the direct acid catalyzed conversion of 2-aminopyridines and acetophenones into 2,3-disubstituted imidazo[1,2-a]pyridines was

tested aiming to improve the reaction yields. It was observed that the carboxylic acids tested catalyzed the transformation insignificantly, while the sulfonic acids led to moderate to excellent yields. It was found that isoquinoline-5-sulfonic acid was the most efficient catalyst, up to 99% total yield. The latter was applied in the reaction between substituted aminopyridines and acetophenones. Significant improvement of the reaction yield was achieved in all cases compared to *p*-TSA and sulfuric acid [33] but the ratios 2-aryl-3-(1-arylethyl) to 2-aryl-3-(1-arylethenyl)imidazo[1,2-a]pyridines were more similar to that obtained with sulfuric acid, i.e. isoquinoline-5-sulfonic acid accelerated the Ortoleva-King type intermediated transformation better than *p*-toluenesulfonic acid. Several chiral acids were also examined but no enantioselectivity was induced. It was found that (*R*)-1,1'-binaphthyl-2,2'-diyl hydrogen phosphate was a very effective catalyst in the transformation studied. Comparison of experimental and theoretically predicted NMR chemical shifts does not allow assignment of the two observed species in the solid state.

Acknowledgements: The financial support by The Bulgarian Science Fund, projects UNA-17/2005 and DRNF-02-13/2009, is gratefully acknowledged.

REFERENCES

1. J. A. Joule, K. Mills, *Heterocyclic Chemistry*, 4th Edition, Blackwell Publishing, Oxford, 2000, Chapter 25, p. 489.
2. H. T. Swainston, G. M. Keating, *CNS Drugs*, **19**, 65 (2005).
3. C. Enguehard-Gueiffier, A. Gueiffier, *Mini-Rev. Med. Chem.*, **7**, 888 (2007).
4. D. Damour, C. Nemecek, P. Nemecek, S. Wentzler, PCT Int. Appl. WO 2010007317, pp. 88 (2010).
5. J. A. Joule, K. Mills, *Heterocyclic Chemistry*, 5th Edition, John Wiley & Sons Ltd, UK, 2010, Chapter 28, p. 539.
6. P. A. Bonnet, A. Michel, F. Laurent, C. Sablayrolles, E. Rechencq, J. C. Mani, M. Boucard, J. P. Chapat, *J. Med. Chem.*, **35**, 3353 (1992).
7. C. Hamdouchi, J. de Blas, M. del Prado, J. Gruber, B. A. Heinz, L. Vance, *J. Med. Chem.*, **42**, 50 (1999).
8. W. M. El-Sayed, W. A. Hussin, Y. S. Al-Faiyz, M. A. Ismail, *Eur. J. Pharmacol.*, **715**, 212 (2013).
9. M. Baumann, I. R. Baxendale, S. V. Ley, N. Nikbin, *Beilstein J. Org. Chem.*, **7**, 442 (2011).
10. W. L. Mosby, *Chem. Heterocycl. Compd.*, **15**, 460 (1961).

11. K. Undheim, in: *Comprehensive Heterocyclic Chemistry I*, A. R. Katritzky, C. W. Rees (Eds.), vol. 6, Pergamon, Oxford, 1984, p. 613.
12. A. S. Howard, in: *Comprehensive Heterocyclic Chemistry II*, A. R. Katritzky, C. W. Rees (Eds.), vol. 8, Pergamon, Oxford, 1996, p. 249.
13. C. Hulme, Y.-S. Lee, *Mol. Divers.*, **12**, 1 (2008).
14. F. Couty, G. Evano, in: *Comprehensive Heterocyclic Chemistry III*, A. R. Katritzky, C. W. Ramsden, E. F. V. Scriven, R. J. K. Taylor (Eds.), vol. 11, chapter 10, Elsevier Ltd., 2008, p. 409.
15. H. Bienayme, K. Bouzid, *Angew. Chem. Int. Ed.*, **37**, 2234 (1998).
16. R. Akbarzadeh, G. Imani Shakibaei, A. Bazgir, *Monatsh. Chem.*, **141**, 1077 (2010).
17. E. Kianmehr, M. Ghanbari, M. Nadiri Niri, R. Faramarzi, *J. Comb. Chem.*, **12**, 41 (2010).
18. P. Liu, L.-s. Fang, X. Lei, G.-q. Lin, *Tetrahedron Lett.*, **51**, 4605 (2010).
19. M. Adib, E. Sheikhi, N. Rezaei, *Tetrahedron Lett.*, **52**, 3191 (2011).
20. S. Mishra, R. Ghosh, *Synthesis*, 3463 (2011).
21. I. R. Siddiqui, P. Rai, Rahila, A. Srivastava, S. Shamim, *Tetrahedron Lett.*, **55**, 1159 (2014).
22. A. L. Rousseau, P. Matlaba, C. J. Parkinson, *Tetrahedron Lett.*, **48**, 4079 (2007).
23. N. Chernyak, V. Gevorgyan, *Angew. Chem. Int. Ed.*, **49**, 2743 (2010).
24. H. Huang, X. Ji, X. Tang, M. Zhang, X. Li, H. Jiang, *Org. Lett.*, **15**, 6254 (2013).
25. J. Zeng, Y. J. Tan, M. L. Leow, X.-W. Liu, *Org. Lett.*, **14**, 4386 (2012).
26. A. Maleki, *Helv. Chim. Acta*, **97**, 587 (2014).
27. B. V. Subba Reddy, P. Sivaramakrishna Reddy, Y. Jayasudhan Reddy, J. S. Yadav, *Tetrahedron Lett.*, **52**, 5789 (2011).
28. Z.-G. Le, Z.-B. Xie, J.-P. Xu, *Molecules*, **17**, 13368 (2012).
29. A. J. Stasyuk, M. Banasiewicz, M. K. Cyrański, D. T. Gryko, *J. Org. Chem.*, **77**, 5552 (2012).
30. Z. Fei, Y.-p. Zhu, M.-c. Liu, F.-c. Jia, A.-x. Wu, *Tetrahedron Lett.*, **54**, 1222 (2013).
31. Y.-L. Chang, H.-M. Wang, R.-S. Hou, I.-J. Kang, L.-C. Chen, *J. Chinese Chem. Soc.*, **57**, 153 (2010).
32. V. B. Kurteva, L. A. Lubenov, D. V. Nedeltcheva, R. P. Nikolova, B. L. Shivachev, *Arkivoc*, **viii**, 282 (2012).
33. V. B. Kurteva, L. A. Lubenov, D. V. Antonova, *RSC Adv.*, **4**, 175 (2014).
34. Topspin 3.2 pl 5, Solid State NMR, AVANCE Solids User Manual.
35. R. K. Harris, E. D. Becker, S. M. Cabral de Menezes, P. Granger, R. E. Hoffman, K. W. Zilm, *Pure Appl. Chem.*, **80**, 59 (2008).
36. P. Bertani, J. Raya, B. Bechinger, *Solid State Nucl. Magn. Reson.*, 2014, accepted.
37. www.wavefun.com.
38. A. V. Marenich, R. M. Olson, C. P. Kelly, C. J. Cramer, D. G. Truhlar, *J. Chem. Theory Comput.*, **3**, 2011 (2007).

2,3-ДИЗАМЕСТЕНИ ИМИДАЗО[1,2-a]ПИРИДИНИ ОТ 2-АМИНОПИРИДИНИ И АЦЕТОФЕНОНИ. ЕФЕКТИВНИ КАТАЛИЗАТОРИ И ЯМР ИЗСЛЕДВАНЕ В ТВЪРДО СЪСТОЯНИЕ.

В. Б. Куртева*, Л. А. Любенов, С. Д. Симова[†]

Институт по Органична Химия с Център по Фитохимия, Българска Академия на Науките, ул. Акад. Г. Бончев, бл. 9, 1113 София, България

Постъпила на 16 юни 2014 г.; Коригирана на 30 юни 2014 г.

(Резюме)

Проверена е ефективността на редица сулфо и карбоксилни киселини като катализатори в директно кисело катализирано превръщане на 2-аминопиридини и ацетофенони в 2,3-дизаместени имидазо[1,2-a]пиридини с цел подобряване на реакционните добиви. Най-ефективният катализатор е използван и при реакция между заместени аминопиридини и ацетофенони. Дискутирани са ефективността на катализаторите и влиянието им върху разпределението на продуктите. Изследвани са и хирални киселини, но стереоселективност не е индуцирана. ЯМР спектрите показват наличие на две форми в твърдо състояние, чието надеждно отнасяне не е възможно с наличните експериментални и теоретични данни.

One-pot synthesis of a chromeno[4,3,2-*de*]-1,6-naphthyridine derivative from 4-chlorocoumarin-3-carbaldehyde

V. T. Angelova¹, W. Frey², I. C. Ivanov^{1*}, N. Vassilev³, T. N. Glasnov⁴

¹Faculty of Pharmacy, Medical University of Sofia, 2 Dunav str., 1000 Sofia, Bulgaria

²Institut für Organische Chemie, Universität Stuttgart, Pfaffenwaldring 55, D-70569 Stuttgart, Germany

³Institute of Organic Chemistry with Centre of Phytochemistry, Bulgarian Academy of Sciences, Acad. G. Bonchev str., bl. 9, 1113 Sofia, Bulgaria

⁴Christian Doppler Laboratory for Flow Chemistry and Institute of Chemistry, Karl-Franzens-University Graz, Heinrichstrasse 28, A-8010 Graz, Austria

Received April 24, 2014; Revised July 16, 2014

Dedicated to Acad. Dimiter Ivanov on the occasion of his 120th birth anniversary

In the reaction of 4-chlorocoumarin-3-carbaldehyde with malononitrile in the presence of piperidine a crystalline piperidinium salt of a novel tetracyclic chromeno[4,3,2-*de*]-1,6-naphthyridine-2-carboxylic acid was isolated instead of the expected product of the “*tert*-amino effect”. The structure of this piperidinium salt and its corresponding acidic form was characterized through spectral methods (IR, NMR, MS) and elemental analysis. In addition, the structure was established by means of X-ray crystallographic analysis. A theoretical multistep mechanism for this one-pot synthesis is discussed.

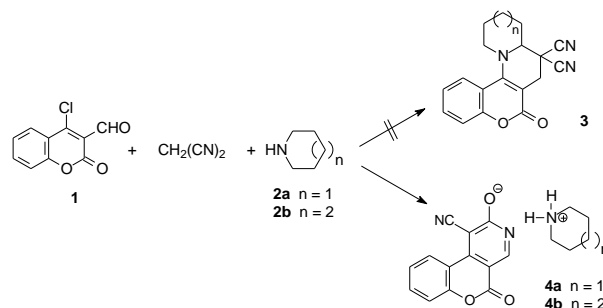
Key words: 4-chlorocoumarin-3-carbaldehyde, chromeno[4,3,2-*de*]-1,6-naphthyridine, X-ray crystallographic analysis, malononitrile

INTRODUCTION

In a previous paper we described some new examples of the so-called “*tert*-amino effect” reaction [1] starting from 4-chlorocoumarin-3-carbaldehyde and ethyl cyanoacetate as a CH-acid in the presence of piperidine. This reaction occurred *via* intermediate Knoevenagel condensation with the formyl group and led to the formation of 1,2 fused 5*H*-chromeno[4,3-*b*]pyridin-5-ones of type **3** (Scheme 1). We found that under the same reaction conditions but employing malononitrile in place of ethyl cyanoacetate [2] the corresponding aminium salts of 2-hydroxy-5-oxo-5*H*-chromeno [3,4-*c*]pyridine-1-carbonitrile (**4a,b**) could be obtained. In continuation of our interest in the development of new and simple methods for the synthesis of poly-functionally substituted heterocycles with anticipated biological activity [3] we now wish to report the use of 4-chlorocoumarin-3-carbaldehyde (**1**) for the one-pot synthesis of a new chromeno[4,3,2-*de*]-1,6-naphthyridine (**5a,b** -Scheme 2).

Many known methods for the preparation of 5*H*-chromeno[4,3-*b*]pyridine or 5*H*-chromeno[3,4-*c*]pyridine derivatives involve coumarin derivatives as starting compounds or intermediates, e. g. [4-6].

Further detailed information on the synthesis and application of various 3,4-fused chromenopyridines is summarized in two review articles [3,7] and a recent paper [8]. We have also developed some synthetic procedures leading to the formation of substituted 5*H*-chromeno[4,3-*b*]pyridines *via* Knoevenagel condensation [9], *via* Wittig reaction followed by Vilsmeier conditions [10], or even *via* the Erlenmeyer-Ploechl reaction [11], all of them starting from coumarin-3-carbaldehydes. The preparation of some novel 5*H*-chromeno[3,4-*c*]pyridines was also reported by us [12,13].

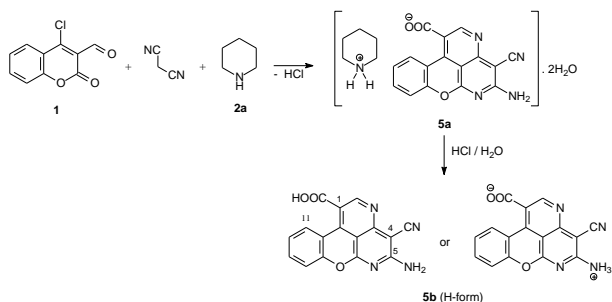


Scheme 1. Reaction of 4-chlorocoumarin-3-carbaldehyde (**1**) with malononitrile, *cf.* [1,2].

The synthesis of some [1]benzopyrano[4,3-*b*]pyrrol-4(1*H*)-ones from 4-chlorocoumarin-3-carb-

* To whom all correspondence should be sent:
E-mail: ivanov43@gmail.com

aldehyde (**1**) has also been described [14]. An efficient preparation of novel chromeno-2,6,9-trioxabicyclo-[3.3.1]nonadiene scaffolds was performed by mild base mediated reaction of 4-chloro-3-formylcoumarin (**1**) and *o*-hydroxy-acetophenones [15]. The synthesis of some novel chromeno [4,3-*b*]pyridine-2,5-diones with antimicrobial activity was reported recently, starting from 4-chloro-3-formylcoumarin (**1**) and acetoacetamides in polyethylene glycol as a recoverable solvent [16].



Scheme 2. Synthesis of 5-amino-4-cyanochromeno[4,3,2-*de*]-1,6-naphthyridine-1-carboxylic acid (**5**) – as piperidinium salt (**5a**) and the acidic form (**5b**).

EXPERIMENTAL

General Remarks

The FTIR spectra were recorded on a Nicolet iS10 FT-IR Spectrometer from Thermo Scientific (USA) using ATR technique. The NMR experiments on Bruker Avance II+ 600 MHz NMR spectrometer in DMSO-*d*₆ allow the assignment of the structures. The precise assignment of the ¹H and ¹³C NMR spectra (resolved signals) was accomplished by measurement of 2D homonuclear correlation (COSY), DEPT-135 and 2D inverse detected heteronuclear (C–H) correlations (HMOC and HMBC). LC-MS: Shimadzu LC-MS 2020 (ESI detector) equipped with a C18 reversed-phase analytical column at 37°C using a mobile phase H₂O-MeCN [90:10 (v/v)] + 0.1% HCOOH. Elemental analyses were performed by the Microanalytical Laboratory, Institute of Chemistry, University of Vienna, Austria. TLC: silica gel 60 GF₂₅₄ Merck pre-coated aluminum sheets, eluted by hexane-chloroform-acetone 5:3:2 (vol. parts); the spots were visualized under UV irradiation ($\lambda = 254$ nm) and/or by treatment with I₂ (vapor).

Piperidinium 5-amino-4-cyano-chromeno[4,3,2-*de*]-1,6-naphthyridine-1-carboxylate dihydrate (**5a**)

Drawn on Scheme 2. To a solution of 1.04 g (5.0 mmol) of 4-chlorocoumarin-3-carbaldehyde (**1**)

(prepared according to lit. [10,17]) and 0.66 g (10 mmol) of malononitrile in 20 ml of anhydr. ethanol, 1.08 ml (0.93 g; 10.9 mmol) of piperidine (**2a**) was added dropwise for 5 min under vigorous stirring at 20–25°C. The reaction mixture turned into a red solution and after stirring for additional 15 min orange-yellow crystals of compound **4a** separated. This product was reported elsewhere [2]. The separated crystals were filtered, recrystallized from ethanol (2 × 10 ml) and air-dried to yield 0.45 g (28%) of **4a** with m.p. 255–256°C.

After a 12 h stay at room temperature a yellow solid crystallized from the ethanolic filtrate. It was filtered, washed with cold ethanol (2 × 10 ml) and air-dried to yield 0.89 g (41%) of crystalline, TLC homogeneous product **5a**. A small sample for X-ray analysis was additionally recrystallized from ethanol to give yellow crystals of **5a** with m.p. 206.5–207.3°C, insoluble in chloroform. FTIR (ATR): ν (cm⁻¹) = 3460 (OH/NH_{assoc.}), 3056 (Ar-H), 3200–2400 (NH_{assoc.}), 2210, 2168, 2144 (CN), 1733 (w) (C=O), 1591, 1557, 1514, 1491, 1444, 1258, etc. ¹H NMR (600 MHz, DMSO-*d*₆): δ (ppm) = 1.62–1.56 (m, 2H, 4'-H), 1.61–1.65 (m, 4H, 3'-H and 5'-H), 3.00–3.02 (m, 4H, 2'-H and 6'-H), 7.42 (dd, $J^3 = 8.3$ Hz, $J^4 = 1.2$ Hz, 1H, 8-H), 7.45 (ddd, $J^4 = 1.2$ Hz, $J^3 = 7.2$ Hz, $J^3 = 8.3$ Hz, 1H, 10-H), 7.70 (ddd, $J^4 = 1.3$ Hz, $J^3 = 7.2$ Hz, $J^3 = 8.3$ Hz, 1H, 9-H), 8.22 (bs, 2H, NH), 8.84 (s, 1H, 2-H), 8.98 (dd, $J^3 = 8.3$ Hz, $J^4 = 1.3$ Hz, 1H, 11-H). ¹³C NMR (150 MHz, DMSO-*d*₆): δ (ppm) = 21.6 (C-4'), 22.3 (C-3' and C-5'), 43.8 (C-2' and C-6'), 83.1 (C-4), 106.0 (C-11c), 115.4 (C-11a), 117.5 (CN), 118.0 (C-8), 119.1 (C-1), 120.5 (C-11b), 124.5 (C-10), 125.3 (C-11), 133.6 (C-9), 144.0 (C-7a), 152.7 (C-6a), 154.1 (C-2), 158.6 (C-3a), 166.3 (C=O). Calcd. for C₂₁H₁₉N₅O₃ (389.41) (water loss on drying): C 64.77, H 4.92, N 17.98; found C 64.70, H 4.49, N 17.80.

5-Amino-4-cyanochromeno[4,3,2-*de*]-1,6-naphthyridine-1-carboxylic acid (**5b**)

Drawn on Scheme 2. After acidification of the aqueous solution of **2b** (0.15 g in 50 ml of water) with HCl (to pH ≈ 2) compound **5b** was isolated as yellow powder with m.p. 313°C (dec.), insoluble in chloroform. FTIR (ATR): ν (cm⁻¹) = 3489 and 3415 (NH₂), 3086 (Ar-H), 2210, 2190 (CN), 1714 (s, C=O), 1589 (s), 1570 (m), 1444, 1423 (w), 1261 (s), 1207 (m), etc. H-Form: ¹H NMR (600 MHz, DMSO-*d*₆): δ (ppm) = 7.42 (dd, $J^3 = 8.3$ Hz, $J^4 = 1.2$ Hz, 1H, 8-H), 7.45 (ddd, $J^3 = 7.2$ Hz, $J^3 = 8.3$ Hz, $J^4 = 1.2$ Hz, 1H, 10-H), 7.70 (ddd, $J^3 = 7.2$ Hz, $J^3 = 8.3$ Hz, $J^4 = 1.3$ Hz, 1H, 9-H), 8.84 (s, 1H, 2-

H), 8.97 (dd, $J^3 = 8.3$ Hz, $J^4 = 1.3$ Hz, 1H, 11-H). 8.97 (dd, Hz, 1H, 8-H), 8.84 (s, 1H, 2-H), 7.70 (m_c, 1H, 9-H), 7.41-7.46 (m, 2H, 10-H and 11-H). ¹³C NMR (150.9 MHz, DMSO-*d*₆): δ (ppm) = 83.2 (C-4), 106.0 (C-11c), 115.4 (C-11a), 117.5 (CN), 118.0 (CH_{arom.}, C-8), 119.1 (C-1), 120.5 (C-11b), 124.5 (CH_{arom.}, C-10), 125.4 (CH_{arom.}, C-11), 133.6 (CH_{arom.}, C-9), 144.1 (C-7a), 152.7 (C-6a), 154.0 (CH_{arom.}, C-2), 158.6 (C-3a), 166.1 (C=O). C₁₆H₈N₄O₃ (304.26). LC-MS (ESI, pos. mode): m/z = 425 [M-CO₂ + 4MeCN + H]⁺, 343 [M-CO₂ + 2MeCN + H]⁺, 327 [M + Na]⁺.

Crystal structure determination of compound 5a
(Table 1)

Data collection: Bruker APEX II Software Suite, 2008; cell refinement: Bruker APEX II Software Suite, 2008; data reduction: Bruker APEX II Software Suite, 2008; program used to solve structure: SHELXS-97 [18]; program used to refine structure: SHELXL-97 [19]; molecular graphics: SHELXTL-Plus, XP [20].

X-ray single-crystal diffraction data were collected on a Bruker Kappa APEX II Duo diffractometer (Bruker AXS GmbH, Karlsruhe, Germany), using graphite monochromatized MoK α radiation ($\lambda = 0.71073$ Å). A single crystal, coated with perfluorinated oil, was mounted on a teflon loop. Unit cell parameters, obtained by indexing the peaks in the first 36 frames, were refined by employing the whole data set. All frames were integrated and corrected for Lorentz and polarization effects. The crystal was measured at low temperature [100 (2) K]. The structure was solved by direct method using SHELXS-97 [18]. Refinement was evaluated on F^2 against all reflections. The weighted R-factor wR and goodness of fit S are based on F^2 , conventional R-factors R are based on F , with F set to zero for negative F^2 . The threshold expression of $F^2 > 2\sigma(F^2)$ is used only for calculating R-factors (gt) etc. and is not relevant to the choice of reflections for refinement. R-factors based on F^2 are statistically about twice as large as those based on F , and R-factors based on all data will be even larger. All nonhydrogen atoms were located and refined anisotropically by full-matrix least squares using SHELXL-97 [19]. The carbon bonded hydrogen atoms were placed in idealized positions. The nitrogen bonded hydrogen atoms were found in the final difference Fourier map and were allowed to refine freely with isotropic displacement para-meters. For the preparation of the structural images the program SHELXTL-Plus [20] was used. The deposition number CCDC

992210 contains the supplementary crystallographic data for this paper. These data can be obtained free of charge from the CCDC via www.ccdc.cam.ac.uk/data_request/cif.

Table 1. Crystal data, data collection and structure refinement details for **5a**.

Chemical formula	C ₁₆ H ₇ N ₄ O ₃ ·C ₅ H ₁₂ N·2(H ₂ O)
M_r	425.44
Crystal system, space group	Triclinic, $P\bar{1}$
Temperature (K)	110
a, b, c (Å)	8.3890 (5), 10.9439 (7), 11.6018 (8)
α, β, γ (°)	98.979 (4), 96.261 (3), 109.626 (3)
V (Å ³)	975.93 (11)
Z	2
Radiation type	Mo $K\alpha$
μ (mm ⁻¹)	0.11
Crystal size (mm)	0.16 × 0.13 × 0.10
<i>Data collection</i>	
Diffractometer	Bruker Kappa APEX II Duo diffractometer
Absorption correction	Multi-scan Blessing, 1995
T_{\min}, T_{\max}	0.717, 0.747
No. of measured, independent and observed [$I > 2\sigma(I)$] reflections	28545, 3992, 3091
R_{int}	0.035
$(\sin \theta/\lambda)_{\text{max}}$ (Å ⁻¹)	0.628
<i>Refinement</i>	
$R[F^2 > 2\sigma(F^2)], wR(F^2), S$	0.043, 0.109, 1.05
No. of reflections	3992
No. of parameters	310
No. of restraints	3
H-atom treatment	H atoms treated by a mixture of independent and constrained refinement
$\Delta\rho_{\text{max}}, \Delta\rho_{\text{min}}$ (e Å ⁻³)	0.32, -0.23

RESULTS AND DISCUSSION

The IR spectra of **5a** displays a split band for cyano group in the range 2144-2210 cm⁻¹ and a carbonyl band at 1733 cm⁻¹. The acidic form **5b** shows absorption at 3489 and 3415 cm⁻¹ for primary amino group whereas the cyano group absorbs at 2210 and 2190 cm⁻¹. In the ¹H NMR spectrum of **5a** a typical singlet for 2-H is observed at $\delta = 8.84$ ppm (same shift in the H-form **5b**) as are the corresponding multiplets for five methylene groups due to the piperidinium ion. Both ¹³C NMR spectra of **5a,b** contain the same ¹³C signals due to the anionic part of **5a,b**, i.e. the only difference

between them is the cationic moiety. The assigned ^{13}C NMR signals are close to those of compounds **5c,d** described by O'Callaghan [21]. The single crystal X-ray crystallography (Table 1) confirmed the structure of the product **5a** (Fig. 1; crystallographic numbering) [Cambridge Crystallographic Data Centre (CCDC): deposit No. 992210].

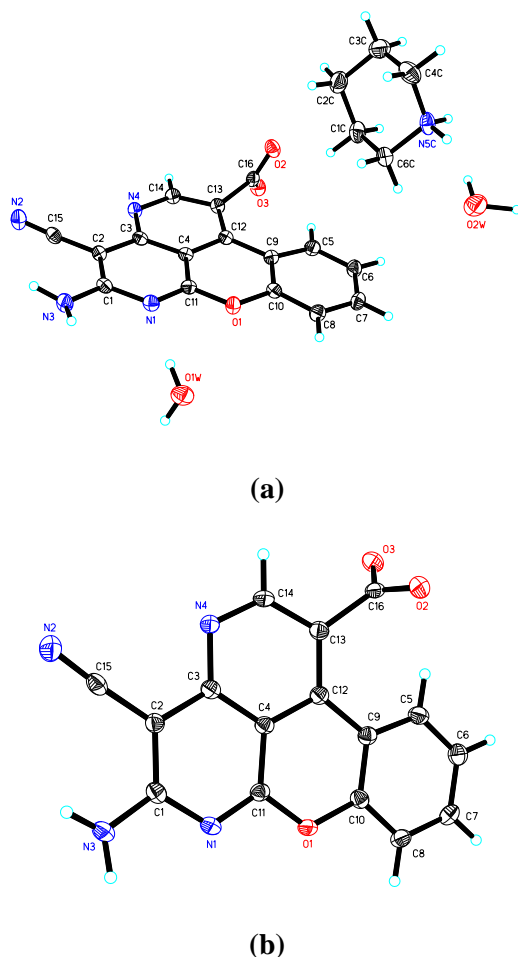
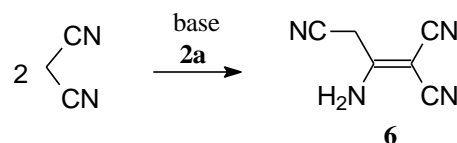


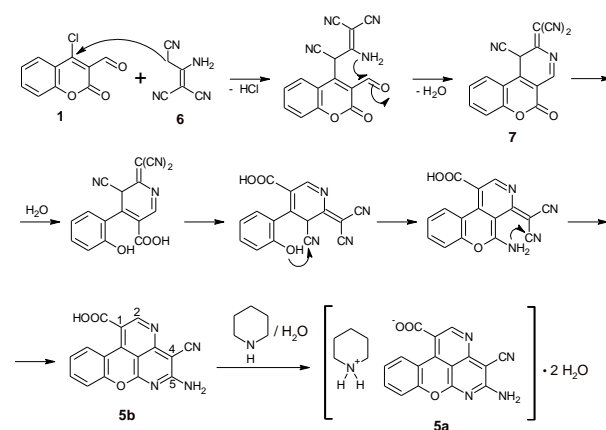
Fig. 1. ORTEP representation of the molecular structure of **5a** in the solid state with displacement ellipsoids at the 50% probability level: (a) whole structure; (b) anion only.

We suggest the following mechanistic sequence for the formation of **5a**: As an initial step, the base-catalyzed dimerization of malononitrile [22,23] into 2-amino-1-propene-1,1,3-tricarbonitrile (**6**) could be assumed (Scheme 3). This dimer has attracted a great deal of interest due to its wide applications in the field of heterocyclic synthesis [24]. The reagent was used for the synthesis of pyridines, pyrimidines, pyridazines, thiophenes, thiazoles and their analogs with diverse pharmaceutical activities including against neurological disorders, as receptor antagonists, as antidiabetics, tubulin inhibitors, kinase inhibitors and anticancer agents [25,26].



Scheme 3. Dimerization of malononitrile.

The next step of the suggested mechanism (Scheme 4) is the nucleophilic addition of the trinitrile **6** to the chloroaldehyde **1** accompanied by elimination of HCl. Further, heterocyclisation to the benzopyrano[4,3-*b*]pyridine derivative **7** is followed by lactone ring opening, re-cyclizing to 2-aminochromene and finally closing of the new pyridine ring to give the stable carboxylic acid **5b** which readily transforms into the crystallizing piperidinium salt **5a**.



Scheme 4. Suggested mechanism for the formation of compounds **5a,b**.

Stable adducts, relevant to **7**, were prepared from salicylaldehyde and malononitrile and were reported earlier [21,27]. They were used for the synthesis of the already known [1]benzo-pyrano[4,3,2-*de*][1,6]naphthyridine derivatives **5c,d** (Fig. 2). The synthetic pathway for these compounds, as described by O'Callaghan [21], differs substantially from that of **5a,b** reported here. The essential difference here is that we used 4-chlorocoumarin-3-carbaldehyde (**1**) as starting material in the presence of piperidine. As a result, a 1-carboxylated compound **5a** without any substituent at position 2 and getting stabilized as a piperidinium salt was formed.

Shaker [28] reported the synthesis of some benzo[5,6]chromeno[4,3,2-*de*][1,6]naphthyridines, related to **5a-d**, starting from a 1*H*-benzo-*f*]chromene trinitrile derivative with CH-acids in order to obtain a series of polyfunctionally substituted heterocyclic compounds with expected biological activity.

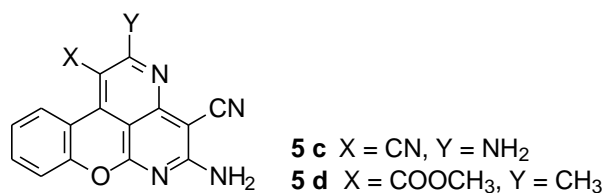


Fig. 2. Known chromeno[4,3,2-de][1,6]naphthyridine derivatives **5c,d**.

CONCLUSION

We developed a rare example of heterocyclic synthesis where a multiply substituted tetracyclic system **5a,b** arises directly in one reaction vessel as a main product. The proposed domino type mechanism (Scheme 4) is based on several one-step processes that are already known from the literature. The possibility the final product to stabilize as a piperidinium salt is obviously an important driving force for this complex multi-step synthetic route to proceed.

Full spectral characterization (IR, NMR and MS) is presented. In addition, suitable crystals of compound **5a** were successfully prepared in order crystallographic X-ray analysis to be carried out (see Table 1 for major X-ray data). Thus, the molecular structure of the product **5a** is unambiguously proven. The acidic form (compound **5b**) of the isolated piperidinium salt has also been characterized.

Acknowledgements: The financial support by the National Research Fund of Bulgaria (Projects UNA-17/2005 and DRNF-02/13) is gratefully acknowledged.

REFERENCES

- I. C. Ivanov, T. N. Glasnov, F. Belaj, *J. Heterocycl. Chem.*, **45**, 177 (2008).
- I. C. Ivanov, V. T. Angelova, I. Tiritiris, T. N. Glasnov, *J. Heterocycl. Chem.* (2014); doi 10.1002/jhet.2103.
- L. J. Núñez-Vergara, J. A. Squella, P. A. Navarrete-Encina, E. Vicente-García, S. Preciado, R. Lavilla (Review article), *Curr. Med. Chem.*, **18**, 4761 (2011).
- K. Tabaković, I. Tabaković, N. Ajdini, O. Leci, *Synthesis*, 308 (1987).
- D. Heber, *Arch. Pharm. (Weinheim)*, **320**, 577 (1987).
- G. E. H. Elgemeie, A. H. H. Elghandour, *Bull. Chem. Soc. Jpn.*, **63**, 1230 (1990).
- M. Darbarwar, V. Sundaramurthy (Review article), *Synthesis*, 337 (1982).
- V. O. Iaroshenko, F. Erben, S. Mkrtchyan, A. Hakobyan, M. Vilches-Herrera, S. Dudkin, A. Bunescu, A. Villinger, V. Y. Sosnovskikh, P. Langer, *Tetrahedron*, **67**, 7946 (2011).
- I. C. Ivanov, S. K. Karagiosov, M. F. Simeonov, *Liebigs Ann. Chem.*, 203 (1992).
- D. Heber, I. C. Ivanov, S. K. Karagiosov, *J. Heterocycl. Chem.*, **32**, 505 (1995).
- I. C. Ivanov, T. N. Glasnov, D. Heber, *J. Heterocycl. Chem.*, **42**, 857 (2005).
- I. C. Ivanov, L. D. Raev, *Liebigs Ann. Chem.*, 1107 (1987).
- L. D. Raev, I. C. Ivanov, W. Frey, H. Astroug, S. G. Agontseva, in preparation.
- A. Alberola, L. Calvo, A. González-Ortega, A. P. Encabo, M. Carmen Sañudo, *Synthesis*, 1941 (2001).
- J. S. Reddy, K. A. Solomon, G. Gayatri, M. Shukla, K. Dorai, G. Gopikrishna, *Tetrahedron*, **69**, 2142 (2013).
- J. S. Reddy, K. A. Solomon, J. V. Prasad, G. S. Kumar, G. Munuswamy-Ramanujam, G. Gopikrishna, *J. Chem. Sci.*, **126**, 187 (2014).
- T. Steinführer, A. Hantschmann, M. Pietsch, M. Weifenfels, *Liebigs Ann. Chem.*, 23 (1992).
- G. M. Sheldrick, SHELXS-97, Program for the Solution of Crystal Structures, University of Göttingen, Göttingen (Germany) 1997. See also: G. M. Sheldrick, *Acta Crystallogr.*, **A46**, 467 (1990).
- G. M. Sheldrick, SHELXL-97, Program for the Refinement of Crystal Structures, University of Göttingen, Göttingen (Germany) 1997. See also: G. M. Sheldrick, *Acta Crystallogr.*, **A64**, 112 (2008).
- G. M. Sheldrick, SHELXTL-Plus. Structure Determination Software Suite. Release 4.1. Siemens Analytical Systems Inc., Madison, Wisconsin, USA 1991.
- C. N. O'Callaghan, T. B. H. McMurry, J. E. O'Brien, *J. Chem. Soc. Perkin Trans. 1*, 417 (1995).
- R. A. Carboni, D. D. Coffman, E. G. Howard, *J. Am. Chem. Soc.*, **80**, 2838 (1958).
- M. Mittelbach, *Monatsh. Chem. / Chem. Monthly*, **116**, 689 (1985).
- N. M. Helmy, F. E. M. El-Baih, M. A. Al-Alshaikh, M. S. Moustafa, *Molecules*, **16**, 298 (2011).
- R. M. Mohareb, H. E. Moustafa, *Acta Pharm.*, **61**, 51 (2011); and the references cited therein.
- R. M. Mohareb, D. H. Fleita, O. K. Sakka, *Heterocycl. Commun.*, **17**, 25 (2011); and the references cited therein.
- R. Ghorbani-Vaghei, Z. Toghræi-Semiromi, R. Karimi-Nami, *J. Braz. Chem. Soc.*, **22**, 905 (2011).
- R. M. Shaker, *ARKIVOC*, **xiv**, 59 (2006).

ЕДНОСТЪПКОВ СИНТЕЗ НА ХРОМЕНО[4,3,2-*d,e*]-1,6-НАФТИРИДИНОВО
ПРОИЗВОДНО ОТ 4-ХЛОРОКУМАРИН-3-КАРБАЛДЕХИД

В. Т. Ангелова¹, В. Фрай², И. Х. Иванов^{1*}, Н. Василев³, Т. Н. Гласнов⁴

¹ Фармацевтичен факултет, Медицински университет - София, ул. Дунав 2, 1000 София, България

² Институт по органична химия на Университета в Щутгарт, ул. Пфафенвалдринг 55, D-70569 Щутгарт,
Германия

³ Институт по Органична химия с Център по Фитохимия, Българска Академия на Науките, ул. Акад. Г. Бончев,
бл. 9, 1113 София, България

⁴ Лаборатория „Кристиан Доплер“ за Flow химия и Институт по химия на Университета „Карл Франц“ -
Грац, Хайнрихсрасе 28, A-8010 Грац, Австрия

Постъпила на 24 април 2014 г.; Коригирана на 16 юли 2014 г.

(Резюме)

Изолирана е пиперидиниевата сол на едно ново тетрациклично производно на хромено[4,3,2-*d,e*]-1,6-нафтиридина вместо очаквания продукт на "трет-амино ефект" при взаимодействие на 4-хлорокумарин-3-карбалдеhid с малонитрил в присъствие на пиперидин. Молекулният строеж на пиперидиниевата сол и на съответната Н-форма е охарактеризиран чрез спектрални методи (ИЧ, ЯМР, МС) и елементарен анализ. Структурата е допълнително потвърдена и с помощта на рентгеноструктурен кристалографски анализ.

Rose hip extract synergistically increase antioxidant activity of fruit and herb extracts

M. G. Kratchanova^{1*}, P. N. Denev^{1,2}, C. G. Kratchanov²

¹Laboratory of biologically active substances, Institute of Organic Chemistry with Centre of Phytochemistry, Bulgarian Academy of Sciences, 139 Ruski blvd., 4000 Plovdiv, Bulgaria

²ITC – Innovative-Technological Centre Ltd., 20 D-r G.M. Dimitrov str., 4000 Plovdiv, Bulgaria

Received May 20, 2014; Revised June 12, 2014

Dedicated to Acad. Dimiter Ivanov on the occasion of his 120th birth anniversary

In the current study, we investigated the possibility to use rosehip extract for synergistic elevation of the antioxidant activity of fruit and herb extracts. The obtained rosehip extract was characteristic with very high antioxidant activity measured by the ORAC method and the addition of the extract to chokeberry, blackberry, blackcurrants or elderflower extracts increased significantly their antioxidant activity. Moreover, there was synergistic effect in ORAC antioxidant activity of the mixed extracts that reached up to 64%. The removal of rosehip polysaccharides inhibited the synergistic effect, indicating that rosehip pectic polysaccharides are at least partially involved in the observed synergism. This opens the possibility to develop rosehip based functional beverages with increased antioxidant activity.

Key words: rosehip, synergism, antioxidant activity, ORAC, fruit, herbs

INTRODUCTION

Increasing amount of evidence indicates the role of reactive oxygen species (ROS) and reactive nitrogen species (RNS) in the pathophysiology of ageing and in the development of degenerative chronic diseases [1,2]. In human body, there is a protective antioxidant system, which impairs oxidative damage and keeps balance between prooxidants and antioxidants. However, because of many factors related to the modern way of life the balance is often broken which lead to a physiological state known as oxidative stress. In such cases to maintain the oxidative balance, an external intake of antioxidant with the diet is required. The definition for antioxidants depends on their application and probably the most widely accepted definition is “any substance that, when present at low concentration compared with those of an oxidizable substrate, significantly delays or prevents oxidation of that substrate” [3]. In food science, term antioxidant has a broader meaning. From one hand, antioxidants are substances that prevent rancidity of foods. On the other hand, these compounds administered with the diet decrease the detrimental effects of ROS and RNS in our bodies [4]. Diet derived antioxidants include free radical scavengers, metal ion chelators, oxidative enzymes inhibitors, and cofactors of antioxidant enzymes. Studying antioxidants in foods is an important issue

because of several reasons: Endogenous or added to foods antioxidants prevent food components from oxidation; Antioxidants taken with the diet are absorbed in human body and exert their beneficial effects *in vivo*. This undoubtedly was found for vitamin E and vitamin C [5], but more and more collected evidence indicates the same for polyphenol compounds [6]. It is quite often that compound with antioxidant activity taken with the diet reveals other health benefits like antiinflammatory effect, antiischemic effect, etc., besides antioxidant activity; Since absorption of phenolic compounds is incomplete, the majority passes through the gastro-intestinal tract (GIT) and enters the colon. Their local action may nevertheless be important because the intestine is particularly exposed to oxidizing agents and may be affected by inflammation and numerous diseases such as cancer. The diet contains various prooxidants, which may induce oxidative stress in the GIT, to induce stomach ulcer and develop stomach, colon, and rectal cancers [7].

The majority of antioxidants taken with the diet are of plant origin and fruit, vegetables, and herbs are the richest sources of natural antioxidants. The most important antioxidants in plants are polyphenols including flavonoids, carotenoids, vitamin C, vitamin E, etc. [1,2,8]. There are numerous studies in the literature demonstrating the correlation between consumption of fresh fruits and vegetables with the prevention of socially significant diseases including cancer, cardiovascular diseases,

* To whom all correspondence should be sent:
E-mail: lbas@plov.omega.bg

Alzheimer disease, etc. [9,10]. Several epidemiologic studies point out that the consumption of polyphenol-rich foods and beverages is associated with lower risk of oxidative stress-related diseases [9,11]. At the laboratory of biologically active substances, Institute of Organic Chemistry with Centre of Phytochemistry, we are dedicated to the development of functional foods, rich in natural antioxidants. In searching of suitable raw materials for functional beverages, we previously investigated the antioxidant activity of 26 Bulgarian fruits [12]. Rosehip appeared to be among the fruits with the highest antioxidant activity and suitable raw material for production of functional foods with antioxidant activity. From the literature, it is known that often plant extracts consisting of several herbs or fruits exert synergistic effect in their antioxidant activity [13]. Synergism is defined as „interaction between two or more entities, factors, substances, etc. that produces an effect greater than the sum of their individual effects”. In the current study, we decided to further explore the applicability of rosehip fruits for the production of mixed herb and fruit extracts with synergistic action in the antioxidant activity. Therefore, the aim of the current work was to investigate the synergism in the antioxidant activity of fruit (chokeberry, blackberry, blackcurrants) and herb extracts (elderflowers) mixed with rosehip fruit extract.

EXPERIMENTAL

Plant materials

All fruit and herb samples were collected from the region of Rhodopi mountain in the stage of full maturity in 2012. The following fruits were used: rosehip, chokeberry, blackcurrant and blackberry. Chokeberries were cultivated, while other fruits were widely collected in the nature. Fresh fruits were frozen immediately and freeze dried in a Cryodos-50 laboratory freeze drier (Telstar Industrial, Spain). Elderflowers (*Sambucus nigra*) were collected from the region of Ravnogor (Rhodopi mountain) in 2012. Fresh flowers were dried at room temperature and dry drug was stored in paper bags at ambient temperature prior to analysis.

Extraction

Plant materials were subjected to extractions under the following conditions:

Fruits: 70 g fruits (rosehip, chokeberry, blackcurrant or blackberry) were mixed with 200 ml

warm water (60°C). Mixtures were homogenized at turbulent conditions and remained at ambient temperature for overnight. After that mixtures were centrifuged (6 000 x g) and supernatants were collected for antioxidant activity determination.

Elderflowers: 1 g of dried elderflowers were mixed with 100 ml warm water (60°C) Mixture was infused at room temperature for 24 hours, centrifuged (6 000 x g) and supernatant was collected for antioxidant activity determination.

Removal of rosehip extract polysaccharides

Rosehip extract polysaccharides were removed via the following procedure: 100 ml extract were mixed with 300 ml 96% ethanol. The mixture was left in refrigerator overnight and centrifuged (6000 x g). The clear supernatant without polysaccharides was collected and investigated for antioxidant activity. Precipitated polysaccharides were collected and dried in a laboratory dryer.

Antioxidant activity

Oxygen Radical Absorbance Capacity (ORAC) assay: ORAC was measured according to the method of Ou *et al.* [14] with some modifications described in details by Denev *et al.* [15]. The method measures the antioxidant scavenging activity against peroxy radical generated by thermal decomposition of 2,2'-azobis[2-methyl-propanamide] dihydrochloride (AAPH) at 37°C. Fluorescein (FL) was used as the fluorescent probe. The loss of fluorescence of FL was an indication of the extent of damage from its reaction with the peroxy radical. The protective effect of an antioxidant was measured by assessing the area under the fluorescence decay curve (AUC) relative to that of a blank in which no antioxidant has been present. Solutions of AAPH, fluorescein and trolox were prepared in a phosphate buffer (75 mmol/l, pH 7.4). Samples were diluted in the phosphate buffer as well. Reaction mixture (total volume 200 µl) contained FL - (170 µl, final concentration 5.36×10^{-8} mol/l), AAPH - (20 µl, final concentration 51.51 mmol/l), and sample - 10 µl. The FL solution and sample were incubated at 37°C for 20 min directly in a microplate reader, and AAPH (dissolved in buffer at 37°C) was added. The mixture was incubated for 30 s before the initial fluorescence was measured. After that, the fluorescence readings were taken at the end of every cycle (1 min) after shaking. For the blank, 10 µl of phosphate buffer were used instead of the extract. The antioxidant activity was expressed in micromole trolox

equivalents ($\mu\text{mol TE}$) per liter of extract. Trolox solutions (6.25; 12.5; 25 and 50 $\mu\text{mol/l}$) were used for defining the standard curve. ORAC analyses were carried out using a FLUOstar OPTIMA plate reader (BMG Labtech, Germany), excitation wavelength of 485 nm and emission wavelength of 520 nm were used.

Statistics

All antioxidant activity tests were repeated 4 times. The results are expressed as means \pm standard deviation (SD).

RESULTS AND DISCUSSION

The Oxygen Radical Absorbance Capacity (ORAC) antioxidant activity of the investigated fruit and herb mixed extracts is presented in Table 1. It is evident from the results that the obtained rosehip extract and mixed extracts are very rich source of natural antioxidants, rendering very high ORAC values. In one of the first attempts to quantify dietary antioxidant needs of the body, Prior *et al.* [16] demonstrated that consumption of certain berries and fruits such as blueberries, mixed grape and kiwifruit was associated with increased ORAC plasma antioxidant capacity in the postprandial state. They estimated that according to the energy

intake of the diet, 5000-15000 $\mu\text{mol TE}$ are necessary to cover human daily antioxidant needs. This indicates that the obtained mixed extracts in our study could serve as functional beverage with high antioxidant activity. For example, only 100 ml of rosehip extract will supply the body with more than 13000 ORAC units. Furthermore, we observed a synergistic effect in the antioxidant activity of the fruit and herb extracts, when mixed with rosehip extract. The effect was concentration-dependent and was up to 64% in the case of mixed rosehip-blackberry extract. The observed synergistic effect opens new possibilities for the production of novel functional foods with increased antioxidant activity. The used fruits and elderflower contain various components with antioxidant activity [7], which could be one of the reasons for the observed synergistic effect. There are reports in the literature that compounds with antioxidant exert synergism in their action when acting together. For example, there was synergism in the common antioxidant activity of β -carotene and α -tocopherol [17]. In another study synergistic effect expressed as elevated lipid peroxidation inhibiting activity was observed for α -tocopherol and quercetin, and quercetin with rutin [18]. Significant synergistic effect was found also between the action of lycopene-lutein, lycopene- β -carotene, and α -tocopherol- β -carotene [19].

Table1. Synergism between rosehip extract and fruit and herb extracts.

Extracts Ratio, %		ORAC, $\mu\text{molTE/l}$	ORAC, $\mu\text{molTE/l}$	synergism, %
Rosehip	Chokeberry	(experimental)	(expected)	
100	0	132408.8 \pm 4058.2	na	na
0	100	15429.2 \pm 1405.2	na	na
75	25	121429.4 \pm 6504.2	103163.9	17.7
50	50	92725.8 \pm 6504.2	73919.0	25.4
25	75	51937.2 \pm 2987.6	44674.1	16.3
Rosehip	Blackberry			
100	0	134889.6 \pm 5049.6	na	na
0	100	12463.0 \pm 985.2	na	na
75	25	118570.7 \pm 5012.3	104283.0	13.7
50	50	91097.9 \pm 3456.2	73676.3	23.6
25	75	70614.1 \pm 4022.2	43069.6	64.0
Rosehip	Blackcurrants			
100	0	134889.6 \pm 5049.6	na	na
0	100	12463.0 \pm 1012.8	na	na
75	25	125698.3 \pm 5069.8	103836.1	21.1
50	50	102088.1 \pm 3985.6	72782.7	40.3
25	75	58014.7 \pm 3046.7	41729.2	39.0
Rosehip	Elderflower			
100	0	126953.9 \pm 5056.3	na	na
0	100	6213.8 \pm 456.2	na	na
75	25	109138.4 \pm 4834.4	96768.8	12.8
50	50	77050.6 \pm 3695.8	66583.8	15.7
25	75	43820.8 \pm 2865.7	36398.8	20.4

na – not applicable

Table2. Synergism between chokeberry extract, elderflower extract and rosehip extract with removed polysaccharide fraction.

Extracts Ratio, %		ORAC, $\mu\text{molTE/l}$ (experimental)	ORAC, $\mu\text{molTE/l}$ (expected)	synergism, %
Rosehip without polysaccharide	Chokeberry			
100	0	68635.6 \pm 3089.9	na	na
0	100	12815.3 \pm 952.1	na	na
75	25	51129.4 \pm 2054.7	54680.5	-6.5
50	50	39223.3 \pm 1114.2	40725.4	-3.7
25	75	26223.5 \pm 2005.7	26770.4	-2.0
Rosehip without polysaccharide		Elderflower		
100	0	68635.6 \pm 3089.9	na	na
0	100	6213.8 \pm 456.2	na	na
75	25	50088.0 \pm 3054.2	53030.2	-5.5
50	50	35484.2 \pm 1865.2	37424.7	-5.2
25	75	20369.4 \pm 1024.5	21819.2	-6.6

na – not applicable

Table3. Synergism between crude polysaccharide isolated from rosehips and chokeberry and elderflower extracts.

Extracts Ratio, %		ORAC, $\mu\text{molTE/l}$ (experimental)	ORAC, $\mu\text{molTE/l}$ (expected)	synergism, %
Crude rosehip polysaccharide (7mg/ml)	Chokeberry			
100	0	24508.6 \pm 1256.3	na	na
0	100	12815.3 \pm 957.2	na	na
75	25	23442.1 \pm 1002.4	21585.3	8.6
50	50	18268.7 \pm 854.2	18662.0	-2.1
25	75	15116.5 \pm 802.2	15738.6	-4.0
Crude rosehip polysaccharide		Elderflower		
100	0	68635.6 \pm 1256.3	na	na
0	100	6213.8 \pm 456.2	na	na
75	25	20466.1 \pm 1235.8	19934.9	2.7
50	50	21850.4 \pm 1078.9	15361.2	42.2
25	75	12068.5 \pm 605.2	10787.5	11.9

na – not applicable

Another example for synergism in antioxidant activity of pure compounds is the ability of rutin and lycopene, and rutin and luteolin to inhibit synergistically the oxidation of LDL cholesterol [20]. Yi *et al.* [21] found out that α -tocopherol and ascorbic acid act in synergism in a model of fish oil oxidation, and Maillard and Berset [22] observed synergism in the antioxidant activity of *p*-coumaric and ferulic acids. Similar effect was observed for caffeic and ascorbic acids, as well [23]. Meyer *et al.* [24] found synergism in mixtures of phenolic acids and flavonoids. Except for pure compounds, synergistic antioxidant action was observed after mixing plant extracts with pure phytochemicals. For example, Hait Darshan *et al.* [25] observed synergistic effect in the antioxidant activity of polyphenol extract from spinach and ferulic acid, caffeic acid, and epigallocatechin-3-gallate. Interesting is the synergistic common action of the three

active components in the Chinese formula ShengMai San, which is one of the most prescribed remedies in the traditional Chinese medicine [26]. Synergistic anti-oxidant effect was observed also for great burdock mixture with α -tocopherol [27] and ascorbic acid with grape seed extract [28]. The polyherbal extracts obtained with green tea also showed higher antioxidant activity compared to the separate components [13]. Chu and Hsu [29] reported 2-3 fold increment of antioxidant activity of peanut oil when using mixtures of antioxidants.

It is well known that rosehips are rich source of various classes of biologically active substances. Besides polyphenols, ascorbic acid and carotenoids that reveal antioxidant activity, fruits contain minerals and sustainable amount of pectic polysaccharides. In order to check whether rosehip polysaccharides take part in the synergistic action we removed the polysaccharide fraction by ethanol

precipitation and measured again the antioxidant activity of the obtained mixed extracts. Results are shown in Table 2. As it is evident from the results, after the removal of the pectic fraction, the synergistic effect was lost. Furthermore, to explore this effect we isolated crude pectic polysaccharide from rosehip extract and combine it with the tested chokeberry and elderflower extract (Table 3). The obtained results show that in the case of elderflower the synergistic effect was partially due to the interaction with polysaccharides.

Several authors have already observed the synergistic effect in the biological activity of polyphenols and polysaccharides. The health effects of apples, especially their cholesterol-lowering properties, were first ascribed to the content of pectin [30-32]. In more recent studies, Aprikian *et al.* [33] found that apple pectin and polyphenolic fractions lowered plasma, liver cholesterol and triglycerides, and were more effective together than were either apple pectin alone or apple phenolics alone. In the intact fruit, the fibres and the phenolic compounds are closely associated; they could reciprocally affect digestibility and possibly exert synergistic effects. The lyophilized apple diet lowered plasma and LDL cholesterol in rats and reduced triglyceride accumulation in heart and liver [34]. Many works [31-33] suggest that there is a beneficial interaction between fruit fibre and polyphenolic components and also support the benefits of eating whole fruits as opposed to dietary supplements.

CONCLUSION

Rosehips are raw material with high antioxidant activity and from the presented results, it is evident that they synergistically increase ORAC antioxidant activity of fruit (chokeberry, blackcurrant and blackberry) and herb (elderflower) extracts. The observed synergistic effect is at least partially due to the presence of pectic polysaccharides in rosehips. However, future studies are necessary to fully investigate this phenomenon. The obtained results indicate that rosehips could be used for the development of functional beverages with increased antioxidant activity. From one hand, this will increase the oxidative stability of the beverages, and from other, probably will increase the health benefits from the consumption of these beverages.

Acknowledgements: This work was funded by project № BG161PO003-1.1.05-0024-C0001 "Development of nutraceuticals with antioxidant

and immune-stimulating action" of Operational Program "Competitiveness" of the EU.

REFERENCES

1. K. J. Davies, *IUBM Life*, **50**, 279 (2000).
2. T. Finkel, N. J. Holbrook, *Nature*, **408**, 240 (2000).
3. B. Halliwell, J. Gutteridge, *Free Radicals in Biology and Medicine* 4th edition. Oxford Univ. Press, 2007.
4. National Academy of Sciences, Institute of Medicine. Dietary reference intakes for vitamin C, vitamin E, selenium, and carotenoids, Washington DC, p. 35 (2000).
5. M. G. Traber, *Adv. Pharmacol.*, **38**, 49 (1997).
6. C. Rice-Evans, *Wake up to flavonoids*. Royal Society of Medicine, London, 2000.
7. P. Denev, M. Kratchanova, M. Ciz, A. Lojek, O. Vasicek, P. Nedelcheva, D. Blazheva, R. Toshkova, E. Gardeva, L. Yossifova, P. Hyrsil, L. Vojtek, *Food Chem.*, **157**, 37 (2014).
8. R. L. Prior, *Am. J. Clin. Nutr.*, **78**, 570S (2003).
9. M. G. Hertog, H. B. Bueno de Mesquita, A. M. Fehily, P. M. Sweetnam, P. C. Elwood, D. Kromhout, *Cancer Epidem. Biomar.*, **5**, 673 (1996).
10. D. Heber, *J. Postgrad. Med.*, **50**, 145 (2004).
11. B. N. Ames, M. K. Shigenaga, T. M. Hagen, *P. Nat. Acad. Sci. USA*, **90**, 7915 (1993).
12. P. Denev, A. Lojek, M. Ciz, M. Kratchanova, *Bulg. J. Agric. Sci.*, **19**, 22 (2013).
13. D. P. Jain, S. S. Pancholi, R. Patel, *J. Adv. Pharm. Technol. Res.*, **2**, 177 (2011).
14. B. Ou, M. Hampsh-Woodill, R. L. Prior, *J. Agric. Food Chem.*, **49**, 4619 (2001).
15. P. Denev, M. Ciz, G. Ambrozova, A. Lojek, I. Yanakieva, M. Kratchanova, *Food Chem.*, **123**, 1055 (2010).
16. R. L. Prior, H. Hoang, L. Gu, X. Wu, R. Jacob, G. Sotoudeh, A. Kader, R. Cook, *J. Am. Coll. Nutr.*, **269**, 170 (2007).
17. P. Palozza, N. Krinsky, *Arch. Biochem. Biophys.*, **297**, 184 (1992).
18. E. M. Becker, G. Ntouma, L. H. Skibsted. *Food Chem.*, **103**, 1288 (2007).
19. Z. Kotíková, A. Hejtmánková, K. Hejtmánková, *LWT- Food Sci. Technol.*, **44**, 1703 (2011).
20. J. Milde, E. F. Elstner, J. Grassmann, *Mol. Nutr. Food Res.*, **51**, 956 (2007).
21. O. S. Yi, D. Han, H. K. Shin, *J. Am. Oil Chem. Soc.*, **68**, 881 (1991).
22. M. N. Maillard, C. Berset, *J. Agr. Food Chem.*, **43**, 1789 (1995).
23. J. J. Cilliers, V. L. Singleton, *J. Agr. Food Chem.*, **38**, 1797 (1990).
24. A. S. Meyer, M. Heinonen, E. N. Frankel, *Food Chem.*, **61**, 71 (1998).
25. R. Hait-Darshan, S. Grossman, M. Bergman, M. Deutsch, N. Zurgil, *Food Res. Int.*, **42**, 246 (2009).
26. Y. Li, M. Gong, T. Konishi, *J. Health Sci.*, **53**, 692 (2007).

27. G. Blekas, D. Boskou, *Grasas Aceites*, **49**, 34 (1998).
28. P.-D. Duh, *J. Am. Oil Chem. Soc.*, **75**, 455 (1998).
29. Y.-H. Chu, H.-F. Hsu, *Food Chem.*, **66**, 29 (1999).
30. J. Groudeva, M. Kratchanova, I. Panchev, C. Kratchanov, *Z. Lebensm. Untres. F. A.*, **204**, 374 (1997).
31. L. Cara, M. Dubois, N. Armand, M. Mekki, M. Senft, H. Portugal, D. Lairon, *Nutrition*, **12**, 66 (1993).
32. R. Sable-Amplis, R. Sicart, E. Bluthe, *Nutr. Rep. Int.*, **27**, 881 (1983).
33. O. Aprikian, V. Duclos, S. Guyot, C. Besson, C. Manach, A. Bernalier, C. Morand, C. Rémésy, C. Demigné, *J. Nutr.*, **133**, 1860 (2003).
34. O. Aprikian, M.-A. Levrat-Verny, C. Besson, J. Busserolles, C. Rémésy, C. Demigné, *Food Chem.*, **75**, 445 (2001).

ЕКСТРАКТ ОТ ШИПКА СИНЕРГИЧНО ПОВИШАВА АНТИОКСИДАНТНАТА АКТИВНОСТ НА ПЛОДОВИ И БИЛКОВИ ЕКСТРАКТИ

М. Г. Крачанова^{1*}, П. Н. Денев^{1,2}, Х. Г. Крачанов²

¹Лаборатория Биологично Активни Вещества, Институт по Органична химия с Център по Фитохимия, Българска Академия на Науките, бул. Руски 139, 4000 Пловдив, България

²ИТЦ – Иновативно-Технологичен Център ООД, ул. Д-р Г. М. Димитров 20, 4000 Пловдив, България

Постъпила на 20 май 2014 г.; Коригирана на 12 юни 2014 г.

(Резюме)

В настоящата работа е изследвана възможността за използване на екстракт от шипкови плодове за синергично повишаване на антиоксидантната активност на плодови и билкови екстракти. Екстрактът от шипки се характеризира с много висока антиоксидантна активност, измерена посредством ORAC метода, а прибавянето му към екстракти от плодове на арония, къпина, черен касис или цвят от бъз повиши значително тяхната антиоксидантна активност. Освен това бе наблюдаван и синергичен ефект в антиоксидантната активност на смесените екстракти, който достигна до 64%. Отстраняването на полизахаридите от шипковите плодове инхибира синергичния ефект, което е индикатор, че пектиновите полизахариди от шипката играят роля в синергичното действие. Наблюдаваният синергичен ефект отваря нови възможности за разработване на функционални напитки с повишена антиоксидантна активност.

Optimization of the key parameters for extraction of polyphenol compounds from tomato fruits (*Solanum lycopersicum* L.). Kinetics of the process.

A. H. Atanasova¹, P. N. Denev^{2*}, I. I. Tringovska¹, S. Y. Grozeva¹, D. G. Ganeva¹, M. G. Kratchanova², I. N. Panchev³

¹Maritsa Vegetable Crops Research Institute, 32 Brezovsko Shosse str., 4003 Plovdiv, Bulgaria

²Institute of Organic Chemistry with Centre of Phytochemistry, Bulgarian Academy of Sciences, 4000 Plovdiv, Bulgaria

³University of Food Technologies, 26 Maritsa str., 4000 Plovdiv, Bulgaria

Received May 20, 2014; Revised June 24, 2014

Dedicated to Acad. Dimiter Ivanov on the occasion of his 120th birth anniversary

The main parameters that affect extraction process of polyphenolic compounds from tomato were investigated. The most suitable solvent for reaching maximum yield of polyphenols was acetone-water mixture 80:20 (v:v). Using this extractant the concentration of extracted polyphenols was approximately 17% higher than using ethanol and methanol. The optimal extraction time, temperature and solid to solvent ratio were 45 min, 60°C and 1:40, respectively. Using these extraction parameters the yield of total polyphenols in tomato variety Desperado was 27.80 GAE/100 g fresh weight. The kinetics of extraction process was investigated and theoretical model describing extraction process was proposed. This mathematical model provides the theoretical initial amount of polyphenols in tomato fruits which could be useful for the breeding programs of varieties with high amount of polyphenol compounds.

Key words: tomatoes, polyphenols, extraction, optimization, kinetics

INTRODUCTION

Polyphenols are secondary metabolites that are synthesized mainly in plants [1,2]. It is known that these components protect plants from pathogens, UV-B light and play role as signal molecules in the interaction between plants and environment [3]. In the recent years polyphenol compounds gained a lot of attention because they act as antioxidants and protect human body from oxidative stress which is the main reason for different degenerative processes. Because of the polyphenol components, the consumption of fruits and vegetables is reversely correlated with the development of chronic diseases [4,5]. Therefore, contemporary breeding programs are directed to the selection of cultivars with increased content of polyphenols and other antioxidant components.

The accurate determination of polyphenols depends on the methods of extraction and analysis. Since the extraction is the main part of sample preparation, there are many methods for isolation of phenolic compounds from different plant matrices. The yield of analytes is influenced by many factors such as: chemical structure, solvent, pH, temperature, etc. Optimization of extraction parameters is

critical for precise and reproducible analysis and there is no protocol, suitable for all classes of phenolic compounds [6]. Therefore, optimization of extraction parameters for different plant matrices is necessary [2].

Tomato is among the most consumed vegetables in the world. Generally, tomato fruits are not very rich of polyphenols, but high consumption of tomato and tomato products make them an important source of these compounds [7]. The main part of the hydrophilic antioxidant capacity of tomatoes is due to the presence of polyphenols [8]. For example, Grozeva *et al.* (2013) compared the polyphenol content and antioxidant activity of cherry and small sized tomatoes and observed that cherry tomato line 1620/10 is distinctive with the highest polyphenol content and the highest antioxidant activity, measured by ORAC (11.54 $\mu\text{mol TE/g}$) and HORAC (6.69 $\mu\text{mol GAE/g}$) methods [9]. Similar results were obtained by Toor *et al.* (2005) who investigated antioxidant properties of tomatoes grown in New Zealand [8].

Predominate phenolic compounds in tomatoes are chlorogenic acid, rutin, naringenin, naringenin chalcone, quercetin [10]. All plant phenolics are conjugated with sugars, rather than free aglycones, which make them more soluble in water. Therefore, for extraction of these compounds mixtures of

* To whom all correspondence should be sent:
E-mail: petkodenev@yahoo.com

ethanol, methanol and acetone with water are most commonly used [11-13]. For obtaining better yield of these compounds optimization of extraction parameters such as temperature, extraction time, solid to solvent ratio is also necessary. These parameters were already optimized in other plant materials but to our knowledge the optimization of these key factors for tomato polyphenols extraction has not been addressed [14,15]. Therefore, the aim of this study was to find the optimal parameters for extraction (temperature, extraction time, solid to solvent ratio) of phenolic compounds from tomatoes and to develop mathematical models describing the process.

EXPERIMENTAL

Reagents, Solvents and Apparatus

Ethanol, methanol and acetone used in experimental work were pure for analysis. Folin-Ciocalteu reagent was from Merck, gallic acid was from Sigma Aldrich. UV/VIS Spectrophotometer used in this work was from Camspec Ltd., Cambridge, UK.

Plant Material

Optimization of extraction parameters was carried out by using freeze-dried tomato samples, variety Desperado (Enza Zaden, the Netherlands). The plants were grown under greenhouse conditions during the period March-July 2012. Randomized samples of tomato fruits were harvested at red ripening state.

Sample Preparation

About 700-800 g of tomatoes were washed, packed in plastic bag and frozen in refrigerator at -20°C. After that, samples were freeze-dried, subsequently crushed to powder using laboratory blender and stored at -20°C prior analysis.

Optimization of Extraction Parameters

The main factors that affect the extraction such as type of solvents (methanol, ethanol and acetone) and their mixtures with water (20%, 40%, 60%, 80% (v:v)), extraction time (15, 30, 45, 60, 75 and 90 min), temperature (room, 40°C and 60°C) and plant material to solvent ratio (1:20, 1:40 and 1:80 (w:v)) were studied. For the extraction two grams of dry powdered sample were weighted accurately and mixed with 40 ml of extragent in extraction

tubes with caps. Samples were extracted in shaking water bath for 1 hour.

Extraction solvent and temperature: Three solvents (acetone, methanol and ethanol) and their mixtures with water (20%, 40%, 60%, 80% (v:v)), as well as three different temperatures of extraction (room temperature, 40°C and 60°C) were studied.

Time of extraction: The influence of time on extraction process was examined in optimal conditions, found for type of extragent and temperature. The tested time intervals were 15, 30, 45, 60, 75 and 90 min.

Sample to solvent ratio: The optimal solvent, temperature and extraction time were used to determine the optimal sample to solvent ratio (v:v) of the extraction process. For that aim 1 gram of the sample were weighted accurately and mixed with 20, 40 or 80 ml of the extragent (80% acetone) to obtain 1:20, 1:40 and 1:80 sample to solvent ratio, respectively. All samples were put in shaking water bath for 45 min at 60°C. After that, samples were filtrated and supernatants were collected for determination of total polyphenol contents.

Determination of Total Polyphenols

The influence of different extraction parameters on the yield of polyphenols was estimated according to the method of Singleton & Rossi (1965) with Folin-Ciocalteu's reagent [16]. Briefly, 100 µl of extract was mixed with 3100 µl water, 200 µl Folin-Ciocalteu's reagent and 600 µl 20% Na₂CO₃. The mixture (final volume 4 ml) was vortexed, incubated for 5 min at 50°C, cooled in ice bath for 5 min and then absorbance was measured spectrophotometrically at 750 nm. The amount of polyphenols was determined by standard curve of seven different concentrations of Gallic acid (0.04; 0.06; 0.08; 0.10; 0.20; 0.40 and 0.60 mg/ml) and results were expressed as mg GAE/100 g fresh weight (FW).

Statistics

Data were subjected to Duncan's Multiple Range Test to evaluate the statistical significance among means. Each sample was measured in triplicates (or quintuplicates) and variations between these technical triplicates in each analysis were less than 1% (data not shown). Method of least squares was also used.

Kinetics of Extraction Process

Based on data obtained from the experiments the rate constants (k_1 , k_2) of the process and the amount

of polyphenols in matrices (A_0) were determined (equation 1). The principal of Nuton-Rafson For was used for determination of nonlinear regression correlation and implementation was performed using NONLIN program compiled on FORTRAN IV, with adapted sub program FUNCTN for the specific mathematical correlation.

RESULTS AND DISCUSSION

We investigated the influence of the main factors that affect the extraction of polyphenols from tomato matrix, namely type of solvent, temperature, solid to liquid ratio (w:v) and extraction time. In Table 1 the results for the influence of temperature and type of solvent on yield of total polyphenols from tomato fruits are presented.

Type of Solvent

From the results in Table 1 it is evident that ethanol-water mixtures have a better extraction efficiency compared to methanol-water mixtures at room temperature and at 40°C. With increasing of the temperature, the yield of total polyphenols for these two solvents has also increased, but differences between obtained values are very low and statistically insignificant (22.79 mg GAE/100 g for methanol-water and 22.97 mg GAE/100 g for ethanol-water). Similar results were reported by Mukhopdhyay *et al.* in 2006 in different plant matrices [6]. In these cases ethanol is preferable solvent

because of its lower toxicity compared to methanol. Among the three solvents used in this investigation acetone exhibited extraction efficiency resulting in up to 17% higher yield of total polyphenols in all studied temperatures. Our results are in line with other studies pointing out acetone as suitable extragent for polyphenol compounds [14]. Acetone has polar index 5.1 which makes it a solvent with intermediate polarity. Phenols, which are present in the tomatoes are compounds with different polarity. Therefore, such types of solvents are preferable for their extraction from this matrix. The higher yield of total polyphenols from tomatoes using acetone extract is probably due to the presence of high molecular polyphenols as tannins that are also extracted with acetone [17].

Temperature

Values obtained for total polyphenol content of tomato extract obtained by methanol-water mixtures at room temperature and 40°C were very close (Table 1). Increasing the temperature intensified the extraction process, yielding higher amounts of extractible polyphenols. The highest yield of polyphenolic compounds was achieved at temperature 60°C. It is known that high temperature promotes high analite solubility and increases mass transfer. Viscosity and solvent surface tension are decreased by high temperature and solvent could easily reach sample matrices which leads to increased extraction rate [13].

Table 1. Influence of type solvent, percentage of solvent with water (v:v), and temperature on yield of total polyphenols from freeze-dried tomato.

Room temperature		Temperature 40°C		Temperature 60°C	
Solvent, %	Polyphenols, mgGAE/100g	Solvent, %	Polyphenols, mgGAE/100g	Solvent, %	Polyphenols, mgGAE/100g
Methanol	18.36±0.36 ^{ef}	Methanol	18.23±0.15 ^{fg}	Methanol	20.91±0.40 ^f
20	18.07±0.38 ^g	20	18.20±0.05 ^{fg}	20	20.67±0.58 ^f
40	19.36±0.26 ^{ef}	40	18.29±0.47 ^{fg}	40	22.79±0.28 ^{de}
60	19.18±0.39 ^{e-g}	60	18.79±0.39 ^f	60	22.07±0.06 ^e
80	19.54±0.36 ^{de}	80	19.58±0.45 ^e	80	22.34±0.33 ^e
Ethanol	15.87±0.49 ^h	Ethanol	17.39±0.23 ^h	Ethanol	18.39±0.58 ^g
20	18.56±0.71 ^{e-g}	20	19.73±0.40 ^e	20	22.78±0.75 ^{cd}
40	19.08±0.47 ^{e-g}	40	21.19±0.11 ^d	40	22.78±0.06 ^{de}
60	22.07±0.80 ^c	60	22.76±0.66 ^c	60	22.57±0.40 ^e
80	22.62±1.06 ^{bc}	80	20.95±0.46 ^d	80	22.97±0.61 ^{de}
Acetone	18.13±0.45 ⁱ	Acetone	17.54±0.31 ^h	Acetone	12.55±0.24 ^h
20	20.40±0.30 ^d	20	21.38±0.20 ^d	20	23.15±0.54 ^{de}
40	23.07±0.54 ^b	40	22.68±0.35 ^c	40	24.34±0.46 ^c
60	26.05±0.53 ^a	60	23.88±0.56 ^b	60	26.21±0.59 ^b
80	25.82±0.42 ^a	80	26.14±0.11 ^a	80	27.80±0.45^a

Results are expressed as mean value ± standard deviation from three measurements. Differences between values marked with different superscript letters are statistically significant at P<0.05 based on Duncan's Multiple Range Test (n = 3).

Solvent Concentration

Obtained results about the influence of different concentrations of organic solvents on the extraction efficiency of polyphenols indicate that pure solvents have the lowest extraction ability in comparison to solvent-water mixtures. Mixtures with water are preferable because water facilitates the penetration of organic solvent into the plant cells and increase polyphenols extraction [6]. In our study, the highest yields were obtained with 60% and 80% water solution of the used organic solvents (Table 1). It has been observed that 80% methanol was better extractant for extraction of some flavonoids from vegetables compared to 50% and 90% methanol [14]. Gyenai *et al.* in 2012 also reported 80% acetone as better solvent for extraction of polyphenols from tomato than methanol and acetonitrile [15].

Extraction Time

The influence of extraction time on polyphenols extraction is shown on Fig. 1.

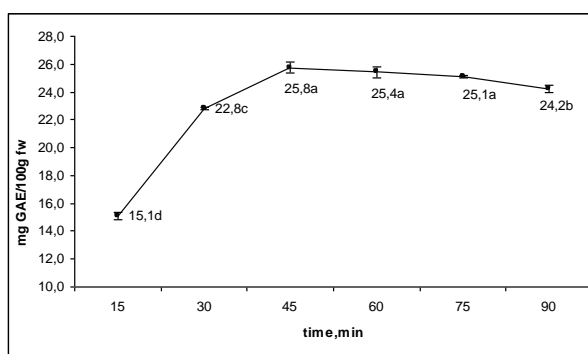


Fig. 1. Influence of extraction time on the yield of total polyphenols in freeze-dried sample tomato.

The lowest yield of total polyphenols was obtained after 15 minutes of extraction at optimum condition (80% acetone at 60°C). Accumulation of polyphenols increased gradually and reached maximum value at the 45th min. After that the yield slightly decreased. Phenolic compounds are not uniformly distributed in plants. Some of them are strongly linked with cellular walls, while others like hydroxycinnamic acid are linked with various cell components and more time is required for their penetration into the solvent. This could explain the low extraction of polyphenols in the first 15 minutes and their gradual increment [1]. On the other hand, polyphenols are prone to degradation if exposed to harsh conditions and long extraction

times, which could lead to reduction of their yield [17]. The values for total polyphenols yield in the 3 time points between 45 and 75 min were very close and mathematical modeling was necessary for prediction of the most effective extraction time.

The influence of solid to solvent ratio (w:v) is shown in Fig. 2. Among the ratios studied, the lowest yield of polyphenols was obtained with 1:20 (w:v). The highest concentration of investigated compounds was achieved with 1:80 (w:v) but the difference between values obtained with 1:80 and 1:40 was not statistically significant. The extraction process is characterized with mass transfer process, where the main driving force is concentration gradient between the solid and the solvent. The transition (moving) of components of solid matrix to the solvents continues until equilibrium of the system is reached. The equilibrium constant of the mass transfer process can be affected by increasing the solid to solvent ratio because the concentration gradient also increases. On the other hand increasing the solid to solvent ratio affects the active coefficient of components and their solubility in the solvent, and thus the yield of analytes is increased [18].

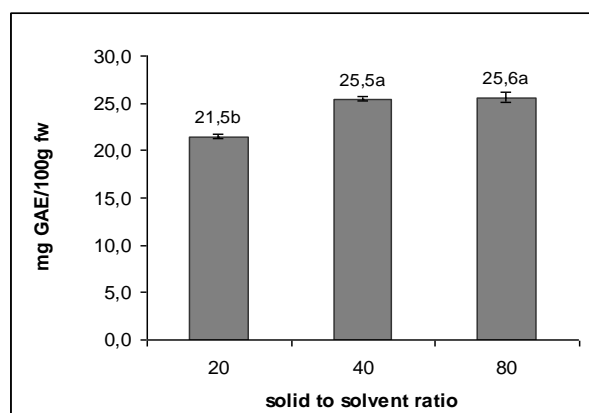


Fig. 2. Influence of ratio sample:solvent (w:v) on the yield of total polyphenols in freeze-dried tomato sample.

Kinetics of Extraction Process in Case of Solid-Liquid Extraction

The extraction processes are dynamic and therefore characterized with their own kinetics. The kinetics of the process is influenced by many factors such as plant matrices, shape and size of participle and especially by temperature and extraction time [19]. The extraction process starts with the crossing of the plant phenolic compounds of the matrix to the extractant. This process is characteri-

zed by rate constant k_1 , which includes a diffusion coefficient. In this case, the extraction of polyphenols for a certain time t can be described by the differential equation 1.

$$\frac{dz(t)}{dt} = -k_1 z(t) \quad (1)$$

where $z(t)$ is the amount of polyphenol remaining in the plant tissue, k_1 is the rate constant and t is time.

The extraction of the polyphenols can also be described as an accumulation in the extractant, and the degradation of the components for a given time t . Degradation is a process which is also characterized by a rate constant k_2 . These processes can be described by a differential equation 2.

$$\frac{dy(t)}{dt} = k_1 z(t) - k_2 y(t) \quad (2)$$

where $y(t)$ is the accumulation and at the same time the decomposition of polyphenols.

Since degradation and accumulation of phenolic compounds are simultaneous processes, they are described by the two differential equations (1 and 2). After mathematical processing, the following equations describing the whole process of extraction are derived:

$$z(t) = A_0 e^{-k_1 t} \quad (3)$$

$$y(t) = A_0 \frac{k_1}{k_2 - k_1} (e^{-k_1 t} - e^{-k_2 t}) \quad (4)$$

$$q(t) = A_0 \left(1 + \frac{k_2}{k_1 - k_2} e^{-k_1 t} - \frac{k_2}{k_2 - k_1} e^{-k_2 t} \right) \quad (5)$$

where $q(t)$ is the amount of degraded polyphenols time t .

$$t_{\max} = \frac{\ln \frac{k_1}{k_2}}{k_1 - k_2} \quad (6)$$

$$y_{\max} = A_0 \left(\frac{k_1}{k_2} \right)^{\frac{k_2}{k_1 - k_2}} \quad (7)$$

The proposed theoretical model describing the extraction and degradation of polyphenols is practically verified by the experimental data shown on Fig. 1. Accumulated experimental data approximated with equation (4) and equations (6) and (7)

are provided for maximum yields during extraction. Data are presented on Fig. 3.

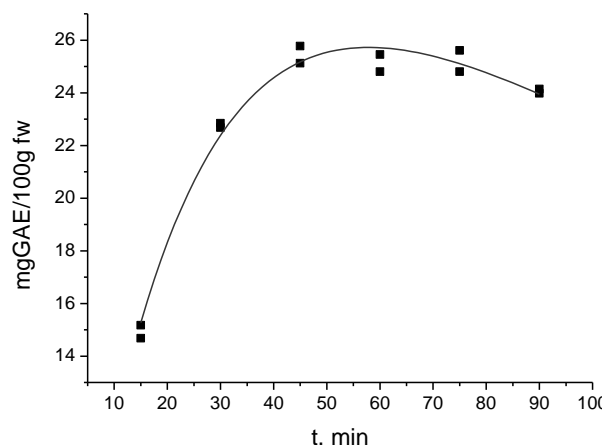


Fig. 3. Theoretical model of the influence of the extraction time on the yield of total polyphenols from tomato: $R^2 = 0.98599$; $A_0 = 34.60136 \pm 2.68647$; $K_1 = 0.04112 \pm 0.00466$; $K_2 = 0.00512 \pm 0.0013$; $t_{\max} = 57.87$ min; $y_{\max} = 25.73$ mg GAE/100g.

From Fig. 3 it is evident that the established theoretical model describes well the experimental data. Statistical processing were performed by the method of least squares and the correlation coefficient is $R^2 = 0.98599$, which shows that more than 98% of the experimental data are described by the model. The optimal extraction time t_{\max} is 57.87 min (6) and the optimal extraction yield of polyphenols y_{\max} is 25.73 mgGAE/100g fresh weight at the selected primary extraction conditions (temperature, solid to liquid/solvent ratio and type of extractant). The coefficient A_0 , known after solving equation (1) is a very important indicator of the model, which theoretically calculates the initial amount of total polyphenols in the matrix. The application of the model could provide valuable information about the theoretical contents of polyphenols in different varieties of tomatoes, and thus allow the choice of polyphenol-rich genotypes for the purposes of tomato breeding.

CONCLUSION

The main extraction parameters that affect extraction process of polyphenolic compounds in tomato were investigated. Maximum amounts of these components were obtained with 80% acetone at 60°C and 1:40 solid to solvent ratio. The kinetics of extraction was also studied. An equation showing what was the theoretical initial quantity of polyphenols in raw material was elaborated, which could be useful for the breeding programs of

varieties with high amount of polyphenol compounds.

Acknowledgements: The research leading to these results has received funding from National Science Fund under Bulgarian Ministry of Education and Science (grant № DMU03/76).

REFERENCES

1. M. Naczek, F. Shahidi, *J. Chromatogr. A*, **1054**, 95 (2004).
2. A. Crozier, B. Jaganath, M. Clifford, in: Phenols, Polyphenols and Tannins: An Overview in Plant Secondary Metabolites: Occurrence, Structure and Role in the Human Diet, A. Crozier, M. N Clifford, H. Ashihara (eds.), 2006.
3. J. H. Makoi, P. A. Ndakidemi, *Afr. J. Biotechnol.*, **6**, 1358 (2007).
4. P. G. Pietta, *J. Nat. Prod.*, **63**, 1035 (2000).
5. C. Iwamura, K. Shinoda, M. Yoshimura, Y. Watanabe, A. Obata, T. Nakayama, *Cells Allergol. Int.*, **59**, 1 (2010).
6. S. Mukhopadhyay, D. L. Luthria, R. J. Robbins, *J. Sci. Food Agr.*, **86**, 156 (2006).
7. M. G. Willits, C. M. Kramer, R. T. Prata, V. De Luca, B. G. Potter, J. C. Steffens, G. Graser, *J. Agric. Food. Chem.*, **53**, 1231 (2005).
8. R. K. Toor, C. E. Lister, G. P. Savage, *Int. J. Food Sci. Nutr.*, **56**, 597 (2005).
9. S. Grozeva, A. Atanasova, P. Denev, D. Ganeva, M. Krachanova, I. Tingovska, *Agrochimica*, **57**, 337 (2013).
10. I. Martinez-Valverde, M. J. Periago, G. Provan, A. Chesson, *J. Sci. Food Agric.*, **82**, 323 (2002).
11. K. Helmja, M. Vaher, J. Gorbatšova, M. Kaljurand, *Proc. Estonian Acad. Sci. Chem.*, **56**, 172 (2007).
12. E. Sarnchez-Rodriguez, M. Rubio-Wilhelmi, L. M. Cervilla, B. Blasco, J. Rios, M. A. Rosales, L. Romero, J. M. Ruiz, *Plant Sci.*, **178**, 30 (2010).
13. J. Dai, R. J. Mumper, *Molecules*, **15**, 7313 (2010).
14. B. Druzynska, A. Stepniewska, R. Wołosiak, *Acta Sci. Pol. Technol. Aliment.*, **6**, 27 (2007).
15. K. Gyenai, N. Mikiashvili, H. Ismail, M. Worku, *Am. J. Anim. Vet. Sci.*, **7**, 126 (2012).
16. V. Singleton, J. Rossi, *Am. J. Enol. Vitic.*, **16**, 144 (1965).
17. L. Y. Nig, Y. K. Ang, H. E. Khoo, H. S. Yim, *J. Phytochem.*, **6**, 61 (2012).
18. Y. C. Shen, S. Chen, S. Zhuang, C. Wang, *J. Food Sci.*, **73**, 1 (2008).
19. P. W. Tan, C. P. Tan, C. W. Ho, *Int. Food Res. J.*, **18**, 557 (2011).

ОПТИМИЗАЦИЯ НА КЛЮЧОВИ ПАРАМЕТРИ НА ЕКСТРАКЦИЯ НА ФЕНОЛНИ КОМПОНЕНТИ ОТ ДОМАТЕНИ ПЛОДОВЕ (*Solanum lycopersicum* L.). КИНЕТИКА НА ПРОЦЕСА.

А. Х. Атанасова¹, П. Н. Денев^{2*}, И. И. Тринговска¹, С. Й. Грозева¹, Д. Г. Ганева¹, М. Г. Крачанова², И. Н. Панчев³

¹Институт по зеленчукови култури „Марица“, ул. Брезовско шосе 32, 4003 Пловдив, България

²Институт по Органична химия с Център по Фитохимия, Българска Академия на Науките, 4000 Пловдив, България

³Университет по хранителни технологии, ул. Марица 26, 4000 Пловдив, България

Постъпила на 20 май 2014 г.; Коригирана на 24 юни 2014 г.

(Резюме)

Проучени бяха основните параметри, оказващи влияние върху процеса на екстракция на полифеноли от домати плодове. Най-подходящ разтворител, с който се достигна максимален добив на полифеноли от плодовете, беше смес от ацетон и вода в съотношение 80:20 (v:v). Използвайки този разтворител, концентрацията на търсените компоненти е приблизително 17% по-висока в сравнение с етанол и метанол. Оптималните време на екстракция, температурата и хидромодел (съотношение проба-екстрагент) бяха съответно 45 мин, 60°C и 1:40. Използвайки оптималните параметри на екстракция, добивът на полифенолни вещества от домати плодове сорт Desperado достигна 27.80 GAE/100g свежо тегло. Кинетиката на екстракционния процес също беше проучена и бе предложен теоретичен модел, описващ екстракционния процес. Този математически модел дава сведения за първоначалното съдържание (теоретично изчислено) на търсените компоненти в домати плодове, което може да бъде използвано успешно за нуждите на селекцията.

Purification and biological activity of pectic polysaccharides from leek

M. Nikolova¹, M. G. Kratchanova^{1*}, E. V. Pavlova¹, I. Ianakieva¹, V. Kussovski²

¹Laboratory of Biologically Active Substances, Institute of Organic Chemistry with Centre of Phytochemistry, Bulgarian Academy of Sciences, 139 Ruski blv., 4000 Plovdiv, Bulgaria

²Institute of Microbiology, Bulgarian Academy of Sciences, Acad. G. Bonchev str., bl. 26, 1113 Sofia, Bulgaria

Received May 20, 2014; Revised July 04, 2014

Dedicated to Acad. Dimiter Ivanov on the occasion of his 120th birth anniversary

The pectic polysaccharides isolated from leek through consecutive water and acid extractions with 0.5% HCl were purified by ion-exchange chromatography on DEAE-Sepharose fast flow. As a result four fractions – W₁, A₁, A₂ and A₃ were obtained, which were partitioned with gel-chromatography on Sephadex G-200 and other fractions were obtained - W₁₁, A₁₁, A₂₁ and A₃₁. All fractions differ on their monosaccharide compositions. In the A₁ fraction obtained through chromatography purification of the acid-extractable polysaccharides prevail neutral sugars (> 58%) whereas the other fractions have higher uronic acid content. It was found that fractions having higher uronic acid content also contain glucuronic acid. The dominant neutral monosaccharides in the pectic polysaccharides from leek are galactose and rhamnose. The molecular mass and the polydispersity of the polysaccharide fractions were determined by HPLC. The purified polysaccharide fractions from leek showed immunomodulating activity, which was determined by the alternative and classical pathway. The activity of the purified polysaccharides increase compared to the activity of the initial polysaccharides.

Key words: pectic polysaccharides, purification, biological activity, leek

INTRODUCTION

The effect of pectic polysaccharides on the physiological processes in the human body, such as lipid exchange [1-4], carbohydrate exchange [2], bile acid metabolism [5,6], etc. has been the subject of a host of experimental and clinical observations. It has been found by international [1,3,7] and local [8,9] studies that the intake of pectin significantly reduces the serum cholesterol levels in the body, which is especially important in cardiovascular diseases. Other biological activities of the pectic polysaccharides, such as immunomodulating, anti-complementary and anti-inflammatory, have also been reported in the recent years [10-13].

Two pectic polysaccharides - W₀ and A₀, were obtained through sequenced water and acid extraction with 0.5% HCl in the course of our previous studies [14]. They were characterised and identified as polysaccharides of a pectic type with a pronounced immunomodulating activity. Definitely, the individual structural fragments from the macromolecule of leek influence on its immunomodulating activity after enzymatic hydrolysis. Obtained hydrolysis products rich in RG-I participated in the activation process of the immune

system [15]. The purification process played an important role in determining the relationship between the structure of the polysaccharides and their biological properties. The purification of the active polysaccharides was carried out through various chromatographic methods depending on the composition of the crude polysaccharides.

The aim of this work was chromatographic purification by means of ion-exchange and gel chromatography of the biologically active pectic polysaccharides from leek and the comparison of their immunomodulating activities.

EXPERIMENTAL

The trials were carried out with leek (*Allium porrum* L.) purchased on the vegetable market. The alcohol insoluble substances (AIS) of leek were obtained by the method described in a previous article of us [16].

Isolation and purification of polysaccharides from leek

Two pectic polysaccharides were isolated by means of a sequenced water and acid extraction with 0.5% HCl from the AIS of leek. The purification procedure is presented in Fig. 1.

* To whom all correspondence should be sent:
E-mail: lbas@plov.omega.bg

The two isolated polysaccharides W_0 and A_0 were subjected to fractionating by means of ion-exchange chromatography on a DEAE-Sepharose fast flow using a semipreparative chromatographic system Pharmacia, Sweden, equipped with a XK 2.6/40 cm column (Pharmacia, Sweden). The eluent was a buffer solution of sodium acetate with pH=4.8 and a linear gradient (0.05-1.0 M). The elution rate was 1 ml/min. Fractions of 10 ml were collected and analyzed for content of neutral sugars and galacturonic acid.

120 mg of polysaccharide B_0 were diluted in 15 ml sodium acetate buffer (pH=4.8), and the solution was centrifuged at 15 000 rpm. 10 ml of the obtained supernatant containing 66.5 mg of B_0 was applied to a column with DEAE-Sepharose fast flow. Chromatography on the polysaccharide led to the emergence of a peak - W_1 , which was collected, dialyzed for 48 h against distilled water and lyophilized on a Cryodos 50 system (Telstar, Spain).

120 mg of polysaccharide A_0 were dissolved in 15 ml sodium acetate buffer (pH=4.8) and the solution was centrifuged at 15 000 rpm. 10 ml of the supernatant containing 71.7 mg of polysaccharide A_0 were subjected to chromatographic purification on a DEAE-Sepharose fast flow. Chromatography on A_0 led to the distinction of three peaks: A_1 , A_2 , A_3 , respectively. The isolated peaks were collected, dialyzed for 48 h against distilled water and lyophilized on a Cryodoc 50 system (Telstar, Spain).

The chromatographically purified fractions W_1 , A_1 , A_2 and A_3 were subjected to gel chromatographic separation on Sephadex G-200, on column XK 1.6/100 cm (Pharmacia, Sweden). The eluent was phosphate buffer (pH=6), and the elution rate was 0.2 ml/min. Fractions of 10 ml were collected in the process of elution and were analyzed for neutral sugars and galacturonic acid.

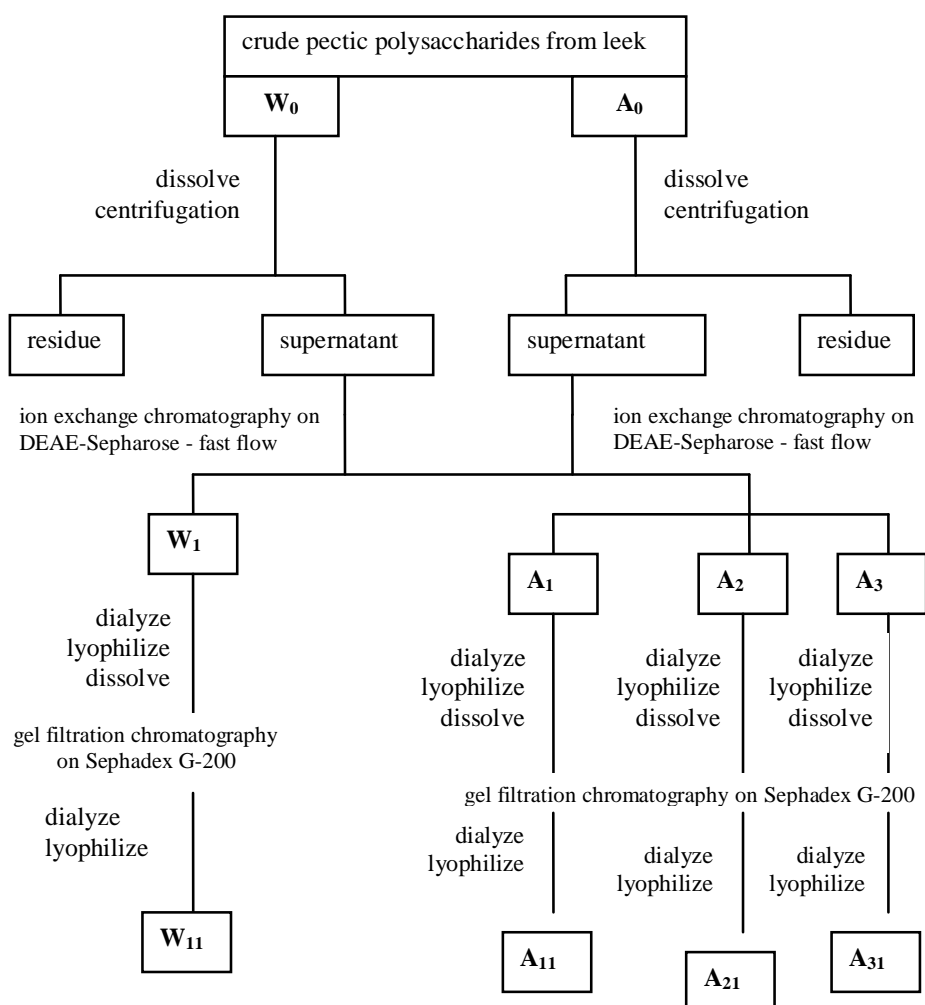


Fig. 1. Purification procedure of anti-complementary pectic polysaccharides from leek.

60 mg of each purified fraction (W_1 , A_1 , A_2 and A_3) were dissolved in 8 ml distilled water. 7 ml of the solution obtained (containing a sample of 52.2 mg) was applied to a column with Sephadex G-200. Fractions W_{11} , A_{11} , A_{21} and A_{31} were isolated during the gel chromatography separation. Each fraction was collected, dialyzed for 48h and lyophilized.

Major analytical methods

Assessment of the total neutral sugars, uronic acids, and protein

The total neutral sugars and uronic acids were assessed by the orcinol [17] and meta-hydroxybiphenyl methods [18], respectively, using arabinose and galacturonic acid as a standard. The separation of galacturonic acid and glucuronic acid was implemented on a Waters HPLC system with RI detector – R401. HPLC analysis was conducted on an Aminex HPX - 87H column with 0.04M H_2SO_4 and the elution rate was 0.3 ml/min. Galacturonic acid and glucuronic acid were identified by the retention time.

The protein content was analyzed by the Lowry method [19] against a standard of bovine serum albumin.

Determination of neutral sugars

Neutral sugars were measured as alditol acetates after hydrolysis. The crude extracted pectic polysaccharides (20 mg) were pretreated with 2M trifluoroacetic acid (TFA) for 3 h at 120°C before conversion to alditol acetates according to the method developed by Blakeney *et al.* [20].

The monosaccharide composition of the pectic polysaccharides was determined by HP gas chromatograph 6890 Series Plus coupled with a 5973 mass-selective detector (Helwett–Packard, Palo Alto, CA), on a column SP-2380 (Supelco). The oven temperature was programmed to 200°C for 3 min, then to 250°C with a rate of 5°C/min. Helium was carrier gas at 1 ml/min. Peak identification was based on retention times, using myo-inositol as internal standard.

Determination of molecular mass

The molar masses of the polysaccharides were assayed through HPSEC on a Waters (Millipore) system. The assay was made on Ultrahydrogel™ 120 and Ultrahydrogel™ 500 column (7.8 x 300 mm, Waters) with bidistilled water as eluent at an elution rate of 0.8 ml/min. The column was

calibrated using the Shodex standard P-82 (Showa DENKO, Japan).

Determination of anti-complementary activity

Complement activity was measured using a microassay method according to Klerx *et al.* [21,22]. The test is based on the colorimetric measurement of hemoglobin released from target erythrocytes after incubation with normal human serum. In the classical pathway assay (CP), veronal buffered saline (25 mM, pH 7.4) containing 0.15 mM $CaCl_2$ and 0.5 mM $MgCl_2$ served as an diluent. Sheep red blood cells (SRBC) sensitized with rabbit anti-SRBC antibodies at a concentration of 2×10^8 cells/ml were used as targets. In the alternative pathway (AP) assay, uncoated (without anti-RRBC antibodies) rabbit erythrocytes (RRBC) at a concentration of 1×10^8 cells/ml as targets were used. Activation of the calcium-dependent classical pathway is prevented by the addition of calcium chelator ethyleneglycol-bis(2-aminoethyl) tetraacetic acid (EGTA) to the assay veronal buffer containing 5 mM $MgCl_2$ and 8 mM EGTA.

The effect of polysaccharides on complement activity was determined after pre-incubation for 45 min at 37°C of equal volumes of normal human serum (dilution giving about 50% lysis of the target cells) and two-fold dilutions of polysaccharides (usually starting with 2 mg/ml). After incubation (1.5h at 37°C) of target erythrocytes and treated sera, hemolysis in cell supernatants was measured at 541 nm. The anti-complementary activity of the samples was expressed as the percentage inhibition of the total complement hemolysis (TCH_{50}) of the control serum given by the formula:

$$\text{Inhibition of } TCH_{50} (\%) = [(TCH_{50} \text{ of control serum} - TCH_{50} \text{ treated with pectin serum}) / TCH_{50} \text{ of control}] \times 100.$$

RESULTS AND DISCUSSION

The isolated pectic polysaccharides, obtained by a sequenced extraction with water were name W_0 and 0.5% hydrochloric acid were name A_0 from AIS of leek, were purified by the procedure shown in Fig. 1.

The polysaccharides were applied to a column with ion-exchange resin DEAE–Sepharose – fast flow and eluted with sodium acetate buffer at a linear gradient (0.05-1.0 M). One fraction, W_1 , was obtained from the water extractable polysaccharide, while three fractions, A_1 , A_2 , A_3 (Fig. 2), were obtained from the acid extractable polysaccharide.

The chemical composition of these fractions is presented in Table 1.

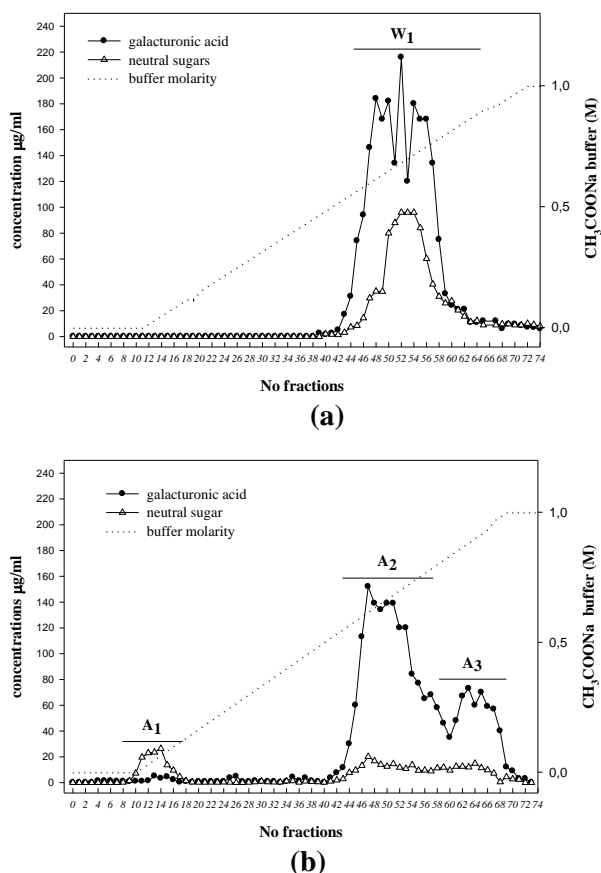


Fig. 2. Elution profile of water extractable (a) and acid extractable (b) pectic polysaccharides on DEAE-Sephacrose fast flow.

The water extractable purified fraction – W_1 had a high content of uronic acids 66.4% (59.7% galacturonic acid and 6.7% glucuronic acid). Galactose (21.2%) was the prevailing neutral monosaccharide in the composition of W_1 .

Fraction A_1 from the acid extractable polysaccharide contained mostly neutral monosaccharides (59.9%) and 38.8% uronic acids, as it can be seen from Table 1. No glucuronic acid was found in this fraction. This polysaccharide had a high molecular mass and the major neutral monosaccharide was galactose (47%). Most probably, it was a polysaccharide of galactan type.

The other two fractions A_2 and A_3 were acidic polysaccharides because they had a higher content of uronic acids: 50.5% and 61.2%, respectively. In both polysaccharides (A_2 and A_3), glucuronic acid was found in addition to galacturonic acid, as it occurred in higher amounts in A_3 . Galactose and rhamnose accounted for the largest share of the monosaccharide.

Dialyzed and lyophilized polysaccharide fractions purified by ion-exchange chromatography (W_1 , A_1 , A_2 and A_3) were subjected to gel chromatography on Sephadex G-200. Each fraction was eluted with a phosphate buffer at pH=6, where fractions W_{11} , A_{11} , A_{21} and A_{31} were obtained (Fig. 3).

Fraction W_{11} was characterized by a higher content of galacturonic acid than W_1 and a lower quantity of glucuronic acid (Table 2). The nonuronic ingredients of W_{11} were dominated by the galactose monosaccharide.

In the purified fraction A_{11} the amount of galacturonic acid increased from 38.8% in A_1 , to 50.7%, respectively. Total neutral monosaccharide in the purified fraction A_{11} was 48.0% mostly that of galactose (42.8%). In the other two SEC purified acidic polysaccharides - A_{21} and A_{31} , a lower content of glucuronic acid was obtained as compared with A_2 and A_3 . As for the nonuronic monosaccharide, the rhamnose content in A_{31} increased to 16.3% in comparison with A_3 (10.7%).

The polysaccharide fraction A_{21} was dominated by the monosaccharide galactose.

Table 1. Chemical compositions of purified anti-complementary extractable polysaccharides on DEAE-Sephacrose fast flow.

	W_1	A_1	A_2	A_3
Uronic acid, %	66.4	38.8	50.5	61.2
Total neutral sugar, %	33.1	59.9	48.0	37.8
Protein, %	0.5	1.3	1.5	1.0
Monosaccharides composition, %				
Rhamnose	5.8	8.2	16.0	10.7
Arabinose	5.2	4.2	8.0	2.5
Xylose	0.8	-	0.4	0.5
Mannose	trace	trace	trace	trace
Galactose	21.2	47.0	19.2	23.6
Glucose	trace	trace	4.5	trace
Galacturonic acid	59.7	38.8	41.2	43.5
Glucuronic acid	6.7	-	9.3	17.7

Table 2. Chemical compositions of purified anti-complementary extractable polysaccharides on Sephadex G-200.

	W ₁₁	A ₁₁	A ₂₁	A ₃₁
Uronic acid, %	66.2	50.7	60.6	67.1
Total neutral sugar, %	33.4	48.0	38.2	31.9
Protein, %	0.4	1.3	1.2	1.0
Monosaccharides composition, %				
Rhamnose	0.6	2.2	5.0	16.3
Arabinose	0.9	1.0	6.2	trace
Xylose	0.8	-	0.4	0.5
Mannose	trace	trace	trace	trace
Galactose	27.9	42.8	24.4	15.1
Glucose	3.2	2.4	2.2	trace
Galacturonic acid	61.6	50.7	53.7	58.2
Glucuronic acid	4.6	-	6.9	8.9

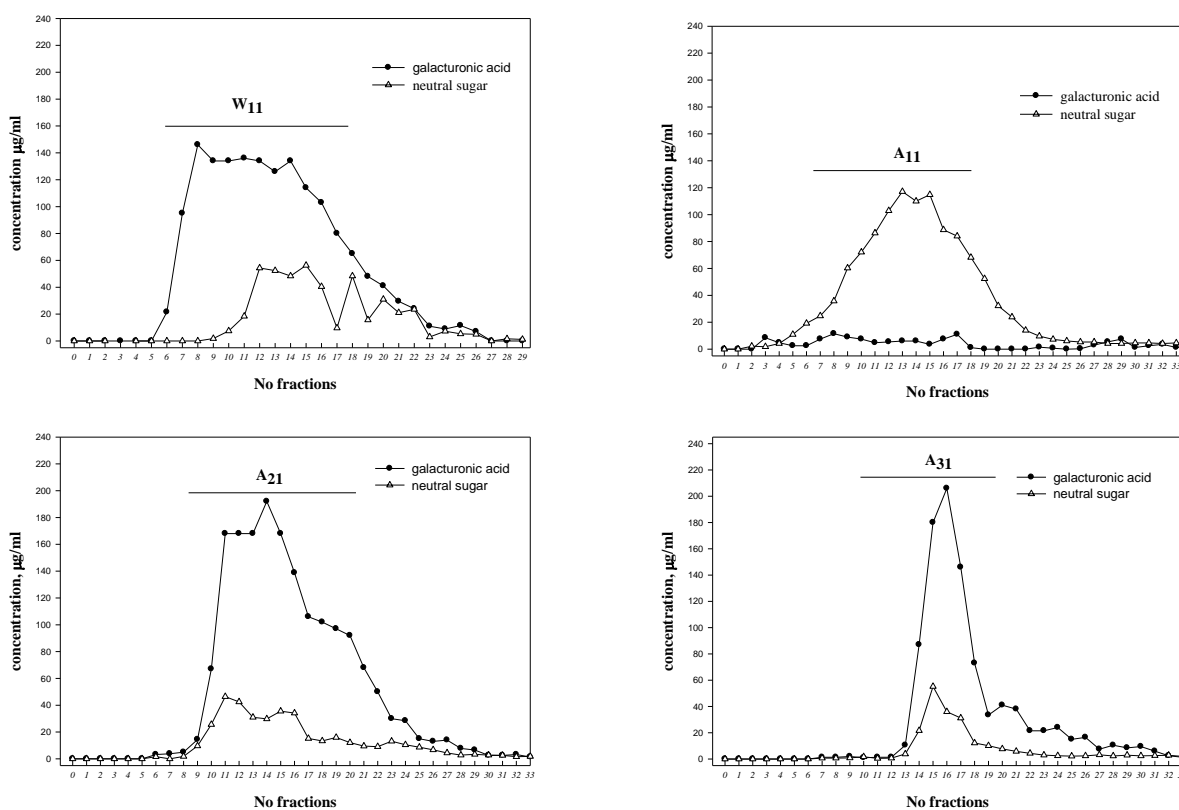


Fig. 3. Elution profile of purified pectic polysaccharides on Sephadex G-200.

The follow-up analyses of the purified samples were related to determining their molecular mass values and their molecular homogeneity (Fig. 4). Fractions W₁ and W₁₁ obtained as a result of the purification and separation of the water-extractable pectic polysaccharide had the highest molecular mass, as well as the highest homogeneity.

Fractions A₁ and A₁₁ made up mostly of neutral monosaccharide showed a high molecular mass and were considerably more homogeneous than the other polysaccharide fractions of the acid extractable pectic polysaccharide. Fractions A₂ and A₂₁ had a higher molecular mass than A₃ and A₃₁.

All polysaccharides tested had some activity in complement-fixation test (Fig. 5). The fractions W₀ and W₁ showed the same low activity. W₁₁ was significantly more active than W₀ and W₁. Neither the anticomplementary activity values of A₀, A₁, and A₂ nor those of A₃ showed significant differences. A₁₁, A₂₁ and A₃₁ were the most active fractions.

The obtained results indicate that the activation of the complement system by these polysaccharides occurs *via* both the classical and alternative pathways.

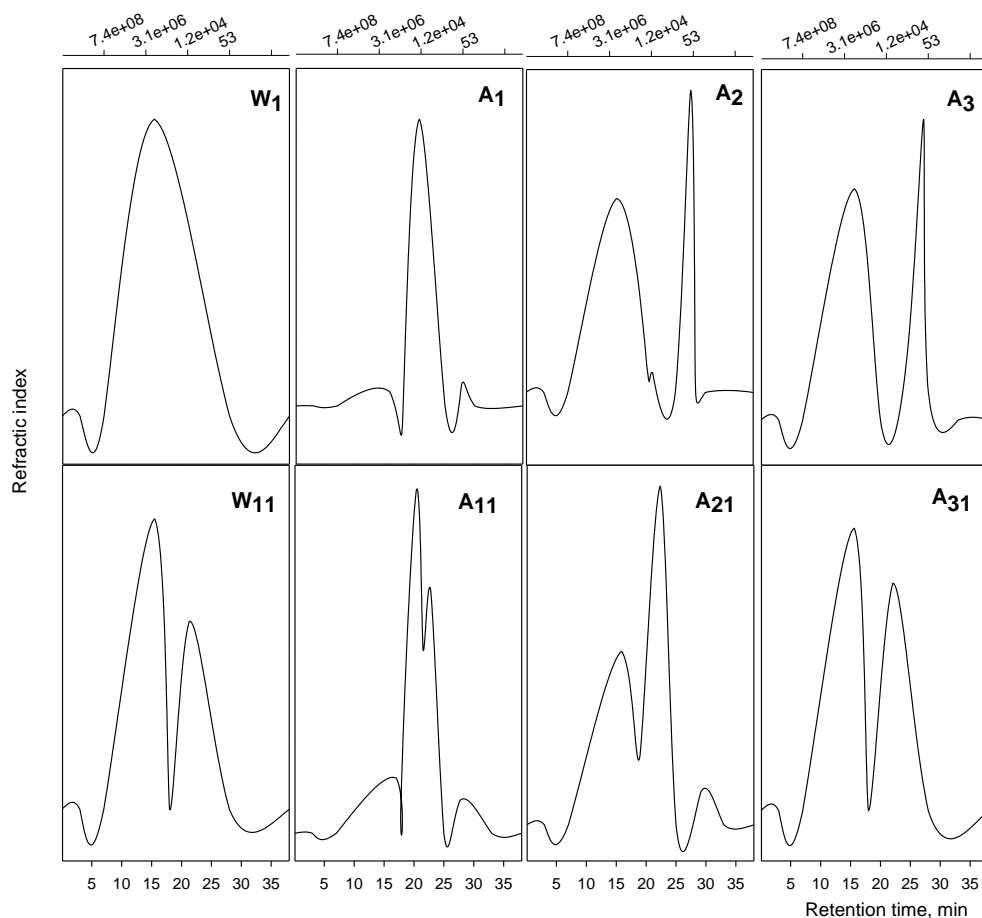


Fig. 4. HPSEC elution patterns to molecular weight of purified on DEAE-Sephacrose fast flow and Sephadex G-200 pectic polysaccharides from leek.

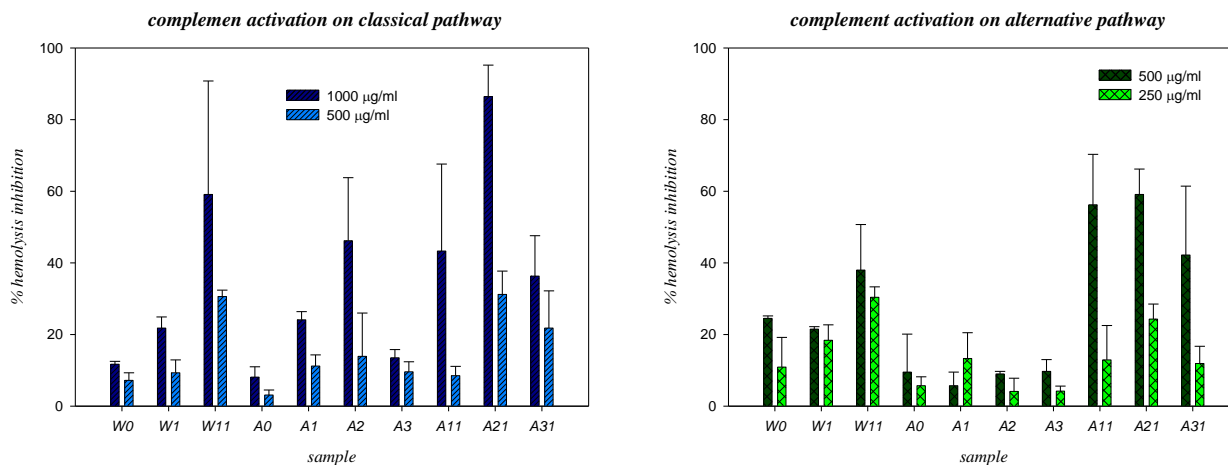


Fig. 5. Immunomodulating activity of purified pectic polysaccharides from leek.

CONCLUSION

It was found, based on the analysis of the polysaccharide fractions obtained by ion-exchange and gel chromatography, that fractions A₂ and A₃ had a higher uronic acid content. The composition of those uronic acids included galacturonic acid

and glucuronic acid. In the process of ion-exchange chromatography, a fraction was isolated that had a high content of neutral monosaccharides, such as fraction A₁ (59.9% neutral sugars). This fraction contained 47.0% galactose. Most probably, there was a presence of galactan type of polysaccharide in the leek.

The analyzed polysaccharide fractions that were by ion-exchange and gel chromatography purified were characterized by a pronounced biological activity which increased in comparison with the source polysaccharides.

Acknowledgements: This work was funded by project No BG161PO003-1.1.05-0024-C0001 "Development of nutraceuticals with antioxidant and immune-stimulating action" of Operational Program "Competitiveness" of the EU.

REFERENCES

1. M. Fernandes, D. M. Sun, M. A. Tosca, D. J. McNamara, *A.m. J. Clin. Nutr.*, **59**, 869 (1994).
2. R. D. Hopewell, R. Yeater, I. Ullrich, *Prog. Food. Nutr. Sci.*, **17**, 159 (1993).
3. M. Thorogood, R. Carter, L. Benfield, *Brit. Med. J.*, **259**, 351 (1987).
4. A. S. Truswell, A. C. Beynen, in: Dietary Fibre, A component of Food Nutritional Function in Health and Disease, Schweizer T.F., Edwards C. A. (eds.), Springer Verlag, 1999.
5. C. Huang, N. Dural, *J. Food Process. Eng.*, **18**, 234 (1995).
6. T. Ide, M. Horil, K. Kawasluma, T. Yamamoto, *Br. J. Nutr.*, **62**, 539 (1989).
7. T. D. Hockaday, *Scand. J. Gastr. Suppl.*, 124 (1987).
8. J. Grudeva, M. Kratchanova, I. Panchev, C. Kratchanov, *Z. Lebensm. Unters. F. A.*, **204**, 374 (1997).
9. J. Grudeva-Popova, M. Kratchanova, A. Djurdjev, C. Kratchanov, *Folia Medica*, **XXXIX**, 1 (1997).
10. R. Labadie, in: Bioactive natural products, S. M. Colegate, R. S. Molyneux (eds.), CRC Press Inc. London, 1993, p. 297.
11. A. Sendi, N. Mulinacci, F. Vincieri, H. Wagner, *Phytochemistry*, **34**, 1357 (1993).
12. R. Srivastara, D. K. Kulshrestha, *Phytochem.*, **28**, 2877 (1989).
13. H. Yamada, H. Kiohara, T. Matsumoto, in: Advances in Pectin and Pectinase Reserch, F. Voragen, H. Schols, R. Visser (eds.), The Netherlands: Kluwer Academic Publishers, 2003, p. 481.
14. M. Kratchanova, M. Nikolova, E. Pavlova, I. Yanakieva, V. Kussovski, *J. Sci. Food Agr.*, **90**, 2046 (2010).
15. M. Ognyanov, M. Nikolova, I. Yanakieva, V. Kussovski, M. Kratchanova, *J. BioSci. Biotech. SE/ONLINE*, **2**, 13 (2013).
16. M. Kratchanova, M. Gocheva, E. Pavlova, I. Yanakiev, D. Nedelcheva, V. Kussovski, A. Slavov, *Bulg. Chem. Commun.*, **40**, 561 (2008).
17. D. W. F. Shannon, *Analyst*, **97**, 209 (1972).
18. M. Blumenkrantz, G. Asboe-Hansen, *Anal. Biochem.*, **54**, 484 (1973).
19. O. H. Lowry, N. J. Rosenbrough, A. L. Farr, R. L. Randall, *J. Biol. Chem.*, **193**, 265 (1951).
20. A. Blakeney, P. Harris, R. Henry, B. Stony, *Carbohydr. Res.*, **113**, 291 (1983).
21. J. P. A. M. Klerx, C. J. Beukelman, V. H. Dijk, J. M. N. Willers, *J. Immunol. Methods*, **63**, 215 (1983).
22. J. P. A. M. Klerx, C. J. Beukelman, H. V. Dijk, F. J. Van Overveld, W. J. Van der Maaden, J. M. N. Willers, *Infect. Immun.*, **49**, 841 (1985).

ПРЕЧИСТВАНЕ И БИОЛОГИЧНА АКТИВНОСТ НА ПЕКТИНОВИ ПОЛИЗАХАРИДИ ОТ ПРАЗ

М. Николова¹, М. Крачанова^{1*}, Е. Павлова¹, И. Янакиева¹, В. Късовски²

¹Лаборатория Биологично Активни Вещества, Институт по Органична химия с Център по Фитохимия, Българска Академия на Науките, бул. Руски 139, 4000 Пловдив, България

²Институт по микробиология, Българска Академия на Науките, ул. Акад. Г. Бончев, бл. 26, 1113 София, България

Постъпила на 20 май 2014 г.; Коригирана на 04 юли 2014 г.

(Резюме)

Осъществено е хроматографско пречистване на пектинови полизахариди от праз, изолирани при последователно екстрахиране с вода и 0,5% солна киселина. Посредством йонообменна хроматография върху DEAE-Sephagrose fast flow от водно и киселинно екстрахируемите полизахариди се получават четири фракции – W₁, A₁, A₂ и A₃, всяка от които е гел хроматографски пречистена на Sephadex G-200, при което са обособени фракциите W₁₁, A₁₁, A₂₁ и A₃₁. Тези фракции се различават по монозахаридния си състав. Във фракцията K₁, получена при йонообменното пречистване на киселинния екстракт, преобладават неутралните захари (> 58%), докато останалите фракции са с високо уронидно съдържание. Установено е, че високо уронидните фракции съдържат и глюкуронова киселина. Доминиращи монозахариди в пектиновите полизахариди от праз са галактоза и рамноза. Чрез HPLC е определена молекулна маса на полизахаридните фракции и тяхната дисперсност. Хроматографски пречистените полизахаридни фракции от праз показват имуномодулираща активност, определена чрез активиране на комплемента по класическия и алтернативния път. В сравнение с изходните полизахариди, активността на пречистените се увеличава.

Chemical composition and anti-complementary activity of enzyme-modified citrus pectins

M. H. Ognyanov¹, Y. N. Georgiev¹, I. Z. Yanakieva¹, V. K. Kussovski², M. G. Kratchanova^{1*}

¹Laboratory of Biologically Active Substances, Institute of Organic Chemistry with Centre of Phytochemistry, Bulgarian Academy of Sciences, 139 Ruski blv., 4000 Plovdiv, Bulgaria

²Department of Infectious Microbiology, Institute of Microbiology, Bulgarian Academy of Sciences, Acad. G. Bonchev str., bl. 26, 1113 Sofia, Bulgaria

Received July 03, 2014; Revised July 26, 2014

Dedicated to Acad. Dimiter Ivanov on the occasion of his 120th birth anniversary

A consecutive enzyme modification of citrus pectin series with *endo*-polygalacturonase (EPG) and combination of β -galactosidase and *endo*- β -(1 \rightarrow 4)-galactanase was conducted. Alcohol precipitation with two volumes of 96% ethanol was used for fractionation of the enzyme hydrolyzate, resulting to recover of alcohol-insoluble and alcohol-soluble (AS) parts. Alcohol-precipitated (AP) rhamnase-enriched fragments were obtained after homogalacturonan (HG) degradation with EPG. Furthermore, it was found that citrus pectins contained xylogalacturonan fragments liberated after EPG treatment. After modification with galactan-degrading enzymes galactose content was reduced between 50-89%, which confirmed predominance of β -(1 \rightarrow 4)-linked galactose in ramified hairy regions of citrus pectins. Anti-complementary activity of investigated pectins was higher through the classical pathway in comparison with alternative ones. Enzyme modification influenced to different extent on the anti-complementary activity. Alcohol precipitation approach led to obtaining of complex mixtures with pectic fragments, hindering the interpretation of biological activity results.

Key words: citrus pectin, enzyme modification, pectinases, monosaccharide composition, immunomodulating polysaccharides

INTRODUCTION

Citrus peels are very rich in pectic constituents and are one of the best sources for commercial pectin production. Pectin is used mainly as a gelling agent in the food industry for manufacturing of jams, jellies and marmalades [1]. As well as pectin has potential uses in many other fields such as pharmaceutical and healthy supplement. For example, modified citrus pectin (MCP) obtained by acid, alkali or enzymatic treatment possesses considerable therapeutic effects on tumor metastasis and apoptosis in experimental animal models and in clinical trials with humans [2]. Regarding the study of anti-complementary activity of citrus pectins there is no enough investigation. During the past few years many efforts for MCP preparation were referred to application of enzymatic and physicochemical techniques. Alcohol precipitation is a method used for isolation and fractionation of polysaccharides from different extracts and at the same way for purification from low molecular weight substances. This approach is used also for isolation of GalA oligomers with different degree

of polymerization after EPG treatment [3,4]. Additionally, alcohol precipitation was used also for separation of mono- and oligosaccharides from stepwise acid hydrolyzed pectic polysaccharide from Siberian fir [5]. In our work alcohol precipitation was used for separation of enzyme-modified high molecular weight fragments from low molecular weight mono- and oligomers. In our previous publication we described the chemical composition, molecular weight and complement-fixing activity of initial water- and acid-extracted orange and lemon peel pectins. All investigated pectins were modified by EPG and AP residues were assessed for their anti-complementary potential [6]. In other earlier studies, Kratchanova *et al.* [7-9] have established a favorable effect of microwave pre-treatment of fresh citrus peels on the yield and quality of pectin. Data on the influence of microwave heating on biological activity was not published.

The aim of the present study was to further elucidate the composition and anti-complementary activity of enzymatic modified by EPG and galactan-degrading enzymes orange and lemon peel pectins, obtained through extraction from alcohol-insoluble solids (AIS) or microwave pretreatment.

* To whom all correspondence should be sent:

E-mail: lbas@plov.omega.bg

© 2014 Bulgarian Academy of Sciences, Union of Chemists in Bulgaria

EXPERIMENTAL

Preparation of AIS

AIS from orange and lemon peels were prepared as described previously [6].

Microwave pretreatment of fresh orange peels

Fresh orange peels (200 g) were placed in a glass vessel and heated in a microwave oven with duration of exposure 10 min, power 0.63 kW, and operating frequency 2450 MHz. Microwave treatment conditions were selected according to Kratchanova *et al.* [9].

Sequential extraction

Sequential extraction of AIS from orange and lemon peels as well as from microwave pretreated fresh orange peels with hot water and 0.5% hydrochloric acid was carried out as previously reported [6]. Water- and acid-extracted orange (WEOP and AEOP), lemon (WELP and AELP) pectins as well as microwave pretreated (AEOP MW) were obtained.

Enzymatic hydrolysis

All enzymes used in these experiments were commercially prepared and were purchased from Megazyme International Ireland Ltd. (Bray, Co. Wicklow, Ireland). They were used without further purification. EPG modification was carried out as previously described elsewhere with slight modification [6]. Briefly: saponified orange or lemon pectins (5 mg/ml) were dissolved in 50 mM sodium acetate buffer (pH 5.0) and incubated with 0.042 IU/5 mg pectin at 40°C for 24 h. Further AP residues after EPG treatment were modified by galactan-degrading enzymes. Modification was performed by combination of *endo*- β -(1 \rightarrow 4)-galactanase (2.5 IU/5 mg substrate) and β -galactosidase (0.8 IU/5 mg substrate) at 40°C for 24 h according to Ognyanov *et al.* [10]. After this modification AP residues were obtained. All enzyme units for applied modifying enzymes were selected after some pretests at different enzyme dosages with saponified AEOP. According to the final kinetic investigation (data not included) the most significant changes in the saponified AEOP after EPG modification were until 7 h. For the subsequent modification with β -(1 \rightarrow 4)-D-Gal-releasing enzymes the most significant changes were observed until 2 h.

Monosaccharide composition

Determination of neutral monosaccharides and glucuronic acid content of AP enzyme-modified pectins were carried out after CF₃CO₂H acid hydrolysis by HPLC without derivatization as previously described else-where [6]. Sugar composition analysis of alcohol-soluble parts was done without acid hydrolysis. Anhydrouronic acid content (AUAC) was assayed by *m*-hydroxy-biphenyl method [11]. Galacturonic acid was calculated on the base of difference between total anhydrouronic acid content and glucuronic acid.

Size-exclusion chromatography (SEC)

SEC was performed on Pharmacia Biotech system. Two milliliters of each sample (3 mg/ml) were centrifuged and loaded on HK 16/100 column filled with Sephacryl S-300 HR and eluted with 0.05 M NaOAc buffer (pH=5.0) at 1.0 ml/min flow rate. Fractions (5.0 ml) were collected and analyzed for uronic acids by a microplate variant of carbazole-sulfuric acid method, using D-GalA as a standard [12]. Additionally molecular weight of separated fractions was determined, using dextran standards (35-200 kDa).

Anti-complementary activity

Anti-complementary activity of alcohol-insoluble residues was measured through the classical and alternative pathway, using a micro-assay method, according to Klerx *et al.* [13]. The anti-complementary activity of the samples was expressed as a percentage inhibition of the total complement hemolysis (TCH₅₀) of target rabbit and sensitized mutton erythrocytes from normal human serum.

RESULTS AND DISCUSSION

In a previous publication we reported sequential extraction of water- and acid-soluble pectins from AIS of orange and lemon peels. Data on the content and further chemical characterization of the initial pectins were published elsewhere [6]. Furthermore in the case of microwave treated peels a higher yield of pectin (5.18% on the fresh peel base) was obtained in comparison with both AIS (4.70%) and control directly dried peels (3.47%). This observation was in agreement with the results published by Kratchanova *et al.* [8,9], and Fishman *et al.* [14]. Keeping in mind higher yield and anti-complementary activity of AEOPMW than water extracted

one, the first was chosen for further investigations. AEOPMW was characterized with high AUAC (80.11%), high degree of methylesterification (58.69%) and low acetyl ester content (0.96%). Sugar composition analysis revealed that the main monosaccharide in AEOPMW was Ara (15.58%), followed by Gal (9.94%), Rha (5.47%) and Xyl (0.22%). It was detected 3.15% GlcA that represented a minor portion of the acidic part. AEOPMW consisted of two populations with different molecular weight 8.4×10^5 Da (91.3%) and 6.0×10^3 Da (8.7%).

All initial pectins were subjected to saponification and enzyme modification with EPG and further with galactan-degrading enzymes as men-

tioned above. The whole enzyme modification scheme is presented on Fig. 1.

In Table 1 are summarized the yield and monosaccharide composition of AP₁ EPG modified pectins. The yield of modified products varied between 28-41%. Modified products contained Rha, Gal, Ara, GalA and GlcA, as their Rha content was higher than those in initial pectins (except for AELP). Also, the amount of GalA decreased between 18% (WEOP) and 60% (AEOPMW) on the base of GalA content in native pectins (68-81%) [6]. These data illustrated that degradation was performed more fully in AEOPMW, contrary to WEOP that was fairly resistant to enzyme action, though saponification. During the degradation of

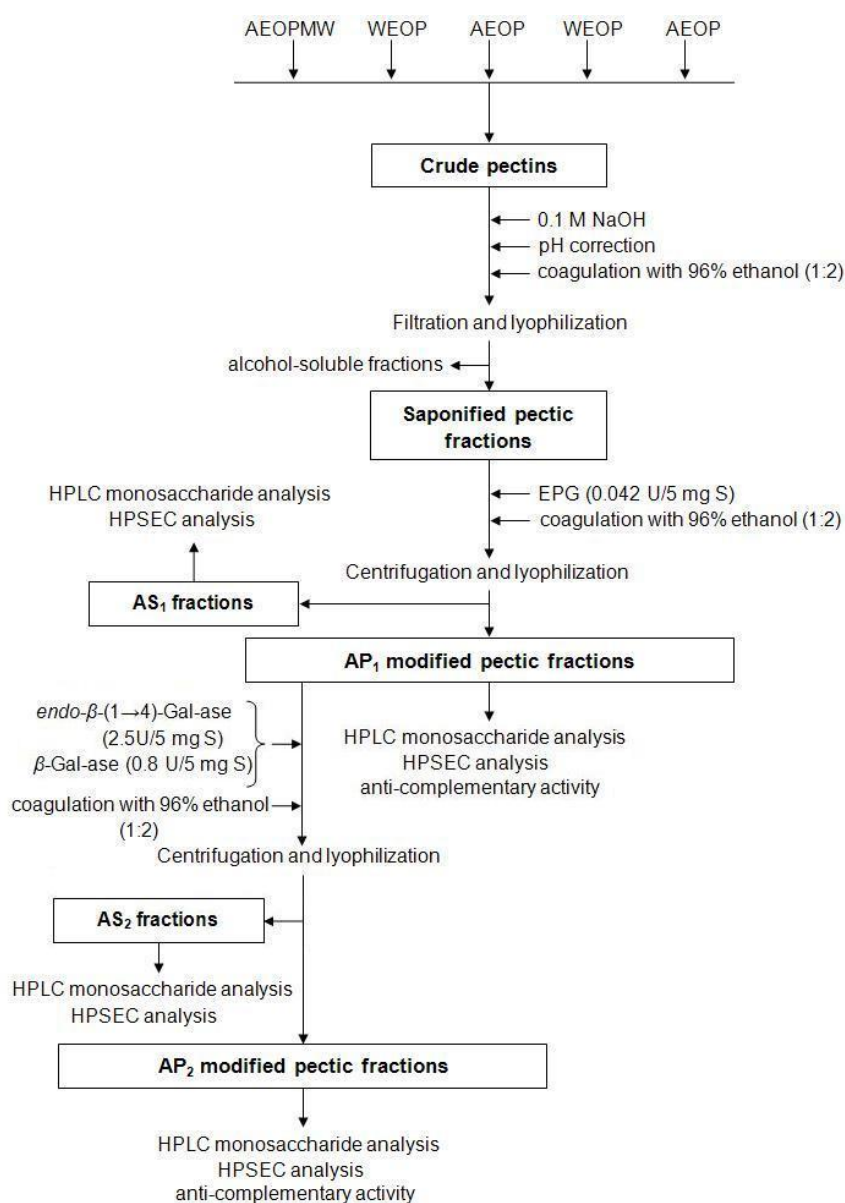


Fig. 1. Scheme for enzyme modification and analysis of different citrus pectins. Extraction procedure was described well in [6]. Abbreviation: EPG (*endo*-polygalacturonase), *endo*- β -(1 \rightarrow 4)-Gal-ase (*endo*- β -(1 \rightarrow 4)-galactanase) and β -Gal-ase (β -galactosidase); Alcohol-precipitated (AP); Alcohol-soluble (AS).

citrus pectins EPG activity could be hindered by neutral sugar side chains and resistant to degradation alcohol-insoluble residue could be isolated. Rhamnogalacturonan I (RG) fraction that was not free of the HG components may be accumulated in AP₁ residue. Indication for this was GalA presence in AP₁ fraction after enzyme treatment (Table 1).

Table 1. Yield and sugar composition (% w/w) of the alcohol-precipitated (AP₁) residue after degradation of citrus pectins with EPG.

	AEOPMW	WEOP	AEOP	WELP	AELP
Yield, %	39	28	39	41	29
Monosaccharides*					
Rha	9.1	11.2	11.0	10.4	12.5
Ara	2.1	1.4	1.5	4.0	2.2
Gal	20.1	9.5	15.6	7.4	11.5
GalA	31	56.4	44.4	53.1	49.2
GlcA	2.6	2.7	3.5	0.7	3.4

*Values are the average of two replicates.

These results were in good agreement with mode of EPG action. The enzyme catalyzes hydrolytic depolymerization of linear HG regions in pectic polysaccharides to oligomers and monomers, but ramified hairy regions remain non-degraded [15]. Therefore a high proportion of pectic RG region is obtained. Surprisingly, after modification Gal and Ara contents were decreased (except AEOPMW). Interestingly, Xyl was not detected in all AP₁ residues, contrary to its presence in AS₁ residue (see Table 2) and this showed that the monosaccharide was in some way released. Quite possible could be the presence of short EPG resistant Xyl-substituted galacturonan segments interspersed with long EPG-degradable HG segments. Thus, it appears that after digestion intact xylosylated oligomers could be accumulated in AS₁ supernatant. Rather, it would be confirmed the statement for Xyl-GalA containing units in initial pectins than for co-extracted hemicelluloses. The presence of mixed AS oligomers could be seen in Table 2, where oligomer's raw data represent the sum of acidic and neutral oligomers. Schols *et al.* [16] and Mort *et al.* [17] have obtained and well-explained the phenomenon with Xyl-substituted HG subunit. Sugar composition was in agreement with another our previous publication, where we reported that in AP part after EPG treatment of leek pectin Rha amount was increased contrary to Gal and Ara contents that were decreased [10]. Suh *et al.* [18] have modified with EPG pectin isolated from mandarin and they obtained a fraction with increased Rha, Gal and Ara contents in comparison with the initial pectin. Inngjerdingen *et al.* [19]

have observed a considerable Xyl decrease in one of the chromatographically purified fractions of EPG treated pectic polysaccharide from *Biophytum petersianum* Klotzsch. It could also be observed that GlcA content after this enzyme modification was increased for some of the products [19]. It was expected because it is well-known that GlcA presents in the RG side chains [20]. Inngjerdingen *et al.* [21] have also found increase of GlcA in a chromatographically purified fraction of pectic polysaccharide from *Glinus oppositifolius* after EPG modification.

Neutral monosaccharides and uronic acids in AS₁ parts after EPG treatment were determined without further acid hydrolysis to investigate enzyme-liberated free monomers. The results are presented in Table 2. Small amounts of free neutral sugars were quantified in all AS₁ products. Data for GalA content illustrated that EPG modification was performed. The presence of Ara and Gal in all samples could be explained with external enzyme activities mentioned in the certificates of used enzymes. Glucuronic acid was not detected in most of the AS₁ parts (except WEOP) as was expected.

Table 2. Sugar composition (% w/w) of the alcohol-soluble (AS₁) part after degradation of citrus pectins with EPG.

Monosaccharides	AEOPMW	WEOP	AEOP	WELP	AELP
Rha	1.7	3.4	2.5	1.3	1.7
Xyl	1.2	0.9	1.2	1.3	1.2
Ara	0.7	0.4	1.1	0.8	0.7
Gal	0.3	0.3	1.6	0.5	0.3
GalA	46.5	10.2	26.9	27.6	22.1
GlcA	-	0.4	-	-	-
Oligomers*	70.4	67.2	69.3	69.7	68.7

* Data for oligomers are directly extracted from chromatograms as % area. Values are the average of two replicates.

For expectation, as many enzymes are involved in the successive stepwise degradation of pectin as more substantial is the reduction in molecular weight and increase of molecular heterogeneity. Because of this fact lower AP products were recovered. The yield of AP₂ products varied in a narrow range between 49-54% calculated on EPG AP₁ residue base (Table 3). Generally, citrus pectins contain predominately arabinogalactan type I, which is a linear chain of β -(1 \rightarrow 4)-linked Gal residues with 20-40% Ara monomers connected mostly to C3 of Gal units [22]. To study the influence of this type of galactan chains on anti-complementary activity of citrus pectins treatment with β -(1 \rightarrow 4)-

galactan-degrading enzymes was performed. Beta-Galactosidase (EC 3.2.1.23) catalyzes hydrolytic decomposition of β -(1 \rightarrow 4)-galactosidic bonds in lactose and different β -D-galactosides towards non-reducing end. The enzyme acts in a synergistic manner with *endo*- β -(1 \rightarrow 4)-D-galactanase (EC 3.2.1.89). The latter catalyzes hydrolytic degradation of different galactans to galactooligosaccharides by *endo* mechanism. These enzymes play a key role in decomposition of β -(1 \rightarrow 4)-D-galactan side chains in pectic arabinogalactan type I from RG I [23,24]. The results in Table 3 show that Gal amount was considerably lower after synergistic action of *endo*- β -(1 \rightarrow 4)-galactanase and β -galactosidase. From Table 1 and 3 could be calculated that Gal content was reduced between 50% (WELP) and 89% (WEOP). The detected Gal amount after this treatment could be related to non-degraded β -(1 \rightarrow 4) glycosidic bonds and the presence of highly branched arabinogalactan type II with chains of galactose residues joint by β -(1 \rightarrow 3,6) linkages. Zhang *et al.* [25] have found that after *endo*- β -(1 \rightarrow 4)-galactanase digestion of arabinogalactan from *Angelica acutiloba* Gal amount was reduced with 30%. Characteristically, pectic ramified regions and more specifically galactan side chains could be substituted with GlcA and/or 4-O-methyl-GlcA, mainly as a non-reducing terminal residue [26]. Therefore digestion with galactan-degrading enzymes leads to liberation of AS galactooligomers substituted with GlcA, which is the reason for its lower quantity in AP₂ products (Table 3). Grønhaug *et al.* [27] have found that after modification with *endo*- β -(1 \rightarrow 4)-galactanase of EPG treated pectic polysaccharide from *Biophytum petersianum* Klotzsch Rha, Gal and Ara contents were increased, but no GlcA was detected. Raw data expressed as %Area and extracted from chromatograms, showing the sum of acidic and neutral AS oligomers are also presented in Table 4. Additionally a small amount of Rha was detected in these fractions because most of the released RG backbone fragments could be AS. Contradictory to previous results for EPG AP₁ residues (Table 1) Xyl was detected in trace amounts in both products after galactose-releasing enzymes (Table 3).

The results, as shown in Table 4, confirmed that the same quality sugar composition was detected as before modification (Table 2). Galactose was the most abundant free neutral monosaccharide because of specificity of conducted enzyme modification. This simply showed that most of Gal was bound by β -(1 \rightarrow 4) linkages.

It should be noted that the absence of monomeric GlcA in AS₂ parts (except AEOPMW) could

be explained with direct sugar analysis without further acid hydrolysis of solubilized GlcA-substituted (galacto)oligomeric residue. This leads to underestimation and masking the GlcA amount in the sample. Detected amounts of GalA in all samples could be related to the mentioned minor external EPG activity in *endo*- β -(1 \rightarrow 4)-galactanase certificate. Actually the same could be said for detected low (trace) amounts of Ara and Xyl.

Table 3. Yield and sugar composition (% w/w) of the alcohol-precipitated (AP₂) residue after degradation of citrus pectins with galactan-degrading enzymes *endo*- β -(1 \rightarrow 4)-galactanase and β -galactosidase.

	AEOPMW	WEOP	AEOP	WELP	AELP
Yield, %	49	54	5152	54	
Monosaccharides*					
Rha	0.7	1.0	1.0	1.2	0.5
Xyl	0.4	0.1	-	trace	0.2
Ara	10.6	13.2	10.5	11.9	11.8
Gal	5.3	1.0	4.3	3.7	4.0
GalA	28.6	54.1	24.8	36.3	21.1
GlcA	0.5	0.6	0.3	1.0	-

*Values are the average of two replicates.

Generally, comparing molecular heterogeneity of all citrus pectins after EPG action AP₁ residues contained higher proportion of molecular fragments with Mw 10⁵ Da and smaller 10⁴ Da. Oppositely, AS₁ parts contained mainly 10⁴ Da population. In result of enzyme hydrolysis with galactose-releasing enzymes AP₂ residues contained predominantly fragments with Mw 10⁴ Da and smaller proportion with 10⁵ Da.

Table 4. Sugar composition (% w/w) of the alcohol-soluble (AS₂) part after degradation of citrus pectins with galactan-degrading enzymes *endo*- β -(1 \rightarrow 4)-galactanase and β -galactosidase.

Monosaccharides	AEOPMW	WEOP	AEOP	WELP	AELP
Rha	1.3	0.5	0.1	0.8	1.6
Xyl	trace	0.1	-	0.2	trace
Ara	0.4	0.7	0.9	1.0	1.1
Gal	11.4	4.9	15.5	1.4	7.5
GalA	2.0	2.3	2.1	2.0	1.0
GlcA	0.4	-	-	-	-
Oligomers*	45.2	80.1	57.6	85	69.7

*Data for oligomers are directly extracted from chromatograms as % area. Values are the average of two replicates.

To access the molecular weight distribution of the initial AEOP and its alcohol-insoluble enzyme-modified products they were analyzed by SEC. AEOP was selected for fractionation because of its higher anti-complementary activity. Fig. 2 shows the elution pattern obtained by fractionation of

AEOP sample before and after enzyme treatment. Also, the found molecular weight value for different peaks was annotated. It was shown by the lower molecular mass of the AP₁ residue that initial high molecular weight substrate was degraded with EPG. In general, initial AEOP consisted of one distinct population in the high molecular weight region and was eluted as a broad peak faster than oligomers.

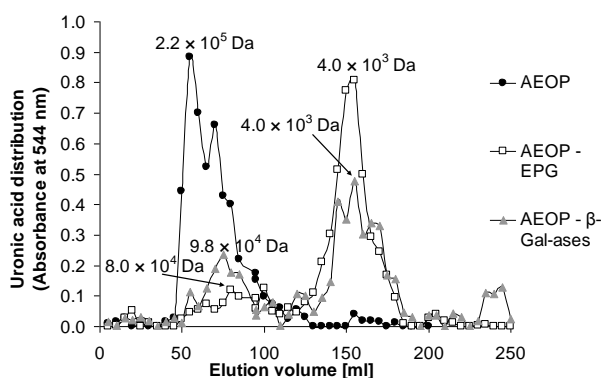


Fig. 2. Size-exclusion chromatography of AEOP and its alcohol-insoluble residues after a consecutive modification with EPG and galactan-degrading enzymes (β -Gal-ases).

Interestingly, two subfractions were separated from AP₁ residue. The higher molecular weight fraction was eluted as a rather broad peak between 50 and 110 ml consisted of lower amount of uronic acids, contrary to the second population that gave a high absorbance, but was eluted later with higher elution volume. Presumably, the first peak represented enzyme-resistant polymeric material and the second either galacturonic acid oligomers with higher molecular weight or mixture of lower molecular weight ramified hairy region fragments that co-eluted with larger oligogalacturonides. The molecular weight distribution and pattern of AP₁ residue after EPG were comparable with this after galactan-degrading enzymes, but as can be seen a small fraction was eluted at elution volume of 250 ml. It could be alcohol co-precipitated acidic oligomers with lower degree of polymerization. Schols *et al.* [28] have shown that by SEC on Sephacryl S-300 was possible the separation of apple pectin EPG hydrolyzate to rich in neutral sugar regions and acidic oligogalacturonides. Authors have determined by HPSEC that molecular weight of obtained hydrolysis products were in the range 10^3 - 10^5 Da. This was in a good agreement with our results. Additionally our results and assumptions were comparative with these of Ros *et al.* [29]. It was also seen that after treatment with galactan-degrading enzymes the peak at elution

volume under 80 ml was retained and absorption maximum of detected uronic acids was slightly increased. This was probably a result from change of uronic acid to neutral sugar ratio in this population as a consequence from Gal release.

The complement system is a basic antimicrobial defense mechanism in humans and normally present in blood in an inactive form. It can be activated through three different enzyme cascades - classical, alternative and lectin pathways by microbial cell wall carbohydrate structures (lipopolysaccharides, mannans, poly-N-acetylglucosamine) and by some plant polysaccharides (pectin, inulin, glucans). It is well-known that the anti-complementary activity of the most biologically active pectins is due to the containing arabinogalactan II side chains in RG I and that pectin could stimulate both classical and alternative pathway [30,31]. For investigation of the influence of linear acidic HG and RG I side chains on the activity was conducted modification by EPG and a successive modification with combination of galactan-degrading enzymes. EPG was used for obtaining of active ramified pectic RGs.

In Table 5 are presented the results from the complement activation test for different citrus pectins and their enzyme-modified alcohol-insoluble products through the classical and alternative pathways. All polysaccharides expressed higher anti-complementary activity through the classical pathway. Acid-extracted pectins were more active than water-extracted ones through this pathway. For example, acid-extracted citrus pectins inhibited mutton erythrocyte hemolysis over 50% at 2500 μ g/ml. Furthermore, AEOP inhibited rabbit erythrocyte hemolysis over 80% at 5000 μ g/ml through alternative pathway. Additionally, polysaccharides were investigated at 2500 μ g/ml, but they did not show any activity through this pathway. Microwave pretreatment of orange peels did not negatively influence on the activity of AEOPMW. Studies dealing with anti-complementary activity of unmodified pectic polysaccharides from different plant sources have been published. For example, Kiyohara *et al.* [32] have obtained by ion-exchange chromatography four acidic fractions AR-2IIa-2IIId from *A. acutiloba* with above 90% AUAC and anti-complementary activity over 50% at 1000 μ g/ml. Paik *et al.* [33] have isolated the biologically active acidic fraction HCAP-0 with hot water from pepper (*Capsicum annuum*), which expressed 85% anti-complementary activity through the classical pathway at 1000 μ g/ml. In comparison with our results AEOP possessed about 80% activity through both pathways, but in significantly higher concen-

Table 5. Anti-complementary activity of citrus pectins and their alcohol-insoluble (AP₁ and AP₂) enzyme-modified products. Mean \pm SD.

Pectins	Inhibition of total complement hemolysis of target animal erythrocytes, %							
	Classical pathway		Alternative pathway	Classical pathway		Alternative pathway	Classical pathway	
	2500 μ g/ml	1250 μ g/ml	5000 μ g/ml	2500 μ g/ml	1250 μ g/ml	5000 μ g/ml	2500 μ g/ml	1250 μ g/ml
	Initial		EPG modified pectins				β -Gal-ases modified pectins	
AEOPMW	74.8 \pm 13.8	14.2 \pm 5.8	20.7 \pm 6.4	34.8 \pm 6.3	4.2 \pm 0.8	35.1 \pm 15.9	60.7 \pm 6.2	10.6 \pm 1.6
WEOP	41.4 \pm 10.7	8.7 \pm 0.9	22.6 \pm 7.6	54.6 \pm 6.6	34.4 \pm 10.1	27.7 \pm 8.4	55.2 \pm 21.4	25.2 \pm 9.8
AEOP	85.8 \pm 7.4	12.6 \pm 1.7	81.5 \pm 15.1	37.3 \pm 4.7	7.7 \pm 4.2	22.4 \pm 2.2	46.4 \pm 15.3	19.1 \pm 11.7
WELP	31.5 \pm 5.6	5.3 \pm 0.6	56.9 \pm 16.2	25.5 \pm 5.8	14.2 \pm 4.1	63.6 \pm 14.6	64.3 \pm 11.4	35.3 \pm 13.2
AELP	57.1 \pm 2.5	11.4 \pm 2.9	19.1 \pm 4.4	28.7 \pm 4.1	14.2 \pm 5.8	29.2 \pm 1.8	44.8 \pm 7.3	25.8 \pm 4.6

trations. Furthermore, Diallo *et al.* [34] have investigated two very potent crude polysaccharide extracts from the leaves of *Trichilia emetica* that showed ICH₅₀ at 35 μ g/ml and 45 μ g/ml, respectively. After ion-exchange chromatography of both extracts they isolated the most potent fraction "Te 100 fraction acidic 4" with ICH₅₀ < 15 μ g/ml rich in GalA, Gal and Rha. Investigated citrus pectins were with considerably lower activity than the mentioned above because of different plant source and polysaccharide preparation.

Clear positive influence after modification with EPG was observed in WEOP through the classical pathway. Except AEOP modification was not negative through the alternative pathway. Interestingly, AEOP was the most potent sample through this pathway before EPG digestion. In agreement with our results Kiyohara *et al.* [32] have observed the same phenomenon after EPG digestion of AR-2IIa and AR-2IIb because their anti-complementary activity decreased from 59.5% to 29.0% and 62.6% to 42.8% at 1000 μ g/ml. But after separation of oligogalacturonides from enzyme resistant fraction on Sephadex G-50 the latter showed higher activity in comparison with the original fraction. Inngjerdingen *et al.* [21] have isolated a pectic polysaccharide GOA2 from *G. oppositifolius*, which inhibited hemolysis of sheep sensitized erythrocytes to about 40% under 1000 μ g/ml. After modification by EPG they obtained chromatographically fractions GOA2-I, II, III, and oligogalacturonides as the first one inhibited hemolysis to 90% and the next two expressed very low activity. As is shown in Table 5 anti-complementary activity is either decreased or not substantially changed. Accumulation of alcohol-insoluble oligogalacturonides could not be excluded because of the mode of action of EPG. The latter may have a nega-

tive masking effect on the activity expression of arabinogalactans. The best way for elucidation of this problem could be fractionation of the obtained products to oligogalacturonides and rich of neutral sugar fraction by ion-exchange chromatography and further investigation of their activity.

Also it was interestingly to study the influence of β -(1 \rightarrow 4)-linked Gal on the anti-complementary activity through the classical pathway. Generally, it could be concluded that this modification did not influence negatively on the activity of citrus pectins (Table 5). For example, WELP (initial) increased its activity from 31.5 \pm 5.6% to 64.3 \pm 11.4%. The higher observed activity for most of the samples could be interpreted with concentration of biologically active oligomers with glycosidic bonds resistant to the catalytic activity of applied enzymes. They should be the active β -(1 \rightarrow 3)-galactans branched with β -(1 \rightarrow 6)-galactans and/or biologically active β -(1 \rightarrow 4)-galactooligosaccharides accumulated in AP residue. Ognyanov *et al.* [10] have determined for acid-extracted leek pectin that modification with EPG led to 3 fold increase in anti-complementary activity of AP residue through the classical pathway, otherwise digestion with *endo*- β -(1 \rightarrow 4)-galactanase led to twofold decrease in activity. Grønhaug *et al.* [27] have reported for pectic polysaccharides from *B. petersianum* that additionally to (1 \rightarrow 3,6)-galactans β -(1 \rightarrow 4)-galactans could also contribute to the immunomodulating activity against immunocompetent Peyer's patch cells. They have shown this fact by digestion with *endo*- β -(1 \rightarrow 4)-galactanase and the aforementioned specific Gal-releasing enzymes and further chromatographic separation. This was in contradiction with our results.

CONCLUSION

In the present study an attempt for characterization of AP enzyme-released pectic oligosaccharides was made. AP₁ rhamnose-enriched fragments were obtained by EPG treatment. It was indicated that investigated citrus pectins contained xylogalacturonan fragments. The predominant presence of β -(1 \rightarrow 4)-linked Gal in investigated pectins using β -(1 \rightarrow 4)-Gal-releasing enzymes was confirmed. Enzyme modification influenced to different extent anti-complementary activity of investigated pectins. Alcohol precipitation is a suitable and relatively prompt strategy for fractionation of enzyme-digested pectins. Introduced approach led to obtaining of a complex mixture of mono- and oligosaccharides that hindered appropriate estimation of influence of enzyme modification on anti-complementary activity. On the base of our investigations it could be concluded that for obtaining more clear results alcohol precipitation procedure should be optimized by applying a stepwise procedure with different alcohol concentrations. For elucidation of the relationship between carbohydrate composition and anti-complementary activity enzymolysis and glycosidic linkage analysis of chromatographically purified pectic arabinogalactan chains are necessary to be used. Moreover for better understanding of pectic monosaccharide composition and structure investigation of more complex AS oligomers after appropriate acid hydrolysis by modern analytical tools (HILIC-ELSD/ESI-MSⁿ, CE-MS/CE-LIF, HPAEC-PAD) are needed.

Acknowledgements: This work was funded by project № BG161PO003-1.1.05-0024-C0001 "Development of nutraceuticals with antioxidant and immune-stimulating action" of Operational Program "Competitiveness" of the EU.

REFERENCES

1. Z. I. Kertesz, The Pectic Substances, Interscience Publishers, New York, 1951.
2. P. S. Bhimanagouda, J. S. Brodbelt, E. G. Miller, N. D. Turner, in: Potential Health Benefits of Citrus, *ACS Sym. Ser.*, **936**, 1 (2006).
3. R. Cameron, G. Luzio, E. Baldwin, J. Narciso, A. Plotto, *Proc. Fla. State Hort. Soc.*, **118**, 406 (2005).
4. R. Cameron, G. Luzio, B. Savary, A. Nuñez, K. Goodner, *Proc. Fla. State Hort. Soc.*, **122**, 295 (2009).
5. E. Makarova, O. Patova, E. Shakhmatov, S. Kuznetsov, Yu. Ovodov, *Carbohydr. Polym.*, **92**, 1817 (2013).
6. Y. Georgiev, M. Ognyanov, I. Yanakieva, V. Kussovski, M. Kratchanova, *J. BioSci. Biotech.*, **1**, 223 (2012).
7. M. Kratchanova, I. Panchev, E. Pavlova, L. Schtereva, *Carbohydr. Polym.*, **25**, 141 (1994).
8. M. Kratchanova, E. Pavlova, I. Panchev, Chr. Kratchanov, *Prog. Biotech.*, **14**, 941 (1996).
9. M. Kratchanova, E. Pavlova, I. Panchev, *Carbohydr. Polym.*, **56**, 181 (2004).
10. M. Ognyanov, M. Nikolova, I. Yanakieva, V. Kussovski, M. Kratchanova, *J. BioSci. Biotech.*, **2**, 13 (2013).
11. N. Blumenkrantz, G. Asboe-Hansen, *Anal. Biochem.*, **54**, 484 (1973).
12. M. Cesaretti, E. Luppi, F. Maccari, N. Volpi, *Carbohydr. Polym.*, **54**, 59 (2003).
13. J. Klerx, C. Beukelman, V. Dijk, J. Willers, *J. Immunol. Methods*, **63**, 215 (1983).
14. M. Fishman, H. Chau, P. Hoagland, A. Hotchkiss, *Food Hydrocolloids*, **20**, 1170 (2006).
15. J. A. E. Benen, J. Visser J. 2003. in: Handbook of Food Enzymology, J. R. Whitaker, A. G. J. Voragen, D. W. S. Wong (eds.), Marcel Dekker, Inc., 2003, ch. 69.
16. H. A. Schols, E. J. Bakx, D. Schipper, A. G. J. Voragen, *Carbohydr. Res.*, **279**, 265 (1995).
17. A. Mort, Y. Zheng, F. Qui, M. Nimtz, G. Bell-Eunice, *Carbohydr. Res.*, **343**, 1212 (2008).
18. H.-J. Suh, H.-S. Yang, K.-S. Ra, D.-O. Noh, K.-H. Kwon, J.-H. Hwang, K.-W. Yu, *Food Chem.*, **138**, 1079 (2013).
19. M. Inngjerdingen, K. T. Inngjerdingen, T. R. Patel, S. Allen, X. Chen, B. Rolstad, G. A. Morris, S. E. Harding, T. E. Michaelsen, D. Diallo, B. S. Paulsen, *Glycobiology*, **18**, 1074 (2008).
20. J. An, M. A. O'Neill, P. Albersheim, A. G. Darvill, *Carbohydr. Res.*, **252**, 235 (1994).
21. K. T. Inngjerdingen, T. R. Patel, X. Chen, L. Kenne, S. Allen, G. A. Morris, S. E. Harding, T. Matsumoto, D. Diallo, H. Yamada, T. E. Michaelsen, M. Inngjerdingen, B. S. Pausen, *Glycobiology*, **17**, 1299 (2007).
22. G. Beldman, H. A. Schols, S. M. Pitson, M. J. F. Searle-Van Leeuwen, A. G. J. Voragen, in: Advances in Macromolecular Carbohydrate Research, R. J. Sturgeon (ed.), vol. 1, 1997, Jai Press, Inc., London, 1997, p. 1.
23. R. R. Mohoney, in: Handbook of Food Enzymology, J. R. Whitaker, A. G. J. Voragen, D. W. S. Wong (eds.), Marcel Dekker, Inc., 2003, ch. 65.
24. R. de Vries, J. Visser, in: Handbook of Food Enzymology, J. R. Whitaker, A. G. J. Voragen, D. W. S. Wong (eds.), Marcel Dekker, Inc., 2003, ch. 70.
25. Y. Zhang, H. Kiyohara, M. H. Sakurai, H. Yamada, *Carbohydr. Polym.*, **31**, 149 (1996).
26. M. Haque, T. Kotake, Y. Tsumuraya, *Biosci. Biotech. & Biochem.*, **69**, 2170 (2005).

27. T. E. Grønhaug, H. Kiyohara, A. Sveaass, D. Diallo, H. Yamada, B. S. Paulsen, *Phytochem.*, **72**, 2139 (2011).
28. H. A. Schols, E. Vierhuis, E. J. Bakx, A. G. J. Voragen, *Carbohydr. Res.*, **275**, 343 (1995).
29. J. M. Ros, H. A. Schols, A. G. J. Voragen, *Carbohydr. Polym.*, **37**, 159 (1998).
30. H. Yamada, H. Kiyohara, in: Immunomodulatory agents from plant, H. Wagner (ed.), 1999, Birkhäuser, Basel, p. 161.
31. H. Yamada, H. Kiyohara, in: Comprehensive Glycoscience – From Chemistry to Systems Biology, J. P. Kamerling (ed.), 2007, Elsevier, Oxford, p. 663.
32. H. Kiyohara, J. C. Cyong, H. Yamada, *Carbohydr. Res.*, **182**, 259 (1988).
33. S.-Y. Paik, K. S. Ra, I. S. Chang, Y. C. Park, H. S. Park, H. S. Baik, J. W. Yun, J. W. Choi, *J. Biochem. Mol. Biol.*, **36**, 230 (2003).
34. D. Diallo, B. S. Pausen, T. H. A. Liljebäck, T. E. Michaelsen, *J. Ethnopharmacol.*, **84**, 279 (2003).

ХИМИЧЕН СЪСТАВ И АНТИКОМПЛЕМЕНТАРНА АКТИВНОСТ НА ЕНЗИМНО-МОДИФИЦИРАНИ ЦИТРУСОВИ ПЕКТИНИ

М. Х. Огнянов¹, Й. Н. Георгиев¹, И. Ж. Янакиева¹, В. К. Късовски², М. Г. Крачанова^{1*}

¹Лаборатория Биологично Активни Вещества, Институт по Органична химия с Център по Фитохимия, Българска Академия на Науките, бул. Руски 139, 4000 Пловдив, България

²Департамент по Инфекциозна Микробиология, Институт по микробиология, Българска Академия на Науките, ул. Акад. Г. Бончев, бл. 26, 1113 София, България

Постъпила на 03 юли 2014 г.; Коригирана на 26 юли 2014 г.

(Резюме)

В настоящото изследване беше проведена последователна ензимна модификация на серия от цитрусови пектини с *ендо*-полигалактуроназа и комбинация от β -галактозидаза и *ендо*- β -(1 \rightarrow 4)-галактаназа. За фракциониране на ензимните хидролизати беше използвано утаяване с двукратен обем 96% етанол, което доведе до получаването на алкохолно-разтворима и алкохолно-неразтворима част. След действието на *ендо*-полигалактуроназа бяха получени алкохолно утаими фракции с повишено съдържание на рамноза и понижено на галактуронова киселина (между 18-60%). Освен това беше установено, че цитрусовите пектини съдържат ксилогалактуронанови фрагменти, които се освобождават след третирането с *ендо*-полигалактуроназа. След последващата ензимна модификация галактозното съдържание на изследваните пектини беше намалено между 50 и 89%, което потвърждава преимуществото на β -(1 \rightarrow 4)-свързаната галактоза в разклонените вериги на цитрусовите пектини. Антикомплементарната активност на цитрусовите пектини беше по-висока по класическия път в сравнение с алтернативния път на активиране на комплемента. Използваният подход за фракциониране с алкохол след ензимната модификация доведе до получаването на комплексни смеси от пектинови фрагменти, проявяващи различно влияние върху антикомплементарната активност на модифицирания продукт.

A new coumarin and total phenolic and flavonoids content of Bulgarian celeriac

M. Popova¹, A. Stoyanova¹, N. Valyovska-Popova², V. Bankova^{1*}, D. Peev²

¹Institute of Organic Chemistry with Centre of Phytochemistry, Bulgarian Academy of Sciences, Acad. G. Bonchev str., bl. 9, 1113 Sofia, Bulgaria

²Institute of Biodiversity and Ecosystem Research, Bulgarian Academy of Sciences, 2 Gagarin str., 1113 Sofia, Bulgaria

Received June 06, 2014; Revised July 02, 2014

Dedicated to Acad. Dimiter Ivanov on the occasion of his 120th birth anniversary

Apium graveolens is a popular vegetable and also a well known medicinal plant. Different extracts have demonstrated diverse useful properties: antioxidant, hipolipidemic, antibacterial, anticancer, etc. In Bulgaria, the most often consumed parts are the leaves (as spice) and the thickened roots of *A. graveolens* var. *rapaceum*, celeriac. We studied the chemical composition of unpolar extract of Bulgarian celeriac. In petroleum ether fraction of the methanol root extract we identified by GC-MS several compounds: neocnidilide, isocnidilide, 3-*n*-butyl phthalide, allyl phenoxyacetate, fatty acids and hydrocarbons; the coumarins xanthotoxin, isopimpinellin, psoralene. A new natural compound 6-(3'-methyl-1'-oxobutyl)-7-hydroxy coumarin was isolated and its structure proved by spectral data. Total phenolic and total flavonoids content of plant material from different locations in Bulgaria was also analyzed spectrophotometrically. We studied methanol extract of leaves and roots from 19 different locations in Bulgaria, including some wild-growing *Apium nodiflorum*. The total phenolics varied between 15-67.2 mg/g GAE in leaves and 8.2-13.6 mg/g GAE in roots, and total flavonoids were between 6-26.5 mg/g in leaves and 1-4.8 mg/g in roots (as quercetin). Our study demonstrated that the roots and leaves of Bulgarian celery are a rich source of biologically active constituents.

Key words: *Apium graveolens* var. *rapaceum*, celeriac, total phenolics, total flavonoids, 6-(3'-methyl-1'-oxobutyl)-7-hydroxy coumarin

INTRODUCTION

Apium graveolens L., belonging to the Apiaceae family, is a plant cultivated and consumed worldwide. In Bulgaria, the most often consumed parts are the leaves (as spice) and the thickened roots of *A. graveolens* var. *rapaceum* known as celeriac. There are abundant literature data reporting a wide spectrum of biological activity of *A. graveolens* [1,2]. Different authors reported that its extracts possessed antimicrobial [3], antifungal [4] and anti-inflammatory activity [5-7], as well as positive effects in treatment of rheumatoid arthritis and osteoarthritis [8]. Further, alcohol extracts of *A. graveolens* have demonstrated significant hepatoprotective [9,10], anticarcinogenic, antiproliferative [11], cytotoxic [12] and hypolipidemic action [13]. Leave and root extracts of *A. graveolens* have potential to scavenge free OH[•] and DPPH[•] radicals and to inhibit lipid peroxidation [14-16].

Phytochemical studies revealed the presence of secondary metabolites belonging to different structural groups: flavonoids (major constituents glycosides of apigenin, kaempferol and quercetin),

phenolic acids (caffeic, ferulic, and their derivatives), phthalides, tannins, steroids, terpenoids, saponins, essential oils [16-24]. Among these, the most important biologically active constituents are phenolics, mainly flavonoids, phenolic acids, and coumarins. It is known that natural products rich in polyphenols are potently effective against dyslipidemia, cardiovascular diseases, inflammation, and underlying mechanisms of other disease processes, mainly because of their antioxidant activity [25].

The aim of the present work was to study the content of bioactive constituents of Bulgarian celeriac roots and leaves from different regions of the country. The quantification of groups of active constituents instead of individual compounds is reasonable because of the well recognized fact that the activity of medicinal plant extracts is mostly due to the simultaneous action of many different constituents [26-29].

EXPERIMENTAL

Extraction of celeriac roots

Commercial Bulgarian celeriac fresh roots (1.4 kg) were cut into small pieces and extracted with

* To whom all correspondence should be sent:
E-mail: bankova@orgchm.bas.bg

MeOH three times successively (1.5 l each) at room temperature for 24h. The extracts were filtered and the combined extracts after concentration *in vacuo* were mixed with water and extracted successively with petroleum ether (PE) (3x, 1:1 v/v). The extract obtained was evaporated to give 880 mg dry residue.

Fractionation of methanol extract of celeriac roots and GC-MS analysis

A part of the PE fraction (20 mg) was subjected to PTLC with mobile phase PE:EtOAc (10:1). Two sub-fractions were gathered and analyzed by GC-MS. The second, more polar fraction was silylated prior to the analysis.

The GC-MS analysis was performed with a Hewlett Packard gas chromatograph 5890 Series II Plus linked to a Hewlett Packard 5972 mass spectrometer system, equipped with a 23m long, 0.25mm i.d. and 0.5 mm film thickness HP-5 capillary column. The temperature was programmed from 100°C to 310°C at a rate of 5°Cmin⁻¹. Helium was used as a carrier gas, at flow rate 0.7mLmin⁻¹, split ratio 1:80, injector temperature 280°C and ionisation voltage 70 eV. For silylation, about 5 mg of the sample was mixed with 75 mL bis(trimethylsilyl)trifluoro-acetamide and 50 mL of dry pyridine, heated at 80°C for 20 min and analysed by GC-MS.

Isolation of individual compounds

Column chromatography was performed on silica gel 60 (Merck, 63-200 mm), normal phase. Analytical TLC was performed on silica gel 60 F254 plates (Merck). Preparative TLC (PTLC) was performed on silica gel 60 F254 glass plates (Merck, 20x20 cm and 0.25 mm). Detection of the spots was achieved under UV light (254 and 366 nm) and by spraying with vanillin-sulphuric acid in methanol, followed by heating at 100°C.

NMR spectra were recorded on a Bruker AV 600 spectrometer (600MHz for ¹H and 150 MHz for ¹³C) in CDCl₃.

A part of the PE extract (750 mg) was subjected to column chromatography on silica gel using a gradient system of PE-EtOAc (1:0-0:1). Nineteen fractions were obtained. Fraction 6 (19 mg, eluted with PE-EtOAc (95:5)) was separated by PTLC with mobile phase CHCl₃-EtOAc (20:1) to yield mixture of neo- and isocnidilide (**3a** and **3b**, 7 mg). Fraction 15 (10 mg, eluted with PE-EtOAc (75:25)) was subjected to PTLC with mobile phase CHCl₃ to yield two compounds: xanthotoxin (**5**, 1 mg) and 6-

(3'-methyl-1'-oxobutyl)-7-hydroxy coumarin (**7**, 1 mg).

Identification of isolated compounds

Compounds **3a** and **3b** (mixture of neo- and isocnidilide) were identified based on comparison of ¹H-NMR spectrum with literature data [30,31].

Xanthotoxin **5** was identified based on comparison of its ¹H-NMR and MS spectra with literature data [32].

6-(3'-methyl-1'-oxobutyl)-7-hydroxy coumarin **7**: ¹H NMR (CDCl₃, 600 MHz) δ: 0.97 (6H, d, J = 6.7 Hz, CH₃-4', CH₃-5'), 2.25 (1H, m, H-3'), 2.81 (2H, d, J = 6.9 Hz, H₂-2'), 6.23 (1H, d, J = 9.5 Hz, H-3), 6.79 (1H, s, H-8), 7.57 (1H, d, J = 9.5 Hz, H-4), 7.83 (1H, s, H-5), 12.81 (1H, s, OH); ¹³C NMR (CDCl₃, 150 MHz) δ: 22.7 (q, C-4', C-5'), 25.5 (d, C-3'), 47.1 (t, C-2'), 105.6 (d, C-8), 111.6 (s, C-4a), 114.1 (d, C-3), 117.3 (s, C-6), 130.9 (d, C-5), 142.9 (d, C-4), 159.0 (s, C-8a), 159.9 (s, C-2), 165.8 (s, C-7), 105.5 (s, C-1'). GC/MS (6-(3'-methyl-1'-oxobutyl)-7-hydroxy coumarin TMS), MS (EI, 70 eV), m/z (relative intensity %): 318 M⁺ (5), 303 [M-CH₃]⁺ (100), 261 [M-C₄H₉]⁺ (75), 233 [M-C₄H₉-CO]⁺ (15), 73 (20).

Plant material. The plant species, the geographic origin and the type of plant material are listed in Table 1.

Extraction of roots and leaves of samples from different regions in Bulgaria. Fresh plant material was extracted twice with methanol, 1:3 (w/v) for leaves and 1:2 (w/v) for roots. The extracts were evaporated to dryness *in vacuo* and 400 mg of the dry extract were dissolved in 70% methanol in a 50 ml volumetric flask (solution **a**) and subjected to spectrophotometric analyses. For every extract, the procedure was performed in triplicate.

Total flavonoids quantification. Methanol solutions of quercetin (0.0095, 0.019, 0.038, 0.076 mg/ml and 0.19 mg/ml) were used to generate the standard curve. In a volumetric flask, 20 ml MeOH and 2 ml of the standard solution were added, and 1 ml 5% AlCl₃ solution in MeOH (w/v) and the volume was made up to 50 ml. The obtained solution was allowed to stay 30 min. Absorbance was measured at 425 nm (blank prepared in the same way, 2 ml of MeOH instead of standard solution). Every analysis was performed in triplicate. For analysis of the plant extracts, 2 ml of solution **a** was applied in the same procedure. Every analysis was performed in triplicate.

Total phenolics quantification. Methanol solutions of gallic acid (0.009; 0.019; 0.037; 0.075 and 0.15 mg/ml) were used to generate the standard

curve. To 1 ml of the standard solution, 10 ml distilled water were added, after that 4 ml of Folin-Ciocalteu reagent and 6 ml of 20% Na_2CO_3 were added and the volume made up to 50 ml (volumetric flask). The solution was allowed to stay for 2 h (± 3 min). Absorbance was measured at 760 nm (blank prepared in the same way, 1 ml of MeOH instead of standard solution). Every analysis was performed in triplicate. For analysis of the plant extracts, 1 ml of solution **a** was applied in the same procedure. Every analysis was performed in triplicate.

RESULTS AND DISCUSSION

The major constituents of the celeriac roots methanol extract are phenolic compounds, including predominantly polar flavonoids and their glycosides, and phenolic acids. However, it contains also other bioactive compounds of lesser polarity and in order to study their chemical profile we used GC-MS. We obtained the petroleum ether fraction of the methanol extracts and divided it into two sub-fractions by preparative TLC. The less polar fraction from the PTLC was analyzed by GC-MS and aliphatic hydrocarbons, fatty acids, allyl phenoxyacetate **1**, and several phtalides were identified, using computer libraries. The phtalides detected were n-butyl phtalide **2** and two isomers of cnidilide (Fig. 1). For complete identification of the cnidilides, they were isolated by PTLC as an inseparable mixture and by comparison with literature NMR data [30,31] they were identified as neocnidilide **3a** and isocnidilide **3b**. N-butyl-phtalide and similar compounds are responsible for the flavor and aroma of celery and extracts thereof [32]. A number of phtalides with diverse biological activity have been found in *A. graveolens* [18,33].

The second, more polar fraction from the PTLC of the petroleum ether fraction, was silylated prior to GC/MS analysis. The data indicated the presence of fatty acids (major constituents), one diterpenic acid (dehydroabiatic acid) and the furocoumarines psoralen **4**, xanthotoxin **5**, and isopimpinellin **6**. Two major compounds of this fraction were isolated by PTLC and one of them was identified as xanthotoxin **5** by comparison of its mass and NMR spectra with literature data [34]. Compound **5** has been isolated from *A. graveolens* [35]. The second compound was identified as 6-(3'-methyl-1'-oxobutyl)-7-hydroxy coumarin **7** based on different NMR experiments (^1H , ^{13}C , DEPT, HSQC, HMBC) and GC/MS after silylation.

The ^1H NMR spectrum of compound **7** showed two one proton doublets at δ 7.57 ($J = 9.5$ Hz) and

6.23 ($J = 9.5$ Hz), typical for olefin protons H-4 and H-3 of α -pyrone ring in coumarins. The HMBC correlation (Fig. 2) between H-4 and quaternary C-2 (δ 159.9, C=O) and C-8a (δ 159.0), H-3 and C-4a (δ 111.6) confirm the base structure.

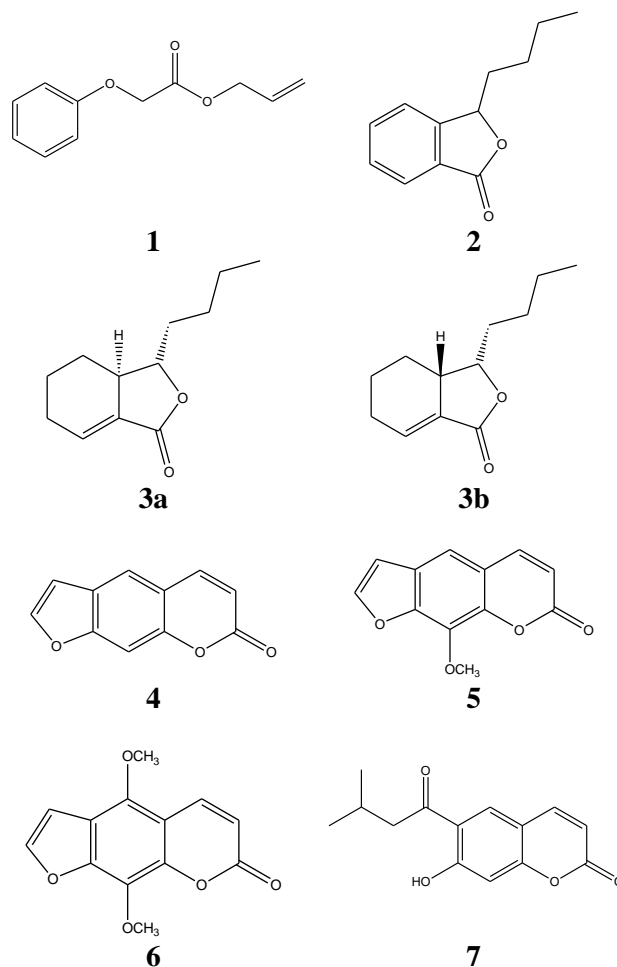


Fig. 1. Compounds, identified in celeriac roots.

Two singlets for one proton each, at δ 7.83 and 6.79 were assigned to *para* aromatic protons H-5 and H-8, respectively. In up field part of ^1H NMR spectrum appeared the signals for the side chain: doublet for two methyl groups at δ 0.97 ($J = 6.7$ Hz), multiplet for one proton at δ 2.25 and doublet for two protons at δ 2.81 ($J = 6.9$ Hz). The corresponding carbon atoms have resonances at δ 22.7 (CH_3 -4', 5'), 25.5 (C-3') and 47.1 (C-2'), respectively. The downfield shifted signal for methylene group at δ_c 47.1 (C-2') and HMBC correlation (Fig. 2) between H_2 -2' and carbon signal at δ 205.5 indicate the side chain as an oxoisopentyl group. The carbon atom C-1' (δ 205.5) was bonded to C-6 (δ 117.3) based on HMBC correlation between H-5 and C-1', and H-8 and C-6. The singlet for one proton at δ 12.81 was assigned to the proton from hydroxy group at C-7

using HMBC data. Correlation between H-5 and C-7 was seen in the same spectrum. Based on these data, the structure of **7** was concluded to be 6-(3'-methyl-1'-oxobutyl)-7-hydroxy-coumarin **7**. Compound **7** has not yet been isolated from a natural source, it has been synthesized back in 1955 [36].

Further, in order to characterize Bulgarian celeriac with respect to the content of potential antioxidants, total phenolics and total flavonoids content was measured spectrophotometrically in methanol extract of leaves and roots of *A. graveolens* var. *rapaceum* from 19 different locations in Bulgaria. The results are represented in Table 1.

The total phenolics varied between 15 - 67.2 mg/g GAE in leaves (mean value 29±13) and 8.2-13.6 mg/g GAE in roots (mean value 11±2), and total flavonoids were between 6 - 26.5 mg/g in leaves (mean value 15±6) and 1 - 4.8 mg/g in roots (as quercetin) (mean value 2±1). The mean values for both compound groups are higher in leaves, the differences being statistically significant ($p < 0.001$).

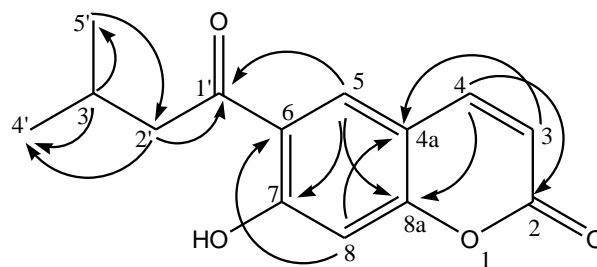


Fig. 2. HMBC (H → C) correlation in **7**.

The samples analyzed originated from regions with different climatic conditions. They demonstrated more or less similar content of phenolics and flavonoids; this fact suggests a possible dominance of genetic rather than ecological factors as determinant for the biosynthesis of these compounds.

Some samples of wild-growing *Apium nodiflorum* were also analyzed. The two leaf samples of *A. nodiflorum* demonstrated total phenolic content and total flavonoids in the range of the samples of celeriac from the same region (Varna).

Table 1. Total phenolics and total flavonoids in extracts of Bulgarian celeriac.

No.	Origin	Organ	Total Phenolics (GAE ^a , mg·g ⁻¹)	Total Flavonoids (QE ^b , mg·g ⁻¹)
1	Varna Region, Oborishte A	leaves	26.9±0.9	19.3±0.5
2	Varna Region, Oborishte B	leaves	15.7±1.1	6.9±0.1
3	Varna Region, Oborishte C	leaves	36±3	11.02±0.03
4	Varna Region, Beloslav A	leaves	20.2±0.1	15.3±0.3
5	Varna Region, Beloslav B	leaves	28.0±1.4	25.6±0.7
6	Varna region, Strashimirovo	leaves	67.2±1.9	26.5±1.6
7	Shabla	leaves	23.3±0.3	21.46±0.02
8	Balgarevo	leaves	38.05±0.05	13.5±1.1
		roots	10.7±0.5	1.45±0.02
9	Aitos Region, Bosilkovo	leaves	33.4±1.1	18.2±0.7
10	Aitos Region, Devetak	leaves	26.9±1.1	16.8±0.3
11	Aitos	leaves	45.8±2.5	18.1±0.1
12	Sofia Region, German	roots	8.2±0.3	1.15±0.1
13	Petrich Region, Drangovo	leaves	18.7±1.3	6.0±0.4
		roots	9.3±0.7	1.6±0.1
14	Petrich Region, Mihievo	roots	13.6±0.8	2.0±0.2
15	Karnobat Region, Gluche	leaves	41.2±0.9	16.9±1.3
16	Karnobat Region, Sokolovo	leaves	20.8±1.0	10.3±0.09
		roots	13.3±0.8	1.31±0.03
17	Karnobat Region, Tserkovsko	leaves	15.0±1.0	8.4±0.1
		roots	8.4±0.7	1.00±0.07
18	Karnobat Region, Dobrilovo	leaves	23.3±0.8	17.2±1.5
		roots	11.1±0.4	1.03±0.05
19	Kardzhali	leaves	16.7±0.8	9.3±0.6
20	Sofia	leaves	38.7±1.4	10.4±0.5
		roots	11.7±0.3	4.8±0.2
21	Bulgaria, commercial sample	roots	8.9±1.1	2.3±0.6
22	Varna Region, Devnya ^c	leaves	24±2	8.1±0.5
		roots	16.1±0.4	7.4±0.1
23	Varna Region, Beloslav ^c	leaves	14.9±0.5	10.7±0.2

^a GAE – gallic acid equivalents; ^b QE – quercetin equivalents; ^c *Apium nodiflorum*.

The only root sample of *A. nodiflorum* had total phenolics and total flavonoids higher than that of the highest values for *A. graveolens* var. *rapaceum*.

CONCLUSION

Our results demonstrate that the roots and leaves of Bulgarian celeriac are a rich source of biologically active constituents. Obviously, Fool's-water-cress roots deserve further, more detailed studies.

Acknowledgements: Partial support of this work by the Bulgarian Science Fund, Contract No. DVU 10 0033 is gratefully acknowledged. The authors wish to thank Dr. D. Antonova for running the GC-MS analyses.

REFERENCES

1. S. S. Fazal, R. K. Singla, *Indo Global J. Pharm. Sci.*, **2**, 36 (2012).
2. H. B. Sowbhagya, *Crit. Rev. Food Sci. Nutr.*, **54**, 389 (2014).
3. A. Sipailiene, P. R. Venskutonis, A. Sarkinas, V. Cypiene, *Acta Hort. (ISHS)*, **677**, 71 (2005).
4. R. A. Momin, M. G. Nair, *J. Agric. Food Chem.*, **49**, 142 (2001).
5. D. A. Lewis, *Int. J. Crude Drug Res.*, **23**, 27 (1985).
6. M. Al-Hindawi, I. Al Deen, M. Nabi, M. Ismail, *J. Ethnopharmacol.*, **26**, 163 (1989).
7. A. H. Atta, A. Alkofahi, *J. Ethnopharmacol.*, **60**, 117 (1998).
8. J. Kolarovic, M. Popovic, J. Zlinska, S. Trivic, M. Vojnovic, *Molecules*, **15**, 6193 (2010).
9. A. Singh, S. S. Handa, *J. Ethnopharmacol.*, **4**, 119 (1995).
10. A. Bahar, T. Alam, M. Varshney, S. A. Khan, *J. Ethnopharmacol.*, **79**, 313 (2002).
11. S. Sultana, S. Ahmad, T. Jahangir, S. Sharma, *Cancer Lett.*, **221**, 11 (2005).
12. V. Subhadradevi, K. Khairunissa, K. Asokkumar, M. Umamaheswari, A. Sivashanmugam, P. Jagannath, *Middle-East J. Sci. Res.*, **9**, 90 (2011).
13. D. Tsi, N. P. Das, B. K. Tan, *Planta Med.*, **6**, 18 (1995).
14. Y. F. Chu; J. Sun, X. Wu, R. H. Liu, *J. Agric. Food Chem.*, **50**, 6910 (2002).
15. M. Popovic, B. Kaurinovic, S. Trivic, N. N. Mimica-Dukic, M. Bursac, *Phytother. Res.*, **20**, 357 (2006).
16. N. Nikolic, D. Cvetkovic, Z. Todorovic, *Italian J. Food Sci.*, **23**, 214 (2011).
17. L. F. Bjeldanes, I.-S. Kim, *J. Org. Chem.*, **42**, 2333 (1977).
18. M. J. M. Gijbels, F. C. Fischer; J. J. C. Scheffer; A. B. Svendsen, *Fitoterapia*, **56**, 17 (1985).
19. A. E. Ataga, H. A. S. Epton, R. R. Frost, *Physiol. Molecular Plant Pathol.*, **42**, 161 (1993).
20. K. H. Miean, S. Mohamed, *J. Agric. Food Chem.*, **49**, 3106 (2001).
21. K. Zhou, F. Zhao, Z. Liu, Y. Zhuang, L. Chen, F. Qiu, *J. Nat. Prod.*, **72**, 1563 (2009).
22. Y. Yao, W. Sang, M. Zhou, G. Ren, *J. Food Sci.*, **75**, 9 (2010).
23. A. A. Shad, H. U. Shah, J. Bakht, M. I. Chiudhary, A. J. Ullah, *J. Med. Plants Res.*, **5**, 5160 (2011).
24. A. Kajser, K. Hartmann, D. Kammerer, R. Carle, *Eur. Food Res. Technol.*, **237**, 353 (2013).
25. K. R. Martin, C. L. Appel, *Nutr. Diet. Suppl.*, **2**, 1 (2010).
26. T. Efferth, E. Koch, *Curr. Drug Targets*, **12**, 122 (2011).
27. D. Marinova, F. Ribarova, M. Atanassova, *J. Univ. Chem. Technol. Metallurgy*, **40**, 255 (2005).
28. E. Souri, G. Amin, H. Farsam, T. M. Barazandeh, *DARU*, **16**, 83 (2008).
29. M. Stankevičius, I. Akuņeca, I. Jākobsone, A. Maruška, *Maisto Chemija ir Technologija*, **44**, 85 (2010).
30. F. C. Fischer, M. J. M. Gijbels, *Planta Med.*, **77** (1987).
31. D. Oguro, H. Watanabe, *Tetrahedron*, **67**, 771 (2011).
32. H. J. Gold, C. W. Wilson III, *J. Org. Chem.*, **28**, 985 (1963).
33. J. J. Beck, S.-C. Chou, *J. Nat. Prod.*, **70**, 891 (2007).
34. J. Intekhab, M. Aslam, *FABAD J. Pharm. Sci.*, **33**, 67 (2008).
35. R. C. Beier, G. W. Ivie, E. H. Oertli, D. L. Holt, *Food Chem. Toxicol.*, **21**, 163 (1983).
36. L. G. Shah, *J. Sci. Indust. Res.*, **14B**, 670 (1955).

НОВ КУМАРИН И СЪДЪРЖАНИЕ НА ТОТАЛНИ ФЛАВОНОИДИ И ТОТАЛНИ ФЕНОЛИ В БЪЛГАРСКА ЦЕЛИНА

М. Попова¹, А. Стоянова¹, Н. Вальовска-Попова², В. Банкова^{1*}, Д. Пеев²

¹Институт по Органична химия с Център по Фитохимия, Българска Академия на Науките, ул. Акад. Г. Бончев, бл. 9, 1113 София, България

²Институт по биорацнообразие и екосистемни изследвания, Българска Академия на Науките, ул. Ю. Гагарин 2, 1113 София, България

Постъпила на 06 юни 2014 г.; Коригирана на 04 юли 2014 г.

(Резюме)

Целината *Apium graveolens* е популярен зеленчук, но също така и добре познато лечебно растение. Различни екстракти от целина са показали разнообразни ценни свойства: антиоксидантни, антибактериални, противоракови, и др. В България най-често се използват листата (като подправка) и удебелените корени на *A. graveolens* var. *rapaceum*. Изследван беше химичният състав на неполярни екстракти от българска целина. В петролевоетерната фракция на метанолния екстракт от корени посредством ГХ-МС идентифицирахме мастни киселини и въглеводороди, алилфеноксиацетат, фталидите неокнидилид, изокнидилид, 3-*n*-бутилфталид и кумарините ксантотоксин, изопимпинелин и псорален. Беше изолирано и едно ново природно съединение, 6-(3'-метил-1'-оксобутил)-7-хидроксикумарин, като структурата му беше доказана с помощта на спектрални данни. Съдържанието на тотални феноли и тотални флаваноиди в растителен материал от различни райони на България беше определено спектрофотометрично. Анализирахме метанолните екстракти от листа и корени от 19 местонаходища в България, както и няколко проби от диворастящ *Apium nodiflorum*. Тоталните феноли варираха в границите 15 - 67,2 mg/g еквиваленти галова киселина (ЕГК) в листа и 8.2 - 13.6 ЕГК в корени, а тоталните флаваноиди – в границите 6 – 26,5 mg/g еквиваленти кверцетин в листа и 1 - 4.8 mg/g еквиваленти кверцетин в корени. Резултатите показват, че корените на българската целина са ценен източник на биологично активни компоненти.

Determination of Benzethonium Chloride in Grapefruit Seed Extracts - a GC/MS alternative

D. V. Nedeltcheva-Antonova*, K. S. Tsandeva, R. D. Dimitrova

Institute of Organic Chemistry with Centre of Phytochemistry, Bulgarian Academy of Sciences, Acad. G. Bonchev str., bl. 9, 1113 Sofia, Bulgaria

Received June 18, 2014; Revised July 03, 2014

Dedicated to Acad. Dimiter Ivanov on the occasion of his 120th birth anniversary

Commercial grapefruit seed extracts, distributed on the market as food supplements, were analysed by gas chromatography-mass spectrometry (GC/MS). Presence of benzethonium chloride, a synthetic antimicrobial agent, in the range of 0.14-22.2% was found in 4 of 5 analysed commercial samples (one of them - especially developed for children). The presence of benzethonium chloride was additionally confirmed by high-performance liquid chromatography with diode-array detection (HPLC/DAD) and direct infusion electrospray ionization mass spectrometry (ESI-MS). This work demonstrates that GC/MS represents a simple, fast, selective and sensitive alternative approach for identification and quantitation of benzethonium chloride in commercial grapefruit seed extracts.

Key words: benzethonium chloride, Grapefruit seed extract, GC/MS

INTRODUCTION

Nowadays, there is a growing interest toward alternative medicine and consumption of herbal drugs and additives. At the same time, many of the herbal products available on the market have not been assessed by regulatory authorities and their chemical composition and pharmacological properties are not always well described. One of the products with most controversial fame in the natural products market is the “grapefruit seed extract” (GSE), labelled as an extract of the seeds and pulp of the common grapefruit (*Citrus paradisi*, Rutaceae). GSE has been promoted over the last three decades as a gentle non-toxic natural product with healing power against a variety of diseases, with very high antimicrobial efficacy and has been used as an ingredient for cosmetic and dermatological formulations, in dietary supplements as well as food/cosmetic preservative. However, in most of the cases, the compositions of commercial GSEs are not defined, and the methods of production being proprietary are not specified.

In 1991 the first analysis of commercial GSE was published by Nishina *et al.* [1], where methyl 4-hydroxybenzoate (methyl paraben), a preservative, and 2,4,4-trichloro-2-hydroxydiphenyl ether (triclosan), a microbicide and disinfectant were found by means of preparative HPLC. Using HPLC

and ESI-MS, Sakamoto *et al.* [2] repeated the analysis of GSE, and compared the commercial GSE with ethanolic extracts of grapefruit seeds prepared by themselves. The presence of methyl paraben and triclosan in the commercial GSE (1.66% and 1.97%, respectively) was confirmed and no trace of these compounds was found in the ethanolic extract of grapefruit seeds. The antimicrobial activity as well as the content of preservative agents (methyl paraben and triclosan) in 6 commercially available GSE were examined by von Woedtke and co-workers [3], who additionally found *N*-Benzyl-*N,N*-dimethyl-2-{2-[4-(2,4,4-trimethylpentan-2-yl)phenoxy]ethoxy}ethanaminium chloride (benzethonium chloride), a synthetic antimicrobial agent commonly used in cosmetics and other topical applications, in these products. The five extracts containing one to three of these preservative agents showed high antimicrobial activity. At the same time, the only GSE product without synthetic preservatives along with the fresh extracts prepared from grapefruit seeds with glycerol, water and ethanol, did not exhibit any antimicrobial activity. The authors concluded that the antimicrobial activity attributed to GSE is due to the synthetic preservative agents with benzethonium chloride being responsible for the majority of activity. Takeoka *et al.* subsequently published two analyses of GSE formulations [4,5]. They have found using HPLC, ESI-MS, nuclear magnetic resonance (NMR) spectroscopy, and elemental

* To whom all correspondence should be sent:
E-mail: dantonova@orgchm.bas.bg

analysis that benzethonium chloride is the main constituent in the analysed commercial GSE in form of a liquid concentrate and a concentrated powder (as 8% of the mass of the liquid GSE, higher amounts of benzethonium chloride were found in powder). Sugimoto *et al.* [6] carried out comprehensive research of the commercial GSE products which are used in Japan as food additives (13 products from 6 manufactures), dietary supplements (5 products from 4 manufactures), cosmetic materials (16 products from 10 manufactures) and disinfectants (7 products from 7 manufactures). By means of LC/MS and NMR analysis, synthetic disinfectant agents such as benzethonium or benzalkonium salts were detected in most of the commercial GSE products. Simultaneous identification and quantification of benzethonium chloride, methyl paraben and triclosan in 9 commercial GSE products, one pomegranate (*Punica granatum*, Punicaceae) seed extract, and a freshly prepared methanolic extract of grapefruit seeds, were performed by Avula *et al.* using HPLC/UV/MS [7]. Benzethonium chloride was found in 8 of 9 commercial GSE preparations. Only the commercial pomegranate seed extract (used as a control sample) and the fresh grapefruit seed extract were free of synthetic additives. An HPLC/UV/MS method was developed and validated by Ganzera *et al.* for simultaneous determination of 18 possible preservatives, disinfectants, and microbicides in GSE and tested on 9 commercial products used for eco-farming [8]. A method for the quantitative analysis of benzethonium chloride in GSE based on ¹H-NMR is also described in the literature [9].

Evidently, there is a serious problem with the adulteration of the commercial GSE, which proves the necessity of development and validation of new methods for analysis of benzethonium chloride. As seen, currently most of the methods are based on high-performance liquid chromatography. In addition to the above described, benzethonium chloride was determined by gas-liquid chromatography as reduction product obtained by treatment of the sample with sodium borohydrate and nickel (II) chloride by Kawase *et al.* [10].

Benzethonium chloride being quaternary ammonium salt (QAS) is non-volatile and at first sight gas chromatography could not be the most suitable method for its direct determination. However, the QAS are thermally unstable and decompose at high temperatures by cleavage at the quaternary nitrogen, forming tertiary amines and other neutral molecules [11-13]. Gas chromatography seems to be an ideal analytical technique for the determination of QAS because the heated inlet

system of the instrument allows *in situ* decomposition of the salts. Consequently, thermal decomposition to neutral molecules, vaporization, and analysis of the characteristic products can be performed in a single step. An injection port pyrolysis method for the analysis of quaternary ammonium compounds (QAC) is reported by Lukazewsky *et al.* [14]. Direct injection GC/MS was used for the analysis of benzyl diethyl (2,6-xylylcarbamoymethyl) ammonium benzoate, a QAS, in various Canadian denatured alcohol formulations [15].

Therefore, the aim of the current communication is to describe a fast, simple and sensitive direct GC/MS method for simultaneous identification and quantification of benzethonium chloride, based on the analysis of N,N-dimethyl-2-{2-[4-(2,4,4-trimethylpentan-2-yl)phenoxy]ethoxy}ethanamine as main pyrolysis product.

EXPERIMENTAL

Materials

Samples of commercial GSE, four of them in form of a liquid concentrate and one as a kid syrup, were purchased from drug stores in Bulgaria, Poland and UK. Benzethonium chloride reference material (99%) was delivered from Sigma-Aldrich. Solvents (methanol, chloroform, acetonitrile) of HPLC gradient grade (Sigma-Aldrich) and de-ionized water ASTM Type I were used. Solid-phase extraction columns SOLA SCX, 10 mg/1ml were purchased from Thermo Scientific.

Sample Preparation

Liquid-liquid extraction. Approximately 2 g of each GSE sample was mixed with 10 ml of water and extracted three times with 30 mL of chloroform. The combined chloroform extracts were evaporated either in a rotary vacuum evaporator or under stream of nitrogen. The dry residues were then dissolved in HPLC mobile phase and filtered through a membrane filter (PTFE, 0.22 μm) before the chromatographic analysis.

Solid Phase Extraction. Approximately 0.1 g of each sample was dissolved in 10 ml of methanol and then an aliquot of 0.5 ml was used for solid phase extraction.

Methods

High-Performance Liquid Chromatography (HPLC). The analyses were performed on a HPLC system consisting of an HP1100 liquid chroma-

tograph equipped with a manual injector (Rheodyne, model 7725), fitted with a 20 μL sample loop and a diode-array detector (G1365B DAD), and controlled by ChemStation software (Rev. B.04.03, Agilent Technologies). Analytical column ChromSep SS, Inertsil 5 ODS-2 (250 x 4.6 mm i.d. 5 μm) equipped with a ChromSep guard column (Varian, Palo Alto, CA) was used. The mobile phase was acetonitrile/water (80:20, v/v) containing 0.1% formic acid (pH 3) at a flow rate of 1.0 ml/min. The detector signal was monitored at 215 and 275 nm.

Gas Chromatography-Mass Spectrometry (GC/MS). The GC/MS analysis was performed on a HP gas chromatograph 6890 Series Plus coupled with a 5973 mass - selective detector (Hewlett-Packard, Palo Alto, CA). The ultra-inert fused silica capillary column DB-5ms UI (J&W Scientific, Folsom, CA) with 30 m column length, 0.25 mm i.d., 0.25 μm film thickness was used. The oven temperature was programmed from 80 to 300°C at a rate of 5°C/min, and a 10 min hold at 300°C was applied. Helium (99.999%) was used as a carrier gas at a constant flow rate of 0.8 ml/min. The split ratio was 1:10, the inlet temperature was set to 280°C and the transfer line temperature was 300°C. Mass - selective detector operated in electron impact ionization (EI) mode at 70 eV electron energy, the ion source temperature was set to 200°C, and the quadrupole temperature was 150°C.

Electrospray Ionization-Mass Spectrometry (ESI-MS). ESI-MS spectra were recorded on a DFS High Resolution magnetic-sector mass spectrometer (Thermo Scientific, Bremen, Germany) under the following operating conditions: positive ion scan mode, capillary temperature of 260°C and capillary voltage of 3.5 kV was applied. Direct infusion mode was used for the introducing of samples into the mass spectrometer via Harvard 11 Plus syringe pump (Harvard Apparatus, Holliston, Massachusetts, USA). Acetonitrile/water (30:70%, v.v) with 0.05% formic acid was used as a mobile phase at a flow rate of 0.05 ml/min. The instrument was controlled and the data was processed by Xcalibur™ software (Rev. 2.0 SR 1, Thermo Scientific).

Calibration Curves

The absolute calibration method (external standard method) was used to establish the calibration curve and quantify the analytes. 0.025 g of benzethonium chloride standard was weighed and diluted in a 25 ml volumetric flask with methanol. Five working standard solutions with concentra-

tions in the range 0.001-0.200 mg/ml were prepared from the stock standard solution with concentration 1 mg/ml. Each working standard solution was then analysed in triplicate by GC/MS, operating in full scan mode and the results were presented graphically, plotting peak area (for the peak at $t_{\text{R}}=20.086$ min) versus concentration.

RESULTS AND DISCUSSION

Benzethonium chloride, being quaternary ammonium salt is non-volatile, but, as seen in Fig. 1, its GC/MS chromatogram exhibits two main peaks. The first one is benzyl chloride (**1**), at retention time $t_{\text{R}}=5.54$ min, and the second one has been identified as N,N-dimethyl-2-{2-[4-(2,4,4-trimethylpentan-2-yl)phenoxy]ethoxy}ethanamine (**2**), at $t_{\text{R}}=20.08$ min. These peaks are result of the thermal dissociation of benzethonium chloride (favored pathway is shown in Scheme 1) in the GC inlet system, following the fact that QAS are unstable at high temperatures. In general, the N-benzyl cleavage is favored over the N-alkyl one in this process. The main pyrolysis product **2** exhibits GC/MS behavior, which makes it suitable for identification and low level quantification of benzethonium chloride.

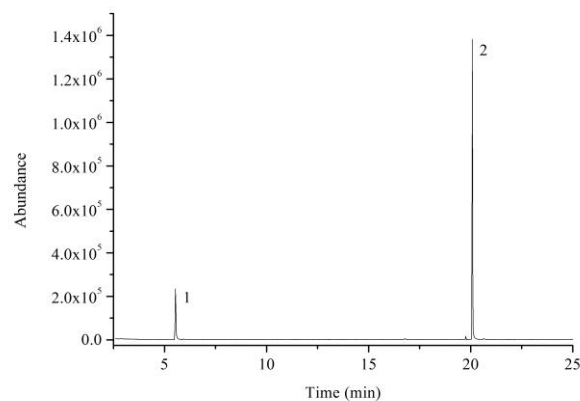


Fig. 1. GC/MS total ion current (TIC) chromatogram of the benzethonium chloride reference material.

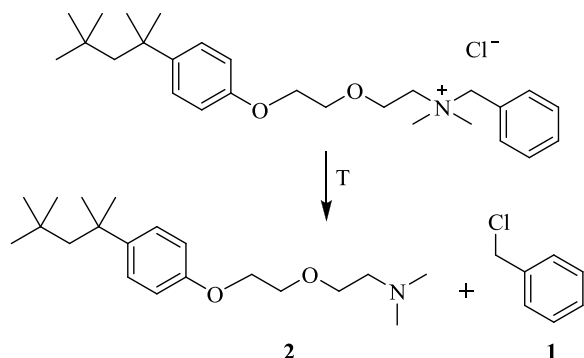
Linear calibration curve with regression coefficient of 0.9997 was established between the EI-MS response of **2** as a function of the benzethonium chloride standard solutions concentration. The corresponding equation is given below:

$$Y = 2.46 \times 10^7 \cdot X + 4.74 \times 10^4,$$

where Y is the total ion current peak area of **2** and X is the concentration of benzethonium chloride in mg/ml.

The linearity was studied in concentration range from 0.001 to 1 mg/ml with limit of quantification

(LOQ) of 0.005 mg/ml (S/N=10) and limit of detection (LOD) of 0.001 mg/ml.



Scheme 1. Thermal dissociation of benzethonium chloride.

Glycerin, used as carrier in the commercial GSE formulations, is moderately volatile and need to be removed from the sample before the GC/MS analysis. Therefore two methods of extraction of benzethonium chloride from the commercial samples have been attempted, namely liquid-liquid extraction with chloroform and solid phase extraction (SPE). In the first case it was impossible to remove glycerin completely and always a white viscous product, containing sufficient amount of glycerin was obtained. The glycerin was fully removed by using only SPE and, therefore, this extraction method was finally selected for sample preparation. The recovery of the SPE, determined by standard addition method, was 0.98.

Using the above discussed procedure, five commercial GSE formulations, available in pharmacies as dietary supplements, with declared ingredients extract of seeds and pulp of grapefruit, plant glycerin and in some cases vitamin C, have been analysed. It is worth to underline that one of these products (sample 1) was introduced as stimulating immune activity syrup, especially designed for kids, with GSE content of 0.1%, containing in addition rose hips extract. The GC/MS analysis has shown availability of benzethonium chloride in four of the samples in range from 0.14 to 22.2%. The corresponding results are collected in Table 1.

These results are stunning, because according to the opinion of the Scientific Committee on Cosmetic Products and Non-Food Products, the scientific advisory body to the European Commission in matters of consumer protection SCCNFP/0762/03, the use of benzethonium chloride as a preservative in leave-on products is safe up to a maximum concentration of 0.1% and absolutely prohibited for internal use.

Table 1. Content of benzethonium chloride in the analysed commercial GSE.

Sample	Benzethonium chloride [%]
1	0.14 ± 0.01
2	8.96 ± 0.39
3	10.6 ± 0.28
4	22.1 ± 0.02
5	< LOD

Benzethonium chloride was identified in the commercial samples by using mass spectral libraries (NIST08, Wiley 275 and MS Search v.2.0), by the retention time of pyrolysis product 2 of the reference material and its mass spectrum with characteristic fragment ions (Fig. 2). As an additional piece of evidence the chromatograms of the analysed samples are shown in Fig. 3.

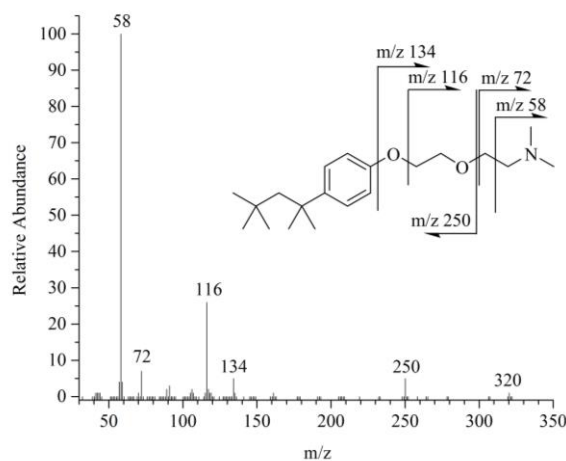


Fig. 2. EI-MS (70 eV) spectrum of 2.

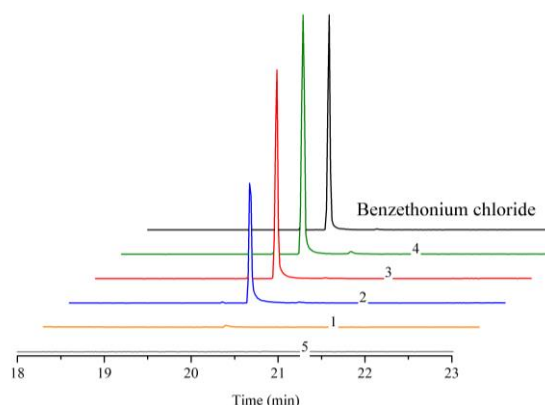


Fig. 3. GC/MS TIC chromatograms of commercial GSE samples.

The identification of benzethonium chloride was additionally confirmed by means of HPLC/DAD and ESI-MS. It is worth to underline that in both cases the samples were analysed at room temperature, which excludes thermal dissociation.

When HPLC/DAD (215 and 275 nm) was used a single peak at $t_R = 8.35$ min has been detected in the samples 1-4, which corresponds to the retention time of the benzethonium chloride standard. The commercial samples and the standard solution of benzethonium chloride in suitable concentrations have been analysed by direct infusion ESI-MS in full scan positive mode. The ESI-MS spectra of the reference benzethonium chloride and the samples 1-4, shown in Fig. 4, are identical, which once again confirms the presence of benzethonium chloride in the samples.

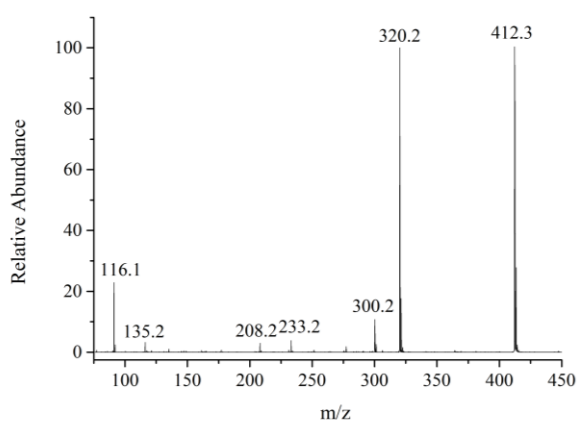


Fig. 4. Positive mode ESI-MS spectrum of benzethonium chloride as reference material and in the samples 1-4.

CONCLUSION

This work demonstrates that direct GC/MS represents a simple, fast, selective and sensitive alternative approach for identification and quantification of benzethonium chloride in commercial GSE. The proposed method seems to be suitable, with small modifications of the sample preparation procedure, for determination of benzethonium chloride and/or other synthetic microbicides based on quaternary ammonium

compounds in various matrices (food additives, cosmetics, etc.).

Acknowledgements: The technical support from Ms E. Dimitrova is gratefully acknowledged.

REFERENCES

1. A. Nishina, H. Kihara, T. Uchibori, T. Oi, *Bokin Bobai (J. Antibact. Antifung. Agents)*, **19**, 401 (1991).
2. S. Sakamoto, K. Sato, T. Maitani, T. Yamada, *Eisei Shikenjo Hokoku (Bull. Natl. Inst. Health Sci.)*, **114**, 38 (1996).
3. T. von Woedtke, B. Schlüter, P. Pflugel, U. Lindequist, D. W. Jülich, *Pharmazie*, **54**, 452 (1999).
4. R. G. Takeoka, D. Lan, Y. R. Wong, R. Lundin, N. Mahoney, *J. Agr. Food Chem.*, **49**, 3316 (2001).
5. R. G. Takeoka, T. L. Dao, Y. R. Wong, A. L. Harden, *J. Agr. Food Chem.*, **53**, 7630 (2005).
6. N. Sugimoto, A. Tada, M. Kuroyanagi, Y. Yoneda, S. Y. Yun, A. Kunugi, K. Sato, T. Yamazaki, K. Tanamoto, *Shokuhin Eiseigaku Zasshi*, **49**, 56 (2008).
7. B. Avula, S. Dentali, A. I. Khan, *Pharmazie*, **62**, 593 (2007).
8. M. Ganzera, A. Aberham, H. Stuppner, *J. Agr. Food Chem.*, **54**, 3768 (2006).
9. S. Bekiroglu, O. Myrberg, K. Ostman, M. Ek, T. Arvidsson, T. Rundlöf, B. Hakkarainen, *J. Pharm. Biomed. Anal.*, **47**, 958 (2008).
10. S. Kawase, S. Kanno, S. Ukai, *J. Chromatogr.*, **247**, 273 (1982).
11. L.-K. Ng, M. Hupe', A. G. Harris, *J. Chromatogr.*, **351**, 554 (1986).
12. B. W. Barry, G. M. Saunders, *J. Pharm. Sci.*, **60**, 645 (1971).
13. A. F. Lopez, M. T. Peralta de Ariza, O. A. Orio, *J. High Resolut. Chromatogr.*, **12**, 503 (1989).
14. T. Lukaszewski, *J. Anal. Toxicol.*, **9**, 101 (1985).
15. K. L. Ng, M. Hupe, J. Harnois, A. Lawrence, *Anal. Chem.*, **70**, 4389 (1998).

ОПРЕДЕЛЯНЕ НА БЕНЗЕТОНИЕВ ХЛОРИД В ЕКСТРАКТИ ОТ СЕМЕНА НА ГРЕЙПФРУТ – АЛТЕРНАТИВЕН ПОДХОД ЧРЕЗ ИЗПОЛЗВАНЕ НА ГАЗОВА ХРОМАТОГРАФИЯ С МАССПЕКТРАЛНА ДЕТЕКЦИЯ

Д. В. Неделчева-Антонова*, К. С. Цандева, Р. Д. Димитрова

Институт по Органична химия с Център по Фитохимия, Българска Академия на Науките, ул. Акад. Г. Бончев, бл. 9, 1113 София, България

Постъпила на 18 юни 2014 г.; Коригирана на 03 юли 2014 г.

(Резюме)

Търговски екстракти от семена на грейпфрут, разпространени в търговската мрежа като хранителни добавки, бяха анализирани чрез газова хроматография – маспектрометрия (ГХ/МС). В четири от пет анализирани търговски продукта (един от които специално разработен за деца) беше намерено присъствие на бензетониев хлорид, синтетичен антимикробен агент, със съдържание от 0.14-22.2%. Наличието на бензетониев хлорид беше допълнително потвърдено чрез високо ефективна течна хроматография с фотометричен детектор с диодна матрица и маспектрометрия с електроспрей йонизация. Публикацията демонстрира възможностите на ГХ/МС като лесен, бърз, селективен и чувствителен алтернативен подход за идентификация и количествено определяне на бензетониев хлорид в търговски екстракти от семена на грейпфрут.

Phospholipid composition of *Cucurbitaceae* seed oils

Z. Y. Petkova*, G. A. Antova

University of Plovdiv 'Paisii Hilendarski', Department of Chemical Technology, 24 Tzar Assen str., 4000 Plovdiv, Bulgaria

Received April 17, 2014; Revised May 27, 2014

Dedicated to Acad. Dimiter Ivanov on the occasion of his 120th birth anniversary

Phospholipid composition of three species of *Cucurbitaceae* family (*Cucurbita moschata*, *Cucurbita pepo* and *Cucurbita maxima*) grown in the southern Bulgaria, was investigated. Oil content of *Cucurbita moschata*, *Cucurbita pepo* and *Cucurbita maxima* seeds was 45.1%, 46.8% and 51.5%, respectively. Phospholipids were determined spectrophotometrically after separation by two dimensional thin layer chromatography. Total phospholipid content in *Cucurbita moschata*, *Cucurbita pepo* and *Cucurbita maxima* seed oils was 0.5%, 1.1% and 1.0%, respectively. Phosphatidylinositol (19.7-29.4%), phosphatidylcholine (34.8-48.6%) and phosphatidylethanolamine (16.0-23.7%) predominated in phospholipid fraction. The quantity of phosphatidic acids was found to be from 2.1% to 5.5%. Fatty acid composition of individual phospholipids was determined by gas chromatography. The predominant fatty acids of phospholipids were palmitic, stearic, oleic and linoleic acids.

Key words: phospholipids, pumpkin seed oil, fatty acids

INTRODUCTION

Phospholipids are the major structural constituents of all biological membranes. They are also present in plants, especially in seeds and kernels of different flora species. Phospholipids are complex lipids which are amphipathic in nature i.e. each molecule consists of a hydrophilic and a hydrophobic parts, thus tending to form lipid bilayers. They are present in many natural sources like human and animal tissues, plants and microbial organisms. Vegetable materials usually contain only small amounts of phospholipids, ranging from 0.3 to 2.5 wt% [1]. The major phospholipids present in plant sources are phosphatidylcholine, phosphatidylinositol and phosphatidylethanolamine. Phospholipids are removed as by-products during the degumming process of vegetable oil refining, too. They are used in food and cosmetic industry [2,3], thence a more detailed study is necessary. Phospholipids are present in pumpkin seeds; therefore the latter could be used as a source of these biologically active components. Their content in pumpkin seeds range from 1.09 to 1.27% [1,4-6]. Nevertheless, the phospholipid content and quantities in pumpkin seed oils have not been investigated in depth.

The most valuable pumpkin species in Bulgaria are *Cucurbita moschata*, *Cucurbita pepo* and *Cucurbita maxima*. There is no information about their phospholipid content and composition, so the

aim of the current study is to present the comparative results of the investigation of phospholipid content and their individual composition in some *Cucurbitaceae* seed oils (three species of pumpkin seed oils) grown in southern Bulgaria. Fatty acid composition of the major phospholipids was investigated, too, and the results were collated to the respective glyceride oils.

MATERIALS AND METHODS

The investigation was carried out with seeds of *Cucurbita moschata*, *Cucurbita pepo*, *Cucurbita maxima* grown in southern Bulgaria, crop 2012. All investigations were carried out with hulled and air-dried seeds. All solvents and reagents were of analytical grade from Merck (Darmstadt, Germany) and were used without additional purification.

Extraction of lipids

The seeds (50 g sample) were ground to powder and the oil was extracted with n-hexane in Soxhlet apparatus for 8 h. After rotation vacuum evaporation of the solvent the extracted oils were dried and weighed [7].

Analysis of phospholipids

Another part (50 g) of air-dried seeds was subjected to Folch extraction [8] and polar lipids were isolated from the total lipids by column

* To whom all correspondence should be sent:
E-mail: jana_petkova@mail.bg

chromatography. The column chromatography was performed according to the procedure reported by Angelova-Romova *et al.* [9]. The sample (about 100 mg oil) was applied into column (2 cm diameter and 40 cm long) filled with silica gel (100-200 mesh). The eluting solvents were chloroform and methanol, respectively. Neutral lipid classes were eluted in sequence of 50 ml chloroform and phospholipids were isolated with 75 ml methanol. The purity of the different classes was verified with thin-layer chromatography. The solvents in the different fractions were evaporated by using N₂. The isolated phospholipid classes were separated by two-dimensional thin-layer chromatography (TLC) on 20 x 20 cm glass plates with 0.2 mm silica gel 60 G layer impregnated with aqueous (NH₄)₂SO₄ (1 g in 100 ml water). In the first direction the plate was developed with chloroform:methanol:ammonia, 65:25:5 (v/v/v) and in the second - with chloroform:acetone:methanol:acetic acid:water, 50:20:10:10:5 (v/v/v/v/v). The individual phospholipids were detected and identified by spraying with specific reagents: Dragendorff test (detection of choline-containing phospholipids), ninhydrin spray (for phospholipids with free amino groups) and Schiff's reagent (for inositol containing phospholipids). Additional identification was performed by comparing the respective R_f values with those of authentic commercial standards subjected to silica gel TLC under identical experimental conditions. The quantification was carried out spectrophotometrically against a standard curve by measuring the phosphorous content at 700 nm after scraping the respective phospholipid zone and mineralization of the substance with a mixture of perchloric acid and sulphuric acid, 1:1 (v/v) [10].

Determination of fatty acid composition of phospholipids

The fatty acids of phospholipids were determined by gas chromatography (GC). The method is based on isolation of phosphatidylcholine (PC), phosphatidylinositol (PI), phosphatidyl-ethanolamine (PE) from the phospholipid fraction by preparative TLC. The obtained free fatty acids after saponification of main phospholipids and acidification [11] were esterified with 2% H₂SO₄ in absolute CH₃OH at 50°C to methyl esters of the fatty acids (FAME) [12]. FAMES were purified by TLC on 20 x 20 cm plates covered with 0.2 mm silica gel 60 G (Merck, Darmstadt, Germany) layer with mobile phase n-hexane:diethyl ether, 97:3 (v/v). GC was performed on a HP 5890 gas

chromatograph (Hewlett Packard GmbH, Austria) equipped with a 60 m x 0.25 mm capillary DB-23 column and a flame ionization detector. The column temperature was programmed from 130°C (1 min), at 6.5°C/min to 170°C, at 3.0°C/min to 215°C (9 min), at 40.0°C/min to 230°C (1 min), injector and detector temperatures were kept at 270°C and 280°C. The carrier gas was hydrogen at a flow rate 0.8 ml/min; split was 1:50. Identification of fatty acids was performed by comparison of retention times with those of a standard mixture of methyl esters of fatty acids subjected to GC under identical experimental conditions [13]. The standard mixture of fatty acid methyl esters was provided by Sigma-Aldrich Chemical Co. (St. Louis, MO, USA).

RESULTS AND DISCUSSION

The content of oil, phospholipids in oil and phospholipids in seeds are presented in Table 1.

Table 1. Oil content, phospholipids in oil and phospholipids in seeds*.

Source	Content, wt %		
	Oil in the seeds	Phospholipids in the oil	Phospholipids in the seeds
<i>Cucurbita moschata</i>	45.1±0.5	0.5±0.1	0.2±0.05
<i>Cucurbita pepo</i>	46.8±0.2	1.1±0.2	0.5±0.1
<i>Cucurbita maxima</i>	51.5±0.3	1.0±0.1	0.5±0.1

*Means of triplicate analysis ± SD.

Based on the data, it is obvious that *Cucurbita maxima* has the highest amount of oil in the seeds (51.5%), followed by *Cucurbita pepo* (46.8%) and *Cucurbita moschata* (45.1%) seeds. According to Kim *et al.* [14], lipid content in *Cucurbita moschata*, *Cucurbita pepo* and *Cucurbita maxima* seed oils was 45.7%, 43.9% and 52.4%, respectively. These results were similar to those obtained in our investigation; according to these authors, only the oil content of *Cucurbita pepo* seeds was a bit lower. On the other hand, according to Ihediohanma *et al.* [15] the lipid content of *Cucurbita pepo* seed oil was 50.3% which was higher than in the species grown in Bulgaria. Fokou *et al.* and Achu *et al.* [16,17] presented the oil content of *Cucurbita moschata* and *Cucurbita maxima* seeds from 48.56 to 52.02% and from 49.05 to 50.81%, respectively.

Cucurbita pepo and *Cucurbita maxima* seeds had the highest amount of phospholipids (0.5%) and phospholipid content in the oil of the same

varieties had also higher amount (1.1 and 1.0%, respectively) than in *Cucurbita moschata* seed oil (0.5% in the oil and 0.2% in the seeds). These values are lower than those in previous publications by Raharjo *et al.* and El-Adawy and Taha [4,6] who report that phospholipid content in *Cucurbita moschata* seeds are 1.27% and 1.09%, respectively. The reasons for the different values of the phospholipids are probably origin and geographic region of the growing [6]. Phospholipid content of pumpkin seed oils is similar to that of sunflower, flaxseed, corn germ, soybean and canola oil (0.7-1.0%) [18-20].

Individual phospholipid composition of pumpkin seed oils is shown in Fig. 1.

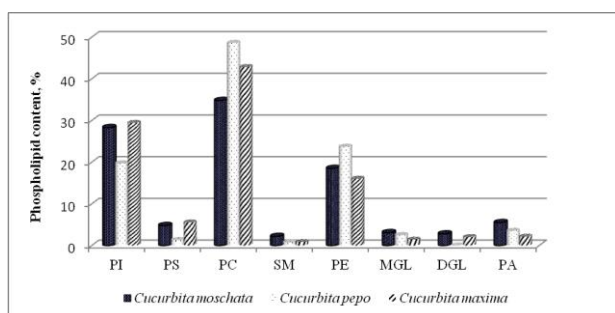


Fig. 1. Individual phospholipid composition of pumpkin seed oils. PI - Phosphatidylinositol; PS - Phosphatidylserine; PC - Phosphatidylcholine; SM - Sphingomyelin; PE - Phosphatidylethanolamine; MGL - Monophosphatidylglycerol; DGL - Diphosphatidylglycerol; PA - Phosphatidic acid.

All main classes of phospholipids were presented in pumpkin seed oils. Phosphatidylcholine was the predominant constituent in all pumpkin seed oils (from 34.8% to 48.6%) followed by phosphatidylinositol (from 19.7% to 29.4%) and phosphatidylethanolamine (from 16.0% to 23.7%). Phosphatidylcholine was detected in highest quantity in *Cucurbita pepo* - 48.6%, while in the other two species its amount was 42.8% in *Cucurbita maxima* and 34.8% in *Cucurbita moschata*. The amount of phosphatidylinositol in *Cucurbita moschata* and *Cucurbita maxima* seed oils was 28.3% and 29.4%, respectively, while the quantity of this class of phospholipids in *Cucurbita pepo* seed oil was 19.7%. The quantity of phosphatidylethanolamine in *Cucurbita pepo* species was 23.7%, while the other two varieties contained lower amounts of it - 18.5% in *Cucurbita moschata* and 16.0% in *Cucurbita maxima* seed oil. Phosphatidylserine (1.3-5.5%), monophosphatidylglycerol (1.4-3.1%) and phosphatidic acids (2.1-5.5%) were presented in small quantities. The amount of sphin-

gomyelin (0.7-2.2%) and diphosphatidylglycerol (~2.8%) was minimal in all pumpkin seed oils.

Fatty acid composition of the main phospholipids (phosphatidylcholine, phosphatidylinositol and phosphatidylethanolamine) is shown in Fig. 2. The most predominant component in all species was palmitic acid, followed by oleic, stearic and linoleic acids.

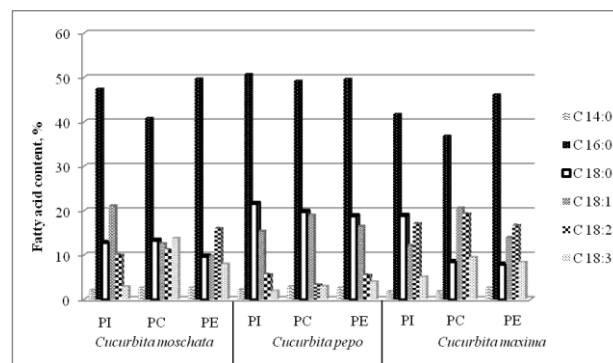


Fig. 2. Fatty acid composition of the main phospholipid classes. C_{14:0}- Myristic acid; C_{16:0}- Palmitic acid; C_{18:0}- Stearic acid; C_{18:1}- Oleic acid; C_{18:2}- Linoleic acid; C_{18:3}- Linolenic acid.

The quantity of palmitic acid in phosphatidylinositol, phosphatidylcholine and phosphatidylethanolamine in *Cucurbita moschata* was 47.4%, 40.9% and 49.7%, respectively. The amount of oleic acid in phosphatidylinositol, phosphatidylcholine and phosphatidylethanolamine was 21.1%, 12.6% and 9.8%, respectively, while the quantity of linoleic acid in the same phospholipids was 10.0%, 11.2% and 16.0%, respectively. The levels of stearic acid were close - 12.8%, 13.3% and 9.7%. Linolenic acid was presented in higher quantity in phosphatidylcholine (13.8%) and in phosphatidylethanolamine (8.0%), while in phosphatidylinositol it was significantly lower (2.1%). Myristic acid in these three phospholipid classes was detected in similar amounts (2.1-2.6%).

The quantity of palmitic acid in phosphatidylinositol, phosphatidylcholine and phosphatidylethanolamine in *Cucurbita pepo* was 50.7%, 49.2% and 49.5%, respectively followed by stearic acid - 21.6%, 19.8% and 18.8%. The levels of oleic acid in phosphatidylinositol, phosphatidylcholine and phosphatidylethanolamine were from 21.6% to 18.8%, respectively. The quantity of linoleic acid in the same phospholipids was a bit higher - 15.4%, 16.5% and 19.0% in phosphatidylinositol, phosphatidylethanolamine and phosphatidylcholine. Linolenic and myristic acids were presented in lower quantities (1.9-4.0% and 2.2-2.9%, respectively), in these phospholipids.

The quantity of palmitic acid in phosphatidylinositol, phosphatidylcholine and phosphatidylethanolamine in *Cucurbita maxima* was 41.7%, 36.8% and 46.1%, respectively, and that of stearic acid was 18.9%, 8.5% and 7.9%. The amount of oleic acid was higher in phosphatidylcholine (20.6%), while in phosphatidylinositol and phosphatidylethanolamine it was 12.2% and 14.0%, respectively. Linoleic acid was presented in a relatively higher amount (17.1% in phosphatidylinositol, 19.3% in phosphatidylcholine and 16.7% in phosphatidylethanolamine). The quantity of linolenic acid was lower - 5.1% in phosphatidylinositol, 9.5% in phosphatidylcholine and 8.4% in phosphatidylethanolamine. There was also a small amount of myristic acid (from 1.8% in phosphatidylinositol and phosphatidylcholine to 2.6% in phosphatidylethanolamine).

These results differ from the data obtained by Vidhute *et al.* [21] who reported that linoleic acid predominated in phospholipid fraction (37.1%), followed by oleic (27.4%) and palmitic acid (24.0%).

The ratio between saturated (SFA), mono-unsaturated (MUFA) and polyunsaturated fatty acids (PUFA) of the main phospholipids was presented in Fig. 3 and these results were collated to the respective triacylglycerols (TAG) reported by Petkova and Antova [22]. Identical fatty acids have been detected in the TAG and phospholipids, but they are in different amounts.

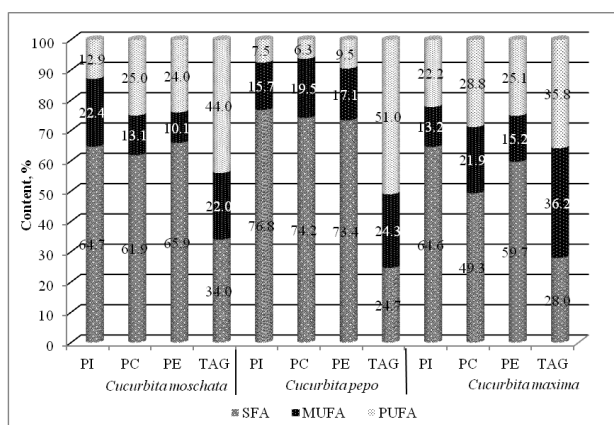


Fig. 3. The ratio between saturated (SFA), monounsaturated (MUFA) and polyunsaturated fatty acids (PUFA) of the main phospholipids and triacylglycerols (TAG).

The highest content of SFAs was detected in *Cucurbita pepo* (73.4-76.8%), while the amount of PUFAs was very low (6.3-9.5%). The phospholipid fraction of *Cucurbita maxima* had a significantly

higher content of PUFAs (25.1-28.8%) which was at the expense of the content of SFAs in the same species (49.3-59.7%). There are considerable differences in the fatty acid composition of phospholipid classes in all pumpkin species. The highest quantity of SFAs was detected in phosphatidylinositol (64.6-76.8%), followed by phosphatidylethanolamine (59.7-73.4%) and phosphatidylcholine (49.3-74.2%). On the other hand, phosphatidylcholine contained the highest level of PUFAs (6.3-28.8%). The differences in the fatty acid composition can be explained by the different individual stages of biosynthesis of the separated phospholipids. Saturated fatty acids were synthesized in the first stage of biosynthesis and were included in phospholipids when the last were synthesized, too [23]. On the other hand, phosphatidylinositol was synthesized first, thus saturated fatty acids were predominant in this phospholipid. Phosphatidylcholine was synthesized last, when the biosynthesis of polyunsaturated fatty acids began. Therefore, polyunsaturated fatty acids predominate in the phosphatidylcholine.

The fatty acid composition of the phospholipids and triacylglycerols was very different. The fatty acid profiles of the phospholipid fraction were characterized by a significant amount of saturated acids, while unsaturated acids predominated in the triacylglycerols [22]. The increase of unsaturated fatty acids was most significant in *Cucurbita pepo* seed oils (from 6.3-9.5% in phospholipids to 51.0% in triacylglycerols), while the changes of the same acids in *Cucurbita maxima* seed oils were only about 10% (from 22.2-28.8% in phospholipids to 35.8% in triacylglycerols).

CONCLUSION

This study shows that the phospholipid content and the fatty acid composition of the main phospholipids classes in pumpkin seed oils do not differ significantly from those in other seed oils as sunflower, canola, corn germ oil, etc. The pumpkin seed oils and seeds have a relatively high content of biologically active compounds, such as phospholipids (0.5-1.1% in the oils and 0.2-0.5% in the seeds). Phospholipids have a similar qualitative and quantitative composition in the studied pumpkin varieties and are similar to those of other vegetable oils, such as sunflower, soybean, flaxseed oils, etc. Palmitic acid is the major component in phospholipids (36.8-50.7%), followed by stearic acid (7.9-21.6%), oleic acid (9.8-21.1%) and linoleic acid (3.3-19.3%). Saturated fatty acids predominate

in phospholipids, while unsaturated fatty acids are predominant in triacylglycerols.

This leads to their complete and versatile examination. The studies about phospholipid content of pumpkin seed oils also contribute to a full assessment of their nutritional value.

Acknowledgements: The investigations were carried out with the partial financial support of contract SI13FC006/2013 of the University of Plovdiv "Paisii Hilendarski".

REFERENCES

1. F. Pasini, Y. Riciputi, V. Verardo, M. Fiorenza Caboni, *Recent Res. Devel. Lipids*, **9**, 139 (2013).
2. S. Kanoh, K. Maeyama, R. Tanaka, T. Takahashi, M. Aoyama, M. Watanabe, K. Lida, E. Niwa, *Dev. Food Sci.*, **42**, 179 (2004).
3. M. Schneider, *Eur. J. Lipid Sci. Technol.*, **103**, 98 (2001).
4. T. A. El-Adawy, K. M. Taha, *Food Chem.*, **74**, 47 (2001).
5. A. Szydłowska-Czeraniak, E. Szlyk, *Food Chem.*, **81**, 613 (2003).
6. T. J. Raharjo, L. Nurliana, S. Mastjeh, *Indo. J. Chem.*, **11**, 48 (2011).
7. ISO 659:2009. Oilseeds – *Determination of oil content* (Reference method), p. 12 (2009).
8. J. Folch, M. Lees, G. H. Sloane-Stanley, *J. Biol. Chem.*, **226**, 498 (1957).
9. M. Angelova-Romova, M. Zlatanov, G. Antova, S. Momchilova, E. Blagoeva, M. Nikolova, *Compt. rend. Acad. Bulg. Sci.*, **66**, 1689 (2013).
10. ISO 10540-1:2003. Animal and vegetable fats and oils. *Determination of phosphorus content – Part 1: Colorimetric method*, p. 10 (2003).
11. N. S. Arutyunyan, E. P. Kornena, Phospholipids of vegetable oils, Agropromizdat Press, Moscow, p. 63 (1986).
12. ISO 5509:2000. Animal and vegetable fats and oils. *Preparation of methyl esters of fatty acids*, p. 30 (2000).
13. ISO 5508:2004. Animal and vegetable fats and oils. *Analysis by gas chromatography of methyl esters of fatty acids*, p. 9 (2004).
14. M. Y. Kim, E. J. Kim, Y.-N. Kim, C. Choi, B.-H. Lee, *Nutr. Res. Pract.*, **6**, 21 (2012).
15. N. C. Ihediohanma, C. N. Ubbaonu, E. N. T. Akobundu, E. O. I. Banigo, *Niger. Food J.*, **24**, 123 (2006).
16. E. Fokou, M. B. Achu, G. Kansci, R. Ponka, M. Fotso, C. Tchiegang, F. M. Tchouanguép, *Pak. J. Nutr.*, **8**, 1325 (2009).
17. M. B. Achu, E. Fokou, C. Tchiegang, M. Fotso, F. M. Tchouanguép, *Afr. J. Biotechnol.*, **4**, 1329 (2005).
18. M. Zlatanov, M. Angelova-Romova, G. Antova, E. Ivanova, B. Damyanova, S. Momchilova, I. Marekov, *Plovdiv University „Paisii Hilendarski“ Bulgaria Scientific Papers-Chemistry*, **36**, 105 (2008).
19. O. Teneva, M. Zlatanov, G. Antova, M. Angelova-Romova, R. Dimitrova, M. Marcheva, *Discourse J. Agric. Food Sci.*, **2**, 59 (2014).
20. D. R. O'Brien, W. E. Farr, P. J. Wan, *Introduction to Fats and Oils Technology*, 2nd ed. AOCS Press, p. 140 (2000).
21. B. P. Vidhute, D. R. Bhide, V. Y. Karadbhajne, A. S. Kulkarni, R. R. Khotpal, *J. Botanic. Sci.*, **2**, 1 (2013).
22. Z. Y. Petkova, G. A. Antova, *J. Food Pack. Sci. Techn. Technol.*, **1**, 43 (2013).
23. S. K. Munshi, S. P. Sukhija, I. S. Bahatia, *Phytochem.*, **22**, 79 (1982).

ФОСФОЛИПИДЕН СЪСТАВ НА МАСЛА ОТ СЕМ. *CUCURBITACEAE*

Ж. Ю. Петкова*, Г. А. Антова

ПУ „Паисий Хилендарски”, Катедра „Химична технология”, ул. „Цар Асен” 24, 4000 Пловдив, България

Постъпила на 17 април 2014 г.; Коригирана на 27 май 2014 г.

(Резюме)

Изследван е фосфолипидният състав на масла от семена на три сорта тиква от сем. *Cucurbitaceae* (*Cucurbita moschata*, *Cucurbita pepo* и *Cucurbita maxima*). Масленото им съдържание е съответно 45.1%, 46.8% и 51.5%. Фосфолипидите са определени спектрофотометрично, след разделянето им чрез двупосочна тънкослойна хроматография. Общото съдържание на фосфолипиди в тиквените масла от семена на сортове *Cucurbita moschata*, *Cucurbita pepo* и *Cucurbita maxima* е съответно 0.5%, 1.1% и 1.0%. Във фосфолипидната фракция преобладават основно фосфатидилинозитол (19.7-29.4%), фосфатидилхолин (34.8-48.6%) и фосфатидилетанол-амин (16.0-23.7%). Количеството на фосфатидните киселини е от 2.1% до 5.5%. Мастнокиселинният състав на индивидуалните фосфолипиди е определен чрез газова хроматография. Установено е, че преобладаващите мастни киселини във фосфолипидната фракция са палмитиновата, стеариновата, олеиновата и линоловата.

Sterol and fatty acid composition of grape seed oils

T. N. Ovcharova¹, M. D. Zlatanov^{1*}, A. S. Ivanov²

¹Department of Chemical Technology, University of Plovdiv "Paisii Hilendarski", 24 Tsar Assen str., 4000 Plovdiv, Bulgaria

²Agricultural University, Faculty of Viticulture and Horticulture, Plovdiv, Bulgaria

Received April 24, 2014; Revised July 01, 2014

Dedicated to Acad. Dimiter Ivanov on the occasion of his 120th birth anniversary

The content and composition of sterols, sterol esters and fatty acid composition of the triacylglycerol and sterol esters fractions isolated from the seed oil of four Bulgarian grape varieties - *Super ran bolgar*, *Bolgar*, *Mavroud* and *Shiroka melnishka loza* - were investigated. The total sterol content was estimated to be 0.3-0.4% with an amount of free sterols - 93.4-97.0% and that of sterol esters - 3.0-6.6%. Sterol composition of both sterol fractions was determined by gas chromatography. β -Sitosterol was the main component in both sterol fractions (66.8-73.2%) followed by campesterol (7.1-24.5%) and stigmasterol (2.7-6.9%). The content of cholesterol and stigmasterol in sterol esters was found to be several times higher than in the fraction of free sterols (1.3-2.0% vs 0.5-0.7% and 3.2-6.9% vs 2.7-3.3% respectively). On the contrary, the percentage of campesterol in the sterol esters (7.1-14.0%) was about two times lower than in the free sterols fraction (19.1-24.5%). Linoleic acid predominated in all samples of sterol esters followed by oleic and palmitic acids (40.7-53.8%, 24.9-35.5% and 13.0-16.7% respectively); the content of these acids in the triacylglycerols fractions were in the ranges 68.5-72.3%, 16.3-18.7% and 8.8-11.5% respectively.

Key words: grape seed oil, sterols, sterol esters, fatty acids

INTRODUCTION

The fruits of grape (*Vitis vinifera* L.) are used as food for raw or dried consumption, as well as a source for the production of wine. Grape seeds represent a by-product obtained after winery exploitation and are a cheap renewable source for the production of glyceride oil. The content of glyceride oil in the seeds was found to be about 11-16% [1,2]. Besides, the seeds contain dietary fiber, galic acid, catechin, tannins [3,4]. The oil is rich in essential fatty acids, such as linoleic and linolenic, and contains some bioactive substances: sterols, tocopherols, carotenoids, phospholipids, polyphenols which have a significant role for the determination of its food value [4,5]. The seeds contain relatively small amounts of oil which is usually extracted by solvent but can also be obtained by pressing [6].

Sterols have a beneficial effect for the prevention of atherosclerosis and coronary heart diseases by lowering the levels of cholesterol. El-Shami *et al.* [7] and Fedeli *et al.* [8] reported predomination of β -sitosterol (73.8%) in sterol fraction followed by stigmasterol (13.7%) and campesterol (10.6%). According to Pironen *et al.*

[9] the total quantity of sterols in the dry pomace was found to be 1390 mg/kg⁻¹, and the main constituents were β -sitosterol, campesterol and stigmasterol. The recent investigations of Madawala *et al.* [10] announced about 0.27% total sterol content in the oil and the sterol fraction included 0.5% brasicasterol, 10.3% campesterol, 9.2% stigmasterol, 74.9% β -sitosterol, 5.1% Δ^5 -avenasterol. Cholesterol was not detected in the oil.

All these investigations have a bearing on composition of total sterol fraction. On the other hand, in glyceride oil, sterols are present in two forms - free sterols and sterol esters.

Sterol composition is an important indicator of the quality of vegetable oils due to the requirement for providing information about the content of cholesterol in foods. However, the information on the type and amount of sterols in grape varieties is rather fragmentary as yet. In addition, separate data on free sterols and sterol esters have not been published so far.

Linoleic acid was found to be the main (63.0-73.1%) constituent in triacylglycerols, followed by oleic (13.7-20.8%) and palmitic acids (6.2-8.5%) according to Fernandes *et al.* [11].

In this connection, the aim of this study was to investigate the seeds recovered from four Bulgarian grape varieties for oil content and to present the

* To whom all correspondence should be sent:
E-mail: magzlat@uni-plovdiv.bg

results about the content and composition of free and esterified sterols separated from the oils as well as the fatty acid composition of sterol esters and triacylglycerol fractions.

MATERIALS AND METHODS

Samples

The seeds of the investigated grape varieties *Super ran bolgar*, *Bolgar*, *Mavroud* and *Shiroka melnishka loza* were obtained from the Agricultural University, Faculty of Viticulture and Horticulture, Plovdiv, Plovdiv region in South Bulgaria, crop 2013. The study was carried out on air dried seeds in technical ripeness.

Glyceride oil

The oil was extracted in Soxhlet apparatus with hexane for 8 h [12]. Then the main part of the solvent was removed in a rotary evaporator, the residue of the solvent was evaporated under a stream of nitrogen and the samples were weighed to determine the oil content.

Sterols

The total oil sample (sample size about 200 mg, precisely measured) was applied on a 20 cm x 20 cm glass plate with 0.5 mm thick silica gel 60 G layer (Merck, Darmstadt, Germany) and developed with hexane-acetone, 100:8 (by volume) to a front of 19 cm. Free ($R_f=0.4$) and esterified ($R_f=0.8$) sterols were detected under UV light by spraying the edges of the plate with 2',7'-dichlorofluorescein and then they were scraped, transferred to small glass columns and eluted with diethyl ether. The solvent was evaporated under a stream of nitrogen, the residue was weighed in small glass containers to a constant weight. Finally, 1% solutions in chloroform were prepared. Free sterols were subjected to gas chromatography (GC) without derivatization.

Sterol esters

Sterol esters were hydrolyzed with ethanolic KOH [13]; free sterols were extracted with light petroleum ether and purified by thin layer chromatography under the above conditions. Sterol composition of both sterol fractions was determined without derivatization on HP 5890 gas chromatograph (Hewlett Packard GmbH, Austria) equipped with 25 m x 0.25 mm HP5 capillary

column (Agilent Technologies, Santa Clara CA, USA) and flame ionization detector (FID). The following temperature gradient was applied: from 90°C (held for 2 min) to 290°C at 15°C/min then to 310°C at 4°C/min and held at this temperature for 10 min; the injector temperature was 300°C and the detector temperature was 320°C. Hydrogen was the carrier gas at a flow rate of 0.8 mL/min; split 100:1. Identification was performed by comparison of the retention times with those of a standard mixture of sterols [14]. The content of total sterols was determined by gas chromatography under the same conditions with betulin as an internal standard [14].

Fatty acids

The fatty acid composition of the triacylglycerols and sterol esters fractions were determined by GC after transmethylation of the respective sample with 2N methanolic KOH at 50°C according to Christie [13]. Fatty acid methyl esters (FAME) were purified by silica gel TLC on 20x20 cm plates covered with 0.2 mm Silica gel 60 G layer (Merck, Darmstadt, Germany) with mobile phase n-hexane:acetone, 100:8 (by volume). GC was performed on a HP 5890 (Hewlett Packard GmbH, Austria) gas chromatograph equipped with a 30 m x 0.25 mm capillary DB-23 column (Hewlett Packard GmbH, Austria) and a FID. The column temperature was programmed from 130°C (1 min) to 170°C at 6.5°C/min; at 3°C/min to 215°C (9 min), at 40°C/min to 230°C (1 min); injector and detector temperatures were 270°C and 280°C respectively. Hydrogen was the carrier gas at a flow rate 0.8 mL/min; split was 100:1. Identification was performed by comparison of retention times with those of a standard mixture of fatty acids subjected to GC under identical experimental conditions [15].

All the analyses were made in triplicate. Data were expressed as mean \pm SD.

RESULTS AND DISCUSSION

The data about oil content in the seeds and sterol content in the oils are presented in Table 1.

The investigated seeds contain low amount of glyceride oil. These values are close to data reported about some varieties of foreign origin [1,16,20]. The sterol content in the oils was found to be similar to data reported earlier by Pironen *et al.* [9] and Madawala *et al.* [10]. Expectedly, the major part of sterols (more than 90%) was in a free form. Since there is no information about free to esterified sterols ratio in grape seed oil, this profile was compared with sterol composition of other vege-

table oils. The quantity of free sterols was found to be rather higher than that in sunflower [17] and tomato [18] seed oils where this content was about 70-75%.

The qualitative and quantitative composition of the free and esterified sterols is given in Table 2.

The qualitative and quantitative sterol composition of the studied oils isolated from all grape varieties was found to be identical. β -Sitosterol predominated in both sterol fractions and was present in relatively close quantities. The content of campesterol in both fractions was relatively high but in the free sterol fraction its value was about 2 times higher than in sterol esters. On the other hand, the quantities of stigmaterol were about 2 times lower in the fraction of free sterols. A substantial difference in cholesterol content of free and esterified sterols fractions was also found. In sterol esters the cholesterol amount was significantly higher than in the free form. A similar ratio between the content of cholesterol in the free and sterol fractions was reported earlier for other glyceride oils of *Asteraceae* family [17] and for tomato seed oil [18]. This picture about ratio between free sterols and sterol esters is a result of different stages for biosynthesis of free sterols and sterol esters and, on the other hand, of different stages for biosynthesis of cholesterol. The presence of a higher content of cholesterol in sterols esters is ascribed to: (i) the fact that sterol esters are the first to biosynthesize and, (ii) cholesterol is biosynthesized firstly in this sterol fraction and is then used as an intermediate for the synthesis of the other sterols [19].

The other sterol components - brasicasterol, Δ^7 -campesterol, Δ^5 -avenasterol, Δ^7 -avenasterol and Δ^7 -stigmaterol - were present in insignificant quantities or in traces in all investigated varieties of grape seed oils.

These amounts of sterols are different from the data reported by El Shami *et al.* [7] and Madawala *et al.* [10], who found the quantities of campesterol to be considerably lower at the expense of the higher values of stigmaterol.

The fatty acid composition of the sterol esters and triacylglycerol fractions are given in Table 3.

Linoleic acid followed by oleic acid predominated in all sterol ester fractions as unsaturated fatty acids. Saturated fatty acids are presented mainly by palmitic and stearic acids. The other constituents are detected in negligible amounts (lower than 1.0%).

Significant differences were established between the separate species. The sterol fraction isolated from *Bolgar* and *Mavroud* seed oils contains higher percentages of oleic acid (32.1% and 35.5% respectively) at the expense of lower levels of linoleic acid (44.6% and 40.7% respectively). On the other hand, the content of oleic acid in the sterol esters of *Shiroka melnishka loza* and *Super ran bolgar* was found to be lower (28.3% and 24.9% respectively) while the quantity of linoleic acid was rather higher (48.6% and 53.8% respectively).

The qualitative and quantitative fatty acid profile of transmethylated triacylglycerols isolated from the oil of all four investigated grape species was similar. Linoleic acid (68.5-72.3%) predominated, followed by oleic and palmitic acids. The ob-

Table 1. Content of oil in the seeds and sterols in the oils*.

Variety	Oil content of seeds, wt %	Sterol content in oil, wt %	Sterol fractions, rel. % from total sterols	
			Free sterols	Esterified sterols
1. <i>Bolgar</i>	11.6 ± 0.2	0.4 ± 0.02	94.3 ± 1.9	5.7 ± 0.2
2. <i>Super ran bolgar</i>	16.5 ± 0.5	0.3 ± 0.01	93.4 ± 2.8	6.6 ± 0.2
3. <i>Mavroud</i>	15.7 ± 0.3	0.3 ± 0.01	93.5 ± 1.9	6.5 ± 0.1
4. <i>Shiroka melnishka loza</i>	13.9 ± 0.6	0.3 ± 0.01	97.0 ± 3.9	3.0 ± 0.1

*Mean ± SD of three determinations.

Table 2. Composition of free and esterified sterols* (rel. %).

Sterols	Varieties							
	<i>Bolgar</i>		<i>Super ran bolgar</i>		<i>Mavroud</i>		<i>Shiroka melnishka loza</i>	
	Free	Esterified	Free	Esterified	Free	Esterified	Free	Esterified
Cholesterol	0.5 ± 0.01	1.6 ± 0.05	0.6 ± 0.02	2.0 ± 0.1	0.5 ± 0.02	1.3 ± 0.04	0.7 ± 0.01	1.9 ± 0.04
Brasicasterol	2.6 ± 0.1	1.8 ± 0.1	2.6 ± 0.1	1.5 ± 0.1	2.4 ± 0.1	1.4 ± 0.04	1.8 ± 0.1	1.9 ± 0.1
Campesterol	20.5 ± 0.4	11.7 ± 0.2	19.1 ± 0.8	7.1 ± 0.1	20.0 ± 0.4	14.0 ± 0.6	24.5 ± 0.7	12.2 ± 0.5
Stigmaterol	3.2 ± 0.1	6.7 ± 0.3	3.3 ± 0.1	6.0 ± 0.1	3.3 ± 0.2	6.9 ± 0.1	2.7 ± 0.1	3.2 ± 0.1
Δ^7 -Campesterol	1.3 ± 0.1	2.4 ± 0.05	1.0 ± 0.02	2.9 ± 0.1	1.7 ± 0.1	2.4 ± 0.1	1.8 ± 0.04	2.7 ± 0.1
β -Sitosterol	70.2 ± 1.4	72.5 ± 2.9	72.1 ± 1.4	72.8 ± 2.2	70.4 ± 1.4	70.9 ± 2.1	66.8 ± 1.3	73.2 ± 2.2
Δ^5 -Avenasterol	0.4 ± 0.01	1.5 ± 0.1	0.4 ± 0.02	1.5 ± 0.03	0.5 ± 0.01	1.4 ± 0.1	0.4 ± 0.02	2.0 ± 0.1
Δ^7 -Avenasterol	0.8 ± 0.02	1.4 ± 0.04	0.5 ± 0.02	2.3 ± 0.1	0.6 ± 0.02	0.8 ± 0.02	0.5 ± 0.02	1.2 ± 0.04
Δ^7 -Stigmaterol	0.5 ± 0.02	2.4 ± 0.05	0.3 ± 0.01	3.9 ± 0.1	0.6 ± 0.01	0.9 ± 0.02	0.9 ± 0.02	1.7 ± 0.1

*Mean ± SD of three determinations.

Table 3. The fatty acid composition of sterol esters and triacylglycerols* (rel. %).

Fatty acids	Grape varieties							
	Bolgar		Shiroka melnishka loza		Mavroud		Super ran Bolgar	
	Sterol esters	Triacyl-glycerols	Sterol esters	Triacyl-glycerols	Sterol esters	Triacyl-glycerols	Sterol esters	Triacyl-glycerols
Lauric (C _{12:0})	0.1 ± 0	0.4 ± 0.02	0.3 ± 0.01	0.1 ± 0	0.3 ± 0.02	0.4 ± 0.02	0.1 ± 0	-
Myristic (C _{14:0})	0.5 ± 0.02	0.1 ± 0	0.5 ± 0.01	0.1 ± 0	1.3 ± 0.04	0.1 ± 0	0.2 ± 0.01	0.1 ± 0
Pentadecanoic (C _{15:0})	0.2 ± 0.01	-	0.1 ± 0	-	0.3 ± 0.01	0.1 ± 0	0.1 ± 0	-
Palmitic (C _{16:0})	16.7 ± 0.3	11.5 ± 0.5	14.4 ± 0.4	10.0 ± 0.4	16.4 ± 0.7	8.8 ± 0.4	13.0 ± 0.3	8.8 ± 0.4
Palmitoleic (C _{16:1})	0.1 ± 0	0.2 ± 0.01	0.1 ± 0	0.3 ± 0.01	0.2 ± 0.01	0.2 ± 0.01	0.1 ± 0	0.1 ± 0
Margarinic (C _{17:0})	0.3 ± 0.01	0.1 ± 0.01	0.2 ± 0.01	0.1 ± 0	0.2 ± 0	0.1 ± 0	0.1 ± 0	0.1 ± 0
Stearic (C _{18:0})	4.2 ± 0.1	1.0 ± 0.03	6.7 ± 0.3	0.7 ± 0.03	3.5 ± 0.1	1.0 ± 0.1	6.1 ± 0.3	0.8 ± 0.03
Oleic (C _{18:1})	32.1 ± 1.3	17.6 ± 0.4	28.3 ± 1.1	16.3 ± 0.7	35.5 ± 1.1	18.7 ± 0.7	24.9 ± 1.2	17.3 ± 0.7
Linoleic (C _{18:2})	44.6 ± 0.9	68.5 ± 2.7	48.6 ± 1.9	71.3 ± 2.9	40.7 ± 1.2	70.1 ± 2.1	53.8 ± 2.2	72.3 ± 2.9
Linolenic (C _{18:3})	0.2 ± 0.01	0.3 ± 0.01	0.1 ± 0	0.5 ± 0.02	0.3 ± 0.01	0.2 ± 0.01	0.1 ± 0	-
Arahinic (C _{20:0})	0.6 ± 0.02	0.2 ± 0.01	0.3 ± 0.01	0.2 ± 0.01	0.8 ± 0.03	0.1 ± 0	0.2 ± 0.01	0.1 ± 0
Gadoleic (C _{20:1})	0.2 ± 0	0.1 ± 0	0.2 ± 0	0.3 ± 0.01	0.3 ± 0.01	0.1 ± 0.01	0.9 ± 0.04	0.1 ± 0
Behenic (C _{22:0})	0.2 ± 0	-	0.3 ± 0.02	0.1 ± 0.01	0.2 ± 0.01	0.1 ± 0	0.3 ± 0.01	0.3 ± 0.01

*Mean ± SD of three determinations.

tained data are close to results reported earlier by [20,21].

This fatty acid profile of the transmethylated triacylglycerol fraction is to a considerable extent different from this of sterol esters. The amount of linoleic acid in triacylglycerols of all investigated varieties was higher at the expense of the lower level of oleic acid. On the other hand, the content of palmitic (8.8-11.5%) and stearic acids (0.7-1.0%) showed decreasing in comparison with fraction of sterol esters.

CONCLUSION

Sterol composition of the glyceride oils isolated from seeds of four Bulgarian grape varieties was found to be similar. The main part of sterol fraction was in free form. β -Sitosterol predominated in both sterol fractions but the content of campesterol in free form was higher than in sterol esters at the expense of the lower quantities of cholesterol and stigmaterol. The qualitative fatty acid profile of sterol esters and triacylglycerols was found to be similar, but higher amounts of saturated and mono-unsaturated fatty acids were present in sterol esters than in triacylglycerols.

Acknowledgements: The investigations were carried out with the partial financial support of contract SI 13 FC 006/2013 of the University of Plovdiv "Paisii Hilendarski".

REFERENCES

1. S. M. Ahmadi, B. A. Siahsar, *Cienc. Investig. Agrar.*, **38**, 291 (2011).
2. A. Akin, A. Altindişli, *BIBAD*, **4**, 13 (2011).
3. T. Maier, A. Schieber, D. R. Kammerer, R. Carle, *Food Chem.*, **112**, 551 (2009).
4. S. Y. Kim, S. M. Jeong, W. P. Park, K. C. Nam, D. U. Ahn, S. C. Lee, *Food Chem.*, **97**, 472 (2006).
5. Codex standard for named vegetable oils, *CODEX-STAN 210 (Amended 2003, 2005)*.
6. C. Da Porto, E. Porretto, D. Decorti, *Ultrason. Sonochem.*, **20**, 1076 (2013).
7. S. M. El-Shami, M. H. El-Mallah, S. S. Mohamed, *Grasas Aceites*, **43**, 157 (1992).
8. E. Fedeli, A. Lanzani, P. Capella, G. Jacini, *J. Am. Oil Chem. Soc.*, **43**, 254 (1966).
9. V. Piironen, J. Toivo, R. Puupponen-Pimiä, A.-M. Lampi, *J. Sci. Food Agr.* **83**, 330 (2003).
10. S. R. P. Madawala, S. P. Kochhar, P. C. Dutta, *Grasas Aceites*, **63**, 143 (2012).
11. L. Fernandes, S. Casal, R. Cruz, J. A. Pereira, E. Ramalhosa, *Food Res. Int.*, **50**, 161 (2013).
12. Oilseeds – determination of oil content (Reference method), *ISO 659* (2009).
13. W. W. Christie, *Lipid Analysis*. The Oily Press: Bridgwater, England, (2003).
14. Animal and vegetable fat and oils – Determination of individual and total sterols contents (Gas chromatographic method), *ISO 12228* (1999).
15. Animal and vegetable fat and oils – Determination of methyl esters of fatty acids- Gas chromatographic method, *ISO 5508* (1990).
16. J. M. Luque-Rodríguez, M. D. Luque de Castro, P. Pérez-Juan, *Talanta*, **68**, 126 (2005).
17. M. D. Zlatanov, M. J. Angelova-Romova, G. A. Antova, R. D. Dimitrova, S. M. Momchilova, B. M. Nikolova-Damyanova, *J. Am. Oil Chem. Soc.*, **86**, 867 (2009).
18. V. Kiosseoglou, D. Boskou, *Oleagineux*, **44**, 113 (1989).
19. S. K. Munshi, S. Sukhija, J. Bahatia, *Phytochemistry*, **22**, 79 (1982).
20. N. G. Baydar, M. Akkurt, *Turk. J. Agric. For.*, **25**, 163 (1999).

21. H. Lutterodt, M. Slavin, M. Whent, E. Turner, L. Yu,
Food Chem., **128**, 391 (2011).

СТЕРОЛОВ И МАСТНО-КИСЕЛИНЕН СЪСТАВ НА МАСЛО ОТ ГРОЗДОВИ СЕМКИ

Т. Овчарова¹, М. Златанов^{1*}, А. Иванов²

¹Пловдивски университет "П. Хилендарски", Катедра Органична Химична Технология, ул. Цар Асен 24, 4000
Пловдив, България

²Аграрен университет, Катедра лозарство и градинарство, Пловдив, България

Постъпила на 24 април 2014 г.; Коригирана на 01 юли 2014 г.

(Резюме)

Изследвано е съдържанието и състава на стеролите, стероловите естери, техния мастно-киселинен състав, както и този на триацилглицероловите фракции, изолирани от семената на четири български сорта грозде: *Супер ран Болгар*, *Болгар*, *Мавруд* и *Широка мелнишка лоза*. Общото съдържание на стероли в маслото е 0.3-0.4%, като свободните стероли са 93.4-97.0%, а стероловите естери-3.0-6.6%. Индивидуалният състав е определен чрез газова хроматография. Основният компонент в двете стеролови фракции е β -ситостерол (66.8-73.2%), следван от кампестерол (7.1-24.5%) и стигмастерол (2.7-6.9%). Съдържанието на холестерол и стигмастерол в стероловите естери е няколко пъти по-високо, отколкото във фракциите на свободните стероли (1.3-2.0% срещу 0.5-0.7% и 3.2-6.9% срещу 2.7-3.3%). Обратно, съдържанието на кампестерол в стероловите естери (7.1-14.0%) е около два пъти по-ниско отколкото в свободната форма (19.1-24.5%). Основните мастни киселини, които преобладават в стероловите естери са линолова (40.7-53.8%), олеинова (24.9-35.5%) и палмитинова (13.0-16.7%); съдържанието на тези киселини в триацилглицеролите е съответно 68.5-72.3%, 16.3-18.7% и 8.8-11.5%.

SDS-induced phenoloxidase activity of *Helix aspersa* maxima hemocyanin

Y. Raynova¹, S. Todinova², D. Yordanov¹, K. Idakieva^{1*}

¹Institute of Organic Chemistry with Centre of Phytochemistry, Bulgarian Academy of Sciences, Acad. G. Bonchev str., bl. 9, 1113 Sofia, Bulgaria

²Institute of Biophysics and Biomedical Engineering, Bulgarian Academy of Sciences, Acad. G. Bonchev str., bl. 21, 1113 Sofia, Bulgaria

Received May 13, 2014; Revised June 13, 2014

Dedicated to Acad. Dimiter Ivanov on the occasion of his 120th birth anniversary

Oxygen-transporting protein of the hemolymph of snails *Helix aspersa* maxima (HaH) was converted from being an oxygen carrier to a form which exhibited phenoloxidase activity by incubation with sodium dodecyl sulfate (SDS). On treatment with 1.73 mM SDS, for 3 min, significant increase of catalytic efficiency of hemocyanin towards substrate catechol ($k_{\text{cat}}/K_m = 34.56 \text{ mM}\cdot\text{min}^{-1}$ versus $k_{\text{cat}}/K_m = 0.093 \text{ mM}\cdot\text{min}^{-1}$ for native hemocyanin) was achieved. The highest *o*-diPO activity and enzyme efficiency of HaH ($k_{\text{cat}}/K_m = 60.94 \text{ mM}^{-1} \text{ min}^{-1}$), after incubation in 1.73 mM SDS for 3 min, was determined towards substrate dopamine. Structural characterization by means of absorption and fluorescence spectroscopy and circular dichroism showed that SDS induced optimal conformational changes in the protein. As a result the active sites become more accessible to the molecules of the substrate and the hemocyanin can function as phenoloxidase.

Key words: hemocyanin; *Helix aspersa* maxima; phenoloxidase activity; enzyme activation

INTRODUCTION

Hemocyanins (Hcs) are high molecular mass copper proteins, freely dissolved in the hemolymph of invertebrates from the phyla *Mollusca* and *Arthropoda* [1,2]. Molecules of molluscan Hcs are structured as decamers (cephalopods) or didecamers (gastropods) of subunits with molecular mass of 350–450 kDa [3]. The subunit polypeptide chains are organized as a linear sequence of seven or eight globular functional units (FUs) of ~ 50 kDa, each containing a binuclear copper active site capable of reversibly binding dioxygen. The binuclear copper active site has two closely spaced copper atoms each coordinated by 3 histidine nitrogen atoms. Dioxygen is reversibly bound to the active site as peroxide in the characteristic side-on bridging ($\mu\text{-}\eta^2\text{:}\eta^2$) geometry (Fig. 1) [4-7]. Similar active site geometry possess the other members of the type-3 copper protein family enzymes i.e. tyrosinase (Ty) and catechol oxidase (CO). Although the binuclear site is highly conserved, as witnessed by its characteristic spectroscopic properties and sequence homology, the functionality of these proteins is different. Namely, Ty catalyzes both the *o*-hydroxylation of monophenols to *o*-diphenols (tyrosinase or monophenoloxidase activity)

and subsequent oxidation of *o*-diphenols to *o*-quinones (catecholase or diphenoloxidase activity), whereas CO catalyzes only the second reaction (Fig. 2) [7].

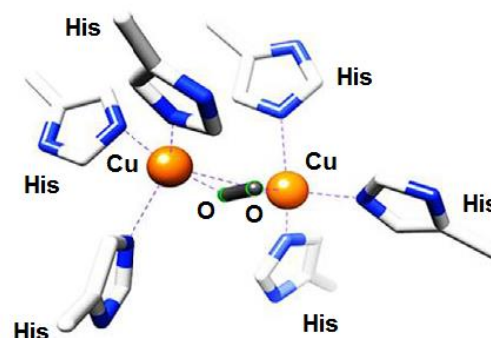


Fig. 1. Binuclear copper active site with six conserved histidine residues, indicative of type-3 copper proteins.

In contrast to these dicopper enzymes, the function of Hcs is restricted to reversible binding of O_2 . The inaccessibility of the type-3 center to potential substrates has been accepted as one of the main reasons for the absence or low level of phenoloxidase (PO) activity in Hcs [8]. After activation of Hcs, making the active sites more accessible to the molecules of the substrate, they can function as POs [9]. Thus, upon treatment of

* To whom all correspondence should be sent:
E-mail: idakieva@orgchm.bas.bg

the Hc, isolated from snails *Helix aspersa maxima* (gastropod) with proteolytic enzyme, more than sixty fold increase in its enzymatic efficiency was achieved [10].

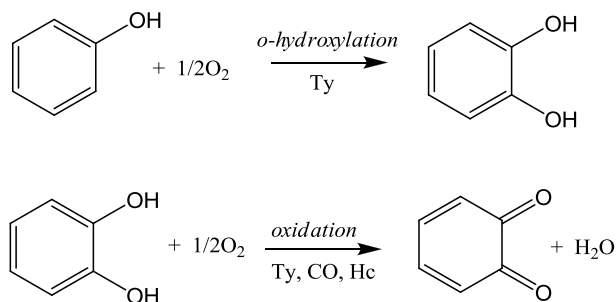


Fig. 2. Hydroxylation step (top) and subsequent oxidation (bottom) mediated by tyrosinase (Ty). The later reaction is also catalyzed by catechol oxidase (CO) and hemocyanin (Hc).

This study presents the SDS-induced phenoloxidase activity of *Helix aspersa maxima* hemocyanin (HaH), as well as an analysis of the accompanying conformational changes in the protein, which gives further insight for the enzymatic properties of these multifunctional proteins.

EXPERIMENTAL

Reagents

L-Dopa and dopamine hydrochloride were purchased from Sigma-Aldrich. Catechol was obtained from Merck. All other chemicals used are of analytical grade.

HaH was isolated from the hemolymph of the snails *Helix aspersa maxima* and purified as described in [10].

Assay of phenoloxidase activity

In the standard procedure, the PO activity of HaH was determined at 25°C in 25 mM sodium phosphate buffer, pH 7.2, at a final concentration of Hc of 0.5 mg/ml. The enzyme reaction was followed by absorbance measurement of quinone derivatives, formed as a result of substrate oxidation at 400 nm (for substrate catechol) or 475 nm (for substrates L-Dopa and dopamine). The absorbance values were corrected for the contribution due to the auto-oxidation of the substrates by running the same assay in the absence of Hc. The reaction rate was measured from the initial quasi-linear portion of the curves (usually 0-3 min). The kinetic parameters [K_m (mM), V_{max} (nmol min⁻¹ mg⁻¹) and k_{cat} (min⁻¹), expressed per copper pair] were derived from non-

linear regression data analysis of the dependence of the initial rates on the substrate concentration (according to Michaelis-Menten kinetics) using HYPER software (Hyperbolic Regression Analysis of Enzyme Kinetic Data, Copyright J. S. Easterby) [11], taking into account the molar absorption coefficient of 1417 M⁻¹cm⁻¹ for *o*-quinone [12] and 3600 M⁻¹cm⁻¹ for dopachrome [13], and the molecular mass of a FU (entity with one active site; 50 kDa). The kinetic parameters were determined from three experiments and reported as mean ± standard deviation.

UV-VIS absorption spectroscopy

UV-VIS spectrophotometer model Evolution 300, Thermo Electron Corporation, equipped with a Peltier temperature control accessory, was used for the kinetic measurements. Specific absorption coefficient $a_{278\text{ nm}} = 1.413\text{ ml mg}^{-1}\text{ cm}^{-1}$ for HaH [14] was used for determining the protein concentration.

Steady-state fluorescence measurements

The fluorescence spectra of HaH were recorded by means of a spectrofluorimeter Perkin Elmer model LS55, at an excitation wavelength of 295 nm. In order to avoid inner filter effects, the optical density of protein samples was < 0.05.

Circular dichroism

Far-UV circular dichroism (CD) measurements were performed at 25°C with a Jobin-Yvon CD6 spectropolarimeter in the 190-250 nm region, using a cell with 0.1 cm pathlength. The protein was dissolved in 25 mM phosphate buffer, pH 7.2, at a concentration of 0.1 mg/ml. Spectra in the near-UV (260-420 nm) were recorded in a rectangular cell of pathlength 0.5 cm, using a protein concentration of 0.3 mg/ml. In each case, five scans were averaged and corrected by subtraction of a spectrum of buffer alone.

RESULTS AND DISCUSSION

Phenoloxidase activation by SDS

Recently, we have established that the native HaH is able to catalyze the reaction of oxidation of catechol to *o*-quinones, i.e. possesses *o*-diPO [10]. The V_{max} value for HaH was obtained to be $22 \pm 0.001\text{ nmol min}^{-1}\text{ mg}^{-1}$, corresponding with a $k_{cat} = 1.1\text{ min}^{-1}$ (expressed per dinuclear copper active site) (Table 1). The native HaH did not show any *o*-

diPO activity with L-Dopa and dopamine as substrates. Similar results have been reported for other molluscan Hcs, namely Hcs isolated from terrestrial snail *Helix pomatia* (β -HpH) and marine snail *Rapana thomasiana* (RtH) [15,16]. Sodium dodecyl sulphate (SDS) is effective in activating Hcs. It has been shown that the micellar form of SDS (present at concentrations > 1 mM in 100 mM sodium phosphate buffer, pH 7.5) is required to induce optimal conformational transitions in the protein, which may result in opening a channel to the di-copper center allowing bulky phenolic substrates to access the catalytic site [17]. Different concentrations of the detergent SDS (0.35-3.81 mM; final concentrations) and incubation times were used in our study to induce *o*-diPO activity in HaH. High degree of increase of the *o*-diPO activity of HaH ($v_i \sim 0.75 \mu\text{mol min}^{-1} \text{mg}^{-1}$) towards substrate catechol, was achieved after 3 min incubation in SDS at concentrations from 1.04 mM to 2.08 mM (Fig. 3).

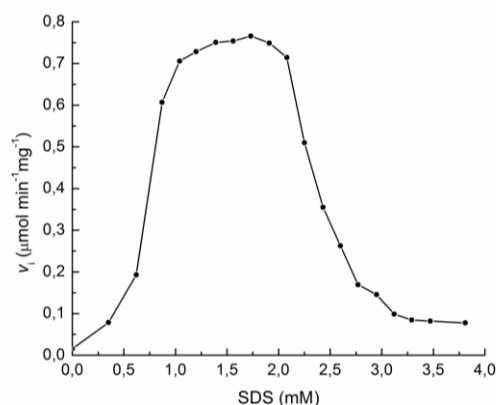


Fig. 3. *o*-diPO activity of HaH, after 3 min incubation with SDS (0.35-3.81 mM; final concentrations). The assay was carried out with catechol (1 mM) as substrate in 25 mM phosphate buffer, pH 7.2, at 25°C and Hc concentration of 0.5 mg/ml.

Higher concentrations of SDS (>2.08 mM SDS) most probably affect the catalytically active conformation of the binuclear copper active sites, thus the induced activity again decreases (Fig. 3). Conformational changes in the protein associated with the

addition of SDS have been analyzed by various biophysical methods.

Effect of SDS on the secondary structure of HaH

The far-UV CD spectrum of native HaH shows two distinct negative Cotton effects at about 208 nm and 222 nm due to the α -helix and β -sheet structures of the protein. CD spectra taken after 3 min of incubation with different concentrations SDS (1.2-2.6 mM) for 3 min at 25°C show changes in the secondary structure, as indicated by the shift of the minimum at 208 nm to lower wavelengths (Fig. 4). This is in agreement with the observations by Baird *et al.* [17] on the Hcs of chelicerates.

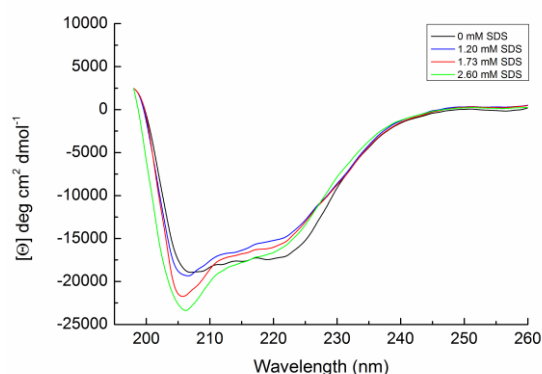


Fig. 4. Far-UV CD spectra of HaH in 25 mM phosphate buffer, pH 7.2, after 3 min incubation in different concentrations of SDS (1.2-2.6 mM).

Effect of SDS on the tertiary structure

SDS-induced changes in the tertiary structure of HaH were characterized by recording intrinsic fluorescence intensities and near-UV CD spectra. After excitation at 295 nm, the fluorescence spectrum of native HaH has maximum at 337 ± 1 nm characteristic for tryptophans “buried” in the hydro phobic interior of the protein molecule. The fluorescence maxima of HaH, incubated in SDS (0.62-2.6 mM) for 3 min, were shifted to longer wavelength (Fig. 5). It appears that after treatment with SDS certain tryptophan side chains turn out to be exposed at the

Table 1. Kinetic parameters of intrinsic and induced *o*-diphenoloxidase activity of *Helix aspersa maxima* hemocyanin towards substrates catechol, L-Dopa and dopamine.

Hemocyanin	Catechol			L-Dopa			Dopamine		
	K_M (mM)	k_{cat} (min^{-1})	k_{cat}/K_M ($\text{mM}^{-1} \text{min}^{-1}$)	K_M (mM)	k_{cat} (min^{-1})	k_{cat}/K_M ($\text{mM}^{-1} \text{min}^{-1}$)	K_M (mM)	k_{cat} (min^{-1})	k_{cat}/K_M ($\text{mM}^{-1} \text{min}^{-1}$)
Native	11.8 \pm 0.5	1.1	0.093	no activity	no activity	no activity	no activity	no activity	no activity
SDS-activated	0.91 \pm 0.23	31.45	34.56	15.26 \pm 0.98	9.58	0.62	0.51 \pm 0.17	31.08	60.94
Proteolytically activated	6.8 \pm 0.2	40.15	5.9	17.3 \pm 0.5	12.45	0.72			

surface of the protein molecule. The presence of SDS also led to increase of the intensity of fluorescence which is indicative for a reduction of internal quenching.

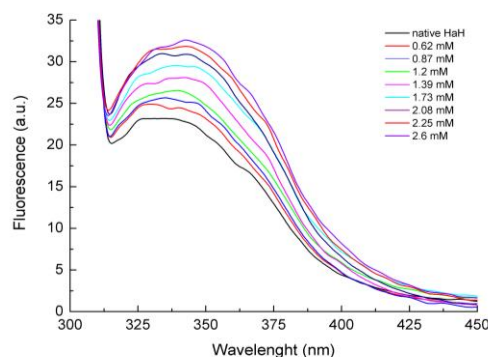


Fig. 5. Fluorescence spectra of HaH in 25 mM phosphate buffer, pH 7.2, excited at 295 nm, after 3 min incubation in different concentrations of SDS (0.62-2.6 mM).

Hcs and POs with bound dioxygen exhibit unique absorption spectra with a characteristic absorption peak at ~ 345 nm [5]. This absorption band results from the peroxide, which is present in a μ - η^2 : η^2 side-on arrangement and acts as a strong σ -donor ligand to the Cu(II) ions. The di-copper center of Hcs is also responsible for the characteristic near UV-CD negative signal at 345 nm [18]. The intensity of the near-UV CD spectra (in the 260- to 320-nm range) of HaH, incubated in SDS (1.2-2.6 mM) for 3 min, was found to decrease substantially (Fig. 6), consistent with conformational changes that alter the microenvironment of at least some of the aromatic residues of the protein. Thus intrinsic fluorescence intensities and near-UV CD spectra both indicate changes in the tertiary structure of HaH upon treatment with SDS.

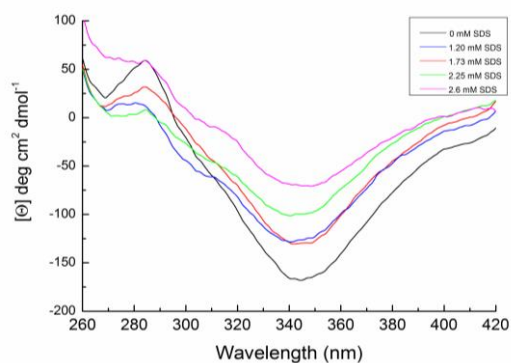
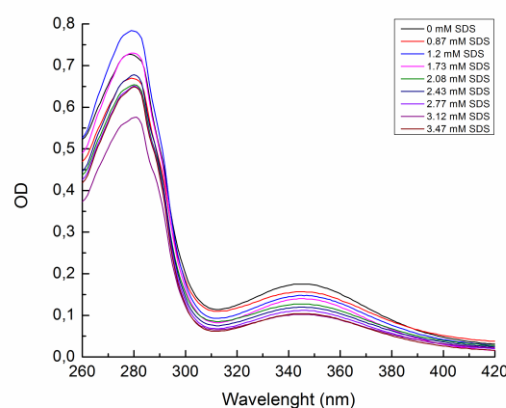
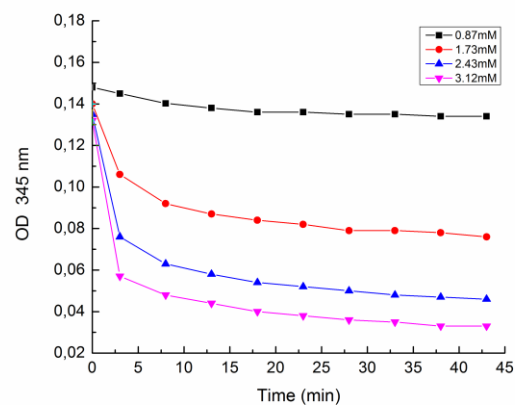


Fig. 6. Near-UV CD spectra of HaH in 25 mM phosphate buffer, pH 7.2, after 3 min incubation in different concentrations of SDS (1.2-2.6 mM).

Absorption spectra taken for HaH at increasing concentration (0.87-3.47 mM) of SDS showed that the intensity of copper-dioxygen band at 345 nm slightly decreased as a function of SDS concentration in the Hc samples (Fig. 7a, b). Therefore, SDS-induced conformational changes did not affect the integrity of the copper active sites in the Hc molecule.



(a)



(b)

Fig. 7. (a) Absorption spectra of HaH in 25 mM phosphate buffer, pH 7.2, after 3 min incubation in different concentrations of SDS (0.87-3.47 mM); (b) Absorbance at 345 nm of HaH in function of time in the presence of SDS at different concentrations (0.87-3.12 mM).

Assay of phenoloxidase activity

Kinetic analysis of the *o*-diPO activity of HaH, activated with SDS, with increasing concentrations of substrates catechol (from 0.1 to 1.2 mM), L-Dopa (from 0.5 to 12 mM) and dopamine (from 0.015 to 0.3 mM) was performed. The kinetic parameters (according to Michaelis-Menten kinetics), obtained by fitting the experimental data using the

software HYPER, are presented in Table 1. High level of SDS-induced activity was detected for HaH towards substrate catechol – V_{\max} increased up to $629 \pm 0.002 \text{ nmol min}^{-1} \text{ mg}^{-1}$, corresponding with a $k_{\text{cat}} = 31.45 \text{ min}^{-1}$ (Table 1). The enzymatic activity of HaH, treated with 1.73 mM SDS for 3 min, is related to that observed with proteolytically activated Hc ($k_{\text{cat}} = 40.15 \text{ min}^{-1}$) [10]. However, the affinity of SDS-activated HaH towards substrate catechol is higher ($K_m = 0.91 \pm 0.2 \text{ mM}$) than the affinity shown by the native HaH ($K_m = 11.8 \pm 0.5 \text{ mM}$) and proteolytically activated HaH ($K_m = 6.8 \pm 0.2 \text{ mM}$) [10]. Moreover, the enzyme efficiency ($k_{\text{cat}}/K_m = 34.56 \text{ mM}^{-1} \text{ min}^{-1}$) of SDS-activated HaH towards catechol is considerably higher than that achieved for proteolytically activated Hc ($k_{\text{cat}}/K_m = 5.9 \text{ mM}^{-1} \text{ min}^{-1}$) [10]. This fact reveals that SDS-activated HaH possesses even higher potential for preparation of biosensors and studies are in progress. Recently, Naresh *et al.* report for a similar sensor for detection of phenols using Hc isolated from a freshwater gastropod *Pila globosa* [19]. The *o*-diPO activity of *P. globosa* Hc has also been enhanced by treatment with SDS.

After activation with SDS, HaH showed *o*-diPO towards the more bulky substrate L-Dopa and dopamine. The V_{\max} value amounted to $192 \pm 0.001 \text{ nmol min}^{-1} \text{ mg}^{-1}$, $k_{\text{cat}} = 9.58 \text{ min}^{-1}$, K_m value of $15.26 \pm 0.98 \text{ mM}$ characterizes the affinity of SDS activated HaH towards substrate L-Dopa. The highest *o*-diPO activity and enzyme efficiency of HaH ($k_{\text{cat}}/K_m = 60.94 \text{ mM}^{-1} \text{ min}^{-1}$), after incubation in 1.73 mM SDS for 3 min, was determined towards substrate dopamine (Fig. 8a, b). Dopamine was also found to be a preferred substrate of SDS-activated Hcs from arthropods *Cancer pagurus* [20] and *Eurypelma californicum* [21]. The physiological importance of this observation represents the fact that dopamine is important metabolite for sclerotization and melanization of the cuticle.

By means of electron cryomicroscopy Cong *et al.* reveal the structural mechanism of SDS-induced enzyme activity of Hc from the scorpion *Pandinus imperator* [22]. They show that secondary and tertiary structural alterations not only provide an increased access of substrates to active sites, but promote novel bridge formation between Hc linker subunits. In this way SDS seems to imitate an allosteric effector.

CONCLUSION

In conclusion, this study demonstrates that micellar concentration of detergent SDS can indu-

ced phenoloxidase activity in the hemocyanin of *Helix aspersa maxima*. The accompanying conformational changes in the protein result in opening a channel to the di-copper center allowing bulky phenolic substrates access to the catalytic site. The high enzyme efficiency of SDS-activated HaH towards catechol ($k_{\text{cat}}/K_m = 34.56 \text{ mM}^{-1} \text{ min}^{-1}$) and dopamine ($k_{\text{cat}}/K_m = 60.94 \text{ mM}^{-1} \text{ min}^{-1}$) reveals the benefit of utilization of PO activity of Hcs for preparation of Hc-based biosensors.

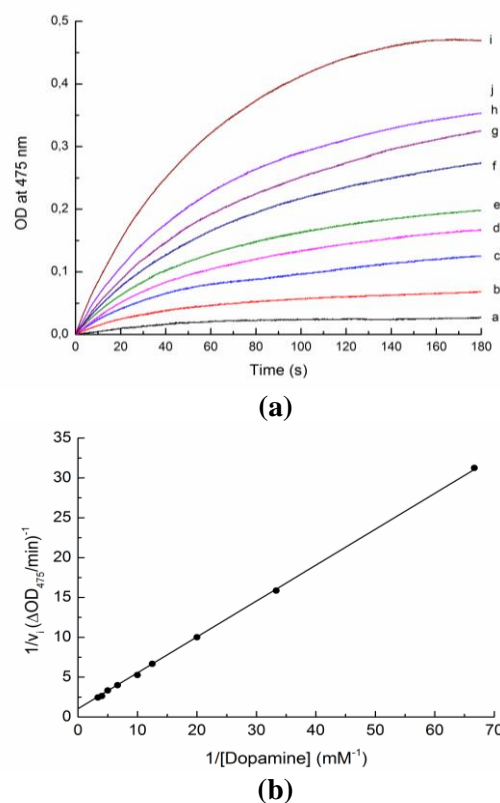


Fig. 8. (a) Kinetic analysis of *o*-diPO activity of HaH with increasing concentration of substrate dopamine: (a) 0.015 mM; (b) 0.03 mM; (c) 0.05 mM; (d) 0.08 mM; (e) 0.1 mM; (f) 0.15 mM; (g) 0.2 mM; (h).25 mM; (i) 0.3 mM. The assay was carried out in 25 mM phosphate buffer, pH 7.2, at 25°C and Hc concentration of 0.5 mg/ml; (b) The corresponding Lineweaver–Burk plot. The derived K_M and k_{cat} values are given in Table 1.

Acknowledgements: Financial support by the National Science Fund of the Ministry of Education and Science, Bulgaria (research grant DTK 02/78), is gratefully acknowledged.

REFERENCES

1. G. Préaux, C. Gielens, Hemocyanins, in: Copper Proteins and Copper Enzymes, Lontie, R. (Ed.), vol. II, CRC Press, Boca Raton, 1984, p. 159.

2. K. E. van Holde, K. I. Miller, *Adv. Protein. Chem.*, **47**, 1 (1995).
3. J. Markl, *Biochim. Biophys. Acta*, **1834**, 1840 (2013).
4. C. J. Coates, J. Nairn, *Dev. Comp. Immunol.*, **45**, 43 (2014).
5. E. I. Solomon, U. M. Sundaram, T. E. Machonkin, *Chem. Rev.*, **96**, 2563 (1996).
6. H. Decker, N. Terwilliger, *J. Exp. Biol.*, **203**, 1777 (2000).
7. M. Rolff, J. Schottenheim, H. Decker, F. Tuczec, *Chem. Soc. Rev.*, **40**, 4077 (2011).
8. H. Decker, F. Tuczec, *Trends Biochem. Sci.*, **25**, 392 (2000).
9. H. Decker, E. Jaenicke, *Dev. Comp. Immunol.*, **28**, 673 (2004).
10. Y. Raynova, L. Doumanova, K. Idakieva, *Protein J.*, **32**, 609 (2013).
11. J. S. Easterby, HYPER.EXE, Version 1.1s: Hyperbolic regression analysis of enzyme kinetic data (1996). <http://homepage.ntlworld.com/john.easterby/index.html>
12. T. Zlateva, P. Di Muro, B. Salvato, M. Beltramini, *FEBS Lett.*, **384**, 251 (1996).
13. J. L. Muñoz-Muñoz, F. Garcia-Molina, R. Varon, J. N. Rodriguez-Lopez, F. Garcia-Canovas, L. Tudel, *Anal. Biochem.*, **351**, 128 (2006).
14. C. Gielens, J. De Sadeleer, G. Preaux, R. Lontie, *Comp. Biochem. Physiol.*, **88B**, 181 (1987).
15. N. I. Siddiqui, R. F. Akosung, C. Gielens, *Biochim. Biophys. Res. Commun.*, **348**, 1138 (2006).
16. K. Idakieva, N. I. Siddiqui, F. Meersman, M. De Maeyer, I. Chakarska, C. Gielens, *Int. J. Biol. Macromol.*, **45**, 181 (2009).
17. S. Baird, S. Kelly, N. Price, E. Jaenicke, Ch. Meesters, D. Nillius, H. Decker, J. Nairn, *Biochim. Biophys. Acta*, **1774**, 1380 (2007).
18. A. M. Tamburro, B. Salvato, P. Zatta, *Comp. Biochem. Physiol.*, **55B**, 347 (1976).
19. K. N. Naresh, S. Krupanidhi, S. S. Rajan, *Protein J.*, **32**, 327 (2013).
20. K. Idakieva, Y. Raynova, F. Meersman, C. Gielens, *Comp. Biochem. Physiol.*, **164B**, 201 (2013).
21. E. Jaenicke, H. Decker, *FEBS J.*, **275**, 1518 (2008).
22. Y. Cong, Q. Zhang, D. Woolford, T. Schweikardt, H. Khant, M. Dougherty, S. Ludtke, W. Chiu, H. Decker, *Structure*, **17**, 749 (2009).

SDS-ИНДУЦИРАНА ФЕНОЛОКСИДАЗНА АКТИВНОСТ НА ХЕМОЦИАНИН ОТ *HELIX ASPERSA MAXIMA*

Ю. Райнова¹, С. Тодинова², Д. Йорданов¹, К. Идакиева^{1*}

¹Институт по Органична химия с Център по Фитохимия, Българска Академия на Науките, ул. Акад. Г. Бончев, бл. 9, 1113 София, България

²Институт по биофизика и биомедицинско инженерство, Българска Академия на Науките, ул. Акад. Г. Бончев, бл. 21, 1113 София, България

Постъпила на 13 май 2014 г.; Коригирана на 13 юни 2014 г.

(Резюме)

Кислород-пренасящият протеин, изолиран от хемолимфата на охлюви от вида *Helix aspersa maxima* (HaH), беше превърнат във форма, която проявява фенолоксидазна активност. Посредством инкубиране на HaH с 1.73 mM SDS, в продължение на 3 мин, беше постигнато значително повишение на каталитичната ефективност на хемоцианина при субстрат катехол ($k_{cat}/K_m = 34.56 \text{ mM} \cdot \text{min}^{-1}$ срещу $k_{cat}/K_m = 0.093 \text{ mM} \cdot \text{min}^{-1}$, определена за нативен HaH). Най-висока SDS-индуцирана *o*-дифенолоксидазна активност и ефективност на HaH, след активиране посредством SDS, беше определена при субстрат допамин ($k_{cat}/K_m = 60.94 \text{ mM}^{-1} \text{ min}^{-1}$). Структурно характеризирани с помощта на абсорбционна и флуоресцентна спектроскопия и кръгов дихроизъм показаха, че мицеларен SDS предизвиква оптимални конформационни промени в протеина, в резултат на което активните центрове стават по-достъпни за молекулите на субстрата и хемоцианинът може да функционира като фенолоксидаза.

Resveratrol loading on mesoporous silica and zeolite carriers by solid state method

M. Popova¹, K. Yoncheva², A. Szegedi³, Y. Kalvachev⁴, N. Benbassat², V. Mavrodinova^{1*}

¹*Institute of Organic Chemistry with Centre of Phytochemistry, Bulgarian Academy of Sciences, Acad. G. Bonchev str., bl. 9, 1113 Sofia, Bulgaria*

²*Faculty of Pharmacy, Medical University of Sofia, 2 Dunav str., 1000 Sofia, Bulgaria*

³*Research Centre for Natural Sciences, Institute of Materials and Environmental Chemistry, Hungarian Academy of Sciences, Magyar tudósok körútja 2, 1117 Budapest, Hungary*

⁴*Institute of Mineralogy and Crystallography, Bulgarian Academy of Sciences, Acad. G. Bonchev str., bl. 107, 1113 Sofia, Bulgaria*

Received April 30, 2014; Revised June 18, 2014

Dedicated to Acad. Dimiter Ivanov on the occasion of his 120th birth anniversary

The feasibility of mesoporous SBA-16 and MCM-41 materials to be used as carriers for the poorly water soluble compound Resveratrol (RES) was studied and compared with that of zeolite Y. A simple procedure of encapsulation in solid-state aiming amorphization of the drug which thus enhancing its solubility has been successfully applied. Investigations using powder XRD, N₂ physisorption, ATR FT-IR and TG analysis demonstrated the effective loading of RES on the surface of the carriers. RES release in buffers with pH=1.2 and pH=6.8 demonstrated faster dissolution of the loaded drug compared to non-loaded resveratrol.

Key words: resveratrol encapsulation, in vitro release, mesoporous silica, zeolite Y carrier

INTRODUCTION

The research and application of natural polyphenols have recently attracted great interest due to their potential in functional food and drug delivery [1-3]. Among these compounds, resveratrol (RES) is recognized mainly as an antioxidant, but also as antiviral, anticancer, an antiinflammatory, antihypersensitive, cardioprotective agent, etc. [4-6]. Despite the promising results in preclinical settings, the extensive use of RES has met only limited success, largely due to its instability [7], poor solubility [8], inefficient systemic delivery and low bioavailability [9]. In this context, the encapsulation of RES into polymeric or lipid-based matrices is a major challenge, and nanotechnology represents a powerful strategy [10]. The development of innovative formulation strategies, capable of overcoming the physicochemical and pharmacokinetic limitations of this compound, is mainly based on discovering suitable carriers able to provide controlled release and protection for RES.

Mesoporous silica nanomaterials of the MCM-41 and SBA-series as well as the microporous zeolites, possess great surface area allowing an efficient drug loading and stabilization of labile drugs during storage or physiological administra-

tion. Further, these carriers could improve water solubility of poorly soluble drugs probably due to the increased surface and/or transformation of the crystal form into amorphous one. Ordered mesoporous silicate MCM-41 and SBA-15 have been widely evaluated as carriers for different poorly soluble compounds [11-15]. In contrast, there has been very limited work dealing with the employment of the cage-like SBA-16 materials as drug carriers [16,17].

The advantages of using zeolites for biomedical applications are their biocompatibility, low toxicity [18-20] and the ability to tune the zeolite properties by varying the SiO₂/Al₂O₃ ratio and the surface functional groups [21,22]. In addition, the smaller zeolite pore size (relative to mesoporous silica) more closely matches the drug molecule size and may better control the drug release kinetics.

The main method applied for loading of active molecules on these carriers is solvent impregnation. This method requires long incubation of the drug and the carrier, usually under heating in appropriate organic solvent. However, some drugs are thermosensitive or insoluble in solvents. Thus, because of this limitation, some new approaches should be developed for the achievement of efficient loading.

The aim of the present study was to evaluate the capacity of three carriers (MCM-41, SBA-16 and Y type zeolite) for RES loading by solid state method.

* To whom all correspondence should be sent:
E-mail: vmavrodinova@orgchm.bas.bg

The method was considered advantageous since no organic solvents or catalysts are required for the encapsulation process and the procedure could be easily performed. Furthermore, the solid state method could be applied as loading method especially for drugs with poor solubility and stability problems like resveratrol.

In our previous publication a thorough examination on the effectiveness of the newly introduced method for solid-state preparation of drug formulations composed of the purely soluble antioxidant resveratrol and nanosized silica materials has been made [23]. In the present contribution a comparison of the loading efficiency and the release kinetics of RES delivery systems based on mesoporous MCM-41 and SBA-16 silicas as well as on Y type zeolite support with different channel structures and morphology, formulated at dry mixing conditions has been made.

EXPERIMENTAL

Synthesis of mesoporous MCM-41 and SBA-16 silica materials. Zeolite Y support

MCM-41 with 100 nm particle size was prepared according to the procedure of Huh *et al.* [24]. This sol-gel procedure is carried out at 80°C without co-solvent, in water solution and applying NaOH as a catalyst. The relative molar composition of the reaction mixture was: 1 TEOS: 0.12 C₁₆TMABr: 0.31 NaOH: 1190 H₂O. The formed gel was aged at 80°C for 2 h, then washed with distilled water until neutral pH and dried at ambient temperature. Structure directing agent removal of MCM-41 materials was carried out in air at 550°C with 1 K/min rate and held at this temperature for 5 h.

SBA-16 has been synthesized according to Zhao *et al.* [25]. F127 triblock copolymer (BASF) is used as template and tetraethylortosilicate (TEOS) as silica source. The relative molar composition of the synthesis mixture is the following: 4 g PEO₁₀₆PPO₇₀PEO₁₀₆: 0.24 HCl: 0.04 TEOS: 7.86 H₂O. The synthesis mixture was stirred at room temperature for 20 h, than hydrothermally treated at 80°C for 48 h. Structure directing agent was removed by calcination in air at 500°C with a heating rate of 1 K/min.

Zeolite Y in its ammonium form was supplied by Zeolyst International (UWE Ohlogge (VF), CBV 500) as a powder with the following characteristics: Si/Al molar ratio of 2.6, Na₂O = 0.2 wt.%, unit cell size = 24.53. The decomposition of the NH₄⁺-form was performed by stepwise heating in dry N₂ as follows: heating up to 300°C, hold for

30min and then heating from 300°C to 550°C, hold 90 min. Heating rate was 8 K/min. The as-obtained initial material is designated as HY(2.6).

Characterization of the samples

X-ray patterns were recorded by a Philips PW 1810/3710 diffractometer with Bragg-Brentano para focusing geometry applying monochromatized CuK α ($\lambda = 0.15418$ nm) radiation (40 kV, 35 mA) and a proportional counter. Philips XPert-MPD apparatus was used for structure characterization of SBA-16.

Nitrogen physisorption measurements were carried out at 77 K using Quantachrome Autosorb 1C apparatus. The specific surface area was calculated by the BET method in the range of relative pressures from 0.01 to 0.1. The pore-size distribution was calculated from desorption branch of the isotherms with the BJH method. The silica supports were pre-treated at 350°C, whereas the drug loaded formulations were heated at 80°C for 5 h before measurements.

Thermogravimetric measurements were performed with a Setaram TG92 instrument. The samples (about 20 mg) were treated in situ in air flow up to 600°C (5°C/min) followed by a hold-up of 1 h. The detected weight loss corresponds to the amount of the deposited resveratrol.

Attenuated Total Reflection Infrared (ATR-FT-IR) spectra were recorded by means of a Varian Scimitar 2000 FT-IR spectrometer equipped with a MCT (mercurycadmium-tellur) detector and a single reflection ATR unit (SPECAC "Golden Gate") with diamond ATR element. In general, 128 scans and 4 cm⁻¹ resolution were applied. For all spectra ATR-correction was performed (Varian ResPro 4.0 software).

Resveratrol loading and in vitro release studies

For the solid state method of RES loading 1:1 weight ratio of RES to the parent mesoporous MCM-41 and SBA-16 materials was used. In case of the zeolite sample 0.8:1.0 ratio was applied. RES was mixed with the carriers at room temperature in a DDR-GM 9458 type vibrational ball mill mixer with stainless holder ($\varnothing = 24$ mm) and one ball ($\varnothing = 9.5$ mm), for 3 minutes without adding any additive for wetting. The as-prepared samples are designated as R/MCM-41(SS), R/SBA-16(SS) and R/Y(2.6)SS indicating their solid-state procedure of preparation. Resveratrol (>99.5%) was provided by Sigma-Aldrich.

For *in vitro* release studies, 5 mg of the drug loaded particles were incubated in 200 ml acid or phosphate buffers (pH=1.2 or pH=6.8, respectively) at 37°C under stirring (100 rpm). At appropriate time intervals, 3 ml samples were withdrawn and replaced by fresh buffer. The withdrawn samples were centrifuged at 15 000 rpm for 15 min and the concentration of the released RES into the supernatant was determined by UV-Vis spectrophotometry (Hewlett Packard 8452A) at a wavelength of 308 nm.

RESULTS AND DISCUSSION

Materials characterization

The XRD reflections of the commercial RES compound and the grinded substance are presented in Fig. 1a. Decrease in the intensity of the diffraction peaks at $2\theta = 17^\circ, 19^\circ, 22^\circ, 23^\circ,$ and 28.3° compared to that of the commercial form of the drug is observed (Fig. 1a). This effect proves that treatment in the vortex mixer leads to partial amorphization of the antioxidant, which was the aim of applying this solid-state preparation procedure. Presence of crystalline RES phase is clearly visible, however, on all loaded samples (Fig. 1a-c). This is evidence that RES is not only introduced in the meso/micropores, but can be found on the outer surface of the nanoparticles or in the voids among them.

The low-angle powder XRD patterns of MCM-41 and SBA-16 show an ordered pore arrangement with the typical reflections at the low angles at $2\theta = 2.4^\circ$ (Fig. 1a) and $2\theta = 1^\circ$ (Fig. 1b) for MCM-41 and SBA-16 respectively which are not destroyed upon RES encapsulation. The X-ray reflections of RES loaded mesoporous carriers reveal clear indication for presence of small RES crystallites on the surface of both MCM-41 and SBA-16 materials.

The X-ray powder diffraction patterns of the calcined zeolite reveal the characteristic of the faujasite topology main diffraction peaks assigned to (1 1 1) and (5 3 3) faces at $2\theta = 6.2^\circ$ and 15.3° respectively (Fig. 1c) the intensity of which decreases to some extent compared to the parent HY zeolite. This effect indicates that the microporous structure was retained, although, the crystallinity has decreased, together with that of RES during the solid-state preparation of the RES containing zeolite formulation (Fig.1c).

The parent and resveratrol loaded MCM-41, SBA-16 and Y samples were characterized by the method of low temperature nitrogen adsorption and the data are presented in Table 1 and in Fig. 2.

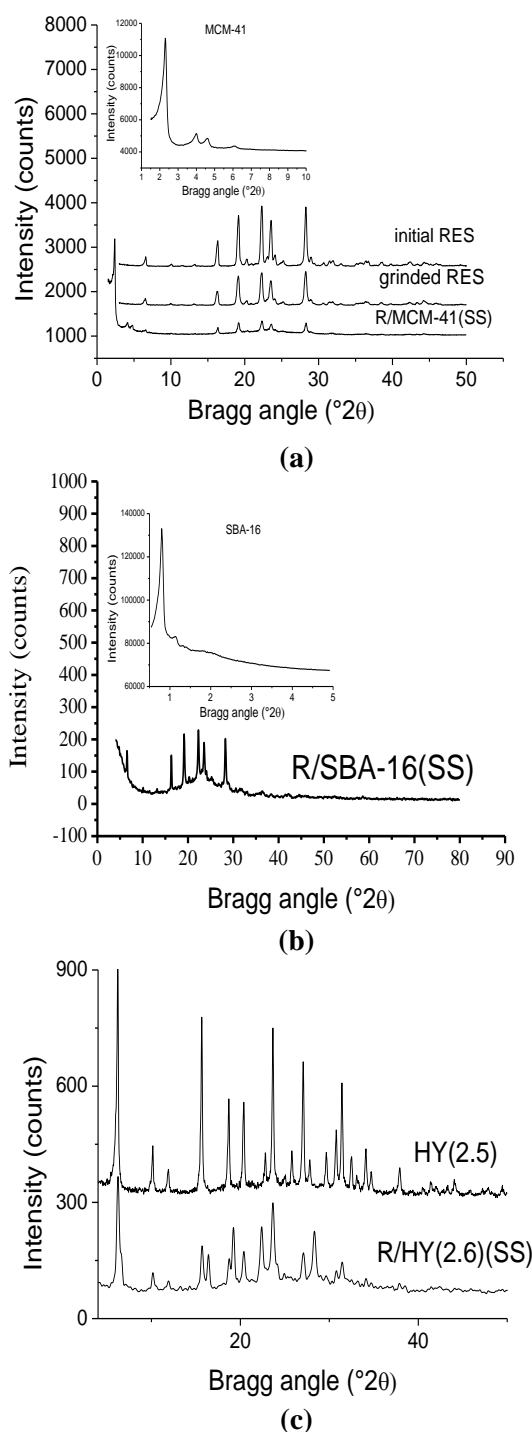


Fig. 1. Powder X-ray diffraction patterns of: (a) initial and grinded RES and RES/MCM-41(SS); (b) RES/SBA-16(SS); (c) parent and RES loaded, RES/HY(2.6)(SS).

As the results reveal, compared to the parent carriers, all loaded with resveratrol compositions exhibit substantial decrease in the surface area and pore volume, as well as some pore diameter reduction in case of the mesoporous carriers (Table 1, Fig. 2). It can be suggested that the pores of the latter supports are not filled entirely with drug, however.

Table 1. Physicochemical properties of the supports and their formulations with RES and concentration of the released RES in pH=1.2 and pH=6.8.

Samples	BET (m ² /g)	Pore diameter (nm)	Pore volume (cm ³ /g)	TG data for loaded RES (%)	Released RES* (%)	
					in pH=1.2	in pH=6.8
MCM-41	1175	2.7	0.97	-	-	-
R/MCM-41(SS)	306	2.5	0.27	50.6	36.7	31.8
SBA-16	1128	2.5-7.9	0.64	-	-	-
R/SBA-16(SS)	105	2.5-4.4	0.10	45.5	36.8	33.5
HY(2.6)	758	0.11	0.34	-	-	-
R/Y(2.6)(SS)	119	n.d. **	0.04	37.1	27.0	31.7

*Determined by TGA by heating from 180°C to 600°C; **no presence of pores detected.

As the results reveal, compared to the parent carriers, all loaded with resveratrol compositions exhibit substantial decrease in the surface area and pore volume, as well as some pore diameter reduction in case of the mesoporous carriers (Table 1, Fig. 2). It can be suggested that the pores of the latter supports are not filled entirely with drug, however.

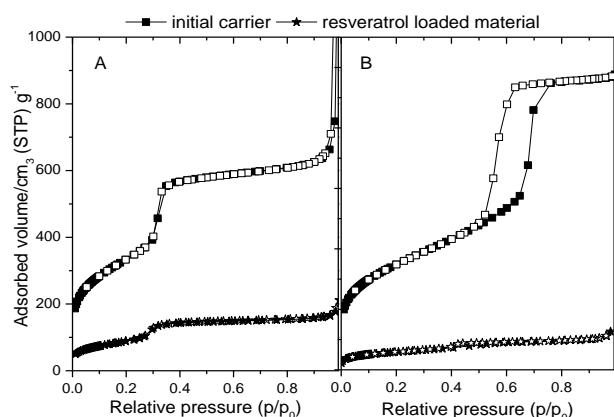


Fig. 2. Nitrogen adsorption/desorption isotherms of the parent materials and resveratrol loaded MCM-41 (a) and SBA-16 (b) composites, respectively.

The change in the isotherms for the loaded Y zeolite, compared to the parent carrier is an indication for total micropore filling or rather plugging. The microporosity of this material with much narrower channel system was actually disappeared and the total pore volume was strongly reduced.

ATR FT-IR method was used to investigate whether some interaction between the adsorbed RES molecule and the nanosized porous carriers (Fig. 3) has occurred upon the drug encapsulation. As was already observed in our previous study [23] that the FT-IR spectrum of resveratrol shows three characteristic strong bands at 1606, 1585 and 1384 cm⁻¹, belonging to RES double bond C=C stretchings of olefinic and aromatic groups, and of ring C-C stretching, respectively. The bands at 1509, 1443 and 1324 cm⁻¹ can be assigned to in

plane and out of plane C-H bending, respectively [26]. After deposition into silica/zeolite framework, a slight blueshift of the resveratrol IR bands corresponding to vinylidene group and a decrease in intensity of the vinylidene C-H in plane band (1324 cm⁻¹) can be observed. These spectral features due to perturbation at vinylidene dipole moments suggest an interaction of resveratrol C=C with the MCM-41 silica and the zeolite framework. For all cases, the out of plane C-H bending of RCH=CHR (965 cm⁻¹, not shown), diagnostic for *trans*-configuration around the di-substituted double bond [27], remains unchanged, indicating that the *trans*-resveratrol configuration is preserved during encapsulation over all supports used.

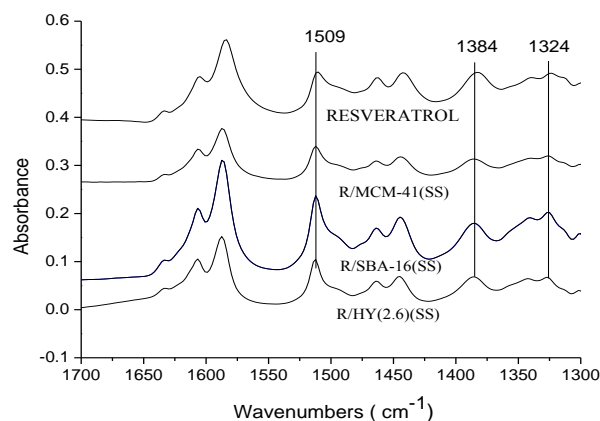


Fig. 3. FT-IR spectra of RES and RES loaded mesoporous and zeolite supports.

Resveratrol loading

The adsorbed amount of RES on the loaded preparations was evaluated by thermogravimetric analysis (TGA) considering the weight loss at heating the formulations in air up to 600°C (Fig. 4). The TGA profile of the pure grinded RES reveals two distinct weight changes starting at 250°C and 400°C which can be attributed to the onset of

melting followed by the decomposition of the RES molecule, respectively. At temperatures below 200°C the drug-host formulations lose the physisorbed water. Above 230°C the onset of a short temperature interval of melting of the supported substance follows, and then fast drug decomposition takes place.

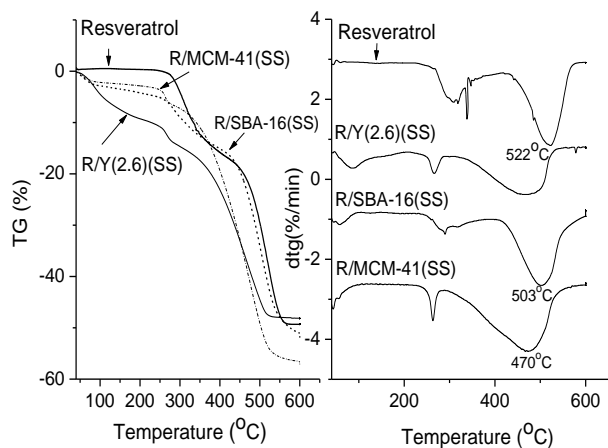


Fig. 4. TGA (a) and DTG (b) profiles of the RES loaded materials.

The calculated from the TGA data values for the amount of encapsulated RES are obtained by subtracting the weight loss due to water released from room temperature to 230°C from the total weight loss registered after heating for 1 h at 600°C.

Compared to the pure RES the loaded RES is released, with the exception of R/SBA-16(SS), at lower temperature, in both regions (Fig. 4). This is an indication for easier release corresponding to the enhanced solubility of the loaded compound compared to the non-supported one. Almost complete adsorption of the deposited RES, corresponding to the envisaged (1:1 for the mesoporous supports and 0.8:1 for the zeolite) RES: carrier weight ratio is registered for the three studied formulations. This result points to the high effectiveness of the simple solid-state procedure of RES deposition used for the preparation of such drug delivery systems.

In vitro drug release

The *in vitro* release process was studied in acid and phosphate buffer with pH values of 1.2 and 6.8, respectively. As shown in Fig. 5, the release rate of RES from the porous carriers was faster than its solubility in the same media. These results were probably due to the transformation of RES from crystal to amorphous state during the loading via grinding procedure. The slightly faster release in acid buffer was associated with the protonation of the carriers that was previously reported [28,29].

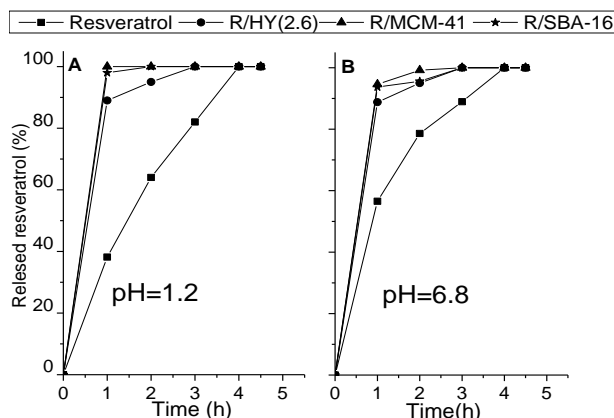


Fig. 5. In vitro release of resveratrol in pH=1.2 (a) and in pH=6.8 (b) from the supported samples.

Comparing the profiles of the three carriers, faster release was observed from both mesoporous carriers (MCM-41 and SBA-16) compared to the microporous Y type zeolite. This behavior could be perhaps explained with the slower diffusion of RES through the narrower zeolite pores. Thus, it appeared that the different pore size (mesoporous for the silica materials and microporous for the zeolite) influenced the release drug kinetics, in accordance to the previously reported findings of M. Vallet-Regi *et al.* [12].

CONCLUSION

Solid, silica-based spherical mesoporous MCM-41 and SBA-16 as well as microporous zeolite Y materials differing in morphology and pore size distribution were used as carriers for the preparation of resveratrol-loaded delivery systems by dry mixing of resveratrol and the respective carrier in solid state. This preparation procedure resulted in better resveratrol solubility compared to the free resveratrol, regardless of the carrier structure. The applied deposition method proved to be effective for encapsulation and stabilization of the drug as well as for its enhanced solubility.

Acknowledgements: Support for this work in the framework of the Hungarian-Bulgarian Inter-Academic Exchange Agreement is gratefully acknowledged.

REFERENCES

1. C. Manach, A. Scalbert, C. Morand, C. Rémésy, L. Jiménez, *Am. J. Clin. Nutr.*, **79**, 727 (2004).
2. A. Scalbert, C. Manach, C. Morand, C. Rémésy, L. Jiménez, *Crit. Rev. Food Sci. Nutr.*, **45**, 287 (2005).

3. A. Scalbert, I. T. Johnson, M. Saltmarsh, *Am. J. Clin. Nutr.*, **81**, 215S (2005).
4. F. Afaq, V. M. Adhami, N. Ahmad, *Toxicol Appl. Pharmacol.*, **186**, 28 (2003).
5. P. R. van Ginkel, D. Sareen, L. Subramanian, *Clin. Cancer Res.*, **13**, 5162 (2007).
6. E. Wenzel, V. Somoza, *Mol. Nutr. Food Res.*, **49**, 472 (2005).
7. P. Signorelli, R. Ghidon, *J. Nutr. Biochem.*, **16**, 449 (2005).
8. Z. Lu, B. Cheng, Y. L. Hu, Y. H. Zhang, G. L. Zou, *Food Chem.*, **113**, 17 (2009).
9. M. E. Juan, J. Buenafuente, I. Casals, J. M. Planas, *Food Res. Int.*, **35**, 195 (2002).
10. A. Amri, J. C. Chaumeil, S. Sfar, C. Charrueau, *J. Control Release*, **158**, 182 (2012).
11. V. Ambrogi, L. Perioli, F. Marmottini, S. Giovagnoli, M. Esposito, C. Rossi, *Eur. J. Pharm. Sci.*, **32**, 216 (2007).
12. M. Vallet-Regi, A. Ramila, R. P. del Real, J. Perez-Pariente, *Chem. Mater.*, **13**, 308 (2001).
13. A. Ramila, B. Munos, J. Perez-Pariente, M. Vallet-Regi, *J. Sol-Gel Sci. Tech.*, **26**, 1199 (2003).
14. S.-C. Shen, W. K. Ng, L. Chia, J. Hu, R. Tan, *Int. J. Pharm.*, **410**, 188 (2011).
15. R. Mellaerts, J. Jammaer, M. van Speybroeck, H. Chen, J. van Humbeek, P. Augustijns, G. van den Mooter, J. Martens, *Langmuir*, **24**, 8651 (2008).
16. S. Shen, W. Ng, L. Chia, Y. Dong, R. Tan, *J. Pharm. Sci.*, **99**, 1997 (2010).
17. Y. Hu, Z. Zhi, Q. Zhao, C. Wu, P. Zhao, H. Jiang, T. Jiang, *Micropor. Mesopor. Mater.*, **14**, 94 (2012).
18. A. Petushkov, N. Ndiege, A. Sale, S. Larsen, *Adv. Mol. Tox.*, **4**, 223 (2010).
19. A. Petushkov, J. Intra, J. B. Graham, S. C. Larsen, A. K. Salem, *Chem. Res. Toxicol.*, **22**, 1359 (2009).
20. I. Fenoglio, A. Croce, F. Di Renzo, R. Tiozzo, B. Fubini, *Chem. Res. Toxicol.*, **13**, 489 (2000).
21. C. H. Cheng, T. H. Bae, B. A. McCool, R. R. Chance, S. Nair, C. W. Jones, *J. Phys. Chem. C*, **112**, 3543 (2008).
22. S. C. Larsen, *J. Phys. Chem. C*, **111**, 18464 (2007).
23. M. Popova, A. Szegedi, V. Mavrodinova, N. Novak-Tusar, J. Mihály, S. Klébert, K. Yoncheva, *J. Solid State Chem.*, (2014) - submitted.
24. S. Huh, J. Wiench, J.-Ch Yoo, M. Pruski, V. S.-Y. Lin, *Chem. Mater.*, **15**, 4247 (2003).
25. D. Zhao, J. Feng, Q. Huo, N. Melosh, G. H. Fredrickson, B. F. Chmelka, G. D. Stucky, *Science*, **279**, 548 (1998).
26. F. Billes, I. Mohammed-Ziegler, H. Mikosch, E. Tyihák, *Spectrochimica Acta Part A*, **68**, 669 (2007).
27. V. Bertacche, N. Lorenzi, D. Nava, E. Pini, C. Sinico, *J. Incl. Phenom. Macrocycl. Chem.*, **55**, 279 (2006).
28. C. H. Lee, L. W. Lo, C. W. Mou, C. S. Yang, *Adv. Funct. Mater.*, **18**, 3283 (2008).
29. B. Tzankov, K. Yoncheva, M. Popova, A. Szegedi, G. Momekov, J. Mihály, N. Lambov, *Micropor. Mesopor. Matter.*, **171**, 131 (2013).

НАТОВАРВАНЕ НА РЕСВЕРАТРОЛ ВЪРХУ МЕЗОПОРЕСТИ СИЛИКАТНИ И ЗЕОЛИТНИ НОСИТЕЛИ ЧРЕЗ ТВЪРДОФАЗЕН МЕТОД

М. Попова¹, К. Йончева², А. Сегеди³, Ю. Кълвачев⁴, Н. Бенбасат², В. Мавродинова^{1*}

¹Институт по Органична химия с Център по Фитохимия, Българска Академия на Науките, ул. Акад. Г. Бончев, бл. 9, 1113 София, България

²Фармацевтичен Факултет, Медицински Университет – София, ул. Дунав 2, 1000 София, България

³Изследователски център за природни науки, Унгарска Академия на Науките, Н-1025 Будапеща, Унгария

⁴Институт по минералогия и кристалография, Българска Академия на Науките, ул. Акад. Г. Бончев, бл. 107, 1113 София, България

Постъпила на 30 април 2014 г.; Коригирана на 18 юни 2014 г.

(Резюме)

Възможността за използване на мезопорестите SBA-16 и MCM-41 силикатни материали като носители за слабо разтворимия във вода ресвератрол (RES) беше изследвана и съпоставена с тази на зеолит тип Y. Успешно беше приложена опростена процедура за натоварване в твърда фаза, съпроводена с аморфизиране на лекарственото вещество и повишаване на разтворимостта му. Изследванията с прахообразна рентгенова дифракция, азотна физисорбция, инфрачервена спектроскопия при пълно вътрешно отражение и термогравиметричен анализ показаха ефективно натоварване на ресвератрола върху повърхността на всички използвани носители. Резултатите от освобождаването в буфери с pH=1.2 и pH=6.8 показаха по-бързо разтваряне на ресвератрола, натоварен в избраните носители, в сравнение с изходния ресвератрол.

Reductive pyrolysis of leonardite humic acids

M. Stefanova^{1*}, L. Gonsalvesh¹, S. P. Marinov¹, J. Czech², R. Carleer², J. Yperman²

¹*Institute of Organic Chemistry with Centre of Phytochemistry, Bulgarian Academy of Sciences, Acad. G. Bonchev str., bl. 9, 1113 Sofia, Bulgaria*

²*Research group of Applied and Analytical Chemistry, Hasselt University, B-3590 Diepenbeek, Belgium*

Received June 16, 2014; Revised July 17, 2014

Dedicated to Acad. Dimiter Ivanov on the occasion of his 120th birth anniversary

Leonardite humic acids from Kaz Daglari (Turkey) are studied by reductive pyrolysis. Sample is pyrolysed in a H₂ flow in the temperature range 250°C–950°C. Volatiles are trapped in two ice-cooled Tenax tubes. Atmosphere Pressure-Temperature Programmed Reduction (AP-TPR) technique coupled “off-line” with thermal desorption gas chromatography - mass spectrometry (TD-GC/MS) apparatus is used to specify organic compounds in the pyrolysate. During sample thermal decomposition a broad range of species is produced. Aliphatic compounds, i.e. *n*-alkenes/*n*-alkanes, i.e. *n*C₆–*n*C₁₄; aromatic compounds, i.e. benzene, alkylated benzenes, naphthalenes, biphenyls; oxygen containing compounds, i.e. phenols, methoxy phenols, furans, benzofurans; sulphur containing compounds, i.e. polysulphides, thiophenes and nitrogen compounds, i.e. benzonitriles, indoles and quinolines. Leonardite organic matter is rich in oxygen, where phenolic structures are the most abundant. Compounds are quantitatively interpreted. According to pyrolysis data “average” structural units of leonardite humic acids from Kaz Daglari deposit are mainly composed by 1-2 aromatic cycles, condensed or coupled. Heteroatom compounds are also admitted. Experimental data argue for sample low maturity as rests of lignin building blocks, i.e. methoxy phenols, and carbohydrate degradation products, i.e., 2-methyl-2-cyclopenten-1-one, are still present.

Key words: leonardite, humic acids, pyrolysis, structural study

INTRODUCTION

Leonardite is a concentrated form of humic and fulvic acids and has appearance of coal but it does not reach its compactness. Leonardite is rich in organic matter (50-75%) and its humic acid content could range between 30-80%. Humic acid and other humic compounds stimulate root and shoot development, increase both available plant nutrients and nutrient uptake from soil, and enhance plants resistance to biotic and abiotic stress factors. Effects of humic acid containing fertilizers on plant yield and nutrient uptake depend on humic acid source, concentration, application type, plant species and cultivars. Therefore leonardite humic acids are of special interest in Turkey and Greece, where they are abundant and serve as raw materials for fertilizers industrial production [1-4]. Nowadays there is a tendency for chemical fertilizers to be gradually replaced by natural products, i.e. leonardite and its derivatives. In such circumstances they should be properly characterized.

Pyrolysis techniques have proved their useful application in fossil material study as they supply

detailed information on a molecular level. Janoš [5] in his review on the separation methods in the chemistry of humic substances from different origin stated that pyrolysis – GC/MS, although not ideal, remained the best technique for structural analysis. Different pyrolytic approaches have been used in our previous studies on coal humic acids, i.e. pyrolysis in a stream of water vapor [6], thermochemolysis [7] and reductive pyrolysis [8].

Atmosphere Pressure - Temperature Programmed Reduction (AP-TPR) technique coupled “off-line” with thermal desorption gas chromatography - mass spectrometry (TD-GC/MS) apparatus can be successfully used to specify qualitatively and quantitatively organic functionalities in coal and its derivatives. This pyrolytic technique has been previously developed and successfully applied for the specification of sulphur species in coals [9]. However, it can be used to track qualitatively and quantitatively the volatile organic compounds as well, like hydrocarbons and aromatic species, released during thermal decomposition of the humic acids. In this way information for composition of the non-extractable portion of the organic matter is obtained.

* To whom all correspondence should be sent:
E-mail: maia@orgchm.bas.bg

The aim of the present study is to analyze products of leonardite humic acids reductive pyrolysis by AP-TPR - TD-GC/MS technique and to relate registered volatile components to the sample organic matter composition.

EXPERIMENTAL

Leonardite from Kaz Daglari (Turkey) is a waxy, brown, shiny, vitreous mineraloid that is easily soluble in alkaline solutions. Its humic acids (HA) are under consideration. HA sample is prepared by 0.1N NaOH extraction and HCl precipitation [10]. Dried sample is milled and sieved < 0.06 mm.

Data for proximate analysis, i.e. moisture, volatile matter (VM), fixed carbon C_{fix} , ash content, are acquired by thermo gravimetric analysis using DuPont 951 instrument. The following programme is applied: i) heating with 20°C/min up to 600°C under nitrogen atmosphere; ii) at 600°C isothermal hold of the temperature for 10 min; iii) the atmosphere is switched to oxygen; iv) after 5 min of isothermal period, heating with 20°C/min up to 800°C under oxygen atmosphere. From the thermo gravimetric curves the following information can be obtained: i) moisture content, from ambient temperature up to 150°C; ii) VM content, from 150°C up to 600°C; iii) combustion of C_{fix} in oxygen atmosphere at temperature > 600°C; iv) ash content is the residue at 800°C.

Elemental analysis is run with a Thermo Electron Flash EA1113 elemental analyzer. By one measurement C, H, N and S can be determined. The instrument is calibrated with 2,5-bis-(5-tert-butylbenzoxazol-2-yl)thiophene (Thermo Electron). All samples are analyzed in duplicate. The oxygen content is calculated by difference as: $O\% = 100\% - (C\% + H\% + N\% + S\% + \text{ash}\%)$.

Pyrolysis is performed in the AP-TPR set-up described previously [11]. Briefly, 40 mg of sample and 20 mg of fumed silica are placed in the reactor under a 100 ml/min flow of pure H_2 . A linear temperature program of 5°C min⁻¹ from ambient temperature up to 950°C is applied. The outlet of the AP-TPR reactor is connected to a set of two ice-cooled tubes containing Tenax (Sigma-Aldrich), a porous polymer of 2,6-diphenyl-*p*-phenylene oxide, as adsorbent. The volatiles are additionally diluted by adding inert gas to the H_2 flow in ratio 5:1 (v/v) in order to prevent the saturation of the adsorption tube. Volatiles are trapped in two separated temperature ranges: i) 250°C÷550°C for the first tube; ii) 550°C-950°C for the second one. Adsorption tubes are separately desorbed and

analyzed by thermal desorption-gas chromatography/mass spectrometry (TD-GC/MS) instrument. The apparatus is used with He as carrier gas at 85 kPa at the following conditions: a) Unity thermal desorber (Marks): primary desorption 20 min at 275°C; Cold trap at -10°C, heated at maximum heating rate up to 320°C, hold time 15 min; flow path temperature 200°C; b) Trace GC Ultra-Gas chromatography (Thermo Instruments): capillary column 30m ZB 5-MS x 0.25 mm x 0.25 µm Phenomenex; temperature program - 3 min at 30°C, heated 8°C/min to 100 °C, heated 12°C/min to 310°C, hold time 5 min; c) DSQ-Mass spectrometer (Thermo Instruments): EI spectra; Ionization energy - 70 eV; Scan range - m/z 33-480 in 0.4s. Deuterated thiophene, d_4 -thiophene, 3 µg, is applied as a standard. NIST library spectra are used for peak identification. Homologous series are MS tracked by single ion monitoring (SIM) technique.

RESULTS AND DISCUSSION

The yield of prepared HA is 45 %. Leonardite HA proximate characteristics are the following, in wt. % as received: Ash - 10.20; Moisture - 11.84; VM - 32.23; C_{fix} - 45.73. Ultimate analysis is calculated on "dry ash free" basis: C - 63.02; H - 6.12; N - 1.16; S - 4.12; O^{diff} - 25.58.

Contents of all compound classes detected in pyrolysate of the leonardite HA subjected to pyrolysis are gathered in Table 1.

Table 1. Contents of compound classes.

Compound classes	Content	
	µg	mg/gC _{org}
Aliphatic:		
n-Alkenes/n-Alkanes	220.0	11.0
Monoaromatic:		
Benzenes	525.8	26.3
Diaromatic:		
Biphenyls	33.6	1.7
Naphthalenes/Acenaphthylenes	168.4	8.4
Oxygen containing:		
Phenols	206.5	10.3
Methoxy phenols	55.5	2.8
Furans/Benzofurans	6.4	0.3
Sulphur containing:		
Di/Tri Sulphides	24.0	1.2
Thiophenes/Benzothiophenes	27.0	1.4
Nitrogen containing:		
Benzonitriles	1.4	0.1
Indoles	3.4	0.3
Quinolines	4.0	0.2
Total	1276.0	63.8

Their sum represents 6.4% from the organic carbon of the pyrolysed material. Compound classes contents in rel. % are illustrated in Fig. 1. TD-GC/MS chromatograms of 250°C÷550°C and 550°C÷950°C pyrolysates are shown in Fig. 2 and Fig.3, respectively.

The main components in the pyrolysate flue gases of HA destruction in the 250°C-550°C region are benzene and its alkylated homologs, being 26.3 mg/g C_{org}, or about 40% of all registered components (Fig.1). Generally, alkylaromatics are considered as a product of the humification of primary plant materials and microbial metabolites that form the skeletons of humic substances. A defined origin of alkyl benzenes could be ascribed only in conjunction with other compounds. Thus, aromatic pyrolysates are ascribed to proteins, and specifically to microbial material, when pyridine and toluene are found simultaneously. A partial microbial origin could be certainly assumed for the HA under study because of the presence of N-containing compounds. However, it should be pointed out that they are in several folds lower amount compared to aromatics (Table 1).

Linear hydrocarbons, nC_6 - nC_{14} , i.e. mono-unsaturated (n -alkenes) and saturated (n -alkanes), are registered only in the first tube. These compounds amount up to 17.2 rel. % (Fig.2). Alkylated naphthalenes are abundant in the second tube. The detection of polycyclic aromatic compounds with higher degree of condensation cannot be expected, bearing in mind the immaturity of the sample under study.

With temperature increase, alkylated aromatic compounds are gradually replaced by phenolic structures. Vanillyl phenols, i.e. phenol-2-methoxy and methyl-2-methoxy phenols, are dominant. It is a proof for the presence of rests from conifer lignin arranged in the structural units of the organic matter from leonardite HA. High contents of phenol and its alkylated homologues are an indication for the proceeding of the coalification accompanied by demethoxylation and subsequent phenolic groups rearrangement [12].

During thermal decomposition of leonardite HA a broad range of other species is released as well. Leonardite organic matter is rich in oxygen (~26%), where beside phenolic structures furans and benzofurans are also detected. However the phenolic structures are more abundant compared to the oxygen in cyclic form.

According to the elemental composition of the sample under study, sulphur in leonardite HA is rather high, 4.12%. The relative low ash content of the sample gave us ground to assume that it is more likely distributed in the organic forms. Based on TD-GC/MS data, it is supposed that sulphur is arranged in bridges and cycles. Mass spectrometrically registered sulphur species are linear aliphatic polysulphides (dimethyl disulphide and dimethyl trisulphide), 1.2%, and cyclic sulphur compounds (thiophenes and benzothiophenes), 1.4%. The concept that with maturation aliphatic sulphur forms are lost and thiophenes represent the organic sulphur in higher rank coals is well documented in the literature. This is confirmed by a

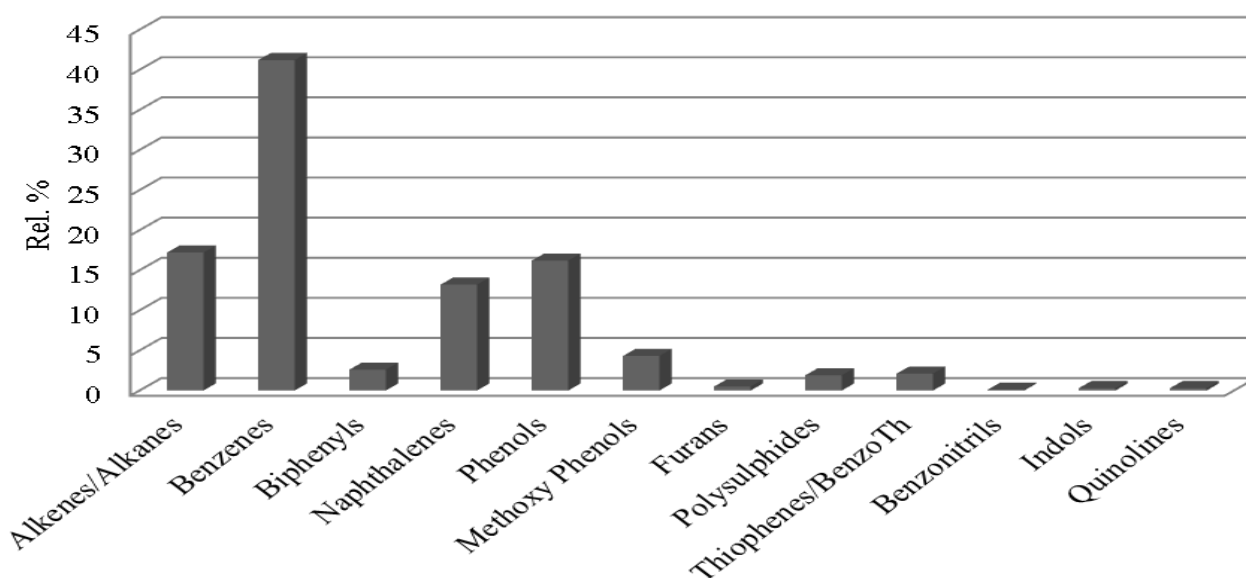


Fig. 1. Distribution of compound classes, in rel. %.

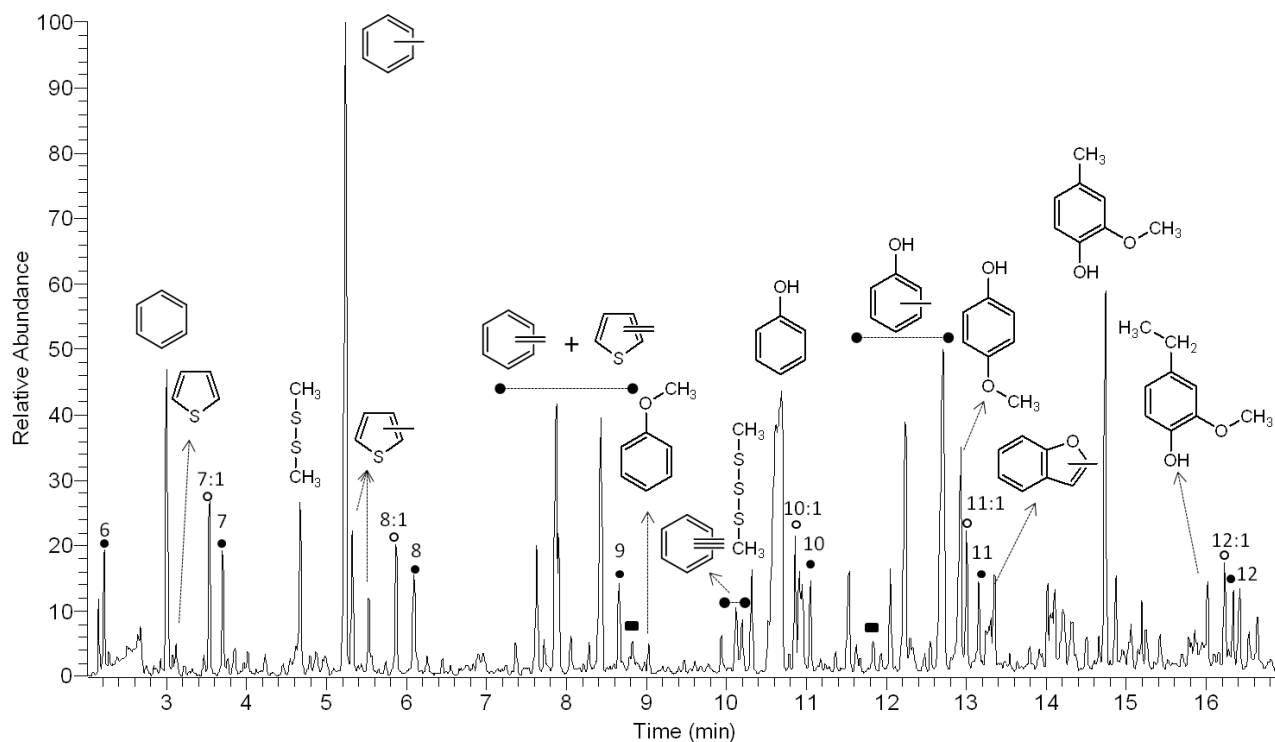


Fig. 2. TD-GC/MS of 250°C-550°C pyrolysis region.

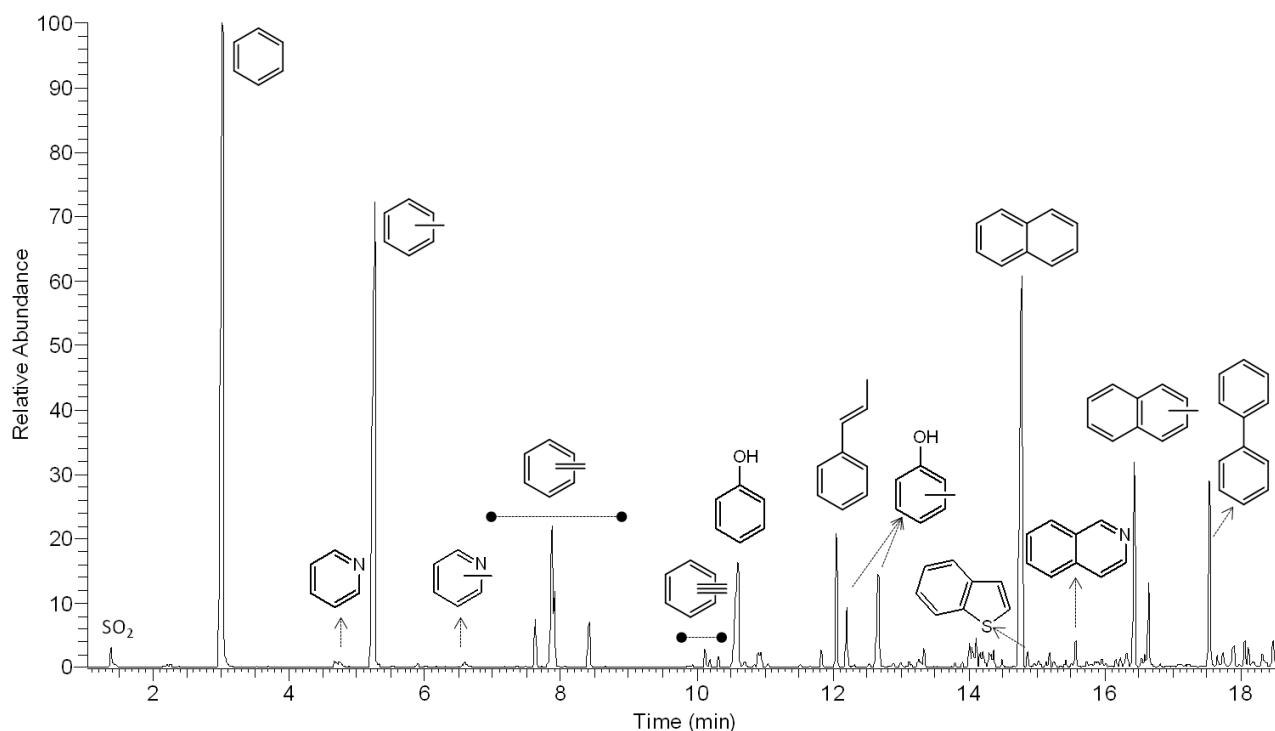


Fig. 3. TD-GC/MS of 550°C-950°C pyrolysis region

variety of instrumental techniques, i.e. non-destructive XPS, XANES and destructive ones, as wet chemical determination, and pyrolytic methods, all reviewed by Olivella et al. [13]. Simultaneously, AP-TPR measurements on different rank coals have

demonstrated that with maturation the amounts of both aliphatic and aromatic sulphides decrease, while the amount of thiophene sulphur increases [14]. Our results show that sulphur in sulphidic and thiophenic structures for leonardite HA is in

comparable amount. However, it should be stressed that pyrolytic experiments are conducted in a reducing atmosphere (hydrogen flow). It is already proved that in such circumstances most of the above mentioned sulphur containing compounds are reduced to H₂S [15]. Therefore a general conclusion on organic sulphur distribution in leonardite HA should be regarded with precaution.

N-containing species are also registered and listed in Table 1. Some of N-compounds could have microbial origin, but others can be both of microbial and plant input [16-17]. Some amounts of N-compounds accompanied by carbohydrate pyrolysis products other than levosugars imply the presence of microbial organic matter. This point needs a special concern in the future.

Cyclopentenones, C_nH_{2n-4}O, with n=6 and 7 (Fig. 2), are largely associated with pyrolysis of plant-derived organic matter, especially when they are accompanied with rests of lignin and small contributions of N-compounds. The negligible contents of 2-methyl-2-cyclopenten-1-one (C₆H₈O, M⁺ 96) and its dimethyl derivative (M⁺ 110) in the pyrogram (Fig.2) could be attributed to products of carbohydrates pyrolysis [18].

CONCLUSION

Structural study of leonardite humic acids from Kaz Daglari (Turkey) revealed some characteristics. From chemical point of view, according to the reductive pyrolysis data, their structural units are mainly composed by 1-2 aromatic cycles, condensed or coupled. Experimental data confirm sample low maturity as lignin residues and products of carbohydrate pyrolysis are still capable for identification. Results of pyrolysis give ground to assume that conifers are the predominant vegetation in the palaeomire. Heteroatoms are also admitted.

Leonardite humic acids from Kaz Daglari (Turkey) are characterized by high oxygen content. Therefore they are promising for an economically sustainable exploration as raw materials for agriculture, horticulture, cosmetics, drilling, filter systems products etc. However, attention should be

paid to the relative high content of the other heteroatoms, i.e. nitrogen 1.16% and sulphur 4.12%, and to consider their eventual harmful impact.

REFERENCES

1. S. Kalaitzidis, S. Papazisimou, A. Giannouli, A. Bouzinos, K. Christanis, *Fuel*, **82**, 859 (2003).
2. M. R. Karaman, M. Turan, A. Tutar, M. Dizman, S. Şahin, *J. Arts & Sci.*, **14**, 457 (2012).
3. A. Sanli, T. Karadogan, M. Tonguc, *Turk. J. Field Crops*, **18**, 20 (2013).
4. V. T. Engin, I. Cocen, U. Inci, *J. Arts & Sci.*, **14**, 435 (2012).
5. P. Janoš, *J. Chromatogr. A*, **983** (2003).
6. S. P. Marinov, M. Stefanova, V. Stamenova, R. Carleer, J. Yperman, *Proc. 16th Int. Sym. Anal. & Appl. Pyr.*, 163 (2004).
7. M. Stefanova, S. P. Marinov, L. Grasset, A. Amblés, *Proc. IHSS*, **2**, 100 (2010)
8. M. Stefanova, S. P. Marinov, R. Carleer, J. Yperman, *Ecol. & Future* **2**, 83 (2003).
9. L. Gonsalvesh, S. P. Marinov, M. Stefanova, R. Carleer, J. Yperman, *Fuel*, **97**, 489 (2012).
10. M. Stefanova, D. Velinova, S.P. Marinov, R. Nikolova, *Fuel*, **72**, 681 (1993).
11. J. Yperman, I. Maes, H. Van de Rul, S. Mullens, J. Van Aelst, D. Franco, *Anal. Chim. Acta*, **395**, 143 (1999).
12. P. G. Hatcher, D. J. Clifford, *Org. Geochem.*, **27**, 251 (1997).
13. M. A. Olivella, J. C. del Rio, J. Palacios, M. A. Vairavamurthy, F. X. C. de las Heras, *J. Anal. & Appl. Pyr.*, **63**, 59 (2002).
14. I. I. Maes, G. Gryglewicz, H. Machnikowska, J. Yperman, D. V. Franco, J. Mullens, L. C. Van Poucke, *Fuel*, **76**, 391 (1997).
15. L. Gonsalvesh, S. P. Marinov, M. Stefanova, Y. Yürüm, A. G. Dumanli, G. Dinler-Doganay, N. Kolankaya, M. Sam, R. Carleer, G. Reggers, E. Thijssen, J. Yperman, *Fuel*, **87**, 2533 (2008).
16. B. Allard, *Geoderma*, **130**, 77 (2006).
17. S. Nasir, T.B. Sarfaraz, T. V. Verheyen, A. L. Chaffee, *Fuel Proc. Tech.*, **92**, 983 (2011).
18. M. Mehrabian, *J. Soil Sci. & Envir. Management*, **4**, 11 (2013).

РЕДУКЦИОНЕН ПИРОЛИЗ НА ХУМИНОВИ КИСЕЛИНИ ОТ ЛЕОНАРДИТ

М. Стефанова^{1*}, Л. Гонсалвеш¹, С. П. Маринов¹, Я. Чех², Р. Карлие², Я. Иперман²

¹Институт по Органична химия с Център по Фитохимия, Българска Академия на Науките, ул. Акад. Г. Бончев, бл. 9, 1113 София, България

²Изследователска група по Приложна и Аналитична Химия, Университет Хаселт, В-3590 Дипенбиик, Белгия

Постъпила на 16 юни 2014 г.; Коригирана на 17 юли 2014 г.

(Резюме)

Хуминови киселини от леонардит от находище Каз Деглари (Турция) са изследвани чрез редукионен пиролиз. Пробата е пиролизирана в ток на водород в температурен интервал 250°C ÷ 950°C. Летливите вещества са задържани в две охладени с ледена баня тубички, запълнени с адсорбент Терах. За доказване на органичните съединения апаратурата за температурно програмирана редукция при атмосферно налягане (AP-TPR) е свързана в режим на “off-line” с апаратура за термично десорбционна газова хроматография - масспектрометрия (TD-GC-MS). По време на термичното разграждане на пробата е получена широка гама органични съединения. Алифатни съединения, в т.ч. *n*-алкени/*n*-алкани, $nC_6 \div nC_{14}$; ароматни съединения в т.ч. бензоли, нафталини, бифенили; кислород съдържащи съединения, в т.ч. феноли, метокси феноли, фурани; сяросъдържащи съединения, в т.ч. ди- и три- полисулфиди, тиофени; и азотни съединения, в т.ч. бензонитрили, индоли и хинолини. Данните са интерпретирани количествено. Органичната маса на леонардита е богата на кислород, като фенолните структури са най-разпространени. Според данните от пиролиза „средните“ структурни единици на хуминови киселини от леонардита най-вероятно са изградени от 1-2 ароматни пръстени и/или ароматни системи от две ароматни ядра при директно свързване на ароматните цикли. Възможно е и участие на хетероатомни съединения на азота и сярата. Експерименталните данни от редукионния пиролиз доказват ниската зрялост на изследваната проба, указание за което са присъствието на остатъци от лигнин (метокси феноли) и разпадни продукти на въглеhidрати (2-циклопентен-1-он, 2-метил).

Conversion of polyolefin wax to carbon adsorbents by thermooxidation treatment

I. G. Racheva^{1*}, B. G. Tsyntsarski¹, B. N. Petrova¹, T. K. Budinova¹, N. V. Petrov¹, B. Nagel², S. Pusz², U. Szeluga²

¹Lab. Chemistry of Solid Fuels, Institute of Organic Chemistry with Centre of Phytochemistry, Bulgarian Academy of Sciences, Acad. G. Bonchev str., bl. 9, 1113 Sofia, Bulgaria

²Center of Polymer and Carbon Materials of the Polish Academy of Sciences, M. Skłodowskiej-Curie 34, 41-819 Zabrze, Poland

Received April 29, 2014; Revised May 26, 2014

Dedicated to Acad. Dimiter Ivanov on the occasion of his 120th birth anniversary

Carbon adsorbents with different properties were obtained from furfural and mixture of furfural and polymer waste (polyolefine wax) with different activation reagents and different conditions of treatment. The carbons obtained have insignificant ash content. It was determined, that pore volume, pore size distribution and the chemical character of the surface of the carbon adsorbents depend on the selected activation reagents and temperature of treatment. The IR spectra and Boehm method show that various oxygen-containing groups with acidic (carboxylic, carboxylic in lactone-like bonding, phenolic, hydroxyl and carbonyl groups) and basic character are present on the carbon surface. Our investigations reveal that on the base of polymer waste, different activated carbons were obtained, and they could be used as effective adsorbents for removal of toxic metal and organic pollutants.

Key words: adsorbents, polymer waste, furfural, surface characterization

INTRODUCTION

Many materials in everyday life are produced from plastics and other petroleum derivatives. Plastics have unique properties and strong chemical bonds, which are not biodegradable, thus contributing to environmental pollution after use. Utilization of plastic waste can be performed by using of various methods of thermal destruction including thermal cracking (pyrolysis), catalytic cracking, gasification and hydrocracking. Pyrolysis is often used as effective method to convert waste plastic into useful products - fuels, lubricant oils, different chemicals, etc.

There are a lot of investigations dedicated on synthesis of carbon materials from polymer materials – polymers, polymer resins and polymer waste [1-21]. Thermoplastic polymers (polyethylene, polypropylene, polyvinyl chloride, polyamide, polystyrene, polyacrylic, etc.) and thermo-setting resins /epoxy resins, formaldehyde resins, melamine resin, etc./ also are suitable precursors. Polyvinyl chloride (PVC) as thermoplastic polymer is suitable precursor for porous activated carbons, synthesized by oxidation and subsequent procedures of carbonization and activation [1-6]. PVC has melting temperature of 160°C (but around 140°C it

starts to decompose), and when heating is first decomposed to hydrogen chloride and unsaturated polymers, which decompose later to other low-molecular products [7,8]. Some authors report about preparation of polystyrene-based activated carbon [9,10]. There are some papers concerning polyethylene terephthalate PET utilization [11-14], however the methods used are complicated, due to the fact that the material is hardly degradable. Some authors produced activated carbon (AC) from polyurethane [15]. Others [11,16] used polyacrylonitril (PAN) fibres to obtain porous carbon. There are also some investigations dedicated to utilization of paper [11] and automobile tyres [17,18].

Polyethylene is also potential precursor. The bags used in grocery stores to carry foods and goods are made of high-density polyethylene (HDPE), and the bags usually used in department and fashion stores are made of low-density polyethylene (LDPE). Polyethylene is a product of petroleum, a non-renewable resource which takes many centuries to break down when put in a landfill. The composition of products from the pyrolysis of pure polyethylene was studied by several researchers [19-21]. Polyolefin wax ($(\text{CH}_2)_n\text{H}_2$, where n ranges between about 50 and 100) is a by-product from polyethylene production, and it is formed as a result of side reactions, i.e. polyethylene cracking at high temperatures ($>400^\circ\text{C}$).

* To whom all correspondence should be sent:
E-mail: racheva89@abv.bg

The aim of this study is to obtain porous activated carbon using polyolefin wax as precursor.

EXPERIMENTAL

The polyolefin wax sample (waste product of polyethylene production at low pressure; from Burgas petroleum plant, Bulgaria) has melting point 115°C, average molecular mass of 1100. When heating in air at 360°C it decomposes (without solid residue) to low-molecular products, which evaporate.

200 g polyolefin wax (POW) was heated up to 115°C until melting. Concentrated sulfuric acid was added by drops during continuous stirring, and the temperature was increased up to 160°C. The obtained solid product was washed with water, dried at 150°C and carbonized at 600°C.

POW carbonizate was subjected to oxidative thermal treatment at 400°C for 1h in a quartz boat in a horizontal tube furnace in a flow of air. The obtained sample is denoted POW-OC.

POW carbonizate was subjected to water steam activation at 800°C for 1 h. The obtained solid product is denoted as POW-AC.

Mixture of 120 g POW and 80 g furfural was heated up to 115°C until melting. The furfural is added for intensification of polymerization and polycondensation, thus decreasing the expense of H₂SO₄. Conc. H₂SO₄ acid was added by drops during continuous stirring, and the temperature was increased up to 160°C. The obtained solid product was washed with water, and then dried at 150°C and carbonized at 600°C. The carbonizate was subjected to water steam activation at 800°C for 1 h. The obtained solid product is denoted as FPOW-AC.

FTIR experiments were performed by spectrometer IFS 113V using pellets with KBr. Textural characterization was carried out by measuring the N₂ adsorption isotherms at -196°C using Micrometrics ASAP 2010. Prior to the adsorption measurements the samples were out-gassed in situ under vacuum at 120°C overnight, to remove any adsorbed moisture and gases.

The isotherms were used to calculate specific surface area S_{BET} , and total pore volume V_t , assuming a slit-shaped pore geometry [22].

The content of oxygen-containing functional groups with acidic character on the carbon surface was determined applying the Boehm method by neutralization with bases of increasing strength: NaHCO₃, Na₂CO₃, NaOH, and sodium ethoxide [23]. About 0.5 g of the sample was put in contact with 100 mL of 0.05 N base solution in sealed

flasks. The suspensions were shaken at least 16 h, and then filtered. The excess of base remaining in the solution was determined from back-titration after adding an excess of standard HCl solution. It was assumed that NaHCO₃ was capable of neutralizing all carboxylic groups, Na₂CO₃-carboxylic and lactonic groups, NaOH-carboxylic, lactonic and phenolic groups, and sodium ethoxide was assumed to neutralize all acidic groups. The total number of basic sites was determined with 0.05 N HCl [24]. The procedure is the same as above mentioned, as back-titration of the excess of HCl was performed using titration with 0.05 N NaOH solution.

Carlo Erba 1106 combustion elemental analyzer was used for C and H. Sulfur content was determined by Eshka method. Oxygen content was determined by the difference.

RESULTS AND DISCUSSION

The results from elemental analysis of the obtained samples are presented on Table 1.

Table 1. Chemical characterization.

Sample	Ash ^{mf} wt. %	C ^a wt. %	H ^a wt. %	S ^b wt. %	O ^c wt. %
POW carbonizate	0.10	87.1	3.7	1.0	8.2
POW-OC	0.10	80.2	3.7	0.9	16.7
POW-AC	0.11	87.4	3.5	0.5	8.6
FPOW-AC	0.12	88.6	1.1	0.3	10.0

^{mf}moisture free sample; ^adata from combustion elemental analyzer; ^bdata from Eshka method; ^cdetermined by the difference.

Elemental analysis shows that activated samples have higher carbon content due to the higher temperature treatment and structure changes of the sample. The oxidation with air leads to significant increase of oxygen content.

The results from N₂ adsorption isotherms (Fig. 1) show that FPOW-AC is characterized with an opening of the knee at low relative pressures. This indicates the development of mesoporosity and a widening of the microporosity in these samples. The surface characteristics are presented in Table 2. The results show that FPOW-AC is distinguished by very high surface area and micropore volume, while POW-AC and POW-OC have considerable amount of micropores and moderate surface area. The oxygen-containing functional groups on the surface of carbons are a very important specific characteristic. The experimental data from Boehm titration (Table 3) show that various oxygen-containing groups (carboxyl groups, carboxyl groups in lactone-like binding, phenolic hydroxyl

and carbonyl groups) of acidic and basic character, and with different chemical properties, are present on the surface of the samples. Basic groups are not detectable in the oxidized samples. These results are confirmed by the elemental analysis.

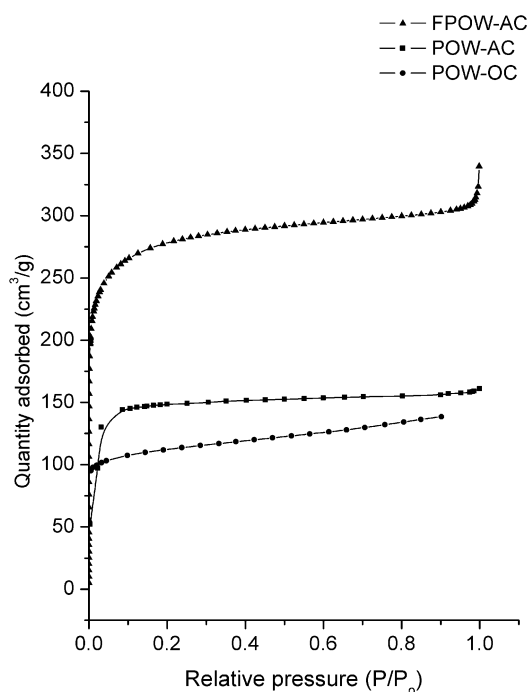


Fig. 1. N₂ adsorption isotherm of investigated carbon samples.

IR spectra of the samples are presented on Fig. 2. Stretch vibrations of associated –OH groups (3400–3230 cm⁻¹) were detected.

The absorption is a consequence of the presence of OH groups in the precursor. The bands at 3000–2800 cm⁻¹ are due to aliphatic stretching vibrations. C-H stretching vibrations in the region of 3000–2800 cm⁻¹ and C-H deformation vibrations in the region 1470–1350 cm⁻¹ are related to aliphatic structures. The band at 1704 cm⁻¹ could be related to the stretching of C=O in linear aliphatic aldehydes, ketones and carboxyls [25]. The bands around 1600 cm⁻¹ cannot be interpreted unequivocally. They could be due to: 1) aromatic ring stretching coupled to highly conjugated carbonyl groups (C=O); 2) stretch vibrations of C=C bonds in aromatic structures; 3) OH groups. The bands in the region of 1360–1150 cm⁻¹ are due to C–O in complex ethers and ring structures. The

IR spectroscopy results confirm the presence of oxygen-containing groups on the surface.

Table 3. Chemical characterization.

Sample	NaHCO ₃	Na ₂ CO ₃	NaOH	NaOEt	Basic groups
POW carbonizate	0.12	0.250	0.340	0.900	0.120
POW-OC	0.69	0.39	2.51	3.510	BDL
POW-AC	BDL	0.100	0.220	2.100	0.600
FPOW-AC	BDL	0.135	0.28	2.334	0.552

BDL-below detection limit.

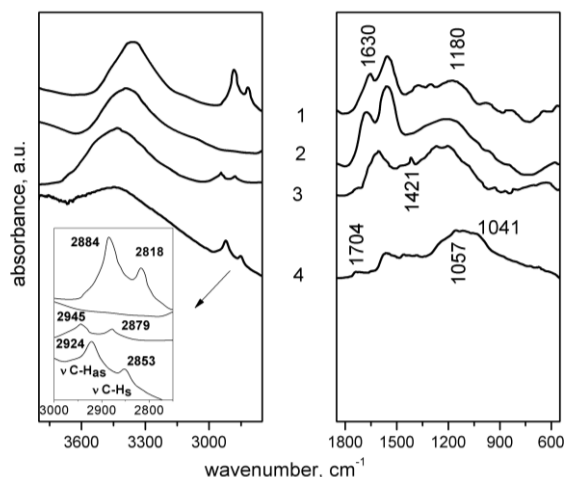


Fig. 2. IR spectra of the investigated samples: 1- POW carbonizate; 2 - POW-OC; 3 - FPOW-AC; 4 - POW-AC.

In summary, oxidized carbons have different properties (hydrophilic character, selective ion-exchange capacity, etc.) than water vapor activated carbons, due to the chemical nature of the surface. The carboxylic groups on oxidized carbon surface have cation exchange properties and oxidized carbons can be used as highly selective cationites.

The carboxylic groups on oxidized carbon surface have cation exchange properties and oxidized carbons can be used as highly selective cationites. Basic surface oxides are always present and carbons exhibit an anion exchange capacity too. The presence of surface oxides, together with chemical and radiation stability of oxidized carbons, provide their advantages over the synthetic resin cationites.

Table 2. BET surface area and pore volume of the samples determined by N₂ adsorption.

Sample	BET m ² /g	V _{tot} cm ³ /g	V _{micro} cm ³ /g	V _{meso} cm ³ /g	V _{macro} cm ³ /g	I ₂ mg/g
POW-OC	500	0.586	0.263	0.120	0.203	490
POW-AC	513	0.600	0.270	0.140	0.190	600
FPOW-AC	1000	0.486	0.338	0.033	0.115	1200

CONCLUSION

Synthetic carbon adsorbents with different properties are obtained from polymer and biomass treatment products. They possess insignificant ash and sulfur content. The results from IR spectroscopy and Boehm titration show the presence of oxygen-containing surface groups. Porous structure and high content of surface groups of the activated carbon samples, produced from polyolefin wax characterize them as potentially effective adsorbents for different pollutants - heavy metals (oxidized sample), organics (physically activated sample), etc.

Acknowledgements: *These studies were carried out in the frame of the Polish - Bulgarian Joint Research Project for Years 2013-2015 entitled "Preparation and characterization of carbon materials from polymer by-products and wastes".*

REFERENCES

1. K. Iguchi, R. Tsunoda, S. Takeshita, *Int. Chem. Eng.*, **14**, 381 (1974).
2. A. Noboru, *J. Chem. Soc. Jpn., Chem. Ind. Chem.*, **7**, 1217 (1975).
3. I. Iguchi, H. Uziki, T. Ishikawa, *J. Chem. Soc. Jpn., Pure Chem. Sect.*, **75**, 634 (1954).
4. C. Pierce, J. W. Wiley, R. N. Smith, *J. Phys. Chem.*, **53**, 669 (1949).
5. S. Ootani, *J. Chem. Soc. Jpn., Ind. Sect.*, **61**, 447 (1958).
6. J. J. Kipling, J. N. Sherwood, P. V. Shooter, N. R. Thompson, *Carbon*, **1**, 315 (1964).
7. C. Huggett, B. C. Levin, *Fire Mater.*, **2**, 131 (1987).
8. R. Miranda, H. Pakdel, C. Roy, C. Vasile, *Polym. Degrad. Stabil.*, **73**, 47 (2001).
9. D. Hines, A. Bagreev, T. J. Bandosz, *Langmuir*, **20**, 3388 (2004).
10. Q. Wang, X. Liang, W. Qiao, Ch. Liu, X. Liu, L. Zhan, L. Ling, *Fuel Process. Technol.*, **90**, 381 (2009).
11. K. Laszlo, A. Bota, L. G. Nagy, I. Cabasso, *Colloid. Surf. A*, **151**, 311 (1999).
12. J. B. Parra, C. O. Ania, A. Arenillas, J. J. Pis, *Stud. Surf. Sci. Catal.*, **144**, 537 (2002).
13. J. B. Parra, C. O. Ania, A. Arenillas, F. Rubiera, J. J. Pis, *Appl. Surf. Sci.*, **238**, 304 (2004).
14. J. B. Parra, C. O. Ania, A. Arenillas, F. Rubiera, J. M. Palacios, J. J. Pis, *J. Alloy. Compd.*, **379**, 280 (2004).
15. W. Yang, Q. Dong, Sh. Liu, H. Xie, L. Liu, J. Li, *Proc. Envir. Sci.*, **16**, 167 (2012).
16. J.-H. Yang, G.-Z. Yang, D.-G. Yu, X. Wang, B. Zhao, L.-L. Zhang, P. Du, X.-K. Zhang, *Carbon*, **53**, 231 (2013).
17. R. Murillo, M. V. Navarro, T. Garcia, J. M. Lopez, M. S. Callen, E. Aylon, A. M. Mastral, *Ind. Eng. Chem. Res.*, **44**, 7228 (2005).
18. R. Murillo, A. Aranda, E. Aylon, M. S. Callen, A. M. Mastral, *Ind. Eng. Chem. Res.*, **45**, 1734 (2006).
19. J. A. Onwudili, N. Insura, P. T. Williams, *J. Anal. Appl. Pyrol.*, **86**, 293 (2009).
20. N. Insura, J. A. Onwudili, P. T. Williams, *Energ. Fuel.*, **24**, 4231 (2010).
21. J. K. Koo, S. W. Kim, Y. H. Seo, *Resour. Conserv. Recycl.*, **5**, 365 (1991).
22. J. P. Olivier, *J. Porous Mater.*, **2**, 9 (1995).
23. H. P. Boehm, in: *Advances in Catalysis and Related Subjects*, D. D. Eley, H. Pines, P. B. Wesz (eds.), vol. 16, Academic Press, New York, 1966, p. 179.
24. E. U. Papier, S. Li, J. Donnet, *Carbon*, **25**, 243 (1987).
25. A. Oberlin, M. Villey, A. Couebay, *Carbon*, **16**, 73 (1978).

ТЕРМООКИСЛИТЕЛНА КОНВЕРСИЯ НА ПОЛИОЛЕФИНОВ ВОСЪК ДО ВЪГЛЕРОДНИ АДСОРБЕНТИ

И. Г. Рачева^{1*}, Б. Г. Цинцарски¹, Б. Н. Петрова¹, Т. К. Будинова¹, Н. В. Петров¹, Б. Нагел², С. Пуш², У. Шелуга²

¹Лаб. Химия на твърдите горива, Институт по органична химия с Център по фитохимия, Българска Академия на Науките, ул. Акад. Г. Бончев, бл. 9, 1113 София, България

²Център за полимерни и въглеродни материал към Полската Академия на Науките, ул. Мария Склодовска-Кюри 34, 41-819 Забже, Полша

Постъпила на 29 април 2014 г.; Коригирана на 26 май 2014 г.

(Резюме)

Въглеродни адсорбенти с различни свойства бяха получени на основата на фурфурол и смеси от фурфурол и полимерни отпадъци (полиолефинов восък) при различни условия на синтез и активиращи агенти. Получените въглени се характеризират с незначително пепелно съдържание. Бе установено, че обемът и разпределението на порите, както и химичният характер на повърхността, зависят от активиращия реагент и от температурата на термохимичната обработка. ИЧ спектрите и охарактеризирането на повърхностните групи по метода да Бьом показаха наличие на различни кислород-съдържащи групи с кисел и основен характер. Нашите изследвания показват, че на основата на полимерни отпадъци са получени различни активни въглени, които поради своите свойства си са перспективни за приложение като ефективни адсорбенти на токсични метални и органични замърсители.

Cobalt and iron modified activated carbons from renewable sources as catalysts in methanol decomposition: Effect of the precursor

I. Genova¹, B. Tsyntsarski¹, M. Dimitrov¹, D. Paneva², D. Kovacheva³, T. Budinova¹, R. Ivanova¹, I. Mitov², N. Petrov¹, T. Tsoncheva^{1*}

¹*Institute of Organic Chemistry with Centre of Phytochemistry, Bulgarian Academy of Sciences, Acad. G. Bonchev str., bl.9, 1113 Sofia, Bulgaria*

²*Institute of Catalysis, Bulgarian Academy of Sciences, Acad. G. Bonchev str., bl.11, 1113 Sofia, Bulgaria*

³*Institute of General and Inorganic Chemistry, Bulgarian Academy of Sciences, Acad. G. Bonchev str., bl.11, 1113 Sofia, Bulgaria*

Received April 24, 2014; Revised May 27, 2014

Dedicated to Acad. Dimiter Ivanov on the occasion of his 120th birth anniversary

Activated carbons, prepared from different biomass waste precursors, such as peach and olive stones, were modified with nanosized cobalt and iron species by incipient wetness impregnation technique. The obtained materials were characterized by nitrogen physisorption, XRD, UV–Vis, FTIR, TPR, Moessbauer spectroscopy and tested as catalysts in methanol decomposition to hydrogen and CO. Both modifications of the activated carbon obtained from peach stones show higher catalytic activity. Among them, the Co modification is more active and significantly more selective and it could be successfully used as a low-cost and efficient catalyst for methanol decomposition to hydrogen and CO.

Key words: iron and cobalt nanoparticles, activated carbon, methanol decomposition

INTRODUCTION

Methanol decomposition attracts growing interest due to the advantage of safe and efficient in situ production of hydrogen which can find application in gas turbines, fuel cells, vehicles and industry [1-7]. Also the high endothermic character of reaction allows recovering the waste heat from vehicle exhausted gases and industrial processes [1-7]. Low-cost, working at relatively low temperatures, highly active and selective catalyst for the decomposition reaction is essential for the utilization of this concept. Activated carbons (ACs) are used worldwide in a huge number of applications that goes from domestic to industrial uses, such as gas storage, removal of pollutants and odours, gas purification and separation, as catalysts or catalyst supports and in a number of medical uses [8,9]. Wood and stones from different lignocellulosic materials are the most used precursors for the production of ACs, but other agricultural by-products have also been investigated, such as date pits, palm shells, almond tree pruning, sugar cane bagasse, sunflower seed hull, olive and peach stones, lignin, coconut shell, cherry stone and rice straws amongst others [8-15]. Thus

obtained ACs possess very high specific surface areas and their pore size distributions can be varied from almost completely microporous to ones containing substantial amount of meso- and macropores as well [9]. Their textural characteristic makes ACs very suitable as catalyst hosts, especially when contain substantial amount of mesoporosity that can facilitate the transportation of reactants and products of a given catalytic reaction. To improve the catalytic activity of activated carbons, usually an active metal component is introduced in order to reduce reaction times and allow working at milder operating conditions [16]. Besides, nanosized Co particles display a wide range of interesting size-dependent structural, electrical, magnetic, and catalytic properties. It was reported [17] that cobalt containing catalysts represent high activity for Fischer-Tropsch synthesis and NO_x reduction [18]. Besides, catalysts based on iron oxide/activated carbon system were found promising in the organic compounds removal from aqueous solution [19], H₂S elimination [20], and NO_x reduction [21]. We have investigated highly active iron and cobalt containing catalysts supported on activated carbon obtained by waste coal treatment by-products for methanol decomposition [22]. We reported that the dispersion and the composition of the loaded metal

* To whom all correspondence should be sent:

E-mail: tsoncheva@orgchm.bas.bg

© 2014 Bulgarian Academy of Sciences, Union of Chemists in Bulgaria

phase depend significantly on the presence of support surface functional groups [22].

The aim of current paper is to elucidate the role of agriculture precursor and the textural properties of the obtained activated carbon support material on the state of the introduced cobalt and iron nanoparticles. XRD, Nitrogen physisorption, UV-Vis, FTIR, temperature programmed reduction with hydrogen (TPR) were used for the samples characterization. The catalytic behaviour of the obtained nanocomposite materials was tested in methanol decomposition to CO and hydrogen.

EXPERIMENTAL

Materials

Biomass based activated carbons were produced by one-step process of hydro-pyrolysis, which includes treatment of 15 g precursor (crushed peach stones and olive stones) with water steam at 1023 K for 1 h at atmospheric pressure, and a heating rate of 10°C/min, in a stainless steel vertical reactor placed in a tube furnace. The obtained activated carbon samples are denoted as PAC and OAC, respectively. Their modification with Fe and Co was performed by incipient wetness impregnation, using the corresponding nitrate precursors. The metal loading in all materials was 8 wt. %. The nitrate precursor decomposition was performed at 773 K for 6 h. The obtained supported samples are denoted as M/S, where M is Co or Fe and S is PAC or OAC.

Methods of characterization

The porous structure of all activated carbons was studied by nitrogen physisorption at 77 K on Micromeritics ASAP 2020 instrument. The amount of various acidic oxygen-containing functional groups was determined by Boehm method using aqueous solutions of NaHCO₃, Na₂CO₃, NaOH, and C₂H₅ONa according the procedure described in [23]. The amount of basic sites was determined with 0.05 N HCl according the procedure described in [24].

Powder X-ray diffraction patterns were collected within the range of 5.3 to 80° 2 θ on a Bruker D8 Advance diffractometer with Cu K α radiation and LynxEye detector. The average crystallite size was evaluated by using the Scherrer equation. The UV-Vis spectra were recorded on a Jasco V-650 UV-Vis spectrophotometer equipped with a diffuse reflectance unit. The IR spectra (KBr pellets) were recorded on a Bruker Vector 22 FTIR spectrometer

at a resolution of 1–2 cm⁻¹, accumulating 64–128 scans. The Moessbauer spectra were obtained in air at room temperature with a Wissel (Wissenschaftliche Elektronik GmbH, Germany) electromechanical spectrometer working in a constant acceleration mode. A ⁵⁷Co/Cr (activity \cong 10 mCi) source and α -Fe standard were used. The experimentally obtained spectra were fitted by the least square-method. The TPR/TG (temperature-programmed reduction/thermo-gravimetric) analyses were performed in a Setaram TG92 instrument in a flow of 50 vol % H₂ in Ar (100 cm³ min⁻¹) and a heating rate of 5 K/min⁻¹.

Catalytic investigation

Methanol conversion was carried out in a fixed bed flow reactor, and argon is being used as carrier gas (50 cm³min⁻¹). The methanol partial pressure was 1.57 kPa. The catalysts (0.055 g) were tested under conditions of a temperature-programmed regime within the range of 350–770 K with a heating rate of 1 Kmin⁻¹. On-line GC analysis was performed on HP 5890 apparatus equipped with flame ionization and thermo-conductivity detectors and a PLOT Q column. The absolute callibration method and carbon based material balance were used for the product yields elucidation. CO selectivity was calculated as X_{CO}/X_{tot}*100, where X_{CO} and X_{tot} are the yield of CO and the amount of converted methanol molecules.

RESULTS AND DISCUSSION

Supports characterization

XRD patterns of parent AC materials (Fig. 1a) represent broad peaks around 26° and 43° 2 θ which are generally assigned to the formation of crystalline carbonaceous structure. The results show that PAC sample is characterized with more ordered structure (more intense 100 hkl reflection at 43°) and higher degree of carbonization than OAC. The OAC XRD pattern also shows additional reflections around 29° and 31° due to small Ca₂CO₃ and NaCl impurities, respectively. The nitrogen adsorption isotherms of parent activated carbons are of type I/IV, according to the IUPAC classification, which is characteristic of materials with well developed micro-mesoporous structure (Fig. 1b). The calculated textural parameters (Table 1) reveal that the activated carbon obtained from the olive stones possesses higher specific surface area and larger portion of micropores.

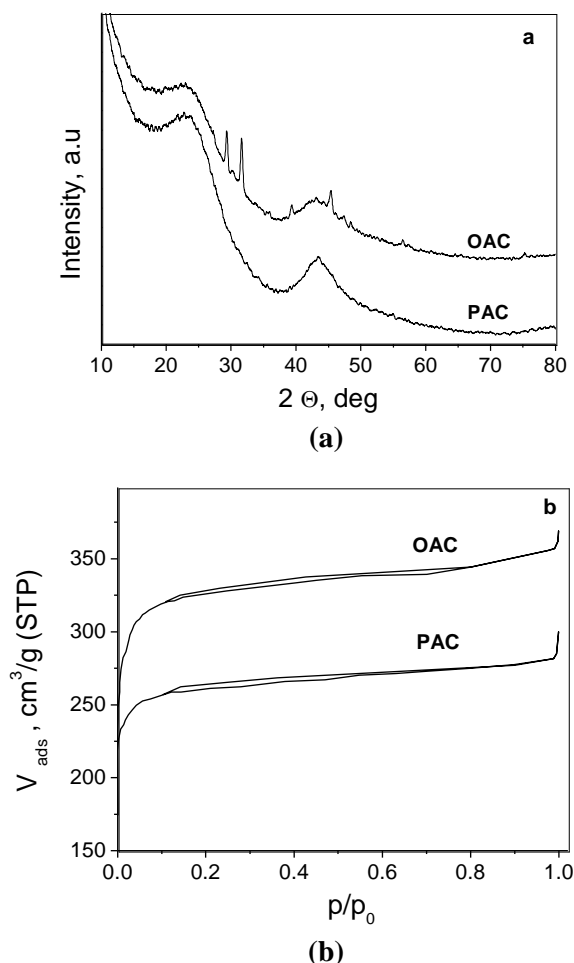


Fig. 1. Nitrogen physisorption isotherms (a) and XRD patterns (b) of pure AC materials.

The FTIR spectra of pure AC materials (not shown) display bands at $3000\text{--}2800\text{ cm}^{-1}$ that indicate the presence of aliphatic C–H stretching vibrations. Besides, the presence of bands at 1743 cm^{-1} and $1600\text{--}1500\text{ cm}^{-1}$ denotes the existence of carbonyl/carboxyl groups and an aromatic C=C ring stretching vibrations, respectively. More precise study of the accessible surface functional groups was performed by Boehm method. The experimental data show predominant presence of hydroxyl and carbonyl groups on both ACs, the latter being significantly more on OAC.

Both ACs represent almost similar amount of basic groups (Table 2).

Physicochemical characterization of Fe and Co modified activated carbons

The preservation of the isotherm shape after impregnation procedure reveals absence of structural collapse of ACs (Fig. 2a). The observed decrease in both BET surface area and total pore volume in comparison with the parent ACs could be assigned to the deposition of metal particles within the support pores or nearby pore openings (Table 1). The observed changes are more significant for OAC modified samples where predominant blocking of micropores could be assumed.

The XRD patterns of Fe/PAC and Fe/OAC (Fig. 2b) represent an intensive reflection at 35.4° and several smaller reflections at 30.5° , 43.5° , 57° , 62.9° 2θ which could be assigned to face-centered cubic (fcc) structure of Fe_3O_4 (PDF#19-0629) with average particle size of 11 and 19 nm, respectively. Intensive reflections at 36.5° , 42.2° and 61.4° 2θ in the XRD pattern of Co/PAC (Fig. 2b), indicate the presence of face centered (fcc) CoO phase (PDF#43-1004) with average particle size of 18 nm. New type of reflections, at 44.3° , 51.7° and 75.6° 2θ , belonging to cubic Co^0 phase (PDF#15-0806) with average particle size of 21 nm is registered for Co/OAC as well.

The FTIR spectra of the iron and cobalt modifications (not shown) display broad bands in the $600\text{--}500\text{ cm}^{-1}$ range, that could be assigned to the absorption of the Me–O bond in iron and cobalt oxide structures. The UV-Vis spectra of all modifications are presented in Fig. 3a. The absorption peaks are not well resolved. However, the slight absorption features with a maximum reflection at about $460\text{--}500\text{ nm}$ for the cobalt modifications could be carefully assigned to the presence of Co^{2+} ions in octahedral coordination and this is in accordance with the XRD data, where CoO was detected. The absorption above $400\text{--}500\text{ nm}$ for the

Table 1. Nitrogen physisorption data of the parent and modified activated carbons.

Sample	S_{BET} , [m^2/g]	V_{tot} , [cm^3/g]	$V_{\text{mic}}(\text{DFT})$, [cm^3/g]	$V_{\text{meso}}(\text{DFT})$, [cm^3/g]	ΔS_{BET} , %	ΔV_{tot} , %
PAC	820	0.41	0.27	0.08		
OAC	910	0.63	0.33	0.09		
Fe/PAC	617	0.28	0.24	0.04	25	32
Fe/OAC	462	0.20	0.16	0.02	49	67
Co/PAC	655	0.28	0.20	0.04	20	30
Co/OAC	502	0.24	0.16	0.03	45	62

Table 2. Quantification of oxygen-containing groups on AC surface (meq/g).

Sample	Acid surface functional groups				Basic groups
	Carboxyl	Lactonic	Hydroxyl	Carbonyl	
PAC	BDL	BDL	0.29	1.07	1.04
OAC	BDL	BDL	0.21	1.69	1.19

BDL – below detection limits

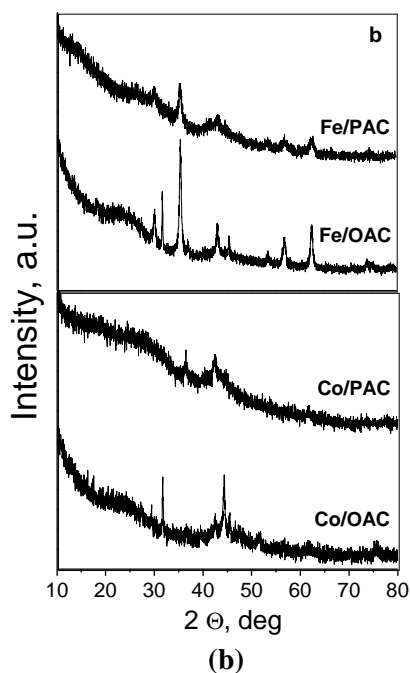
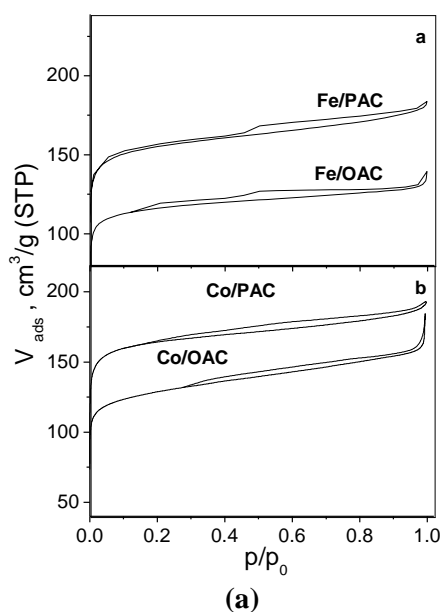


Fig. 2. Nitrogen physisorption isotherms with pore size distributions as insets (a) and XRD patterns (b) of iron and cobalt modified AC materials, respectively.

cobalt modifications could be carefully assigned to the presence of Co^{2+} ions in octahedral coordination and this is in accordance with the XRD data, where CoO was detected. The absorption above 400-500 nm in the spectra of iron modifications could be

assigned to $\text{Fe}^{n+} \leftarrow \text{O}^{2-}$ CT transitions in FeO_x particles.

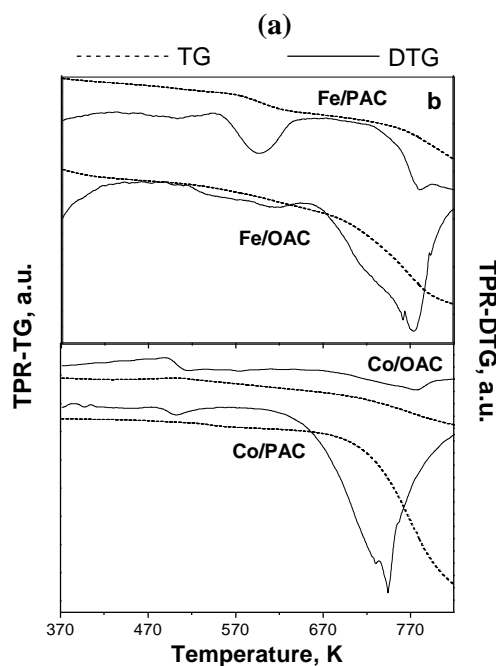
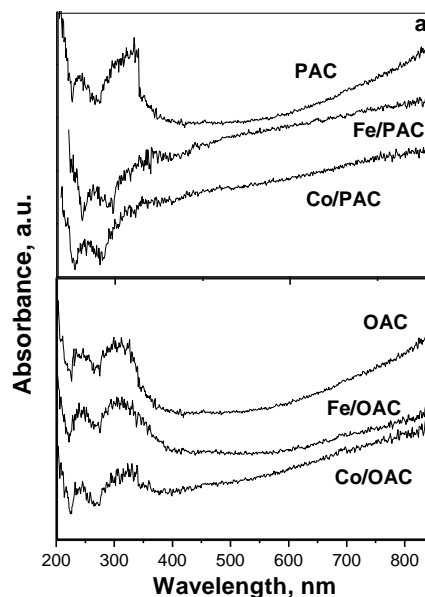


Fig. 3. UV-Vis spectra (a) and TPR data (b) of Fe- and Co- modified AC materials.

More information for the state of loaded iron species in the corresponding iron modifications is

Table 3. Moessbauer parameters of Fe/PAC and Fe/OAC samples before and after the catalytic test (*).

Sample	Components	IS, mm/s	QS, mm/s	Heff, T	FWHM, mm/s	G, %
Fe/PAC	Sx1- α -Fe ₂ O ₃	0.32	-0.10	49.8	0.50	3
	Sx2-Fe ₃ O ₄	0.30	0.01	47.6	0.42	10
	Sx3-Fe ₃ O ₄	0.64	0.01	43.7	1.35	61
	Db1-Fe ³⁺ _{octa} -SPM	0.34	0.72	-	0.52	12
	Db2-Fe ³⁺ _{octa} -SPM	0.31	1.05	-	0.73	14
Fe/OAC	Sx1-Fe ₃ O ₄	0.27	0.00	48.9	0.30	25
	Sx2-Fe ₃ O ₄	0.63	0.00	45.8	0.54	66
	Db1-Fe ³⁺ _{octa} -SPM	0.31	1.45	-	0.50	3
	Db2-Fe ³⁺ _{octa} -SPM	0.31	0.55	-	0.50	7
Fe/PAC*	Sx1-Fe ₃ O ₄	0.28	0.00	48.4	0.50	17
	Sx2-Fe ₃ O ₄	0.60	0.00	44.6	0.95	43
	Sx3-Fe ₃ C	0.20	0.02	20.5	0.69	19
	Db1-Fe ³⁺ _{octa} -SPM	0.35	0.58	-	0.45	10
	Db2-Fe ³⁺ _{octa} -SPM	0.35	1.02	-	0.58	11
Fe/OAC*	Sx1-Fe ₃ O ₄	0.29	0.00	48.2	0.50	5
	Sx2-Fe ₃ O ₄	0.65	0.00	45.1	0.75	7
	Sx3- α -Fe	0.00	0.00	33.2	0.28	39
	Sx4-Fe ₃ C	0.19	0.00	21.1	0.39	29
	Db1-Fe ²⁺ _{octa} -FeO	1.14	0.02	-	0.76	7
	Db2-Fe ³⁺ _{octa} -SPM	0.31	0.66	-	0.54	13

obtained by Moessbauer spectroscopy. The spectra of all iron modifications (not shown) are well fitted with sextets and doublets components. The calculated Moessbauer parameters (Table 3) of Fe/PAC show presence of hematite (Sx1- α -Fe₂O₃) particles with a relative weight of about 3%. The spectra of both iron samples consist mainly of sextets (Sx2 and Sx3) with parameters corresponding to highly dispersed magnetite phase with particle size below 30 nm and their relative weight is higher for Fe/OAC. The doublet part in the spectra reveals presence of ultra-dispersed iron oxide particles (up to 3-4 nm) with super paramagnetic (SPM) behaviour (Table 3).

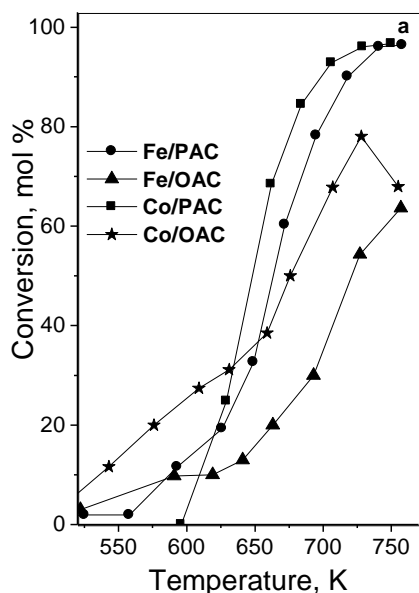
Additional information for the type and environment of metal ions was obtained by temperature programmed reduction with hydrogen (Fig. 3b). For the cobalt modifications, the observed effects up to 650 K could be assigned to the reduction to metallic cobalt of a mixture of Co₃O₄ and CoO species with different dispersion and location into the support porous structure [25]. In the case of Co/OAC, the reduction degree is smaller than the expected one. In accordance with XRD data this is due to the presence of substantial amount of metallic cobalt. Above 700 K, a significant weight loss was observed for both cobalt modifications that could be ascribed to the gasification of activated carbons promoted by the

presence of metallic Co, and this is much pronounced for the PAC modification.

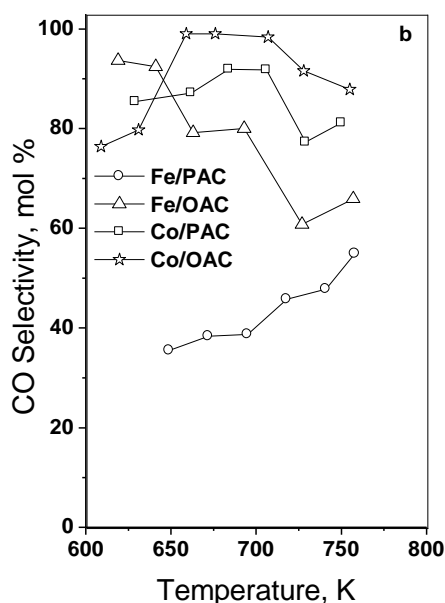
The TPR profiles for both iron modifications (Fig. 3b) represent broad reduction effect in the range of 400-650 K, which in accordance with XRD and Moessbauer data can be predominantly ascribed to step-wise reduction of Fe₃O₄ to FeO and then to Fe⁰. The TPR profile for Fe/OAC is broader and slightly shifted to higher temperature. Taking into account Moessbauer and nitrogen physisorption data, this could be due to lower dispersion of Fe₃O₄ and/or due to blocking of iron oxide particles into the micropores of the support. The significant weight loss is registered for both iron modifications above 660 K, which could be ascribed to gasification of the activated carbon supports, and again this is more pronounced for Fe/PAC.

The temperature dependencies of methanol conversion and CO selectivity on all modifications are presented in Fig. 4. The pure AC samples do not show any catalytic activity, and hence the influence of the observed by XRD impurities could be neglected. Among the iron modifications, Fe/PAC exhibits higher catalytic activity but lower selectivity to CO (below 60%) due to the formation of methane and CO₂. The Moessbauer data of Fe/PAC after the catalytic test (Table 3) show disappearance of the hematite phase and a decrease in the relative weight of Fe₃O₄ with the formation

of Fe₃C instead. At the same time, the ultra-dispersed nanoparticles with SPM behaviour remain almost unchanged, indicating that the reduction transformations affect only the larger particles. More pronounced reduction transformations of magnetite particles to α -Fe and Fe₃C under the influence of the reaction medium were established for Fe/OAC (Table 3).



(a)



(b)

Fig. 4. Methanol conversion (a) and CO selectivity (b) vs temperature on Fe- and Co- modifications of PAC and OAC.

Appearance of new phase of FeO nanoparticles with SPM behaviour was also registered. So, the observed differences in the catalytic behaviour of iron modifications (Fig. 4b) reflects in a complex way by the variations in the initial state of loaded iron (dispersion, location) and the reductive changes with it under the reaction medium. Obviously, the more pronounced blocking of micropores in OAC by the loaded iron species renders difficult the accessibility to the reactant molecules, leading to lower catalytic activity. However the more pronounced reduction changes with the iron oxide phase for Co/OAC seems to increase the CO selectivity. Among cobalt modifications, Co/PAC exhibits increase in the catalytic activity in a narrow temperature range above 600 K up to about 100% (Fig. 4a) and formation mainly of H₂ and CO (Fig. 4b). At the same time, Co/OAC (Fig. 2b) facilitates the methanol conversion even below 500 K, which is probably related to the presence of active metallic Co phase. However, the conversion curve for this sample is smoother with a maximum at 720 K due to fast deactivation, and this could be assigned to partial blocking of active phase into the micropores.

CONCLUSION

Highly active catalysts for methanol decomposition were prepared by deposition of cobalt and iron nanoparticles on activated carbons, obtained from waste biomass precursors, such as peach and olive stones. The dispersion, oxidative state and location of loaded particles could be successfully controlled by the textural peculiarities of the AC matrix. The best catalytic activity and selectivity is observed for cobalt modified AC from peach shells and it could be successfully used as low-cost efficient catalyst for methanol decomposition to hydrogen and CO.

Acknowledgements: Financial support from BAS and Bulgarian National Science Fund at the Ministry of Education and Science under Project DFNI-E01/7/2012 is gratefully acknowledged.

REFERENCES

1. J. R. Croy, S. Mostafa, J. Liu, Y. Sohn, B. R. Cuenya, *Catal. Lett.*, **118**, 1 (2007).
2. G. A. Olah, *Catal. Lett.*, **93**, 1 (2004).
3. P. Mizsey, E. Newson, T. B. Truong, P. Hottinger, *Appl. Catal. B*, **213**, 233 (2001).

4. K. W. Park, D. S. Han, Y. E. Sung, *J. Power Sources*, **163**, 82 (2006).
5. M. Borasio, O. R. de la Fuente, G. Rupprechter, H. J. Freund, *J. Phys. Chem. B*, **109**, 17791 (2005).
6. H. Borchert, B. Jurgens, T. Nowitzki, P. Behrend, Y. Borchert, V. Zielasek, S. Giorgio, C. R. Henry, M. Baumer, *J. Catal.*, **256**, 24 (2008).
7. J. C. Brown, E. Gulari, *Catal. Commun.*, **5**, 431 (2004).
8. K. Y. Foo, B. H. Hameed, *Chem. Eng. J.*, **184**, 57 (2012).
9. T. Budinova, D. Savova, B. Tsintsarski, C. O. Ania, B. Cabal, J. B. Parra, N. Petrov, *Appl. Surf. Sci.*, **255**, 4650 (2009).
10. W. Li, L. B. Zhang, J. H. Peng, N. Li, X. Y. Zhu, *Ind. Crop. Prod.*, **27**, 341 (2008).
11. J. Gñán, J. F. González, C. M. González-García, A. Ramiro, E. Sabio, S. Román, *Appl. Surf. Sci.*, **252**, 5993 (2006).
12. M. Olivares-Marín, C. Fernández-González, A. Macías-García, V. Gómez-Serrano, *Appl. Surf. Sci.*, **252**, 5967 (2006).
13. S. Guo, J. Peng, W. Li, K. Yang, L. Zhang, S. Zhang, H. Xia, *Appl. Surf. Sci.*, **255**, 8443 (2009).
14. W. C. Lim, C. Srinivasakannan, N. Balasubramanian, *J. Anal. Appl. Pyrolysis* **88**, 181 (2010).
15. I. I. Gurten, M. Ozmak, E. Yagmur, Z. Aktas, *Biomass Bioenergy*, **37**, 73 (2002).
16. A. Quintanilla, J. A. Casas, J. J. Rodríguez, *Appl. Catal. B*, **76**, 135 (2007).
17. M. Arsalanfar, A. A. Mirzaei, H. R. Bozorgzadeh, H. Atashi, S. Shahriari, A. Pourdolat, *J. Nat. Gas Sci. Eng.*, **9**, 119 (2012).
18. Z. H. Zhu, L. R. Radovic, G. Q. Lu, *Carbon*, **38**, 451 (2000).
19. M. H. Do, N. H. Phan, T. D. Nguyen, T. T. S. Pham, V. Nguyen, T. T. Vu, T. K. Nguyen, *Chemosphere*, **85**, 1269 (2011).
20. X. Yonghou, W. Shudong, W. Diyong, Y. Quan, *Separ. Pur. Tech.*, **59**, 326 (2008).
21. X. Gao, S. Liu, Y. Zhang, Z. Luo, K. Cen, *J. Hazard. Mater.*, **188**, 58 (2011).
22. T. Tsoncheva, I. Genova, B. Tsintsarski, M. Dimitrov, D. Paneva, Z. Cherkezova-Zheleva, T. Budinova, R. Ivanova, I. Mitov, N. Petrov, *J. Porous Mater.*, DOI: 10.1007/s10934-014-9797-4, in press.
23. H. P. Boehm, in: *Advances in Catalysis and Related Subjects*, D. D. Eley, H. Pines, P. B. Weisz (eds.), vol. 16, Academic Press, New York, 1966, p. 179.
24. E. Papier, S. Li, J. B. Donnet, *Carbon*, **25**, 243 (1987).
25. Y. Du, Q. Meng, J. Wang, J. Yan, H. Fan, Y. Liu, H. Dai, *Micropor. Mesopor. Mater.*, **162**, 199 (2012).

КАТАЛИЗАТОРИ ЗА РАЗЛАГАНЕ НА МЕТАНОЛ НА ОСНОВАТА НА КОБАЛТ И ЖЕЛЯЗО МОДИФИЦИРАН АКТИВЕН ВЪГЛЕН ОТ ВЪЗОБНОВЯЕМИ ИЗТОЧНИЦИ: ВЛИЯНИЕ НА ПРЕКУРСОРА

И. Генова¹, Б. Цинцарски¹, М. Димитров¹, Д. Панева², Д. Ковачева³, Т. Будинова¹, Р. Ивановна¹, И. Митов², Н. Петров¹, Т. Цончева^{1*}

¹ *Институт по органична химия с Център по фитохимия, Българска Академия на Науките, ул. Акад. Г. Бончев, бл. 9, 1113 София, България*

² *Институт по катализ, Българска Академия на Науките, ул. Акад. Г. Бончев, бл. 11, 1113 София, България*

³ *Институт по обща и неорганична химия, Българска Академия на Науките, ул. Акад. Г. Бончев, бл. 11, 1113 София, България*

Постъпила на 24 април 2014 г.; Коригирана на 27 май 2014 г.

(Резюме)

Два вида активен въглен, получени от различни прекурсори на основата на отпадъчна биомаса, съответно костилки от праскови и маслини, бяха модифициран с железни и кобалтови наночастици чрез импрегниране. Получените материали бяха охарактеризирани с помощта на физична адсорбция на азот, рентгенова дифракция (XRD), температурно-програмирана редукция с водород (TPR), UV-Vis, ИЧ- (FTIR) и Мьосбауерова спектроскопия и тествани като катализатори в реакция на разпадане на метанол до водород и СО. По-висока каталитична активност показаха модификациите на въглена, получен от прасковени костилки. Измежду тях, Со-съдържащият активен въглен е най-активен и значително по-селективен, и може с успех да бъде използван като евтин и ефективен катализатор в реакцията на разпадане на метанол до водород и СО.

Study on the catalytic activity of nanosized NiOx for oxidative degradation of 2,4-dichlorophenol in aqueous solutions

V. V. Ivanova, M. K. Stoyanova, S. G. Christoskova*

Department of Physical Chemistry, University of Plovdiv, 24 Tzar Assen str, 4000 Plovdiv, Bulgaria

Received May 04, 2014; Revised May 26, 2014

Dedicated to Acad. Dimiter Ivanov on the occasion of his 120th birth anniversary

Nanosized NiOx was prepared and tested as heterogeneous catalyst for low-temperature oxidation of 2,4-dichlorophenol in aqueous solution using air as an oxidant. The catalyst employed was synthesized by non-conventional ultrasound assisted precipitation-oxidation method with reverse order of precipitation. The physicochemical properties of the as-prepared catalyst were characterized by several techniques, such as XRD, TEM, SAED, FT-IR spectroscopy and chemical analysis. Characterization data reveal that the applied synthesis yields highly dispersed oxide material with a high content of over-stoichiometric active oxygen (O*~8 %), loosely bonded to the surface Ni- ions. The catalyst studied exhibited high activity in degradation of 2,4-dichlorophenol and 100% decomposition could be achieved in short duration of 5 minutes at the optimum conditions, while complete oxidation could be attained in 120 minutes. The effect of several operational parameters, such as catalyst loading, temperature, and pH on the efficiency of the oxidation process was investigated.

Key words: 2,4-dichlorophenol, heterogeneous catalytic oxidation, Ni-oxide system, active oxygen, wastewater treatment

INTRODUCTION

Chlorophenols (CPs) constitute an important group of aromatic compounds which are widely used in the production of pesticides, herbicides, disinfectants and preservatives in wood, dyes, and leather. The large scale production and heavy consumption of CPs generate wastewaters containing these substances at high concentrations. Owing to their high potential of phytotoxicity and zootoxicity, CPs represent one of the most abundant families of industrial environmental pollutants. Chlorophenols could be produced when drinking and industrial waters are disinfected with chlorine but could also be formed as a result of bioaccumulation of compounds with lower molecular weight in natural bodies of water [1-3]. In particular, 2,4-dichlorophenol (2,4-DCP), listed by US EPA as a priority pollutant, is a precursor to the manufacture of the widely used herbicide 2,4-dichlorophenoxyacetic acid. It is also the main by-product of sun induced photolysis of 2,4-dichlorophenoxyacetic acid in soil and water [4]. Due to high toxicity of 2,4-DCP even at low concentrations, resistance for biodegradation as well as its capacity to form organic macromolecules it is

necessary to treat effluents containing chlorophenols prior to its discharge into water [5,6].

At present, the conventional methods used to treat wastewater containing such organic pollutants include biological treatments, adsorption, incineration, air stripping, etc. In general these treatments are inexpensive and safe but have several disadvantages. Biological oxidation can be affected by the toxicity of CPs and requires longer retention time. Non-destructive adsorption method is proven to be effective, however, new secondary waste could be generated that required further treatment and thus increasing the operational cost. Incineration present considerable emission of other hazardous compounds. These essential drawbacks limit considerably practical application of these treatment technologies [7].

Recently, advanced oxidation processes (AOPs) have attracted great scientific and technological interest in the area of water treatment. AOPs are generally based on the production of highly reactive and non-selective hydroxyl radicals through employment of different approaches. These radicals are capable of readily attacking organic contaminants in water, thereby transforming them into harmless end products [8-10]. One of the methods for generation of hydroxyl radical employs photocatalytic processes under exposure of UV light in the presence of semiconductors. The photocatalytic

* To whom all correspondence should be sent:
E-mail: christ@uni-plovdiv.bg

activity of nanosized TiO₂ and ZnO for oxidation of 2,4-DCP has been studied [11]. The results show that 98% extent of 2,4-DCP oxidation could be achieved for 90 and 60 minutes, respectively, in the presence of these photo-catalysts. The main disadvantage of TiO₂ as a photocatalyst is its inability to absorb visible light that represents 97% of the solar spectrum. This is the reason why scientists have focused their attention on modification of TiO₂ in order to increase its adsorption ability within the visible spectrum.

The photocatalytic activity of TiO₂ modified with porphyrin has been studied in order to evaluate the degree of oxidative destruction of 2,4-DCP under irradiation with visible light. The results indicate that in 4 hours a degree of reduction of the substrate is in the range from 42% to 81% has been achieved when pH=10 [12]. The low level of destruction of toxic substance when visible light is used and the high price of the method when combination with UV light is used limits the possibilities for large scale application of photocatalysis.

An effective and economically feasible process for destruction of a variety of hazardous pollutants in wastewater is based on heterogeneous catalytic reactions providing complete oxidation. Using both suitable catalytic systems and reaction conditions a high selectivity towards environmentally harmless products can be achieved at mild conditions (room temperature and atmospheric pressure).

Our previous studies showed that NiOx is highly effective catalyst for low-temperature oxidative liquid-phase degradation of phenol using air as oxidant. The results obtained show that phenol is completely oxidized for 30 minutes to harmless products - carboxylic acids and CO₂ at ambient temperature and pH 6.0-7.0 [15].

The primary objective of this study is to investigate the effectiveness of Ni-oxide system as heterogeneous catalyst for the oxidative degradation of 2,4-DCP in aqueous solutions. The kinetics of the oxidation process and the effect of various operating parameters influencing 2,4-DCP removal efficiency such as catalyst loading, temperature, and solution pH were studied.

EXPERIMENTAL

Preparation of catalyst

The procedure applied for the synthesis of the catalytic sample was in accordance with the basic requirements to the environmental low-temperature catalysts for complete oxidation in aqueous solution. Some of the typical features of these catalysts include: high dispersity of the catalytically

active phase; high content of active oxygen; high oxidation state and octahedral coordination of metal ions; low binding energy of the M-O bond on the catalyst surface, presence of OH-groups. In order to synthesize the Ni-oxide system complying with these requirements a non-conventional precipitation-oxidation method with reversed order of feeding the precipitator to the system was applied. The synthesis process was assisted by ultrasonic activation using ultrasonic homogenizer UP100H [16]. On the one hand ultrasonic treatment contributes for the more effective homogenization of the reaction mixture and on the other hand it is a prerequisite for the production of nanosized systems with high dispersity and higher specific surface. A certain volume of nickel nitrate aqueous solution (1 M) was added to a mixture of aqueous solutions of NaOH (4M) and NaOCl (1 M) under continuous stirring. The resulting black precipitate was pretreated for 20 min with the ultrasonic homogenizer and allowed to stay in mother liquor for 24 hours. Then it was filtered, washed with distilled water until negative reaction for Cl⁻ and neutral pH, followed by drying at 105°C overnight.

Catalyst characterization

XRD analysis was conducted using X-ray diffractometer TUR-MA 62 equipped with a computerized HZG-3, operated at U = 37kV, Cu K α radiation ($\lambda = 1.5406 \text{ \AA}$) and I=20mA. The sample was scanned in the $2\theta = 10-80^\circ$ range.

The infrared spectra were recorded with a model 1750 Perkin Elmer FT-IR spectrophotometer in KBr tablets (2 mg of the respective sample in 200 mg KBr).

The structural analysis of the samples has been made with high-resolution transmission electron microscope JEOL JEM 2100 at acceleration tension of 200 kV. The two basic operation modes of the microscope have been used namely bright field transmission electron microscopy (BF TEM) and selected area diffraction (SAED).

The chemical analysis of the synthesized catalyst included measurement of the total amount of active oxygen (O*), represented in both % and g.at.g⁻¹.

Active oxygen is the amount of over-stoichiometric oxygen in the oxide above that corresponding to the lowest stable oxidation state. The total active oxygen content of the catalysts was determined iodometrically. A known amount catalyst (0.1 g \pm 0.001) was added to 25 cm³ dilute (1:10) sulfuric acid containing 2g of potassium iodide in a flask supplied with a ground stopper. After complete

dissolution of the sample, the solution is allowed to stand for 10 min and the liberated iodine is titrated with 0.1 N sodium thiosulfate solution using starch as indicator. The relative standard deviation of the method is 4.71%.

The total active oxygen content in g-at.g⁻¹ and % was determined according to the Eq. (1) and Eq. (2):

$$O^* = \frac{N \times V \times mgE_{O_2}}{m \times 16}, g-at/g \quad (1)$$

$$O^* = \frac{N \times V \times mgE_{O_2}}{m} \times 100\% \quad (2)$$

where: N – normality of the titrant; V – volume of the consumed titrant solution, cm³; m- catalyst amount, g; $mgE_{O_2} = 0.008$, milligram equiv. O₂.

Catalytic activity test

Heterogeneous catalytic oxidation of 2,4-DCP in aqueous solution was conducted in a thermostated glass reactor of 150 cm³ capacity at batch mode with constant stirring at around 400 rpm using magnetic stirrer. All experiments followed the following procedure: 100 cm³ 50 mg dm⁻³ aqueous solution of 2,4-DCP was transferred into the reactor and was saturated with air for 20 minutes. Then a fixed amount of catalyst in powder form was added. The reaction was carried out under continuous airflow passing through the system, thus maintaining stationary concentration of oxygen dissolved in water. At given intervals of oxidation process, samples of 4 ml were withdrawn from the suspension, centrifuged at 4000 rpm for 1 min to remove the catalyst and analyzed for residual content of 2,4-DCP and oxidation products.

The reaction progress was followed by UV-Vis spectroscopy and HPLC. The UV-Vis spectra of the samples were recorded from 200 to 500 nm using a UV-Vis double beam spectrophotometer (Cintra 101, GBS, Australia). Due to the very fast catalytic transformation of the substrate (2,4-DCP) in the presence of NiOx, the reaction kinetics was determined by monitoring decrease in absorbance at the maximum wavelength (254 nm) of the intermediate compound produced during the oxidation process.

HPLC analyses were performed using a Knauer Series HPLC system equipped with DAD detector. Separations were carried out by a Purospher Rstar RP-18e column (250 mm × 4.6 mm i.d.; silica

particle size 5 μm). The mobile phase consisted of acetonitrile mixed with water (v/v; 50:50) at a flow rate of 1 mL/ min; an isocratic elution mode was used. Detection was performed at 254 nm.

pH values of the reaction mixture were measured by digital pH meter (inoLab 740, WTW).

The catalytic activity of the NiOx was evaluated through the degree of conversion of the formed intermediate compound (α, %), calculated according to the Eq. (3) as well as by the rate constant (k, min⁻¹), determined in accordance with a first-order kinetics equation (Eq. 4):

$$\alpha = \frac{A_0 - A}{A} \cdot 100 \quad (3)$$

$$k = \frac{1}{t} \ln \frac{A_0}{A} \quad (4)$$

where A₀ and A are the measured absorptions of the intermediate compound at the moment of its formation and at a any instant time t, respectively.

RESULTS AND DISCUSSION

Powder X-ray diffraction

The XRD measurements of the NiO_x show that the catalyst is X-ray amorphous. The amorphous character of the as-prepared sample determines the chemical and structural isotropy of the active sites centers on the catalytic system surface area which is a prerequisite for high selectivity in the oxidation processes. Although not detectable by the XRD technique, the crystallographic structure of the catalyst was determined through application of TEM and SAED analyses.

TEM and SAED analyses

Fig. 1 shows the typical TEM and the corresponding SAED image of NiO_x, deposited on a carbon coated copper grid. As observed in Fig.1a, the catalyst's nanoparticles have spherical form and diameter in the range 5 nm- 20 nm forming large agglomerates amounting hundreds of particles. The SAED patterns (Fig.1b) obtained from the TEM showed well-defined rings characteristic of the nanocrystalline materials. After the indexation of the diffraction pattern it has been found that they correspond to reflections from non-stoichiometric monoclinic Ni₁₅O₁₆ [PDF 72-1464].

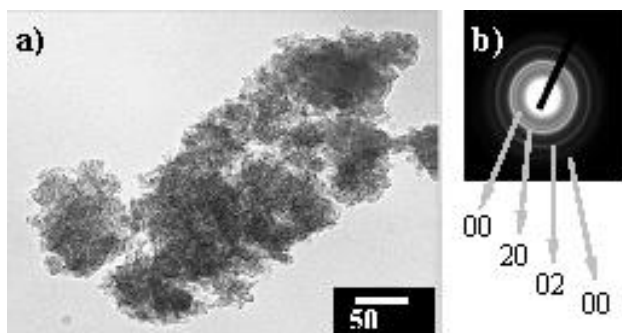


Fig. 1. SAED (b) and TEM (a) micrographs of bulk NiOx catalyst.

FT-IR spectroscopy

The FT-IR spectrum of the synthesized catalyst is shown in Fig. 2. Characteristic feature of the spectrum is the presence of wide and intense absorption band located at 573 cm^{-1} . This band is provided by stretching vibrations of the Ni-O bond on the oxide and indicates the presence of active oxygen. Thereupon the intensity of the indicated bands is proportional to the content of O^* . The spectral range of appearance of these bands is an evidence for the covalent character of oxygen bonding to the metal ions of the surface, which in its turn justifies the assumption of high activity of the synthesized samples in reactions of complete oxidation.

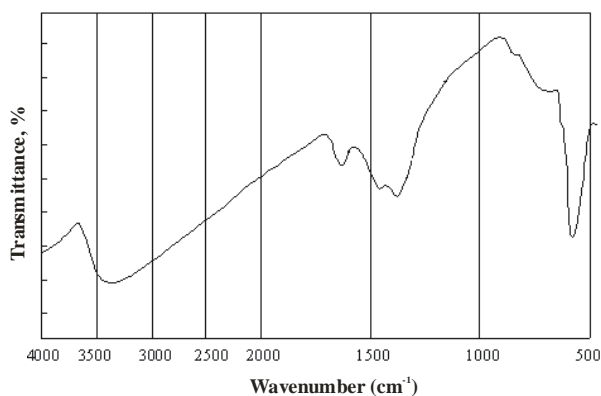


Fig. 2. IR spectrum of bulk NiOx.

The infrared spectrum of the studied catalytic system show also a broad band with a maximum centered at about 3370 cm^{-1} (O-H stretching), together with a band at 1630 cm^{-1} (H-O-H bending). The band at 3370 cm^{-1} can be ascribed to hydroxyl groups bonded through hydrogen bonds, whereas the band at 1630 cm^{-1} corresponds to adsorbed molecular water. The inclusion of OH – groups in the composition of the oxide system (as a result of the reverse order of feeding of the precipitator) is

considered appropriate, since they are involved in the oxidation mechanism of the studied process.

Chemical analysis

Data from the chemical analysis of the synthesized oxide system indicated that NiOx is characterized with high total content of active oxygen (5.33%) and about 80% of it is located on the sample surface. This loosely bonded surface oxygen is a key factor determining high activity of the catalyst in complete oxidation reactions.

It should also be noted that the incorporation of over-stoichiometric (i.e. active) oxygen into oxide system is a direct consequence of the applied synthesis method. As a result of the electron transfer between the precursor $\text{Ni}(\text{OH})_2$ and the oxygen from NaOCl the oxidation state of metal ions in the oxide system increases and high concentration of ionic oxygen species (O^- , O_2^-) on the surface is provided. The latter play a basic role in oxidation catalysis. Most probably the active oxygen is formed as a result of chemisorption of the nascent oxygen (produced on decomposition of NaOCl in strongly alkaline medium) on the precursor surface during the synthesis.

The experimental results obtained from characterization of NiOx give grounds to conclude that the applied synthesis method meets the preliminary requirements described in part 2.1.

Liquid-phase catalytic oxidation of 2,4-DCP over Ni-oxide system

Initially, in order to assess the contribution of non-catalytic oxidation of 2,4-DCP with air on the overall degree of its degradation a preliminary control test was carried out without adding of catalyst to the reaction mixture. It was found that a negligible destruction of 2,4- DCP occurred with air alone (Fig.3, curve 2). The removal efficiency was less than 1% after reaction for 6 hours, indicating that chemical oxidation of substrate is very slow.

However, the simultaneous presence of NiO_x and oxidant significantly improved the removal rate of 2,4-DCP under the certain conditions. The gradual decrease in 2,4-DCP concentration in the course of oxidation reaction was followed by recording the UV spectra illustrated in Fig.3. It should be underlined that almost complete reduction of the intensity of the absorption band at 286 nm corresponding to the maximum absorption wavelength of 2,4-DCP is achieved in very short duration of about 5 minutes. Considering the negli-

gible parallel removal of contaminant molecules by oxidation with air alone it may be concluded that the very fast destruction of 2,4-DCP under heterogeneous oxidation mode is due to its catalytic transformation.

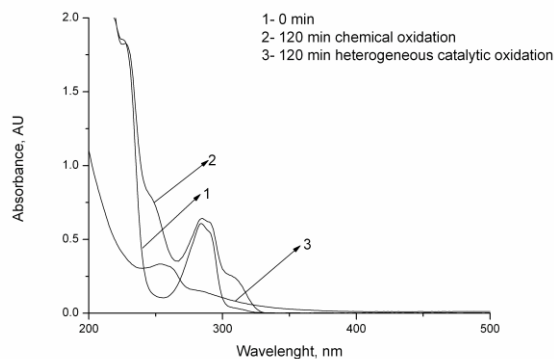


Fig. 3. UV spectrum profiles of the reaction mixture during chemical oxidation (2) and heterogeneous catalytic oxidation (3) on NiOx; ($C_o = 50 \text{ mg dm}^{-3}$; $\text{pH} = 6.0$, $t = 60^\circ\text{C}$, $C_{\text{cat}} = 2 \text{ g dm}^{-3}$).

In the meantime, a new absorbance band at about 254 nm appears at the very beginning of reaction (even at 1 min), but subsequently almost disappears after 120 min, implying that a new structure unit is formed from destruction of 2,4-DCP molecules which further is also complete degraded. The latter is confirmed by results obtained from HPLC analysis.

Fig. 4 shows HPLC chromatograms at 254 nm of 50 mg dm^{-3} 2,4-DCP before and after catalytic oxidation over NiO_x. It is evident that as the catalytic reaction occurs, the intensity of 2,4-DCP peak at $t_r=10.70 \text{ min}$ significantly declined and disappeared after 5 minutes. Simultaneously, a new well resolved peak at $t_r=5.87 \text{ min}$ is registered, implying generation of one intermediate compound as a result of 2,4-DCP oxidation over NiO_x. According to literature reference this peak most likely corresponds to chlorocatechol [17]. Considering very fast catalytic destruction of 2,4-DCP, the kinetic parameters of the oxidation process - reaction rate constant (κ, min^{-1}) and degree of 2,4-DCP conversion ($\alpha, \%$) were calculated on the basis of the gradual decrease of the intensity of the absorption band of intermediate compound. The linear plot of $\ln(A_o/A)$ versus time confirms the assumed first-order kinetics (not shown).

The influence of the main operational parameters such as pH, amount of the catalyst and temperature on the efficiency and selectivity of the oxidation process were studied.

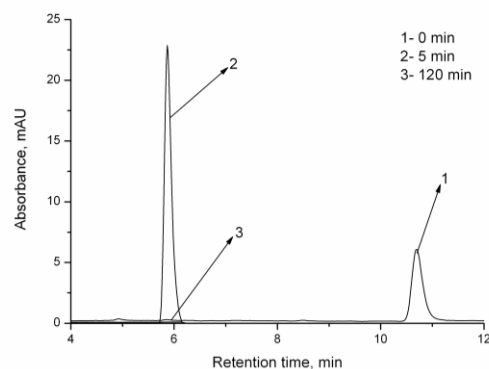


Fig. 4. HPLC chromatograms of the reaction mixture during heterogeneous oxidation on NiOx; ($C_o = 50 \text{ mg dm}^{-3}$; $\text{pH} = 6.0$, $t = 60^\circ\text{C}$, $C_{\text{cat}} = 2 \text{ g dm}^{-3}$).

Fig. 5 illustrates the effect of temperature on the effectiveness of 2,4-DCP oxidative degradation. Experiments were carried out at three different temperatures – 25°C , 40°C and 60°C . Results indicate that at 25°C and 40°C an insignificant destruction of the formed intermediate compound is observed even for 120 min, while at temperature of 60°C a complete oxidation is attained within the same reaction period. Therefore, further studies on the influence of pH and catalyst amount on the reaction kinetics were conducted at a constant temperature of 60°C .

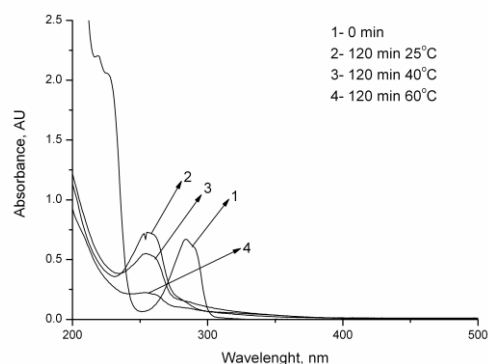


Fig. 5. UV spectrum profiles of the reaction mixture during oxidation with NiOx at different reaction temperatures. ($C_o=50 \text{ mg dm}^{-3}$; $\text{pH} = 6.0$, $C_{\text{cat}} = 2 \text{ g dm}^{-3}$)

Fig. 6 depicts the kinetic curves of catalytic oxidation of 2,4-DCP at 60°C using three different concentrations of NiOx - 0.5 g dm^{-3} , 2 g dm^{-3} and 5 g dm^{-3} . It was found that four-fold increase in catalyst amount led to complete complete degradation of the intermediate compound in 120 min. Moreover, there is no change in reaction rate constant when the catalyst concentration is increased from 2 g dm^{-3} to 5 g dm^{-3} (Table 1). These results imply that a catalyst concentration of 2 g dm^{-3}

dm⁻³ is still enough to achieve complete oxidation of the intermediate absorbing at 254 nm and further incremental addition of the catalyst does not influence the reaction kinetics.

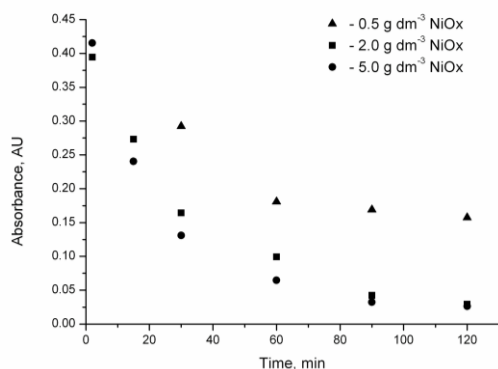


Fig. 6. Effect of catalyst loading on 2,4-DCP degradation. ($C_o = 50 \text{ mg dm}^{-3}$; $\text{pH} = 6.0$; $t = 60^\circ\text{C}$).

Table 1. Rate constants of 2,4-DCP oxidation with different catalyst's concentrations. ($C_o = 50 \text{ mg dm}^{-3}$; $\text{pH} = 6.0$; $t = 60^\circ\text{C}$).

Catalyst dosage (g dm^{-3})	First-order rate constants, $k \cdot 10^2 \text{ (min}^{-1}\text{)}$
0.5	0.6
2.0	3.6
5.0	3.8

In order to determine the optimal conditions for complete oxidation of 2,4-DCP to harmless products the influence of pH on the efficiency and selectivity of the process was investigated. The results obtained are presented in Fig. 7.

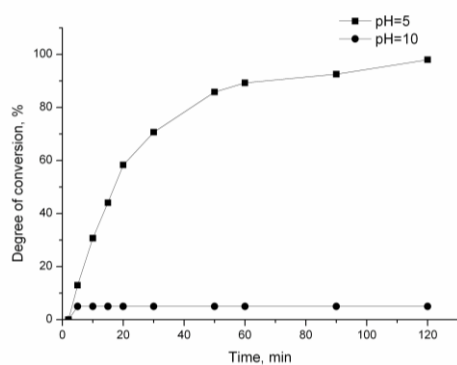


Fig. 7. Effect of pH on the effectiveness of the oxidation process. ($C_o = 50 \text{ mg dm}^{-3}$, $C_{\text{cat}} = 2 \text{ g dm}^{-3}$, $t = 60^\circ\text{C}$).

It is seen that the higher conversion degree of intermediate compound is achieved when the oxidation process is conducted at $\text{pH} = 5.0$ (α is $\sim 100\%$ in 120 minute). The increase of the alkalinity (with other constant parameters) causes a decrease in the conversion degree and the process is

strongly retarded. At $\text{pH} = 10.0$ only 5% of 2,4-DCP was converted into intermediate for 60 minutes and the latter does not further oxidize. Similar effect of pH was observed during liquid phase oxidation of phenol using the same catalytic system [15] and could be explained by comparing the UV spectra of initial solution of 2,4-DCP at $\text{pH} = 5$ and $\text{pH} = 10$ (Fig. 8). A bathochromic shift of the absorption maximum of 2,4-DCP in alkaline medium is registered which is caused by the formation of phenolate anion characterized with $\lambda_{\text{max}} = 303 \text{ nm}$.

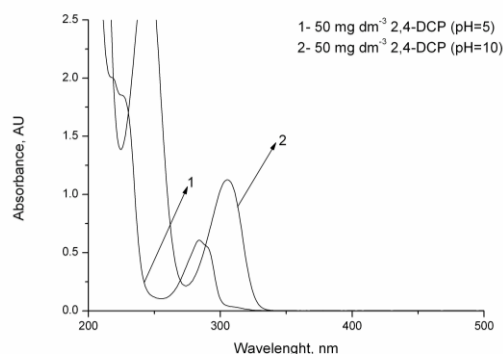


Fig. 8. UV spectrum profiles of the 50 mg dm^{-3} 2,4-DCP initial solutions at $\text{pH} = 5$ and $\text{pH} = 10$.

Based on these results it could be suggested that the oxidation process is most probably initiated by dissociative adsorption of the substrate on the catalyst surface through tearing of an H atom off from the phenolic OH group. The latter interacts with the active oxygen of the catalyst, thus forming highly reactive surface $\cdot\text{OH}$ radicals that attack the 2,4-DCP molecule and cause its destruction. The reduced surface of the catalyst becomes reoxidized by oxygen from air continuously bubbled during oxidation. At $\text{pH} = 10.0$ 2,4-DCP is found mostly in the form of phenolate anion in the solution which makes impossible the formation of $\cdot\text{OH}$ radicals and respectively the oxidation of substrate. Furthermore, when the oxidation was carried out without bubbling of air in the reaction mixture (depletive oxidation) a different 2,4-DCP degradation profile is observed. Initially, the depletive 2,4-DCP oxidation occurs as fast as the reaction carried out in the presence of oxygen and then a strong decrease of the oxidation rate with reaction time is observed. Chemical analysis also showed a decrease in the active oxygen content of the catalyst after depletive oxidation experiment (from 5.33% in the fresh NiO_x to 1.09% in used sample). However, the active oxygen content could be completely recovered on the regeneration of the reduced catalyst

with NaOCl. These results give us ground to conclude that the catalytic oxidation of 2,4-DCP in an aqueous phase with the participation of NiO_x follows the Mars-van Krevelen oxidation-reduction mechanism. The observed relationship between the amount of Ni-oxide system and the effectiveness of the oxidation process also supports the proposed mechanism of heterogeneous catalytic oxidation, i.e. that the active oxygen of the catalyst takes part in the oxidation process. The larger is the amount of the active oxygen (the mass of the oxide, respectively), more OH are formed resulting in higher rate of the process.

The long-term stability is an important property for effective catalyst and is crucial for its practical application. To evaluate the stability of the NiO_x catalyst, three rounds of the 2,4-DCP degradation reaction was conducted with the recycling of the catalyst under the same reaction conditions. After the degradation was finished, the catalyst was recovered from the reaction mixture, washed thoroughly with double distilled water and dried overnight before the next run. The recycling test results showed that the catalyst activity remained unaffected in the second round reuse and decreased slightly in the third test whereupon 2,4-DCP removal was still about 90% at 5 minute.

CONCLUSION

Nickel oxide catalyst was prepared by employing non-conventional ultrasound assisted precipitation-oxidation method with reverse order of feeding of the precipitator to the system. The catalytic performance of the as-prepared NiO_x for low-temperature oxidation of 2,4-DCP in aqueous solutions with air was studied. The obtained results show that 2,4-DCP could be completely degraded in aqueous solutions by heterogeneous catalytic oxidation over NiO_x in 120 min at temperature 60°C. The high catalytic activity of the sample is due to the high content of active oxygen and the nano-dimension of the catalyst's particles, resulting from the applied non-conventional synthesis procedure. The effect of the main operating parameters on the reaction kinetics and 2,4-DCP degradation efficiency were investigated as well. The obtained results indicate that 2,4-DCP is completely oxidized to harmless products at temperature 60°C, pH 5.0-6.0. and concentration of the catalyst 2 g dm⁻³. The simple scheme for the synthesis of the Ni-oxide system and its efficiency

for degradation of 2,4-DCP is a prerequisite for its practical application for purification of wastewaters containing toxic organic compounds.

Acknowledgements: The authors gratefully acknowledge financial support by the National Science Fund (Projects DDVU 02-7/10, DFNI-E01/7) and by the University of Plovdiv Research Fund (Project HF-13-006).

REFERENCES

1. M. Czaplicka, *Sci. Total Environ.*, **322**, 21 (2004).
2. M. Fukushima, K. Tatsumi, *Environ. Sci. Technol.*, **35**, 1771 (2001).
3. J. F. Peng, J. F. Liu, X. L. Hu, G. B. Jiang, *J. Chromatogr. A*, **1139**, 165 (2007).
4. M. M. Ba-Abbada, A. A. H. Kadhum, A. B. Mohamad, M. S. Takriff, K. Sopian, *Int. J. Thermal Envir. Eng.*, **1**, 37 (2010).
5. US EPA. National Emission Standards for Hazardous Air Pollutants: Miscellaneous Organic Chemical Manufacturing; Final Rule, Federal Register Part V, 40 CFR Part 63, United States Environmental Protection Agency, 2006.
6. US EPA/OSHA, US EPA Office of pollution prevention and toxics and occupational safety and health administration, USA, 2000.
7. B. Bayarri, J. Giménez, D. Curcó, S. Esplugas, *Catal. Today*, **101**, 227 (2005)
8. S. Esplugas, J. Gimenez, S. Contreras, E. Pascual, M. Rodriguez, *Water Res.*, **36**, 1034 (2002).
9. M. Pera-Titus, V. García-Molina, M. A. Baños, J. Giménez, S. Esplugas, *Appl. Catal. B- Environ.*, **47**, 219 (2004).
10. R. Andreozzi, V. Caprio, A. Insola, R. Marotta, *Catal. Today*, **53**, 51 (1999).
11. M. M. Ba-Abbad, A. A. H. Kadhum, A. B. Mohamad, M. S. Takriff, K. Sopian, *Int. J. Electrochem. Sci.*, **7**, 4871 (2012).
12. M.-Y. Chang, Y.-H. Hsieh, T.-C. Cheng, K.-S. Yao, M.-C. Wei, C.-Y. Chang, *Thin Solid Films*, **517**, 3888 (2009).
13. T. Thornton, D. LaDue, P. Savage, *Environ. Sci. Technol.* **25**, 1507 (1991).
14. U. S. Ozkan, R. B. Watson, *Catal. Today*, **100**, 101 (2005).
15. S. Christoskova, M. Stoyanova, *Wat. Res.*, **35**, 2073 (2001).
16. S. Christoskova, M. Stoyanova, M. Georgieva, D. Mehandzhiev, *Appl. Catal. A- Gen.*, **173**, 95 (1998).
17. S. Chaliha, K. Bhattacharyya, *Catal. Today*, **141**, 225 (2009).

ИЗСЛЕДВАНЕ НА КАТАЛИТИЧНАТА АКТИВНОСТ НА НАНОРАЗМЕРЕН NiOx ЗА ОКИСЛИТЕЛНА ДЕСТРУКЦИЯ НА 2,4-ДИХЛОРФЕНОЛ ВЪВ ВОДНИ РАЗТВОРИ

В. В. Иванова, М. К. Стоянова, С. Г. Христоскова*

Пловдивски университет „Паисий Хилендарски”, Химически факултет, ул. Цар Асен 24, 4000 Пловдив, България

Постъпила на 04 май 2014 г.; Коригирана на 26 май 2014 г.

(Резюме)

Синтезиран е наноразмерен NiOx и е проучена каталитичната му активност за нискотемпературно окисление на 2,4-ДХФ във водни разтвори с въздух. За получаването на каталитичния образец беше приложен неконвенционален утаечно-окислителен метод с обратен порядък на утаяване, подпомогнат с ултразвукова активация. Синтезираната по посочения метод наноразмерна каталитична система беше охарактеризирана чрез XRD, FTIR, TEM, SAED и химичен анализ. Данните от охарактеризирането показаха, че приложеният метод за синтез благоприятства получаването на високо дисперсни наноразмерни оксидни материали, характеризиращи се с високо съдържание на силно подвижен свръхстехиометричен активен кислород ($O^{*} \sim 8\%$). Резултатите от настоящото проучване показват, че изследваният катализатор проявява висока каталитична активност относно окислителната деструкция на 2,4-ДХФ във водни разтвори с въздух. Пълно превръщане на субстрата се постига за реакционен период от 5 мин. при оптималните условия на процеса, а минерализацията и на интермедиата се извършва за реакционен период от 120 мин.. Изследвано е влиянието на основни операционни параметри върху ефективността на процеса- температура, рН и маса на катализатора.

Experimental and DFT studies on the IR spectral and structural changes arising from the conversion of 4-amino-N-[amino(imino)methyl] benzenesulfonamide (sulfaguanidine) into azanion

A. Popova*, B. Stamboliyska, E. Velcheva

Institute of Organic Chemistry with Centre of Phytochemistry, Bulgarian Academy of Sciences, Acad. G. Bonchev str., bl. 9, 1113 Sofia, Bulgaria

Received May 10, 2014; Revised July 15, 2014

Dedicated to Acad. Dimiter Ivanov on the occasion of his 120th birth anniversary

The structure of 4-amino-N-[amino(imino)methyl] benzenesulfonamide (sulfaguanidine) and of its azanion have been studied on the basis of both infrared spectra and DFT calculations. A good agreement has been found between the theoretical and experimental vibrational characteristic of the particles studied. The theoretical method used gives a good description of the strong spectral changes caused by the conversion of the sulfaguanidine molecule into the corresponding azanion. The structural changes which accompany this conversion take place *at* and *next to* azanionic centre. According to the present calculations, the new (anionic) charge of azanion is distributed, as follows: $-0.07 e^-$, $-0.37 e^-$ and $-0.56 e^-$ over the amino group, phenylene ring and sulfonylguanidine fragment, respectively.

Key words: sulfaguanidine, azanion, IR, DFT

INTRODUCTION

4-Amino-N-[amino(imino)methyl]benzenesulfonamide (sulfanilylguanidine, sulfaguanidine, SG) is the first sulfanilamide antimicrobial agent that is used to treat enteric infections such as bacillary dysentery. In April, 1940, Roblin *et al.* [1] presented the synthesis and physical properties of sulfanilylguanidine to the Division of Medicinal Chemistry at the meeting of the American Chemical Society. In September, 1940, Marshall, Jr., *et al.* [2] published a report of their experiments with sulfanilylguanidine. They had studied its antibacterial properties and its absorbability when given orally and intra-peritoneally. Although fairly soluble in water, sulfanilylguanidine is poorly absorbed from the intestinal tract, but it is a very effective antimicrobial agent.

The crystalline forms of sulfaguanidine have been studied extensively [3-8]. Yang and Guillory [5] found four polymorphic forms and discuss the possibilities of the system of hydrogen bonds. The crystal structure of sulfaguanidine monohydrate [6,7] and molecular structure of anhydrous sulfaguanidine is defined by means of X-ray diffraction [8].

The infrared (IR) spectra of SG in the solid state together with the main band assignments were

reported long time ago [9,10] Trius using infrared spectroscopy for the identification of sulfonamide drugs [11]. The most recent IR spectroscopic investigation, complemented by theoretical studies of the SG has been reported by Chandran *et al.* [12]. However, this investigation is incomplete, as only one tautomeric form (imino) was examined. It is known from NMR spectroscopic [9,13] and X-ray studies [6-8] that the preferred form assumed by the molecule of SG is the symmetrical structure (amino form).

Neither the IR spectra nor structure of sulfaguanidine azanion have been studied theoretically or experimentally. The conversions of neutral molecules into radical anions, carbanions, azanions, etc., are accompanied with essential changes in the vibration spectra. So these changes are very informative for the structural variations that result from the above conversions [14-18]. The purpose of the present investigation is to follow the spectral and structural changes, caused by the conversion of sulfaguanidine molecule into the corresponding azanion on the basis of both DFT computations and IR spectroscopic experiments.

EXPERIMENTAL AND COMPUTATIONS

The sulfaguanidine anion (counter ion Na⁺) was prepared by adding 0.05 and 0.2 mol/l DMSO/DMSO-d₆ solutions of the parent sulfaguanidine to

* To whom all correspondence should be sent:
E-mail: ani_popova@orgchm.bas.bg

equimolar quantities of dry alkali-metal methoxides -d₀ and -d₃ under argon. The conversion was practically complete (no bands of the parent compound were seen in the spectra after metalation).

The IR spectra were measured on a Bruker Tensor 27 spectrophotometer in a CaF₂ cell of 0.13 mm path length for DMSO/DMSO-d₆ solutions and in KBr disk, at a resolution of 1 cm⁻¹ and 64 scans.

The quantum chemical calculations were performed using the Gaussian 09 package [19]. The geometry optimizations of the structures investigated were done without symmetry restrictions, using density functional theory (DFT). We employed B3LYP hybrid functional, which combines Becke's three-parameter nonlocal exchange with the correlation functional of Lee *et al.* [20,21], adopting 6-31+G* and 6-311+G(2df,p) basis sets. The stationary points found on the molecular potential energy hypersurfaces were characterized using standard harmonic vibrational analysis. The theoretical vibrational spectra were interpreted by means of potential energy distributions (PEDs) using VEDA 4 program [22]. For a better correspondence between experimental and calculated values, we modified the results using the empirical scaling factors [23].

RESULTS AND DISCUSSION

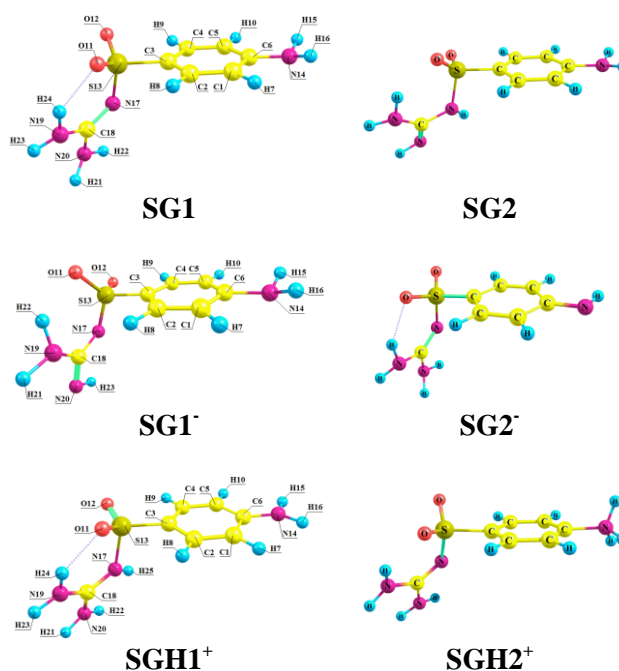
Energies and conformational isomers

The sulfaguanidine molecule can exist as two tautomers, SG1 and SG2 which have its guanidine group in amino and imino form, respectively. All tautomers of sulfaguanidine and its protonated and deprotonated forms have different conformers resulting from rotation about C-S, S-N and N-C bonds. After a systematic conformation search on the B3LYP/6-31+G* potential energy of studied species, four different minima for molecule and six – for anion and cation are located. The structure of the most stable conformers were reoptimized at B3LYP/6-311(2df,p)G** and can be seen in Scheme 1; their total energies are compared in Table 1. The following comments can be made on the basis of the corresponding energy values:

- The tautomer SG1 is predicted to be more stable than SG2 one by more than 40 kJ.mol⁻¹. According to Minkin *et al.* [24] prototropic conversions are probable in case when the energy differences between the initial and the final structure do not exceed 25 kJ.mol⁻¹, with activation barrier not higher than 105 kJ.mol⁻¹. As it could be seen in Table 1 the energy

difference is larger in the present case, and convinces that only SG1 should be expected to exist in real system. The presence of the same amino tautomer SG1 was established by crystallographic analysis [6,8] and experimental NMR spectral data in DMSO [9]. In recently published DFT vibrational analysis, Chandran and co-workers [12] computed only imino SG2 structure, which is less stable.

- The anion SG1⁻ is the most stable among the possible anionic isomers, obtained through elimination of a proton from the guanidine group and with the 45 kJ.mol⁻¹ more stable than anion SG2⁻ obtained through elimination of a proton from amino group.
- SG1H⁺ protonated at the guanidine group is the significantly more stable protonated isomer. The other isomer protonated at the N atom connected with phenyl ring highly improbable in gas state.



Scheme 1. B3LYP/6311+G(2df,p) optimized structures of the tautomers of sulfaguanidine molecule SG1 and SG2 and their protonated and deprotonated species.

The deprotonation energy (E^D) of a given species can be calculated as a difference between ZPVE-corrected energies of the most stable conformer of this species and of the corresponding deprotonated form. So, for species studied we can calculate from the data in Table 1:

Table 1. Total E_{tot} (in hartree) and relative E_{rel} (in kJ/mol) energies of sulfaguanidine molecule, its protonated and deprotonated species.

Species ^a	B3LYP/6-31+G*		B3LYP/6-311+G(2df,p)	
	E_{tot}	E_{rel}	E_{tot}	E_{rel}
SG1	-1040.41404		-1040.66028	
SG2	-1040.39780	42.55	-1040.64383	43.19
SG1H ⁺	-1040.79436		-1041.04101	
SG2H ⁺	-1040.75752	96.72	-1041.00436	96.20
SG1 ⁻	-1039.85858		-1040.10438	
SG2 ⁻	-1039.84153	44.74	-1040.08710	45.36

^a Numbering according Scheme 1. E^{D} of the sulfaguanidine:

$$E_{\text{SG1}}^{\text{D}} = 1459.52 \text{ kJ/mol}$$

 E^{D} of the protonated sulfaguanidine:

$$E_{\text{SG1H}^+}^{\text{D}} = 999.60 \text{ kJ/mol}$$

The E^{D} values are related qualitatively with the acidities of the C–H, C–N etc. acids in DMSO and other solvents (lower E^{D} , higher acidity, lower pK_{a} 's). In the present case the above E^{D} value are also in a qualitative agreement with the experiment: the protonated sulfaguanidine is a strong acid ($\text{pK}_{\text{a}}=2.75$ [25]) and sulfaguanidine itself is a weak acid ($\text{pK}_{\text{a}}=12.1$ [26]).

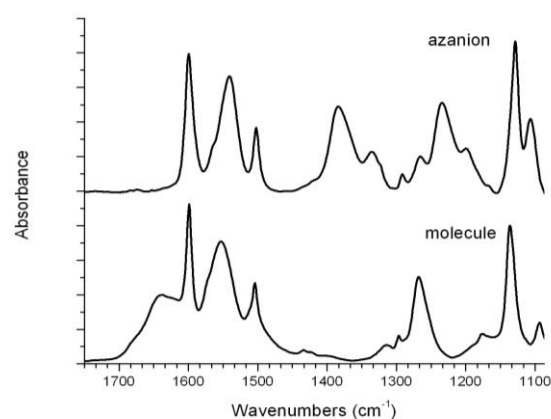
Spectral analysis

The theoretical and experimental IR data, measured in DMSO solvent for the sulfaguanidine molecule are compared in Table 2. We can see there a good agreement between experimental and scaled theoretical frequencies. The mean absolute deviation between them is nearly 13 cm^{-1} .

The largest differences between theoretical and experimental IR data correspond to the NH_2 stretching vibrations. The calculations predict that the highest frequency band (3572 cm^{-1}) corresponds to the asymmetric deformation of amino group, the following frequencies (3561 cm^{-1} , 3560 cm^{-1}) correspond to the asymmetric NH_2 modes of guanidine structural motif, whereas the other ones (3464 cm^{-1} , 3463 cm^{-1} , 3387 cm^{-1}) are assigned respectively to the symmetric ones. The measured amino frequencies are significantly lower than theoretically predicted ones, due to the formation of strong hydrogen bonds between the sulfaguanidine molecules and DMSO-d_6 solvent. The theory predicted well the low intensities of the $\nu(\text{PhH})$ bands. The stretching $\nu(\text{NC})$ strongly coupled with deformation vibrations of $\delta(\text{NH}_2)$ of guanidine frag-

ment is predicted to appear at 1626 cm^{-1} as a very intense band. Experimentally, a strong band was detected at 1640 cm^{-1} . Deformation vibration of the amino group is predicted as pure in 1607 cm^{-1} and found at 1600 cm^{-1} . The strong bands of the $\nu^{\text{as}}(\text{SO}_2)$ and $\nu^{\text{as}}(\text{SO}_2)$ frequencies, appear at 1269 cm^{-1} and 1137 cm^{-1} , respectively. For comparison the corresponding bands of the saccharin molecule have been found at 1326 cm^{-1} and 1177 cm^{-1} (in DMSO solvent) [27] and we have found those of sulfanilamide molecule at 1317 cm^{-1} and 1153 cm^{-1} (in DMSO solvent) [16].

The theoretical and experimental IR data for the sulfaguanidine anion are compared in Table 3. As above we can find there a good agreement between experimental and scaled theoretical frequencies. The mean deviation between them is 13 cm^{-1} within the corresponding interval of $9\text{--}25 \text{ cm}^{-1}$, typical for DFT calculations of frequencies for series of carbanions [28,29], azanions [14] and oxyanions [15] (and references therein). The conversion of sulfaguanidine into the azanion results in very essential changes in the IR spectrum (Tables 2 and 3; Fig. 1). In agreement between theory and experiment, the conversion results in considerable frequency decreases in both $\nu^{\text{as}}(\text{SO}_2)$ and $\nu^{\text{as}}(\text{SO}_2)$ bands, which sum is: predicted 115 cm^{-1} , measured 110 cm^{-1} . The latter value is rationally larger than the corresponding values for other molecule-azanion pairs, containing additional electron-withdrawing groups (compound, SO_2 sum): o-sulfobenzimide (saccharin), 93 cm^{-1} [28]; o-sulfothiobenzimide (thiosaccharin), 60 cm^{-1} [30] and less than in sulfanilamide, 140 cm^{-1} [16].

**Fig. 1.** Experimental IR spectra of sulfaguanidine and its azanion.

A new band was registered and it was attributed to the deformation $\delta(\text{CNH}^-)$ of deprotonated guanidine fragment. The band at 1600 cm^{-1} assigned as $\delta(\text{NH}_2)$ remained unchanged.

Table 2. Theoretical (B3LYP/6-311+G(2df,p)) and experimental (DMSO) IR data of sulfaguanidine molecule.

No.	B3LYP/6311+G(2df,p)			Approximate description ^b	Experimental data
	ν (cm ⁻¹)	ν^a (cm ⁻¹)	Λ (km/mol)		
1	3687	3572	36.5	99 $\nu_{NH_2}^{as}$	3508 sh.
2	3676	3561	97.5	100 $\nu_{NH_2}^{as}$	3420
3	3676	3561	22.2	100 $\nu_{NH_2}^{as}$	- ^c
4	3576	3464	39.4	98 $\nu_{NH_2}^s$	3336
5	3576	3463	37.3	98 $\nu_{NH_2}^s$	- ^c
6	3496	3387	134.4	99 $\nu_{NH_2}^s$	3218
7	3199	3099	2.3	97 ν_{CH}	3088
8	3198	3098	1.5	96 ν_{CH}	3068
9	3160	3060	18.2	96 ν_{CH}	3056
10	3159	3060	12.3	97 ν_{CH}	3033
11	1679	1626	750.8	45 $\delta_{NH_2}^{guanine}$, 26 $\nu_{N=C}$	1640
12	1659	1607	274.5	72 $\delta_{NH_2}^{amino}$	1600
13	1639	1587	90.8	32 ν_{CC} , 15 $\delta_{NH_2}^{amino}$	- ^c
14	1629	1578	230.8	68 $\delta_{NH_2}^{guanine}$	1574
15	1613	1563	10.4	54 ν_{CC} , 13 δ_{CCC}	1554
16	1582	1533	238.8	49 $\delta_{NH_2}^{guanine}$, 31 $\nu_{N=C}$	1509
17	1535	1487	55.9	61 δ_{CCH}	- ^c
18	1465	1419	66.8	32 ν_{CC} , 10 δ_{CCC} , 11 δ_{NCN}	1436
19	1462	1416	116.2	42 ν_{C-NH_2} , 10 δ_{NCN}	1420
20	1356	1314	3.9	40 ν_{CC} , 32 δ_{CCC} , 12 $\delta_{NH_2}^{amino}$	1316
21	1330	1289	70.4	54 δ_{CCH} , 31 ν_{CC}	1297
22	1313	1272	101.2	52 $\nu_{C-NH_2}^{amino}$	- ^c
23	1299	1258	201.1	92 $\nu_{SO_2}^{as}$	1269
24	1207	1169	4.0	68 δ_{CCH}	- ^c
25	1198	1160	115.6	46 $\delta_{NH_2}^{rock}$, 23 $\nu_{N=C}$, δ_{CCH}	1179
26	1151	1115	12.7	58 δ_{CCH} , 23 ν_{CC} , 10 $\delta_{NH_2}^{rock}$ (amino)	- ^c
27	1137	1101	213.6	39 $\nu_{SO_2}^s$, 22 ν_{CC} , 13 ν_{SC}	1137
28	1101	1063	23.2	48 δ_{CNH} , 23 ν_{C-NH_2}	1083
29 ^d	1084	1047	88.1	25 $\nu_{SO_2}^s$, 18 δ_{CNH}	- ^c

^a Scaled by 0.9858 [23]. ^b Vibrational modes: ν , stretching; δ , bendings. The numbers before the mode symbols indicate % contribution (10 or more) of a given mode to the corresponding normal vibration, according to the potential energy distribution matrix. ^c These bands were not detected in the experimental spectrum. ^d Followed by 37 lower-frequency normal vibrations.

Table 3. Theoretical (B3LYP/6-311+G(2df,p) and experimental (DMSO) IR data of sulfaguanidine anion.

No.	B3LYP/6311+G(2df,p)			Approximate description ^b	Experimental data
	ν (cm ⁻¹)	ν^a (cm ⁻¹)	A (km/mol)		
1	3636	3522	32.0	99 $\nu_{NH_2}^{as}$	- ^c
2	3632	3518	7.1	100 $\nu_{NH_2}^{as}$	- ^c
3	3540	3428	2.1	100 $\nu_{NH_2}^{as}$	- ^c
4	3502	3392	50.1	98 $\nu_{NH_2}^s$	- ^c
5	3490	3381	3.0	98 ν_{N-H}	- ^c
6	3194	3094	5.0	97 ν_{CH}	- ^c
7	3180	3081	9.2	96 ν_{CH}	3030
8	3137	3039	31.6	96 ν_{CH}	- ^c
9	3134	3035	39.2	97 ν_{CH}	3080
10	1650	1598	93.9	67 $\delta_{NH_2}^{amino}$	1600
11	1636	1585	24.1	55 ν_{CC} , 15 $\delta_{NH_2}^{amino}$	- ^c
12	1621	1570	167.5	44 δ_{NH_2} , 19 ν_{C-N^-}	1564sh
13	1618	1567	12.6	45 ν_{CC} , 13 $\delta_{NH_2}^{guanidine}$	- ^c
14	1600	1550	654.8	48 ν_{C-N^-} , 28 $\delta_{NH_2}^{guanidine}$	1540
15	1530	1482	80.8	68 δ_{CCH}	1502
16	1453	1407	5.3	30 δ_{CCH} , 26 ν_{CC}	- ^c
17	1417	1373	273.5	33 δ_{C-N-H} , 16 δ_{NH_2}	1384
18	1352	1309	1.1	53 δ_{CCH} , 22 ν_{CC}	1335
19	1324	1282	16.7	29 ν_{CC} , 20 δ_{CCH}	1291
20	1275	1235	65.2	48 $\nu_{C-NH_2}^{amino}$, 20 δ_{CCH}	1255
21	1241	1202	310.3	76 $\nu_{SO_2}^{as}$	1234
22	1219	1181	19.6	32 δ_{C-N-H} , 16 ν_{C-NS} , 10 $\delta_{NH_2}^{guanidine}$	1199
23	1202	1164	12.8	82 δ_{CCH}	1166
24	1168	1131	192.9	51 $\delta_{NH_2}^{guanidine}$, 16 ν_{C-NS}	1128
25	1143	1108	8.5	60 δ_{CCH} , 17 $\delta_{NH_2}^{rock(amino)}$	- ^c
26 ^d	1115	1080	162.0	42 $\nu_{SO_2}^s$, 26 ν_{CC} , 13 ν_{SC}	1106

^a Scaled by 0.9858 [23]. ^b Vibrational modes: ν , stretching; δ , bendings. The numbers before the mode symbols indicate % contribution (10 or more) of a given mode to the corresponding normal vibration, according to the potential energy distribution matrix. ^c These bands were not detected in the experimental spectrum. ^d Followed by 37 lower-frequency normal vibrations.

Structural analysis

According to both X-ray diffraction experimental data [6] and DFT calculations the sulfaguanidine molecule is composed of atoms lying approximately in two planes: one of the phenylene rings and amino group, and the other of

the guanidine moiety. The angle between these planes has been experimentally found to be 94.4°; the same angle for the isolated sulfaguanidine molecule has been theoretically estimated at 96.7°. The corresponding value for the free sulfaguanidine anion is 82.1°.

The theoretical and experimental bond lengths and angles in the sulfaguanidine and its azanion are listed in Table 4. As seen, there is a good agreement between the experimental and the theoretical values. The largest deviation from 0.053 Å is in bond S₁₃ - N₁₇ and can be associated with the formation of hydrogen bonds in the solid state. The mean absolute deviations (m.a.d.) between theoretical and experimental bond lengths and angles of sulfaguanidine molecule are 0.017 Å and 1.06, respectively. This result leads us to

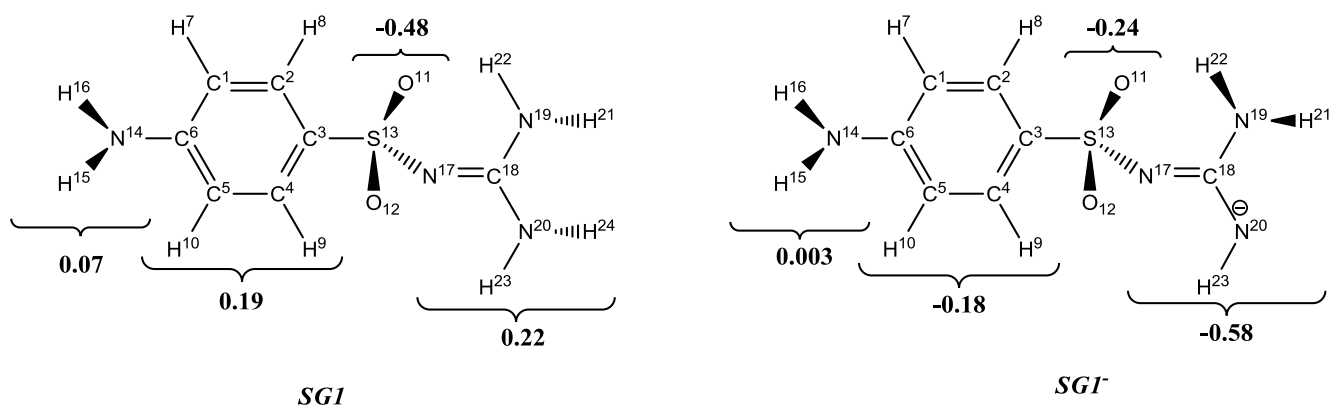
believe that the theoretical bonds lengths and angle for the sulfaguanidine anion are also reliable. The most significant changes caused by the conversion molecule azanion take place both at the azanionic center and next to it, with agrees the data for other azanions [14,16,28,30]. They are strong shortening of the N₂₀-C₁₈ and S₁₃-N₁₇ bonds, strong lengthening of the C₁₈-N₁₇ and C₁₈-N₁₉ bonds.

The net electric charges q_i of the fragments of the species studied are given in Scheme 2. The charge change values Δq_i= q_i (anion) - q_i (molecule)

Table 4. Theoretical (B3LYP/6-311+G(2df,p)) and experimental bond lengths R (Å), angles A (°) in the sulfaguanidine molecule and its azanion.

	Molecule			Anion		
	Experimental ^a	Theoretical	Δ ^b	Theoretical	∇ ^c	
<i>Bond lengths^d</i>						
R(C ¹ C ²)	1.379	1.380	1.384	0.004	1.387	0.003
R(C ¹ C ⁶)	1.401	1.389	1.401	0.006	1.398	-0.003
R(C ² C ³)	1.387	1.387	1.391	0.004	1.393	0.002
R(C ³ C ⁴)	1.388	1.388	1.392	0.004	1.389	-0.003
R(C ³ S ¹³)	1.767	1.763	1.773	0.008	1.814	0.041
R(C ⁴ C ⁵)	1.378	1.386	1.383	0.001	1.391	0.008
R(C ⁵ C ⁶)	1.379	1.380	1.402	0.023	1.395	-0.007
R(C ⁶ N ¹⁴)	1.399	1.396	1.386	-0.012	1.410	0.024
R(O ¹¹ S ¹³)	1.445	1.450	1.466	0.019	1.476	0.010
R(O ¹² S ¹³)	1.442	1.430	1.446	0.010	1.458	0.012
R(N ¹⁷ S ¹³)	4.589	1.587	1.642	0.053	1.576	-0.066
R(N ¹⁷ C ¹⁸)	1.343	1.340	1.302	-0.039	1.374	0.072
R(C ¹⁸ N ¹⁹)	1.336	1.326	1.356	0.025	1.401	0.045
R(C ¹⁸ N ²⁰)	1.322	1.337	1.372	0.043	1.296	-0.076
<i>Bond angles^d</i>						
A(C ² C ¹ C ⁶)	121.0	120.5	120.6	-0.150	120.7	0.100
A(C ¹ C ² C ³)	120.1	120.0	120.0	-0.050	120.4	0.400
A(C ² C ³ C ⁴)	119.6	119.8	120.1	0.400	119.1	-1.000
A(C ² C ³ S ¹³)	121.8	121.2	120.3	-1.200	120.5	0.200
A(C ⁴ C ³ S ¹³)	118.5	119.0	119.7	0.950	120.3	0.600
A(C ³ C ⁴ C ⁵)	120.4	119.9	120.0	-0.150	120.6	0.600
A(C ⁴ C ⁵ C ⁶)	120.5	120.8	120.7	0.050	120.6	-0.100
A(C ¹ C ⁶ C ⁵)	118.3	119.0	118.7	0.050	118.6	-0.100
A(C ¹ C ⁶ N ¹⁴)	120.4	121.2	120.7	-0.100	120.6	-0.100
A(C ⁵ C ⁶ N ¹⁴)	121.2	119.8	120.6	0.100	120.8	0.200
A(C ³ S ¹³ O ¹¹)	107.0	107.2	107.5	0.400	104.7	-2.800
A(C ³ S ¹³ O ¹²)	107.7	107.9	108.1	0.300	104.5	-3.600
A(C ³ S ¹³ N ¹⁷)	106.0	106.1	101.9	-4.150	106.7	4.800
A(O ¹¹ S ¹³ O ¹²)	115.0	116.5	118.0	2.250	115.6	-2.400
A(O ¹¹ S ¹³ N ¹⁷)	114.3	112.6	111.9	-1.550	115.2	3.300
A(O ¹² S ¹³ N ¹⁷)	106.2	105.9	108.3	2.250	109.2	0.900
A(S ¹³ N ¹⁷ C ¹⁸)	121.5	121.6	123.6	2.050	126.1	2.500
A(N ¹⁷ C ¹⁸ N ¹⁹)	124.7	126.5	127.4	1.800	120.3	-7.100
A(N ¹⁷ C ¹⁸ N ²⁰)	116.5	116.2	117.1	0.750	122.8	5.700

^aSee Ref. [8]. ^bAlgebraic deviations (Å, degrees) between theoretical and experimental values. ^cAlgebraic deviations (Å, degrees) between theoretical values of the anion and molecule. ^dAtom numbering according to Scheme 1.



Scheme 2. Mulliken net electric charges q_i over fragments of sulfaguandine molecule **SG1** and its azanion **SG1⁻**.

are usually quite informative in showing the distributions of the new charges in anions (Refs. [28-30] and references therein). According to the present calculations, the anionic charge of azanion is distributed, as follows: $-0.07 e^-$, $-0.37 e^-$ and $-0.56 e^-$ are delocalized over the amino group, phenylene ring and sulfonylguanidine fragment, respectively.

CONCLUSION

The spectral and structural changes, caused by the conversion of the sulfaguandine molecule into the corresponding azanion have been studied by IR spectra DFT method at B3LYP/6-311+G(2df,p) level.

A comparison of calculated with measured infrared data can be used as a test for the reliability of the structural predictions for various molecules and anions of this and similar types. These predictions can be very useful in cases of molecules and ions for which experimental structural parameters are inaccessible or unknown. IR spectral changes, which take place as a result of the conversion of molecule into azanion, were adequate predicted by same theoretical method.

Acknowledgements: Financial support of National Science Fund, Bulgaria (DID02/33/2009 and DRNF-02/13/2009) is gratefully acknowledged.

REFERENCES

1. R. O. Roblin Jr., J. H. Williams, Ph. S. Winnek, J. P. English, *J. Am. Chem. Soc.*, **62**, 2002 (1940).
2. E. K. Marshall, A. C. Bratton, H. J. White, J. T. Litchfield, *Johns Hopkins Hosp. Bull.*, **67**, 163 (1940).
3. M. Kuhnert-Brandstätter, *Oesterr. Apoth. Ztg.*, **13**, 297 (1959).
4. M. Kuhnert-Brandstätter, S. Wunsch, *Microchim. Acta*, 1297 (1969).
5. S. S. Yang, J. K. Guillory, *J. Pharm. Sci.*, **61** (1972) 26.
6. C. H. Koo, H. S. Kim, W. Shin, C. Choe, *J. Kor. Chem. Soc.*, **18**, 97 (1974).
7. M. Alleaume, *Acta Cryst.*, **B32**, 669 (1976).
8. A. Kalman, M. Czugler, G. Argay, *Acta Cryst.*, **B37**, 868 (1981).
9. G. Schwenker, *Arch Pharm.* **295**, 753 (1962).
10. M. Brandstätter, F. Bachleitner-Hofmann, *Spectrochim. Acta*, **A27**, 191 (1971).
11. N. V. Trius, *Khim.-Farm. Zh.*, **13**, 103 (1979).
12. A. Chandran, H. T. Varghese, C. Yohannan, G. Rajendran, *Orient. J. Chem.*, **27**, 611 (2011).
13. G. R. Sullivan, J. D. Roberts, *J. Org. Chem.*, **42**, 1095 (1977).
14. A. D. Popova, E. A. Velcheva, B. A. Stamboliyska, *J. Mol. Struct.*, **1009**, 23 (2012).
15. E. A. Velcheva, B. A. Stamboliyska, P. J. Boyadjieva, *J. Mol. Struct.*, **963**, 57 (2010).
16. A. D. Popova, M. K. Georgieva, O. I. Petrov, K.V. Petrova, E. A. Velcheva, *Int. J. Quant. Chem.*, **107**, 1752 (2007).
17. S. Stoyanov, J. A. Tsenov, D. Y. Yancheva, *J. Mol. Struct.*, **1009**, 42 (2012).
18. S. Stoyanov, *J. Phys. Chem.*, **114** 5149 (2010).
19. M. J. Frisch, G. W. Trucks, H. B. Schlegel, G. E. Scuseria, M. A. Robb, J. R. Cheeseman, G. Scalmani, V. Barone, B. Mennucci, G. A. Petersson, H. Nakatsuji, M. Caricato, X. Li, H. P. Hratchian, A. F. Izmaylov, J. Bloino, G. Zheng, J. L. Sonnenberg, M. Hada, M. Ehara, K. Toyota, R. Fukuda, J. Hasegawa, M. Ishida, T. Nakajima, Y. Honda, O. Kitao, H. Nakai, T. Vreven, J.A. Montgomery, Jr., J. E. Peralta, F. Ogliaro, M. Bearpark, J. J. Heyd, E. Brothers, K. N. Kudin, V. N. Staroverov, R. Kobayashi, J. Normand, K. Raghavachari, A. Rendell, J. C. Burant, S. S. Iyengar, J. Tomasi, M. Cossi, N. Rega, J. M. Millam, M. Klene, J. E. Knox, J. B. Cross, V. Bakken, C. Adamo, J. Jaramillo, R. Gomperts, R. E. Stratmann, O. Yazyev, A.J. Austin, R. Cammi, C. Pomelli, J. W. Ochterski, R. L. Martin, K. Morokuma, V. G. Zakrzewski, G. A. Voth, P.

- Salvador, J. J. Dannenberg, S. Dapprich, A. D. Daniels, Ö. Farkas, J. B. Foresman, J. V. Ortiz, J. Cioslowski, D. J. Fox, Gaussian 09, Revision A1, Gaussian Inc., Wallingford CT, 2009.
20. A. D. Becke, *J. Chem. Phys.*, **98**, 5648 (1993).
21. C. Lee, W. Yang, G. R. Parr, *Phys. Rev.*, **B37**, 785 (1998).
22. H. J. Michal, VEDA 4, Warsaw, 2004.
23. J. P. Merrick, D. Moran, L. Radom, *J. Phys. Chem.*, **A111**, 11683 (2007).
24. I. Minkin, B. Y. Simkin, R. M. Minyaev, Quantum chemistry of organic compounds. Mechanisms of reactions, Springer, Heidelberg, 1990.
25. B. E. Ballard, E. Nelson, *J. Pharmacol. Exp. Ther.*, **135**, 120 (1962).
26. B. C. Rudy, B. Z. Senkowski, *Analyt Profiles.*, **2**, 234 (1973).
27. I. G. Binev, B. A. Stamboliyska, E. A. Velcheva, *Spectrochim. Acta Part A*, **52**, 1135 (1996).
28. J. A. Tsenov, S. S. Stoyanov, I. G. Binev, *Bulg. Chem. Commun.*, **40**, 538 (2008).
29. J. A. Tsenov, S. S. Stoyanov, I. G. Binev, *Bulg. Chem. Commun.*, **37**, 361 (2005).
30. Y. G. Binev, C. T. Petkov, L. Pejov, *Spectrochim. Acta*, **A56**, 1949 (2000).

ЕКСПЕРИМЕНТАЛНО И ТЕОРЕТИЧНО ИЗСЛЕДВАНЕ НА ИЧ СПЕКТРАЛНИ И СТРУКТУРНИ ПРОМЕНИ, ПРОИЗТИЧАЩИ ОТ ПРЕВРЪЩАНЕТО НА 4-АМИНО-N-[АМИНО(ИМИНО)МЕТИЛ] БЕНЗЕНСУЛФОНАМИД (СУЛФАГУАНИДИН) В АЗАНИОН

А. Попова*, Б. Стамболийска, Е. Велчева

Институт по Органична химия с Център по Фитохимия, Българска Академия на Науките, ул. Акад. Г. Бончев, бл. 9, 1113 София, България

Постъпила на 10 май 2014 г.; Коригирана на 15 юли 2014 г.

(Резюме)

Структурата на amino-N-[амино(имино)метил]бензенсулфонамид (сулфагуанидин) и неговия азанион са изследвани с помощта на инфрачервени спектри и DFT пресмятания. Намерено е добро съответствие между експерименталните и теоретичните вибрационни характеристики на изследваните частици. Използваният теоретичен метод добре предсказва силните спектрални промени, възникващи при превръщането на молекулата на сулфагуанидина в азанион. Превръщането в азанион поражда и значителни промени в структурата *при* и *непосредствено до* азанионния център. Според изчисленията новият (азанионен) заряд е разпределен както следва: $-0.07 e^-$, $-0.37 e^-$ и $-0.56 e^-$ върху amino групата, фениленовото ядро и сулфонилгуанидиновия фрагмент, съответно.

IR spectral and structural changes, caused by the conversion of 4-cyanobenzenesulfonamide into azanion

A. D. Popova*, E. A. Velcheva

Institute of Organic Chemistry with Centre of Phytochemistry, Bulgarian Academy of Sciences, Acad. G. Bonchev str., bl. 9, 1113 Sofia, Bulgaria

Received May 28, 2014; Revised July 14, 2014

Dedicated to Acad. Dimiter Ivanov on the occasion of his 120th birth anniversary

A combined IR experimental/DFT computational approach has been applied to follow the spectral and structural changes, caused by the conversion of 4-cyanobenzenesulfonamide into azanion. The conversion has shown a weak effect on the cyano stretching band $\nu_{C\equiv N}$ and strong effects on both $\nu_{SO_2}^{as}$ and $\nu_{SO_2}^s$ stretching bands. According to the computations, the strong structural changes, caused by the conversion, take place *at* and *next to* the azanionic center. The new (azanionic) charge is distributed as follows: 0.08 e⁻, 0.25 e⁻ and 0.10 e⁻ are delocalized over the cyano, phenylene and sulfonyl groups, respectively, and 0.57 e⁻ of it remain localized in the azanionic center.

Key words: IR spectra, DFT/B3LYP, 4-cyanobenzenesulfonamideamide, azanion

INTRODUCTION

Sulfonamides (SA) are well known for their various biological activities: antibacterial, diuretic, antidiabetic etc. [1]. The unsubstituted in sulfamide group aromatic/heterocyclic SA are known as inhibitors of the zinc-enzyme Carbonic anhydrase (CA) with diuretic activities, hypoglycemic activity and anticancer properties [2,3]. This enzyme catalyzes the reversible hydration of carbon dioxide and both meta- and para- substituted SAs are specific and potent inhibitors of CA. The inhibition mechanism seems to be mainly connected with the generation of an electrostatic field of the zinc ion which favors the correct orientation of the SO₂NH₂ group and its anticipated deprotonation. So, the inhibitory action is caused by the binding of the sulfamide anion to the Zn²⁺ of the enzyme, mimicking the bicarbonate anion in the transition state [3-5]. Due to their pharmacology applications and widespread use in medicine, these compounds have gained attention in many fields of drug chemistry.

4-Cyanobenzenesulfonamide is a representative of the benzenesulfonamides with primary sulfonamide group. 4-Cyanobenzenesulfonamide was first prepared almost 120 years ago by Remsen et al. [6] using a multistep synthesis, starting with 4-(aminosulfonyl)benzoic acid. There is a recent study of the

title compound by Camí and coworkers [7]. They have synthesized 4-cyanobenzenesulfonamide and its copper complex and reported their UV, IR and Raman spectra and B3LYP calculations. The structure and IR spectra of 4-cyanobenzenesulfonamide azanion itself have never been studied experimentally or theoretically. The conversions of neutral molecules into radical anions, carbanions, azanions, etc., are accompanied with essential changes in the vibration spectra. So, these changes are very informative for the structural variations that result from the above conversions [8-11].

The purpose of the present investigation is to follow the spectral and structural changes, caused by the conversion of 4-cyanobenzenesulfonamide molecule into the corresponding azanion on the basis of both DFT computations and IR spectroscopic experiments.

EXPERIMENTAL

The sample of p-cyanobenzenesulfonamide (Manchester Organic Limited, spectroscopic grade) was used without any additional purification. Its azanion was prepared by adding dimethyl sulfoxide (DMSO/DMSO-d₆) solutions of the parent compound to excess of dry CD₃O⁻Na⁺ under argon, and collecting the clear azanion solution with a syringe-filter. We prepared the sample of CD₃O⁻Na⁺ itself by reacting CD₃OD (Fluka, 99% at. enrichment) with Na and evaporating the excess of methanol *in vacuo*. p-Cyanobenzenesulfonamide reacted with

* To whom all correspondence should be sent:
E-mail: ani_popova@orgchm.bas.bg

$\text{CD}_3\text{O}^-\text{Na}^+$ to form the azanion in DMSO/DMSO- d_6 promptly (within 1-2 min) and practically completely: no bands of the parent compound were seen in the spectra after metalation.

The IR spectra are recorded on a Bruker Tensor 27 FTIR spectrophotometer in a CaF_2 cell of 0.129 mm path length (for DMSO/ DMSO- d_6 solutions), a KBr cells of 0.6 mm path length (for saturated CDCl_3 solutions) and in KBr and CsI disks, at a resolution of 1cm^{-1} and 64 scans.

COMPUTATIONS

The quantum chemical calculations were performed using the Gaussian 09 package [12] on a MADARA grid. The geometry optimizations of the structures investigated were done without symmetry restrictions, using density functional theory (DFT). We employed B3LYP hybrid functional, which combines Becke's three-parameter nonlocal exchange with the correlation functional of Lee, Yang and Parr [13,14], adopting 6-31++G(d,p), 6-311+G(2df,p) and aug-cc-pVTZ basis sets. The stationary points found on the molecular potential energy hypersurfaces were characterized using standard harmonic vibrational analysis. The absence of imaginary frequencies confirmed that the stationary points corresponded to minima on the potential energy hypersurfaces. In order to check statistically which basis set performed agrees best with the experimental data for the species studied, we have treated the correlations between their theoretical and experimental IR frequencies. The comparison has shown that the B3LYP/6-311+G(2df,p) IR data correlate best with the experimental ones. For a better correspondence between experimental and calculated values, we modified the results using the empirical scaling factors [15].

RESULTS AND DISCUSSION

Energy analysis

The full conformational search on the potential energy surface of the molecule and azanion of 4-cyanobenzenesulfonamide allowed the identification of two different minima of the molecule, all of them bearing the sulfamide nitrogen atom placed in the perpendicular orientation relatively to the aromatic ring and differing from each other in the orientation of the amide hydrogen atoms and one minimum of the azanion. The conformers of the species studied are shown in Fig. 1 and their energies are compared in Table 1. The depro-

tonation energy of a given Brønsted acid can be defined [16,17] (and references therein) as

$$E^D = E_{corr}^{anion} - E_{corr}^{molecule}$$

(for the most stable conformers of these species). Georgieva and Velcheva [16] have found that E^D (B3LYP/6-31++G(d,p)) values correlate fairly well with pKa 's of Brønsted acids, containing cyano or carbonyl groups, measured in DMSO solvent, according to correlation equation:

$$\text{pKa}(\text{DMSO}) = 0.11507 \times E^D - 150.04 (\text{kJ/mol}).$$

So, having in mind E_{corr} of 1 and 2 in Table 1, we can estimate pKa (DMSO) of 4-cyanobenzenesulfonamide near 9.4. Hence, 4-cyanobenzenesulfonamide should be a moderately weak N-H acid, (for comparison literature data for pKa (DMSO) of benzenesulfonamide is 16.1 [18]).

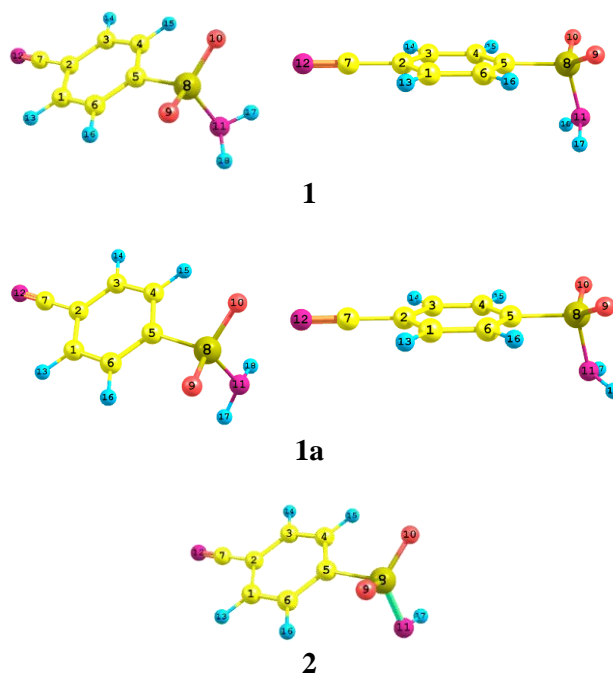


Fig. 1. B3LYP/6-311+G(2df,p) optimized structures of the species studied.

Spectral analysis

Theoretical and experimental IR data for 4-cyanobenzenesulfonamide molecule are compared in Table 2. We can see there is a good agreement between experimental and scaled theoretical frequencies. M.a.d between them is 12.9cm^{-1} , which value lies within the interval of $9\text{-}20\text{cm}^{-1}$, typical for the DFT calculations for molecules containing

cyano or carbonyl groups [17,19-23] (and references therein). We include in Table 2 the frequencies $\nu_{NH_2}^{as}$ and $\nu_{NH_2}^s$ measured in $CDCl_3$, as the stretching frequencies of $-XHn$ groups ($X=$

O, N, etc.), measured in DMSO, are strongly underestimated, and the bending ones strong $-XHn \cdots O=S(CH_3)_2$ hydrogen bonds, which effects can be estimated only qualitatively

Table 1. Zero-point vibrational energy (ZPVE) corrected total energies ($E^{corr.}$ in hartree) of 4-cyanobenzenesulfonamide molecule **1** and of its azanion **2**, as well as their differences (ΔE in kJ/mol).

Species	B3LYP 6-31++G(d,p)		B3LYP/aug-cc-pVTZ		B3LYP/6-311+(2df,p)	
	$E^{corr.}$	ΔE	$E^{corr.}$	ΔE	$E^{corr.}$	ΔE
Molecule 1	-928.322889	0.00	-928.679457	0.00	-928.539333	0
Molecule 1a	-928.320810	5.46	-928.678335	2.95	-928.538131	3.16
Azanion 2	-927.795230	1385.37	-928.138421	1420.49	-928.012712	1382.64

Table 2. Theoretical B3LYP/6-311+(2df,p) and experimental (in DMSO/DMSO- d_6) IR frequencies (ν in cm^{-1}) and integrated intensities (A in km/mol) of 4-cyanobenzenesulfonamide molecule.

No.	ν	B3LYP/6-311+(2df,p)			Approximate description ^b	Experimental data ν^c
		A	ν^a			
1	3642	57.6	3595		$\nu_{NH_2}^{as}$	3456 ^d
2	3527	61.9	3481		$\nu_{NH_2}^s$	3350 ^d
3	3220	2.2	3178		ν_{PhH}	3153 ^d
4	3218	0.0	3177		ν_{PhH}	- ^e
5	3204	1.0	3162		ν_{PhH}	3096 ^d
6	3203	0.0	3162		ν_{PhH}	- ^e
7	2334	26.1	2303		$\nu_{C\equiv N}$	2232 m
8	1628	0.2	1607		ν_{CC}, δ_{PhH}	1601 sh
9	1594	2.1	1573		ν_{CC}, δ_{PhH}	1570 broad
10	1574	34.0	1554		$\delta_{NH_2}^{sc}$	1554 sh
11	1514	6.0	1495		δ_{PhH}, ν_{CC}	1491 m
12	1419	20.6	1400		δ_{PhH}, ν_{CC}	1397 m
13	1371	175.7	1353		$\nu_{SO_2}^{as}, \delta_{NH_2}^{rock}, \nu_{CC}$	1342 vs
14	1327	2.3	1310		$\nu_{PhH}, \nu_{C-S}, \delta_{CCC}$	- ^e
15	1320	20.5	1303		ν_{PhH}, δ_{CCC}	1282 m
16	1215	1.6	1199		ν_{PhH}, ν_{C-CN}	1197 sh
17	1201	1.3	1186		δ_{PhH}, ν_{C-CN}	1185 m
18	1156	216.7	1141		$\nu_{SO_2}^s, \delta_{NH_2}^{sc}, \nu_{C-S}, \delta_{CCC}$	1165 vs
19	1131	4.3	1116		δ_{PhH}	1111 vw
20	1093	26.6	1079		ν_{C-S}, δ_{PhH}	1095 m
21	1071	1.2	1057		$\delta_{NH_2}^{rock}$	- ^e
22 ^d	1028	4.7	1015		δ_{CCC}	- ^e

^a Scaled by 0.9686 [15]. ^b Vibrational modes: ν , stretching; δ , bendings. ^c Relative intensities: vs, very strong; s, strong; m, moderate; w, weak; vw, very weak; sh, shoulder. ^d Solvent $CDCl_3$. ^e These bands were not detected in the experimental spectrum. ^d Followed by 26 lower-frequency normal vibrations.

Table 3. Theoretical B3LYP/6-311+(2df,p) and experimental (in DMSO/DMSO-d₆) IR frequencies (ν in cm⁻¹) and integrated intensities (A in km/mol) of 4-cyanobenzenesulfonamide azanion.

No.	B3LYP/6-311+(2df,p)			Approximate description ^b	Experimental data
	ν	A	ν^a		ν^c
1	3496	6.2	3451	ν_{NH^-}	- ^d
2	3204	4.4	3162	ν_{PhH}	- ^d
3	3203	7.1	3161	ν_{PhH}	- ^d
4	3178	9.9	3137	ν_{PhH}	3076 vw
5	3176	9.9	3135	ν_{PhH}	- ^d
6	2301	225.7	2271	$\nu_{C\equiv N}$	2227 s
7	1612	102.2	1592	ν_{CC}, δ_{PhH}	1593 m
8	1574	3.2	1554	δ_{PhH}, ν_{CC}	- ^d
9	1503	10.3	1483	δ_{PhH}, ν_{CC}	1487 m
10	1417	7.5	1398	δ_{PhH}, ν_{CC}	1396 w
11	1326	0.5	1309	δ_{CCC}	- ^d
12	1313	0.4	1296	ν_{PhH}	1295 vw
13	1248	220.2	1231	$\nu_{SO_2}^{as}, \delta_{CNH^-}, \delta_{PhH}$	1228 vs
14	1213	15.2	1197	$\nu_{C-CN}, \delta_{PhH}, \delta_{CC}$	1190 vw
15	1190	11.5	1174	δ_{PhH}	1177 vw
16	1132	167.5	1117	$\nu_{SO_2}^s, \delta_{PhH}, \delta_{SNH}$	1134 vs
17	1116	24.4	1102	$\delta_{PhH}, \delta_{CNH^-}$	- ^d
18	1091	46.8	1077	$\delta_{CNH^-}, \nu_{C-S}$	1096 s
19	1077	113.6	1063	$\delta_{SNH}, \delta_{CCC}, \nu_{C-S}$	- ^d
20 ^e	1029	2.7	1015	δ_{CCC}	- ^c

^a Scaled by 0.9686 [15]. ^b Vibrational modes: ν , stretching; δ , bendings. ^c Relative intensities: vs, very strong; s, strong; m, moderate; w, weak; vw, very weak. ^d These bands were not detected in the experimental spectrum. ^e Followed by 25 lower-frequency normal vibrations.

within the Onzeger's approach [24]. There are no peculiarities of the cyano stretching band: moderately high frequency $\nu_{C\equiv N}$ and intensity $A_{C\equiv N}$, as the cyano and phenylene groups are in resonance. The frequencies of the strongest in the spectrum sulfonyl stretching bands $\nu_{SO_2}^{as}$ and $\nu_{SO_2}^s$ measured in DMSO agree well with those measured in solid state (Fig. 2 curves **a** and **b**). Its frequencies of 1342 cm⁻¹ and 1165 cm⁻¹ are higher with 37 cm⁻¹ (sum) than corresponding values of sulfanilamide (solvent DMSO-d₆) [9] due to electron-withdrawing effect of cyano group.

We compare in Table 3 theoretical and experimental IR data for the azanion of 4-cyanobenzenesulfonamide (2 in Fig. 1). The agreement between experimental and scaled theoretical frequencies is essentially better than above. M.a.d between them is 10.1 cm⁻¹ only, close to the lower limit of the corresponding integral of 9-25 cm⁻¹, typical for DFT calculations of vibrational frequencies for anions containing cyano or carbonyl groups [17, 19-23] (and references therein). The experimental IR spectra of azanion and molecule (in DMSO/ DMSO-d₆) are compared in Fig. 2 (curves c and b).

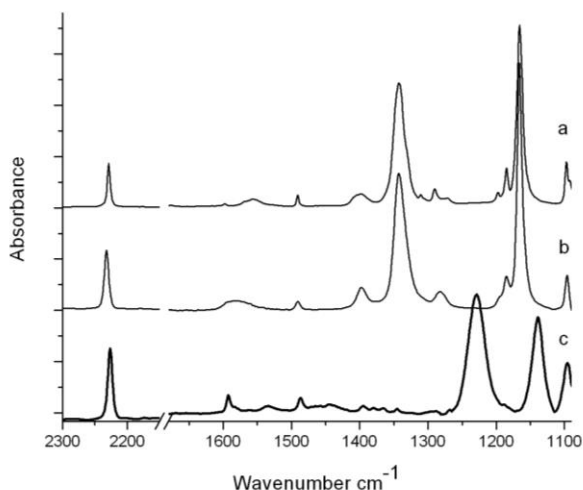


Fig. 2. Experimental spectra of 4-cyanobenzenesulfonamide (**a** in KBr; **b** in DMSO/DMSO- d_6) and its azanion **c** (0.1 mol^{-1} solutions in DMSO/DMSO- d_6).

The following spectral changes take place as a result of the conversion of 4-cyanobenzene-sulfonamide into azanion:

- i) According to the computations, both $\nu_{SO_2}^{as}$ and $\nu_{SO_2}^s$ undergo essential frequency decreases, which sum is: predicted 146 cm^{-1} , measured 145 cm^{-1} . The latter value is rationally larger than the corresponding values for other cases of molecule-azanion pairs, containing additional electron-withdrawing groups (compound, ν_{SO_2} sum): o-sulfobenzimide (saccharin), 93 cm^{-1} [25]; o-sulfothiobenzimide (thiosaccharin), 60 cm^{-1} [26] and similar than in sulfanilamide, 140 cm^{-1} [9].
- ii) The computational method used predicts only qualitatively the changes in the cyano stretching band characteristics, viz.: $\nu_{C\equiv N}$ decreases: predicted 32 cm^{-1} , measured 5 cm^{-1} only.
- iii) According to the calculations, in the azanion a new δ_{CNH^-} mode takes essential parts in vibrations Nos. 13, 18, and 19 (Table 3).

Structural analysis

We can see in Table 4 a good agreement between experimental [7] and theoretical bond lengths of 4-cyanobenzenesulfonamide molecule **1**: the mean absolute deviation between them is 0.019 \AA . There are no experimental structural data for 4-cyanobenzenesulfonamide azanion. According to our computations, the conversion of the molecule into azanion causes certain essential steric structure

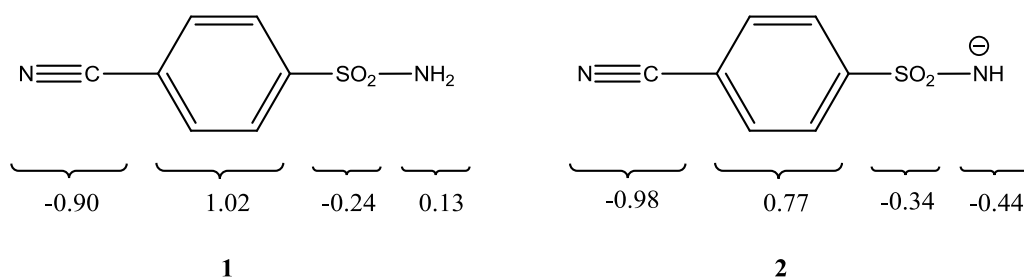
variations (Table 4). It is seen in there that the largest bond length changes should take place at the azanionic center (shortening of the S^8-N^{11} bond by 0.106 \AA) and next to it (lengthening of the C^5-S^8 bond by 0.037 \AA) etc. The same rule is also valid for the corresponding bond angles changes.

Table 4. Selected B3LYP/6-311+G(2df,p) bond lengths R (\AA), bond angles A(degrees) and dihedral angle D(degrees) of 4-cyanobenzenesulfonamide molecule **1** and its azanion **2**.

Indices ^a	Molecule		Azanion	∇^c
	Theor.	Exper. ^b		
R(1,2)	1.403	1.383	1.409	0.006
R(1,6)	1.390	1.387	1.386	-0.004
R(2,3)	1.403	1.383	1.404	0.001
R(2,7)	1.433	1.462	1.429	-0.004
R(3,4)	1.390	1.387	1.391	0.001
R(4,5)	1.395	1.377	1.398	0.003
R(5,6)	1.394	1.377	1.401	0.007
R(5,8)	1.792	1.777	1.829	0.037
R(7,12)	1.158	1.130	1.162	0.004
R(8,9)	1.444	1.420	1.464	0.020
R(8,10)	1.444	1.420	1.473	0.029
R(8,11)	1.667	1.601	1.561	-0.106
A(4,5,8)	119.3	118.7	121.1	1.8
A(5,8,9)	107.3	107.4	102.4	-4.9
A(5,8,10)	107.3	107.4	103.1	-4.2
A(5,8,11)	103.4	108.7	106.0	2.6
A(9,8,10)	122.7	119.6	116.8	-5.9
A(9,8,11)	107.3	106.6	110.7	3.4
D(6,5,8,9)	-22.6	-26.4	-45.8	-23.2
D(6,5,8,11)	90.6	88.7	70.3	-20.3
D(10,8,11,17)	2.9	-	26.1	-23.2

^a Atomic numbering, according to Figure 1. ^b See Ref. [7]. ^c Algebraic deviations (\AA , degrees) between theoretical and experimental values of the anion and molecule. The largest values are given in bold.

The changes in the *electronic structure* of 4-cyanobenzenesulfonamide, caused by its conversion into azanion, can be demonstrated on the basis of net electronic charges. Scheme 1 contains values of net electric charges q_i over fragments of molecule **1** and azanion **2** studied. The electric charge changes $\Delta q_i = q_i^{\text{anion}} - q_i^{\text{molecule}}$ are usually quite informative to demonstrate the distribution of the new (carbanionic, azanionic, etc.) charge between individual fragments of anions [8,9,17,27,28] (and references therein). According to our calculations, the anionic charge in 4-cyanobenzenesulfonamide azanion is distributed, as follows: 0.08 , 0.25 and $0.10 e^-$ are delocalized over the cyano, phenylene and sulfonyl groups, respectively, and $0.57 e^-$ of it remains localized in the azanionic center.



Scheme 1. Mulliken net electric charge q_i over fragments of molecule **1** and azanion **2** of 4-cyanobenzenesulfonamide.

CONCLUSION

We found on the basis of both experimental and computational IR data that the effect of the conversion of 4-cyanobenzenesulfonamide into azanion on the cyano group was weak and was essential on the pharmacological important sulfonamide group. This statement was confirmed by the analysis of both steric and electronic structures, computed for the species studied.

REFERENCES

1. T. H. Maren, *Annu. Rev. Pharmacol. Toxicol.*, **16**, 309 (1976).
2. T. Mann, D. Keilin, *Nature*, **146**, 164 (1940).
3. M. A. Ilies, *Drug Design of Zinc-Enzyme Inhibitors: Functional, Structural, and Disease Applications*, John Wiley & Sons, Inc., Hoboken, NJ, USA (2009).
4. K. Kanamori, J. D. Roberts, *Biochem.*, **22**, 2658 (1983).
5. M. C. Menziani, M. Cocchi, P. G. D. Benedetti, *J. Mol. Struct. (THEOCHEM)*, **88**, 217 (1992).
6. I. Remsen, R. N. Hartman, A. M. Muckenfuss, *Am. Chem. J.*, **18**, 163 (1896).
7. G. E. Cami, M. E. C. Villalba, P. Colinas, G. A. Echeverria, G. Estiu, D. B. Soria, *J. Mol. Struct.*, **1024**, 110 (2012).
8. A. D. Popova, E. A. Velcheva, B. A. Stamboliyska, *J. Mol. Struct.*, **1009**, 23 (2012).
9. A. D. Popova, M. K. Georgieva, O. I. Petrov, K. V. Petrova, E. A. Velcheva, *Int. J. Quant. Chem.*, **107**, 1752 (2007).
10. S. S. Stoyanov, J. A. Tsenov, D. Y. Yancheva, *J. Mol. Struct.*, **1009**, 42 (2012).
11. S. Stoyanov, *J. Phys. Chem.*, **114**, 5149 (2010).
12. M. J. Frisch, G. W. Trucks, H. B. Schlegel, G. E. Scuseria, M. A. Robb, J. R. Cheeseman, G. Scalmani, V. Barone, B. Mennucci, G. A. Petersson, H. Nakatsuji, M. Caricato, X. Li, H. P. Hratchian, A. F. Izmaylov, J. Bloino, G. Zheng, J. L. Sonnenberg, M. Hada, M. Ehara, K. Toyota, R. Fukuda, J. Hasegawa, M. Ishida, T. Nakajima, Y. Honda, O. Kitao, H. Nakai, T. Vreven, J. A. Montgomery, Jr., J. E. Peralta, F. Ogliaro, M. Bearpark, J. J. Heyd, E. Brothers, K. N. Kudin, V. N. Staroverov, R. Kobayashi, J. Normand, K. Raghavachari, A. Rendell, J. C. Burant, S. S. Iyengar, J. Tomasi, M. Cossi, N. Rega, J. M. Millam, M. Klene, J. E. Knox, J. B. Cross, V. Bakken, C. Adamo, J. Jaramillo, R. Gomperts, R. E. Stratmann, O. Yazyev, A. J. Austin, R. Cammi, C. Pomelli, J. W. Ochterski, R. L. Martin, K. Morokuma, V. G. Zakrzewski, G. A. Voth, P. Salvador, J. J. Dannenberg, S. Dapprich, A. D. Daniels, O. Farkas, J. B. Foresman, J. V. Ortiz, J. Cioslowski, and D. J. Fox, Gaussian 09, Revision A.02, Gaussian, Inc., Wallingford CT, 2009.
13. C. Lee, W. Yang, R.G. Parr, *Phys. Rev.*, **B 37**, 785 (1988).
14. A. D. Becke, *J. Chem. Phys.*, **98**, 56548 (1993).
15. J. Merrick, D. Moran, L. Radom, *J. Phys. Chem. A*, **111**, 11683 (2007).
16. M. K. Georgieva, E. A. Velcheva, *Int. J. Quantum. Chem.*, **106**, 1316 (2006).
17. L. I. Daskalova, *J. Mol. Struct. (THEOCHEM)*, **848**, 9 (2008).
18. F. G. Bordwell, *Acc. Chem. Res.*, **21**, 456 (1988).
19. M. K. Georgieva, N. B. Nedelchev, I. N. Juchnovski, *Bulg. Chem. Commun.*, **37**, 235 (2005).
20. S. S. Stoyanov, A. D. Popova, J. A. Tsenov, *Bulg. Chem. Commun.*, **40**, 538 (2008).
21. M. K. Georgieva, P. J. Vassileva-Boyadjieva, P. N. Angelova, *Bulg. Chem. Commun.*, **37**, 366 (2005).
22. L. I. Daskalova, E. A. Velcheva, I. G. Binev, *J. Mol. Struct.*, **826**, 198 (2007).
23. A. D. Popova, E. A. Velcheva, I. G. Binev, *Asian Chem. Lett.*, **13**, 187 (2009).
24. E. A. Velcheva, L. I. Daskalova, I. G. Binev, *Bulg. Chem. Commun.*, **36**, 230 (2004).
25. I. G. Binev, B. A. Stamboliyska, E. A. Velcheva, *Spectrochim. Acta*, **A52**, 1135 (1996).
26. Y. Binev, C. Petkov, L. Pejov, *Spectrochim. Acta*, **56A**, 1949 (2000).
27. J. A. Tsenov, S. S. Stoyanov, I. G. Binev, *Bulg. Chem. Commun.*, **37**, 361 (2005).
28. J. A. Tsenov, S. S. Stoyanov, I. G. Binev, *Bulg. Chem. Commun.*, **40**, 320 (2008).

ИЧ-СПЕКТРАЛНИ И СТРУКТУРНИ ПРОМЕНИ, ПОРОДЕНИ ОТ ПРЕВРЪЩАНЕТО НА 4-ЦИАНОБЕНЗЕНСУЛФОНАМИД В АЗАНИОН

А. Попова*, Е. Велчева

Институт по Органична химия с Център по Фитохимия, Българска Академия на Науките, ул. Акад. Г. Бончев, бл. 9, 1113 София, България

Постъпила на 28 май 2014 г.; Коригирана на 14 юли 2014 г.

(Резюме)

Приложен е комбиниран ИЧ експериментален/DFT теоретичен подход за проследяване на спектралните и структурни промени, породени от превръщането на 4-цианобензенсулфонамида в азанион. Ефектът на превръщането се проявява слабо върху валентното трептене на нитрилната група $\nu_{C\equiv N}$ и силно върху двете валентни трептения на сулфонамидната група $\nu_{SO_2}^{as}$ и $\nu_{SO_2}^s$. Според изчисленията, превръщането в азанион поражда значителни промени в структурата *при* и *непосредствено до* азанионния център. Според нашите изчисления новият (азанионен) заряд се разпределя както следва: 0.08 e⁻, 0.25 e⁻ и 0.10 e⁻ са делокализирани съответно върху циано, фенилен и сулфонилната групи и 0.57 e⁻ от него остават локализирани при азанионния център.

Development of FTIR spectra database of reference art and archaeological materials

Z. I. Glavcheva^{1*}, D. Y. Yancheva¹, Y. K. Kancheva², E. A. Velcheva¹, B. A. Stamboliyska¹

¹*Institute of Organic Chemistry with Centre of Phytochemistry, Bulgarian Academy of Sciences, Acad. G. Bonchev str., bl. 9, 1113 Sofia, Bulgaria*

²*National Gallery of Foreign Art, St. A. Nevsky Square, 1 19 Feb. str., 1000 Sofia, Bulgaria*

Received June 06, 2014; Revised July 21, 2014

Dedicated to Acad. Dimiter Ivanov on the occasion of his 120th birth anniversary

Fourier Transform Infrared (FTIR) spectroscopy is a reliable analytical technique to study both organic and inorganic materials. FTIR spectroscopy has been widely applied in investigation of art and archaeological objects. The specificity and complexity of such analysis require the availability of comprehensive database containing standards of cultural heritage materials. In this paper, the development of FTIR spectra database of art and archaeological materials is presented. The database provides absorption FTIR spectra, total attenuated reflectance (ATR) spectra, as well as information on a number of pigments and dyes, adhesives, oils, resins, gums and other binders, bulk components, fillers and etc. The composition of several ancient art and archaeological materials was determined by means of our spectral database.

Key words: art and archaeological materials, database, FTIR, ATR

INTRODUCTION

Globally, there is a huge interest in preservation of the cultural heritage. The care, maintenance and investigation of the Bulgarian museums' collections play significant role in the conservation of the Bulgarian cultural heritage. Protection, conservation and restoration of cultural valuables are needed in order to preserve them ensuring national and worldwide appreciation. Archaeological, historical and artistic objects bear not only aesthetical value but also can be considered for their historical and cultural context. [1,2] In the field of fine arts, archeological and monumental conservation, science and technology play fundamental role for the characterization of the materials constituting the cultural heritage (historical buildings, monuments, archaeological objects, works of art, ancient papers, manuscripts, etc.) [3]. FTIR spectroscopic techniques are widely used in investigation of both organic and inorganic art and archaeological materials [1,3,4]. The main advantages of this spectroscopic method are the speed, accessibility and the requirement for very small sample amount, the latter being very important factor when studying artworks. Thanks to these characteristics and the broader scope of application for analysis of cultural heritage objects, the FTIR spectroscopy has been selected as main analytical method in many different types of

artwork investigations [3,4]. A large number of papers have been published showing the importance of FTIR spectroscopy and covering all kinds of specimens and materials used in different art techniques in wall paintings [5-7], icons [8-11] pottery [12,13], metal artifacts [14,15], polychromed sculptures [16,17], etc.

In the process of artwork creation, various inorganic and organic materials are used. Natural aging and changes in environmental conditions have specific impact on the cultural heritage objects. In order to have an appropriate identification of an artwork material, it is essential to use spectral database of standard art and archaeological materials. In general, the available spectral databases [4,18-20] provide one spectrum per compound, typically as an image file, thus the spectra cannot be used with the appropriate spectroscopic software and the information given about the material is not sufficiently detailed.

The scope of the paper is focusing on developing FTIR spectra database of art and archaeological materials. All tested samples of reference materials and Bulgarian art and archaeological artwork samples are classified according to their type, chemical composition and historical period in which they were used. A matter of particular interest is the availability of their FTIR-ATR spectra.

This paper illustrates the usefulness of FTIR spectroscopy as an applied method for the study of cultural heritage presenting example spectra of

* To whom all correspondence should be sent:
E-mail: zornitza@orgchm.bas.bg

some reference and artefacts materials. The e-library would be a particularly useful tool for analysing unknown cultural valuables by comparison with similar artworks available in the database.

MATERIALS AND METHODS

Commercially available materials have been selected on the basis of their chemical properties, and their application as art and archaeological materials. The main part of standard materials (pigments and dyes, some natural and synthetic resins and gums) has been kindly provided by the conservator-restorers Yoana Kancheva and Elitsa Tzvetkova and by the National Academy of Art, Sofia. The remaining materials under study have been purchased from Aldrich (e. g. calcium carbonate, barium sulphate, gypsum) and from food supermarkets (e. g. egg, honey, beeswax, oils produced from walnut, sunflower, almond, sesame, soybeans, etc.). Some substances were synthesised in the laboratory (e.g. Punic wax) or obtained from natural sources (e.g. cherry gum).

All samples were characterized by means of FTIR spectral methods. Vibrational spectra were taken at standard conditions:

(a) Absorption spectra in the middle IR region (4000-400 cm^{-1})

(b) Reflection (ATR) spectra in the middle (4000-600 cm^{-1}) IR region

Reference art and archaeological materials of pigments and/or dyes, waxes, oils, resins, proteins, gums, and different carbonates, sulphates, silicates, etc., as well as ancient art and archaeological materials were studied. The ancient art and archaeological materials of organic origin were obtained from the samples by extraction with a suitable solvent. Commercially available spectral quality solvents were used. The extracted solutions were kept at room temperature for several days and the dry materials were analysed.

All samples were measured in solid state (KBr pellet) and/ or in the case of ATR technique they were directly applied on a diamond crystal. The spectra were recorded on Bruker Tensor 27 FT spectrometer with MIRacle-Diamond ATR accessory (Pike technologies). For KBr pellet technique, a resolution of 2 cm^{-1} and 64 scans were applied with background spectrum of pure KBr. In the ATR measurements, the spectra were recorded with a resolution of 2 cm^{-1} and 128 scans referencing to the air as background spectrum.

DATA PROCESSING

All spectra were recorded and processed by OPUS software (Bruker Optics). The absorptions of the atmospheric moisture and carbon dioxide were removed in all cases by automatic compensation which is included in the software package OPUS, version 6.5.

Spectral data were saved in several formats (spectral-JCAM-DX and ASCII, and graphics-GIF, JPG or PDF) in order to be easily compared with the spectra of materials from real artistic and archaeological objects, as well as to be processed with the available spectrum software. For each spectra the frequencies and intensities of the characteristic bands were described.

RESULTS AND DISCUSSION

Multi-layered structure of each cultural heritage object is a complex and complicated issue for analysis. FTIR spectroscopy provides molecular and structural information for the organic as well as for inorganic materials. FTIR spectra of art and archaeological standards (reference materials) were measured. In order to provide more detailed spectroscopic information, it is necessary to record more than one spectrum for each sample.

Total attenuated reflectance (ATR) is a very suitable and useful technique for the analysis of artefacts, especially using high refractive index crystal such as diamond. Due to its durability and chemical inertness, it allows direct deposition on the crystal without sample preparation for a wide range of solid and liquid samples. Furthermore, the ATR accessory available in our laboratory has a very small diamond crystal, 2 mm across.

It diminishes the amount of sample required for analysis to a few milligrams. When obtaining spectra with this technique, it should be taken into account that the absorption peak intensity shows wavenumber dependency. As a result, the spectral bands in the low wavenumber region appear with enhanced intensity compared to those obtained with absorption measurement with KBr technique. Also peak deformation toward the first-order differential form is possible in the ATR spectra of inorganic and other high-refractive-index samples due to the anomalous dispersion of the refractive index. Some differences in the intensities, bands shapes and peak's position could appear depending on the different spectra collection technique or sample origin. As an example, the spectra of Gum Arabic obtained by absorption measurement with KBr and ATR are illustrated in Fig. 1. The stretching of

polysaccharides O-H group at 3429 cm^{-1} is shifted at 3291 cm^{-1} in the case of ATR spectrum. Other notable FTIR pattern differences are the two intense C-O stretching bands at 1073 cm^{-1} and 1032 cm^{-1} in the absorption spectrum and the corresponding shoulder at 1063 cm^{-1} and peak at 1026 cm^{-1} in the ATR spectrum.

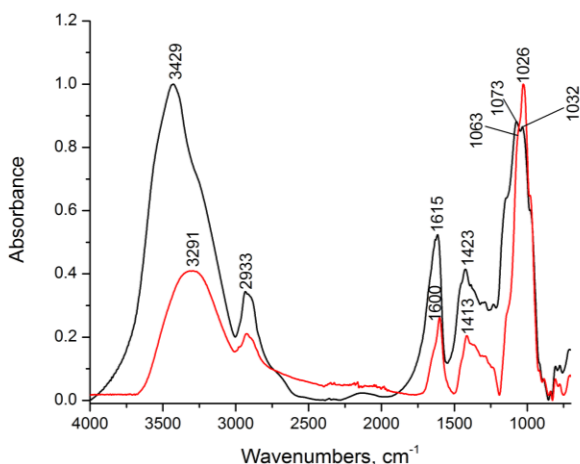


Fig. 1. Normalized FTIR spectra of Arabic gum: KBr pellet (black line), ATR-FTIR on a diamond crystal (red line).

The data for each standard contains spectral and additional (name, synonyms, origin, etc.) information (example- Gum Arabic Fig. 1 and Animal glue Table 1). The presence of such additional information is quite helpful. For example, identical names have been used to describe more than one pigment in antiquity. In Roman times, minium was reserved for cinnabar (HgS) but was applied increasingly to red lead (Pb_3O_4) by the Renaissance [21]. On the other hand, most of the varnishes, binders, dyes, pigments and etc. included in the artworks have their own history of occurrence and certain (historical) periods of use as well as geographical areas of distribution. This information can be added to the results of chemical analyses (and sometimes by the method of exclusion) in order to specify and limit the search. Some materials used in artworks are not commercially available. Such example is the Punic wax, which is produced by boiling beeswax with alkaline carbonates or hydroxides. In this way, the esters and free fatty acids in the beeswax are partially converted into alkaline salts (soaps). Emulsions of Punic wax in water were used as paint vehicle. In order to provide a reference spectrum of Punic wax, a sample of beeswax purchased from the local market was subjected to saponification by potassium carbonate (potash) according to a

literature recipe [22]. The obtained emulsion was dried on glass and the spectrum was measured by ATR technique. The superimposed spectra of beeswax and Punic wax are presented in Fig. 2. The main difference between the spectra of beeswax and Punic wax is the appearance of IR bands for the carboxylate stretching vibrations at 1561 and 1414 cm^{-1} . Saponification was carried out also by potassium hydroxide and led to the same spectral changes.

Table 1. Animal glue information.

Name	Animal glue
Obsolete and synonym names/Varieties	Hide glue, bone glue, skin glue, fish glue, etc. tutkal (in Bulgarian)
Origin	Animal (rabbit, fish, goats, sheep, etc.) Natural organic product extracted from animal tissues and bones.
Chemical composition	It consists primarily of gelatine and other proteins, residues of collagen, keratin or elastin. It swells when it is soaked in cold water and it may be dissolved by gentle heating.
Compatibility and permanence	When dry it hardens but do not change chemically. Thus it can be dissolved again in water.
Use and applications	Adhesive, binder of pigments and grounds (primers), consolidating agent.
Possible adulterations and mixtures	The addition of a bulking agent to the glue causes some changes in the chemical and physical properties of the protein network, most of these correlate to changes seen in cross-linked polymers.
FTIR Spectrum	sample 1, sample 2, sample 3,....
ATR-FTIR Spectrum	sample 1, sample 2, sample 3,....

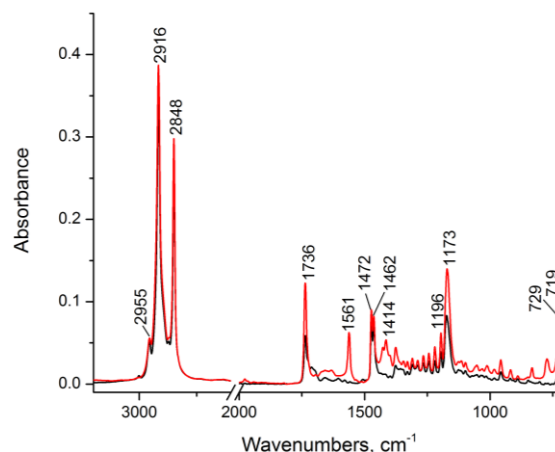


Fig. 2. ATR-FTIR spectra of reference beeswax (black line) and Punic wax (red line).

Vegetable drying oils (sometimes with or without the addition of siccativ) were used in the paintings as binding media. In order to provide more versatile examples, including some oils

typically used in Bulgarian artistic objects, several reference spectra were recorded. This group includes linseed oil which is commonly used in the painting art in many countries and oils from some other locally grown seeds - sunflower, walnut, corn etc. Vegetable oils consist basically of triglycerides with different substitution patterns whose main differences are the degree and the form of unsaturation of the acyl groups and their length. Despite of these differences, the IR spectra of vegetable oils show a great similarity (Fig. 3). The discrimination is possible based on the position of band of the C-H stretching of the *cis*-double bond above 3000 cm^{-1} . The oil composition affects the exact position of this band which for vegetable oils rich in polyunsaturated fatty acids such as linseed oil, is about 3010 cm^{-1} . In oils with higher content of monounsaturated fatty acids, such as olive and almond oil, the band appears about 3005 cm^{-1} . The ratio of the absorbance of the bands responsible for the C-H stretching of the *cis*-double bonds and the asymmetric C-H stretching the methylene bonds at 2925 cm^{-1} could also be used for differentiation.

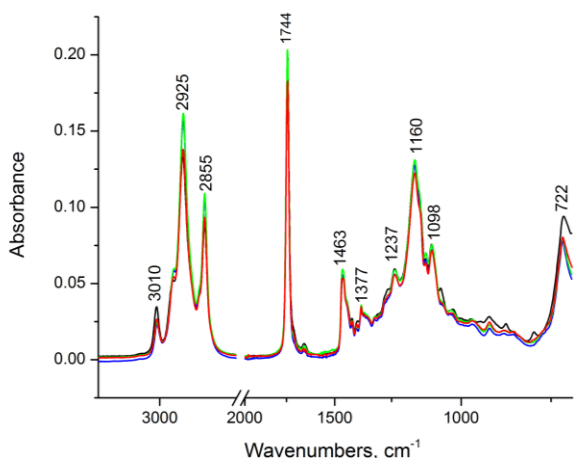


Fig. 3. FTIR-ATR spectra of linseed (black line), walnut (red line), sunflower (blue line) and corn oils (green line).

The interpretation of the spectra of art and archaeological samples were carried out by comparing the spectra of the reference materials. This allows identification of the materials of interest in actual samples and establishing their age. When it was impossible to use "automatic search" for analysing the vibrational spectra from the available electronic spectral database (since this method is only reliable for pure samples and the investigated materials usually are complex mixture of different substances), it was more appropriate to apply an analytical approach, namely: "peak by

peak" comparison of the spectrum of the sample with the characteristic bands in the spectrum of reference material taking into account aging, atmospheric and degradation process, as well as applying of the fundamental analytical approach in IR spectral analysis. This method is slower but gives much better results and usually all peaks of the samples could be identified. As an illustration the spectrum of a red sample from the Thracian tomb wall paintings at Alexandrovo, Bulgaria (fourth century BC), is given in Fig.4, together with spectra of CaCO_3 and red ochre standards. It is obvious that this archaeological sample contains both materials CaCO_3 (characteristic bands at 2512, 1797, 1427, 876 and 712 cm^{-1}) and red ochre (characteristic bands at 3698, 3621, 3427, 1092, 1032, 1009, 913, 799, 778, 538 and 472 cm^{-1}).

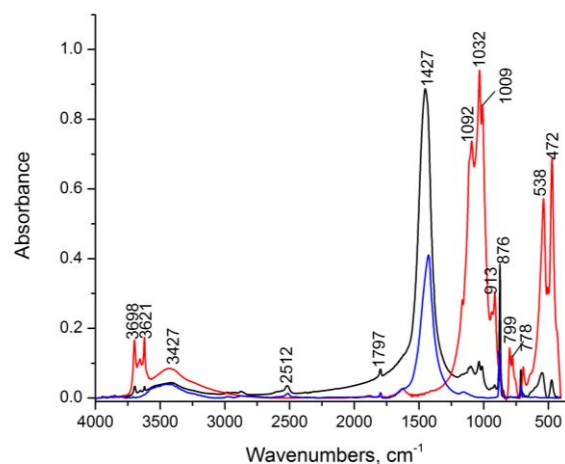


Fig. 4. FTIR spectra (KBr pellet) of Alexandrovo Thracian tomb wall paintings red sample (black line); standard CaCO_3 (blue line) and standard red ochre (red line).

Thanks to the high sensitivity for organic compounds, FTIR spectroscopy is indispensable when studying organic materials used in artworks and archaeological sites. However, since usually the analysed sample is a complex matrix of several materials, FTIR spectrum often includes collective information for the primer, pigment and/or binder, etc. This leads to complications when identifying individual components due to overlapping of spectral bands and relative signal intensity. As an example, the spectra of archaeological sample (decoration with white incrustation paste) from Deneva Mogila (dated in the early or in the late Chalcolithic period), located south-east from the village of Salmanovo, Bulgaria are presented (Fig. 5). The predominant compound in the studied archaeological sample is CaCO_3 . The binder was

extracted with distilled water. After water evaporation white medium was obtained. The exact composition of the binder is under investigation. According to historical information and the FTIR spectrum of water-extracted mass (aggregation) (Fig. 5, red line) the closest presumable binder compound is gum from a plant origin (such as Gum Arabic or Cherry gum).

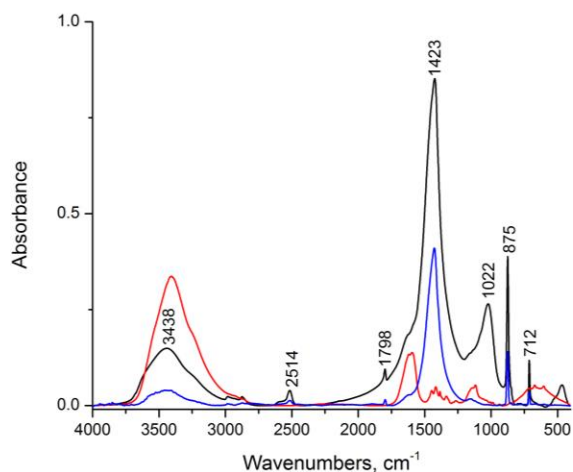


Fig. 5. FTIR spectra (KBr pellet) of Devina Mogila white sample (black line); reference CaCO_3 (blue line) and binder in Devina Mogila sample (red line).

CONCLUSION

The necessity and usefulness of FTIR database of reference art and archaeological materials have been demonstrated using various examples. Taking into account the collected spectroscopic, art, archaeological and historical information, it is possible to gain appropriate and complete artefact information.

The currently available FTIR database of reference art and archaeological materials needs to be constantly updated. Also fluorescence spectroscopic analysis, additional information and materials (modern art materials, conservation products, mixtures, etc.) will be included. The provision of a much wider and more comprehensive database of standards would facilitate more accurate study and description of art and archaeological materials. Moreover, the data on newly studied cultural heritage objects will be included in order to create artefacts' database which will be useful in investigation of other art and archaeological objects. This will be of great benefit

to the cultural heritage preservation science and society in Bulgaria and worldwide.

REFERENCES

1. I. Kuleff, *Archaeometry*, Sv. Kliment Ohridski, Sofia, 2012.
2. H. G. M. Edwards, J. M. Chalmers, *Raman Spectroscopy in Archaeology and Art History*, Royal Society of Chemistry, Cambridge, 2005.
3. G. Bitoss, R. Giorgi, M. Mauro, B. Salvadori, L. Dei, *Appl. Spectros. Rev.*, **40**, 187 (2005).
4. M. R. Derrick, D. Stulik, J. M. Landry, *Infrared Spectroscopy in Conservation Science*, The Getty Conservation Institute Los Angeles, 1999.
5. C. Maruțoiu, I. Bratu, A. Trifa, M. Botiș, V. C. Maruțoiu, *Int. J. Conserv. Sci.*, **2**, 29 (2011).
6. J. Cuni, P. Cuni, B. Eisen, R. Savizky, J. Bové, *Anal. Methods*, **4**, 659 (2012).
7. M. L. V. de Ágredos Pascual, M. T. D. Carbó, A. D. Carbó, *J. Cult. Herit.*, **12**, 140 (2011).
8. D. Kovala-Demertzi, L. Papathanasis, R. Mazzeo, M. A. Demertzis, E. A. Varella, S. Prati, *J. Cult. Herit.*, **13**, 107 (2012).
9. I. C. A. Sandu, S. Bracci, I. Sandu, M. Lobefaro, *Microsc. Res. Techniq.*, **72**, 755 (2009).
10. I. C. A. Sandu, C. Luca, I. Sandu, V. Vasilache, M. Hayashi, *Rev. Chem. (Bucuresti)*, **59**, 384 (2008).
11. A. Baci, Z. Moldovan, I. Bratu, O.F. Măruțoiu, I. Kacsó, I. Glăjar, A. Hernanz, C. Măruțoiu, *Curr. Anal. Chem.*, **6**, 53 (2010).
12. D. Barilaro, G. Barone, V. Crupi, D. Majolino, P. Mazzoleni, G. Tigano, V. Venuti, *Vib. Spectrosc.*, **48**, 269 (2008).
13. S. Legnaioli, F. A. Garcia, A. Andreotti, E. Bramanti, D. D. Pace, S. Formola, G. Lorenzetti, M. Martini, L. Pardini, E. Ribechini, E. Sibilina, R. Spiniello, V. Palleschi, *Spectrochim. Acta A*, **100**, 144 (2013).
14. J. Baeten, K. Romanus, P. Degryse, W. De Clercq, H. Poelman, K. Verbeke, A. Luybaerts, M. Walton, P. Jacobs, D. De Vos, M. Waelkens, *Microchem. J.*, **95**, 227 (2010).
15. W. Luo, T. Li, C. Wang, F. Huang, *J. Archaeol. Sci.*, **39**, 1227 (2012).
16. D. Cauzzi, G. Chiavari, S. Montalbani, D. Melucci, D. Cam, H. Ling, *J. Cult. Herit.*, **14**, 70 (2013).
17. A. Sarmiento, M. Pérez-Alonso, M. Olivares, K. Castro, I. Martínez-Arkarazo, L. A. Fernández, J. M. Madariaga, *Anal. Bioanal. Chem.*, **399**, 3601 (2011).
18. C. Montagner, M. Bacci, S. Bracci, R. Freeman, M. Picollo, *Spectrochim. Acta A*, **79**, 1669 (2011).
19. <http://www.irug.org>
20. http://www.ut.ee/katsekoda/IR_Spectra/index1.htm
21. H. G. M. Edwards, D. W. Farwell, E. M. Newton, F. R. P. Mium, *Analyst*, **124**, 1323 (1999).
22. H. Kühn, *Stud. Conserv.*, **2**, 71 (1960).

СЪЗДАВАНЕ НА СПЕКТРАЛНА БАЗА ДАННИ ОТ РЕФЕРЕНТНИ ХУДОЖЕСТВЕНИ И АРХЕОЛОГИЧЕСКИ МАТЕРИАЛИ

З. И. Главчева^{1*}, Д. Я. Янчева¹, Й. К. Кънчева², Е. А. Велчева¹, Б. А. Стамболийска¹

¹Институт по Органична химия с Център по Фитохимия, Българска Академия на Науките, ул. Акад. Г. Бончев, бл. 9, 1113 София, България

²Национална галерия за чуждестранно изкуство, Площад "Св. Александър Невски", ул. 19 февруари 1, 1000 София, България

Постъпила на 06 юни 2014 г.; Коригирана на 21 юли 2014 г.

(Резюме)

ИЧ спектроскопията е надеждна аналитична техника за изследване както на органични, така и на неорганични материали. Тя намира широко приложение при анализа на художествени и археологически обекти. Спецификата и сложността на подобни анализи изисква наличието на обширна база данни на референтни художествени и археологически материали. Настоящата работа представя създаването на спектрална ИЧ база данни на такива материали. Базата данни съдържа набор от абсорбционни и отразителни (ATR) спектри, както и информация за голям брой пигменти, багрила, лепила, масла, смоли, гуми, и други свързватели, градивни материали, пълнители и т.н. Материалният състав на различни старинни художествени и археологически обекти беше определен с помощта на създадената спектрална база данни.

IR spectra and structure of 1,1,3,3-tetracyanopropane and its carbanions: experimental and quantum chemical study

S. S. Stoyanov*, J. A. Tsenov

Institute of Organic Chemistry with Centre of Phytochemistry, Bulgarian Academy of Sciences, Acad. G. Bonchev str., bl. 9, 1113 Sofia, Bulgaria

Received June 10, 2014; Revised July 21, 2014

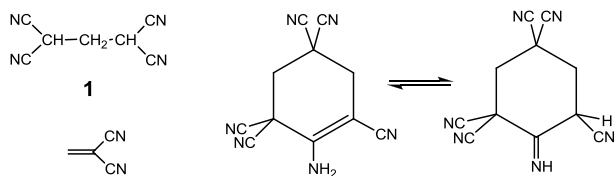
Dedicated to Acad. Dimiter Ivanov on the occasion of his 120th birth anniversary

A combined IR experimental/DFT computational approach has been applied to follow the spectral and structural changes, caused by the conversion of 1,1,3,3-tetracyanopropane in mono-, di-, and trianion. The conversion of molecule into carbanion has shown a weak effect on the cyano stretching band $\nu(\text{C}\equiv\text{N})$ of cyanogroups remote of anionic center (down to 13 cm^{-1}) and strong on the cyano stretching band $\nu(\text{C}\equiv\text{N})$ of cyanogroups which are directly bonded with anionic center (down to 140 cm^{-1}). The carbanionic charge is distributed mainly at anionic centre and cyanogroups which are directly bonded to it (overall 0.85 e^-). The conversion of the molecule into di- and trianion are pursued with stronger lowering of $\nu(\text{C}\equiv\text{N})$ down to 300 cm^{-1} . A very good agreement between experimental and theoretical data has been found. According to the computations the anionic charge formed by second and third step of deprotonation is distributed nearly uniformly over all fragments.

Key words: IR spectra, DFT B3LYP, structure, 1,1,3,3-tetracyanopropane, anion

INTRODUCTION

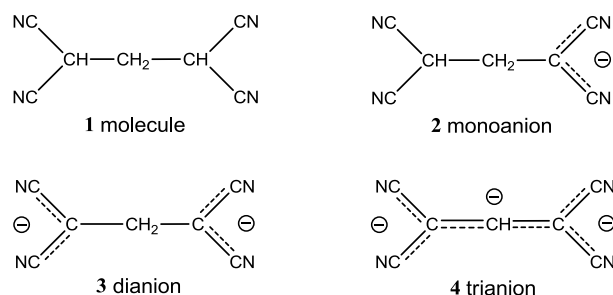
1,1,3,3-Tetracyanopropane (methylene-bis-malononitrile) **1** in Scheme 1 was synthesized for the first time by Diels as early as in 1922 [1] from formaldehyde and malononitrile, with vinylidene cyanide **2** (1,1-dicyanoetan) as intermediate [1-3].



Scheme 1. Methylene-bis-malononitrile **1** and some possible products of its decomposition.

Compound **1** and its derivatives undergo reaction of cyclo-dimerization (Michael-Thorpe) [2-5], leading to the formation of cyano-containing cyclohexane amines and imines (see Scheme 1) or decomposition to vinylidene cyanide ("reverse" Michael) [2]. There are complexes of **1** with transition metals such as Au and Pt [6,7]. A detailed study of the structure on **1** by IR, Raman, mass spectra and X-ray diffraction has been reported [8]. Although the structure, chemistry and covalent complexes of methylene-bis-malononitrile with

transition metals are studied, there are no data about its anions available in the literature.



Scheme 2. Methylene-bis-malononitrile **1** and its anions **2-4**.

Its mono- and dianion **2, 3** (Fig. 1) are clearly intermediates in many of the above reactions. The purpose of the present study is to generate the anions of methylene-bis-malono-nitrile and investigate their structure and IR spectra on the basis of experimental/DFT computational approach.

EXPERIMENTAL

Synthesis of neutral compound

Malononitrile is highly reactive and polymerize on being kept. For this reason commercial malono-

* To whom all correspondence should be sent:

E-mail: S_Stoyanov@orgchem.bas.bg

© 2014 Bulgarian Academy of Sciences, Union of Chemists in Bulgaria

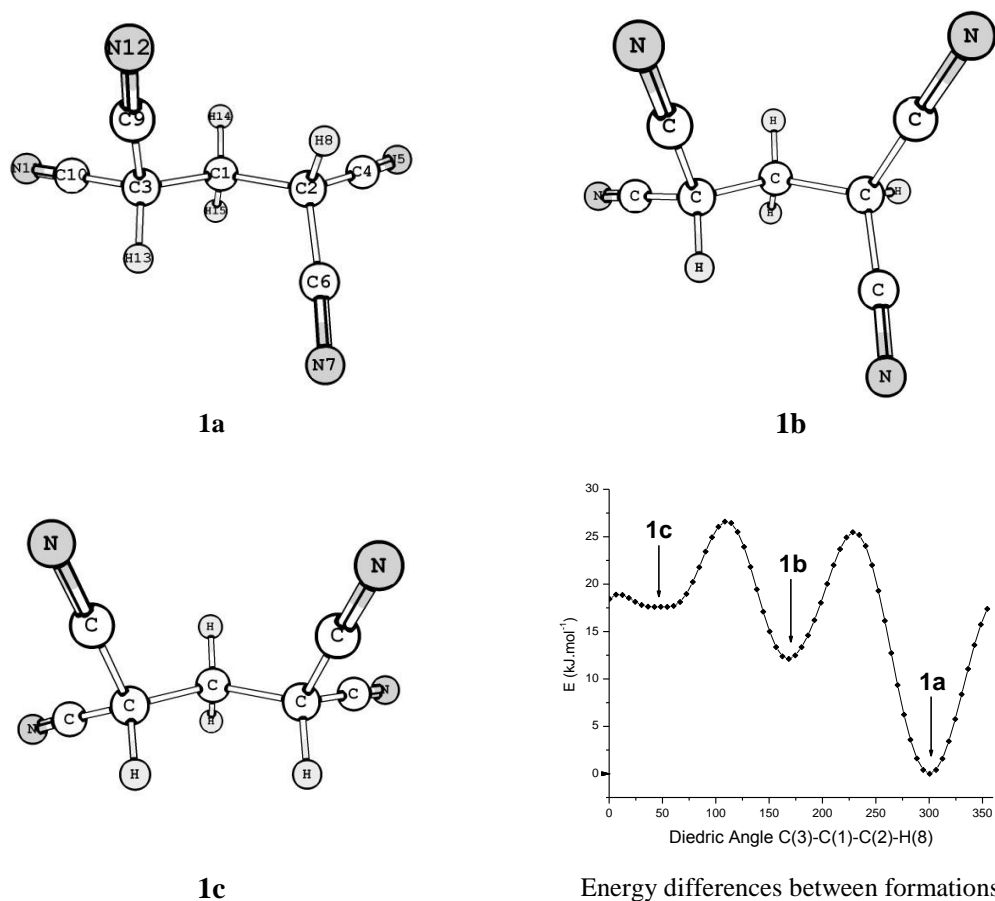
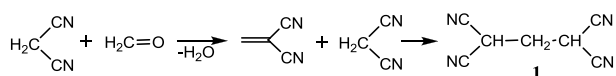


Fig. 1. Stability of conformers of methylene-bis-malononitrile **1**.

nitrile (Aldrich) was used in present study after purification by vacuum distillation. The resulting distillate was crystallized in colorless crystals of melting point 30°C. 1,1,3,3-Tetracyanopropane **1** was synthesized by modifying the method of Bell *et al.* [6] (Scheme 3).



Scheme 3. Synthesis of **1** by Bell *et al.* [6].

In a round bottom flask equipped with a stirrer and thermometer 7.5 ml 96% ethanol were mixed with 1.5 g (0.0227 mol) of purified malononitrile. The mixture was heated to 40°C and stirred until malononitrile was completely dissolved. The solution was cooled in ice bath to 10-12°C, and 0.86 ml (0.0144 mol) of 37% formaldehyde, and a few crystals of β-alanine as catalyst were added. The stirring was continued at this temperature, the solution became yellow (formation of vinylidene cyanide). When the solution became cloudy (app. 1

hour after the start) the reaction was stopped. 15 minutes after the crystallization started the mixture was filtered and washed several times with ice cold ethanol. The product was used without further purification. The product was dried and showed m. p. 132-135°C. The reaction is highly influenced by the temperature and stoichiometry and several adverse reactions such as polymerization and cyclo-dimerization to side products are possible to occur (Scheme 1).

Conversion of neutral compound into anions

The monoanion of methylene-bis-malononitrile (DMSO solution) was prepared by adding dimethyl sulfoxide solution of the parent compound to excess of dry CH₃O⁻ Na⁺ under argon, stirring and collecting the clear anion solution with a syringe-filter. We prepared the sample of dry CH₃O⁻ Na⁺ itself by reacting CH₃OH with Na and evaporating the excess of methanol *in vacuo*. Methylene-bis-malononitrile **1** reacted with CH₃O⁻ Na⁺ to form monoanion in DMSO promptly (within 1-2 min)

and practically completely: no bands of the parent compound were shown in the spectra after metalation. The IR spectra were recorded on Bruker Tensor 27 FTIR spectrometers in a CaF₂ cell of 0.129 mm path length, at a resolution of 1cm⁻¹ and 64 scans.

The dianion of the methylene-bis-malononitrile was prepared by reacting with dimsyl sodium (Sodium salt of dimethylsulfoxide). Dimsyl sodium was formed by reacting sodium metal with excess of DMSO. The solution of this reagent (excess) was added to the solution of the neutral compound **1** and transferred to IR cell, previously flushed with argon. The conversion was nearly complete. The IR bands, corresponding to dianion strongly dominate over those, corresponding to monoanion. The latter bands appeared like little shoulders.

Trianions of methylene-bis-malononitrile **1** were prepared by reacting with red naphthalene lithium, naphthalene sodium and naphthalene potassium in THF solution. Alkali reagents (dianions of naphthalene) were formed previously in ampulla with excess of alkali metals in dry THF. The metal reagents (more than 3-fold excess) were added to the solution of neutral compound **1** and were transferred immediately into IR cell, previously flushed with argon. The conversion into trianions

was incomplete, as in all spectra bands corresponding to their dianions appeared.

COMPUTATIONS

Full optimization of geometries was done using Gaussian-98 program package [9]. We performed DFT B3LYP computations, the latter combined Becke's three-parameter nonlocal exchange [10] with the correlational functional of Lee, Yang and Parr [11-12], adopting a 6-31++G** basis set without any symmetry restrictions. The stationary points found on the potential energy hypersurfaces for each structure, were characterized using the standard harmonic vibrational analysis. The absence of imaginary frequencies confirmed that the stationary points corresponded to local minima on the potential hypersurfaces. A standard least-squares program was used to calculate the single-parameter linear regression indices.

RESULTS AND DISCUSSION

Energy analysis

B3LYP/6-31++G** theoretical level has been chosen to perform all computations. This level

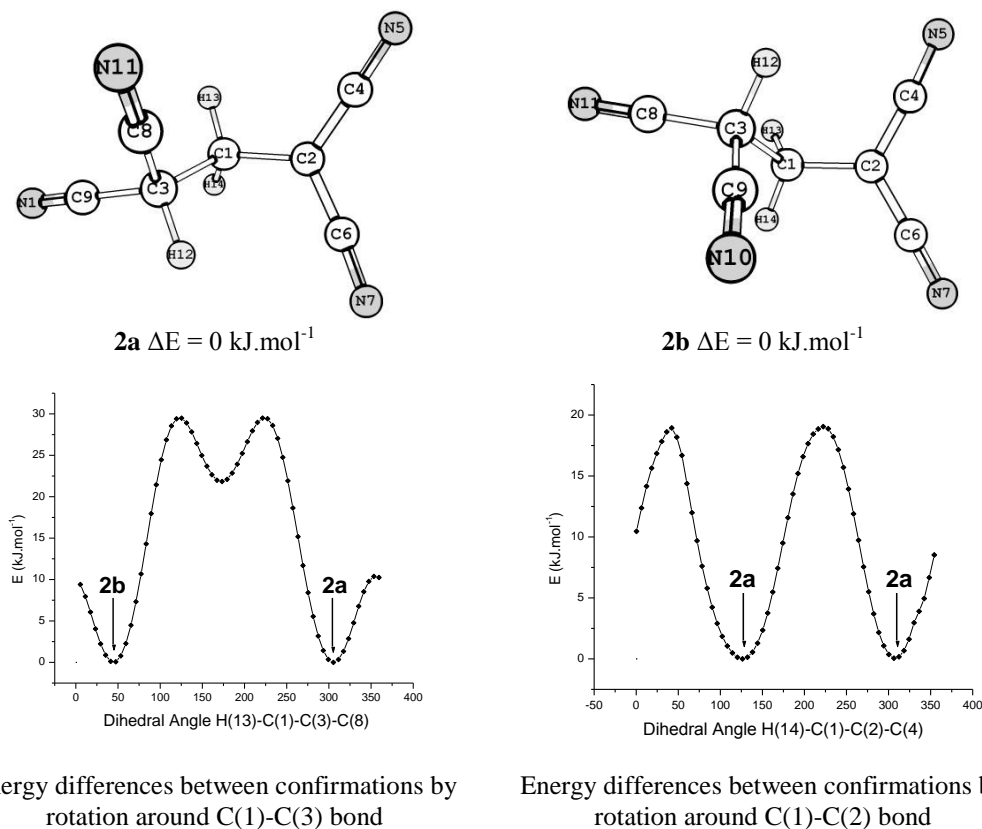


Fig. 2. Stabilities of the conformers of methylene-bis-malononitrile carbanion **2**.

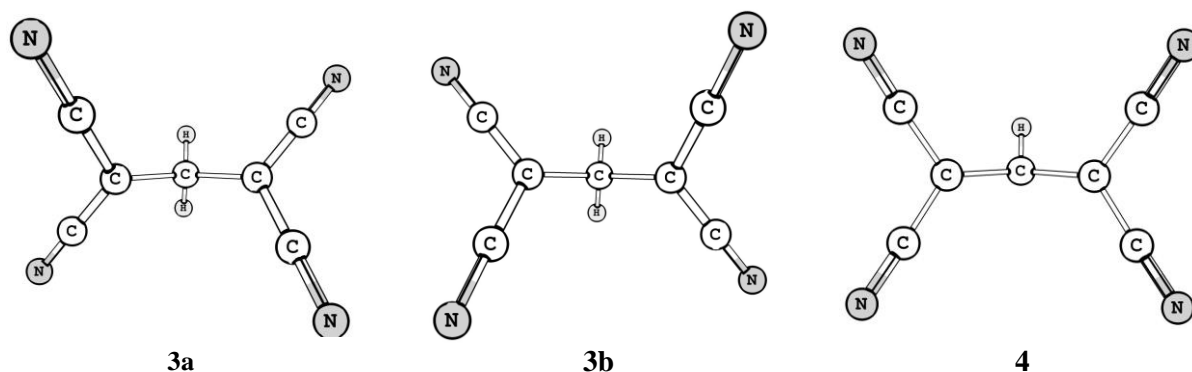


Fig. 3. Optimized structures of di- **3a-3b** and trianion **4** of methylene-bis-malononitrile.

shows a good prediction of IR spectra of nitriles and their anions [13-19]. The mean absolute deviation (MAD) of predicted values of cyano stretching frequencies for a large series of nitriles is 6 cm^{-1} and 11 cm^{-1} in a series of nitrile anions [19]. Different conformations of the molecule of methylene-bis-malononitrile **1** by rotation around C(1)-C(3) and C(1)-C(2) bonds in steps of 6° are presented in Fig 1. According to the theoretical calculations, among all possible conformations of the molecule **1** the three most stable conformers **1a-1c** should exist. **1a** possess the lowest energy among them, and the energy difference between **1a** and the other two is approximately 12 and 17 $\text{kJ}\cdot\text{mol}^{-1}$. According to the X-ray diffraction [8], only **1a** exists in the crystalline state. IR spectra measured in DMSO, THF and CHCl_3 solutions show no evidences for the presence of more than one conformer. So, we can assume, that only **1a** exists in solution. We have calculated the energy of the different conformations of the anion **2** (Fig. 2), by rotation around C(1)-C(3) and C(1)-C(2) bonds in steps of 6° . Four minima were found by this procedure. By reason of symmetry of anionic dicyanomethanide fragment three of them correspond to identical structure - **2a**. The fourth structure **2b** in fact is a chiral conformer of **2a**, which is energetically degenerated. For di- and trianion **3-4** there is only one stable conformer (Fig 3). However, **3** possesses a chiral axis and two enantiomers **3a** and **3b**.

Spectral analysis

In Table 1 the theoretical and experimental frequencies of the molecule of methylene-bis-malononitrile **1** measured in solid state are presented. They show a very good correlation: correlation coefficient $R=0.99985$; standard deviation $SD = 14.75$; number of points $n = 28$. The

resulting correlation Equation (1) is used for scaling the theoretical frequencies:

$$\nu^{\text{scaled}} = 0.94388\nu^{\text{native}} + 43.0 \quad (1)$$

The mean absolute deviation (MAD) is 11 cm^{-1} . This value lies within the range $9\text{-}25\text{ cm}^{-1}$, typical for molecules and anions containing cyano and carbonyl groups [20-24].

In the IR spectra of methylene-bis-malononitrile **1** nitrile vibrations are four, two of them are symmetrical and degenerated and two are asymmetrical also degenerated (see Table 2). The splitting between them is only several cm^{-1} , so only a single band was observed in the solid-state and solution IR spectra. However a distinct high-frequency shoulder is present corresponding to $\nu^s(\text{C}\equiv\text{N})$. In the IR spectra measured in DMSO-d_6 solution the bands responsible for $\nu_{\text{C-H}}$ stretching vibrations decrease around $30\text{-}70\text{ cm}^{-1}$ in comparison to the corresponding bands observed in KBr tablet. These shifts are due to hydrogen bonding with the molecules of solvent DMSO.

Similar to molecule **1** in the IR spectra of di- and trianions **3, 4**, the stretching vibrations of the cyano group have mixed origin (see Table 2). In the molecule the frequencies of both symmetric and asymmetric vibrations are very close to each other, and they have in phase and anti-phase components (Table 2). The differences in the frequencies are a bit larger in the free di- and trianion **3, 4** than observed in the molecule **1**. They also have in-phase and anti-phase components. Only in the free carbanion **2** the four nitrile vibrations are isolated. The $\nu_{\text{C}\equiv\text{N}}$ in the anionic fragment are lower than those corresponding to the fragment which is remote from the anionic centre and they are strongly decoupled. The frequencies and intensities of former bands are very similar to those, observed in other dicyanomethanides [14,15,17,21-23]. They

interact much less with $\nu_{\text{C}\equiv\text{N}}$ of the cyano groups remote from carbanion centre. In general, the relative intensities of the latter are very low and the frequencies are close to those observed in the molecule **1**.

Fig. 4 illustrates the experimental and theoretical spectral changes caused by the conversion of the molecule in the anions. Given the data in Table 2 and Figure 4, we can conclude that the conversion of the molecule **1** in anion **2** causes a decrease in nitrile frequencies of the cyano group in carbanion center predicted by theory as 98 ($\nu^{\text{s}}\text{C}\equiv\text{N}$) and 139 cm^{-1} ($\nu^{\text{as}}\text{C}\equiv\text{N}$), and observed in practice - 96 and 135 cm^{-1} respectively. The conversion of the carbanion **2** into dianion **3** leads to further decrease of nitrile frequencies. It is larger in the cyano group directly bonded to the second carb-

anionic center: predicted 128, measured 126 cm^{-1} . The lowering of the nitrile frequency at the first carbanionic center is smaller: predicted 52, measured 35 cm^{-1} . Theory provides further lowering in the nitrile frequencies at conversion of the dianion **3** into trianion **4** of about 50-70 cm^{-1} . We could not obtain measurable amounts of trianion in DMSO solution, which generally can be expected to exist as free (uncoordinated) anion. However the IR spectra in THF solution show presence of mixture of di- and trianion. The conversion to trianion is significant when counterion is K^+ , higher when counterion is Na^+ , and dominant when counterion is Li^+ . This fact allowed to decompose the complex bands into components. The polarity of THF as a

Table 1. B3LYP 6-31++G** theoretical and experimental (KBr tablet) frequencies (ν в cm^{-1}) and relative intensities of methylene-bis-malononitrile molecule **1**.

No.	Theoretical data			Experimental data ^a	
	ν^{b}	A	Approximate description ^c	ν	A ^d
1	3020	0.2	$\nu^{\text{as}}(\text{CH}_2)$	3020	m
2	2965	0.6	$\nu^{\text{s}}(\text{CH}_2)$	2959	m
3	2916	2.2	$\nu(\text{CH})$	}2912	vw
4	2915	4.9	$\nu(\text{CH})$		
5	2282	1.8	$\nu^{\text{s}}(\text{C}\equiv\text{N})$	}2278	sh
6	2281	0.1	$\nu^{\text{s}}(\text{C}\equiv\text{N})$		
7	2275	0.4	$\nu^{\text{as}}(\text{C}\equiv\text{N})$	}2266	m
8	2275	0.5	$\nu^{\text{as}}(\text{C}\equiv\text{N})$		
9	1452	6.7	$\delta^{\text{sciss}}(\text{CH}_2) + \delta(\text{CH})$	1450	s
10	1349	6.5	$\gamma^{\text{wag}}(\text{CH}_2) + \delta(\text{CH})$	1370	w
11	1325	5.3	$\gamma^{\text{twist}}(\text{CH}_2) + \delta(\text{CH})$	1340	w
12	1293	3.8	$\nu(\text{CC}) + \delta(\text{CH}) + \gamma^{\text{wag}}(\text{CH}_2)$	1293	m
13	1287	2.7	$\delta(\text{CH}) + \gamma^{\text{twist}}(\text{CH}_2)$	1284	m
14	1243	3.7	$\delta(\text{CH}) + \gamma^{\text{wag}}(\text{CH}_2)$	1247	s
15	1177	0.6	$\nu(\text{CC}) + \delta(\text{CH}) + \gamma^{\text{wag}}(\text{CH}_2)$	1181	m
16	1056	4.9	$\nu(\text{CC}) + \nu(\text{C-CN})$	1072	m
17	1054	7.7	$\nu(\text{CC}) + \nu(\text{C-CN})$	1072	m
18	1018	7.0	$\nu(\text{CC})$	1058	s
19	992	0.1	$\nu(\text{CC}) + \delta(\text{CH})$	1020	s
20	948	7.3	$\nu(\text{CC})$	953	m
21	854	0.1	$\nu(\text{C-CN}) + \nu(\text{CC})$	850	w
22	792	4.6	$\nu(\text{C-CN}) + \nu(\text{CC})$	787	w
23	621	7.4	$\delta(\text{C-CN}) + \delta(\text{skeletal})$	602	m
24	587	0.2	$\delta(\text{C-CN}) + \delta(\text{skeletal})$	571	m
25	585	0.4	$\delta(\text{C-CN}) + \delta(\text{skeletal})$	571	m
26	579	0.8	$\delta(\text{C-CN}) + \delta(\text{skeletal})$	562	m
27	500	0.6	$\delta(\text{skeletal}) + \delta(\text{C-CN})$	482	m
28 ^e	479	0.4	$\delta(\text{skeletal}) + \delta(\text{C-CN})$	464	m
MAD^f	10.86	-	-	-	-

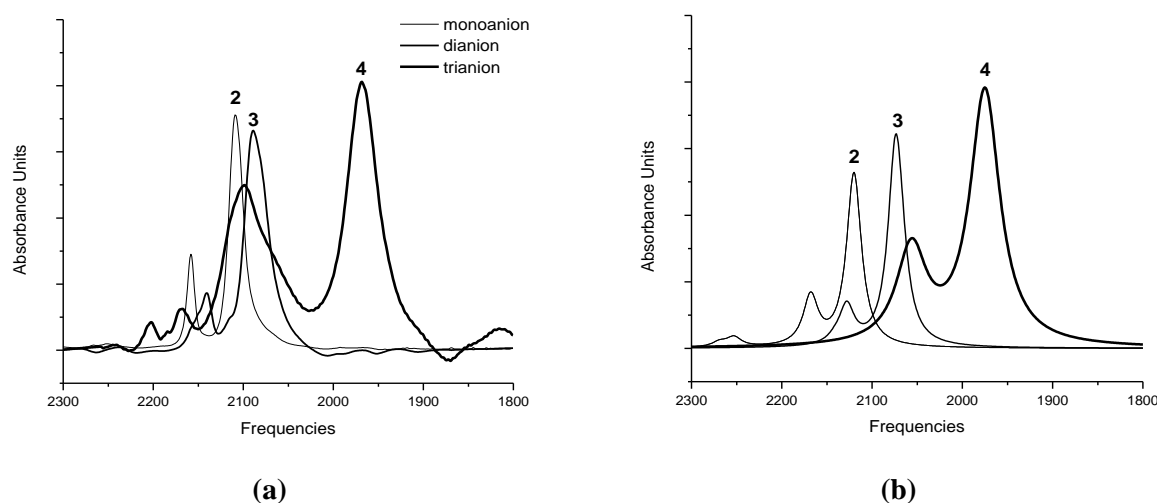
^aMeasured after having decomposed the complex bands into components. ^bScaled, according to correlation Eqn. (1).

^cVibrational modes: ν , stretching; δ , in-plane bending; γ , out-of-plane bending; superscripts: s, symmetrical; as, asymmetrical; sciss, scissoring; wag, wagging. ^dRelative intensities: s, strong; m, moderate; w, weak; v, very; sh, shoulder. ^eFollowed by 11 lower-frequency vibrations. ^fMean absolute deviation.

Table 2. B3LYP/6-31++G** theoretical and experimental (ν in cm^{-1} DMSO solutions) nitrile frequencies and relative intensities for methylene-bis-malononitrile molecule **1** and their anions **2-4**.

No.	Theoretical data			Experimental data ^a	
	ν^b	A ^c	Approximate description ^d	ν	A ^e
1	2266	0.7	$\nu_{af}^s(\text{C}\equiv\text{N})$	2264	sh
	2265	0.0	$\nu_{sf}^s(\text{C}\equiv\text{N})$	2264	sh
	2259	0.1	$\nu_{sf}^{as}(\text{C}\equiv\text{N})$	2258	vw
	2259	0.2	$\nu_{af}^{as}(\text{C}\equiv\text{N})$	2258	vw
2	2269	7.2	$\nu^s(\text{C}\equiv\text{N})$	2268	w
	2253	14.4	$\nu^s(\text{C}\equiv\text{N})$	2251	w
	2168	73.9	$\nu^{as}(\text{C}\equiv\text{N})$	2161	m
	2120	261.2	$\nu^{as}(\text{C}\equiv\text{N})$	2113	s
3	2141	16.9	$\nu_{sf}^s(\text{C}\equiv\text{N})$	2142	m
	2128	157.8	$\nu_{af}^s(\text{C}\equiv\text{N})$	2115	vw
	2074	679.9	$\nu_{sf}^{as}(\text{C}\equiv\text{N})$	2091	s
	2068	114.0	$\nu_{af}^{as}(\text{C}\equiv\text{N})$	2078	s
4	2061	21.7	$\nu_{sf}^s(\text{C}\equiv\text{N})$	2111 ^f	m
	2056	266.1	$\nu_{af}^s(\text{C}\equiv\text{N})$	2071 ^f	m
	1975	764.3	$\nu_{sf}^{as}(\text{C}\equiv\text{N})$	1975 ^f	s
	1969	3.2	$\nu_{af}^{as}(\text{C}\equiv\text{N})$	1969 ^f	m
MAD^f	8.0	-	-	-	-

^aMeasured after having decomposed the complex bands into components. ^bScaled with 0.9552 for $\nu_{\text{C}\equiv\text{N}}$ for molecule of **1** and 0.9642 for anions **2-4** [19]. ^cScaled theoretical intensities with 0.4010 [19] ^dVibrational modes: ν , stretching; s-symmetrical, as-asymmetrical, sf-sinphase, af-antiphase. ^eRelative intensities: m, moderate; w, weak; v, very; sh, shoulder. ^fMeasured in THF solution, counter-ion Na^+ .

**Fig. 4.** Experimental (a) and theoretical (b) IR spectra of anions **2-4** in nitrile stretch region 2300-1800 cm^{-1} .

solvent is significantly lower than DMSO and we have no doubts in the existence of ion aggregation. The position of nitrile bands varies within 10 cm^{-1} depending on counterion (Li^+ , Na^+ , K^+). Nevertheless, the nitrile frequencies of trianion **4** are predicted satisfactorily by the computations performed for the free trianion.

As we can see in Table 2, the theory predicts very well the frequencies of the bands observed in

the nitrile stretch region. By analogy with other studied anionic dicyanometanides we believe that the same can be said about the intensity. The theoretical values of intensities of carbanion **2** lies in the interval 50-100 $\text{km}\cdot\text{mol}^{-1}$ for $\nu^s(\text{C}\equiv\text{N})$ and 200-300 $\text{km}\cdot\text{mol}^{-1}$ for $\nu^{as}(\text{C}\equiv\text{N})$ typical for other dicyanometanides [14-19]. The mean absolute deviation (MAD) for nitrile frequencies is only 8

cm⁻¹ and it is smaller than those observed in a wide variety of nitriles, and their anions [18,19].

Structural analysis

The experimental [8] and theoretical data on the structure of the molecule **1** are compared in Table 3. It is interesting, to note that according to the experimental data the comparison of methylene-bis-malononitrile with malononitrile shows a significant lengthening of the triple bond of the cyano group: 1.157 Å [25] (Table 3), malononitrile 1.132 Å [8]. The theory does not provide similar effect and the differences are in the fourth digit. However bond angles, are predicted good by the theory, as the average absolute deviation is in the first digit.

According to the computations, the conversion of the molecule **1** into monoanion **2** and the monoanion **2** into dianion **3** (Scheme 1, Fig 2, 3) leads to change of the configuration of the carbanionic centres from sp³ to sp² (atom C(2) and atom C(3)). Only the formation of third anionic center (atom C(1)) leads to preservation of the tetragonal configuration. According to the data listed in Table 3 the largest structural changes are at and near to the carbanionic centers. On every step of deprotonation C≡N bonds are lengthened, and C-CN bonds are

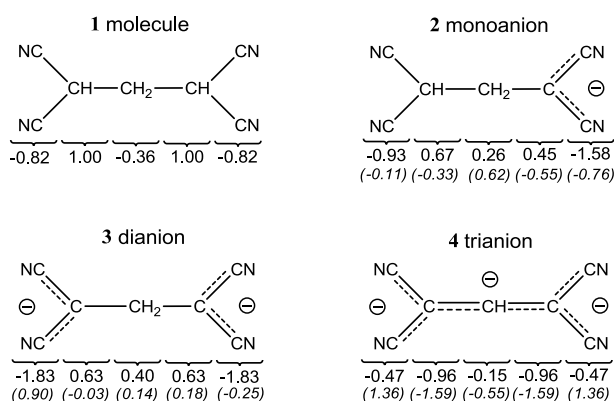
shortened. The changes in bond lengths and bond angles remote from the carbanionic center are smaller.

The electronic structure of the molecule and the anions of methylene-bis-malononitrile is presented in Scheme 4. The electronic charge changes $\Delta q_i = q_i(\text{anion}) - q_i(\text{molecule})$ are usually quite informative to demonstrate the distribution of the new carbanionic charge over individual fragments of anions. These charge changes of the fragments at each step of deprotonation are given in parentheses. According to the theory, the changes in electron density are greatest in and near to the newly created carbanion centers, and yet they are distributed in all fragments. Upon conversion of the molecule **1** to carbanion **2** and the carbanion **2** to dianion **3** the electron density of cyano groups situated far from the new carbanionic centers increases by 0.08 e⁻ and 0.14 e⁻ respectively. The electronic density of the newly created charge in **2** and **3** is distributed almost uniformly between the carbanion center and the cyano groups (0.42 to 0.49 e⁻) attached to it. 0.56 e⁻ of the third carbanionic charge remains localized in the middle fragment and the remaining electron density is distributed over the four cyano groups.

Table 3. B3LYP/6-31++G** theoretical and experimental (Roentgen diffraction) bond lengths (Å) and bond angles (degree) of methylene-bis-malononitrile **1** and its anions **2-4**. The largest changes in the values are given in bold.

bond lengths and bond angles ^a	Molecule 1		Monoanion 2	Dianion 3	Trianion 4
	Theoretical data	Experimental data [8]	Theoretical data ^b	Theoretical data ^b	Theoretical data ^b
C(4)≡N(5)	1.160	1.132(3)	1.178	1.183	1.195
C(6)≡N(7)	1.160	1.132(3)	1.179	1.185	1.191
C(8)≡N(11)	1.160	1.132(3)	1.161	1.183	1.195
C(9)≡N(10)	1.160	1.132(3)	1.162	1.185	1.191
C(1)–C(2)	1.556	1.546(3)	1.501	1.153	1.527
C(2)–C(4)	1.475	1.486(3)	1.402	1.400	1.408
C(2)–C(6)	1.473	1.478(3)	1.402	1.398	1.402
C(1)–H(14)	1.092	1.03(2)	1.099	1.100	1.099
C(2)–H(8)	1.099	1.04(2)	-	-	-
MAD	0.029	-	-	-	-
<C(2)C(4)N(5)	178.0	177.9(3)	175.5	179.2	175.4
<C(2)C(6)N(7)	176.6	176.6(3)	178.2	178.5	178.1
<C(1)C(2)C(4)	110.1	108.8(2)	117.9	121.7	121.1
<C(4)C(2)C(6)	111.0	110.3(2)	120.8	119.9	113.7
<C(2)C(1)C(3)	112.6	112.5(2)	113.0	120.1	121.2
<C(1)C(2)C(6)	111.4	111.7(2)	120.8	120.6	124.4
<C(2)C(1)H(14)	108.4	109(1)	112.5	109.4	107.3
<C(2)C(1)H(15)	109.6	109(1)	110.7	105.7	-
<C(1)C(2)H(8)	109.3	111(1)	-	-	-
<C(6)C(2)H(8)	107.6	107(1)	-	-	-
<H(14)C(1)H(15)	108.2	109(2)	107.	105.7	-
MAD	0.6	-	-	-	-

^aAtom numbering according to Figure 1. ^bThe largest changes towards values of molecule **1** are given in bold.



Scheme 4. NBO electronic charges of methylene-bis-malononitrile **1** and its anions.

CONCLUSION

We found on the basis of both experimental and computational IR data that the effect of conversion of 1,1,3,3-tetracyanopropane into anions is strong. The cyano stretching frequencies at the first step of deprotonation decreases by maximum 140 cm^{-1} upon deprotonation and further to 200 and 300 cm^{-1} upon the next steps of deprotonation. At every step a large change in the geometry occurs and significant part of the electronic charge generated by the formation of carbanionic centers is distributed over the cyanogroups. 0.42 e^- , 0.49 e^- and 0.56 e^- from the newly generated anionic charge remains localized over the first, second and third carbanionic center respectively. This findings are in agreement with the observed spectral change.

REFERENCES

- O. Diels, B. Conn, *Berichte*, **56B**, 2076 (1923).
- A. Ardis, S. Averill, H. Gilbert, F. Miller, R. Schmidt, F. Stewart, H. Trumbull, *J. Am. Chem. Soc.*, **72**, 1305 (1950).
- J. Krajewski, J. Moyer, *Can. J. Chem.*, **52**, 3626 (1974).
- T. J. Johnson, K. W. Hipps, R. D. Willett, *J. Phys. Chem.*, **92**, 6892 (1988).
- J. Westfahl, T. Gresham, *J. Org. Chem.*, **21**, 319 (1956).
- D. Yarrow, J. Ibers, M. Lenarda, M. Graziani, *J. Organomet. Chem.*, **65**, 133 (1974).
- M. Dinger, W. Henderson, *J. Organomet. Chem.* **577**, 219 (1999).
- R. A. Bell, B. E. Brown, M. Durate, H. E. Howard-Lock, *Can. J. Chem.*, **65**, 261 (1987).
- M. J. Frisch, G.W. Trucks, H. B. Schlegel, G. E. Scuseria, M. A. Robb, J. R. Cheeseman, V. G. Zakrzewski, J. A. Montgomery, Jr., R. E. Stratmann, J. C. Burant, S. Dapprich, J. M. Millam, A. D. Daniels, K. N. Kudin, M. C. Strain, O. Farkas, J. Tomasi, V. Barone, M. Cossi, R. Cammi, B. Mennucci, C. Pomelli, C. Adamo, S. Clifford, J. Ochterski, G. A. Petersson, P. Y. Ayala, Q. Cui, K. Morokuma, D. K. Malick, A. D. Rabuck, K. Raghavachari, J. B. Foresman, J. Cioslowski, J. V. Ortiz, A. G. Baboul, B. B. Stefanov, G. Liu, A. Liashenko, P. Piskorz, I. Komaromi, R. Gomperts, R. L. Martin, D. J. Fox, T. Keith, M. A. Al-Laham, C. Y. Peng, A. Nanayakkara, C. Gonzalez, M. Challacombe, P. M. W. Gill, B. Johnson, W. Chen, M. W. Wong, J. L. Andres, M. Head-Gordon, E. S. Replogle and J. A. Pople, *Gaussian 98*, Revision A.7, Gaussian, Inc., Pittsburgh PA, 1998.
- A. D. Becke, *J. Chem., Phys.*, **98**, 5648 (1993).
- C. Lee, W. Yang, G. R. Parr, *Phys. Rev. B*, **37**, 785 (1988).
- P. J. Stephens, F. J. Devlin, C. F. Chabalowski, M. J. Frisch, *J. Phys. Chem.*, **98**, 623 (1994).
- J. A. Tsenov, S. S. Stoyanov, I. G. Binev, *Bulg. Chem. Commun.*, **40**, 520 (2008).
- S. S. Stoyanov, A. D. Popova, A. D. Tsenov, *Bulg. Chem. Commun.*, **40**, 538 (2008)
- S. S. Stoyanov, J. A. Tsenov, I. G. Binev, *Assian Chem. Lett.* **13**, 155 (2009).
- S. S. Stoyanov, J. A. Tsenov, I. G. Binev, *Assian Chem. Lett.* **13**, 171 (2009).
- S. S. Stoyanov, J. A. Tsenov, D. Y. Yancheva, *J. Mol. Struct.*, **1009**, 42 (2012).
- S. S. Stoyanov, *Compt. Rend. L'Acad. Bulg. Sci.* **62**, 445 (2009).
- S. S. Stoyanov, *J. Phys. Chem. A*, **114**, 5149 (2010).
- A. D. Popova, M. K. Georgieva, O. I. Petrov, K. V. Petrova, E. A. Velcheva. *Int. J. Quant. Chem.*, **107**, 1752 (2007) (and references therein)
- I. N. Juchnovski, I. G. Binev, *Chem. Phys. Lett.*, **12**, 40 (1971).
- Y. I. Binev, J. A. Tsenov, I. N. Juchnovski, I. G. Binev, *J. Mol. Struct. THEOCHEM*, **625**, 207, (2003).
- I. G. Binev, Y. I. Binev, B. A. Stamboliyska, I. N. Juchnovski, *J. Mol. Struct.*, **435**, 235 (1997).
- E. A. Velcheva, Y. I. Binev, M. J. Petrova, *J. Mol. Struct.*, **475**, 65 (1999).
- J. Demaison, G. Wlodarezak, H. Rueck, K. N. Wiedenmann, H. D. Rudolph, *J. Mol. Struct.*, **376**, 399 (1996).

ИЧ-СПЕКТРИ И СТРУКТУРА НА 1,1,3,3-ТЕТРАЦИАНОПРОПАН И НЕГОВИТЕ КАРБАНИОНИ: ЕКСПЕРИМЕНТАЛНО И КВАНТОВОХИМИЧНО ИЗСЛЕДВАНЕ

С. С. Стоянов*, Й. А. Ценов

*Институт по Органична химия с Център по Фитохимия, Българска Академия на Науките, ул. Акад. Г. Бончев,
бл. 9, 1113 София, България*

Постъпила на 10 юни 2014 г.; Коригирана на 21 юли 2014 г.

(Резюме)

Приложен е комбиниран ИЧ експериментален/DFT теоретичен подход за проследяване на спектралните и структурни промени, породени от превръщането на 1,1,3,3-тетрацианопропан в моно-, ди- и трианион. Превръщането на молекулата в моноион се отразява слабо върху валентното трептене на $\nu(\text{C}\equiv\text{N})$ на отдалечените от карбанионния център цианогрупи (13 cm^{-1}) и силно върху близкоразположените цианогрупи (140 cm^{-1}). Карбанионният заряд е разпределен главно в анионния център и цианогрупите директно свързани с него (общо $0,85\text{ e}^-$). Превръщането на молекулата в ди- и трианион е съпроводено с по-силно понижение на $\nu(\text{C}\equiv\text{N})$, достигащо до 300 cm^{-1} . Установено е много добро съответствие между експерименталните и теоретичните данни. Според изчисленията разпределението на карбанионния заряд, получен при второто и третото депротониране се разпределя почти равномерно във всички фрагменти.

Influence of the environment on the antioxidant action of two 6-(propan-2-yl)-4-methyl-morpholine-2,5-diones

D. Yancheva^{1*}, S. Stoyanov¹, B. Stambolyiska¹, L. Daskalova¹, E. Cherneva², A. Smelcerovic³

¹*Institute of Organic Chemistry with Centre of Phytochemistry, Bulgarian Academy of Sciences, Acad. G. Bonchev str., bl. 9, 1113 Sofia, Bulgaria*

²*Department of Chemistry, Faculty of Pharmacy, Medical University of Sofia, 2 Dunav str., 1000 Sofia, Bulgaria*

³*Department of Chemistry, Faculty of Medicine, University of Niš, 81 Dr. Zorana Djindjica blv., 18000 Niš, Serbia*

Received May 21, 2014; Revised August 11, 2014

Dedicated to Acad. Dimiter Ivanov on the occasion of his 120th birth anniversary

Density functional theory was used to study diketo and enol structures of two cyclodipeptides, 3-(2-methylpropyl)-6-(propan-2-yl)-4-methyl-morpholine-2,5-dione and 3,6-di(propan-2-yl)-4-methyl-morpholine-2,5-dione, able to form radicals and act as reducing agents. Three possible mechanisms of antioxidant action were considered: H-atom abstraction (HAT), single electron transfer (SET), and sequential proton loss electron transfer (SPLET). The influence of the environment was elucidated by calculating the respective dissociation enthalpy (BDE), ionization potential (IP), proton dissociation enthalpy (PDE), proton affinity (PA), and electron transfer enthalpy (ETE) in non polar solvent benzene, and polar solvents methanol and water. The preferred mechanism in different environment was outlined based on the obtained reaction enthalpies and showed that the reaction pathway depends on the environment polarity. HAT is the most probable mechanism in nonpolar phase, while SPLET is the preferred one in polar environment.

Key words: cyclodipeptide, 6-(propan-2-yl)-3-methyl-morpholine-2,5-dione, antioxidant activity, reaction mechanism, solvent polarity

INTRODUCTION

Cyclodipeptides are the simplest members of cyclodipeptides family, which have an ester group and an amide group in the same 6-membered ring. They contain only one residue of amino acid and one residue of lactic, α -hydroxyisovaleric or other α -hydroxy acid. The cyclodipeptides exhibit antimicrobial [1,2], immunomodulating [1,3,4], anticoagulant [5], and inhibitory activity towards acyl-CoA:cholesterol acyltransferase [6], α -glucosidase [7-9] and xanthin oxidase (XO) [10]. In this way they are interesting candidates for pharmacological application. As a part of our continuing study of identification [11], synthesis [11,2] and biological activities [1,2,4,10] of cyclic dipeptides, recently we elucidated the antioxidant activity of the two synthesized cyclodipeptides 3-(2-methylpropyl)-6-(propan-2-yl)-4-methyl-morpholine-2,5-dione (**1a**) and 3,6-di(propan-2-yl)-4-methyl-morpholine-2,5-dione (**2a**), by applying two assays, 2,2-diphenyl-1-picrylhydrazyl (DPPH)-radical scavenging capacity and total reducing power [12]. Our data indicate moderate antioxidant

potentials of the two studied cyclodipeptides. A high correlation between DPPH-radical scavenging capacity and total reducing power were found. Diketo, enol and dienol structures of compounds **1** and **2** (Fig. 1), able to form radicals and act as reducing agents, were examined using density functional theory (DFT) calculations in gas phase. The calculated total energies indicate the diketo form "a" as the most stable.

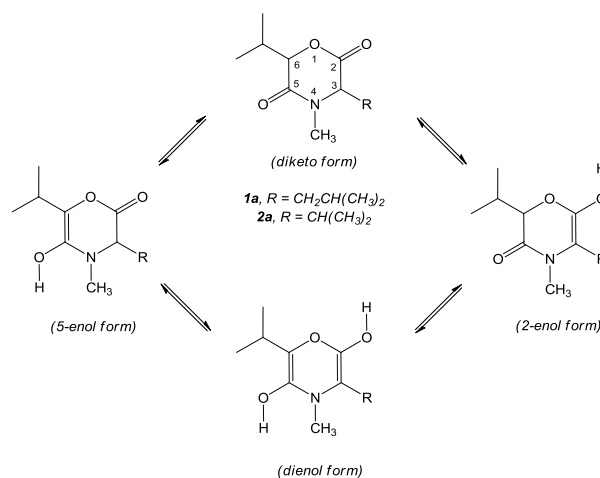
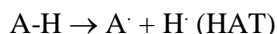


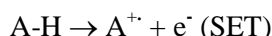
Fig. 1. Tautomeric structures of compounds **1** and **2**.

* To whom all correspondence should be sent:
E-mail: deni@orgchem.bas.bg

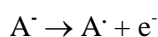
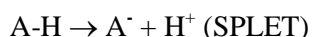
One possible mechanism by which the antioxidants can deactivate a free radical is H-atom abstraction (HAT mechanism) [13-16]:



The efficacy of the antioxidant to react via HAT is characterized by the bond dissociation enthalpy (BDE). Higher stability of A, i.e., lower BDE values, corresponds to good antioxidant capacity of A-H. Another possible mechanism is electron transfer (SET mechanism), in which the radical cation is first formed followed by deprotonation [16-19]:



For evaluation of reactivity via SET, the ionization potential (IP) is used. A lower IP implies an easier electron release. More recently a third mechanism has been discussed – sequential proton loss electron transfer (SPLET) [13, 20]:



In the first step of this mechanism an anion is formed by initial proton transfer, followed by an electron transfer. The proton affinity (PA) of the formed anion is used as a measure for reactivity via SPLET. Higher stability of A⁻, i.e., lower PA values, indicates an easier extraction of the proton.

The net result of the three antioxidant action mechanisms is the same. SET and SPLET mechanisms are favoured in polar environment because the generated charged species are stabilized by the solvent. Based on calculation of the reaction enthalpies for each of the mechanisms, it is possible to suggest the most probable mechanism of action of a particular group of compounds [13].

In the case of the two cyclodipeptides **1** and **2** studied by us, hydrogen atom abstraction from the activated C-H group at 3-position in the diketo form was found to be the most probable mechanism of antioxidant action in gas phase. However, these calculations do not account for the influence of the polarity of the surrounding medium. For this reason, the main goal of the present contribution is to determine the preferred mechanism of antioxidant action in polar environment as a description of the processes taking place in the living organism. Calculations in benzene will be performed in order to improve the description of the antioxidant action of **1** and **2** in nonpolar

environment representing the biological membranes. The polar medium is also very important as illustration of the biological liquids and therefore the relevant enthalpies will be calculated in water. Based on the obtained enthalpies it will be clarified which of the three possible mechanisms of antioxidant action (HAT, SET or SPLET) is the most probable in polar liquid environment. In this way, the expected mechanism of antioxidant action of the title compounds will be described for all potential sites in the living organism. The study will be complemented also by computations in methanol in order to take account of the conditions used in the *in vitro* radical scavenging assays [12].

COMPUTATIONAL DETAILS

All theoretical calculations were performed using the Gaussian 09 package [21] of programs. Geometry and vibrational frequencies of species studied were performed by analytical gradient technique without any symmetry constraint. All the results were obtained using the density functional theory (DFT), employing the B3LYP (Becke's three-parameter non-local exchange [22] and Lee *et al.* correlation [21] potentials). To establish the stability order for the neutral, radical and ionic species in solvent we used the Integral Equation Formalism Polarizable Continuum Model (IEF-PCM) [23] at the same level of theory.

The geometries of all possible isomers of the studied compounds, radicals, radical cations were fully optimized by application of the UB3LYP functional in conjunction with the 6-311++G** basis set. The optimized structures were further characterized by analytical computations of harmonic vibrational frequencies at the same level. Dissociation enthalpy (BDE), ionization potential (IP), proton dissociation enthalpy (PDE), proton affinity (PA), and electron transfer enthalpy (ETE) were calculated according the equations given by Klein *et al.* [13].

$$\text{BDE} = H(\text{A}^\cdot) + H(\text{H}^\cdot) - H(\text{A-H})$$

$$\text{IP} = H(\text{A}^{+\cdot}) + H(\text{e}^-) - H(\text{A-H})$$

$$\text{PDE} = H(\text{A}^\cdot) + H(\text{H}^+) - H(\text{A}^{\cdot+})$$

$$\text{PA} = H(\text{A}^-) + H(\text{H}^+) - H(\text{A-H})$$

$$\text{ETE} = H(\text{A}^\cdot) + H(\text{e}^-) - H(\text{A}^\cdot)$$

The enthalpy of hydrogen atom, $H(\text{H}^\cdot)$, for each solvent was obtained by the same method and basis set. All reaction enthalpies were calculated for 298 K. Solvation enthalpies of proton $H(\text{H}^+)$, electron,

$H(e^-)$, in organic solvents, determined using IEF-PCM DFT/B3LYP/6-311++G** calculations, were taken from the literature [24].

Natural bond orbitals (NBO) analysis [25-27] has been performed to characterize the delocalization of electron density within the molecule.

RESULTS AND DISCUSSION

In order to determine the preferred geometry of the compounds studied, a large number of probable geometries should be constructed taking into account the flexibility of the ring system and the change-over to chair- and boat-conformations. For each boat or chair ring conformation, all relevant combinations of axial and equatorial positions of the 3- and 6-alkyl groups should also be considered. In previous studies [2,11,28], it was demonstrated that in all cases the morpholine-2,5-dione ring adopts boat conformation and the most favourable orientation of the larger 3- and 6-substituents is equatorial/axial and axial/equatorial.

The title compounds, **1a** and **2a**, are synthesized in a condensation reaction of 2-bromo-3-methylbutanoyl chloride with (*L*)-*N*-methylleucine or (*L*)-*N*-methylvaline, respectively, followed by intramolecular cyclization [11]. The mechanism of the amide group formation does not involve

conversion of the stereo configuration of the amino acid residues, therefore only the (*3S*) diastereoisomers could be considered in the structure optimizations. In gas phase the most stable among them is the (*3S,6R*) form [11]. It was also found that the higher polarity of the environment (in solvents such as water and DMSO) does not influence the stability order of diastereoisomers of a related compound 6-(propan-2-yl)-3-methyl-morpholine-2,5-dione [2]. For this reason, in the present study, only the most stable gas-phase diastereoisomers of **1a** and **2a** were taken for the optimization in benzene, water and methanol. The structural parameters of **1a** and **2a** in all employed solvents are similar. The morpholine-2,5-dione rings are in boat conformations with the sp^3 C3 and C6 atoms displaced by 25-35° out of the plane formed by O1, C2, N4 and C5.

For the antioxidant action, the interconversion between diketo, enol and dienol structures is more important as it leads to the formation of different radicals able to act as reducing agents. In order to examine the prototropic tautomerism, the relative stability of the two most stable gas-phase structures of **1** and **2** – diketo “**a**” and 2-enol “**b**” were optimized in the different solvents. The calculated total energies are summarized in Table 1.

Table 1. Calculated total and relative energies, and dipole moments of neutral, radical and ionic species of **1** and **2**.

Species		E_{tot} , (Hartree)	ΔE , kJ/mol	μ , D		E_{tot} , (Hartree)	ΔE , kJ/mol	μ , D
<i>Benzene (2.271)^a</i>								
Molecule	1a	-750.593201		4.08	2a	-711.261514		4.27
Enol	1b	-750.567096	68.53 ^b	3.35	2b	-711.239677	57.3 ^a	3.28
Radical	1c	-749.963946		4.46	2c	-710.636419		4.37
	1d	-749.946488	45.83 ^c	2.91	2d	-710.615411	55.1 ^b	3.23
Radical cation	1e	-750.310199		3.52	2e	-710.981092		3.33
Anion	1f	-750.065192		6.80	2f	-710.737265		5.31
	1g	-750.047205	47.2 ^d	6.56	2g	-710.719960	45.4 ^c	4.33
<i>Methanol (32.613)^a</i>								
Molecule	1a	-750.600900		5.00	2a	-711.269287		5.13
Enol	1b	-750.573064	73.1 ^b	4.23	2b	-711.245598	62.2 ^a	4.18
Radical	1c	-749.971607		5.40	2c	-710.643888		5.38
	1d	-749.952652	49.7 ^c	3.51	2d	-710.621738	58.1 ^b	3.84
Radical cation	1e	-750.345624		4.81	2e	-711.015835		4.16
Anion	1f	-750.103919		8.67	2f	-710.775302		6.95
	1g	-750.083373	53.9 ^d	4.97	2g	-710.757432	46.9 ^c	3.28
<i>Water (78.355)^a</i>								
Molecule	1a	-750.601392		5.07	2a	-711.269769		5.19
Enol	1b	-750.573430	73.4 ^b	4.29	2b	-711.245968	62.5 ^a	4.24
Radical	1c	-749.972081		5.47	2c	-710.644359		5.45
	1d	-749.953045	50.0 ^c	3.56	2d	-710.622133	58.3 ^b	3.88
Radical cation	1e	-750.347428		4.91	2e	-711.017557		4.21
Anion	1f	-750.105869		8.80	2f	-710.777227		7.07
	1g	-750.085170	54.3 ^d	4.93	2g	-710.759315	47.1 ^c	3.25

^a Relative dielectric permittivity [35 and references therein]; ^b $\Delta E = E_{(\text{enol})} - E_{(\text{keto})}$; ^c $\Delta E = E_{(\text{radical } 1c)} - E_{(\text{radical } 1d)}$; ^d $\Delta E = E_{(\text{anion } 1f)} - E_{(\text{anion } 1g)}$.

In all cases the energy differences between diketo and enol forms are much higher than 50 kJ/mol; therefore prototropic conversion is not expected to occur. The values in water are higher than the corresponding in benzene (Table 1) showing in this way that the diketo structures of **1** and **2** are further stabilized by the polar environment. This result is in accordance with the experimental NMR and IR data for **1** and **2** showing that both compounds are present in diketo form in solid state and chloroform. The possibility of prototropic tautomerism of a related compound, 6-(propan-2-yl)-3-methyl-morpholine-2,5-dione, was recently studied in solution and in this case again no evidence of enol formation was found neither in polar nor in nonpolar environment [2]. So further only diketo forms will be taken into account for evaluation of their capability to form radicals and act as reducing agents via HAT, SET and SPLET mechanisms in different environment.

The calculated reaction enthalpies, involved in the three mechanisms of antiradical activity of **1** and **2**, are presented in Table 2. Two possible sites for hydrogen atom abstraction were estimated – C3 (radicals “c”) and C6 (radicals “d”, respectively) as well as for generation of anion species – deprotonation at C3 (anions “f”) and C6 (anions “g”, respectively).

Table 2. DFT bond dissociation enthalpy (BDE), ionization potential (IP), proton dissociation enthalpy (PDE), proton affinity (PA), and electron transfer enthalpy (ETE) values of **1a** and **2a** in kJ/mol.

Species	BDE	IP	PDE	PA	ETE
<i>Gas phase</i> ^a					
1a	306	824	782	1439	167
2a	294	818	776	1427	167
<i>Benzene (2.271)</i> ^b					
1a	312	733	-7	459	267
2a	301	727	-12	449	266
<i>Methanol (32.613)</i> ^b					
1a	311	583	-78	235	269
2a	300	578	-85	226	267
<i>Water (78.355)</i> ^b					
1a	302	559	-59	246	254
2a	291	555	-65	238	252

^a According to [12]; ^b Relative dielectric permittivity [35 and references therein].

Site C3 is more reactive both via HAT and SPLET as demonstrated by the relative stability of the radicals produced by proton transfer from C3 and C6 (HAT) and the anions produced by deprotonation at C3 and C6 (SPLET). The energy differences between the more stable radicals of **1c** and **2c** and the less stable **1d** and **2d** in benzene is

smaller than in water. The same trend is observed also with the stability of anions **1f** and **2f** versus **1g** and **2g**.

Important information for the radical stability could be derived also from atomic spin population analysis. The energy of a free radical can be efficiently decreased if the odd electrons are delocalized through the conjugated system. Fig. 2 illustrates the spin density distribution over the fragments in **1c**, **1d**, **2c** and **2d** in benzene and water obtained by NBO population analysis. Approximately 0.5 of the spin density in **1c** and **2c** is localized on C3 and the rest is distributed equally between the ester and the amide moiety. The spin density in the radicals generated by abstraction of a hydrogen atom from C6 is less effectively delocalized indicating lower stability of the respective radicals. Comparing the values in benzene and water, it could be concluded the in polar environment **1c** and **2c** show slightly higher stability which would be favourable for their radical scavenging efficiency.

In order to rationalize the solvent polarity significance for the stabilization of the molecules and their derivatives (enols, radicals, and ions), data for their dipole moments are presented in Table 1. As could be seen there, the polarity of the anionic derivatives is considerably higher than those of the radical species. Therefore, the polarity of the environment is expected to have a bigger impact on the processes involving anionic species. In accordance with this, when analysing the reaction enthalpies for the HAT, SET and SPLET mechanisms in gas phase [12] and in different solvents presented in Table 2, it can be noted the C-H bond dissociation enthalpies (BDEs) are similar in all solvents i.e. the energy requirements for HAT do not change much with the environment polarity. On the other hand, the solvation of the electron and the positively charged radical species of **1a** and **2a** exerted even by nonpolar solvents such as benzene lowers the IP values in liquid phase. As a result of the greater stabilisation in polar environment (water) the corresponding IPs are significantly lower than in benzene. As the SPLET mechanism is also involving charged species, the respective reaction enthalpies are affected by the solvation and the medium polarity. Mainly due to the large enthalpy of H⁺ solvation, the PAs in benzene differ dramatically from those in gas-phase. They are further lowered in aqueous environment.

The comparison of the respective BDE, IP and PA values outlines clearly the most probable mechanism of antioxidant activity of **1a** and **2a** in

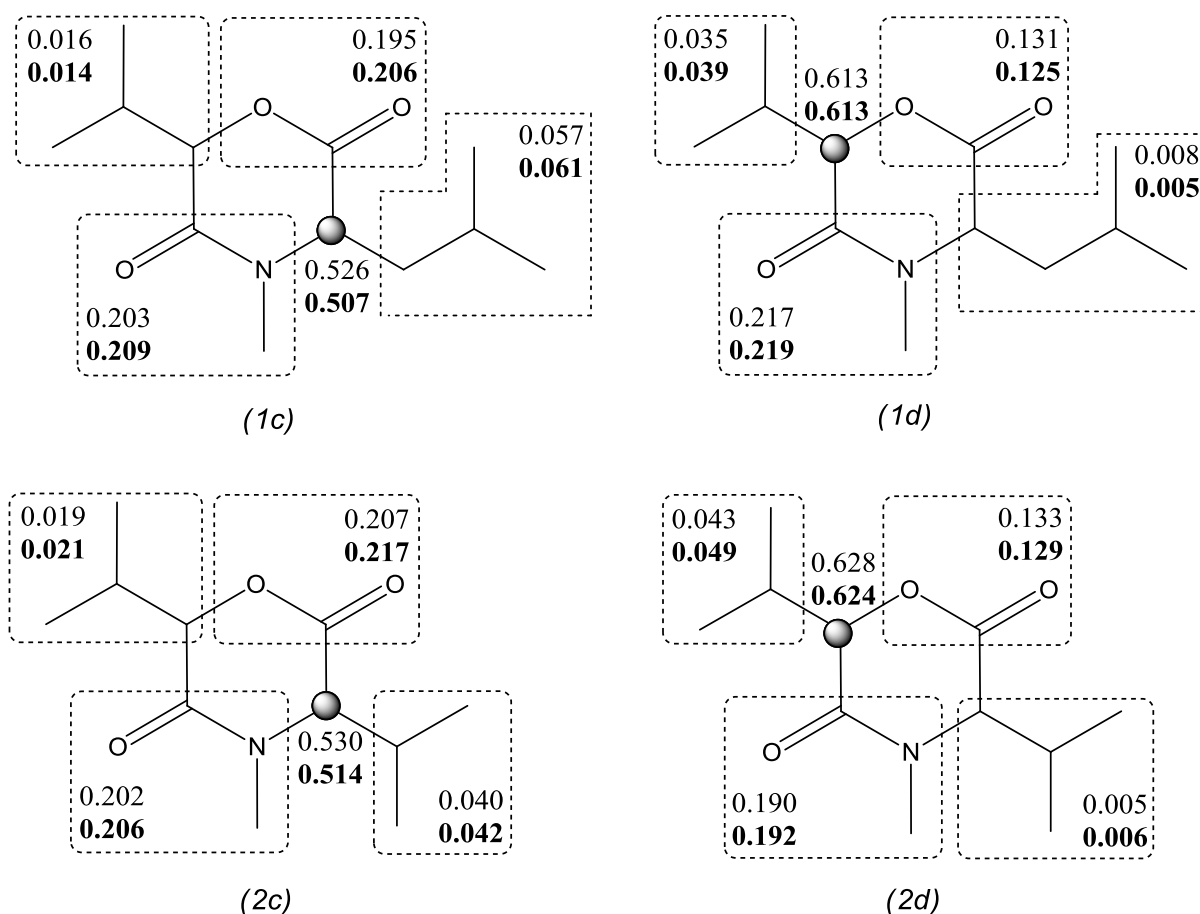


Fig. 2. Calculated NBO spin density over fragments of radicals **1c**, **1d**, **2c** and **2d** in benzene and water (in bold).

the polar and nonpolar environment. Similarly to the gas phase, in benzene the BDE values of **1a** and **2a** are lower than the IPs and PAs which supports the assumption of HAT as the most probable mechanism in nonpolar environment. Taking into account the interactions with the surrounding nonpolar molecules is necessary to conclude accurately on the preferred mechanism in nonpolar environment. These interactions change dramatically the thermodynamic requirements of the SPLET reaction and examination of the gas-phase reaction enthalpies alone might not lead to the right conclusions.

Clarification of the possible mechanism of antioxidant action of **1a** and **2a** in nonpolar environment is very important in relation to the lipophilic nature of both compounds and their favourable physico-chemical properties for efficient blood penetration and intestinal absorption [28]. This would allow their transportation to different possible sites of action. Their partition into lipid bilayers would provide increased local concentration and thus antiradical activity. Free lipid-peroxyl radicals of the type LOO[•] typically display a

BDE of about 367 kJ/mol [29]. Thus, an effective chain-breaking antioxidant that could prevent lipid peroxidation should have a lower BDE value. A well-known antioxidant that reacts via HAT is α -tocopherol, for which a BDE values of 327 kJ/mol was calculated in gas-phase and 293 kJ/mol in water using the same computational scheme [13]. In the present case, the calculated BDE values are also within this range and suggest good potential of **1a** and **2a** to prevent lipid peroxidation. Compounds **1a** and **2a** exhibit antimicrobial [1] and antioxidant [12] activity. Furthermore, they were excellent inhibitors of XO and significantly suppressed the activation of the nuclear factor κ B (NF- κ B) [10]. NF- κ B is a redox-associated transcription factor that is required for maximal transcription of a wide array of pro-inflammatory mediators. It is well known that Reactive Oxygen Species (ROS) stimulate the NF- κ B pathway in the cytoplasm through I κ B (inhibitor of kappa B) degradation. Overexpression of the antioxidant proteins was shown to inhibit NF- κ B activation [28]. Xu *et al.* [30] have found NF- κ B binding site on human xanthine dehydrogenase (XDH) gene, and it is

known that XDH conversion to XO may represent a feed-forward mechanism for stimulation of ROS production [31]. It can be concluded that NF- κ B may directly affect the XO activity and ROS production. **1a** and **2a** were confirmed as non-toxic in thymocytes [1] and therefore may give a promise to be used in the treatment of gout and other excessive uric acid production or inflammatory conditions [10].

The feasibility of the three mechanisms of antioxidant action in polar environment will give us a clue to the processes in physiological liquids whose main constituent is water. The BDE values in the three polar solvents are similar to those in nonpolar environment, so the preferred reaction pathway depends on the changes in the IP and PA induced by the polar solvent. The reactivity of **1a** and **2a** via SET was estimated according to the principle defined by Wright *et al.* [16], i.e., when IPs drop to *ca.* 167 kJ/mol below phenol, the SET mechanism gains importance in solution. The IP value of phenol in water is calculated at the same theoretical level as 346 kJ/mol [13]. In all studied polar solvents, the IPs of **1a** and **2a** are higher than 500 kJ/mol. It implies that the SET mechanism is not preferred for this type of compounds in any kind of environment. SET mechanism is typical mainly for electron-donating compounds containing a conjugated system of double bonds. Such example are the pyrrolopyrimidines, which were described as effective *in vitro* and *in vivo* antioxidants possessing neuroprotective activity in brain injury and ischemia models [32]. Another class of compounds reported recently to act as lipid peroxidation inhibitors presumably via SET mechanism are the 2-amino-5-alkylidenethiazol-4-ones [33].

As can be seen in Table 2, the first step of SPLET has lower energy requirements than HAT and SET in water. This indicates the SPLET as the most probable mechanism in polar environment in general. In some cases, the HAT mechanism could be competitive to the SPLET one, because in spite of the low values of PA, the second step of the SPLET mechanism, i.e., electron transfer might require higher energy than the corresponding hydrogen atom abstraction [34]. However, in the present case not only the PAs, but also the ETE values are lower than the BDEs which confirms that the SPLET mechanism is the most probable mechanism of antioxidant action in polar environment.

The PAs in methanol are slightly lower than in water due to the greater solvation enthalpy of the proton [24]. Similarly to water solution, the expected mechanism of antioxidant action is SPLET.

CONCLUSION

Density functional theory (DFT) calculations in benzene, methanol and water were used to study diketo and enol structures of compounds **1** and **2**, able to form radicals and act as reducing agents. The calculated energy differences between diketo and enol forms are much higher than 50 kJ/mol and therefore prototropic conversion is not expected to occur. The ability of compounds **1** and **2** to be oxidized according to HAT, SET and SPLET mechanisms was estimated in the above-mentioned solvents. The environment polarity hardly affects the BDEs of the C-H bond, while the IPs and PAs are significantly lowered in the polar environment. The dramatic change of the reaction enthalpy of SPLET (three times less compared to the gas phase) results in a reversal of the antioxidant mechanism of **1** and **2** in polar solvents. Hence, HAT is the most probable mechanism in nonpolar phase, while SPLET is expected to be the preferred one in polar environment. Hydrogen atom abstraction and deprotonation might occur at two possible sites (C3 and C6), but C3 is found to be more reactive both via HAT and SPLET in all media.

Acknowledgments: *The financial support of this work by the National Science Fund of Bulgaria (Contracts: DMU-03/66 and RNF01/0110) and the Ministry of Education and Science of the Republic of Serbia (Grant No.172044) is gratefully acknowledged.*

REFERENCES

1. V. Pavlovic, A. Djordjevic, E. Cherneva, D. Yancheva, A. Smelcerovic, *Food Chem. Toxicol.*, **50**, 761 (2012).
2. D. Yancheva, L. Daskalova, E. Cherneva, B. Mikhova, A. Djordjevic, Z. Smelcerovic, A. Smelcerovic, *J. Mol. Struct.*, **1016**, 147(2012).
3. M. Iijima, T. Masuda, H. Nakamura, H. Naganawa, S. Kurasawa, Y. Okami, M. Ishizuka, T. Takeuchi, Y. Iitaka, *J. Antibiot.*, **45**, 1553 (1992).
4. V. Pavlovic, E. Cherneva, D. Yancheva, A. Smelcerovic, *Food Chem. Toxicol.*, **50**, 3014 (2012).
5. T. Kagamizono, E. Nishino, K. Matsumoto, A. Kawashima, M. Kishimoto, N. Sakai, B. M. He, Z. X. Chen, T. Adachi, S. Morimoto, K. Hanada, *J. Antibiot.*, **48**, 1407 (1995).
6. K. Hasumi, C. Shinohara, T. Iwanaga, A. Endo, *J. Antibiot.*, **46**, 1782 (1993).
7. A. Arcelli, D. Balducci, A. Grandi, G. Porzi, M. Sandri, S. Sandri, *Monatsh. Chem.*, **135**, 951 (2004).

8. A. Arcelli, D. Balducci, A. Grandi, G. Porzi, M. Sandri, S. Sandri, *Tetrahedron: Asymmetry*, **16**, 1495 (2005).
9. A. Arcelli, D. Balducci, S. F. E Neto, G. Porzi, M. Sandri, *Tetrahedron: Asymmetry*, **18**, 562 (2007).
10. A. Smelcerovic, M. Rangelov, Z. Smelcerovic, A. Veljkovic, E. Cherneva, D. Yancheva, G. M. Nikolic, Z. Petronijevic, G. Kocic, *Food Chem. Toxicol.*, **55**, 493 (2013).
11. A. Smelcerovic, D. Yancheva, E. Cherneva, Z. Petronijevic, M. Lamshoeft, D. Herebian, *J. Mol. Struct.*, **985**, 397 (2011).
12. V. Stankov-Jovanovic, J. C. Tabet, P. Dzodic, L. Daskalova, E. Cherneva, D. Yancheva, A. Smelcerovic, *Acta Chim. Slov.*, **59**, 939 (2012).
13. E. Klein, V. Lukes, M. Ilcin, *Chem. Phys.*, **336**, 51 (2007).
14. G. W. Burton, T. Doba, E. J. Gabe, L. Hughes, F. L. Lee, L. Prasad, K. U. Ingold, *J. Am. Chem. Soc.*, **107**, 7053 (1985).
15. M. I. de Heer, P. Mulder, H. Korth, K. U. Ingold, J. Luszyk, *J. Am. Chem. Soc.*, **122**, 2355 (2000).
16. J. S. Wright, E. R. Johnson, G. A. DiLabio, *J. Am. Chem. Soc.*, **122**, 1173. (2001).
17. M. Musialik, G. Litwinienko, *Org. Lett.*, **7**, 4951 (2005).
18. A. P. Vafiadis, E. G. Bakalbassis, *Chem. Phys.*, **316**, 195 (2005).
19. J. Rimarcik, V. Lukes, E. Klein, M. Ilcin, *J. Mol. Struct. (Theochem)*, **952**, 25 (2010).
20. M. Musialik, R. Kuzmicz, T. S. Pawlowski, G. Litwinienko, *J. Org. Chem.*, **74**, 2699 (2009).
21. M. J. Frisch, G. W. Trucks, H. B. Schlegel, G. E. Scuseria, M. A. Robb, J. R. Cheeseman, G. Scalmani, V. Barone, B. Mennucci, G. A. Petersson, H. Nakatsuji, M. Caricato, X. Li, H. P. Hratchian, A. F. Izmaylov, J. Bloino, G. Zheng, J. L. Sonnenberg, M. Hada, M. Ehara, K. Toyota, R. Fukuda, J. Hasegawa, M. Ishida, T. Nakajima, Y. Honda, O. Kitao, H. Nakai, T. Vreven, J. A. Montgomery, Jr., J. E. Peralta, F. Ogliaro, M. Bearpark, J. J. Heyd, E. Brothers, K. N. Kudin, V. N. Staroverov, R. Kobayashi, J. Normand, K. Raghavachari, A. Rendell, J. C. Burant, S. S. Iyengar, J. Tomasi, M. Cossi, N. Rega, J. M. Millam, M. Klene, J. E. Knox, J. B. Cross, V. Bakken, C. Adamo, J. Jaramillo, R. Gomperts, R. E. Stratmann, O. Yazyev, A. J. Austin, R. Cammi, C. Pomelli, J. W. Ochterski, R. L. Martin, K. Morokuma, V. G. Zakrzewski, G. A. Voth, P. Salvador, J. J. Dannenberg, S. Dapprich, A. D. Daniels, O. Farkas, J. B. Foresman, J. V. Ortiz, J. Cioslowski, and D. J. Fox, Gaussian 09, Revision A.1, Gaussian Inc., Wallingford CT, 2009.
22. S. F. Nelsen, M. N. Weaver, J. I. Zink, J. P. Telo, *J. Am. Chem. Soc.*, **127**, 10611 (2005).
23. J. Tomasi, B. Mennucci, E. Cancès, *J. Mol. Struct. (THEOCHEM)*, **464**, 211 (1999).
24. J. Rimarčič, V. Lukeš, E. Klein, M. Ilčin, *J. Mol. Struct. (Theochem.)*, **952**, 25 (2010).
25. A. E. Reed, L. A. Curtiss, F. Weinhold, *Chem. Rev.*, **88**, 899 (1988).
26. J. E. Carpenter, F. Weinhold, *J. Mol. Struct. (Theochem)*, **46**, 41 (1988).
27. F. Weinhold, J. E. Carpenter, in: *The Structure of Small Molecules and Ions*, R. Naaman, Z. Vager (eds), Plenum, 1988, p. 227.
28. A. Smelcerovic, P. Dzodic, V. Pavlovic, E. Cherneva, D. Yancheva, *Amino Acids*, **46**, 825 (2014).
29. J. Berkowitz, G. B. Ellison, D. Gutman, *J. Phys. Chem.*, **98**, 2744 (1994).
30. P. Xu, T. P. Huecksteadt, J. R. Hoidal, *Genomics*, **34**, 173 (1996).
31. J. S. McNally, A. Saxena, H. Cai, S. Dikalov, D. G. Harrison, *Arterioscler. Thromb. Vasc. Biol.*, **25**, 1623 (2005).
32. E. D. Hall, P. K. Andrus, S. L. Smith, T. J. Fleck, H. M. Scherch, B. S. Lutzke, G. A. Sawada, J. S. Althaus, P. F. Vonvoigtlander, G. E. Padbury, P. G. Larson, J. R. Palmer, G. L. Bundy, *J. Pharmacol. Exp. Ther.*, **281**, 895 (1997).
33. J. Zvezdanovic, L. Daskalova, D. Yancheva, D. Cvetkovic, D. Markovic, M. Anderluh, A. Smelcerovic, *Monatsh. Chem.*, **145**, 945 (2014).
34. Z. Marković, D. Milenković, J. Đorović, J. M. Dimitrić Marković, V. Stepanić, B. Lučić, D. Amić, *Food Chem.*, **135**, 2070 (2012).
35. E. Wilhelm, R. Battino, *Chem. Rev.*, **73**, 1 (1973).

ВЛИЯНИЕ НА ОБКРЪЖАВАЩАТА СРЕДА ВЪРХУ АНТИОКСИДАНТНОТО ДЕЙСТВИЕ НА ДВА 6-(ПРОПАН-2-ИЛ)-4-МЕТИЛ-МОРФОЛИН-2,5-ДИОНА

Д. Янчева^{1*}, С. Стоянов¹, Б. Стамболийска¹, Л. Даскалова¹, Е. Чернева², А. Шмелцерович³

¹Институт по Органична химия с Център по Фитохимия, Българска Академия на Науките, ул. Акад. Г. Бончев, бл. 9, 1113 София, България

²Фармацевтичен Факултет, Медицински Университет - София, ул. Дунав 2, 1000 София, България

³Факултет по медицина, Университет - Ниш, бул. Д-р Зоран Джинджич 81, 18000 Ниш, Сърбия

Постъпила на 21 май 2014 г.; Коригирана на 11 август 2014 г.

(Резюме)

Теорията на плътностния функционал беше използвана за изследване на дикето и енолни форми на два циклодипептида, 3-(2-метилпропил)-6-(пропан-2-ил)-4-метил-морфолин-2,5-дион и 3,6-ди(пропан-2-ил)-4-метил-морфолин-2,5-дион, способни да образуват радикали и да действат като редуктори. Бяха разгледани три възможни механизма на антиоксидантно действие: откъсване на водороден атом (НАТ), пренос на електрон (SET) и отделяне на протон, последвано от пренос на електрон (SPLET). Влиянието на полярността на средата беше изследвано чрез определяне на съответните енталпии на дисоциация (BDE), йонизационни потенциали (IP), енталпии на дисоциация на протона (PDE), протонни афинитети (PA) и енталпии на електронния пренос (ETE) в неполярен разтворител бензен и полярни разтворители вода и метанол. Предпочетеният механизъм в различните обкръжения беше изяснен на базата на получените енталпии. Резултатът показва, че реакционният път зависи от полярността на средата. Откъсването на водороден атом е най-вероятният процес в неполярна среда, докато в полярна среда предпочетен механизъм е отделянето на протон, последвано от пренос на електрон.

DFT/B3LYP calculated bond-dissociation enthalpies, radical-scavenging and antioxidant activities of natural-like coumarins

S. E. Angelova^{1*}, A. K. Slavova-Kazakova¹, L. Saso², S. Malhotra^{3,4}, A. K. Prasad³, M. E. Bracke⁵, V. S. Parmar^{3,5}, V. D. Kancheva¹

¹*Institute of Organic Chemistry with Centre of Phytochemistry, Bulgarian Academy of Sciences, Acad. G. Bonchev str., bl. 9, 1113 Sofia, Bulgaria*

²*Department of Human Physiology and Pharmacology "Vittorio Erspamer", University of Rome "La Sapienza", 00185 Rome, Italy*

³*Bioorganic Laboratory, Department of Chemistry, University of Delhi, 110 007 Delhi, India*

⁴*Institut für Chemie und Biochemie, Freie Universität Berlin, 14195 Berlin, Germany*

⁵*Laboratory of Experimental Cancer Research, University Hospital, University of Gent, B-9000 Gent, Belgium*

Received May 28, 2014; Revised August 04, 2014

Dedicated to Acad. Dimiter Ivanov on the occasion of his 120th birth anniversary

Bond dissociation enthalpies (BDEs) of O-H groups of a set of hydroxy- and dihydroxy-4-methylcoumarins have been calculated in gas phase and in acetone by means of density functional theory calculations at B3LYP/6-31+G(d,p) level. The study has been done to determine the capacity of bond-dissociation enthalpy to explain the observed radical-scavenging and chain-breaking antioxidant activities of the studied coumarins. DPPH radical scavenging activity (RSA) in acetone solution [as %RSA and stoichiometry coefficient (n) for the fast (2 min) and total (20 min) kinetics] and the chain-breaking antioxidant activity (as protection factor, PF) during bulk phase lipid autoxidation have been used in the experimental study. The experimental results for the studied compounds show that the two phenolic groups at *ortho* position work in tandem, while the same at *meta* position work independent of each other. According to the theoretical results, the substitution in the benzene ring of the coumarin system is very important for the chain-breaking antioxidant activity. At the same time, theoretical calculations reveal that the introduction of methyl group and/or various substituents at the C-3 and C-4 positions of the pyrone ring affects the BDEs insignificantly. Interestingly, the radical scavenging activity towards DPPH radical of 7,8-dihydroxy-4-methylcoumarins are much higher than that of the 6,7-dihydroxy-4-methylcoumarins, 5,7-dihydroxy-4-methylcoumarin and 7-hydroxy-4-methylcoumarin. Differences in RSA of studied coumarins could be explained with the solvent effect of acetone. Our findings revealed that BDE can serve as a probe for radical scavenging and antioxidant activities and even have predictive capacity, but for some tiny effects a precise description of the solvent effects is required.

Key words: coumarins, hydroxycoumarins, DFT, bond-dissociation enthalpy, chain-breaking antioxidant activity, radical-scavenging activity

INTRODUCTION

In nature, coumarins are abundantly found in plants and are formed via the shikimate pathway [1,2]. Natural coumarins and their synthetic analogues manifest a wide range of activities such as anticoagulant, antitumor, antiviral, anti-inflammatory, antimicrobial, antioxidant (radical-scavenging), and enzyme inhibition activity [3-6]. The presence of different substituents on the coumarin ring system strongly influences the antioxidant and biological activities of the resulting derivatives [5,7]. The pharmacological applications of coumarins are limited by the tendency to form mutagenic

and toxic C-3, C-4 coumarin epoxide intermediates during their metabolic degradation [8,9]. Introduction of methyl group at the C-4 position is a possible way to prevent formation of these dangerous C-3, C-4 epoxides during the metabolic degradation of the coumarins [10]. In a detailed investigation of the structure-activity relationship of dihydroxy-4-methylcoumarins by Kancheva *et al.* [11], the effects of the substituents in both rings of the coumarin system have been substantiated: the substituents in the benzene ring are responsible for the antioxidant activity of the studied hydroxy-4-methylcoumarins, while the effect of substituents in the pyrone ring (at positions C-3 and C-4) is insignificant for the biological activity.

In the present study, a set of coumarin derivatives has been selected in order to correlate

* To whom all correspondence should be sent:
E-mail: sea@orgchem.bas.bg

the structural differences with alternations in the radical scavenging and chain-breaking antioxidant activities (taking in mind the above mentioned parameters) by means of DFT calculation. The following structural modifications have been taken into consideration: number and positions of the OH-groups, presence or absence of the methyl group at the C-4 position and different substituents at the C-3 position. The chief emphasis of our investigation has been towards the direct hydrogen atom transfer between the antioxidant and the active radical. The descriptor related to this mechanism is the bond-dissociation enthalpy (BDE). The theoretical (*ab initio* and DFT) calculations are helpful in the explanation of the structure-activity relationship [9,12,13]. Successful applications of BDE on polyphenolic compounds as theoretical descriptors of antioxidant activity/efficiency has already been reported by us [14,15]. It is well known that the antioxidant power of phytochemicals (including coumarins), as well as other biochemical properties, depend not only on the

substitution in the parent molecule(s), but also on the reaction medium and from the nature of the involved free radicals/reactive species [16]. Therefore, the structure-activity relationship needs to be explored in different environments. Taking into account the report of Yordanov [17] about the higher stability of DPPH radical in acetone solution than in ethanol, the DPPH test was run in acetone solution. Chain-breaking antioxidant activity of the studied coumarins was tested during bulk phase lipid autoxidation.

EXPERIMENTAL AND COMPUTATIONAL DETAILS

Chemicals

All coumarins used in the experimental study (Fig. 1, Table 1) were synthesized and characterized at the Department of Chemistry, University of Delhi, Delhi as described previously [18-21]. DPPH was purchased from Sigma-Aldrich.

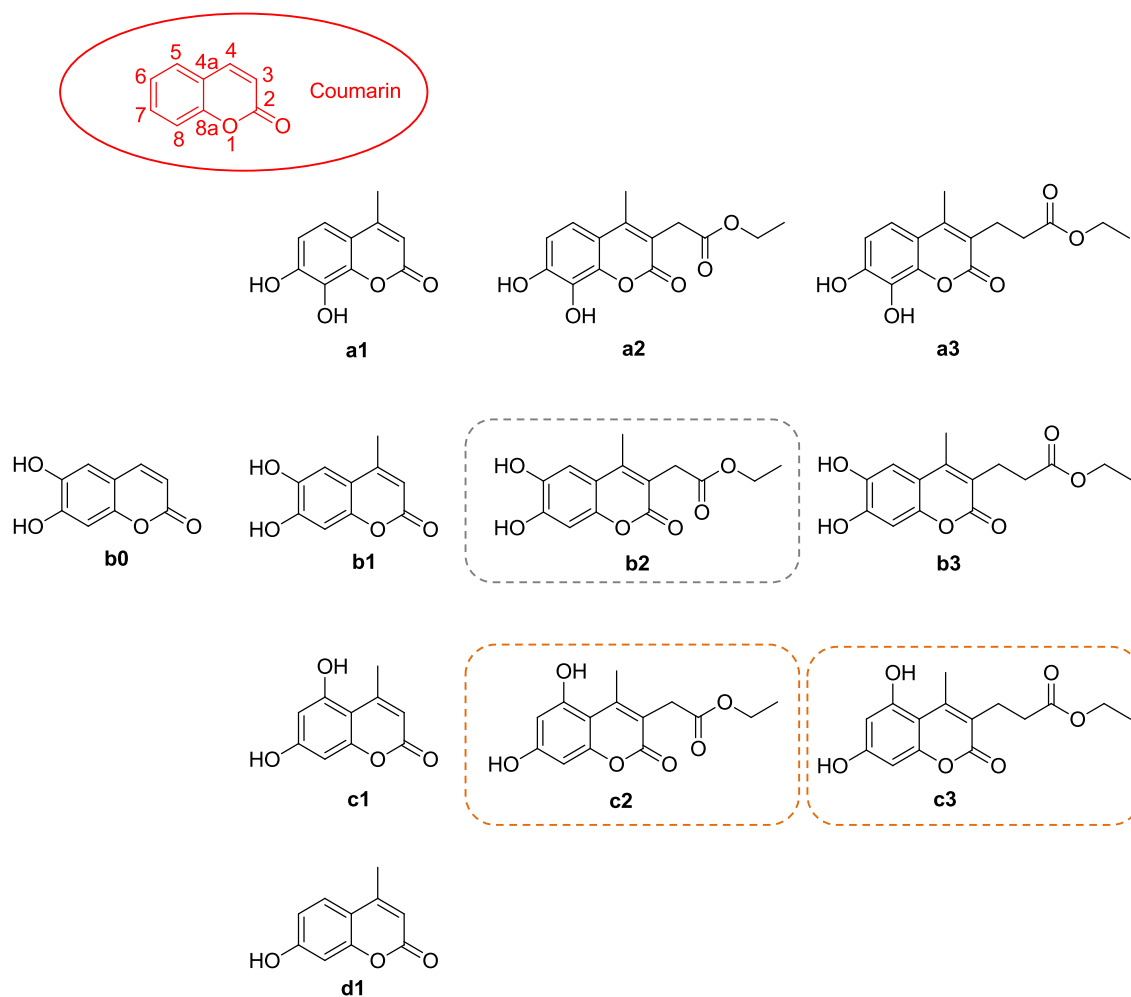


Fig. 1. Structures of coumarin and compounds **a1-a3**, **b0-b3**, **c1-c3**, **d1**. In rounded rectangle boxes are structures of the compounds for which only theoretical data are available (grey box) or for which experimental results are derived after theoretical predictions (orange boxes).

Table 1. Compound names.

Coumarin	2H-chromen-2-one
a1	7,8-dihydroxy-4-methyl-2H-chromen-2-one
a2	ethyl 2(7,8-dihydroxy-4-methyl-2-oxo-2H-chromen-3-yl)acetate
a3	ethyl 3-(7,8-dihydroxy-4-methyl-2-oxo-2H-chromen-3-yl)propanoate
b0	6,7-dihydroxy-2H-chromen-2-one
b1	6,7-dihydroxy-4-methyl-2H-chromen-2-one
b2	ethyl 2(6,7-dihydroxy-4-methyl-2-oxo-2H-chromen-3-yl)acetate
b3	ethyl 3-(6,7-dihydroxy-4-methyl-2-oxo-2H-chromen-3-yl)propanoate
c1	5,7-dihydroxy-4-methyl-2H-chromen-2-one
c2	ethyl 2(5,7-dihydroxy-4-methyl-2-oxo-2H-chromen-3-yl)acetate
c3	ethyl 3-(5,7-dihydroxy-4-methyl-2-oxo-2H-chromen-3-yl)propanoate
d1	7-hydroxy-4-methyl-2H-chromen-2-one

Screening for free radical scavengers by DPPH test

Kinetics of DPPH absorbance decrease for a quantitative determination of radical scavenging activity at the ratio antioxidant (AH) and DPPH $[AH]/[DPPH] = 0.40$ and physiological temperature 37°C was studied. For experimental details, please see ref.10. The main kinetic parameters for the fast kinetics ($\Delta t=2$ min) $\%RSA_{\text{fast}}$ and n_{fast} and for the total kinetics ($\Delta t=20$ min) $\%RSA_{\text{tot}}$ and n_{tot} were determined by the following formulae:

$$\%RSA = [(Abs_0 - Abs_t)/Abs_0] \times 100,$$

$$n = [(Abs_0 - Abs_t)]/\varepsilon[AH],$$

where: Abs_0 and Abs_t stay for the DPPH absorption at 517 nm for time $t=0$ and $t=2$ min (fast kinetics) or $t=20$ min (total kinetics), n is the stoichiometric coefficient, meaning how many DPPH radicals were trapped from 1 molecule of AH, molar extinction coefficient $\varepsilon = 1.2 \times 10^4 \text{ M}^{-1}\text{s}^{-1}$.

Chain-breaking antioxidant activity of coumarins under study presented as protection factor (PF), means how many times the added antioxidant AH can increase the oxidation stability of lipid substrate was studied as described in our earlier publication [11]. Here we report new data about **a₃** and **b₃** coumarins.

Computational details

As a descriptor of antiradical/antioxidant activity, calculated homolytic bond dissociation enthalpy (BDE) was utilized. B3LYP calculations were chosen for this study because this functional provides reliable geometries, frequencies, and bond lengths [22]. The geometries of compounds studied and their radicals were optimized using unrestricted open-shell approach (UB3LYP) and 6-31+G(d,p) basis set [23-25] without symmetry constraints with

the default convergence criteria. Frequency calculations at the same level of theory were carried out to confirm that the obtained structures correspond to energy minima. Unscaled thermal corrections to enthalpy were added to the total energy values. The BDEs for the generation of the respective radicals from the parent compounds are calculated by the formula $BDE = H_{298}(A\bullet) + E_T(H\bullet) - H_{298}(AH)$ where $H_{298}(A\bullet)$ and $H_{298}(AH)$ are enthalpies calculated at 298 K for radical species $A\bullet$ and neutral molecule AH, respectively, and $E_T(H\bullet)$ (calculated total energy of $H\bullet$) is $-313.93 \text{ kcal mol}^{-1}$. In order to take into account the solvent effect, the integral equation formalism (IEF) of the polarizable continuum model (PCM) [26-28] was employed for acetone and all the structures were optimized in this surrounding environment. All quantum chemical calculations were carried out using GAUSSIAN 09 program package [29].

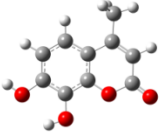
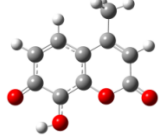
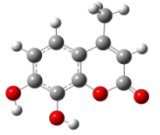
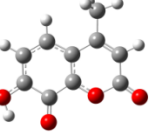
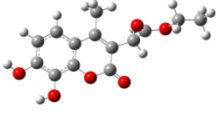
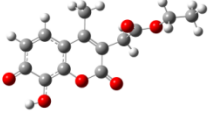
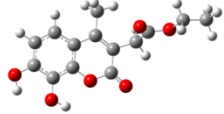
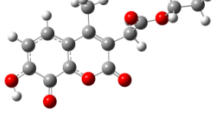
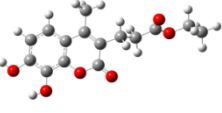
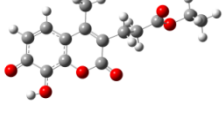
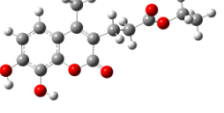
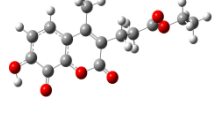
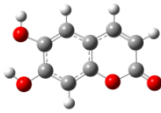
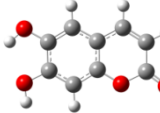
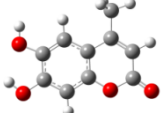
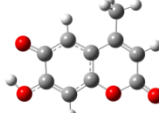
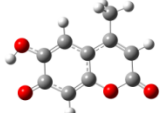
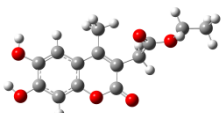
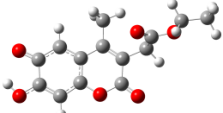
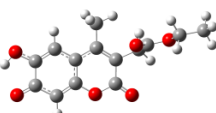
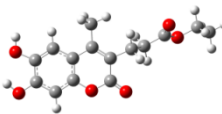
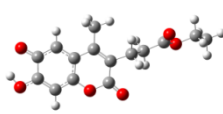
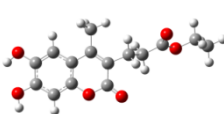
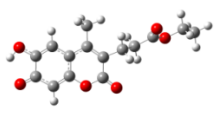
RESULTS AND DISCUSSION

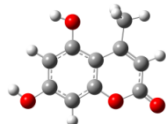
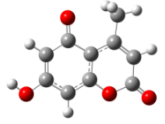
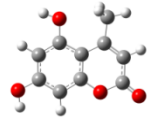
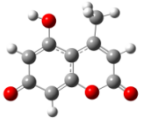
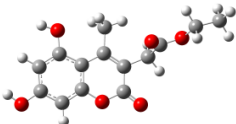
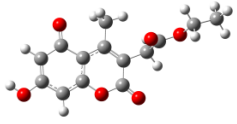
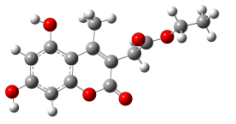
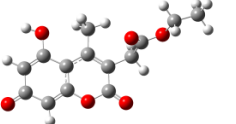
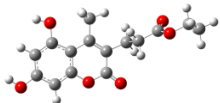
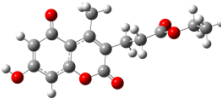
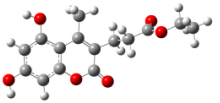
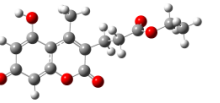
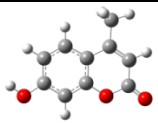
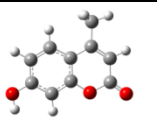
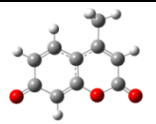
UB3LYP/6-31+G(d,p) calculated enthalpies (H_{298}) at 298 K, enthalpy differences (ΔH_{298}) between rotamers of the compounds studied and their radicals and bond dissociation enthalpy (BDE) in gas phase and in solvent acetone are listed in Table 2. For the coumarins belonging to group **a** and **b**, only rotamers with intramolecular hydrogen bonds are studied. These rotamers differ in the position of the hydrogen atoms from the hydroxyl groups in the coumarin moiety. The structures of the denoted "rotamers 1 & 2" are shown in Table 2. Two rotamers of compounds from group **c** with different orientation of the OH hydrogen atoms in position 7 are also considered. In gas phase the following relations can be noticed: for all the compounds, rotamer 2 is more stable than rotamer 1, and the BDEs of the radicals formed from this rotamer are considered (in spite of the lower BDE values characterizing the radical, formed from rota-

mer 1). The enthalpy difference between the rotamers of group **a** compounds is about 5 kcal mol⁻¹,

of group **c** compounds is about 1 kcal mol⁻¹, while rotamers of group **b** compounds have almost equal

Table 2. UB3LYP/6-31+G(d,p) calculated enthalpies (H_{298}) at 298 K (in Hartree), enthalpy differences (ΔH_{298}) between rotamers of compounds studied and their radicals (in kcal mol⁻¹) and bond dissociation enthalpy (BDE) (in kcal mol⁻¹). The values in acetone are given in parentheses.

	Rotamer 1	Radical 1: 7(7,8)	Rotamer 2	Radical 2: 8(7,8)
a1	 $H_{298}=-686.645831$ (-686.661963) $\Delta H_{298}=5.50$ (1.86)	 $H_{298}=-686.028641$ (-686.041754) BDE=73.37 (75.26)	 $H_{298}=-686.654589$ (-686.664920) $\Delta H_{298}=0.00$ (0.00)	 $H_{298}=-686.030393$ (-686.044250) BDE=77.76 (75.54)
a2	 $H_{298}=-993.064035$ (-993.081013) $\Delta H_{298}=5.26$ (1.94)	 $H_{298}=-992.447700$ (-992.461856) BDE=72.83 (74.59)	 $H_{298}=-993.072418$ (-993.084112) $\Delta H_{298}=0.00$ (0.00)	 $H_{298}=-992.448975$ (-992.464084) BDE=77.29 (75.14)
a3	 $H_{298}=-1032.352843$ (-1032.369799) $\Delta H_{298}=5.18$ (2.86)	 $H_{298}=-1031.736581$ (-1031.752441) BDE=72.78 (73.47)	 $H_{298}=-1032.361095$ (-1032.37436) $\Delta H_{298}=0.00$ (0.00)	 $H_{298}=-1031.737713$ (-1031.754311) BDE=77.25 (75.15)
	Rotamer 1	Radical 1: 6(6,7)	Rotamer 2	Radical 2: 7(6,7)
b0	 $H_{298}=-647.357275$ (-647.371649) $\Delta H_{298}=0.06$ (0.00)	 $H_{298}=-646.741251$ (-646.751778) BDE=72.63 (75.04)	 $H_{298}=-647.357375$ (-647.371162) $\Delta H_{298}=0.00$ (0.31)	 $H_{298}=-646.740335$ (-646.751314) BDE=73.21 (75.33)
b1	 $H_{298}=-686.650881$ (-686.665921) $\Delta H_{298}=0.26$ (0.00)	 $H_{298}=-686.035698$ (-686.046682) BDE=72.11(74.65)	 $H_{298}=-686.651300$ (-686.665549) $\Delta H_{298}=0.00$ (0.23)	 $H_{298}=-686.034081$ (-686.045675) BDE=73.38 (75.04)
b2	 $H_{298}=-993.069272$ (-993.084718) $\Delta H_{298}=0.12$ (0.00)	 $H_{298}=-992.454061$ (-992.466346) BDE=72.12 (74.10)	 $H_{298}=-993.069462$ (-993.084623) $\Delta H_{298}=0.00$ (0.06)	 $H_{298}=-992.453109$ (-992.465771) BDE=72.84 (74.40)
b3	 $H_{298}=-1032.357886$ (-1032.375617) $\Delta H_{298}=0.21$ (0.00)	 $H_{298}=-1031.742831$ (-1031.756799) BDE=72.03 (74.38)	 $H_{298}=-1032.358213$ (-1032.375137) $\Delta H_{298}=0.00$ (0.30)	 $H_{298}=-1031.742023$ (-1031.756515) BDE=72.74 (74.26)

	Rotamer 1	Radical 1: 5(5,7)	Rotamer 2	Radical 2: 7(5,7)
c1	 $H_{298} = -686.647224$ (-686.661877) $\Delta H_{298} = 1.15$ (0.27)	 $H_{298} = -686.022300$ (-686.034022) BDE=78.22 (80.05)	 $H_{298} = -686.649058$ (-686.662311) $\Delta H_{298} = 0.00$ (0.00)	 $H_{298} = -686.016344$ (-686.029859) BDE=81.96 (82.67)
c2	 $H_{298} = -993.064037$ (-993.081188) $\Delta H_{298} = 1.13$ (0.26)	 $H_{298} = -992.440251$ (-992.454364) BDE=77.51 (79.41)	 $H_{298} = -993.065837$ (-993.08161) $\Delta H_{298} = 0.00$ (0.00)	 $H_{298} = -992.434172$ (-992.449879) BDE=81.32 (82.22)
c3	 $H_{298} = -1032.352611$ (-1032.369611) $\Delta H_{298} = 1.12$ (0.29)	 $H_{298} = -1031.729210$ (-1031.74345) BDE=77.26 (78.99)	 $H_{298} = -1032.354388$ (-1032.370074) $\Delta H_{298} = 0.00$ (0.00)	 $H_{298} = -1031.723117$ (-1031.739294) BDE=81.09 (81.60)
	Rotamer 1		Rotamer 2	Radical: 7
d1	 $H_{298} = -611.431360$ (-611.443368) $\Delta H_{298} = 0.44$ (0.03)		 $H_{298} = -611.432056$ (-611.443410) $\Delta H_{298} = 0.00$ (0.00)	 $H_{298} = -610.799536$ (-610.811495) BDE=82.55 (82.57)

enthalpies ($\Delta H_{298} = 0.06 \div 0.21$ kcal mol⁻¹). For **d1** the difference is also very low – 0.44 kcal mol⁻¹. In acetone medium the enthalpy difference between the rotamers of the compounds from **a** and **c** groups decreases but with different scale, the rotamers 1 of group **b** are preferred with very low ΔH_{298} ($0.06 \div 0.31$ kcal mol⁻¹), for **d1** both rotamers are isoenergetic ($\Delta H_{298} = 0.03$ kcal mol⁻¹). It can be concluded that the addition of acetone (as surrounding environment) equalize the BDEs for both OH-groups of the dihydroxy compounds as for compounds **c** this trend is not so strong.

The BDEs for the preferred rotamers of compounds **a1-a3**, **c1-c3**, both rotamers of compounds from **b** group and of **d1** are presented graphically on Fig. 2. The values in gas phase and in acetone are compared. In gas phase compounds from **b** group are characterized with the lowest BDE values, followed by **a** group with higher BDEs, while the compounds with OH-groups in positions 5,7 (**c1-c3**) and with one OH group (**d1**) are with highest BDEs. The substituent in position 3 does not affect ($BDE_{6(6,7)}$) or affect weakly the BDEs, as in almost all cases (exception – group **c**) the lengthening of substituent's chain in this

position leads to lower BDE values. When the solvent is taken into account, the BDEs of compounds **a1-a3** decrease, the BDE of **d1** is not affected, while the BDEs of compounds **b** and **c** increase (exception - **c2**). As a result, the BDEs of **a** and **b** groups are equalized in acetone medium, but the separation of compounds in two groups (with and without catechol moiety) is preserved, i. e. the BDE values of **a** and **b** groups remain lower than those of **c** and **d** groups. The observed tendency is in accordance with the conclusion of Zhang *et al.* that the catechol moiety in the coumarins is a beneficial structural factor that reduces BDE and the coumarins with this fragment are strong antioxidants [13].

The effect of the CH₃-group on the BDE can be estimated from the comparison of the BDEs of **b0** and **b1**. The presence of CH₃-group at position 4 in the tested coumarins does not act equally on both the OH-groups in gas phase: **b0** is characterized with higher $BDE_{6(6,7)}$ and lower $BDE_{7(6,7)}$ in comparison to **b1**, while in acetone both OH-groups of **b1** have lower BDEs than **b0**.

The BDE of the more stable rotamers (respectively in gas phase and in solvent acetone)

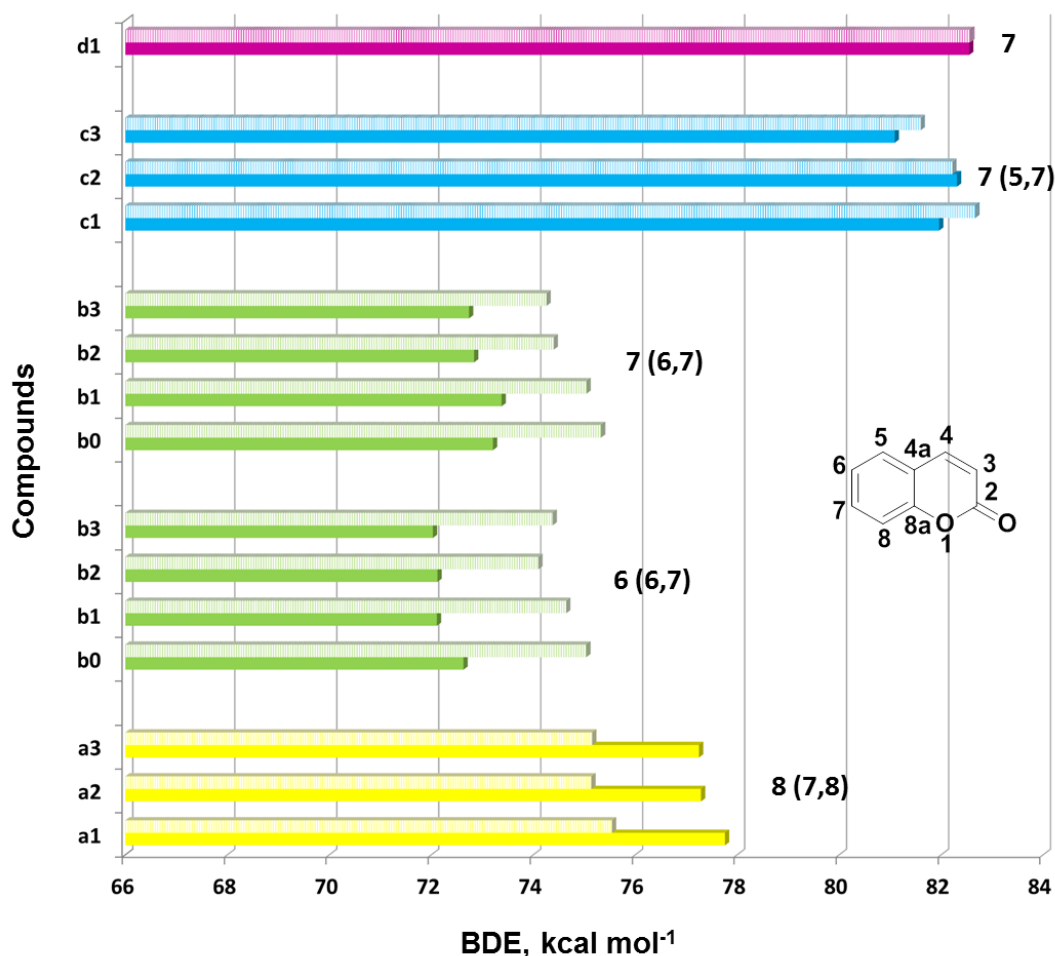


Fig. 2. Selected BDEs (in kcal mol⁻¹) in gas phase (solid fill) and in acetone (pattern fill). The position of OH group from which H atom is abstracted and the positions of OH groups in the coumarin main structure (in parentheses) are denoted.

Table 3. Theoretical parameters (BDE in gas phase and in acetone) and the main experimental kinetic parameters: antioxidant efficiency, presented as a protection factor (PF) during lipid autoxidation, % RSA and stoichiometry (n) for the fast (t=2 min) and total (t=20 min) kinetics of DPPH radical absorption decrease at 516-517 nm.

	BDE (gas phase), kcal mol ⁻¹	PF	BDE (acetone) kcal mol ⁻¹	RSA _{fast} , %	n _{fast} , M ⁻¹ s ⁻¹	RSA _{tot} , %	n _{tot} , M ⁻¹ s ⁻¹
a1	77.76	1.3	75.54	35.8	0.9	49.1	1.1
a2	77.29	1.5	75.14	-	-	-	-
a3	77.25	1.4	75.15	48.8	1.2	64.2	1.6
b0	73.21 ^a	3.7	75.04 ^b	-	-	-	-
b1	73.38 ^a	3.4	74.65 ^b	16.3	0.4	17.3	0.4
b3	72.74 ^a	3.4	74.38 ^b	18.6	0.5	21.2	0.5
c1	81.96	1.2	82.67	3.0	0.1	3.0	0.1
c2	81.32	1.2	82.22	-	-	-	-
c3	81.09	1.1	81.60	-	-	-	-
d1	82.55	1.0	82.57	2.2	0.1	2.2	0.1

^a - BDE 7(6,7); ^b - BDE 6(6,7).

for each structure is compared to the experimentally derived data in Table 3. The presented experimental data are chain-breaking antioxidant activity (as PF) and DPPH scavenging (as %RSA and \underline{n}) for the fast

and total kinetics. The protection factors (PF) of **b0**, **b1** and **b3** are in the range 3.4-3.7 while the rest of compounds are characterized with values in the range of 1.0-1.5, i.e. compounds from **b**-group have

the highest antioxidant efficiency during lipid autoxidation. The gas phase calculated BDEs are in agreement with these results: the compounds with high PF have low BDE values and *vice versa*. The coumarins from group **a** (**a3** and **a1**) demonstrate strong RSA (%RSA > 40%), coumarins from group **b** (**b1** and **b3**) – moderate RSA (15% < %RSA < 40%), **c1** and **d1** – weak RSA (%RSA < 15%). The much lower value of %RSA for **c1** (*meta*-dihydroxy-coumarin) than *ortho*-dihydroxy-coumarins is not unforeseen considering the position of OH groups. The OH groups of compound **c** react individually with DPPH radical, not in tandem (like *ortho*-dihydroxy-coumarins) and %RSA is close to the value for the mono-hydroxycoumarin (**d1**). The compounds from **b** group are characterized with lower %RSA_{tot} values (17.3 and 21.2) than those from **a** group (41.9 and 64.2) in spite of the *ortho* positioning of the OH-groups in all of them. The BDEs in acetone for both groups **a** and **b** of *ortho*-dihydroxy-coumarins are close, all values being in the range of 74.38-75.54 kcal mol⁻¹. The failure of the calculations to distinguish these groups could be explained with the incomplete description of the solvent-solute interactions by the model used (PCM). The difference in the RSAs of compounds from **a** and **b** groups is probably due to the formation of different active intermediates from 7,8-diOH and 6,7-diOH, which react with different rates with DPPH. Monophenolic coumarin **d1** in the cross-recombination reaction form inactive products. *Meta*-dihydroxy coumarin reacts as two mono-phenolic antioxidants. Each OH-group reacts individually (not in tandem as *ortho*-substituted) and thus the formation of active intermediates cannot increase their RSA. *Meta*-dihydroxy coumarin **c1** shows RSA close to that of the monophenolic coumarin and much lower than that of *ortho*-dihydroxycoumarins. The stoichiometric coefficients n_{tot} for *ortho*-dihydroxycoumarins (group **b**) are lower than 1 (0.4 and 0.5 for **b1** and **b3** respectively) and much lower for **c1** and **d1** ($n_{tot} =$

0.1). Compounds **a1** and **a3** are characterized with different stoichiometric coefficients $n_{tot} - 1.1$ and $1.6 \text{ M}^{-1}\text{s}^{-1}$. The proposed mechanisms which explain the different values of the experimentally derived stoichiometry coefficient for **a1** and **a3** are listed in Table 4. One molecule **a1** can trap one DPPH radical ($n = 1$), while one molecule **a3** can trap 1.5 DPPH radicals ($n = 1.5$).

DFT calculated BDEs in gas phase and in acetone are able to distinguish the effects of the substituents at positions 3 and 4, but failed in the description of the activity of the systems sensible to the solvent effects (*ortho*-dihydroxy-coumarins from **a** and **b** groups).

CONCLUSION

In this study, the power (capacity) of DFT calculations for the explanation of radical-scavenging and antioxidant activities of mono- and dihydroxycoumarins is tested. A relatively good correlation between antioxidant efficiency (PF) of lipid autoxidation and O-H BDEs in gas phase is found. The studied hydroxycoumarins are divided into three groups: strong (PF=3.4-3.7, BDE=72.74-73.21 kcal mol⁻¹), moderate (PF=1.3-1.5, BDE=77.25-77.76 kcal mol⁻¹) and weak antioxidants (PF=1.0-1.2, BDE=81.96-82.55 kcal mol⁻¹), i.e. the compounds with high PF have low BDE values and *vice versa*. We observed that in acetone BDE values are grouped into two groups: 1) *ortho*-dihydroxy-coumarins **a1-a3** and **b0-b3** (BDE=74.10-75.54 kcal mol⁻¹) and 2) *meta*-dihydroxy-coumarins **c1-c3** and monohydroxy-coumarin **d1** (BDE=81.60-82.64 kcal mol⁻¹). Calculated BDEs in acetone for compounds of the series **a** and **b** are close and do not explain the difference in the experimentally derived RSA and stoichiometry coefficient n for the fast and total kinetics of the decreased DPPH radical absorption of the *ortho*-dihydroxycoumarins. We propose that

Table 4. The proposed mechanism of action between DPPH radical and coumarins of group **a** (**a1** and **a3**) for explanation of the experimentally observed total stoichiometry (n_{tot}).

	$n_{tot}, \text{M}^{-1}\text{s}^{-1}$	Mechanism A ₁ H and A ₃ H- the correspond coumarins; A ₁ • and A ₃ •- coumarins', radicals; A-A – unactive dimer	Stoichiometry coefficient for the proposed mechanism
a1	1.1	A ₁ H + DPPH• → A ₁ • + DPPH – H x2; H atom transfer 2 A ₁ • → A ₁ -A ₁ ; homo-recombinaton reaction 2 A₁H + 2DPPH• → 2DPPH – H + A₁-A₁	n = 1
a3	1.6	A ₃ H + DPPH• → A ₃ • + DPPH – H x2; H atom transfer A ₃ • + DPPH• → A ₃ -DPPH; cross-recombination reaction 2 A ₃ • → A ₃ -A ₃ ; homo-recombinaton reaction 2 A₃H + 3DPPH• → 2DPPH – H + A₃-DPPH + A₃-A₃	n = 1.5

DFT calculated BDEs have the potential as a probe for radical scavenging and antioxidant activities but more precise description of the solvent effects where the specific interactions are taken into account is highly recommended and the results must be handled carefully.

Acknowledgements: The authors appreciate the possibility to run DPPH absorbance kinetics on UV-Vis spectrophotometer in the laboratory of Prof. L. Antonov, IOCCP-BAS. Partial financial support by the Project BG051PO001-3.3.06-0025 operative program "Development of human resources" is gratefully acknowledged. The part of the calculations was performed on the computer system installed at IOCCP – BAS with the financial support of the Bulgarian Scientific Fund under Project "MADARA" (RNF01/0110, contract N_DO02-52/2008). V. Parmar was supported by a Grant from EU under its Erasmus Mundus EMA-2 Svaagata Programme.

REFERENCES

1. A. R. Knaggs, *Nat. Prod. Rep.*, **20**, 119 (2003).
2. P. M. Dewick, Chapter 4. The Shikimate Pathway: Aromatic Amino Acids and Phenylpropanoids, Medicinal Natural Products: A Biosynthetic Approach, Second Edition, Wiley, 2002.
3. J. R. Hoult, M. Payá, *Gen. Pharmacol.*, **27**, 713 (1996).
4. K. C. Fylaktakidou, D. J. Hadjipavlou-Litina, K. E. Litinas, D. N. Nicolaidis, *Curr. Pharm. Des.*, **10**, 3813 (2004).
5. F. Borges, F. Roleira, N. Milhazes, L. Santana, E. Uriarte, *Curr. Med. Chem.*, **12**, 887 (2005).
6. I. Kostova, S. Bhatia, P. Grigorov, S. Balkansky, V. S. Parmar, A. K. Prasad, *Curr. Med. Chem.*, **18**, 3929 (2011).
7. D. Egan, R. O'Kennedy, E. Moran, D. Cox, E. Prosser, R. D. Thornes., *Drug Metab. Rev.*, **22**, 503 (1990).
8. H. G. Raj, V. S. Parmar, S. C. Jain, S. Goel, P. Himanshu, S. Malhotra, A. Singh, C. E. Olsen, J. Wengel, *Bioorg. Med. Chem.*, **6**, 833 (1998).
9. A. Barzegar, M. D. Davari, N. Chaparzadeh, N. Zarghami, J. Z. Pedersen, S. Incerpi, L. Saso, A. A. Moosavi-Movahedi, *J. Iranian Chem. Soc.*, **8**, 973-982 (2011).
10. J. Z. Pedersen, C. Oliveira, S. Incerpi, V. Kumar, A. M. Fiore, P. De Vito, A. K. Prasad, S. V. Malhotra, V. S. Parmar, L. Saso, *J. Pharm. Pharmacol.*, **59**, 1721, (2007).
11. V. D. Kancheva, L. Saso, P. V. Boranova, M. K. Pandey, S. Malhorta, J. T. Nechev, A. K. Prasad, M. B. Georgieva, A. L. DePass, V. S. Parmar, *Biochimie*, **92**, 1089 (2010).
12. M. C. Foti, *J. Pharm. Pharmacol.*, **59**, 1673 (2007).
13. H.-Y. Zhang, L.-F. Wang, *J. Mol. Struct. (Theochem)*, **673**, 199 (2004).
14. S. Angelova, V. Kancheva, A. Slavova-Kasakova, L. Saso, G. Delogu, D. Fabbri, M. A. Dettori, M. C. Foti, A. Prasad, V. S. Parmar, 10th Indo-Italian Workshop on Chemistry and Biology of Antioxidants, 9-13 Nov. 2011, Department of Biochemical Sciences, Sapienza University, Rome, Italy, Abstracts, p. 83.
15. S. Angelova, L. Saso, V. Kancheva, A. Slavova-Kasakova, M. Foti, C. Daquino, O. Firuzi, V. Enchev, J. Nechev, Fifth National Pharmaceutical Congress with International Participation, 1-3 April 2011, Hisarya, Bulgaria, Abstracts, p. 31.
16. V. D. Kancheva, in: Phytochemicals and Human Health: Pharmacological and Molecular Aspects, Nova Science Publishers Inc., USA, A. A. Farooqui (ed.), 2012, Chapter I, pp. 1-45.
17. N. D. Yordanov, *Appl. Magn. Reson.*, **10**, 330 (1996).
18. V. Kumar, S. Tomar, R. Patel, A. Yousaf, V. S. Parmar, S. V. Malhorta, *Synth. Commun.*, **38**, 2646 (2008).
19. S. Tomar, PhD Thesis, Department of Chemistry, University of Delhi, 2010.
20. S. S. Bahekar, D. B. Shinde, *Tetrahedron Lett.*, **45**, 7999 (2004).
21. V. S. Parmar, S. Singh, P. M. Boll, *Magn. Reson. Chem.*, **26**, 430 (1988).
22. T. Brinck, M. Haeberlein, M. Jonsson, *J. Phys. Chem.*, **119**, 4239 (1997).
23. W. J. Hehre, R. Ditchfield, J. A. Pople, *J. Chem. Phys.*, **56**, 2257 (1972).
24. T. Clark, J. Chandrasekhar, G. W. Spitznagel, P. v. R. Schleyer, *J. Comp. Chem.*, **4**, 294 (1983).
25. M. J. Frisch, I. A. Pople, J. S. Binkley, *J. Chem. Phys.*, **80**, 3265 (1984).
26. R. Cammi, M. Cossi, J. Tomasi, *J. Chem. Phys.*, **104**, 4611 (1996).
27. R. Cammi, M. Cossi, B. Mennucci, J. Tomasi, *J. Chem. Phys.*, **105**, 10556 (1996).
28. J. Tomasi, R. Cammi, B. Mennucci, C. Cappelli, S. Corni, *Phys. Chem. Chem. Phys.*, **4**, 5697 (2002).
29. M. J. Frisch, G. W. Trucks, H. B. Schlegel, G. E. Scuseria, M. A. Robb, J. R. Cheeseman, G. Scalmani, V. Barone, B. Mennucci, G. A. Petersson, H. Nakatsuji, M. Caricato, X. Li, H. P. Hratchian, A. F. Izmaylov, J. Bloino, G. Zheng, J. L. Sonnenberg, M. Hada, M. Ehara, K. Toyota, R. Fukuda, J. Hasegawa, M. Ishida, T. Nakajima, Y. Honda, O. Kitao, H. Nakai, T. Vreven, J. A. Montgomery, Jr., J. E. Peralta, F. Ogliaro, M. Bearpark, J. J. Heyd, E. Brothers, K. N. Kudin, V. N. Staroverov, R. Kobayashi, J. Normand, K. Raghavachari, A. Rendell, J. C. Burant, S. S. Iyengar, J. Tomasi, M. Cossi, N. Rega, J. M. Millam, M. Klene, J. E. Knox, J. B. Cross, V. Bakken, C. Adamo, J. Jaramillo, R.

Gomperts, R. E. Stratmann, O. Yazyev, A. J. Austin, R. Cammi, C. Pomelli, J. W. Ochterski, R. L. Martin, K. Morokuma, V. G. Zakrzewski, G. A. Voth, P. Salvador, J. J. Dannenberg, S. Dapprich, A. D. Daniels, O. Farkas, J. B. Foresman, J. V. Ortiz, J.

Cioslowski, D. J. Fox, Gaussian 09, Revision A.02, Gaussian, Inc., Wallingford CT, 2009.

DFT/B3LYP ИЗЧИСЛИТЕЛНИ ЕНТАЛПИИ НА ДИСОЦИАЦИЯ НА ВРЪЗКА, РАДИКАЛОВО-УЛОВИТЕЛНА И АНТИОКСИДАНТНА АКТИВНОСТ НА СИНТЕТИЧНИ АНАЛОЗИ НА ПРИРОДНИ КУМАРИНИ

С. Е. Ангелова^{1*}, А. К. Славова-Казакова¹, Л. Сасо², Ш. Малхотра^{3,4}, А. К. Прасад³, М. Е. Браке⁵, В. С. Пармар^{3,5}, В. Д. Кънчева¹

¹Институт по Органична химия с Център по Фитохимия, Българска Академия на Науките, ул. Акад. Г. Бончев, бл. 9, 1113 София, България

²Департамент по физиология на човека и фармакология "Виторио Ерспамер", Университет на Рим, "Ла Сапиенца", 00185 Рим, Италия

³Биоорганична лаборатория, Департамент по химия, Университет на Делхи, 110 007 Делхи, Индия

⁴Институт по химия и биохимия, Свободен университет на Берлин, 14195 Берлин, Германия

⁵Лаборатория за експериментално изследване на рака, Университетска болница, Университет на Гент, В-9000 Гент, Белгия

Постъпила на 28 май 2014 г.; Коригирана на 04 август 2014 г.

(Резюме)

Енталпиите на дисоциация на връзка (ЕДВ) в О-Н групи на серия от хидрокси и дихидрокси-4-метил кумарини са изчислени в газова фаза и в ацетон чрез използване на теория на функционала на плътността на B3LYP/6-31+G(d,p) ниво. Изследването е проведено с цел да се определи способността на енталпиите на дисоциация на връзка да обяснят наблюдаваните радикалоулавяща и прекъсваща окислителната верига антиоксидантна активности на изследваните кумарини. При експерименталното изследване са използвани дифенилпикрилхидразил (ДФПХ) радикалоулавяща активност в разтвор на ацетон [като %RSA и стехиометричен коефициент ρ за бърза (2 мин.) и тотална (20 мин.) кинетика] и прекъсваща окислителната верига антиоксидантна активност (като фактор на стабилизиране, PF) по време на липидно автоокисление в хомогенна среда. Експерименталните резултати за изследваните съединения показват, че двете фенолни групи в *ortho* положение действат съвместно, докато в *meta* положение не зависят една от друга. Според теоретичните данни заместването в бензеновия пръстен на кумариновата система е много важно за прекъсващата окислителната верига антиоксидантна активност. Също така според теоретичните изчисления въвеждането на метилова група и/или други заместители в положение С-4 и С-3 на пириновия пръстен влияе върху ЕДВ незначително. Интересното е, че радикалоулавящата активност (РУА) спрямо ДФПХ радикал на 7,8-дихидрокси-4-метил-кумарините е много по-висока от тази на 6,7-дихидрокси-4-метил-кумарините, 5,7-мета-дихидрокси-4-метил-кумарина и 7-хидрокси-4-метил-кумарина. Разликите в РУА на изследваните съединения вероятно се дължи на влиянието на разтворителя (ацетон). ЕДВ може да се използва като мярка за радикалоулавяща и прекъсваща окислителната верига антиоксидантна активности и има предсказваща способност, но за някои фини ефекти се налага да се отчитат детайлно ефектите на разтворителя.

Metal-ligand interactions in transition metal complexes of glyoxilic acid oxime

I. Georgieva, N. Trendafilova*

Institute of General and Inorganic Chemistry, Bulgarian Academy of Sciences, Acad. G. Bonchev str., bl. 11, 1113 Sofia, Bulgaria

Received April 04, 2014; Revised May 16, 2014

Dedicated to Acad. Dimiter Ivanov on the occasion of his 120th birth anniversary

The simplest derivative of 2-(hydroxyimino)carboxylic acids, glyoxilic acid oxime ($gaoH_2$), was used as a model compound for investigation of the metal-ligand interactions in a series of metal complexes: $Cu(gaoH)_2(H_2O)_2$, $Zn(gaoH)_2(H_2O)_2$, $Co(gaoH)_2(H_2O)_2$, $Ni(gaoH)_2(H_2O)_2$, $[Cd(gaoH)_2(H_2O)_2]H_2O$, $K[Pd(gao)(gaoH)]$ and $K[Pt(gao)(gaoH)]3/4H_2O$. The coordination abilities of the active ligand forms, $gaoH^-$ and gao^{2-} , in gas phase and in solution have been studied and discussed at theoretical level. In agreement with X-ray data for Cu(II), Zn(II), Cd(II), Pt(II) and Pd(II) complexes, the calculations have shown that the most preferred binding is the bidentate one through the carboxylic oxygen and the oxime nitrogen atoms (M- $gaoH(N,O)$). The solvent polarization and the second $gaoH^-$ ligand play crucial role for the preferred M- $gaoH(N,O)$ binding mode. The nature and the strength of the metal-ligand interactions were estimated in terms of molecular orbital analysis at the DFT(B3LYP/TZVP) level of theory. The largest interaction energy, accompanying by significant net charge transfer from the gao ligand to the metal ion was found for Cu(II) and Pt(II) complexes.

Key words: metal-ligand interactions, transition metal complexes, glyoxilic acid oxime, DFT, ab initio

INTRODUCTION

Glyoxilic acid oxime ($gaoH_2$, (H)O-N=C(H)-C(O)-O(H), (IUPAC name: 2-(hydroxyimino)acetic acid)) (oxime analogue of glycine) is the simplest representative of 2-(hydroxyimino)carboxylic acids which exhibit original coordination properties to metal ions. The oxime derivatives are used as suitable matrices for organometallic reactions [1], as very effective complexing agents in the analytical chemistry [2-5], as low temperature precursors for metal oxide ceramic [6] for design and synthesis of magnetic polynuclear assemblies [7] and as model compounds for investigation of metal-protein interactions [8-10]. Metal complexes of $gaoH_2$ have also shown versatile bioactivity as chelation therapy agents, drugs, inhibitors of enzymes and as intermediates in the biosynthesis of nitrogen oxide [11,12]. The alternative donor centers of the oxime group (N, O_N) and of the carboxylic group (O,O) lead to many different metal-ligand bindings: monodentate, bidentate chelate (forming four-, five- and six-membered stable rings) and bridging. The O,N-bidentate complexes were found as *cis* [12] and *trans* [13] isomers, the first one being stabilized by hydrogen bonding between the protonated and deprotonated

oxime groups. The present work aims to demonstrate the potential of the theoretical methods to gain deeper insight into the coordination properties of the glyoxilic acid oxime to metal ions as well as to estimate the nature and the strength of the metal-ligand interactions in the Zn(II), Cu(II), Ni(II), Co(II), Pt(II) and Pd(II) complexes. The theoretical estimations were done by means of the calculated M-O/N(gao) bond lengths, M(II)- gao interaction energies, NPA metal charges, M-O/N(gao) 2-center Wiberg (Mayer) bond orders (BO), polarization energy contributions, donation and back-donation $M \leftrightarrow gao$ contributions to the bond energy.

RESULTS AND DISCUSSION

Glyoxilic acid oxime is a small molecule with 16 possible conformations which arise from internal rotations around the C-O, C-C, C=N and N-O bonds [14,15]. DFT(BHLYP/6-311G(d,p), B3LYP/6-31++G(d)), HF, MP_n and QCISD(T) calculations have successfully predicted the lowest energy conformer of $gaoH_2$, *ectt*, (Fig. 1). Single crystal XRD data confirmed the prediction made and showed that in the solid state four $gaoH_2$ molecules in *ectt* conformation are linked by $O \cdots H-O$ and $N \cdots H-O$ hydrogen bonds, forming stable tetramer structure, (Fig. 1) [16]. Vibrational

* To whom all correspondence should be sent:
E-mail: ntrend@svr.igic.bas.bg

analysis at B3LYP/6-31G(d) level suggested cooperativity in the cyclic H-bonded aggregates in the solid state [17].

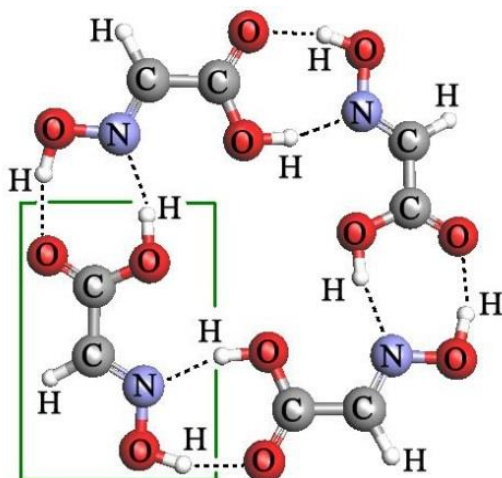


Fig. 1. Cyclic tetramer of glyoxilic acid oxime (*ectt* conformation) with “head-to-tail” bondings, as obtained from single crystal XRD analysis [16]. The lowest energy monomer conformation, *ectt*, is given in a frame.

The most important properties of the glyoxilic acid oxime, however, are revealed in solvent environment. Mono- and doubly deprotonated species of the ligand exist in water solution and they are the active forms of the ligand in complexation reactions with metal ions [15]. O–H bond deprotonation energies (BDE), proton affinity (PA), gas-phase basicity (GB) as well as reactive sites for electrophilic attack were theoretically predicted by detailed comprehensive DFT, MP2 and CCSD(T) studies of *gaoH₂*, *gaoH⁻* and *gao²⁻* in gas phase and in solution (SCRF-PCM method) [15]. For the neutral *gaoH₂*, the calculations in solution predicted lower O–H bond deprotonation energy of the COOH group as compared to the NOH group and thus the carboxylic group should firstly be deprotonated in solution [12,13]. The molecular electrostatic potential (MEP) values obtained for *gaoH⁻* and *gao²⁻* predicted bidentate coordination to metal(II) ions through both the carboxylic oxygen atoms (O,O) or through the oxime nitrogen and the carboxylic oxygen (N,O) (Fig. 2). The theoretical predictions for the coordination properties of the *gaoH⁻* and *gao²⁻* ligand species made on the basis of *ab initio* and DFT computations were proved by experimental studies of Zn(II), Ni(II), Cu(II), Co(II), Cd(II), Pt(II) and Pd(II) complexes of this ligand: single crystal XRD analysis, magnetic measurements, electronic-, NMR-, IR- and Raman spectroscopies [12,13,17,18].

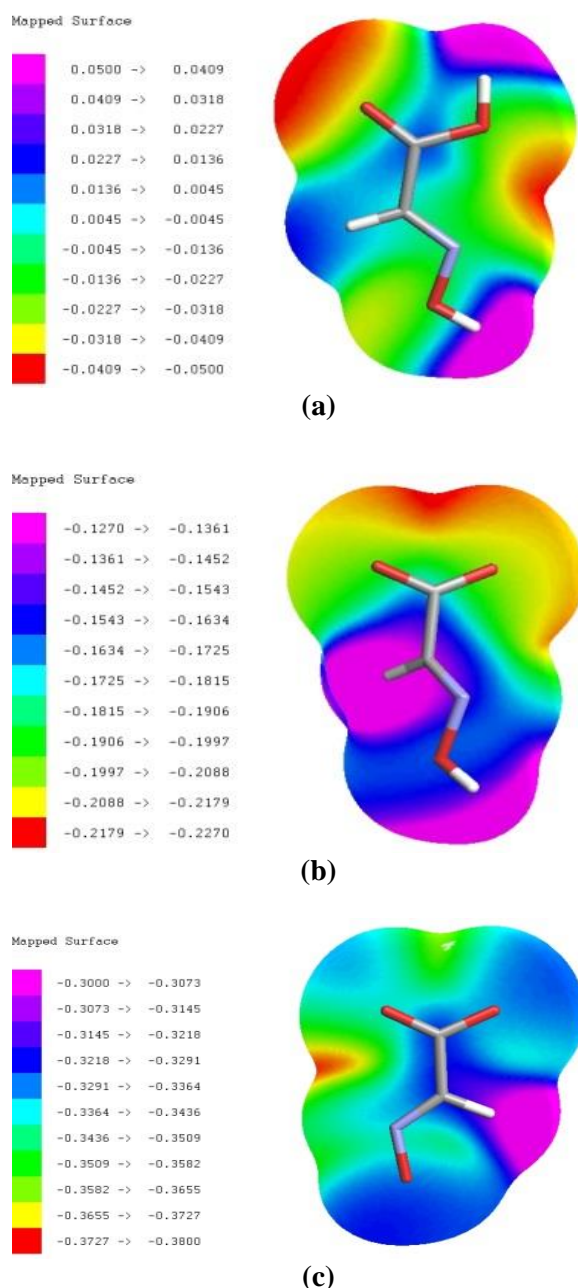


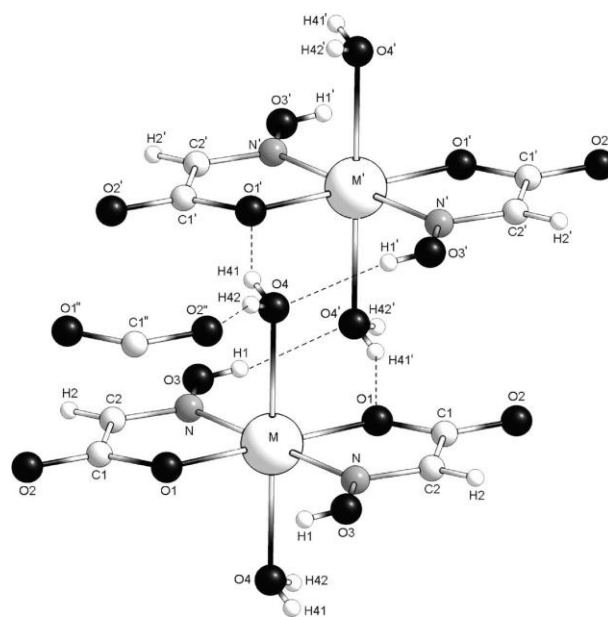
Fig. 2. Molecular electrostatic potential (MEP) of (a) *gaoH₂*; (b) *gaoH⁻*; (c) *gao²⁻* species, mapped onto an isosurface of electron density with $0.001 \text{ e}^{-1}/\text{bohr}^3$.

Zn(II), Ni(II), Cu(II), Co(II) and Cd(II) complexes of glyoxilic acid oxime

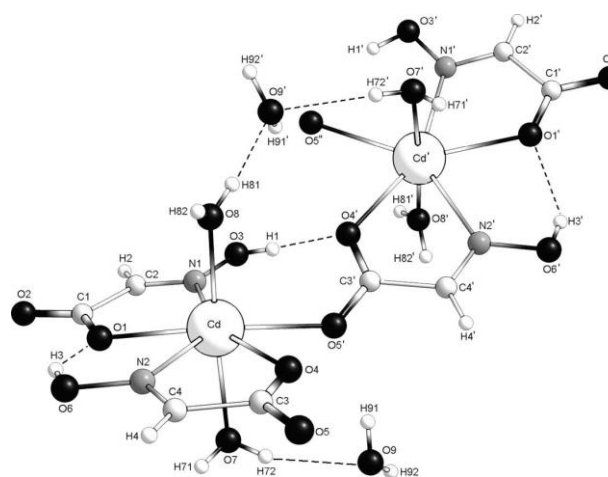
The coordination properties of the deprotonated ligand to Cu(II) were previously studied through calculations of different isomer models for Cu(II):*gao* = 1:1 in gas phase [19]. As a result, a stabilization of the [Cu-*gaoH*(O,O)]⁺ (bidentate ligand binding through both carboxylic oxygens) was predicted. This finding however does not correspond to the experimentally observed M-L

binding mode in the complexes studied, $[\text{Cu}(\text{gaoH}(\text{N},\text{O}))]^+$. Therefore, in the present study we extend the theoretical investigation with modeling species $\text{Cu}(\text{II}):\text{gao} = 1:2$ both in gas phase and in solution. The calculations were performed at DFT(B3LYP/6-31++G(d,p)/6-311++G(d)) levels using the Gaussian09 program package [20]. Two $[\text{Cu}(\text{gaoH})]^+$, two $[\text{Cu}(\text{gaoH})_2]$ and two $[\text{Cu}(\text{gao})]$ structures were computed with the most stable anionic and dianionic conformers both in gas phase and in aqueous solution. The calculations of the $[\text{Cu}(\text{gaoH}(\text{O},\text{O}))]^+$ and $[\text{Cu}(\text{gaoH}(\text{N},\text{O}))]^+$ structures in gas phase predicted more stable $[\text{Cu}(\text{gaoH}(\text{O},\text{O}))]^+$ structure by 4.0 kcal/mol. In solution, however, the (N,O) coordination in the $[\text{Cu}(\text{gaoH}(\text{N},\text{O}))]^+$ structure is by 6.6 kcal/mol more stable. With addition of a second gaoH^- ligand the $[\text{Cu}(\text{gaoH}(\text{N},\text{O}))_2]$ structure appeared more stable both in the gas phase and in polar solution (by ~11 and 14 kcal/mol, respectively). Obviously, the inclusion of the solvent and of the second gaoH^- ligand stabilized the M- $\text{gaoH}(\text{N},\text{O})$ bidentate binding, which is in agreement with X-ray data obtained for Cu(II), Zn(II), Cd(II) (Fig. 3), Pt(II) and Pd(II) complexes (Fig. 4) [12,13]. In the case of gao^{2-} -Cu(II) coordination mode, the calculations in the gas phase predicted slight stabilization of the $[\text{Cu}(\text{gao}(\text{O},\text{O}))]$ structure (by 1.1 kcal/mol) as compared to $[\text{Cu}(\text{gao}(\text{N},\text{O}))]$. In solution, however, the $[\text{Cu}(\text{gao}(\text{N},\text{O}))]$ binding appears more stable by 7.6 kcal/mol which is consistent with the experimentally observed $\text{gao}^{2-}(\text{N},\text{O})$ coordination realized in the studied complexes [12]. In the Cu(II) and Zn(II) complexes (Fig. 3a), the gaoH^- ligands form two planar five-membered chelate rings in *trans* position. Two water molecules complete the coordination sphere of the metal atoms taking the axial positions of a distorted octahedron with equal M-O4 bond distances. In the Cd(II) complex of gaoH^- (Fig. 3b), Cd(II) is seven-coordinated and in addition to the two gaoH^- (N,O) ligands in *trans* position, the third gaoH^- molecule acts simultaneously as bridging (through the COO^- group) and chelating ligand (it lies in a plane different from that of the other two gaoH^- ligands). Two free coordination sites of the Cd(II) complex are occupied with water molecules which are located above and below the plane of the other two ligands.

Pt(II) and Pd(II) bis-chelate square-planar complexes, $\text{K}[\text{Pt}(\text{gaoH})(\text{gao})]\cdot 3/4\text{H}_2\text{O}$ and $\text{K}[\text{Pd}(\text{gaoH})(\text{gao})]$, have been synthesized and characterized by IR, Raman, NMR and UV-vis spectroscopies as well as by single crystal XRD analysis [12,18].



(a)



(b)

Fig. 3. Molecular structure of: a) $\text{M}(\text{gaoH})_2(\text{H}_2\text{O})_2$ ($\text{M} = \text{Cu}(\text{II}), \text{Zn}(\text{II})$) and b) $[\text{Cd}(\text{gaoH})_2(\text{H}_2\text{O})_2]\cdot\text{H}_2\text{O}$, as obtained from X-ray diffraction analysis.

Pt(II) and Pd(II) complexes of glyoxilic acid oxime

Each complex contains one mono- and one doubly deprotonated ligand coordinated to Pt(II) and Pd(II) via the carboxylic oxygen and oxime nitrogen atoms (O,N), forming two *cis*-oriented five-membered planar chelate rings, as shown in Fig. 4. The two ligands are connected via intramolecular hydrogen bond of the $\text{N}-\text{O}\cdots\text{H}-\text{O}-\text{N}$ type.

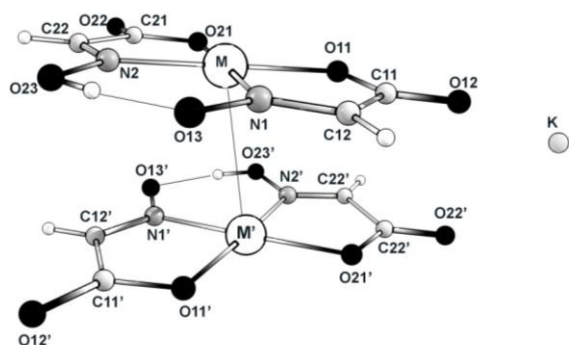


Fig. 4. Molecular structure of *cis*-K[M(*gaoH*)(*gao*)] (M = Pt(II) and Pd(II)), as obtained from X-ray diffraction analysis.

Theoretical estimation of the metal(II)-*gao* interactions

The molecular structures of complexes studied were optimized at the B3LYP level with 6-311+G(d) basis sets for Co(II), Ni(II), Cu(II), Zn(II), ECPs (SDD) for Pt(II) and Pd(II) and 6-31++G(d,p) for all other atoms. Metal(II)-*gao* interactions in the neutral $M(gaoH)_2(H_2O)_2$ (M = Co, Ni, Cu, Zn) and in the ionic $K[M(gaoH)(gao)]$ complexes (M = Pd, Pt) were analyzed by means of the calculated M-O/N(*gao*) bond lengths, M(II)-*gao* interaction energies, charge-transfer and polarization energy contributions, donation and back-donation $M \leftrightarrow gao$ contributions to the M(II)-*gao* bond energy (Charge Decomposition Analysis, CDA) [21,22] (in the frame of 2 fragment orbitals calculations), NPA metal charges, M-O/N(*gao*) 2-center (atoms) Wiberg (Mayer) bond order (BO) indices. The CDA and BO components help to analyze the chemical bonding in molecular systems and to monitor changes in the electron density distribution. The CDA approach decomposes the Kohn-Sham determinant of a complex [ML] in terms of fragment orbitals of the ligand, L and the metal [M]. The $[M] \leftarrow L$ donation is then given by mixing of the occupied orbitals of L and vacant orbitals of [M]. The $[M] \rightarrow L$ back-donation is given by the mixing of the occupied orbitals of [M] and vacant orbitals of L. The mixing of the occupied orbitals of both fragments gives the repulsive polarization and the mixing of the unoccupied orbitals - residual term. The 2-center “generalized” Wiberg and Mayer indices, calculated from the canonical MOs in the AO basis resemble the “classical” bond order in diatomic molecule defined as one half of the difference between the number of electrons in the bonding and antibonding states in the corresponding bond. BO value suggests how “strong” the bond is (for single

bond the value is close to 1). The Mayer bond orders are:

$$B_{AB} = B_{AB}^{\alpha} + B_{AB}^{\beta} = 2 \sum_{a \in A} \sum_{b \in B} [(P^{\alpha} S)_{ba} (P^{\alpha} S)_{ab} + (P^{\beta} S)_{ba} (P^{\beta} S)_{ab}]$$

where P ($P = P^{\alpha} + P^{\beta}$) and P^s ($P^s = P^{\alpha} - P^{\beta}$) are the density and spin-density matrices, respectively, P^{α} and P^{β} are α - and β -electron density matrices and S is the overlap matrix. In closed-shell spin-singlet state calculations, $P^{\alpha} = P^{\beta}$, $B_{AB}^{\alpha} = B_{AB}^{\beta}$ and B_{AB} (Mayer) = B_{AB} (Wiberg). In a general case with $P^{\alpha} \neq P^{\beta}$, the generalized Wiberg and Mayer bond orders are not equal.

The molecular orbital analysis, BO and CDA computations were performed with the B3LYP/TZVP method applying the AOMix program [23,24]. The metal-ligand interactions/bond in the studied metal complexes were estimated in terms of two fragments: $M(gaoH)(H_2O)_2^+$ (1) and $gaoH^-$ (2) for Cu(II), Zn(II), Ni(II) and Co(II) complexes and two types fragments $M(gaoH)^+$ (1) and $gaoK^-$ (2), and $K[M(gao)]^+$ (1) and $gaoH^-$ (2) for the Pt(II) and Pd(II) complexes. The two-fragment approach used for Cu(II), Zn(II), Ni(II) and Co(II) complexes better describes the metal-*gao* bonding in the complexes since it takes into account the perturbation of metal ions by one *gao* ligand and two water molecules. The results are listed in Table 1 for the Co(II), Ni(II), Cu(II), Zn(II) complexes and in Table 2 for the Pt(II) and Pd(II) complexes.

In keeping with the experimental effective magnetic moments [13], the Co(II), Ni(II) and Cu(II) complexes were calculated in high spin states: multiplicity = 4, 3 and 2, respectively. The calculated bond lengths and bond orders for the neutral Co(II), Ni(II), Cu(II) and Zn(II) complexes (Table 1) predicted a stronger M-O bond than the M-N one. The calculated M-*gao* interaction energy, M-O/N bond lengths, M-O/N bond orders and overlap populations suggested the strongest M-*gao* bonding in the $Cu(gaoH)_2(H_2O)_2$ complex and the weakest one in the high spin $Co(gaoH)_2(H_2O)_2$ complex. The same conclusions were derived by previous analyses of the spectral behavior of $\nu(COO)$, $\nu(M-O)$ and $\nu(M-N)$ frequencies [13]. The charge decomposition analysis results listed in Table 1 showed that at equilibrium Cu-*gao* distance the $gaoH^- \rightarrow Cu^+$ donation is the most significant one, 0.846 e (including the largest net charge donation from the ligand to the metal and the electron polarization contribution), whereas the back-donation $Cu^+ \rightarrow gaoH^-$ is very small. The cal-

Table 1. NBO and CDA data for neutral $M(gaoH)_2(H_2O)_2$ complexes ($M = Co(II), Ni(II), Cu(II), Zn(II)$)*

Complex	R_{M-gao} (Å)	q_M (a.u.)	E (kcal/mol)	BO (a.u.)	overlap population		Electronic polarization PL(1)-PL(2)	Net charge donation CT(2→1)-CT(1→2)	d	b	r
					α	β					
Co(<i>gaoH</i>) ₂ (H ₂ O) ₂	1.997 ^{M-O}	0.97	-181.3/ -651.4 ^t	0.503	0.140	0.205	0.053	0.529	0.681	-0.021	-0.272
	2.120 ^{M-N}			0.343	0.087	0.158					
	2.268 ^{M-Ow}			0.199	0.053	0.096					
Ni(<i>gaoH</i>) ₂ (H ₂ O) ₂	2.003 ^{M-O}	0.90	-182.6/ -674.4 ^t	0.476	0.136	0.193	0.063	0.564	0.712	-0.011	-0.279
	2.047 ^{M-N}			0.413	0.119	0.186					
	2.191 ^{M-Ow}			0.237	0.061	0.114					
Cu(<i>gaoH</i>) ₂ (H ₂ O) ₂	1.944 ^{M-O} /1.944 ^{exp}	0.96	-191.4/ -691.8 ^t	0.579	0.160	0.207	0.123	0.788	0.846	-0.030	-0.258
	1.981 ^{M-N} /2.063 ^{exp}			0.510	0.132	0.218					
	2.598 ^{M-Ow}			0.031	0.016	0.013					
Zn(<i>gaoH</i>) ₂ (H ₂ O) ₂	1.983 ^{M-O} /2.042 ^{exp}	1.21	-182.7/ -653.2 ^t	0.475	0.183	0.183	0.019	0.508	0.683	-0.026	-0.214
	2.175 ^{M-N} /2.178 ^{exp}			0.286	0.111	0.111					
	2.319 ^{M-Ow}			0.156	0.065	0.065					

*Geometry optimizations - at B3LYP/6-31++G(d,p)/6-311+G(d) level (the latter for Co(II), Ni(II), Cu(II), Zn(II)); population analysis - at B3LYP/TZVP level; BO and CDA calculations with AOMix program. R_{M-gao} - optimized M-O and M-N bond lengths; q_M - NPA charge of metal ion in the complex; E - interaction energy between $M(gaoH)(H_2O)_2^+(1) - gaoH^-(2)$ fragments ($M = Cu, Ni, Co$); BO- 2-centers Bond Order (Mayer BO - for open shell complexes, Wiberg BO - for closed shell complexes); net charge donation ($gaoH^- \rightarrow M(gaoH)(H_2O)_2^+$); $gaoH^- \rightarrow M(gaoH)(H_2O)_2^+$ donation d (including charge donation and electronic polarization); $M(gaoH)(H_2O)_2^+ \rightarrow gaoH^-$ back-donation b; $M(gaoH)(H_2O)_2^+ \leftrightarrow gaoH^-$ repulsive polarization r.

Table 2. NBO and CDA data for ionic $K[M(gaoH)(gao)]$ complexes ($M = Pt(II), Pd(II)$)^a

Complex	R_{M-gao} (Å)	q_M (a.u.)	E (kcal/mol)	BO (a.u.)	overlap population		Electronic polarization PL(1)-PL(2)	Net charge donation CT(2→1)-CT(1→2)	d	b	r
					α	β					
K[Pd(<i>gaoH</i>)(<i>gao</i>)]	2.054 ^{M-O*} /2.036 ^{exp}	0.62	-191.9* -280.5**	0.512	0.153	0.153	0.033	0.657	0.719	0.176	-0.504
	1.996 ^{M-N*} /1.957 ^{exp}			0.590	0.204	0.204					
	2.054 ^{M-O**} /2.021 ^{exp}			0.421	0.105	0.105					
	1.997 ^{M-N**} /1.948 ^{exp}			0.608	0.201	0.201					
K[Pt(<i>gaoH</i>)(<i>gao</i>)]	2.069 ^{M-O*}	0.30	-212.3* -298.4**	0.521	0.138	0.138	0.016	0.688	0.728	0.153	-0.624
	1.986 ^{M-N*}			0.659	0.176	0.176					
	2.059 ^{M-O**}			0.457	0.106	0.106					
	1.994 ^{M-N**}			0.655	0.159	0.159					

^aMolecular optimizations are performed at B3LYP/6-31++G(d,p)/SDD level (the latter - for Pt(II) and Pd(II)); population analysis - at B3LYP/TZVP level; WBO and CDA calculations with AOMix program. R_{M-gao} - optimized M-O and M-N bond lengths; q_M - NPA charge of metal ion in the complex; E* - interaction energy between $M(gaoH)^+(1) - gaoH^-(2)$ fragments ($M = Pt, Pd$); BO- 2-center Bond Order (Wiberg); net charge donation (* $gaoH^- \rightarrow M(gao)K^+$ and ** $Kgao^- \rightarrow MgaoH^+$); * $gaoH^- \rightarrow M(gao)K^+$ and ** $Kgao^- \rightarrow MgaoH^+$ donation d (including charge donation and electronic polarization); * $K[M(gao)]^+ \rightarrow gaoH^-$ and ** $MgaoH^+ \rightarrow gaoK^-$ back-donation b; * $K[M(gao)]^+ \leftrightarrow gaoH^-$ and ** $MgaoH^+ \leftrightarrow gaoK^-$ repulsive polarization r.

culations revealed that the *gaoH*⁻ ligand is a strong donor and a weak acceptor in all the neutral complexes studied.

The calculated M(II)-N/O bond lengths and the corresponding BOs for the ionic Pt(II) and Pd(II) complexes of *gao* predicted stronger M(II)-N bonds than M(II)-O ones which is in contrast to the results obtained for the neutral Co(II), Ni(II), Cu(II) and Zn(II) complexes of *gao*. The interaction energies of Pt(II)-*gaoH*⁻/*gao*²⁻ are larger as compared to the corresponding Pd(II)-*gaoH*⁻/*gao*²⁻ ones. More negative interaction energy and stronger metal-ligand bonding (larger donation contribution to the M(II)-*gao*²⁻ bond energy) were predicted for the metal-dianion binding (Pt(II)/Pd(II)-*gao*²⁻) than for the metal-monoanion binding (Pt(II)/Pd(II)-*gaoH*⁻).

CONCLUSION

As the simplest derivative of the 2-(hydroxyimino) carboxylic acids the glyoxilic acid oxime is a very suitable model compound for investigation of metal-ligand interactions in transition-metal complexes. The coordination abilities of the active *gaoH*⁻ and *gao*²⁻ forms in solution were predicted by MEP calculations and different metal-ligand bonding isomers. The largest stabilization was found for the structures with *M-gaoH*(N,O) bidentate binding through the carboxylic oxygen and the oxime nitrogen atoms, which is in agreement with X-ray data for Cu(II), Zn(II), Cd(II), Pt(II) and Pd(II) complexes. The solvent polarization and the second *gaoH*⁻ ligand play crucial role for the preferred *M-gaoH*(N,O) binding

mode. The calculated M(II)-N/O bond lengths and the corresponding bond orders for the ionic Pt(II) and Pd(II) complexes of *gao* predicted a stronger M(II)-N bond than the M(II)-O one, which is in contrast to the results obtained for the Co(II), Ni(II), Cu(II) and Zn(II) neutral complexes of *gao*, where the M(II)-O interaction is stronger than the M(II)-N one. Among the studied neutral transition metal complexes, the largest interaction energy was found for Cu(II)-(*gaoH*)₂ and among the ionic metal complexes, the larger interaction energy is predicted for Pt(II)-*gaoH*²⁻/*gao*²⁻. For these complexes, the net charge transfer energy contribution from the *gao* ligand to the metal ion is the largest one in the series of complexes studied.

Acknowledgements: *The authors thank the Computer Center for Advanced Studies in Molecular Design, New Materials and Nanotechnology (MADARA) at the Bulgarian Academy of Sciences (Institute of Organic Chemistry with Center of Phytochemistry) where all computations were performed.*

REFERENCES

- V. Y. Kukushkin, D. Tudela, A. J. L. Pombeiro, *Coor. Chem. Rev.*, **156**, 333 (1996).
- I. O. Fritsky, R. Lampeka, V. Skopenko, Y. Simonov, T. Malinovski, *Z. Naturforsch. B*, **48**, 270 (1993).
- V. V. Skopenko, I. O. Fritskii, R. D. Lampeka, *Zh. Neorg. Khim.*, **39**, 1478 (1994).
- V. V. Skopenko, T. Yu. Sliva, Yu. A. Simonov, A. A. Dvornik, M. D. Mazus, R. D. Lampeka, T. I. Malinovski, *Zh. Neorg. Khim.*, **35**, 1743 (1990).
- A. A. Dvorkin, Yu. A. Simonov, T. Yu Sliva, R. D. Lampeka, M. D. Mazus, V. V. Skopenko, T. I. Malinovski, *Zh. Neorg. Khim.*, **34**, 2582 (1989).
- A. W. Apblett, G. D. Georgieva, *Phosphorus Sulfur*, **93**, 479 (1994).
- R. Ruiz, J. Sanz, B. Cervera, F. Lloret, M. Julve, C. Bois, J. Faus, M. Carmen Munoz, *J. Chem. Soc. Dalton Trans.*, 1623 (1993).
- D. Mansuy, P. Battioni, J. P. Battioni, *Eur. J. Biochem.*, **184**, 267 (1989).
- B. Meunier, *Chem. Rev.*, **92**, 1411 (1992).
- J. Custot, J.-L. Boucher, S. Vadov, C. Guedes, S. Dijols, M. Delaforge, D. Mansuy, *J. Biol. Inorg. Chem.*, **1**, 73 (1996).
- A. Garoufis, S. K. Hadjikakou, N. Hadjiliadis, *Coor. Chem. Rev.*, **253**, 1384 (2009).
- N. I. Dodoff, M. Kubiak, J. Kuduk-Jaworska, A. Mastalarz, A. Kochel, V. Vassilieva, N. Vassilev, N. Trendafilova, I. Georgieva, M. Lalia-Kantouri, M. Apostolova, *Chemija*, **20**, 208 (2009).
- I. Georgieva, N. Trendafilova, G. Bauer, *Spectrochim. Acta A*, **63**, 403 (2006).
- N. Trendafilova, G. Bauer, I. Georgieva, V. Delchev, *J. Mol. Struct.*, **604**, 211 (2002).
- I. Georgieva, N. Trendafilova, *Chem. Phys.*, **321**, 311 (2006).
- I. Georgieva, D. Binev, N. Trendafilova, G. Bauer, *Chem. Phys.*, **286**, 205 (2003).
- I. Georgieva, N. Trendafilova, D. Binev, *Vib. Spectrosc.*, **31**, 143 (2003).
- I. Georgieva, N. Trendafilova, N. I. Dodoff, *J. Photoch. Photobiol. A*, **267**, 35 (2013).
- I. Georgieva, N. Trendafilova, L. Rodriguez-Santiago, M. Sodupe, *J. Phys. Chem. A*, **109**, 5668 (2005).
- R. D. Gaussian 09, Revision A.02, M. J. Frisch, G. W. Trucks, H. B. Schlegel, G. E. Scuseria, M. A. Robb, J. R. Cheeseman, G. Scalmani, V. Barone, B. Mennucci, G. A. Petersson, H. Nakatsuji, M. Caricato, X. Li, H. P. Hratchian, A. F. Izmaylov, J. Bloino, G. Zheng, J. L. Sonnenberg, M. Hada, M. Ehara, K. Toyota, R. Fukuda, J. Hasegawa, M. Ishida, T. Nakajima, Y. Honda, O. Kitao, H. Nakai, T. Vreven, J. A. Montgomery, Jr., J. E. Peralta, F. Ogliaro, M. Bearpark, J. J. Heyd, E. Brothers, K. N. Kudin, V. N. Staroverov, R. Kobayashi, J. Normand, K. Raghavachari, A. Rendell, J. C. Burant, S. S. Iyengar, J. Tomasi, M. Cossi, N. Rega, J. M. Millam, M. Klene, J. E. Knox, J. B. Cross, V. Bakken, C. Adamo, J. Jaramillo, R. Gomperts, R. E. Stratmann, O. Yazyev, A. J. Austin, R. Cammi, C. Pomelli, J. W. Ochterski, R. L. Martin, K. Morokuma, V. G. Zakrzewski, G. A. Voth, P. Salvador, J. J. Dannenberg, S. Dapprich, A. D. Daniels, Ö. Farkas, J. B. Foresman, J. V. Ortiz, J. Cioslowski, and D. J. Fox, Gaussian, Inc., Wallingford CT, 2009.
- S. Dapprich, G. Frenking, *J. Phys. Chem. A*, **99**, 9352 (1995).
- G. Frenking, N. Frohlich, *Chem. Rev.*, **100**, 717 (2000).
- S. I. Gorelsky, AOMix: Program for Molecular Orbital Analysis; University of Ottawa (2011), <http://www.sg-chem.net/>.
- S. I. Gorelsky, A. B. P. Lever, *J. Organomet. Chem.*, **635**, 187 (2001).

МЕТАЛ-ЛИГАНД ВЗАИМОДЕЙСТВИЯ В КОМПЛЕКСИ НА ПРЕХОДНИ МЕТАЛИ С ОКСИМА НА ГЛИОКСИЛОВАТА КИСЕЛИНА

И. Георгиева, Н. Трендафилова*

Институт по обща и неорганична химия, Българска Академия на Науките, ул. Акад. Г. Бончев, бл. 11, 1113
София, България

Постъпила на 4 април 2014 г.; Коригирана на 19 май 2014 г.

(Резюме)

Оксимът на глиоксилната киселина ($gaoH_2$) е използван като модел за изследване на метал-лиганд взаимодействията в серия комплекси на преходни метали с този лиганд: $Cu(gaoH)_2(H_2O)_2$, $Zn(gaoH)_2(H_2O)_2$, $Co(gaoH)_2(H_2O)_2$, $Ni(gaoH)_2(H_2O)_2$, $[Cd(gaoH)_2(H_2O)_2]H_2O$, $K[Pt(gao)(gaoH)]3/4H_2O$ and $K[Pd(gao)(gaoH)]$. Координационната способност на активните форми на лиганда, $gaoH^-$ и gao^{2-} , в газова фаза и в разтвор е изследвана на теоретично ниво. В съгласие с рентгеноструктурни данни за комплексите на Cu(II), Zn(II), Cd(II), Pt(II) и Pd(II) изчисленията показват, че най-предпочетеното свързване е бидентатно чрез карбоксилния кислороден атом и азотния атом от оксимната група, M- $gaoH(N,O)$. Установено е, че ефектът на полярния разтворител и присъствието на втори лиганд в молекулата имат определяща роля при реализиране на свързването M- $gaoH(N,O)$. Природата и силата на метал-лиганд взаимодействията в изследваните комплекси са оценени чрез МО изчисления на DFT(B3LYP/TZVP) ниво на теорията. Най-голяма стойност на енергията на взаимодействие и най-голям пренос на заряд от лиганда към металния йон е намерен за комплексите на Cu(II) и Pt(II).

Xanthine and hypoxanthine: in a search for conical intersections S_0/S_1 connected with deformations of pyrimidine residue of the purine ring

V. B. Delchev*

Department of Physical Chemistry, University of Plovdiv, Tzar Assen 24 str., 4000 Plovdiv, Bulgaria

Received March 19, 2014; Revised April 09, 2014

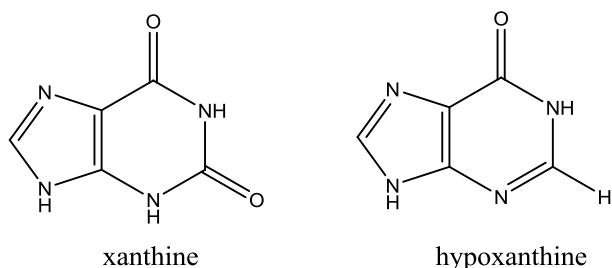
Dedicated to Acad. Dimiter Ivanov on the occasion of his 120th birth anniversary

The oxo N9H tautomers of xanthine and hypoxanthine were studied theoretically at the CC2/aug-cc-pVDZ level in order to find conical intersections S_0/S_1 , which show deformations of the pyrimidine rings. The conical intersections were characterized locally by adiabatic surfaces constructed on the narrow grid. The accessibility of the conical intersections from the excited state was also implied.

Key words: CC2 method, conical intersections, hypoxanthine, xanthine

INTRODUCTION

Xanthine (**XA**) is a purine base, which can be found in most human body tissues. This compound is produced through purine degradation. It is obtained enzymatically from guanine and hypoxanthine (**HXA**) by deamination and oxidation respectively. Hypoxanthine is a naturally occurring deaminated form of adenine. It is obtained as an intermediate in the purine catabolism reaction. It is also included in the anticodon of tRNA as the nucleoside base inosine [1].



Scheme 1. Canonical structures of xanthine and hypoxanthine N9H tautomers.

The canonical structures of N9H tautomers of xanthine and hypoxanthine are given in Scheme 1. As one can see, hypoxanthine has one extra C=N bond in pyrimidine residue (canonical structure) than xanthine. To our knowledge, the internal conversions of the excited states of pyrimidines and purines occur through a twisting around the double bond(s) within the rings [2-6]. These mechanisms

are known to be main channels for a non-radiative decay of the excited states [7,8], which determine their high photostability with respect to UV radiation. Unfortunately for purines, especially for (hypo)xanthine, these reactions are not very well clarified, even though some excited states have been an object of the theoretical research of Farrokhpour *et al.* [9], who have tried to explain the photoelectron spectra of both compounds. However, no information for the excited states' deactivation channels has been given [9]. Some excited-state non-radiative decay paths of xanthine through conical intersections S_0/S_1 have been studied theoretically; however they concern only the imidazole part of the ring [10].

Theoretical calculations and experimental UV spectral investigations have revealed that in aqueous solution the N9H tautomer of hypoxanthine is dominant over the keto-N7H form [11-14]. In the crystalline phase this tautomer is the most stable one either [15]. The keto and enol tautomers, and their stability in aqueous solution have been reported in the paper of Stimson *et al.* [16]. They have been established by UV spectroscopy that in acid solution the enol forms of hypoxanthine and xanthine dominate [16]. Some recent investigations have revealed that hypoxanthine in aqueous solution shows absorption maximum at 250 nm [17]. It was found also that the lifetimes of hypoxanthine in aqueous media are 2.3 ± 0.3 ps (probe 250 nm) and 130 ± 20 fs (probe 570 nm) [17]. The major conclusion of the latter research is that hypoxanthine appears to decay non-radiatively by puckering of the six-membered ring

* To whom all correspondence should be sent:
E-mail: vdelchev@uni-plovdiv.net

in aqueous media. However, a concrete mechanism has not been proposed and commented.

The aim of the reported research is to throw light upon the deformation mechanisms of pyrimidine fragments of xanthine and hypoxanthine and to clarify their contribution to internal conversions S_0/S_1 or fluorescence in both compounds. The study requires a search of accessible and reliable conical intersection(s) mediating the $S_1 \rightarrow S_0$ decay (internal conversion). Such conical intersections and their accessibility could explain the high UV photostability of both compounds. In the cases of excited state decay either internal conversion or fluorescence may dominate. The knowledge which process prevails is important to the understanding of whether the compound could find application as photoprotector or not.

THEORETICAL METHODS

The ground-state equilibrium geometries of the N9H tautomers of xanthine and hypoxanthine were optimized at the CC2 level [18,19]. Their structures were used to calculate subsequently the vertical excitation energies of the minima with no symmetry restrictions.

The emission energies were found with the optimized structures of the excited states (CC2). The optimizations of the excited state equilibrium geometries were carried out using symmetry restrictions - C_s . This approach allows distinguishing of the excited states under consideration by symmetry, which is always useful in the studies of electronic states involving a large number of configurations. Thus, the ${}^1\pi\pi^*$ excited states have symmetry A' , while the ${}^1n\pi^*$ and ${}^1\pi\sigma^*$ excited states have symmetry A'' . The optimizations of the excited states without symmetry restrictions led to a mixing of excited states and the assignment of the states is not always possible.

For the generation of adiabatic structures on the narrow grid around the conical intersections we orthogonalized the vectors $\mathbf{g}=2GD$ and $\mathbf{h}=DC$ by the Yarkony's procedure [20]. Further procedure for the PESs' constructions is described in the paper of Woywod [20]. The adiabatic PESs were constructed using the normal modes of the geometry-minimum, as obtained from CASSCF computations [21,22].

All computations were performed at the CC2/aug-cc-pVDZ level with the TURBOMOLE program package [18,23]. Only the optimizations of the conical intersections and the geometries-minima for the adiabatic PESs were performed at the

CASSCF(6,6)/6-31G* level with the program GAUSSIAN 03 [24].

RESULTS AND DISCUSSION

Equilibrium geometries

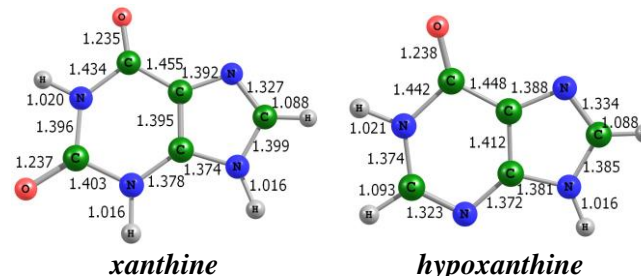


Fig. 1. CC2 ground-state equilibrium geometries of xanthine and hypoxanthine.

The ground-state equilibrium geometries of **XA** and **HXA** found at the CC2 level are illustrated in Fig. 1. The structures are planar which allows using symmetry (C_s) to study the excited states which are vertically located over the ground-state minima. As seen **HXA** has one extra C=N bond in the pyrimidine residue than **XA**. This bond implies twisting around which is usually favored in the excited state than in the ground state.

Vertical excitation and emission energies

Table 1. Vertical excitation and emission energies of xanthine and hypoxanthine.

XA			HXA		
State	eV	nm	State	eV	nm
<u>vertical excitation energies</u>					
${}^1\pi\sigma^*$	4.918	252	${}^1\pi\pi^*$	4.884	254
${}^1n\pi^*$	5.080	244	${}^1n\pi^*$	5.253	236
${}^1\pi\pi^*$	5.297	234	${}^1n\pi^*$	5.422	229
${}^1\pi\pi^*$	5.821	213	${}^1\pi\pi^*$	5.429	229
${}^1\pi\sigma^*$	5.827	213	${}^1\pi\sigma^*$	5.436	228
<u>emission energies (C_s symmetry)</u>					
${}^1\pi\pi^*(A')$	4.659	266	${}^1\pi\pi^*(A')$	3.574	347
${}^1\pi\sigma^*(A'')$	4.307	288	${}^1\pi\sigma^*(A'')$	3.574	248

The calculated vertical excitation energies of the tautomers of both compounds are presented in Table 1. The data show that the bright ${}^1\pi\pi^*$ excited state of xanthine (at 5.297 eV) is the third excited state (ordered by energy), while it is the lowest excited state in hypoxanthine (at 4.884 eV). That could be explained with the extra oxygen atom, which is present in xanthine as compared to hypoxanthine; such bases with carbonyl groups have ${}^1n\pi^*$ excited states with lower energies than those of ${}^1\pi\pi^*$ excited states [8,10,11]. The molecular orbitals under consideration are illustrated in Fig. 2.

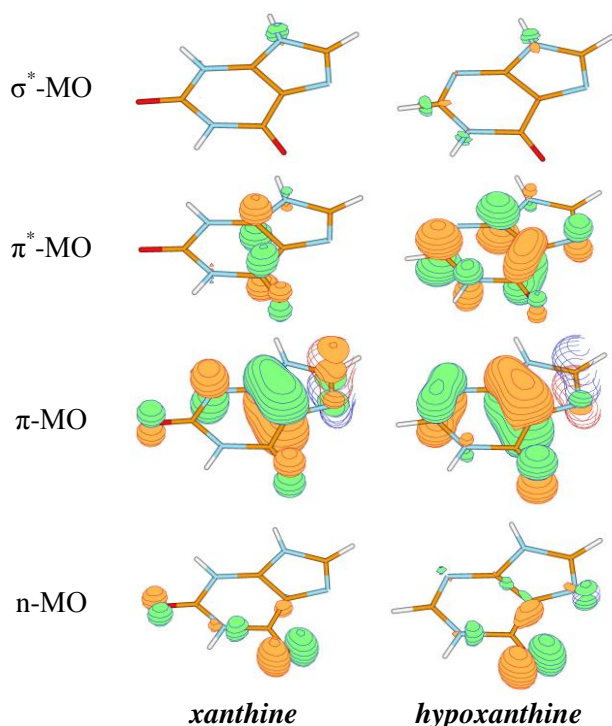


Fig. 2. Selected molecular orbitals involved in the electronic transitions leading to the excited states under consideration.

The calculated ${}^1\pi\pi^*$ emission energy (in eV) of hypoxanthine is considerably lower than this of xanthine. In other words, the fluorescence maximum of xanthine is expected to be blue-shifted with respect to this of hypoxanthine. To the contrary, the emission energy of the ${}^1\pi\sigma^*$ excited state (if any maximum of this state can be measured) of xanthine should be red-shifted as compared to hypoxanthine.

Conical intersections

The structures of the optimized conical intersections are illustrated in Fig. 3.

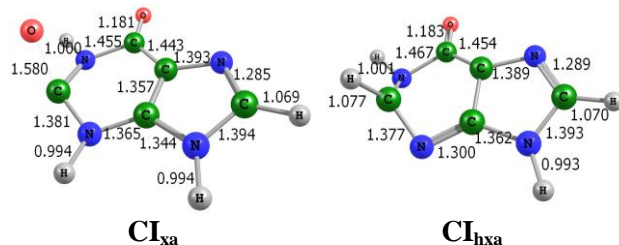
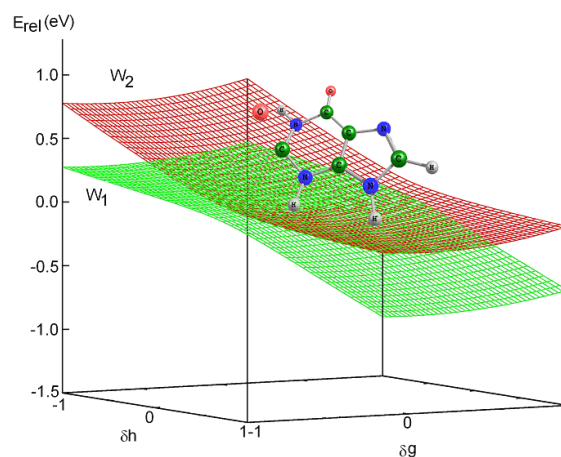


Fig. 3. Conical intersections of xanthine and hypoxanthine obtained through deformations of the pyrimidine residues of purine rings.

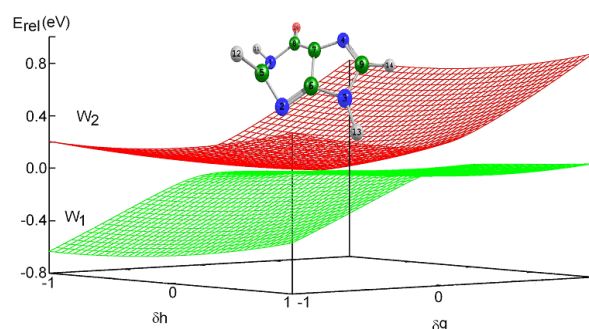
They both show deformations in pyrimidine fragment of the purine ring. As seen, the conical intersection S_0/S_1 of **XA** shows deformation of the carbonyl oxygen at the second position (IUPAC). The C=O bond is star-ched to 1.580 Å as compared

to the minimum (Fig. 1). The carbonyl oxygen is located in the upper side of the purine ring.

The optimized intersection S_0/S_1 of **HXA** shows a typical twisting of the C=N bond of pyrimidine ring. As expected, this twisting is accompanied by a deviation of the hydrogen atom of the nearest carbon atom out of the molecular plane.



(a)



(b)

Fig. 4. Adiabatic potential energy surfaces of the electronic states S_0 (W_1) and S_1 (W_2) of a) xanthine and b) hypoxanthine.

The adiabatic surfaces W_1 and W_2 of the electronic states S_0 and S_1 are presented in Fig. 4. As seen in both cases, for **XA** and **HXA**, the two electronic states are degenerated in the point 0/0: the conical intersection S_0/S_1 is located there. The slope of the S_0 -surface after the conical intersection is indicative enough for the course of the reaction since it shows in which direction the reaction could proceed. In other words, the steeper the slope, the higher probability for the reaction to proceed. The S_0 -surface of **XA** shows the steepest slope in the direction 1/-1 (these are the end values of δg and δh correspondingly). The S_0 -surface of **HXA** indicates the steepest slope in the direction -1/-1.

Energy-level diagrams

In Fig. 5 are depicted the energy-level diagrams and the possible pathways (dashed arrows) of the deactivation processes of the excited states as well as the basic optical transitions (full arrows).

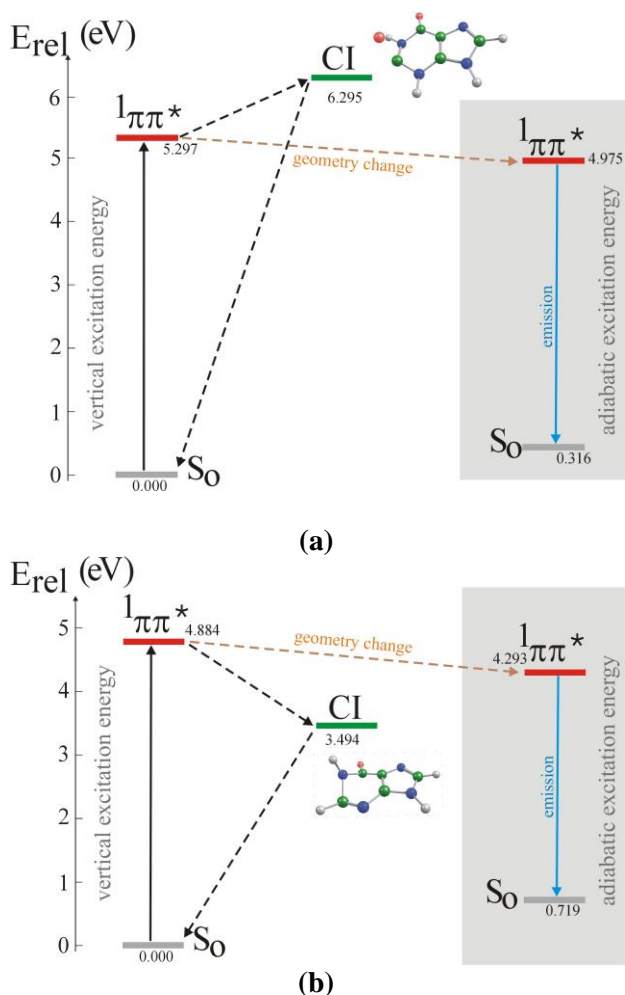


Fig. 5. Energy-level diagrams of the possible deactivation pathways of the N9H tautomers of a) xanthine and b) hypoxanthine – CC2/aug-cc-pVDZ level (gas phase).

As seen, the conical intersection S_0/S_1 of **XA** has higher energy than the energy of the spectroscopically active $^1\pi\pi^*$ excited state. In other words, this conical intersection is not accessible through the lowest bright state. The second bright $^1\pi\pi^*$ excited state of **XA** (Table 1) has lower energy either than the energy of the conical intersection S_0/S_1 . As seen from Fig. 5a, the $^1\pi\pi^*$ excited state equilibrium geometry is of lower energy than the vertical excitation energy of this state. It indicates a Stokes shift of 0.638 eV between absorption and fluorescence energies. The experiment has shown fluorescence maximum at 435 nm but in strong acid

media (pH=1) [25]. This value is not directly comparable to the calculated one here since, as it was mentioned in the introduction section, it can be associated with the enol tautomer, which is dominant at pH=1 [16]. At pH=7.2 the fluorescence is about 325 nm [26]. Obviously, the fluorescence maximum is approaching the predicted here value despite the fact that the calculations are referred to molecules in the gas phase.

Fig. 5b shows the energy-level diagram of **HXA**. The picture shows that the conical intersection S_0/S_1 has lower energy than the lowest bright $^1\pi\pi^*$ excited state, and thus it can be accessed through this state and a proper excited-state decay path. Our future research will be dedicated to a search of such path connecting both stationary points on the W_2 -adiabatic-PES of **HXA**. Perhaps, this conical intersection could be also accessed from the equilibrium geometry of the $^1\pi\pi^*$ excited state, whose energy is lower (the gray area of the picture). The results imply a Stokes shift of 1.31 eV between absorption and fluorescence maxima.

CONCLUSION

The oxo N9H tautomers of xanthine and hypoxanthine were studied theoretically at the CC2/aug-cc-pVDZ level in order to find conical intersections S_0/S_1 which correspond to deformations of the pyrimidine fragment of the purine ring. The energies of the conical intersections and the minima were summarized in energy-level diagrams which shed light upon the possible deactivation channels of the two compounds. It was shown that the conical intersection S_0/S_1 of **XA** cannot be accessed through the spectroscopically active $^1\pi\pi^*$ excited state. Obviously, with respect to these mechanisms only fluorescence is expected; in other words the compound does not exhibit photoprotective properties. To the contrary, the conical intersection S_0/S_1 of **HXA** could be easily accessed through the lowest bright active $^1\pi\pi^*$ excited state of the compound. The domination of the internal conversion of **HXA** shows that the compound can exhibit photoprotective properties. We found also that **HXA** should show larger Stokes shift than **XA** between the absorption and fluorescence maxima.

Acknowledgements: The author thanks prof. Petko Ivanov (Institute of Organic Chemistry – Bulgarian Academy of Sciences) for the given computational quota and the technical support of the CC2 calculations (Linux-cluster MADARA), Project RNF01/0110.

REFERENCES

1. J. M. Berg, J. L. Tymoczko, L. Stryer, *Biochemistry* (5th ed.), W. H. Freeman, New York, 2002.
2. K. A. Kistler, S. Matsika, *J. Chem. Phys.*, **128**, 215102 (2008).
3. S. Matsika, P. Krause, *Annu. Rev. Phys. Chem.*, **62**, 621 (2011).
4. S. Matsika, *J. Phys. Chem. A*, **108**, 7584 (2004).
5. S. Yamazaki, W. Domcke, A. Sobolewski, *J. Phys. Chem. A*, **112**, 11965 (2008).
6. S. Yamazaki, W. Domcke, *J. Phys. Chem. A*, **112**, 7090 (2008).
7. C. Canuel, M. Mons, F. Piuze, B. Tardivel, I. Dimicoli, M. Elhanine, *J. Chem. Phys.*, **122**, 074316 (2005).
8. V. B. Delchev, A. L. Sobolewski, W. Domcke, *Phys. Chem. Chem. Phys.*, **12**, 5007 (2010).
9. H. Farrokhpour, F. Fathi, *J. Comput. Chem.*, **32**, 2479 (2011).
10. S. Yamazaki, A. L. Sobolewski, W. Domcke, *Phys. Chem. Chem. Phys.*, **11**, 10165 (2009).
11. M. Shukla, J. Leszczynski (ed.), *Radiation induced molecular phenomena in nucleic acids: a comprehensive theoretical and experimental analysis*, Springer, 2008.
12. M. K. Shukla, J. Leszczynski, *J. Phys. Chem. A*, **104**, 3021 (2000).
13. M. K. Shukla, J. Leszczynski, *J. Mol. Struct. (Theochem)*, **529**, 99 (2000).
14. B. Hernandez, F.T. Luque, M. Orozco, *J. Org. Chem.*, **61**, 5964 (1996).
15. D. Lichtenberg, F. Bergmann, Z. Neiman, *Isr. J. Chem.*, **10**, 805 (1972).
16. M. M. Stimson, M. A. Reuter, *J. Am. Chem. Soc.*, **65**, 153 (1943).
17. J. Chen, B. Kohler, *Phys. Chem. Chem. Phys.*, **14**, 10677 (2012).
18. C. Hättig, F. Weigend, *J. Chem. Phys.*, **113**, 5154 (2000).
19. C. Hättig, *J. Chem. Phys.*, **118**, 7751 (2003).
20. C. Woywod, W. Domcke, A. L. Sobolewski, H.-J. Werner, *J. Chem. Phys.*, **100**, 1400 (1994).
21. R. H. A. Eade, M. A. Robb, *Chem. Phys. Lett.*, **83**, 362 (1981).
22. H. B. Schlegel, M. A. Robb, *Chem. Phys. Lett.*, **93**, 43 (1982).
23. R. Ahlrichs, M. Baer, M. Haeser, H. Horn, C. Koelmel, *Chem. Phys. Lett.*, **162**, 165 (1989).
24. M. J. Frisch, G. W. Trucks, H. B. Schlegel, G. E. Scuseria, M. A. Robb, J. R. Cheeseman, J. A. Montgomery, Jr., T. Vreven, K. N. Kudin, J. C. Burant, J. M. Millam, S. S. Iyengar, J. Tomasi, V. Barone, B. Mennucci, M. Cossi, G. Scalmani, N. Rega, G. A. Petersson, H. Nakatsuji, M. Hada, M. Ehara, K. Toyota, R. Fukuda, J. Hasegawa, M. Ishida, T. Nakajima, Y. Honda, O. Kitao, H. Nakai, M. Klene, X. Li, J. E. Knox, H. P. Hratchian, J. B. Cross, V. Bakken, C. Adamo, J. Jaramillo, R. Gomperts, R. E. Stratmann, O. Yazyev, A. J. Austin, R. Cammi, C. Pomelli, J. W. Ochterski, P. Y. Ayala, K. Morokuma, G. A. Voth, P. Salvador, J. J. Dannenberg, V. G. Zakrzewski, S. Dapprich, A. D. Daniels, M. C. Strain, O. Farkas, D. K. Malick, A. D. Rabuck, K. Raghavachari, J. B. Foresman, J. V. Ortiz, Q. Cui, A. G. Baboul, S. Clifford, J. Cioslowski, B. B. Stefanov, G. Liu, A. Liashenko, P. Piskorz, I. Komaromi, R. L. Martin, D. J. Fox, T. Keith, M. A. Al-Laham, C. Y. Peng, A. Nanayakkara, M. Challacombe, P. M. W. Gill, B. Johnson, W. Chen, M. W. Wong, C. Gonzalez, J. A. Pople, Gaussian 03, Revision D.01, Gaussian, Inc., Wallingford CT, 2004.
25. D. E. Duggan, R. L. Bowman, B. B. Brodie, S. Udenfriend, *Arch. Biochem. Biophys.*, **68**, 1 (1957).
26. M. K. Shukla, P. C. Mishra, *J. Mol. Struct.*, **324**, 241 (1994).

КСАНТИН И ХИПОКСАНТИН: В ТЪРСЕНЕ НА КОНИЧНИ СЕЧЕНИЯ S_0/S_1 , СВЪРЗАНИ С ДЕФОРМАЦИЯ НА ПИРИМИДИНОВИЯ ФРАГМЕНТ НА ПУРИНОВИЯ ПРЪСТЕН

В. Б. Делчев

Пловдивски университет "П. Хилендарски", Катедра Физикохимия, ул. Цар Асен 24, 4000 Пловдив, България

Постъпила на 19 март 2014 г.; Коригирана на 9 април 2014 г.

(Резюме)

Н₉Н тавтомерите на оксо ксантина и хипоксантина са изследвани на CC2/aug-cc-pVDZ теоретично ниво с цел да се намерят конични сечения от типа S_0/S_1 , за да се изучат механизмите на безизлъчвателна дезактивация на възбудените им състояния, които са свързани с деформации на пиримидиновите остатъци в пуриновите пръстени. Намерените конични сечения са охарактеризирани чрез адиабатните повърхнини на двете електронни състояния S_0 и S_1 , построени в ограничено пространство около тях.

Use of the descriptor fingerprints to clustering of chemical datasets

B. P. Stoyanov¹, P. R. Kostadinov¹, M. V. Kolev¹, Z. A. Mustafa², M. N. Moskovkina³, R. S. Milina², I. P. Bangov^{3*}

¹Department of Computer Informatics, Faculty of Mathematics and Informatics, Konstantin Preslavski University of Shumen, 115 Universitetska str., 9712 Shumen, Bulgaria

²Central Research Laboratory, Faculty of Natural Sciences, Prof. Assen Zlatarov University, 62 San Stefano str., 8001 Burgas, Bulgaria

³General Chemistry Chair, Faculty of Natural Sciences, Konstantin Preslavski University of Shumen, 115 Universitetska str., 9712 Shumen, Bulgaria

Received April 28, 2014; Revised May 20, 2014

Dedicated to Acad. Dimiter Ivanov on the occasion of his 120th birth anniversary

A novel approach in the area of chemoinformatics, the use of descriptor fingerprints has been applied to the problem of clustering of chemical databases. This approach coupled with the clustering method of Butina (originally created for structural fingerprints) was tested with a set of 96 biodiesel fuels. The influence of the threshold values from 0.0 to 1.0 of the Tanimoto index on the clustering results was studied. The results show a good discrimination power of the method, biodiesels of the same oils fall in one the same clusters. It was also shown that similar cetane number (CN) values of biodiesels within the statistical accuracy fall in the same cluster.

Key words: clustering analysis, descriptor fingerprints, Tanimoto index, biodiesels

INTRODUCTION

There are many methods developed in the field of chemoinformatics, such as neuronal networks, partial least square (PLS), multivariable regression, discriminant analysis etc. They have their advantages and drawbacks. For a year we have developing a novel approach - *descriptor fingerprints* devised by one of the authors (IB) [1-3], toward the similarity of different chemical and/or non-chemical materials. Its potentials have been demonstrated with the creation of a server on the net for allergen and non allergen food proteins compared with servers based on the traditional chemoinformatics methods [2]. Hence, the purpose of this work is to study the influence of the *threshold value* on the results from similarity clustering with descriptor fingerprints.

The basic idea of descriptor fingerprints comes from the well known structural fingerprints [4-6]. Both structural and descriptor fingerprints are defined either as a character or binary string of 0s and 1s.

In the case of structural fingerprint an array of structural fragments is juxtaposed to the fingerprint array, each element of the former corresponding to the element of the latter being at the same location.

The general scheme is shown on Fig. 1.

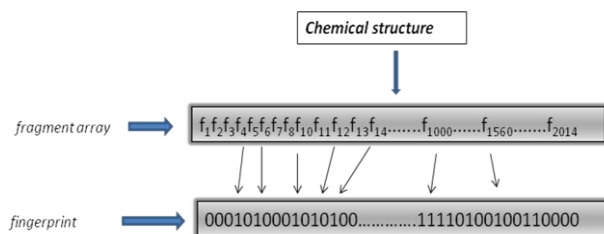


Fig. 1. Fingerprint generation of chemical structures.

The program automatically determines these minimum and maximum values for each descriptor from all the descriptors in the set. A precision (resolution) - *resValue* of each descriptor is user defined. Hence, for each real value descriptor its interval is divided into $N = (\text{initValue} - \text{endValue}) / \text{resValue}$ discrete sub-intervals. Some descriptor could be binary, e.g. the presence or absence of a property. They are encoded by one interval. Thus, the formation of the fingerprint from all its descriptors is carried out by concatenation of all their sub-intervals. In case a descriptor real value falls in an interval a 1 is put in the corresponding position of the fingerprint array, the other elements corresponding to the descriptor remaining 0s. The formation of a descriptor fingerprint is illustrated in Fig. 2.

* To whom all correspondence should be sent:
E-mail: ivan.bangov@gmail.com

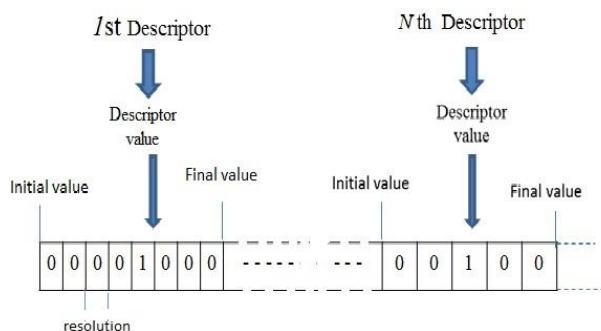


Fig. 2. Formation of a descriptor fingerprint.

The similarity search of two objects (chemical structures, materials, etc.) is carried out by comparing their fingerprints using any similarity measure [7,8]. In this work the Tanimoto measure has been employed to this end. It has the following form:

$$T = N_C / (N_A + N_B - N_C). \quad (1)$$

Here, N_A is the number of elements having value 1 in the first fingerprint A, N_B is the number of elements having value 1 in the second fingerprint B, and N_C is the number of the common elements (being in the same position in both fingerprints) having value 1. This index has real values between 0.0 and 1.0. The higher is the value the more similar are the two objects.

CLUSTERING OF SETS OF OBJECTS

Clustering of set of objects is based on the cluster analysis. Here is a definition from Wikipedia [9]:

“Cluster analysis or clustering is the task of grouping a set of objects in such a way that objects in the same group (called a cluster) are more similar (in some sense or another) to each other than to those in other groups (clusters). It is a main task of exploratory data mining, and a common technique for statistical data analysis, used in many fields, including machine learning, pattern recognition, image analysis, information retrieval, and bioinformatics.”

There are several algorithms for clustering of different sets of objects. Some of them are the *connectivity based*, *distance measure based*, other are *centroid based* approaches. Here we use the clustering algorithm of Butina [10]. It consists of the following procedures:

- ◆ First, the Tanimoto index is calculated pairwise for all the objects in the set within the given threshold value (the smallest Tanimoto value accepted for a pair).

- ◆ Second, the objects are sorted according to the number of their neighbours, i.e. forming from most to less numerous pairs within the given threshold value, i.e., with Tanimoto value between the threshold value and 1.0.

- ◆ Further, another pass of pairwise fingerprint Tanimoto calculation is carried out, starting from the first pair of the sorted set. All its neighbours form the first cluster and are subsequently flagged as “used”. Then, follows the same procedure with the second unused object, applied to the remaining unused fingerprints only, and the second cluster is formed, then the next clusters are formed in the same way. A last cluster is formed from the objects having 1 neighbour only.

- ◆ An additional procedure of automatic perception of the threshold value (TV) was developed by us. An extra preliminary pairwise Tanimoto calculation of the data set with a subsequent ranking of the pairs was carried out. Further a procedure scan the names of the ranked pairs and finds out at what value the Tanimoto index produces false result. This value increase by 0.00001 is taken for a threshold value (TV_{auto}).

APPLICATION, RESULTS AND DISCUSSION

We applied this clustering approach to a set of 96 biodiesel fuels of several vegetable oils: sunflower (SF), soya beans (SB), corn (CR), rape seed (RS), peanut (PN), palm (PM) and some mixed cases (MIX). They have been selected from different feed stocks (with different composition and properties respectively). In as much as the biodiesel fuel is a mixture of fatty acid methyl esters (FAME) its properties depend on the chemical structure of the individual FAME and their contents (FAME profile) [11-14]. Hence, the descriptor fingerprint method has been based on their gas chromatographic FAME profiles [15-19]. To the aim some available literature data on FAME profiles of biodiesels from several types of oils were used [11,14,20-22].

Our method of descriptor fingerprint clustering was applied to a set of different biodiesel fuels in order to derive a new alignment for them into some groups (clusters).

In this paper we study the influence of the threshold value (TV) on the clustering. The results are provided in Table 1.

One can see from Table 1, that the best clustering is with threshold value TV=0.7. Thus, it is seen that a perfect discrimination leading to separation of the different biodiesels, say, all sun-

Table 1. Results of the biodiesel oils clustering.

Cluster No	Vegetable oils in biodiesels	TV= 0.0	TV= 0.1	TV= 0.2	TV= 0.3	TV= 0.4	TV= 0.5	TV= 0.6	TV= 0.7	TV= 0.8	TV= 0.9	TV= 1.0	TVauto= 0.5263158
1	SF	33	33	32	30	28	25	21			5	3	13
	SB	19	19	19	18	12	1		11	7			
	CR	8	8	8	7	2							
	PN	6	5										
	RS	19	19	12									
	PM	6	6	5									
	Mix	5	5	1	1								
2	SF			1	3	2			11	6			
	SB				1	1	14	15			3	2	12
	CR					2							
	Mix			2									
3	SF						2	2	4	5	3	2	2
	SB					6	1						
	CR					2	2						
	RS			7	18								
	Mix			2									
4	SF						4	1	3	3			4
	PN			6									
	RS					14							
	PM				6								
	SB										2		
	CR							1					
5	SB						2			2	2		
	PN				4								
	RS					2							5
	SF							2					
	PM									4			
6	RS						6						
	PM					6							
	Mix				3								
	SF								3	3			
	SB							1			2		2
	CR							2					
7	CR					2							
	PN				2								
	PM						5						
	SF										2		
	SB								2	2			1
	RS							5					
8	SF					2		3					
	RS						3		3	2	2		
	SB												1
9	CR						3						
	PN					3							
	SF									2			3
	RS								3				
	PM							5					
10	RS						2	4	2	2			3
	Mix					2							
11	PN					2			2				
	RS						4	3					
	PM									2			
	CR												2

12	RS				3			2			
	SF						2				
	PN					3					
13	PN				3						
	RS						2				
	PM									3	
14	PN				2						
	SF						2			2	
15	SF				2						
	RS						2				
Last	SF				1		2	10	14	23	25
	SB					1	3	6	8	10	17
	CR			1		3	5	8	8	8	8
	PN	1		1		3	4	6	6	6	6
	RS			1	3		3	11	13	17	19
	PM		1			1	1	2	4	6	6
	Mix			1	3	5	5	5	5	5	5

Table 2. Statistical data concerning cetane number of biodiesel fuels for the highest Tanimoto index values.

Cluster	N class	CN	Mean	Standard deviation	Confidence level (95%)
T=1					
1	14 SF	48.695	48.508	0.166	0.413
1	17 SF	48.453			
1	21 SF	48.377			
2	61 SB	49.260	49.020	0.340	3.056
2	67 SB	48.779			
3	6 SF	47.758	47.884	0.177	1.595
3	7 SF	48.009			
T=0.9					
1	14 SF	48.695	48.467	0.182	0.226
1	15 SF	48.584			
1	16 SF	48.224			
1	17 SF	48.453			
1	21 SF	45.377			
2	61 SB	49.260			
2	67 SB	48.779	48.774	0.489	1.214
2	76 SB	48.283			
3	5 SF	48.191			
3	6 SF	47.758	47.986	0.217	0.540
3	7 SF	48.009			

flower biodiesels in one cluster, all soy bean biodiesels in another etc., is not achieved. We have two clusters of sunflower biodiesels, two clusters of soy bean biodiesels. This situation can be explained with different fatty acid composition of vegetable oils.

The results from TV=0.6, TV=0.7, TV=0.8, and TV=0.9 providing best discrimination are visualized in Fig. 3, Fig.4, Fig. 5, and Fig. 6.

One can see from Table 1 and Fig. 3, Fig. 4, Fig. 5, and Fig. 6 that the number of biodiesels grouped in a separate cluster depends on the value of TV. At low TVs the number of objects in a cluster increases but the number of clusters decreases.

Thus, at TV=0.0, and TV=0.1 we have only 1 cluster.

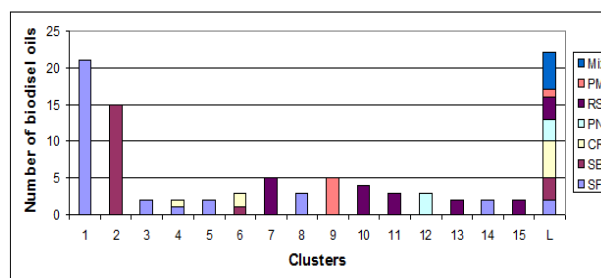


Fig. 3. Distribution of the different biodiesels at TV=0.6.

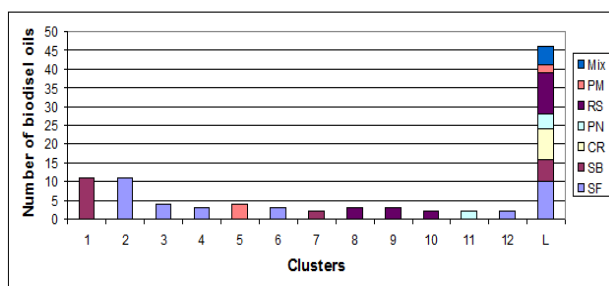


Fig. 4. Distribution of the different biodiesels at TV=0.7.

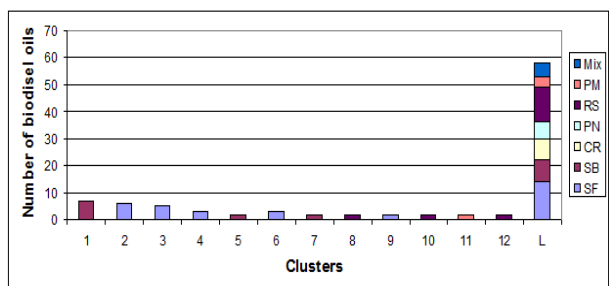


Fig. 5. Distribution of the different biodiesels at TV=0.8.

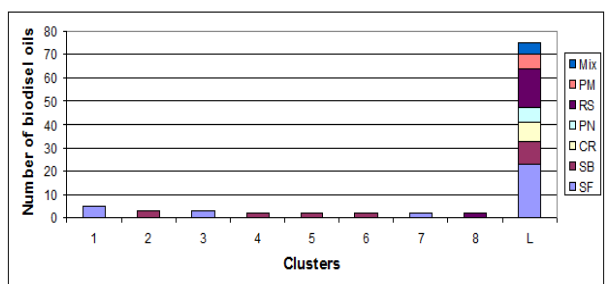


Fig. 6. Distribution of the different biodiesels at TV=0.9.

There are various parameters, used for characterization of different biodiesel grades. The determination of the cetane number (CN) is an important index from our clustering analyses. The CN values of the biodiesel fuels, grouped in clusters having T-values 1.0 and T=0.9 are shown in Table 2. Some statistical indicators such as mean and standard deviation (confidence level 95%) are presented also in Table 2.

One can see that the oils grouped in a given cluster are of the same type on the one hand and on the other hand they produce similar CN values.

The lowering of Tanimoto index value extends the frontiers of the cluster; this tendency is characterized by the statistical indicator of the Standard Deviation value, presented in Table 2.

CONCLUSION

A group of 96 biodiesel oils of different origin was used for creation of descriptor fingerprints

based on their gas chromatographic FAME profiles. The influence of the threshold value on the clustering results was studied. As a result of the clustering analysis based on descriptor fingerprints biodiesel oils of the same type were grouped into distinct clusters. It was observed that in general, biodiesels having similar values of some important parameters (properties) fall in the same clusters. It was shown the CN values are correlating with the Tanimoto index are within the statistical accuracy. The obtained results allow us to carry out in-depth studies on the ability of the method of descriptor fingerprints for prediction of various analytical properties.

REFERENCES

1. I. Bangov, L. Naneva, M. N. Moskovkina, I. Dimitrov, I. Doytchinova, *Annual of Konstantin Preslavski University of Shumen, Natural Sciences, Chemistry*, **XXII B1**, 28 (2013).
2. I. Dimitrov, L. Naneva, I. Doytchinova, I. Bangov, *Bioinformatics*, **30**, 846 (2014).
3. I. Dimitrov, N. Kochev, M. Moskovkina, L. Naneva, V. Paskaleva, R. Milina, Z. Mustafa, I. Doytchinova, I. Bangov, *Acta Sci. Natur.*, (2013) submitted.
4. J. M. Barnard, in *Handbook of Chemoinformatics*, **1**, 27 (2003).
5. J. Tomczak, in *Handbook of Chemoinformatics*, **2**, 392 (2003).
6. T. Engel, in *Chemoinformatics. A textbook*, 15 (2003).
7. P. Willett, in *Handbook of Chemoinformatics*, **2**, 904 (2003).
8. N. Kochev, V. Monev, I. Bangov, in *Chemoinformatics. A textbook*, 291 (2003).
9. http://en.wikipedia.org/wiki/Cluster_analysis.
10. D. Butina, *J. Chem. Inf. Comput. Sci.*, **39**, 747 (1999).
11. S. K. Hoekman, A. Broch, C. Robbins, E. Ceniceros, M. Natarajan, *Renew. Sust. Energ. Rev.*, **16**, 143 (2012).
12. Y. C. Sharma, B. Singh, S. N. Upadhyay, *Fuel*, **87**, 2355 (2008).
13. A. E. Atabania, A. S. Silitonga, I. A. Badruddina, T. M. I. Mahlia, H. H. Masjuki, S. Mekhilef, *Renew. Sust. Energ. Rev.*, **16**, 2070 (2012).
14. M. J. Ramos, C. M. Fernandez, A. Casas, L. Rodriguez, A. Perez, *Bioresource Technol.*, **100**, 261 (2009).
15. C. P. Prados, D. R. Rezende, L. R. Batista, M. I. R. Alves, N. R. A. Filho, *Fuel*, **96**, 476 (2011).
16. E. D. Dodds, M. R. McCoy, L. D. Rea, M. J. Kennish, *Lipids*, **40**, 419 (2005).
17. L. Mondello, A. Casilli, P. Q. Tranchida, R. Costa, B. Chiofalo, P. Dugo, *J. Chromatogr. A*, **1035**, 237 (2004).
18. E. Bravy, G. Perrey, L. Montanary, *J. Chromatogr. A*, **1134**, 210 (2006).

19. R. Milina, Z. Mustafa, *Petroleum & Coal*, **55**, 12 (2013).
20. B. R. Moser, S. F. Vaughn, *Biomass Bioenerg.*, **37**, 31 (2012).
21. D. Brodnjak-Voncina, Z. C. Kodba, M. Novich, *Chemometr. Intell. Lab.*, **75**, 31 (2005).
22. E. G. Giakoumis, *Renew. Energ.*, **50**, 858 (2013).

ИЗПОЛЗВАНЕ НА ДЕСКРИПТОРНИТЕ ОТПЕЧАТЪЦИ НА ПРЪСТИТЕ ЗА КЛЪСТЕРИРАНЕ НА ХИМИЧНИ МНОЖЕСТВА ОТ ДАННИ

Б. П. Стоянов¹, П. Р. Костадинов¹, М. В. Колев¹, З. А. Мустафа², М. Н. Московкина³, Р. С. Милина², И. П. Бангов^{3*}

¹Катедра по компютърна информатика, Факултет по математика и информатика, Шуменски университет "Константин Преславски", ул. Университетска 115, 9712 Шумен, България

²Централна изследователска лаборатория, Факултет по природни науки, Университет "Проф. Асен Златаров", ул. Сан Стефано 62., 8001 Бургас, България

³Катедра Обща химия, Факултет по природни науки, Шуменски университет "Константин Преславски", ул. Университетска 115, 9712 Шумен, България

Постъпила на 28 април 2014 г.; Коригирана на 20 май 2014 г.

(Резюме)

Един нов подход в областта на хемоинформатиката - използването на дескрипторните отпечатъци на пръстите е приложен към проблема за клъстериране на бази от химически данни. Този подход, придружен с метода на Бутина (първоначално създаден за структурни дескриптори) беше тестват с група от 96 биодизелни горива. Влиянието на праговата стойност от 0.0 до 1.0 на индекса на Танимото върху резултатите от клъстерирането беше изследвано. Резултатите показаха една добра разделителна способност на метода, като биодизели с еднакви масла попадат в едни и същи клъстери. Беше показано също, че подобни стойности на цетановото число на биодизелите попадат в едни и същи клъстери в рамките на статистическата точност.

A novel program for computer-aided generation of 2D chemical structures

B. P. Stoyanov¹, E. P. Petrov¹, N. T. Kochev², I. P. Bangov^{3*}

¹Department of Computer Informatics, Faculty of Mathematics and Informatics, Konstantin Preslavski University of Shumen, 115 Universitetska str., 9712 Shumen, Bulgaria

²Plovdiv University "Paisii Hilendarski", Faculty of Chemistry, Department of Analytical Chemistry and Computer Chemistry, 24 Tsar Assen str., 4000 Plovdiv, Bulgaria

³Department of Chemistry, Faculty of Natural Sciences, Konstantin Preslavski University of Shumen, 115 Universitetska str., 9712 Shumen, Bulgaria

Received April 30, 2014; Revised July 01, 2014

Dedicated to Acad. Dimiter Ivanov on the occasion of his 120th birth anniversary

A novel software product STRGEN-2D for generation of 2D chemical structures from a gross formula is implemented. It is based on an approach developed by one of the authors (IB). Various functionalities and options of the program are discussed. The output of STRGEN-2D software is compared with the generated structures by MOLGEN software. The generation efficiency and correctness of obtained structure sets are proved.

Key words: structure generation, 2D chemical structures, generation tree, depth-first approach

INTRODUCTION

2D computer-aided structure-generation plays a special role in QSAR/QSPR investigations. Structure-generator software provides new prospective candidate-structures for both biological activity and chemical and physical properties studies in these fields.

The implementation of 2D chemical structure generator programs comes across on some specific mathematical problems. Its algorithm is exponential which leads to the so called combinatorial explosion. This explosion is conducive to generation of enormous number of structures with the increase of number of atoms participating in the generation process. Hence it is challenging to be processed by the most powerful computer equipment on the one hand, and on the other hand it is virtually impossible to be inspected by the users. Furthermore, the generation is a blind process which leads to so called isomorphism problem i.e. generation of isomorphic (duplicated) structures. Thus, if we have N atoms a permutation of 2 atoms will produce $(N-2)!$ duplicated structures.

During the 80's a novel approach to the solution of these problems was devised by one of the authors (IB) [1-12]. This approach was oriented towards the development of a computer-assisted structure elucidation based on ¹³C spectral information [8]. Our new development is oriented

toward QSAR/QSPR problems. The software was implemented in C++ programming language. The aim of this paper is to study the efficiency and correctness of our new software by comparing the generated structures with structures from other sources.

ALGORITHM DESCRIPTION

A chemical structure is mathematically considered a chemical graph $G(A,B)$. Here A is a set of atoms (vertices of the graph), and B is a set of bonds (edges of the graph). Efficient two-row representation of the chemical structure is used [1-3] as it is illustrated in Fig. 1. In order to alleviate the combinatorial process we devised the following separation of the chemical graph vertices. Consider a chemical structure represented by a directed graph (the orientations of the edges are given by arrows) depicted in Fig. 1.

Hence, we separate the vertices into two groups, vertices presented in Fig. 1 with arrows pointing to other vertices (we call them Saturating Valences - SVs), and vertices which accept the arrows, called Saturation Sites, SSs). One can see that each atom except the first has 1 SV and $n-1$ SSs. Here n is the atom valency. The first atom has all its n valencies of SS type. In case of a cycle closure (see atom 6 from Fig. 1) a SS is transformed into SV. Accordingly the generation process is carried out by level by level saturation of the SS with the SVs, each level represented by one SV as shown in Fig. 1.

* To whom all correspondence should be sent:
E-mail: ivan.bangov@gmail.com

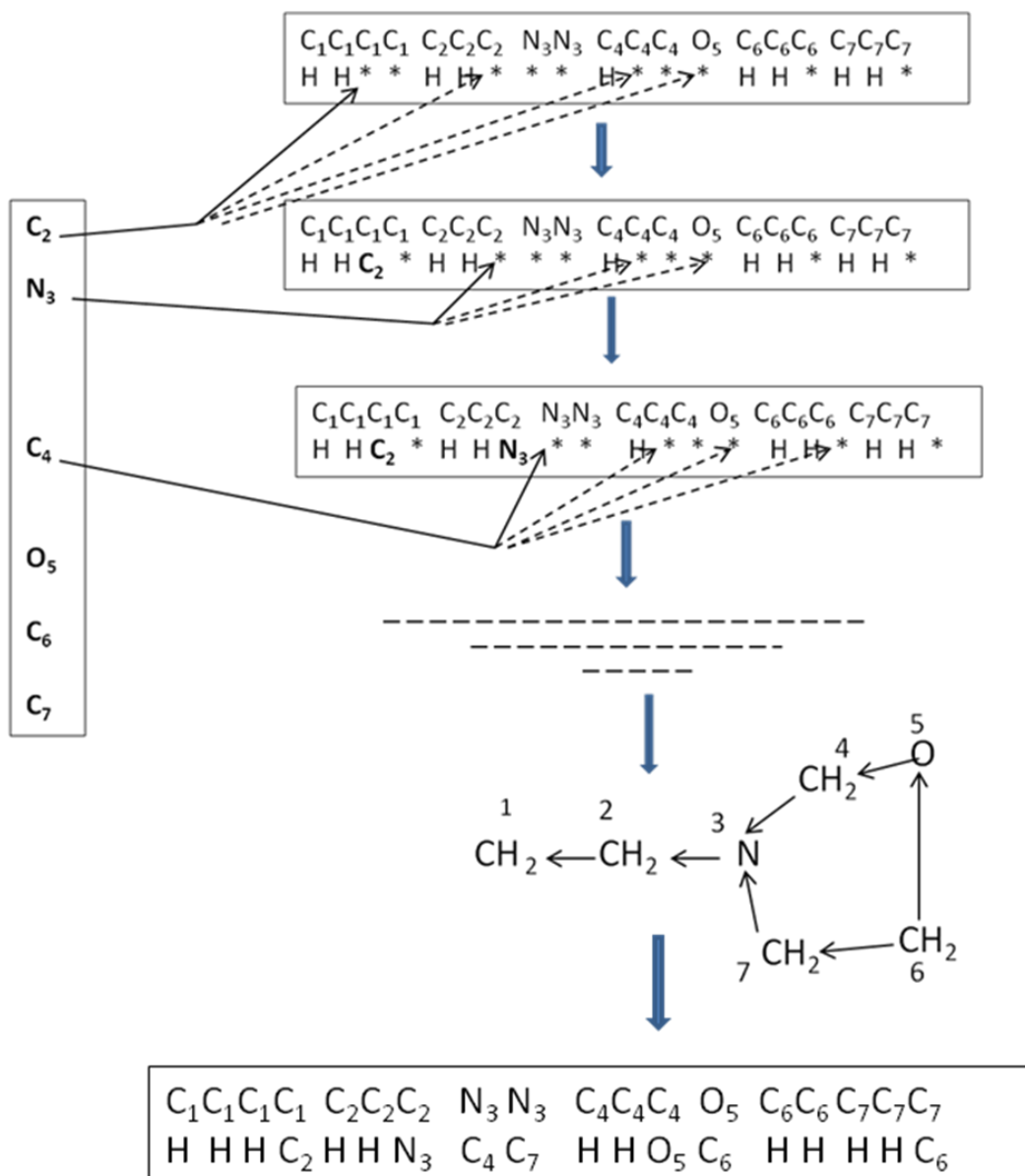


Fig. 1. Two-dimensional matrix structure representation and depiction of level-by-level structure generation.

Each saturation produces a fragment which is practically an extension to the formation of complete chemical structures. Thus, a structure generation tree shown in Fig. 2 is formed.

The process of saturation can be carried in two ways: either depth-first with backtracking. In this case the formation of a structure goes to its end and then follows backtracking over the generation tree and generation of a new structure. The other approach is breath-first approach. In this case all the SSs of a given level are saturated producing fragments the their SSs are saturated at the next level, and so on, to the generation of the full set of structure at the highest level.

For our QSAR/QSPR we have found the latter approach to be more appropriate. This allows some further developments towards pruning any chemically and physically inappropriate extensions, on the one hand, and the introduction of parallel processing on the other [9].

Our approach toward the isomorphism problem lies on the following principles:

- ❖ as it was suggested [4-6] the isomorphism is a consequence of the automorphism (vertex equivalence) the equivalence of the different vertices at each extension is studied by using the following local charge-related index (LCI):

$$Li = n_v + q - N_H \quad (1)$$

- ❖ where n_v is the atom valence, q is the atom charge and N_H is the number of attached hydrogen atoms. The equivalent vertices (atoms) give the same value L_i s within the computer-word accuracy we accept up to 6th sign after decimal point. Hence, permutations between equivalent atoms are forbidden. Such permutations are generated if two equivalent SVs saturate two equivalent SSs and then exchange their SSs. As shown in Fig. 1. Hence, in case of equivalent SVs saturating equivalent SSs, each next level starts from the atom next to the atom that has been saturated in the previous level.
- ❖ Besides the previous principle some duplications still remain because of the mirror symmetry of some structures cannot be predicted during the course of generation.

Further, the CTI index for each extension has been calculated and compared with the CTI indices [3,13-15] of the extensions at the current level. The CTI has the following form:

$$CTI = 1/2 \sum_i \sum_j \frac{L_i L_j}{D_{ij}} \quad (2)$$

Here L_i are the local indices (1) and D_{ij} are topological distance matrix elements. In a recent paper [15] it was shown by us that CTI s provide extremely good discriminating power, the equivalent (isomorphic) structures have the same CTI , whereas the different structures possess different CTI s within a computer word precision up to 7th sign after the decimal point. Thus, all the remaining branches containing isomorphic structures are pruned from the generation tree.

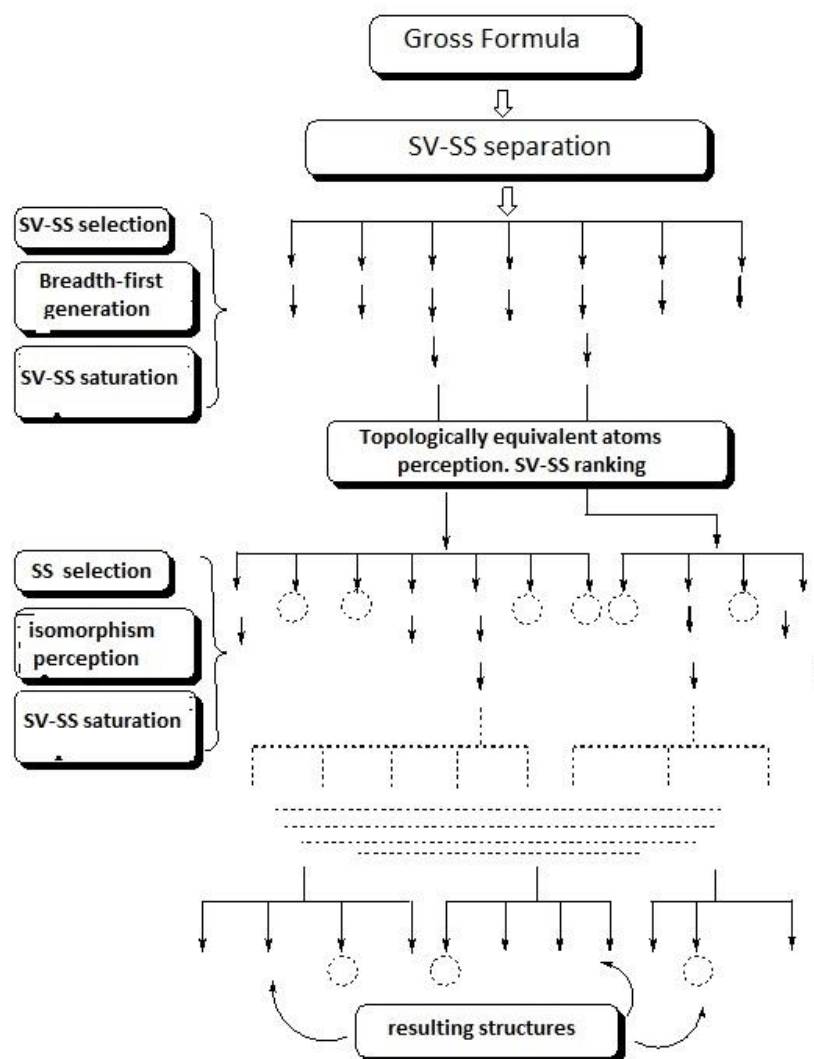


Fig. 2. Structure generation tree with depiction of the steps of structure generation algorithm.

TEST RESULTS

In order to test the correctness of the result structure set from STRGEN-2D software we performed analogous calculation with MOLGEN [16,17] method for various gross formulas. The results from MOLGEN were exported as *.MOL files and additionally converted into canonical linear notations SMILES. The STRGEN-2D program transforms internally the structures into SMILES forms. The generated from the two programs structures were compared on the base of both the SMILES canonical linear notation and with the *CTI* index mentioned above. The comparison results for some gross formulas are provided in Table 1. One can see that the numbers of generated structures by our method are the same with these generated by MOLGEN method.

Table 1. Number of generated structures by MOLGEN and STRGEN-2D programs and times of generation by STRGEN-2D program.

Gross formula	MolGen (number of structures)	STRGEN 2D	
		Number of structures	Time in seconds
C6N1H11	1111	1111	4.85
C6N2H14	2338	2338	11.82
C6N3H17	1395	1395	7.56
C6N2O1H14	31984	31984	2478.30
C6N3O1H17	20368	20368	1754.04
C6O2H12	1313	1313	4.72
C6O3H12	6171	6171	83.27
C6O4H12	24562	24562	2059.28

The times of generation from the STRGEN-2D software are also provided in Table 1. However they cannot be compared with these from the MOLGEN program for several reasons. Our program runs on a 64bit processor while the MOLGEN program on a 32bit processor. Furthermore, the two programs have different output which produces different times. And more important, our breadth-first approach with exploring each level makes the program slower. Instead of simple combinatorial process the program generates SMILES codes of the fragments at each level. However, we need this approach for our further QSAR/QSPR developments. Accordingly, it was clear for us that the STRGEN-2D is slower than the other programs for structure enumeration, only.

Additionally some results generated by using fragments which obviously reduce the number of generated structures are provided in Table 2.

Table 2. Number of generated structures having certain fragments.

Gross Formula	Fragments		Number of generated structures
C6N2O2H14	CC	C-C	32192
	C=N	C=N	
	CO		
C6N1H11	C=NC	C=N-C	141
C6N1H11	C=C=N	N=C=C	18
C6O3H12	C=O	C=O	703
C6N3H17	NN	N-N	708
	CN	C-N	
C6N2H14	C1CC1		63
	NN	N-N	
C6N2H14	C1CCN1		198
			

CONCLUSION

A software product for two dimensional structure generation was created. It was developed towards the perception of novel chemical structures for a further QSAR/QSPR processing. It is based on a multilevel breath-first approach, at each level a set of substructures (fragments) is generated and transformed in SMILES codes.

Acknowledgements: We acknowledge the Bulgarian Science Fund for its financial support (Grant SFSI I01/7).

REFERENCES

1. I. P. Bangov, *MATCH Commun. Math. Comput. Chem.*, **14**, 235 (1983).
2. I. P. Bangov, K. D. Kanev, *J. Mathem. Chem.*, **2**, 31 (1988).
3. I. P. Bangov, *J. Chem. Inform. Comput. Sci.*, **30**, 277 (1990).
4. I. P. Bangov, *J. Chem. Inf. Comput. Sci.*, **32**, 167 (1992).
5. I. P. Bangov, *MATCH Commun. Math. Comput. Chem.*, **27**, 3 (1992).
6. I. P. Bangov, *J. Chem. Inf. Comput. Sci.*, **34**, 318 (1994).
7. I. P. Bangov, M. I. Spassova, *Bulgarian Chem. Commun.*, **28**, 443 (1997).
8. T. Laidboeur, I. Laude, D. Cabrol-Bass, I. P. Bangov, *J. Chem. Inf. Comput. Sci.*, **34**, 171 (1994).
9. I. Bangov, S. Simova, I. Laude, D. Cabrol-Bass, *J. Chem. Inf. Comput. Sci.*, **34**, 546 (1994).
10. I. P. Bangov, *Discrete Appl. Math.*, **67**, 27 (1996).

11. I. P. Bangov, in: Handbook of Chemoinformatics, **1**, 178 (2003).
12. I. P. Bangov, *Annual of Konstantin Preslavski Shumen University, Natural Sciences, Chemistry*, **XXI B1**, 29 (2011).
13. P. A. Demirev, A. Dyulgerov, I. P. Bangov, *J. Math. Chem.*, **8**, 367 (1991).
14. N. Kochev, V. Monev, I. P. Bangov, in: Chemoinformatics. A Textbook, 291 (2003).
15. E. Petrov, B. Stoyanov, N. Kochev, I. Bangov, *MATCH Commun. Math. Comput. Chem.*, **71**, 645 (2014).
16. C. Benecke, R. Grund, R. Hohberger, A. Kerber, R. Laue, T. Wieland, *Anal. Chim. Acta*, **314**, 141 (1995).
17. MOLGEN (Molecule Structure Generation), <http://www.molgen.de/> (last accessed 25 April, 2014).

ЕДНА НОВА ПРОГРАМА ЗА ГЕНЕРИРАНЕ НА 2D ХИМИЧНИ СТРУКТУРИ С ПОМОЩТА НА КОМПЮТРИ

Б. П. Стоянов¹, Е. П. Петров¹, Н. Т. Кочев², И. П. Бангов^{3*}

¹Катедра по компютърна информатика, Факултет по математика и информатика, Шуменски университет "Константин Преславски", ул. Университетска 115, 9712 Шумен, България

²Катедра по аналитична химия и компютърна химия, Пловдивски университет "Паисий Хилендарски", ул. Цар Асен 24, 4000 Пловдив, България

³Катедра Обща химия, Факултет по природни науки, Шуменски университет "Константин Преславски", ул. Университетска 115, 9712 Шумен, България

Постъпила на 30 април 2014 г.; Коригирана на 01 юли 2014 г.

(Резюме)

Един нов софтуерен продукт STRGEN-2D за генериране на 2D химични структури от брутна формула бе създаден. Той се основава на един подход разработен от един от авторите (ИБ). Различните функции и опции са дискутирани. Изходните резултати от софтуера STRGEN-2D са сравнени с генерираните структури със софтуерния продукт MOLGEN. Ефективността и правилността на получените структури при генерацията са доказани.

Stereoselectivity in intramolecular Diels-Alder reactions of 2,4-pentadienyl butadienamides in the “Remote Stereocontrol Group” approach

A. Z. Patleeva*, D. D. Enchev, G. D. Neykov

Department of Organic Chemistry and Technology, Faculty of Natural Sciences, University of Shumen, Shumen, Bulgaria

Received May 12, 2014; Revised May 26, 2014

Dedicated to Acad. Dimiter Ivanov on the occasion of his 120th birth anniversary

The possible reaction paths of intramolecular pericyclic reactions of buta-2,3-dienoic penta-2,4-dienylamide ([1,5]-sigmatropic shift and subsequent Intramolecular [4+2] cycloaddition, Alder-ene reaction and Intramolecular [4+2] cycloaddition) were modeled as asynchronous concerted processes at semi-empirical, ab initio and DFT theoretical level. The endo/exo and π -diastereofacial stereoselectivity of the amide-tethered IMDA reaction of 2,4-pentadienyl butadienamides was investigated using the “Remote Stereocontrol Group” (RSG) approach. The localized transition states (TS) of the investigated reactions were fully optimized at MP2/6-31G(d) and DFT B3LYP/6-31G(d) levels. The relative TS free energies were calculated to determine the stereochemical outcome of the kinetically controlled reactions.

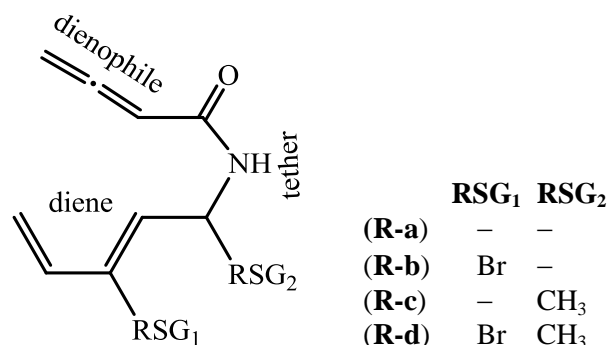
Key words: stereoselectivity, Diels-Alder reaction, Remote Stereocontrol Group, ab initio, DFT, pentadienyl butadienamides

INTRODUCTION

The intramolecular Diels-Alder (IMDA) reaction, popular in organic synthesis for producing polycyclic structures, draws the attention of many theoretical chemists. The computational investigation of IMDA reactions enables predicting chemo-, regio- and stereoselectivities and gives opportunity to examine ways to alter the expected structures, varying conformational, steric and electronic effects independently. It has been established that the stereoselectivity of IMDA reactions could be changed by a suitable choice of diene, dienophile and the type of the tether [1,2]. A large amount of experimental and theoretical studies have investigated the origin of chemical stereoselectivity in intramolecular cycloadditions – reactions of 1,3,8-nonatrienes, 1,3,9-decatrienes and 1,3,10-undecatrienes [3], substituted 3,5-hexadienyl acrylates and acrylamides [4], pentadienyl acrylates [5,6], diene and dienophile linked by a $-(CH_2)_n-$ chain, ($n=1, 2, 3$ и 4) [7]. Despite the existence of computational models of *allene* as *dienophile* in the *intermolecular* Diels-Alder reaction [8,9], models of *intramolecular* cycloadditions are not available.

In this respect we have been interested in modeling the transition structures (TS), predicting and

varying, using *Remote Stereocontrol Group* (RSG), the stereochemical outcome of the IMDA reactions of pentadienyl butadienamides (**R-a**), (**R-b**), (**R-c**) and (**R-d**).



COMPUTATIONAL PROCEDURE

Geometries of the reactants, transition structures (TS) and products were fully optimized at B3LYP/6-31G(d) and MP2/6-31G(d) level. The precursors and the expected products were connected via transition structures using the IRC procedure, Gonzalez-Schlegel method. All structures were characterized as minima (no imaginary frequencies) or a saddle point (1 imaginary frequency) on the potential energy surface (PES) by frequency calculations at the same computational

* To whom all correspondence should be sent:
E-mail: a.patleeva@shu-bg.net

level. The calculated total energies, enthalpies and free energies were corrected by zero-point energy (unscaled), estimated from the harmonic frequency calculations under atmospheric pressure and temperature 373K, which we believe is typical for modeled reactions. The relative free energies of the TS at the 373K were calculated to determine the stereochemical outcome of the kinetically controlled reactions.

All calculations were performed using the Firefly QC package [10], which is partially based on the GAMESS (US) [11] source code.

RESULTS AND DISCUSSION

The calculations of the three reaction pathways of the competing intramolecular pericyclic reactions (Fig. 1) were performed at the semi-empirical (AM1, PM3) theoretical level. The aim of the preliminary computations was to evaluate the activation and reaction energies, to determine whether the reactions are feasible, which is particularly important in the absence of experimental data and to compare the competing

processes. Reasonable pericyclic reactions (*reaction path 1* - Intramolecular [4+2] cycloaddition, *reaction path 2* - [1,5]-sigmatropic shift and subsequent Intramolecular [4+2] cycloaddition, *reaction path 3* - Alder-ene reaction) of (**R-a**, **b**, **c**, **d**) were modeled as *asynchronous concerted* processes. The *reaction path 3* (Alder-ene reaction, Fig. 1) was definitely eliminated. Nevertheless, to obtain accurate energies and hence the correct prediction of the preferred cycloadducts, higher levels of theory were required. An adequate geometry for the asynchronous TS, reactants and products was furnished by calculations at the semi-empirical level.

To perform higher level calculations, we used the hybrid B3LYP functional with the 6-31G(d) basis set which has been proven to be particularly successful for modeling TS and energetics of pericyclic reactions [12-14], and the many-body perturbation method of Møller and Plesset (MP2) with the same basis, for estimating the effect of dynamic electron correlation. Despite of the limitations of DFT methods leading to overestima-

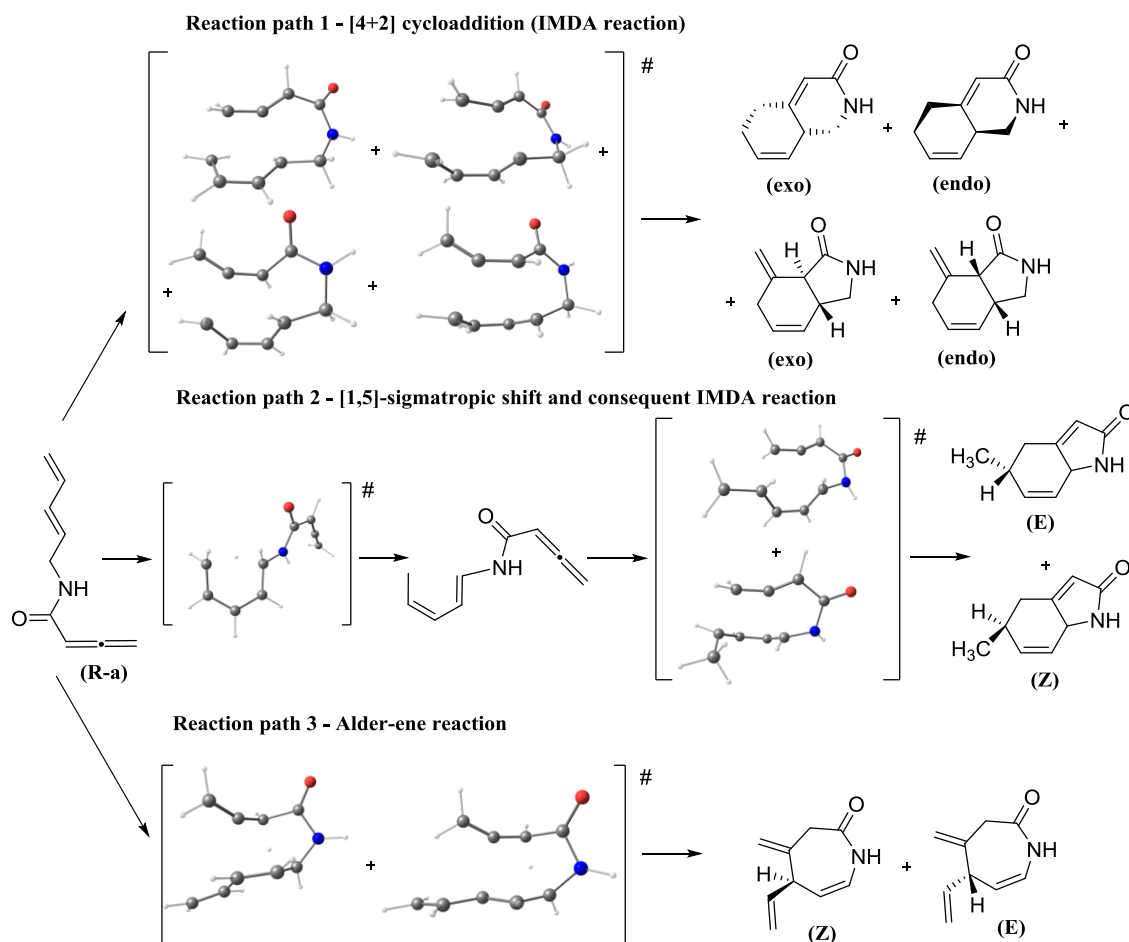


Fig. 1. Modeled pericyclic reactions of buta-2,3-dienoic penta-2,4-dienylamide (**R-a**) at AM1 (presented TS models) semi-empirical computational level.

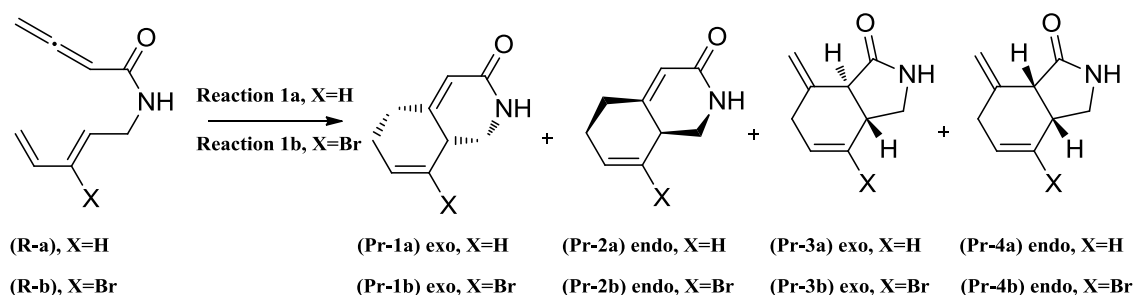


Fig. 2. Modeled IMDA reactions of precursors (R-a) and (R-b); Reactions 1a and 1b.

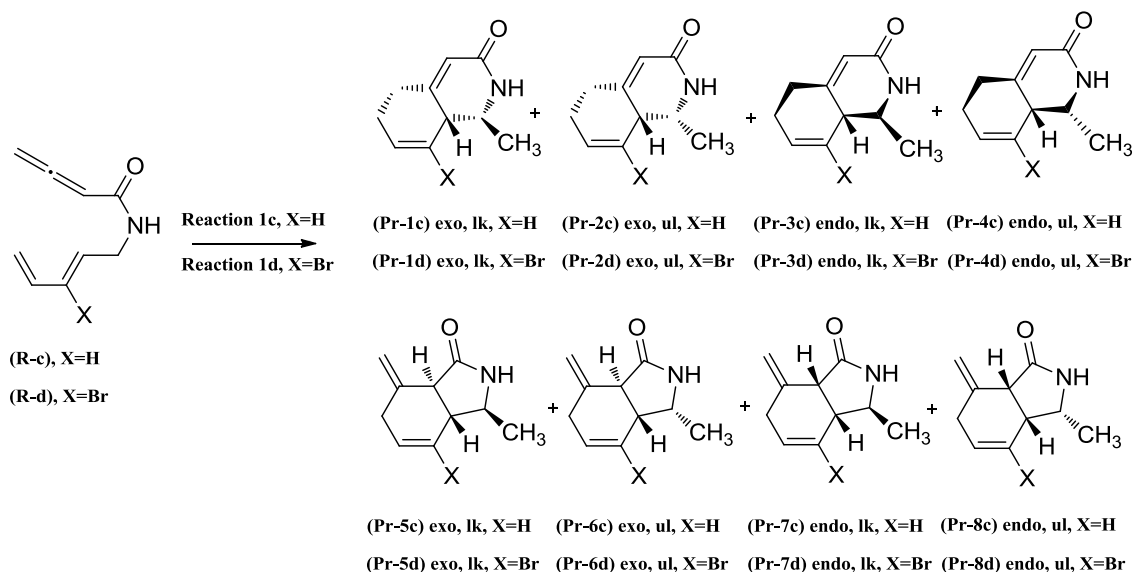


Fig. 3. Modeled IMDA reactions of precursors (R-c) and (R-d); Reactions 1c and 1d.

tion of the energy of conversion of π bonds into σ bonds, which might result in errors in DFT energetics of electrocyclic reactions [15], the functional B3LYP remains very popular due to the balance between accuracy and efficiency.

The Diels-Alder reaction goes primarily in an *endo* rather than an *exo* direction when the product formation is kinetically controlled. It is known that C3 substituent manipulates the stereochemical outcome of IMDA reaction and shifts product distribution toward trans-fused (*exo*) bicyclic products [1], so we have used *bromine*, reported as a successful *RSG* and the *5-methyl tether substituent* - another stereo controlling element which also effectively accelerates the rate of IMDA reactions [3].

Competing IMDA reactions (*reaction paths 1a, 1b, 1c, 1d*) and corresponding [1,5]-sigmatropic shifts (*reaction paths 2a, 2b, 2c, 2d*) are presented on Fig. 2, Fig. 3 and Fig. 4. Computed relative free energies for the competing IMDA Reactions and

corresponding [1,5]-sigmatropic shifts at DFT and ab initio MP2 level are given in Table 1.

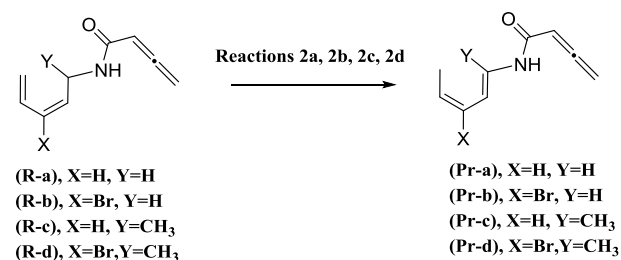


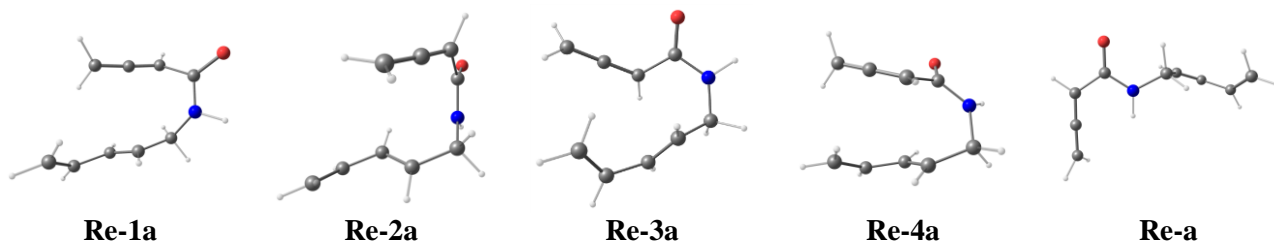
Fig. 4. Modeled [1,5]-sigmatropic shifts of precursors (R-a, R-b, R-c, R-d), Reactions 2a, 2b, 2c, 2d.

The reagents (R-a, b, c, d) are presented by the conformation having the lowest energy. The relative free energy of the proper conformer (Re-n, Fig.5) is the "cost" of reaching suitable configuration for the corresponding transition state and could reach 10-12 kcal.mol⁻¹ (Table 1).

Table 1. Computed free energies (ΔG^\ddagger and ΔG , kcal.mol⁻¹) at 373 K for the competing IMDA Reactions **1a-d** (Fig. 2, Fig. 3) and corresponding [1,5]-sigmatropic shifts (Reactions **2a-d**, Fig. 4) at DFT and ab initio MP2 level.

		$\Delta G^\ddagger/\Delta G$, kcal.mol ⁻¹							
		B3LYP/6-31G(d)				MP2/6-31G(d)			
		a (X=H)	b (X=Br)	c (X=H)	d (X=Br)	a (X=H)	b (X=Br)	c (X=H)	d (X=Br)
Reaction 1	R*	0.00	0.00	0.00	0.00	0.00	0.00	0.00	0.00
	Re-1	11.32	12.38	5.02	4.79	4.44	10.82	7.03	1.97
	Re-2	7.87	9.19	8.95	8.13	4.25	7.43	10.50	7.54
	Re-3	7.39	8.76	9.94	9.24	2.69	10.70	11.66	8.63
	Re-4	7.84	10.73	3.44	6.35	2.52	7.19	4.79	7.09
	(TS-1)	34.53	33.98	28.99	30.08	23.53	25.64	25.36	22.71
	(TS-2)	35.31	35.79	30.87	35.19	23.31	26.19	26.91	27.95
	(TS-3)	39.11	37.73	30.73	32.32	26.07	27.49	26.04	25.86
	(TS-4)	39.83	39.88	29.77	32.57	26.77	27.61	24.90	24.02
	Pr-1	-34.53	-35.08	-39.79	-35.53	-48.44	-42.61	-48.84	-47.73
	Pr-2	-33.18	-31.16	-38.81	-37.87	-51.37	-44.08	-48.69	-50.81
	Pr-3	-26.66	-26.48	-38.29	-37.45	-45.25	-36.63	-45.72	-47.18
Pr-4	-28.46	-27.58	-37.66	-31.11	-47.25	-42.43	-45.22	-44.25	
Reaction 2	a (X=H)	5.27	2.93	0.48	2.33	0.88	3.23	5.54	2.98
	(TS)	31.94	32.19	32.94	34.46	27.10	31.38	34.05	32.91
	Pr	-4.06	-6.24	-5.61	-7.77	-7.46	-4.04	-1.60	-2.19

* The reagents, TS and products are marked as “**Re-n**, **Pr-n**, **TS-n**, **exo/endo**, **lk/ul**”, where lk/ul – Seebach-Prelog descriptors, **n** – the number of the relevant product (Fig. 3). The substrates, TS and cycloadducts of the reactions **1c** and **1d** having high activation energy and hence negligible product distribution are omitted.

**Fig. 5.** The models of the conformations (**Re-1a**, **Re-2a**, **Re-3a** and **Re-4a**, **Re-a**) of the reagent (**R-a**) computed at MP2 level for reactions **1a** and **2a**.

Geometries of the TS having lowest value of ΔG^\ddagger_{rel} for the IMDA reactions **1a**, **1b** and corresponding competing [1,5]-sigmatropic shift, reactions **2a**, **2b** (**TS-a**, **TS-b**) are shown in Fig. 6.

Models of the TS for reactions **1c** and **1d** are shown in Fig. 7. All computed TS are asynchronous with a longer developing peripheral bond (r_1 , Å) then the developing internal bond (r_2 , Å). Calculated differences between r_1 and r_2 (Δr) were used as a measure of asynchronicity (Table 3).

The *exo*-TS are less asynchronous and closer to the TS in Intermolecular Diels-Alder reaction of propadiene and 1,3-butadiene [8]. MP2 calculations significantly increased reaction asynchronicity. The computed forming and breaking bond lengths of the TS are reasonable for pericyclic reactions [13].

The free energy profile of all reactions **1a-1d**, **2a-2d** (Table 1, Fig. 8-reaction **1a**) estimated with MP2 level disfavored reactions **2a-d** – sigmatropic shift. The comparison of the relative free energy of the computed MP2 TS predicted as preferable (**Pr-2a**, no RSG) and (**Pr-4c**, 5-methyl RSG) (*endo*) cycloadducts. Bromine as RSG shifted distribution toward *trans*-fused (*exo*) products (**Pr-1b**, **Pr-1d**) (Table 1, Table 2). In fact, the MP2 calculations determined reaction **1a** as stereo unselective, reaction **1b** – as a reaction with moderate stereoselectivity in favor of the (*exo*) product, reaction **1c** – as a reaction with moderate stereoselectivity toward *cis*-fused (*endo*) product. Using two RSG – bromine and methyl substituents led to increasing amount of (*exo*) products considerably – (**Pr-1d**, *exo*, lk; **Pr-5d**, *exo*, lk).

Table 2. Computed free energies (ΔG^\ddagger and ΔG , kcal.mol⁻¹) at 373 K for the competing IMDA Reactions **1a-d** (Fig. 2, Fig. 3) and corresponding [1,5]-sigmatropic shifts (Reactions **2a-d**, Fig. 4) at DFT and ab initio MP2 level.

		ΔG^\ddagger_{rel} , kcal.mol ⁻¹			
		B3LYP/6-31G(d)		MP2/6-31G(d)	
		a (X=H)	b (X=Br)	a (X=H)	b (X=Br)
Reaction 2	(TS)	0.0	0.0	0.2	5.7
Reaction 1	(TS-1) exo	2.6	1.8	0.0	0.0
	(TS-2) endo	3.4	3.6	2.8	0.6
	(TS-3) exo	7.2	5.5	3.5	1.9
	(TS-4) endo	7.9	7.7	3.8	2.0
		c (X=H)	d (X=Br)	c (X=H)	d (X=Br)
Reaction 2	(TS)	3.9	4.4	9.1	10.2
Reaction 1	(TS-1) exo, lk	0.0	0.0	0.5	0.0
	(TS-2) exo, ul	1.9	5.1	2.0	5.2
	(TS-3) endo, lk	1.7	2.2	1.1	3.2
	(TS-4) endo, ul	0.8	2.5	0.0	1.3
	(TS-5) exo, lk	4.2	2.8	2.7	3.1
	(TS-6) exo, ul	5.5	8.1	3.8	6.5
	(TS-7) endo, lk	5.4	5.0	3.8	2.9
	(TS-8) endo, ul	6.5	8.4	4.6	4.9

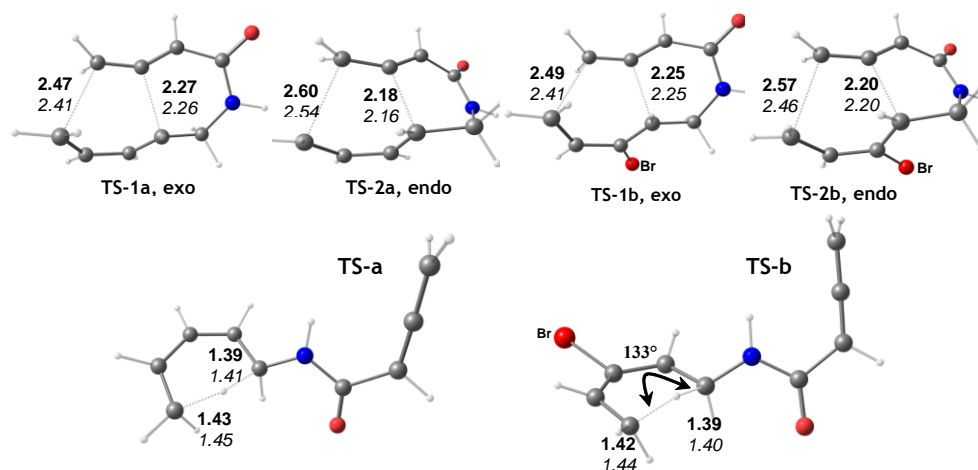
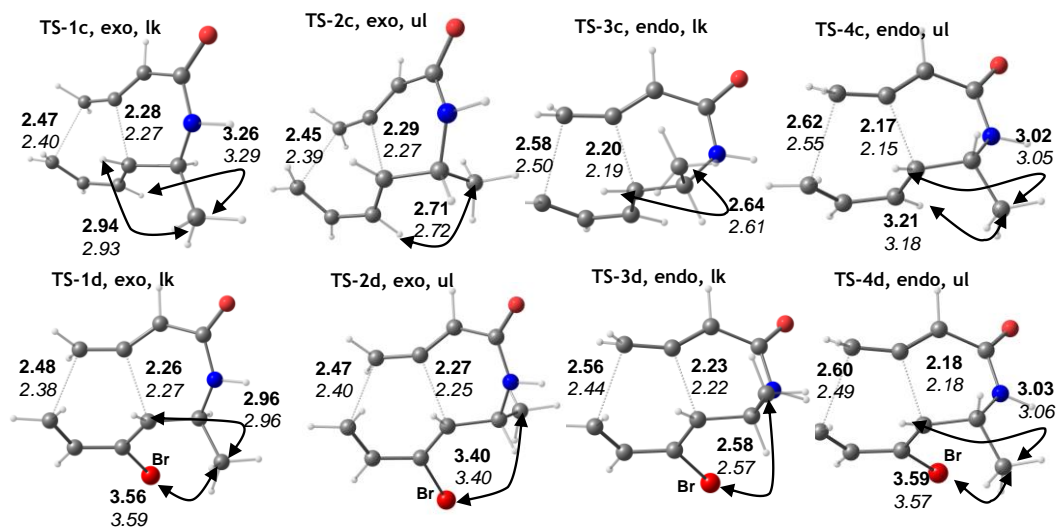
**Fig. 6.** Computed length (Å) of developing bonds for TS (Reactions **1a**, **1b**, **2a** and **2b**) at MP2/6-31G(d) (bold) and B3LYP/6-31G(d) (italics) level.**Fig. 7.** Computed geometries for TS (reactions **1c** and **1d**) at MP2/6-31G(d) (bold) and B3LYP/6-31G(d) (italics) level. Bond lengths are given in Å. Geometries for TS having a low product distribution are not presented.

Table 3. Computed bond lengths of the developing peripheral bond (r_1 , Å) and the developing internal bond (r_2 , Å) in TS* of IMDA Reactions **1a-d** (Fig. 2, Fig. 3).

TS	r_1 , Å		r_2 , Å		$\Delta r = r_1 - r_2$, Å	
	B3LYP/6-31G(d)	MP2/6-31G(d)	B3LYP/6-31G(d)	MP2/6-31G(d)	B3LYP/6-31G(d)	MP2/6-31G(d)
Intermolecular TS**	2.357		2.261		0.10	
TS-1a, exo	2.408	2.469	2.258	2.274	0.15	0.20
TS-2a, endo	2.540	2.602	2.158	2.179	0.38	0.42
TS-1b, exo	2.407	2.489	2.247	2.253	0.16	0.24
TS-2b, endo	2.464	2.573	2.203	2.198	0.26	0.38
TS-1c, exo, lk	2.397	2.471	2.269	2.278	0.13	0.19
TS-2c, exo, ul	2.386	2.453	2.268	2.285	0.12	0.16
TS-3c, endo, lk	2.499	2.580	2.187	2.202	0.31	0.38
TS-4c, endo, ul	2.546	2.616	2.152	2.174	0.39	0.44
TS-1d, exo, lk	2.381	2.479	2.269	2.264	0.11	0.22
TS-2d, exo, ul	2.400	2.468	2.252	2.269	0.15	0.20
TS-3d, endo, lk	2.439	2.545	2.218	2.226	0.22	0.32
TS-4d, endo, ul	2.489	2.597	2.178	2.183	0.31	0.41

* Bond lengths for the TS having a low product distribution are not presented; ** TS of Intermolecular Diels-Alder reaction of propadiene and 1,3-butadiene [8].

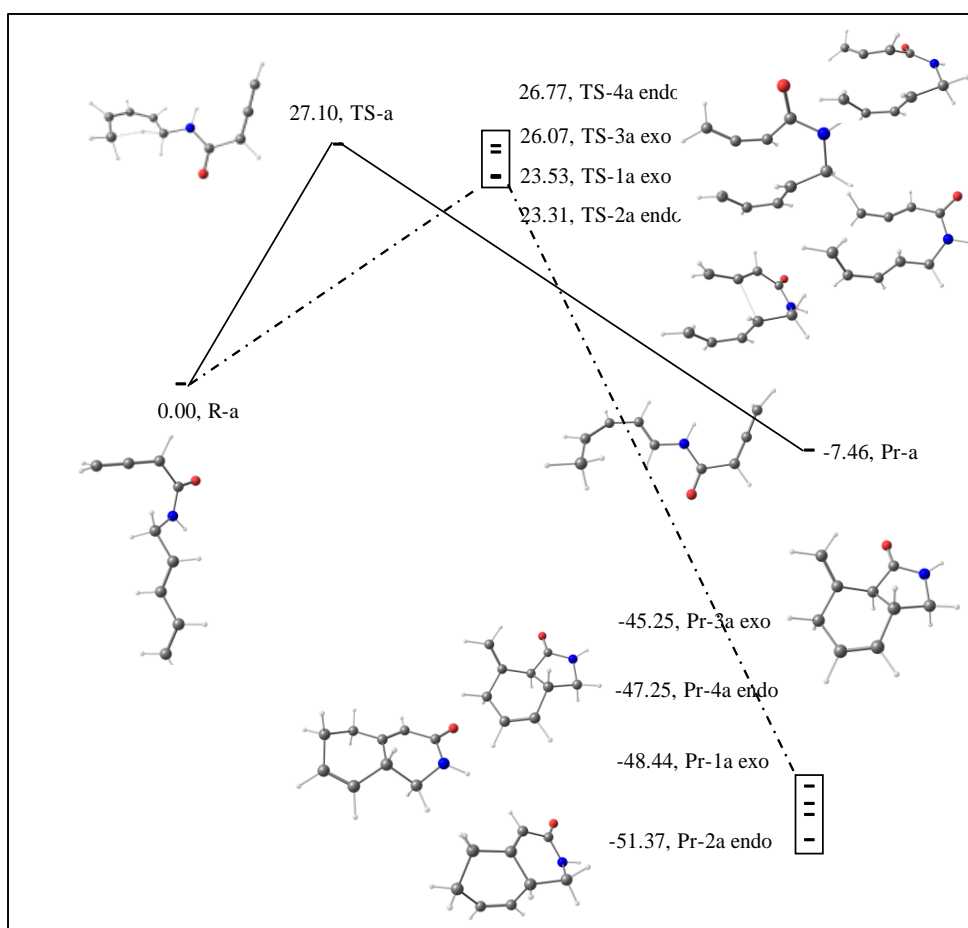


Fig. 8. Free energy profiles for reactions **1a** (—) and **2a** (- - -). The relative free energies (ΔG^\ddagger and ΔG) given in kcal.mol⁻¹ are computed at MP2/6-31G(d) level of theory (Table 1).

In contrast, DFT computations favored *reaction paths 2a, 2b* (Fig. 4) [1,5]-sigmatropic shift and subsequent Intramolecular [4+2] cycloaddition and hence the yielding of (**Z**) and (**E**) cycloadducts (Fig. 1, *reaction path 2*) with a more active in

IMDA reactions 1-methyl substituted diene moiety. The methyl SDG shifted reaction path toward Diels-Alder reaction and hence the group changed *regioselectivity*. The B3LYP/6-31G(d) exo cycloadducts - (**Pr-1a**), **exo** (*reaction 1a*) and (**Pr-**

1b), **exo** (reaction **1b**) - were preferred. Bromine SDG shifted the product ratio towards the trans-fused (**exo**) cycloadduct (Fig. 2). Use of SDG led to decreasing activation free energy of Diels-Alder reaction and accelerates the reaction rate (Table 1). Computed relative free energy differences of the favored products (**Pr-1c**) **exo**, **lk** and (**Pr-4c**), **endo**, **ul** by DFT and MP2 methods for reaction **1c** were opposite (Table 2).

Distances between C5 substituent and C3 connected H atom (causing destabilizing ^{1,3}A strain) and C5 substituent and C4 connected H atom (causing destabilizing eclipsing interactions) were optimized in the preferred products (**Pr-1c**) **exo**, **lk** and (**Pr-4c**), **endo**, **ul** (Fig. 7). When C3 and C5 substituents were incorporated in the precursor (**R-d**) a similar results were computed at MP2/6-31G(d) and B3LYP/6-31G(d) levels and reaction **1d** (Fig. 3) was found to be stereoselective.

Generally, the *steric effects* appear more important than the *electronic* ones in the IMDA reactions, especially in the presence of C3 and C5 substituents. C5 methyl substituent switches reaction paths **1** and **2** according to DFT calculations. Both methods are in agreement that in the presence of bromine and methyl substituents at C3 and C5 positions stereochemical outcome shifts toward (**exo**) cycloadduct.

Acknowledgements: This paper is supported by the Project BG051PO001-3.3.06-0003 "Building and steady development of PhD students, post-PhD and young scientists in the areas of the natural, technical and mathematical sciences". The Project is realized by the financial support of the Operative Program "Development of the human resources" of the European social fund of the European Union. The calculations were performed on Supermicro A+ Server 4042G-TRF, CPU AMD

Opteron 16 Cores Abu Dhabi 6376 2.30GHz, purchased with funds from the Project DFNI IO1/7, realized by financial support of Bulgarian National Science Fund.

REFERENCES

1. A. G. Fallis, *Can. J. Chem.*, **62**, 183 (1984).
2. D. Craig, *Chem. Soc. Rev.*, **16**, 187 (1987).
3. M. K. Diedrich, F-G. Klärner, B. R. Beno, K. N. Houk, H. Senderowitz, W. Clark Still, *J. Am. Chem. Soc.*, **119**, 10255 (1997).
4. D. J. Tantillo, K. N. Houk, M. E. Jung, *J. Org. Chem.*, **66**, 1938 (2001).
5. M. J. Lilly, M. N. Paddon-Row, M. S. Sherburn, C. I. Turner, *Chem. Commun.*, 2213 (2000).
6. T. Cayzer, L. Wong, P. Turner, M. N. Paddon-Row, M. S. Sherburn, *Chemistry*, 739 (2002).
7. R. Vijaya, G. N. Sastry, *J. Mol. Struct.: THEOCHEM*, **617**, 201 (2002).
8. M. Nendel, L. Tolbert, L. Herring, M. Islam, K. N. Houk, *J. Org. Chem.*, **64**, 976 (1999).
9. M. Manohan, P. Venuvanalingam, *J. Chem. Soc., Perkin Trans. 2*, 1423 (1996).
10. A. A. Granovsky, Firefly version 8.0.0, <http://classic.chem.msu.su/gran/firefly/index.html>
11. M. W. Schmidt, K. K. Baldrige, J. A. Boatz, S. T. Elbert, M. S. Gordon, J. J. Jensen, S. Koseki, N. Matsunaga, K. A. Nguyen, S. Su, T. L. Windus, M. Dupuis, J. A. Montgomery, *J. Comput. Chem.*, **14**, 1347 (1993).
12. V. Guner, K. S. Khuong, A. G. Leach, P. S. Lee, M. D. Bartberger, K. N. Houk, *J. Phys. Chem. A*, **107**, 11445 (2003).
13. V. A. Guner, K. S. Khuong, K. N. Houk, A. Chuma, P. Pulay, *J. Phys. Chem. A*, **108**, 2959 (2004).
14. D. H. Ess, K. N. Houk, *J. Phys. Chem. A*, **109**, 9542 (2005).
15. S. N. Pieniazek, F. R. Clemente, K. N. Houk, *Angew. Chem. Int. Ed. Engl.*, **47**, 7746 (2008).

ТЕОРЕТИЧНО ИЗСЛЕДВАНЕ НА СТЕРЕОСЕЛЕКТИВНОСТТА НА
ВЪТРЕШНОМОЛЕКУЛНА РЕАКЦИЯ НА ДИЛС-АЛДЕР НА 2,4-ПЕНТАДИЕНИЛ
БУТАДИЕНАМИДИ С УЧАСТИЕТО НА КОНТРОЛИРАЩИ
СТЕРЕОСЕЛЕКТИВНОСТТА ГРУПИ

А. Ж. Патлеева*, Д. Д. Енчев, Г. Д. Нейков

Факултет по природни науки, Шуменски университет „Епископ Константин Преславски“, Шумен, България

Постъпила на 29 април 2014 г.; Коригирана на 26 май 2014 г.

(Резюме)

Конкуриращи се вътрешномолекулни перициклични реакции на 2,4-пентадиенил бутадиенамиди (вътрешномолекулна реакция на Дилс-Алдер; [1,5]-сигматропна прегрупировка и следващо [4+2] циклоприсъединяване; Алдер-ене реакция) са моделирани като асинхронни съгласувани процеси с полуемпирични, *ab initio* и DFT теоретични методи. Изследвана е промяната в регио- и стереоселективността на вътрешномолекулните реакции с помощта на контролиращи съотношението между стереоизомерите заместители на C3 и C5 позиция. Предпочитаните циклоадукти са определени от относителните енергии на моделираните преходни структури.

Prediction of the color of dyes by using time-dependent density functional theory (TD-DFT)

S. Kawauchi^{1*}, L. Antonov^{1,2*}, Y. Okuno³

¹Department of Organic and Polymeric Materials, Tokyo Institute of Technology, 2-12-1 O-okayama, Meguro-ku, 152-8552 Tokyo, Japan

¹Institute of Organic Chemistry with Centre of Phytochemistry, Bulgarian Academy of Sciences, Acad. G. Bonchev str., bl. 9, 1113 Sofia, Bulgaria

³Center for Information Science, Kokushikan University, 4-28-1, Setagaya, Setagaya-ku, 154-8515 Tokyo, Japan

Received May 16, 2014; Revised June 17, 2014

Dedicated to Acad. Dimiter Ivanov on the occasion of his 120th birth anniversary

Time-dependent density functional theory calculations (6-31+G* basis set) at four functional levels of theory (B3LYP, ω B97XD, M06-2X, and PBE0) have been performed in order to estimate their applicability to predict the visible spectra of organic colorants. The absorption wavelength calculations give the following order of performance: M06-2X > ω B97XD > PBE0 > B3LYP when set of ionic and neutral dyes is used. In the case of neutral dyes only, the performance at all time-dependent PBE0, ω B97XD and M06-2X methods is statistically comparable. The importance of the specific interactions on the λ_{\max} prediction in the case of anionic phenylhydrazone dyes is shown. The comparison between experimental and calculated oscillator strengths was possible only in the case of anthraquinone dyes and has shown that all four methods predict reasonably well the trend of change of the oscillator strength as function of the substituents.

Key words: UV-Vis spectra, organic dyes, TD-DFT, ω B97XD, M06-2X, PBE0

INTRODUCTION

A correct prediction of the color (as position of the long-wavelength absorption band, measured as λ_{\max}) and its intensity (as molar absorptivity of this band and/or the oscillator strength of the corresponding transition) are of crucial importance for the development of new dyes and pigments for traditional and high-technology use [1-3]. During last two decades many attempts to find computational tools that predict the colouristic properties of the most intensively used dyes have been made by applying semi-empirical [4-7] and density functional theory (DFT) [8-12] methods.

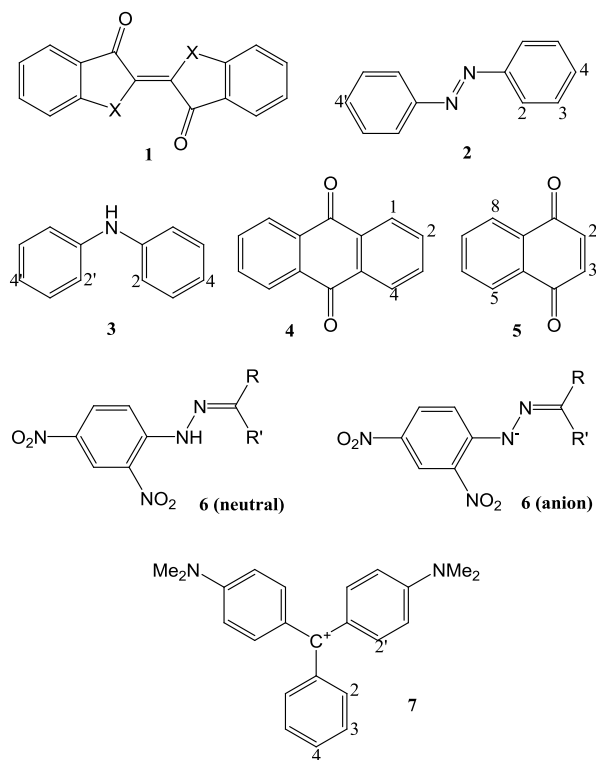
Currently the DFT method [13,14] is the most popular technique for electronic structure calculations with good computational cost/ molecular size ratio, which makes it suitable for electronic structure study of relatively large organic compounds in ground state. The number of the research applications by using time-dependent DFT (TD-DFT) [15] in the prediction of the spectral characteristics in the UV-Vis area is also growing [16,17]. Although its performance in this case had been found mode-

rate for charge-transfer system, which comes as a consequence of the DFT inborn defects, the development of the new functionals tends to improve significantly the situation. Unfortunately, no systematic way for such improvement is known up to now, in contrast to some of the traditional wavefunction-based methods like configuration interaction or coupled cluster theory, and the current approach is to test the TD-DFT results obtained by using various functionals against experimentally measured spectral data (λ_{\max} and in some rare cases - oscillator strengths) of selected organic dyes. In many of the cases direct conclusions about the performance of the different density functionals is impossible, because on one side different basis sets are used and on the other side there is no standardized spectral data set to test on. The most intensively used set of spectral data containing 30 dye structures (neutral and ionized, Scheme 1) had been introduced by Adachi and Nakamura [5] and has been used to estimate the performance of B3LYP and BPW91 [8] functionals. Later, this set has been enlarged to 100 structures by Jacquemin et al. [11], who used them to test five conventional and long-range corrected DFT functionals (PBE, PBE0, LC-PBE, LC- ω PBE and CAM-B3LYP).

* To whom all correspondence should be sent:

E-mails: skawauch@polymer.titech.ac.jp (SK) © 2014 Bulgarian Academy of Sciences, Union of Chemists in Bulgaria
lantnov@orgchm.bas.bg (LA)

Recently, intensive TD-DFT benchmarking (~500 compounds) has been performed using 29 DFT functionals (LDA, GGA, meta-GGA, global and long-range corrected hybrids), showing that any conclusion is strongly dependent on the set of organic molecules selected [18].



Scheme 1. Investigated dye structures.

In the present study, we estimate the ability of four DFT functionals (B3LYP [19-22], ω B97XD [23], M06-2X [24], and PBE0 [25,26]) to predict the λ_{\max} of organic dyes using a balanced spectral data set of 50 organic dyes (enlarged set of Adachi and Nakamura [5] including neutral and ionic dyes), where special emphasis has been given to find in the literature spectral data in non-polar solvents, when possible, and to avoid the complications of solvent effects description.

COMPUTATIONAL METHOD

For the current study representative compounds from several classes of dyes have been selected (Scheme 1): indigo (**1**), azobenzene (**2**), diphenylamine (**3**), anthraquinone (**4**), naphthoquinone (**5**), 2,4-dinitrophenylhydrazone (**6**), malachite green cation (**7**). The structural modifications include change of the skeleton atom(s) and/or adding substituent(s) as presented in Tables 1-7.

Initially the structures were built using SPARTAN [27] interface, and then structural relaxation with Merck molecular force field [28] have been performed. This was carried out for each compound in order to determine a global minimum structure among one or more of minimum structures including local minimum structures.

Then, structures were optimized without any restrictions by using Gaussian 09 program suite [29] at four levels of theory, namely B3LYP, ω B97XD, M06-2X and PBE0, and then were characterized as true minima by vibrational frequency calculations. In all cases 6-31+G(d) basis set [30] was applied. After the structure optimization, TD-DFT calculations were carried out at the same basis set in order to get straightforward conclusions about the effect of the basis set size on the reliability of the spectral predictions [31]. The largest absorption wavelength (i.e. lowest excitation energy) having more than 0.01 oscillator strength (this avoids in most of the cases the low intensive $n\text{-}\pi^*$ transitions) is used to compare with the experimental results. In order to model the solvent effect the Polarizable Continuum Model (PCM), using the integral equation formalism variant (IEFPCM [32]), has been used as implemented in Gaussian 09 [24]. The corresponding solvents are listed in Tables 1-7. In the case of the anionic 4,6-dinitrophenylhydrazone dyes (**6a**, **6c**, **6e**) ethanol was used as a solvent, while acetic acid was the solvent medium for the malachite green family **7**.

In the case of the anionic 4,6-dinitrophenylhydrazone dyes (**6a**, **6c**, **6e**) two type of complexes (with Na^+ and with ethanol molecule) were modeled by optimization in vacuum using 6-31+G** basis set using full counterpoise (CP) method [33,34] to correct the basis set superposition error. The corresponding TD-DFT calculations were carried out at 6-31+G* basis set at these optimized structures to be comparable with the result for the rest of the calculated dyes. It is worth to be noted that the DFT functionals chosen for this study are hybrid ones obtained by fitting against various training sets of molecules. The B3LYP is one of the most popular and intensively used functionals [18]. The PBE0 functional is also well known [21]. In comparison to them, the functional ω B97XD is a range-separated functional, where the switching between DFT and HF exchange is controlled by $\omega=0.2$, the short range HF exchange is ~22%, while the long-range one is 100% [19]. It yields high accuracy in thermochemistry, kinetics and noncovalent interactions. The M06-2X functional developed by Zhao and Truhlar [20] is a high-nonlocality functional with doubled amount of nonlocal

exchange (54% HF exchange), parameterized only chemistry, kinetics, and noncovalent interactions. for nonmetals, but reproduces well thermo-

Table 1. Indigo dyes: calculated and observed values of λ_{\max} [nm].

Dye		Calculated				Observed	Solvent
		B3LYP	ω B97XD	M06-2X	PBE0		
1a	X=NH	553	481	483	535	605 [35]	CHCl ₃
1b	X=NMe	586	517	524	569	650 [36]	
1c	X=O	430	364	359	411	420 [37]	

Table 2. Azo dyes: calculated and observed values of λ_{\max} [nm].

Dye		Calculated				Observed	Solvent
		B3LYP	ω B97XD	M06-2X	PBE0		
2a	-	338	302	297	326	317 [38]	C ₆ H ₁₂
2b	2-NH ₂	410	357	354	395	417 [5]	EtOH
2c	3-NH ₂	415	328	324	392	315 [2]	hexane
2d	3-NO ₂	353	301	296	327	317 [6]	hexane
2e	4-Cl	348	308	304	337	324 [6]	C ₆ H ₁₂
2f	4-CN	352	310	306	339	324 [6]	EtOH
2g	4-Me	346	308	303	334	324 [6]	C ₆ H ₁₂
2h	4-NEt ₂	402	347	349	388	407 [39]	C ₆ H ₁₂
2i	4-NEt ₂ -4'-NO ₂	472	374	382	444	480 [40]	2-methyl THF
2j	4-NH ₂	374	328	326	361	363 [2]	hexane
2k	4-NHMe	385	335	334	372	380 [2]	C ₆ H ₁₂
2l	4-NMe ₂	397	343	344	383	399 [2]	hexane
2m	4-NMe ₂ -4'-NO ₂	465	369	376	437	444 [6]	C ₆ H ₁₂
2n	4-NO ₂	368	314	309	350	329 [6]	hexane
2o	4-OH	354	314	310	342	339 [6]	C ₆ H ₁₂
2p	4-OMe	358	316	312	346	342 [6]	hexane

Table 3. Diphenylamino dyes: calculated and observed values of λ_{\max} [nm].

Dye		Calculated				Observed	Solvent
		B3LYP	ω B97XD	M06-2X	PBE0		
3a	2-NO ₂	451	357	347	416	415 [41]	hexane
3b	4-NO ₂	369	311	313	347	362 [37]	
3c	2,4-diNO ₂	423	343	338	392	411 [37]	

Table 4. Anthraquinone dyes: calculated and observed [42] values of λ_{\max} [nm].

Dye		Calculated				Observed	Solvent
		B3LYP	ω B97XD	M06-2X	PBE0		
4a	1-NH ₂	457	383	378	438	465	CH ₂ Cl ₂
4b	1-OH	410	347	340	393	405	
4c	1,2-diOH	436	358	352	418	416	
4d	1,4-diNH ₂	517	447	445	502	550	
4e	1,4-diOH	466	400	394	451	476	
4f	2-NH ₂	428	345	341	407	410	
4g	2-NMe ₂	475	371	370	449	470	

Table 5. Naphthoquinone dyes: calculated and observed [43] values of λ_{\max} [nm].

Dye		Calculated				Observed	Solvent
		B3LYP	ω B97XD	M06-2X	PBE0		
5a	2,3-diCl-5-NH ₂ -8-OMe	501	420	416	482	540	C ₆ H ₁₂
5b	5-NH ₂	493	408	400	471	484	
5c	5-NH ₂ -8-OMe	499	417	405	480	512	
5d	5-OMe	372	309	300	354	387	

Table 6. Neutral and deprotonated hydrazone dyes: calculated and observed [44] values of λ_{\max} [nm].

Dye	Calculated				Observed	Solvent
	B3LYP	ω B97XD	M06-2X	PBE0		
6a H, H (anion)	501	414	404	466	500	EtOH/NaOH
6b H, H (neutral)	392	331	322	369	345	CHCl ₃
6c <i>p</i> -NH ₂ C ₆ H ₄ , Me (anion)	539	427	419	500	461	EtOH/NaOH
6d <i>p</i> -NH ₂ C ₆ H ₄ , Me (neutral)	510	366	366	465	403	CHCl ₃
6e <i>p</i> -NO ₂ C ₆ H ₄ , Me (anion)	601	484	501	566	540	EtOH/NaOH
6f <i>p</i> -NO ₂ C ₆ H ₄ , Me (neutral)	435	349	344	403	382	CHCl ₃

Table 7. Malachite green dyes: calculated and observed [45-48] values of λ_{\max} [nm].

Dye	Calculated				Observed	Solvent
	B3LYP	ω B97XD	M06-2X	PBE0		
7a None	489	448	460	476	621	
7b 2-NO ₂	502	461	474	487	637	
7c 2-OMe	496	454	468	482	625	
7d 2,2'-diMe	499	460	473	487	634	
7e 3-OMe	506	449	461	482	623	
7f 4-Cl	493	451	463	480	628	
7g 4-CN	505	460	472	492	643	
7h 4-Me	488	445	458	475	617	
7i 4-NO ₂	516	463	476	499	645	
7j 4-OH	487	441	454	474	603	
7k 4-OMe	487	439	453	474	608	98% acetic acid

RESULTS AND DISCUSSION

The predicted band positions in vacuum are compared with the experimental ones in Tables 1-7 and the overall performance of the used TD-DFT methods is shown in Fig. 1.

The visual inspection of Fig. 1 allows several interesting conclusions to be pointed out. In the case of TD-B3LYP and TD-PBE0 there are obvious correlation trends where compounds **6c**, **6e** and **6d**, and the whole class of dyes **7**, i.e., Malachite green dyes, are outliers. In the case of TD- ω B97XD and TD-M06-2X the Malachite green dyes are part of the linear tendency, while **6c** and **6e** remain, to a certain extent, deviated from the relation along with **5d**. Visually the performance of TD- ω B97XD and TD-M06-2X is better than the TD-B3LYP and TD-PBE0.

The statistical information collected in Table 8 support these initial conclusions.

The statistical analysis, comparing predicted and experimentally observed λ_{\max} , shows substantially lower mean average errors in the cases of B3LYP and PBE0. This is not in contradiction with Fig. 1 since these two methods do not give systematical shift of the predicted band positions, i.e. there are large negative and positive deviations, which at end

neutralize each other. According to the deviations given in Table 8, the observed values for **7** are underestimated by the calculations (largest positive deviations are 138 nm and 151 nm for B3LYP and PBE0 respectively, both in the case of **7g**), while the band positions for the anionic dyes are overestimated (with 107 nm for TD-B3LYP and 64 nm for TD-PBE0, both in the case of **6d**).

The TD- ω B97XD and TD-M06-2X calculated λ_{\max} quantities are systematically deviated, underestimating the experiment, which leads to larger mean absolute error (MAE) and root mean square (RMS) values. However, according to our results and the previously published prediction of band positions by various DFT functionals [9-12] there is no DFT method that directly predict the real band positions, i.e. there is inherent problem associated with the TD calculation with the hybrid DFT methods.

The practical solution is to find a DFT method whose predictions correlate with the experiment and to use this correlation for additional correction of the calculated λ_{\max} values. Actually this has been performed and the linear regression parameters are collected in Table 8. In the ideal case the linear fit coefficients *a* and *b* must tend to 1 and 0

respectively, but as we mentioned above the tested functionals do not directly predict experimentally observed band positions. The data in Table 8 show very clearly that ω B97XD and M06-2X results correlate very satisfactory with the experiment and substantially better than those of B3LYP and PBE0. This leads to substantially lower MAE and RMS values and narrow limits of the maximal positive and negative deviations. As seen after the fitting the Malachite green dyes remain problematic for B3LYP, while in the case of the rest three DFT methods largest positive deviation is obtained at **5d**.

The anionic dyes also remain problematic, but in smaller extent for M06-2X.

Taking into account the all statistical data we can conclude that the order of performance of the tested four functionals is as follows: M06-2X> ω B97XD>PBE0>B3LYP. According to the recent data of Jacquemin et al. [11], obtained with 6-311+G(2d,p) basis set (at PBE0/6-311G** geometry), the performance of their tested functionals with a set of 100 neutral dyes follows the PBE>PBE0>CAM-B3LYP>LC-PBE>LC- ω PBE>HF sequence. Since the used sets of dyes overlap and although the used basis sets are different we

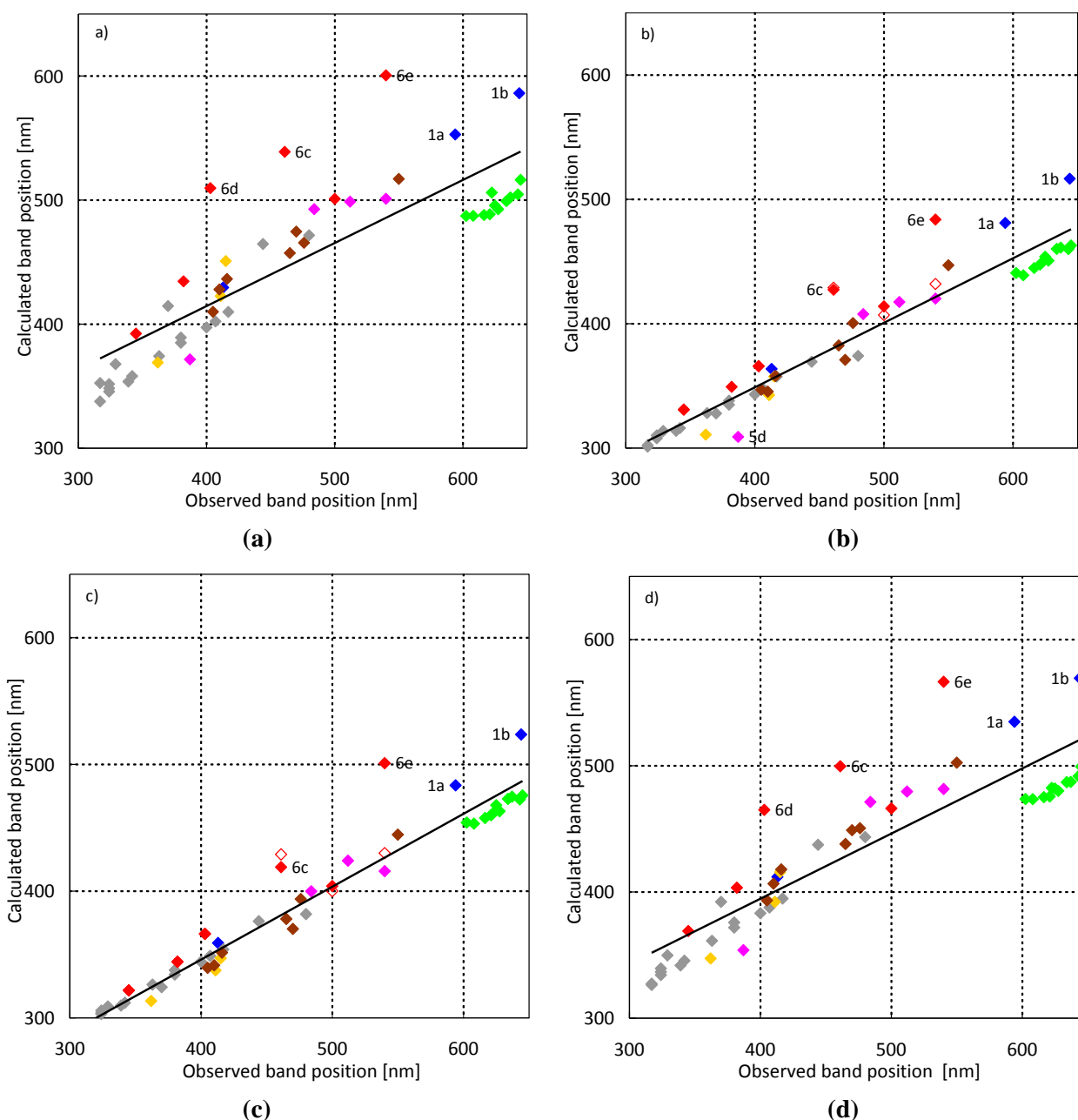


Fig. 1. Comparison between calculated (in vacuum) and experimental band positions at: a) B3LYP; b) ω B97XD; c) M06-2X; d) PBE0. The families of dyes are presented as following colors: **1** – blue; **2** – grey; **3** – orange; **4** – brown; **5** – pink; **6** – red; **7** – green. The calculated values for the complexes of **6a,c,e** with Na⁺ are given with empty symbols.

Table 8. Statistical analysis of the prediction capacity in vacuum and in solution (underlined). The corresponding values obtained by taking into account the interaction between anionic phenylhydrazone dyes and Na⁺ are presented in curly brackets.

Parameter	B3LYP	ω B97XD	M06-2X	PBE0
<i>without fit</i>				
MAE* [nm]	47 <u>52</u>	83 {84} <u>63 {65}</u>	82 {83} <u>63 {64}</u>	48 <u>44</u>
RMS** [nm]	69 <u>65</u>	99 {100} <u>81 {81}</u>	96 {97} <u>76 {77}</u>	71 <u>59</u>
largest positive deviation*** [nm]	138 (7g) <u>106 (7d)</u>	183 (7g) <u>148 (7g)</u>	171 (7g) <u>133 (7g)</u>	151 (7g) <u>116 (7d)</u>
largest negative deviation [nm]	-107 (6d) <u>-169 (6d)</u>	- <u>-7 (6c)</u>	- <u>-</u>	-62 (6d) <u>-108 (6c,6d)</u>
<i>with correction equation**** $a \cdot \lambda_{calc} - b$, obtained by linear fit between λ_{obs} and λ_{calc}</i>				
<i>a</i>	1.968 <u>1.704</u>	1.927 {1.953} <u>1.724 {1.736}</u>	1.739 {1.767} <u>1.560 {1.572}</u>	1.938 <u>1.724</u>
<i>b</i>	415 <u>348</u>	293 {279} <u>228 {231}</u>	202 {210} <u>162 {165}</u>	364 <u>317</u>
R ²	0.712 <u>0.672</u>	0.917 {0.936} <u>0.929 {0.940}</u>	0.936 {0.955} <u>0.947 {0.954}</u>	0.785 <u>0.773</u>
MAE [nm]	56 <u>59</u>	23 {20} <u>20 {18}</u>	18 {16} <u>18 {16}</u>	46 <u>45</u>
RMS [nm]	70 <u>77</u>	33 {29} <u>30 {28}</u>	29 {24} <u>26 {24}</u>	57 <u>59</u>
largest positive deviation [nm]	76 (7a) <u>85 (7h)</u>	64 (5d) <u>66 (5d)</u>	67 (5d) <u>67 (5d)</u>	66 (5d) <u>76 (5d)</u>
largest negative deviation [nm]	-226 (6e) <u>-258 (6c)</u>	-120 (6e) <u>-119 (6c)</u>	-129 (6e) <u>-94 (6c)</u>	-193 (6e) <u>-204 (6c)</u>

* mean absolute error; ** root mean square; *** deviations are calculated as difference between observed and calculated band position, namely: $\lambda_{obs} - \lambda_{calc}$; in this case the statistical analysis (MAE, RMS and deviations) is based on comparison between $\lambda'_{calc} (\lambda'_{calc} = a \cdot \lambda_{calc} + b)$ and λ_{obs} .

can conclude that M06-2X method could be used for practical prediction of the experimental spectra of organic dyes. The exclusion of the ionic dyes (**6** and **7**) from the linear fitting leads to correlation (R²) 0.9725, 0.9530 and 0.9690 for TD-PBE0, TD- ω B97XD and TD-M06-2X respectively, which means that these three methods are comparable in the case of neutral dyes, but the M06-2X performs much better (Table 8) when ionic dyes are included.

According to Table 8 and Fig. 2 the introduction of the solvent effect does not improve substantially the performance of the tested functionals, even in two of them (B3LYP and PBE0) decrease of the correlation is observed. Generally the solvent inclusion leads to decrease of both slope and intercept of the liner fit, but the systematic deviation in the case of ionic dyes remain unaffected (Fig. 2).

As seen from Fig. 1b,c and 2b,c in the case of ω B97XD and M06-2X functionals the anionic dyes of phenylhydrazone family are substantially deviated from the linear tendency and the situation is practically not affected by introducing solvent environment. This means that the effects are either systematically related to DFT performance or rela-

ted to specific, intermolecular, effects in solution. Compounds **6b**, **6d** and **6f** are treated with NaOH in ethanol solution to give the deprotonated species **6a**, **6c** and **6e**, resp., which could lead to hypothesis for specific interaction with Na⁺ or with ethanol molecule. According to the calculations, the optimized complexes with Na⁺ have shown much more stability in both vacuum and solvent field in all three anionic dyes comparing to the corresponding ethanol complexes. As seen from Fig. 1 and 2 the use of the Na complexes of the anionic phenylhydrazones leads to some improvement of the overall performance, but it does not substantially changes the overall statistical parameters (as shown in Table 8). Evidently latter comes from the fact that the three anionic dyes have negligible weight in the whole set of 50 compounds.

As it was mentioned before, the prediction of the band position is only one side of the overall color/properties elucidation. The real dye development needs information for the intensity of the color in the same extend, or even in larger, as the information for the long-wavelength band position. Such information is provided by the TD-DFT as

oscillator strength (f), which fundamental value defines how probable is the corresponding transition [49].

The corresponding values for the studied dyes and the used DFT functionals are available from the authors upon request. Unfortunately in most of the cases there is no way for direct comparison with the experiment. Where available, the experimental data are presented as molar absorptivity (ϵ_{\max}) at λ_{\max} . The fundamental relation between f and ϵ_{\max} is well known:

$$f \cong 4.39 \cdot 10^{-9} \cdot \int \epsilon(\tilde{\nu}) d\tilde{\nu}$$

where the spectrum must be presented in wave numbers ($\tilde{\nu}$). If the spectral band is individual (resolved mathematically [50] or experimentally) and its shape is assumed to be Gaussian function [29,30], as it is in UV-Vis spectra, the integral band can be presented as follows:

$$\int \epsilon(\tilde{\nu}) d\tilde{\nu} = 1.063 \cdot \epsilon_{\max}^o \cdot \Delta\tilde{\nu}_{1/2}$$

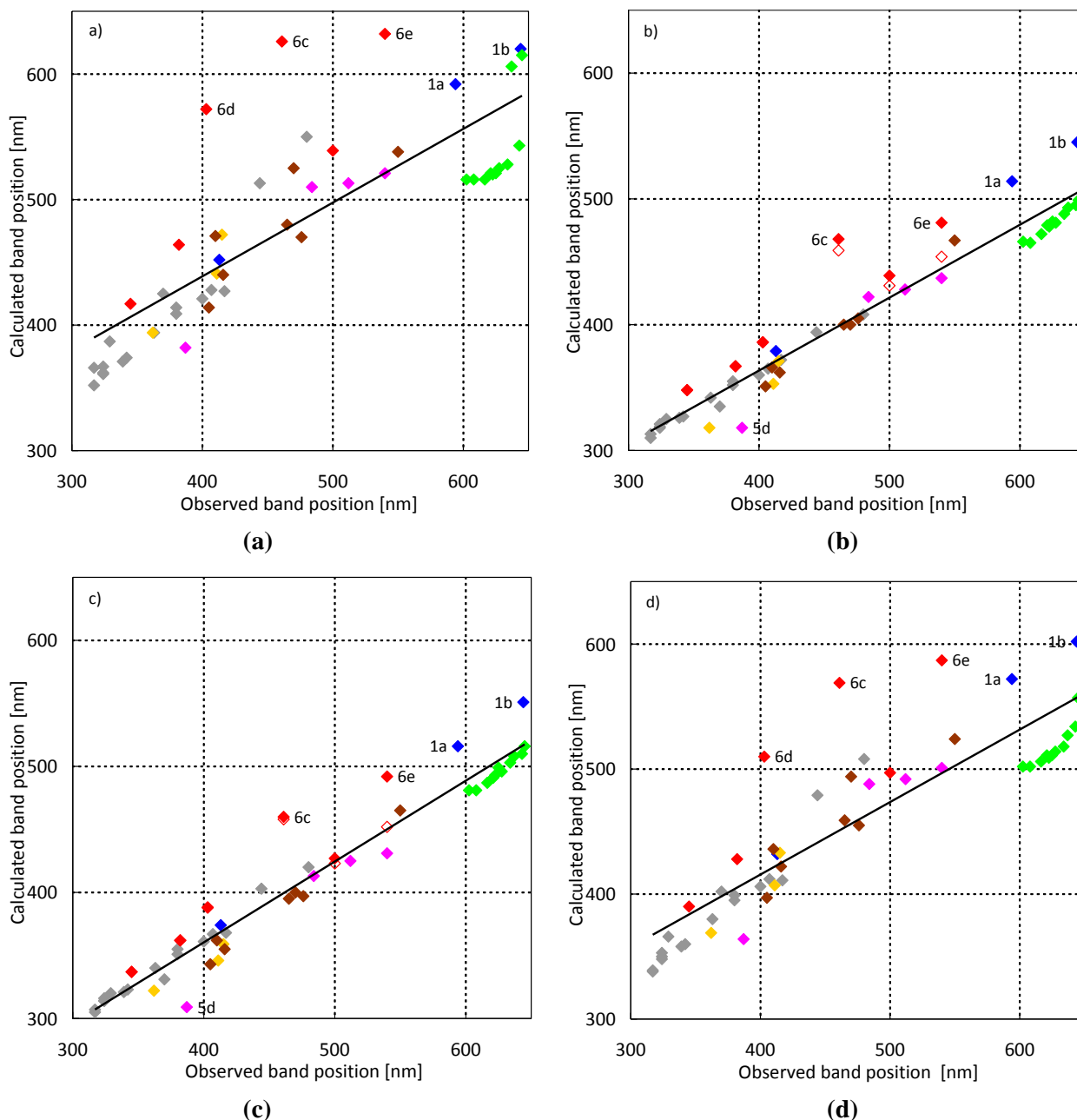


Fig. 2. Comparison between calculated (in corresponding solvents) and experimental band positions at: a) B3LYP; b) ω B97XD; c) M06-2X; d) PBE0. The families of dyes are presented as following colors: 1 – blue; 2 – grey; 3 – orange; 4 – brown; 5 – pink; 6 – red; 7 – green. The calculated values for the complexes of **6a,c,e** with Na^+ are given with empty symbols.

Table 9. Anthraquinone dyes: calculated and observed [38] oscillator strengths.

Dye	Calculated				Observed	
	B3LYP	ω B97XD	M06-2X	PBE0		
4a	1-NH ₂	0.119	0.1692	0.1595	0.128	0.114
4b	1-OH	0.1238	0.1737	0.1621	0.1334	0.113
4c	1,2-diOH	0.0952	0.1495	0.1342	0.1052	0.119
4d	1,4-diNH ₂	0.1866	0.235	0.2242	0.1988	0.157
4e	1,4-diOH	0.1727	0.2263	0.213	0.1848	0.131
4f	2-NH ₂	0.0495	0.0742	0.0762	0.0488	0.091
4g	2-NMe ₂	0.07	0.1096	0.1117	0.0773	0.109

Depending on the extent of band overlapping in the visible area (which is usually substantial) the experimental maximal molar absorptivity (ϵ_{\max}) differs from the individual one (ϵ_{\max}^o). In addition there is no way of estimation of the band width ($\Delta\tilde{\nu}_{1/2}$) from the experimental spectrum without resolving it mathematically [29]. For these reasons, assuming a universal value for the band width of 4000 cm⁻¹ as it was made [8] does not have physical meaning and finally cannot bring any conclusions.

In the experimental dye set used by us the experimentally determined oscillator strengths are available for the anthraquinone dyes **4** (Table 9), which allows a direct comparison. This comparison shows that the DFT methods tested in this study correctly predict the tendency (with statistically comparable correlation in all four cases), but the data are not sufficient to make statistically valid conclusions about the overall performance.

CONCLUSION

TD-DFT calculations with 6-31+G* basis set at four functional levels of theory, namely B3LYP, ω B97XD, M06-2X, and PBE0, have been performed in order to estimate their applicability to predict the visible spectra of organic colorants. For this purpose a set of 50 dye structures, including ionic and neutral, has been used. It has been found that there are good correlation relationships between the calculated wavelength values and the observed wavelength values. The absorption wavelength calculations at the M06-2X and ω B97XD functional levels were found to provide better prediction than those at the B3LYP and PBE0 functional levels. Comparing our data and data, previously published by other authors, we can conclude that M06-2X could be recommended for predicting visible spectra of organic dyes. The use of solvent effect description (as PCM) leads also to improvement of the results.

The comparison between experimental and calculated oscillator strengths was possible only in the case of anthraquinone dyes and has shown that all four methods predict reasonably well the trend of change of the oscillator strength.

This study has shown that there is need for establishment of a standard set of dyes (as structures with colors equally distributed through the visible area and strictly determined oscillator strengths), which to be used for comparative testing of various methods and basis sets.

Acknowledgements: LA is indebted to JSPS for the fellowship provided. The numerical calculations were carried out on the TSUBAME2.5 supercomputer at the Tokyo Institute of Technology, Tokyo, Japan, and on the supercomputer at the Research Center for Computational Science, Okazaki, Japan.

REFERENCES

1. H. Zollinger, *Color - A Multidisciplinary Approach*, Wiley-VCH, Weinheim, 1999.
2. J. Fabian, H. Hartmann, *Light Absorption of Organic Colorants: Theoretical Treatment and Empirical Rules*, Springer-Verlag, Berlin, 1980.
3. J. Griffiths, *Colour and Constitution of Organic Molecules*, Academic Press, London, 1976.
4. C. Forber, E. Kelusky, N. Bunce, M. Zerner, *J. Am. Chem. Soc.*, **107**, 5884 (1985).
5. M. Adachi, S. Nakamura, *Dyes Pigm.*, **17**, 287 (1991).
6. A. Matsuura, H. Sato, W. Sotoyama, A. Takahashi, M. Sakurai, *J. Mol. Struct.: Theochem*, **860**, 119 (2008).
7. S. Kawauchi, K. Mita, M. Satoh, J. Komiyama, J. Watanabe, Y. Tamura, K. Mori, K. Suzuki, *Nonlinear Optics*, **26**, 221 (2000).
8. D. Guillaumont, S. Nakamura, *Dyes Pigm.*, **46**, 85 (2000).
9. P. C. Chen, Y. C. Chieh, J. C. Wu, *J. Mol. Struct.: Theochem*, **715**, 183 (2005).
10. C. Adamo, D. Jacquemin, *Chem. Soc. Rev.*, **42**, 845 (2013).

11. A. D. Laurent, D. Jacquemin, *Int. J. Quant. Chem.*, **17**, 2019 (2013).
12. D. Jacquemin, J. Preat, E. A. Perpète, D. P. Vercauteren, J.-M. Andre, I. Ciofini, C. Adamo, *Int. J. Quant. Chem.*, **111**, 4224 (2011).
13. P. Hohenberg, W. Kohn, *Phys. Rev.*, **136B**, 864 (1964).
14. W. Kohn, L. J. Sham, *Phys. Rev.*, **140**, A1133 (1965).
15. R. E. Stratman, G. E. Scuseria, M. J. Frisch, *J. Chem. Phys.*, **109**, 8218 (1998).
16. B. Mennucci Computational Spectroscopy, Ed. J. Grunenberg, Wiley-VCH, Weinheim, 2010, pp. 151-168.
17. P. H. P. Harbach, A. Dreuw, Modeling of Molecular Properties, ed. by P. Comba, Wiley-VCH, Weinheim, 2011, pp. 29-45.
18. D. Jacquemin, V. Watherlet, E. A. Perpète, G. E. Scuseria, C. Adamo, *J. Chem. Theory Comput.*, **5**, 2420 (2009) and the references cited therein in respect of the available training sets.
19. A. D. Becke, *J. Chem. Phys.*, **98**, 5648 (1993).
20. C. Lee, W. Yang, R.G. Parr, *Phys. Rev.*, **37B**, 785 (1988).
21. S. H. Vosko, L. Wilk, M. Nusair, *Can. J. Phys.*, **58**, 1200 (1980).
22. P. J. Stephens, F. J. Devlin, C. F. Chabalowski, M. J. Frisch, *J. Phys. Chem.*, **98**, 11623 (1994).
23. J.-D. Chai, M. Head-Gordon, *Phys. Chem. Chem. Phys.*, **10**, 6615 (2008).
24. Y. Zhao, D. G. Truhlar, *Theor. Chem. Acc.*, **120**, 215 (2008).
25. J. P. Perdew, K. Burke, M. Ernzerhof, *Phys. Rev. Lett.*, **77**, 3865 (1996).
26. C. Adamo, V. Barone, *J. Chem. Phys.*, **110**, 6158 (1999).
27. Y. Shao, L.F. Molnar, Y. Jung, J. Kussmann, C. Ochsenfeld, *Phys. Chem. Chem. Phys.*, **8**, 3172 (2006).
28. T. A. Halgren, *J. Comp. Chem.*, **17**, 490 (1996).
29. M. J. Frisch, G. W. Trucks, H. B. Schlegel, G. E. Scuseria, M. A. Robb, J. R. Cheeseman, G. Scalmani, V. Barone, B. Mennucci, G. A. Petersson, H. Nakatsuji, M. Caricato, X. Li, H. P. Hratchian, A. F. Izmaylov, J. Bloino, G. Zheng, J. L. Sonnenberg, M. Hada, M. Ehara, K. Toyota, R. Fukuda, J. Hasegawa, M. Ishida, T. Nakajima, Y. Honda, O. Kitao, H. Nakai, T. Vreven, J. A. Montgomery, Jr., J. E. Peralta, F. Ogliaro, M. Bearpark, J. J. Heyd, E. Brothers, K. N. Kudin, V. N. Staroverov, R. Kobayashi, J. Normand, K. Raghavachari, A. Rendell, J. C. Burant, S. S. Iyengar, J. Tomasi, M. Cossi, N. Rega, J. M. Millam, M. Klene, J. E. Knox, J. B. Cross, V. Bakken, C. Adamo, J. Jaramillo, R. Gomperts, R. E. Stratmann, O. Yazyev, A. J. Austin, R. Cammi, C. Pomelli, J. W. Ochterski, R. L. Martin, K. Morokuma, V. G. Zakrzewski, G. A. Voth, P. Salvador, J. J. Dannenberg, S. Dapprich, A. D. Daniels, O. Farkas, J. B. Foresman, J. V. Ortiz, J. Cioslowski, D. J. Fox, Gaussian 09, Revision A.02, Gaussian, Inc., Wallingford CT, 2009.
30. J. S. Binkley, J. A. Pople, W. J. Hehre, *J. Am. Chem. Soc.*, **102**, 939 (1980).
31. R. Improta, UV-Visible Absorption and Emission Energies in Condensed Phase by PCM/TD-DFT Methods, in Computational Strategies for Spectroscopy, V. Barone (Ed.), Wiley-VCH, Weinheim, 2012.
32. J. Tomasi, B. Mennucci, R. Cammi, *Chem. Rev.*, **105**, 2999 (2005).
33. S. B. Boys, F. Bernardi, *Mol. Phys.*, **19**, 553 (1970).
34. S. Simon, M. Duran, J. J. Dannenberg, *J. Chem. Phys.*, **105**, 11024 (1996).
35. W. R. Brode, E. G. Pearson, G. M. Wyman, *J. Am. Chem. Soc.*, **76**, 1034 (1954).
36. R. Pummerer, G. Marondel, *Liebigs Ann. Chem.*, **602**, 228 (1957).
37. R. Pummerer, G. Marondel, *Chem. Ber.*, **93**, 2834 (1960).
38. S. Yamamoto, N. Nishimura, S. Hasegawa, *Bull. Chem. Soc. Jpn.*, **44**, 2018 (1971).
39. H. Mustroph, *Dyes Pigm.*, **15**, 129 (1991).
40. S. Lunak Jr., M. Nepas, R. Hrdina, H. Mustroph, *Chem. Phys.*, **184**, 255 (1994).
41. M. G. W. Bell, M. Day, A. T. Peters, *J. Soc. Dyers Colour.*, **82**, 410 (1966).
42. H. Labhart, *Helv. Chim. Acta*, **40**, 1410 (1957).
43. K.-Y. Chu, J. Griffiths, *J. Chem. Res. (S)*, 180 (1978).
44. L. A. Jones, C. K. Hancock, *J. Org. Chem.*, **25**, 226 (1960).
45. C. C. Barker, M. H. Bride, G. Hallas, A. Stamp, *J. Chem. Soc.*, 1285 (1961).
46. C. C. Barker, G. Hallas, *J. Chem. Soc.*, 1529 (1961).
47. A. S. Ferguson, G. Hallas, *J. Soc. Dyers Colour.*, **87**, 187 (1971).
48. A. S. Ferguson, G. Hallas, *J. Soc. Dyers Colour.*, **89**, 22 (1973).
49. L. Antonov, D. Nedeltcheva, *Chem. Soc. Rev.*, **29**, 217 (2000).
50. L. Antonov, S. Stoyanov, *Appl. Spectrosc.*, **47**, 1030 (1993).

ПРЕДСКАЗВАНЕ НА ЦВЕТА НА БАГРИЛА ПОСРЕДСТВОМ ЗАВИСЕЩА ОТ ВРЕМЕТО ТЕОРИЯ НА ФУНКЦИОНАЛА НА ПЛЪТНОСТТА (TD-DFT)

С. Каваучи^{1*}, Л. Антонов^{1,2*}, И. Окуно³

¹Департамент по Органични и полимерни материали, Токийски Технологичен институт, 152-8552 Токио, Япония

²Институт по Органична химия с Център по Фитохимия, Българска Академия на Науките, ул. Акад. Г. Бончев, бл. 9, 1113 София, България

³Център по Информационни науки, Университет Кокушикан, 154-8515 Токио, Япония

Постъпила на 16 май 2014 г.; Коригирана на 17 юни 2014 г.

(Резюме)

Беше проверена приложимостта на четири TD-DFT метода (B3LYP, ω B97XD, M06-2X, and PBE0) при базичен набор 6-31+G* за предсказване на спектрите на органични багрила във видимата област на спектъра. При използване на набор от неутрални и йонни багрила най-добри резултати за положението на дълго-вълновите спектрални максимуми са получени в реда M06-2X> ω B97XD>PBE0>B3LYP. При използване само на неутрални багрила трите метода, PBE0, ω B97XD и M06-2X, показват статистически сравними резултати. При фенилхидразоновите багрила е показана важноста на специфичните взаимодействия в разтвор върху коректното предсказване на λ max. Сравнението на експериментално наблюдаваните и предсказаните сили на осцилатора, което беше възможно само при серията антрахинонови багрила, показа, че и четирите метода предсказват добре общата тенденция на промяна като функция от ефекта на заместителите.

Further studies on the conformations of large-ring cyclodextrins

P. Ivanov

¹*Institute of Organic Chemistry with Centre of Phytochemistry, Bulgarian Academy of Sciences, Acad. G. Bonchev str., bl. 9, 1113 Sofia, Bulgaria*

Received May 07, 2014; Revised June 18, 2014

Dedicated to Acad. Dimiter Ivanov on the occasion of his 120th birth anniversary

The dependence of the results from the conformational search on the starting geometry of large-ring cyclodextrins (LR-CDs) was examined for the set of macrorings CD_n, n = 16, 17, 18, 19, 20, 21. The structures obtained earlier for CD_n, n=16, 17, 18, 19 were confirmed, but not those for CD₂₀ and CD₂₁, although the tendency is evident for opening of the macrorings. Results from DFT studies on a model system, using different functionals, justify our choice to use the AMBER Glycam04 parameterization for modeling the conformations of large-ring cyclodextrins. The configurations of hydrogen bonds that determine the geometries of the preferred *syn* and *anti* conformations were also examined.

Key words: large-ring cyclodextrins, molecular dynamics, Glycam04 and Glycam06 AMBER parameterizations, DFT

INTRODUCTION

As a natural consequence of the long-lasting interest and the numerous applications of the native cyclodextrins (small cyclodextrins; α -CD, β -CD and γ -CD, respectively, cyclohexa-, cyclohepta-, and cyclooctaamylose), their larger analogues, the large-ring cyclodextrins (LR-CDs; CDs with a degree of polymerization (DP) higher than eight) [1-5], also attracted attention in recent years, and advances were marked in the study of their physicochemical properties [6,7], in spite of existing difficulties in their synthesis, isolation and purification. The existence of LR-CDs has been proven as products from the action of 4- α -glucanotransferases on amylose and amylopectin [2] almost a century later after the first evidences for the existence of cyclodextrins [8]. The expectations were that, in addition to the numerous well-known useful for the practice properties of the small cyclodextrins, namely to provide heterogeneous microenvironment to molecules, accommodated in their cavities, that acquire significantly modified properties compared to the free forms, some of the LR-CDs may have new, specific properties.

It took about twenty years after the first report for the existence of LR-CDs (DP = 9-14) [9] preparation method for LR-CDs mixtures to be worked out and δ -CD (DP = 9) [10] to be isolated and its crystal structure to be characterized [11].

This opened the renewed interest on LR-CDs: within very short time the crystal determinations of CD₁₀ (ϵ -CD) [12-14], CD₁₄ (ι -CD) [12, 13], CD₂₆ (ν -CD) [15,16] were reported. Important further steps related with the development of an effective purification method for LR-CDs [4] was the first chemical synthesis of a LR-CD, as well as the synthesis of the first chemically modified LR-CD (CD₉). The experimental information about the conformations of LR-CDs is scarce. Crystal structure determinations were so far successful only for four of them. The difficulties in forming intramolecular and intermolecular hydrogen bonds, due to the high flexibility of their macrocyclic rings, as well as the low nucleation rates of sugars, that has to precede crystal growth [3], are considered to be the main cause for the low crystallinity of most LR-CDs.

An advantage of the LR-CDs in comparison with the small CDs, especially with α -CD and β -CD, is that they are without any significant toxicity and that nutritionally they can be regarded as starch [2]. Commercially available CD-mixtures containing LR-CDs with a degree of polymerization from 9 to 21 were examined as additives to food (retrogradation retardant in breads, for freeze resistant jellies and for production of non-sticky rice) and drink products (high energy additive to soft drinks) for improving their texture, mouth feeling, flavor, taste, and palatability [6]. Others were studied as stabilization and solubilization for drugs. LR-CDs mixtures with a degree of polymerization from 22 to 45, and greater than 50 exhibited an efficient

* To whom all correspondence should be sent:
E-mail: ivanov@bas.bg

artificial chaperone effect for protein refolding (a protein refolding kit containing a mixture of LR-CDs as one of the active components is on the market [3] - the first practical application of LR-CDs in biotechnology). Such LR-CDs mixtures were able to strip detergent molecules of unfolded protein-detergent complexes, thus allowing the protein molecules to refold to their proper, folded, active state [2]. LR-CDs have been suggested for applications in the paper industry as an improved paper coating material and as starch substitutes in adhesives and biodegradable plastics.

LR-CDs may be good host molecules for relatively large guest compounds [6]. An increased flexibility of these molecules allows them either to present a more suitable cavity prior to complex formation or adapt to the guest molecules by an *induced fit* mechanism [2]. Since the large CDs are able to present a variety of cavity sizes, compared to the small CDs, they may be useful for special applications. δ -CD, for example, has demonstrated to form a stable complex with C70 Buckminsterfullerene that allows its solubilization in water [17]. It has been proven that η -CD (12 glucoses) is effective in the partial separation of carbon nanotubes [18], i.e. not only fullerenes, but also single-wall carbon nanotubes were dissolved into water using LR-CD [3]. Increased interest is evident from the literature on developing techniques for isolation of LR-CDs [19,20] and for examining the properties of these macromolecules as new polysaccharide-based biomaterials [21].

In view of the difficulties with the experimental examination of the conformations of large-ring cyclodextrins, computational modeling and simulation methods provide useful tool to gain information about their conformational dynamics, the energetics, and the complex-forming ability. The conformations of some LR-CDs were systematically examined using molecular dynamics simulations as conformational search protocol [22,23-29]. Representative conformations of the macrocycles were obtained for different ranges of DP. There still exist however some problems that deserve further elucidation:

1. The range of DP from 16 to 21 was considered as appropriate test cases to examine alternative starting conformations for the conformational searches. This is the range of macroring sizes that differ significantly from the reference structures CD14 and CD26 for which experimental crystal structure determinations are available.

2. We used the AMBER (parm99) force field in our earlier studies [22]. The parameterization for carbohydrates, Glycam04 (AMBER v.8) [30] was

later adopted [23,24,28]. The most recent development of the Glycam series of parameterizations, Glycam06 (in AMBER v. 11) [31], is recommended to be used instead of Glycam04. It is natural now to adopt this new development. We tested however different methods on representative *syn* and *anti* conformations of α -D-glucopyranosyl-(1 \rightarrow 4)- α -D-glucopyranoside (all they have six intramolecular hydrogen bonds). A *syn* conformation was estimated to have the lowest energy, whereas the following relative energies of the flipped (*anti*) conformation of the lowest energy were obtained (in kcal mol⁻¹): DFT(6-311++G**): 5.7 (B3LYP), 5.7 (LC-wPBE), 6.1 (CAM-B3LYP), 6.4 (wB97XD); SE-MO: 7.6 (AM1), 6.0 (PM3), 6.5 (PM6); UFF: 3.8; MMFF94: 5.7; Glycam04: 4.6; Glycam06: 2.9, i.e. Glycam06 estimated too low relative energy for the flipped conformation. How this result will reflect on the outcome from the Glycam06 modeling studies? Thus we consider important to justify our choice of using the Glycam04 parameterization for modeling the conformations of LR-CDs by comparing results for a model structure obtained with Glycam04 and DFT methods.

COMPUTATIONAL DETAILS

The MD simulation trajectories were obtained with the AMBER program (version 11 [30]) using the parameterization for carbohydrates, Glycam04 [30]. The molecular dynamics simulations were run for aqueous solution (a box with TIP4P water molecules) using the particle mesh Ewald (PME) method for the treatment of the long-range electrostatics. A 9.0 Å distance cutoff was used for direct space nonbonded calculations and a 1.0×10^{-5} Ewald convergence tolerance for the inclusion of long-range electrostatic contributions. The 'solvateBox' command of LEaP was used to create cubic solvent box around the CD with buffer distances 15.0 Å between the walls of the box and the closest atoms of the solute. The SHAKE option (tolerance 5.0×10^{-5} Å) was used for constraining bonds involving hydrogen atoms. The starting geometries were derived following schemes based on the X-ray geometries of CD14 and CD26 as key reference structures and adding or removing residues. The same protocol from our previous studies was used for the preparation of the systems for the simulation [24,28,29]. Additional 500.0 ps simulation (NPT) was executed before starting the productive runs. The productive runs were performed with the recommended maximum time-step 2.0 fs when SHAKE is used, at 300 K and an average

pressure 1.0 bar with isotropic position scaling. The simulation time was 100.0 ns. Samplings were taken every 2.0 ps.

RESULTS AND DISCUSSION

For the purpose of the representation we have to introduce some designations. Fig. 1 displays a schematic representation of a fragment of a cyclodextrin macroring with the numbering of the atoms and examples for *syn* and *anti* orientations of neighbouring glucose units.

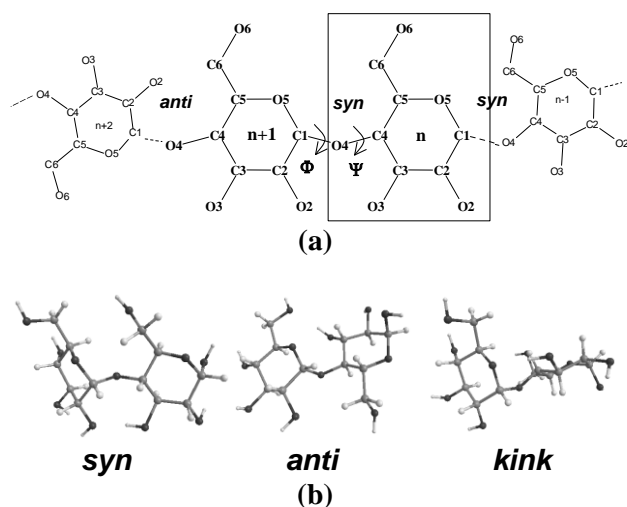


Fig. 1. a) Schematic representation for a cyclodextrin showing the atomic numbering. Each individual glucose unit is designated by a number “n”. Atoms are identified by a letter and a number that indicates its position in the glucose. (b) Relative conformations of neighbor glucoses: *syn*, *anti* and *kink*.

Dependence of the results from the starting geometry

The three groups of LR-CDs examined by us so far [25-27] present structures from different ranges of values for the degree of polymerization. The starting geometries in two of these cases were derived from the experimental crystal structures of cyclodextrins which were closer in size, CD14 [26] and CD26 [25]. It should not be surprising that for the third group of cyclodextrins, CD_n (n=18, 19, 20) [27], averaged geometries of CD20 were obtained that differ from the structures of the same macroring obtained earlier using different starting geometry (Fig. 2) [25]. This prompted us to examine in more detail the conformations of these LR-CDs using different starting geometries. The systems studied were CD_n, n=16, 17, 18, 19, 20, 21. Indeed we found that such dependences exist.

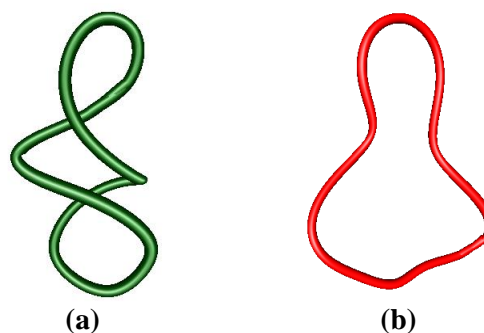


Fig. 2. Averaged structures of CD20 derived after conformational searches with different starting geometries for the molecular dynamics simulations: a) Results from Ref. 27; b) Results from Ref. 25.

The scheme for generating the starting geometries differs considerably from the one we used before. The starting geometries in the earlier study were derived following a scheme based on the X-ray geometry of CD14 as a key reference structure and adding or removing residues: CD14→CD15→CD16→CD18→CD20→CD19. The leading idea in the present examination was to start from *flips*-free geometries (Fig. 3).

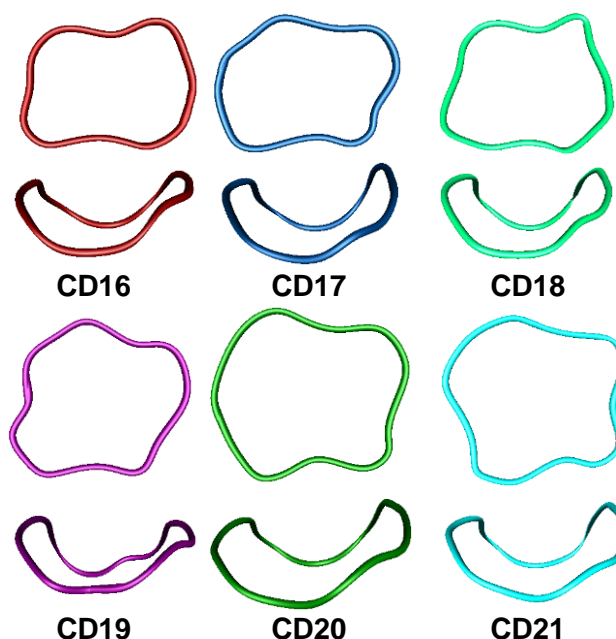


Fig. 3. Starting geometries for the conformational searches.

We prepared for the purpose starting geometry of CD16 using molecular graphics, whereas the other necessary structures were derived according to the sequence CD16→CD18→CD17→CD19→CD20, CD19→CD21. Fig. 4 contains average

geometries for 10.0 ns simulation time intervals of the conformational searches. CD20 was used also to examine the dependence of the results from the value of the buffer parameter for the thickness of the water layer (Fig. 4). Using the same starting geometry, the value 15.0 Å for the solvent buffer

parameter was used in this study, whereas the results designated with CD20s were obtained with the smaller value 10.0 Å.

The structures obtained earlier for CDn, n=16, 17, 18, 19 were confirmed [26,27], but not those for

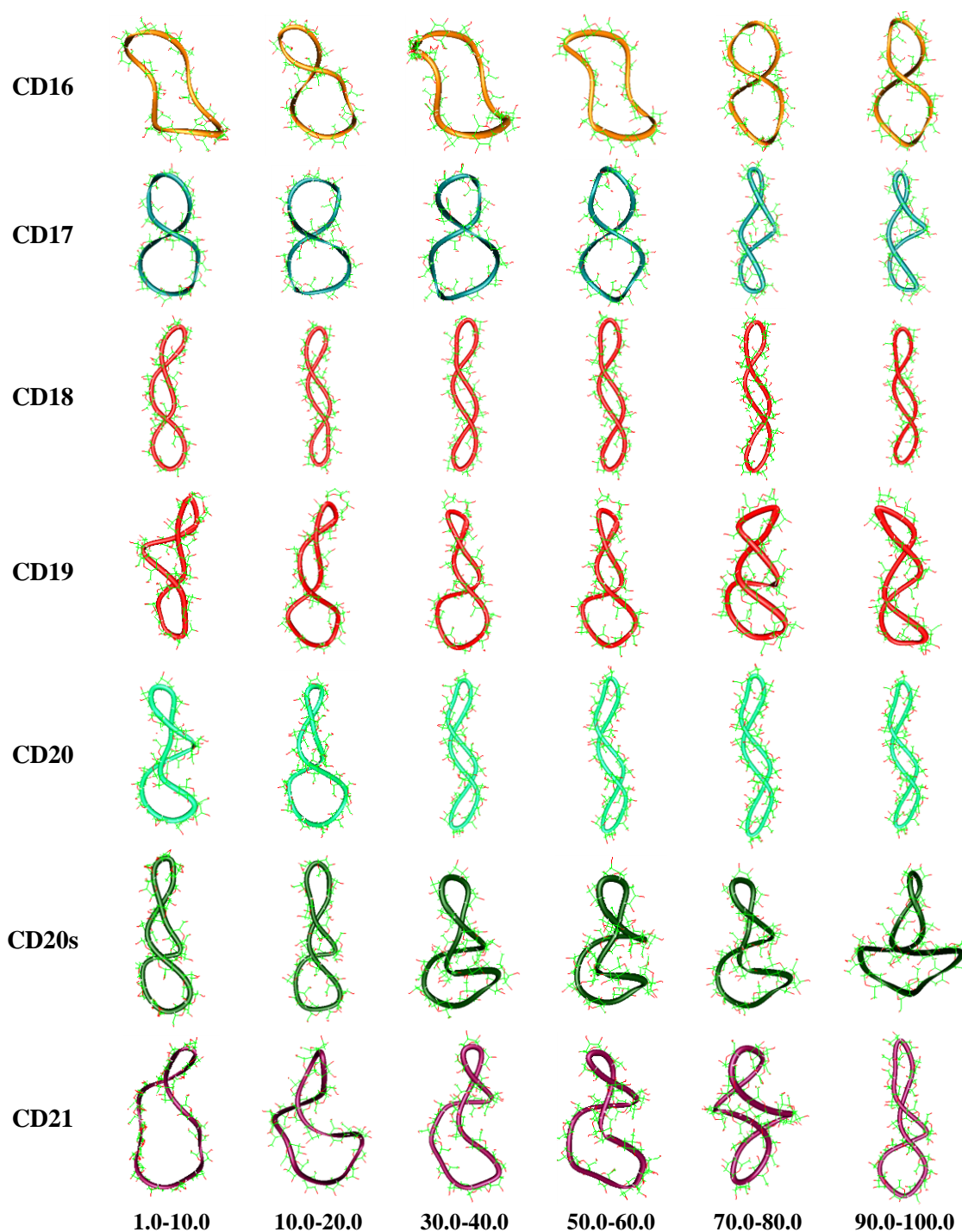


Fig. 4. Averaged geometries of CDn (n=16, 17, 18, 19, 20, 21) for different 10.0 ns intervals of the conformational searches.

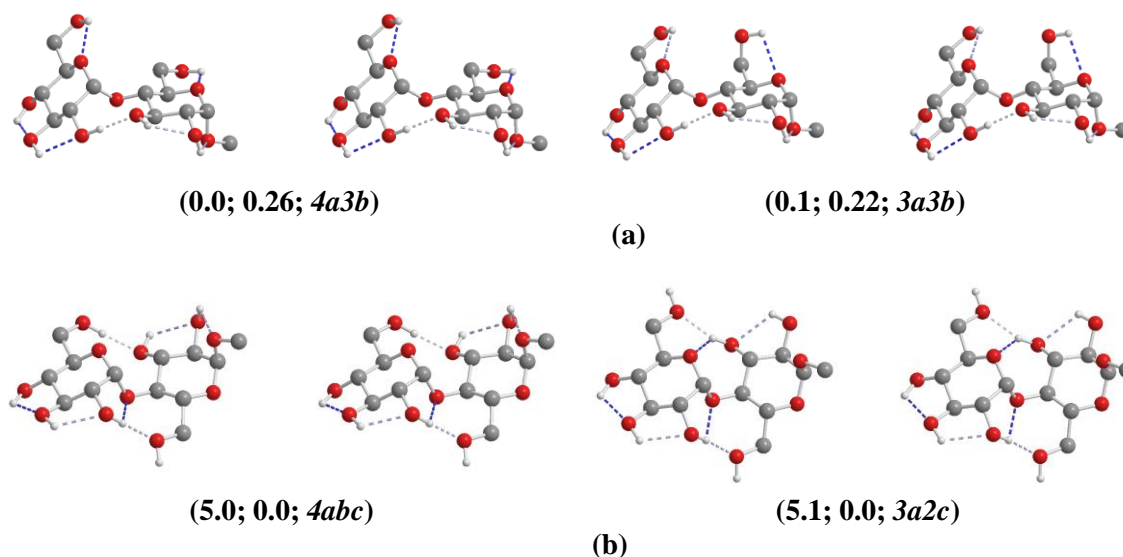


Fig. 5. Stereo views of optimized geometries of the lowest-energy conformations of α -D-glucopyranosyl-(1 \rightarrow 4)- α -D-glucopyranoside obtained with the MMFF94S force field: (a) *syn* conformations; (b) *anti* conformations. In parentheses are given the relative steric energies, the populations of the conformations and the letter-code describing the hydrogen bonding.

CD20 and CD21 [25], although the tendency is evident for opening of the macrorings. Longer duration of the simulations most probably may manifest also the geometries of CD20 and CD21 in Fig. 25 in Ref. 28. The observation of extended narrow antiparallel double helices for the cyclodextrins with DP in the range of 18 to 20 (Fig. 4), when using two different starting geometries, one of which has opened macroring, is additional evidence in support for the existence of such structures. Thicker water layer enhances the appearance of narrow extended geometries (Fig. 4, results for CD20). CD16 and CD17 display the figure-eight-like conformations with two β -CD pseudocavities. The cyclodextrins with even number of glucose residues, CD18 and CD20, present more symmetrical extended structures, probably due to more favorable torsional deformations about glycosidic bonds diametrically positioned along the perimeter of the macrocycle. Three segments, each of 6-7 glucoses, may produce more open cavities for CD21 (Fig. 4).

Validation of the Glycam04 AMBER parameterization for conformational studies on large-ring cyclodextrins – a DFT study on a model system α -D-glucopyranosyl-(1 \rightarrow 4)- α -D-glucopyranoside

We will recall again the reasons hidden behind this examination. Tests with the Glycam06 parameterization (*vide supra*) gave too low relative

energy for the flipped conformation. A consequence of this result, when applying Glycam06 on the flexible LR-CD systems, could be unreliable modeling of local *syn/anti* transitions. In order to validate our preference for using the Glycam04 parameterization (adopted not only because of this reason), we examined with molecular mechanics (MMFF94S force field) the conformations of α -D-glucopyranosyl-(1 \rightarrow 4)- α -D-glucopyranoside. The total of 6697 conformations were obtained with relative energies less than 24.0 kcal mol⁻¹. The first 130 lowest-energy conformations were further modeled also with four DFT functional [32]. The results for some of them are given in Table 1. We used two “standard” hybrid functionals not including dispersion (B3LYP, PBEh1PBE), one functional that has been constructed to account for dispersion (wB97XD) and the Zhao-Truhlar’s high-nonlocality functional M06 with double the amount of nonlocal exchange (2X) that has been recommended for noncovalent interactions. Fig. 5 presents MMFF94S optimized geometries of the lowest-energy *syn* and *anti* conformations. Table 1 contains also data for the dihedral angles of low-energy structures. For simplicity a letter-code was used to designate the values of the dihedral angles: *s* – dihedral angles in the range -30.0° – (+30.0°); *g*⁺ – dihedral angles in the range 30.0° – 130.0°; *g*⁻ – dihedral angles in the range -30.0° – (-130.0°); *a* – dihedral angles in the range 130.0° – (-130.0°). The pair of dihedrals (Φ , Ψ) determines whether a particular conformation can be characterized as *syn*,

kink or *anti*. The four DFT methods estimate relative energies of ‘*band-flipped*’ conformations in accord with the Glycam04 results. The results justify our choice to use Glycam04 for modeling the conformations of large-ring cyclodextrins.

Let us examine the configurations of hydrogen bonds that determine the geometries of the preferred *syn* and *anti* conformations. For simplicity of the presentation we will introduce a letter-code for designation of the type of hydrogen bonding: *a* - a hydrogen bond between hydroxyl groups; *b* - a hydrogen bond between a hydroxyl group and a ring-oxygen atom or glycosidic oxygen; *c* - bifurcated hydrogen bond with proton acceptors hydroxyl oxygen and glycosidic or ring-oxygen atoms. Then, *4a2bc* will designate the case with four hydrogen bonds of type *a*, two hydrogen bonds of type *b* and one hydrogen bonding of type *c*.

The typical chain of four hydrogen bonds (*4a*) between the secondary hydroxyl groups determine the geometry of the lowest energy conformation optimized with molecular mechanics. The two primary hydroxyls form hydrogen bond with the ring-oxygen atoms. This is the typical case encountered in cyclodextrins. The second low-energy conformation has the same hydrogen bonds, the only difference being the orientation of the primary hydroxyl group with respect to the C5(n)-O5(n) bond. This hydrogen bonding is not present in the third conformation. The same type of hydrogen bonding of conformations one and two characterizes also conformations four (*kink* conformation) and five, but some dihedral angles have different values. Five hydrogen bonds of type *a*, constituting a ‘proton-relay’-like fragment, determine the conformation of the sixth *syn* conformation. One and

Table 1. Relative energies (kcal mol⁻¹) of some low-energy conformations of α-D-glucopyranosyl-(1→4)-α-D-glucopyranoside determined with molecular mechanics and DFT methods.

No.	ΔE ^a					Dihedral angles ^{d,e,f}												
	B3LYP	wB97XD	PBEh1PBE	M062X	MMFF94S	Φ	Ψ	θ ₁ ¹	θ ₁ ²	θ ₃ ¹	θ ₄ ¹	θ ₁ ²	θ ₂ ²	θ ₃ ²	θ ₄ ²	φ _{OH}	φ _{OG+}	
1	1.6	1.8	1.7	2.6	0.0	g ⁺	g ⁺	g ⁺	g ⁺	g ⁻	g ⁻	g ⁺	g ⁻	s	g ⁻	g ⁺	g ⁺	
2	0.0	0.0	0.0	0.0	0.1	g ⁺	g ⁺	g ⁺	g ⁺	g ⁻	g ⁻	g ⁺	g ⁻	s	g ⁻	g ⁺	g ⁺	
3	1.1	0.5	0.7	0.6	0.1	g ⁺	g ⁺	g ⁺	a	g ⁻	g ⁻	g ⁺	g ⁻	s	g ⁻	g ⁺	g ⁺	
4 ^b	0.0	0.0	0.0	0.0	0.8	a	a	g ⁺	g ⁺	g ⁻	g ⁻	g ⁺	g ⁻	s	g ⁻	g ⁺	g ⁺	
5	1.6	1.6	1.7	2.7	1.0	g ⁺	g ⁺	g ⁺	g ⁺	g ⁻	g ⁻	g ⁺	g ⁻	s	g ⁻	g ⁺	g ⁺	
6	1.7	1.7	1.7	2.8	1.1	g ⁺	g ⁺	g ⁺	g ⁺	g ⁻	g ⁻	g ⁺	a	s	g ⁻	g ⁺	g ⁺	
7	2.0	2.3	2.2	2.9	1.6	g ⁺	g ⁺	g ⁺	g ⁺	g ⁻	g ⁻	g ⁺	g ⁻	g ⁻	g ⁻	g ⁺	g ⁺	
8	0.2	0.6	0.2	0.8	1.7	g ⁺	g ⁺	g ⁺	g ⁺	g ⁻	g ⁻	g ⁺	g ⁻	s	g ⁻	g ⁺	g ⁺	
9	1.1	0.5	0.9	1.1	1.7	g ⁺	g ⁺	g ⁺	a	g ⁻	g ⁻	g ⁺	g ⁻	s	g ⁻	g ⁺	g ⁺	
10 ^b	1.4	1.8	1.5	2.6	1.8	a	a	g ⁺	g ⁺	g ⁻	g ⁻	g ⁺	g ⁻	g ⁻	g ⁻	g ⁺	g ⁺	
11	1.7	1.4	1.5	1.8	1.9	g ⁺	g ⁺	g ⁺	g ⁺	g ⁻	g ⁻	g ⁺	g ⁻	s	g ⁻	g ⁺	g ⁺	
12	0.0	0.6	0.0	0.9	1.9	g ⁺	g ⁺	g ⁺	g ⁺	g ⁻	g ⁻	a	g ⁺	s	g ⁻	g ⁺	g ⁺	
13	2.2	3.2	2.4	3.4	2.1	g ⁺	g ⁺	g ⁺	g ⁺	a	a	a	a	a	a	a	g ⁺	
14	1.1	0.7	0.8	0.7	2.1	g ⁺	g ⁺	g ⁺	g ⁺	g ⁻	g ⁻	g ⁺	a	s	g ⁻	g ⁺	g ⁺	
15 ^b	0.2	0.6	0.2	0.8	2.1	a	a	g ⁺	g ⁺	g ⁻	g ⁻	g ⁺	g ⁻	g ⁻	g ⁻	g ⁺	g ⁺	
16 ^b	0.0	0.6	0.0	0.9	2.3	a	a	g ⁺	g ⁺	g ⁻	g ⁻	a	g ⁺	g ⁻	g ⁻	g ⁺	g ⁺	
17	3.0	3.4	3.2	4.2	2.4	g ⁺	g ⁺	g ⁺	g ⁺	g ⁻	g ⁻	g ⁺	g ⁻	s	g ⁻	g ⁺	g ⁺	
18 ^b	2.2	2.5	2.4	2.6	2.4	a	a	g ⁺	g ⁺	g ⁻	g ⁻	g ⁺	g ⁻	g ⁻	g ⁻	g ⁺	g ⁺	
19	2.2	2.5	2.4	2.6	2.5	g ⁺	g ⁺	g ⁺	g ⁺	a	a	a	a	a	a	a	g ⁺	
20	2.9	3.6	3.1	4.1	2.6	g ⁺	g ⁺	g ⁺	g ⁺	g ⁻	g ⁻	g ⁺	a	s	g ⁻	g ⁺	g ⁺	
21 ^b	1.0	1.6	1.1	2.2	2.8	a	a	g ⁺	g ⁺	g ⁻	g ⁻	g ⁺	g ⁻	g ⁻	g ⁻	g ⁺	g ⁺	
71 ^c	6.7	6.2	6.3	6.2	5.0	g ⁺	g ⁻	a	a	g ⁻	g ⁻	g ⁺	s	s	g ⁻	g ⁺	g ⁺	
72 ^c	4.7	4.1	4.4	3.8	5.1	g ⁺	g ⁻	a	a	a	a	g ⁺	a	s	g ⁻	g ⁺	g ⁺	

^a Total energies of the lowest-energy conformations: $(E_o)_g^{B3LYP} = -1337.662286$ a.u., $(E_o)_g^{wB97XD} = -1337.269492$ a.u., $(E_o)_g^{PBEh1PBE} = -1336.333340$ a.u., $(E_o)_g^{M062X} = -1337.1721753$ a.u., $(E_o)_g^{MMFF94S} = 176.1$ kcal mol⁻¹. ^b *kink*-conformations. ^c *band-flipped* conformations. ^d Definition of the dihedral angles according to the numbering of the atoms in Fig. 1: Φ = C4(n)-O4(n)-C1(n+1)-O5(n+1); Ψ = C3(n)-C4(n)-O4(n)-C1(n+1); θ₁¹ = O5(n)-C5(n)-C6(n)-O6(n); θ₁² = C5(n)-C6(n)-O6(n)-H; θ₃¹ = C1(n)-C2(n)-O2(n)-H; θ₄¹ = C2(n)-C3(n)-O3(n)-H; θ₁² = O5(n+1)-C5(n+1)-C6(n+1)-O6(n+1); θ₂² = C5(n+1)-C6(n+1)-O6(n+1)-H; θ₃² = C1(n+1)-C2(n+1)-O2(n+1)-H; θ₄² = C2(n+1)-C3(n+1)-O3(n+1)-H; φ_{OH} = C3(n+1)-C4(n+1)-O4(n+1)-H; φ_{OG+} = C4(n-1)-O4(n-1)-C1(n)-H. ^e Results with MMFF94S. ^f A letter-code: *s* - dihedral angles in the range -30.0° - (+30.0°); *g*⁺ - dihedral angles in the range 30.0° - 130.0°; *g*⁻ - dihedral angles in the range -30.0° - (-130.0°); *a* - dihedral angles in the range 130.0° - (-130.0°).

the same **4abc**-type *anti* conformation was found by all methods used. In addition to the two sets of three hydrogen bonds, a bifurcated hydrogen bond is also formed with the participation of the glycosidic oxygen atom. With the same energy, determined with MMFF94S, and with lower energy, determined by all DFT methods, is another *anti* conformation characterized by **4ac** or **3a2c** types of hydrogen bonding. The lowest energy *anti* conformation has one or two hydrogen bonds less than the corresponding *syn* counterpart. What is more interesting however is that the lowest energy *anti* form has one hydrogen bond less than the other *anti* conformation.

CONCLUSION

Evidences were acquired on the validation of the modeling and simulation results on large-ring cyclodextrins from the starting geometry for the conformational search. The dependence of the results from the starting geometries was examined for the set of macrorings CD_n, n= 16, 17, 18, 19, 20, 21. The structures obtained earlier for CD_n, n=16, 17, 18, 19 were confirmed, but not those for CD20 and CD21, although the tendency is evident for opening of the macrorings. Results from DFT studies on a model system using different functionals (B3LYP, wB97XD, PBEh1PBE, M06-2X) justify our choice to use Glycam04 for modeling the conformations of large-ring cyclodextrins. The configurations of hydrogen bonds that determine the geometries of the preferred *syn* and *anti* conformations were also examined.

Acknowledgements: The financial support is from the National Science Fund within the project TK01/0167. CPU-hours grants from HPC-EUROPA2 (RII3-CT-2003-506079 – Research Infrastructure Action under the FP6 and the FP7 “Structuring the European Research Area” Programme) and RNF01/0110 (NSF-Bulgaria) projects, as well as stimulating discussions with partners in the COST action CM1002 are also acknowledged.

REFERENCES

1. W. Saenger, J. Jacob, K. Gessler, T. Steiner, D. Hoffmann, H. Sanbe, K. Koizumi, S. Smith, T. Takaha, *Chem. Rev.*, **98**, 1787 (1998).
2. K. L. Larsen, *J. Incl. Phenom. Mol. Recognit. Chem.*, **43**, 1 (2002).
3. T. Endo, H. Ueda, *J. Pharm. Sci.*, **29**, 27 (2004).
4. H. Ueda, T. Endo, in: Cyclodextrins and their complexes. Chemistry, analytical methods, applications; H. Dodziuk, Ed.; Weinheim: Wiley-VCH, 2006; pp. 370-380.
5. T. Endo, *Trends Glycosci. Glycotechnol.*, **23**, 79 (2011).
6. H. Ueda, *J. Incl. Phenom. Macrocyclic Chem.*, **44**, 53 (2002).
7. K. L. Larsen, F. Mathiesen, W. Zimmermann, *Carbohydr. Res.*, **298**, 59 (1997).
8. M. A. Villier, *Comptes. Rendus. Acad. Sci.*, **112**, 536 (1891).
9. D. French, A. O. Pulley, J. A. Effenberger, M. A. Rougvie, M. Abdullah, *Arch. Biochem. Biophys.*, **111**, 153 (1965).
10. S. Kobayashi, M. Fukuda, M. Monma, T. Harumi, M. Kubo, Abstracts of Papers, the Annual Meeting of the Agricultural Chemical Society of Japan, Kyoto, April 1986, p. 649 (in Japanese).
11. T. Fujiwara, N. Tanaka, S. Kobayashi, *Chem. Lett.*, 739 (1990).
12. J. Jacob, K. Gessler, D. Hoffmann, H. Sanbe, K. Koizumi, S. M. Smith, T. Takaha, W. Saenger, *Angew. Chem. Int. Ed. Eng.*, **37**, 606 (1998).
13. J. Jacob, K. Gessler, D. Hoffmann, H. Sanbe, K. Koizumi, S. M. Smith, T. Takaha, W. Saenger, *Carbohydr. Res.*, **322**, 228 (1999).
14. K. Imamura, O. Nimz, J. Jacob, D. Myles, S. A. Mason, S. Kitamura, T. Aree, W. Saenger, *Acta Cryst. B*, **B57**, 833 (2001).
15. K. Gessler, I. Uson, T. Takaha, N. Krauss, S. M. Smith, S. Okada, G. M. Sheldrick, W. Saenger, *Proc. Natl. Acad. Sci. USA*, **96**, 4246 (1999).
16. O. Nimz, K. Gessler, I. Uson, S. Laettig, H. Welfle, G. M. Sheldrick, W. Saenger, *Carbohydr. Res.*, **338**, 977 (2003).
17. T. Furuishi, T. Endo, H. Nagase, H. Ueda, T. Nagai, *Chem. Pharm. Bull.*, **46**, 1658 (1998).
18. H. Dodziuk, A. Ejchart, W. Anczewski, H. Ueda, E. Krinichnaya, G. Dolgonos, W. Kutner, *Chem. Commun.*, 986 (2003).
19. F. Ellouze, N. Ben Amar, A. Deratani, W. Zimmermann, Results presented at the 15th International Cyclodextrin Symposium, O12, May 9-12, 2010, Vienna, Austria.
20. J. Wang, A. Jiao, Y. Tian, X. Xu, Z. Jin, Y. Li, *J. Chromatography A*, **1218**, 863 (2011).
21. S. Toita, N. Morimoto, K. Akiyoshim, *Biomacromolecules*, **11**, 397 (2010).
22. P. M. Ivanov, C. Jaime, *J. Phys. Chem. B*, **108**, 6261 (2004).
23. M. G. Gotsev, P. M. Ivanov, *J. Phys. Chem. B*, **113**, 5752 (2009).
24. P. M. Ivanov, *J. Phys. Chem. B*, **114**, 2650 (2010).
25. P. M. Ivanov, *Chirality*, **23**, 628 (2011).
26. P. M. Ivanov, *J. Mol. Struct.*, **1009**, 3 (2012).

27. P. M. Ivanov, in: Nanoscience & Nanotechnology - Nanostructured materials - Application and Innovation Transfer, E. Balabanova, E.; I. Dragieva, I. Eds., 2011, issue 11, 14.
28. P. Ivanov, *Curr. Phys. Chem.*, **2**, 413 (2012), and references cited therein.
29. P. Ivanov, E. Atanassov, C. Jaime, *J. Mol. Struct.*, **1056-1057**, 238 (2014).
30. D. A. Case, T. A. Darden, T. E. Cheatham III, C. L. Simmerling, J. Wang, R. E. Duke, R. Luo, M. Crowley, R. C. Walker, W. Zhang, K. M. Merz, B. Roberts, B. Wang, S. Hayik, A. Roitberg, G. Seabra, I. Kolossvary, K. F. Wong, F. Paesani, J. Vanicek, X. Wu, S. Brozell, T. Steinbrecher, H. Gohlke, Q. Cai, X. Ye, J. Wang, M.-J. Hsieh, G. Cui, D. R. Roe, D. H. Mathews, M. G. Seetin, C. Sagui, V. Babin, T. Luchko, S. Gusarov, A. Kovalenko, P. A. Kollman, (2010), AMBER 11, University of California, San Francisco.
31. K. N. Kirschner, A. B. Yongye, S. M. Tschampel, J. González-Outeiriño, C. R. Daniels, B. L. Foley, R. J. Woods, *J. Comput. Chem.*, **29**, 622 (2007).
32. Gaussian 09, Revision A.1, M. J. Frisch, G. W. Trucks, H. B. Schlegel, G. E. Scuseria, M. A. Robb, J. R. Cheeseman, G. Scalmani, V. Barone, B. Mennucci, G. A. Petersson, H. Nakatsuji, M. Caricato, X. Li, H. P. Hratchian, A. F. Izmaylov, J. Bloino, G. Zheng, J. L. Sonnenberg, M. Hada, M. Ehara, K. Toyota, R. Fukuda, J. Hasegawa, M. Ishida, T. Nakajima, Y. Honda, O. Kitao, H. Nakai, T. Vreven, J. A. Montgomery, Jr., J. E. Peralta, F. Ogliaro, M. Bearpark, J. J. Heyd, E. Brothers, K. N. Kudin, V. N. Staroverov, R. Kobayashi, J. Normand, K. Raghavachari, A. Rendell, J. C. Burant, S. S. Iyengar, J. Tomasi, M. Cossi, N. Rega, J. M. Millam, M. Klene, J. E. Knox, J. B. Cross, V. Bakken, C. Adamo, J. Jaramillo, R. Gomperts, R. E. Stratmann, O. Yazyev, A. J. Austin, R. Cammi, C. Pomelli, J. W. Ochterski, R. L. Martin, K. Morokuma, V. G. Zakrzewski, G. A. Voth, P. Salvador, J. J. Dannenberg, S. Dapprich, A. D. Daniels, Ö. Farkas, J. B. Foresman, J. V. Ortiz, J. Cioslowski, D. J. Fox, Gaussian, Inc., Wallingford CT, 2009.

ИЗСЛЕДВАНЕ ВЪРХУ КОНФОРМАЦИИТЕ НА ГОЛЕМИ ЦИКЛОДЕКСТРИНИ

П. Иванов

Институт по Органична химия с Център по Фитохимия, Българска Академия на Науките, ул. Акад. Г. Бончев, бл. 9, 1113 София, България

Постъпила на 07 май 2014 г.; Коригирана на 18 юни 2014 г.

(Резюме)

Изследвана е зависимостта на резултатите от изходните геометрии при конформационно търсене за набор от големи циклодекстрини, CD_n, n = 16, 17, 18, 19, 20, 21, Потвърдени бяха получени по-рано структури за CD_n, n=16, 17, 18, 19, но не и такива за CD₂₀ и CD₂₁, но се наблюдава тенденция към разтваряне на макропръстените, установено по-рано при тях. Резултати от DFT пресмятания с различни функционали на моделна система са в подкрепа на направения от нас избор на силово поле, Amber Glucam04, за моделиране на конформациите на големи циклодекстрини. Проучени са и конфигурациите от вътрешномолекулни водородни връзки, определящи геометриите на предпочетените *syn* и *anti* конформации.

Application of Isohypses method for AES quantification of semiconductor solid solutions

G. S. Spasov

Institute of Optical Materials and Technologies "Academician Jordan Malinovski", Bulgarian Academy of Sciences, Acad. G. Bonchev str., bl. 109, 1113 Sofia, Bulgaria

Received April 17, 2014; Revised May 26, 2014

Dedicated to Acad. Dimiter Ivanov on the occasion of his 120th birth anniversary

The Isohypses method (IHM), previously used in energy dispersive X-ray microanalysis, is discussed as a tool for AES quantification of ternary and quaternary semiconductor quasi-binary solid solutions. It is with standards, which components are mainly with an unit less than those of the analyzed compound (The standards are peripheral points on the concentration triangle/square). For that reason a less number of standards are requested, which is a principal advantage of the IHM compared to the method of a complete standards' description. The method is based on the assumption, that when mixing binary systems in which the values of response of the A element are equal to each other, the response is not changed. As a procedure it consists of: I. Construction of a nomograph according to Auger standards data and, II. Determination by it the sample composition from the Auger intensities. The essence of the method is presented in the paper and the specifications required by the considered class compounds. Applications for $\text{Al}_x\text{Ga}_{1-x}\text{As}$, $\text{In}_x\text{Ga}_{1-x}\text{As}$ and $\text{In}_x\text{Ga}_{1-x}\text{P}_y\text{As}_{1-y}$ are discussed.

Key words: Auger electron spectroscopy, AES analysis, Semiconductor solid solutions

INTRODUCTION

Three reasons make us to remind the already proposed Auger quantification by isohypses [1]: I. The semiconductor solid solutions continue to be of interest and a subject of scientific research; II. Miniaturization strengthens the AES analyses importance, but III. Still the accurate Auger quantification is problematic. The total calibration by standard compositions perhaps is most accurate, but the method' use is limited when the number of components is more than three.

The Isohypses method (IHM) for AES quantification is developed by analogy of its use in energy dispersive X-ray microanalysis [2]. The term "isohypse" (from Greek "hypsos" – height) is cartographic. There it means a line connecting the points with equal altitude, in our case, respectively, equal Auger signal.

The method is based on the assumption, that when mixing binary systems in which the values of response of the element A are equal to each other, the response is not changed. It can be shown that this leads to the conclusion that the composition' isohypses for ternary and quaternary solid solutions are straight lines.

It is not known someone to have used into Auger practice the IHM. Hoping to have followers we submit an IHM application for $\text{Al}_x\text{Ga}_{1-x}\text{As}$, $\text{In}_x\text{Ga}_{1-x}\text{As}$ and $\text{In}_x\text{Ga}_{1-x}\text{P}_y\text{As}_{1-y}$ systems. This is new at this work and its essence. But preliminary the general IHM procedure is exposed briefly according to our work [1].

THEORY

First IHM quantification will be demonstrated for three-component system (A, B, C). The concentration triangle sides AB, BC and AC conform to the homonymous binary systems. Their Auger response characteristics (experimentally or theoretically obtained) are plotted on the ordinates K_A , K_B , K_C (Fig. 1). Through them, the binary compositions a' , a'' , etc., are constructed by the signal intensities K_A^S , K_B^S , K_C^S of the analyzed specimen. They define the isohypses $a'-a''$, $b'-b''$, $c'-c''$, which crossings form the searched composition triangle A'B'C'. Its sizes reflect the experiment precision and the applicability of the IHM. If they are small, it is possible to treat A'B'C' as a point. The atomic part of i^{th} -element, c_i^S , is equal to the distance from this point, O, to the ABC side, opposite to the i^{th} -apex, normalized to the altitude (e.g., $c_B^S = \text{OM}/\text{BS}$). Otherwise these operations are performed toward the centre of gravity of A'B'C'.

* To whom all correspondence should be sent:
E-mail: gspasov@clf.bas.bg

Now it will be presented the possibility of applying the IHM to four-component solid solutions of the type $AB_{1-x-y}C_xD_y$ and $A_xB_{1-x}C_{1-y}D_y$. The concentration triangle is replaced by a tetrahedron. The composition of first type semiconductors (e.g., $GaAs_{1-x-y}P_xSb_y$) is represented by a triangle with apexes the binary compounds AB, AC, AD (GaAs, GaP, GaSb). The availability of the intrinsic standard ($c_A = 50\%$) allows analysing similar to that from Fig. 1.

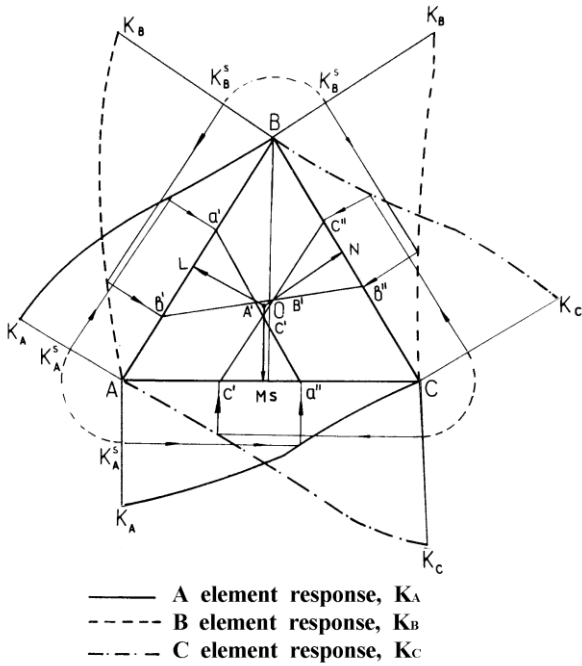


Fig. 1. IHM for a three-component system.

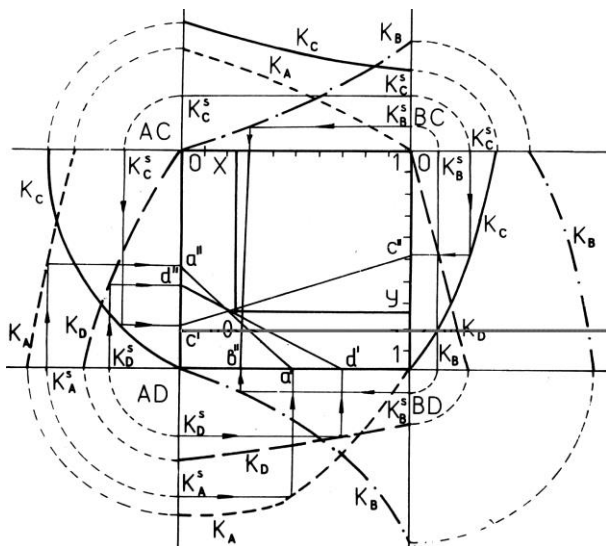


Fig. 2. IHM for a 4-component system $A_xB_{1-x}C_{1-y}D_y$.

The case of $A_xB_{1-x}C_{1-y}D_y$ appears to be more general and requires a detailed examination. All these compositions ($0 \leq x \leq 1$, $0 \leq y \leq 1$) correspond to the square tetrahedron' section with apexes AC, AD, BD, BC, shown on Fig. 2.

Again Auger response characteristics (now 3 each) are constructed on the figure' sides. The Auger signal of the i^{th} -element (for example, A) has intensity 0 along the side BC-BD. Starting at 0, it increases along BC-AC cut, it is biggest – but changes less – in AC-AD cut and decreases along BD-AD cut. The quantification is similar to that for the three-component system. The Auger signals obtained from the analyzed specimen K_i^s lead to the isohypsens $a'-a''$, etc. The figure of the errors is now a tetragon with its median point O. Since x varies (from 0 to 1) along the horizontal square' side and y – along the vertical, the distances of point O to the square side are just x and y content.

Nomograph Construction

IHM will be applied to the systems $Al_xGa_{1-x}As$ and $In_xGa_{1-x}As$ at first. Their quasi-binarity is of main importance, giving the As contents $c_{As} = 0.5$. For $Al_xGa_{1-x}As$, it is located along the cut AlAs-GaAs (coincident with the As-isohypse) of the concentration triangle. The exclusion of As-side allows to present Fig. 1 simplified, as AlGaAs triangle tear in the top As and stood up straight: As-Al-Ga-As, Fig. 3 and Fig. 4. The points a' and a'' (determining the isohypse for Al) and b' and b'' (determining the isohypse for Ga) are found as in Fig. 1. The sought x is the medial between the points of intersection of these isohypsens with the cut AlAs-GaAs. Now it becomes convenient to work with relative (toward As) Auger signals. The normalization is done by the value of the As-intensity from the stoichiometric binary composition (e.g., GaAs for the side As-Ga).

It seems a difficulty that on the mentioned sides there may not be the continuous solid solutions. But the ends and the middle point (i.e., As, GaAs, Ga) are enough to construct a "rough" response characteristic true reflecting analyses specificity. The fitting curve "Auger intensity vs. Ga contents" must be of "matrix correction" type:

$$y = x/[F + x(1 - F)] \quad (1)$$

where F is the matrix correction factor (comprising the ion etching effects). The Ga (or As) contents in GaAs after etching must be known for curve' theoretic determination. The surface composition Ga/As (1keV Ar^+) is 1/0.92 [3] and the calculated "atomic density – attenuation length [4] – back-scattering factor" correction for Ga in GaAs is 0.94. So the dependence (1), (which is 0 at As and 1 at Ga), decreases with about 2% from the linear at 0.5, Fig. 3 and Fig. 4.

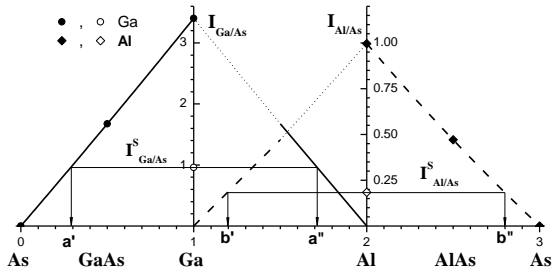


Fig. 3. IHM for the system $Al_xGa_{1-x}As$ (after Arthur's data [11]). The concentration triangle sides As-Ga, Ga-Al, Al-As are unfolded on the axis x, corresponding to 0-1, 1-2, 2-3.

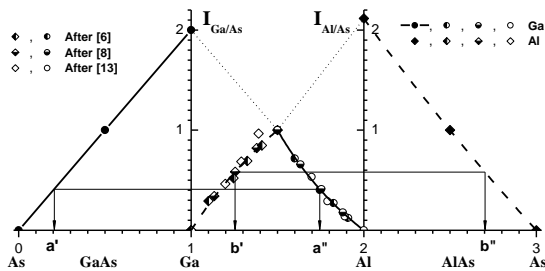


Fig. 4. IHM for the system $Al_xGa_{1-x}As$ (Bulk composition determined by the surface data).

But for the side Al-As we have neither AlAs standard, nor its sputtering data. Therefore getting the experimental intensity ratio Al/As^{GaAs} (The last symbol means that As is from GaAs) and correcting it by 1.14 (average from [5-8] for As^{AlAs}/As^{GaAs}), we obtain Al/As^{AlAs} 1.10. I.e. the relative (to As) Al-intensity is 0.55. This value for the compound AlAs is 0.51 (average from [9-12]), which gives for the mean of the side Al-As a decrease with about 7% compared to the linear dependency, Fig. 3 and Fig. 4.

As to the nomograph's part of the two elements from III group, it should not be forgotten that quasi-binary compounds are of analytical interest. So Auger behaviour of III-III alloys may not be useful to the response characteristics. It is more reliable the reconstruction to be made by the quasi-binaries themselves. Assuming that these characteristics are proportional to the corresponding ones from the quasi-binary cut ($Al_xGa_{1-x}As$; $0 \leq x \leq 1$), so, the normalized Al characteristic at $x \leq 0.5$ is Al/As from $Al_xGa_{1-x}As$ and that of Ga at $x \geq 0.5$ is Ga/As from $Al_xGa_{1-x}As$. (For the rest parts of the range these characteristics are not important: Ga and Al don't surpass 50% in the analyzed compositions.) If some of the metals (e.g., Ga) is characterized theoretically (in Part As-Ga of the x axis) and experimentally (in Part Ga-Al of the x axis), it is

necessary to fit one curve to the other at the binary stoichiometric composition. This is most visible for In of Fig. 5.

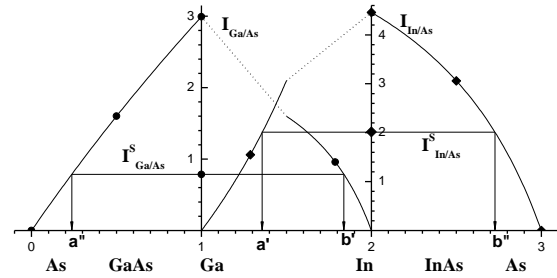


Fig. 5. IHM for the system $In_xGa_{1-x}As$.

The first $Al_xGa_{1-x}As$ application is after Arthur and LePore's work [11]. They analyse the surface composition, receiving linear dependency of x to Al/As (0.47 for AlAs) and Ga/As (1.67 for GaAs). As a standard we used their sample with (AlAs)-atomic part 0.42. Its relative intensities Al/As 0.18 and Ga/As 0.96 are constructed on Fig. 3, setting the points a' and a'' for Ga' isohypse, and b' and b'' for Al' isohypse. The concentrations are found from these points by a calculating procedure.

At the next application the bulk composition of $Al_xGa_{1-x}As$ layer is determined by the surface data. Influenced by the ion etching, now the Auger intensities are a non-linear function of x. They are found by a "matrix corrected" fitting of the data of several literary sets [6,10,13] (conformed with the analytical regime), Fig. 4. The medial composition from [10] is viewed as a sample, because it is located closest to the fitted curve.

By analogy the nomograph for the system $In_xGa_{1-x}As$ is constructed, Fig. 5. Now the construction of the response characteristics on the side Ga-In is by one experimental point. The ion etching is with 3 keV Ar^+ . The composition of both standard and sample ($3\mu m$ liquid-epitaxial layers on GaAs substrate) is measured by the electron probe microanalysis. The very different sputtering behaviour of $In_xGa_{1-x}As$ and InAs makes worse the IHM analysis' result for this system.

$In_xGa_{1-x}P_yAs_{1-y}$ analysis is made by a specimen, which composition is measured by EPMA. Its Auger intensities (in arbitrary units) are Ga(30.5), In(133.0), As(52.5), P(22.0). We use the simplest model, accepting all response characteristics are straight lines connecting the binary apexes. The measured Auger intensities (in arbitrary units) are GaAs(132; 86), InAs(189; 58), InP(140; 116), GaP(104; 136); the figures in brackets correspond to the order of the elements in the formula. As this model allows to determine the isohypes' cuts by

simple trigonometric calculations, Fig. 6 displays only the isohypeses.

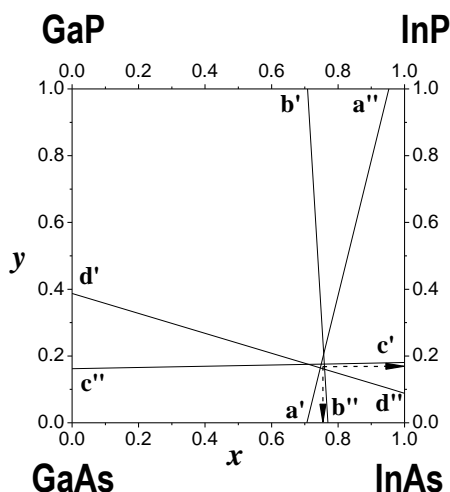


Fig. 6. IHM for the system $\text{In}_x\text{Ga}_{1-x}\text{P}_{1-y}\text{As}_y$.

RESULTS AND DISCUSSION

The test of one method for quantification usually consists of evaluation by it of a standard (specimen with known composition), what we do. All received results are listed in Table 1.

Table 1. Quantification results

Specimen	True x	IHM x	$\Delta x/x, \%$	$\Delta I/I, \%$
$\text{Al}_x\text{Ga}_{1-x}\text{As}$ [11]	0.42	0.41	2.4	1.2
$\text{Al}_x\text{Ga}_{1-x}\text{As}$ [10]	0.51	0.56	10.1	1
$\text{In}_x\text{Ga}_{1-x}\text{As}$	0.73	0.59	19.3	1
$\text{In}_x\text{Ga}_{1-x}\text{P}_y\text{As}_{1-y}$	0.74	0.75	2.4	0.7
(this row is to y)	0.17	0.17	1.6	0.8

The presented analytic applications prove that the isohypeses method (IHM) is a useful and accurate tool for a quantitative Auger analysis (let remember that the elemental sensitivity factors method is semi-quantitative; the methods with one or two standards are very erroneous, while the method with fully tabulation is practically inapplicable for four-component compositions because of the great number of necessary standards). The standards' number for IHM is at least an order less (equidistant traveling over the figure periphery compared to that of its area).

Simpler compositions are used as the standards. Since their components number is usually less by one compared to the one of the analyzed, their preparation would offer no difficulty, too.

These standards are close to the analyzed specimen from physicochemical point of view (lattice type and constant, orientation, density, etc.). On the other hand, this closeness is the general

condition for the matrix effects decrease, which increases the linearity of the analysis.

The IHM combines the taking into account of all matrix effects (inherent of the method used a series of compositions as standards) with applicability to quaternary compounds.

The IHM procedure is easy and leads to unambiguous result.

The work demonstrates that the Auger response characteristics can be received not only experimentally, but also by modelling. That's why a partial lack of experimental data is not an obstacle to the method utilization.

CONCLUSION

The Isohypeses method is concretized and tested for AES quantification of a few ternary and quaternary quasi-binary solid solutions. It proves to be adaptable and accurate enough.

The Isohypeses method' advantage is the using of less in number and simpler in composition standards, close to the analyzed sample.

REFERENCES

- V. A. Moshnikov, G. S. Spasov, 12th Intern. Congress X-Ray Optics & Microanal. (Ed. S. Jasienska, L. J. Maksymowicz), Academy of Mining & Metallurgy, Cracow, Vol. I, 308, 1989.
- V. B. Nesterenko, X-ray Spectroscopic and Electron Microscopic Methods for the Structure and the Properties of Materials Examination, Science and Technics, Minsk, 1980 (in Russian).
- J. B. Malherbe, *Crit. Rev. Sol. St. Mater. Sci.*, **19**, 129 (1994).
- M. P. Seah, W. A. Dench, *Surf. Interface Anal.*, **1**, 2 (1979).
- C. M. Garner, Y. D. Shen, J. S. Kim, G. L. Pearson, W. E. Spicer, *J. Appl. Phys.*, **48**, 3147 (1977).
- W. D. Chen, H. Bender, A. Demesmaeker, H. E. Maes, *Surf. Interface Anal.*, **12**, 156 (1988).
- K. Kajiwara, H. Kawai, *Surf. Interface Anal.*, **15**, 433 (1990).
- K. Satori, Y. Haga, R. Minatoya, M. Aoki, K. Kajiwara, *J. Vac. Sci. Technol.*, **A 15**, 478 (1997).
- R. Ludeke, L. Esaki, L. L. Chang, *Appl. Phys. Lett.*, **24**, 417 (1974).
- L. L. Chang, A. Koma, *Appl. Phys. Lett.*, **29**, 138 (1976).
- J. R. Arthur, J. J. LePore, *J. Vac. Sci. Technol.*, **14**, 979 (1977).
- T. S. Stewart, S. I. Boldish, J. A. Osmer, N. Marquez, D. G. Heflinger, G. A. Evans, J. B. Kirk, A. Mantie, T. Stockton, *Proc. SPIE*, **323**, 164 (1982).
- S. L. Wright, R. F. Marks, R. J. Savoy, *J. Vac. Sci. Technol.*, **B 6**, 1105 (1988).

ПРИЛОЖЕНИЕ НА МЕТОДА НА ИЗОХИПСИТЕ ЗА ЕЛЕКТРОНЕН ОЖЕ
СПЕКТРОСКОПСКИ КОЛИЧЕСТВЕН АНАЛИЗ НА ПОЛУПРОВОДНИКОВИ ТВЪРДИ
РАЗТВОРИ

Г. С. Спасов

*Институт по оптични материали и технологии, Българска Академия на Науките, ул. Акад. Г. Бончев, бл. 109,
1113 София, България*

Постъпила на 17 април 2014 г.; Коригирана на 26 май 2014 г.

(Резюме)

Разисква се количествен Оже електронен спектроскопски анализ на тройни и четворни полупроводникови квазибинарни твърди разтвори посредством Метода на изохипсите, МИХ (вече използван в рьонгеновия микроанализ). Методът е със стандарти, като броят на елементите, които те съдържат, е поне с единица по-малък от този на анализиращия състав – стандартите се явяват точки от периферията на концентрационния триъгълник/квадрат. Оттук, по-малкият брой необходими стандарти – основно предимство на МИХ спрямо метода на пълно привързване към стандарти. В основата на МИХ е приемането, че при смесване на бинарни системи с равни сигнали от елемента А, сигналът не се променя. Процедурно методът се състои от: I. Построяване на номограма по данните на стандартите; и II. Определяне чрез нея на състава на образеца по Оже интензитетите му. В статията е представена същността на метода и спецификата, налагана за разглеждания клас съединения. Разисквани са 4 приложения за $Al_xGa_{1-x}As$, $In_xGa_{1-x}As$ и $In_xGa_{1-x}P_yAs_{1-y}$.

Optical properties of silver-doped organic polymer films as solar control coating materials for advanced architectural glazing application

R. Todorov^{1*}, Y. Ilieva², V. Lozanova¹, A. Lalova¹

¹*Institute of Optical Materials and Technologies "Acad. J. Malinowski", Bulgarian Academy of Sciences, Acad. G. Bonchev str., bl. 109, 1113 Sofia, Bulgaria*

²*Faculty of Architecture, Higher School of Construction Engineering "L. Karavelov", 175 Suhodolska str., 1373 Sofia, Bulgaria*

Received May 01, 2014; Revised July 02, 2014

Dedicated to Acad. Dimiter Ivanov on the occasion of his 120th birth anniversary

Metal-polymer nanocomposites possess a great potential for minimization of heat transfer losses and heat gains through the building envelope, finding application in the field of solar control coating materials. In the present paper we report the optical properties of a metal-polymer from Ag and polymethyl methacrylate (PMMA) nanocomposite fabricated by layer-by layer deposition technique. The X-ray diffraction pattern confirms the presence of silver particles in the thin films. The average size of silver particles was calculated by Debye-Scherrer formula. An absorbance band in the spectral range 350-550 nm due to the surface plasmon resonance of the silver nanoparticles was observed in transmittance spectra. The position of the absorbance band has been analyzed by the Bruggeman's model for the effective media. On the base of the obtained results the polymer-inorganic hybrid coatings were suggested for application as sun protective coatings.

Key words: nanocomposite films, silver, polymethyl methacrylate, Bruggeman's model

INTRODUCTION

Glazing elements are significant portion of the building envelope, although traditionally more attention is paid to the solid part of walls and roofs and they are one of the weakest thermal control points in building interiors. For example in a standard family residence, 10-20 % of all heat loss occurs through the windows [1]. Therefore in the glazing design, it is necessary to consider performance in terms of heat transfer, thermal comfort, light transmission, and appearance. To achieve good thermal insulation effect, the solar-protected glasses must be manufactured with a special coating that provides high transmittance of the visible light and reflected the IR beams. All coating must reflected the infrared beams in the spectral range 5-12 μm . In this region of the electromagnetic spectra the electrical appliances, heaters and the human body, i.e. internal heat sources for the building emit their thermal energy. Window glazing that reduces the entry of the infrared solar radiation (spectral range 0.8-2 μm) is most effective in summer and reduces the cooling demand. In contrast, in winter, this type of glazing increases the need for heating because it hinders the use of solar

energy for passive heating. The development of glazing that reduces the quantity of solar radiation should not affect the possibility of seeing through windows, especially when a large amount of natural light is required, such as in office buildings. A reduction in natural daylight causes a corresponding increase in artificial light. This signifies higher energy costs as well as an increase in indoor temperature.

In [2] it is shown that the coatings which consist of alternating dielectric and metal (D/M/D) films on glass exhibit great energy saving effects by reflecting the IR radiation by the infrared reflective metal film and transmitting visible and near IR radiation. Film-plating glazing is treated with layers of another material to improve its thermal performance. The most common coatings are done with metals (Cr, Ti, Ag and stainless steel), metal nitrides (CrN, TiN, ZrN), or metal oxides (SnO₂, TiO₂, ZnO). The coating layers can be low-emissivity films, reflective films, tinted films or spectrally selective coating [1]. Many different polymers also can be incorporated in prototype solar energy control devices, e.g. poly- and monomeric pyrrole, viologens, 4,40-diaminodiphenyl sulfone, poly(3-me-tylthiophene) or diclofenac, polyaniline (PANI) and poly(3,4-ethylene-dioxy-thiophene) (PEDOT) [3]. According to [2], the ideal

* To whom all correspondence should be sent:
E-mail: rossen@iomt.bas.bg

film thickness is between 40 and 80 nm. Metal-polymer nanocomposites have an advantage over the oxide/noble metal multilayers in terms of ease of synthesis. There have been several co-evaporation and co-sputtering approaches to synthesize the nanocomposite structure [4]. They possess good adhesion to the organic polymer materials such as urethane-acrylate and poly-carbonate (PC) which are well known as a glazing material [2,5]. The special advantage of PC panels is that they can transmit to 90% from the visible light and they have good resistance to external conditions.

When nanoparticles embedded in a dielectric matrix are excited by light, the electric vector of the electromagnetic wave induces a charge density oscillation [6] corresponding to the plasmon frequency (ν_p) of metal particles, resulting in strong absorption of light at a particular wavelength ($\lambda_p = c/\nu_p$, where c is the velocity of light). Apart from the optical, applications as bandpass filters [7], there is a tremendous interest in achieving an optical absorber extending from the visible to the far-IR region [8] for a variety of applications. The broad absorption band in visible spectral range and increase of conductivity of metal-polymer films make them potential materials for applications in the field of solar absorbers.

In the present work, we report the synthesis and optical properties of a metal-polymer (Ag-poly-methyl methacrylate, hereafter referred to as Ag-PMMA) nanocomposite by layer-by layer deposition technique. The possibility of deposition of coatings for control of the spectrum of the transmitted true the window sunlight is discussed.

EXPERIMENTAL

The coatings were formed in one cycle of thermal evaporation in high vacuum of 10^{-3} Pa from two sources - of silver and PMMA, respectively. The ratio between the evaporation rates of the two substances was controlled during the process. The films were deposited at 0.2 - 0.3 nm/s. To obtain thin films uniform in composition, the substrates were rotated continuously during the process of thermal evaporation. The substrate holder is a dome-shaped calotte that can be considered as a segment of a sphere. The evaporation sources are located approximately at the geometric centre of this sphere. The coatings consist of 6 alternating layers from silver and PMMA with three different thickness's ratio Ag/PMMA - 0.3, 0.13 and 0.25. The thickness of the silver layers was kept a constant ~ 5 nm. The phase structure of thin films was probed by X - ray diffraction (XRD). The

substrate holder is a dome-shaped calotte that can be considered as a segment of a sphere. The evaporation sources are located approximately at the geometric centre of this sphere. Optical transmittance and reflectance measurements at normal incidence of light beam were carried out in the spectral range from 300 to 2000 nm using an UV-VIS-NIR spectrophotometer (Cary 05E, Australia).

RESULTS AND DISCUSSION

The transmittance and reflectance spectra of Ag-PMMA coatings in the spectral range 300-2000 nm are shown in Fig. 1.

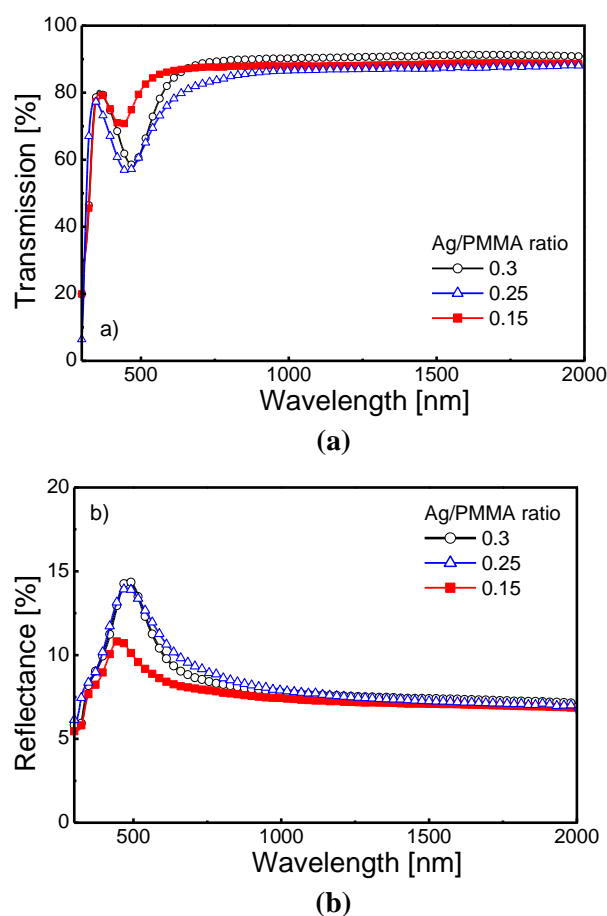


Fig. 1. Transmittance (a) and reflectance (b) spectra of thin Ag-PMMA coatings with different Ag contain.

The transmittance spectra showed that the Ag-PMMA coatings possess transmission higher than 80% in the infrared spectral range. All spectra demonstrate an absorption band situated in the 400-550 nm due to silver surface plasmon resonance. The plasmon peak in the spectra of the thin films indicates that the silver is included in the coatings in the form of small particles. According to [9] the increase of the particle's size leads to shift of the

absorption band due to plasmon excitation at longer wavelengths and can explain the shift of the absorption band at higher Ag/PMMA ratios. The width and magnitude of the absorption band depend on the metal fraction in the nanocomposite, and therefore can be engineered. The spectra of the composite coatings show that the color appearance can be tailored, which presents a potential for applications in architectural windows and automotive glazing.

The X-ray diffraction pattern of the nanocomposite Ag-PMMA film at ratio 0.15 is shown in Fig. 2. Peaks due to the diffraction from the crystallographic planes (111) and (200) of silver are seen in the pattern. Two diffraction peaks at 32.8° and 35.6° indicate for the presence of Ag₂O in Ag-PMMA. The possible reason for the presence of Ag₂O in the thin films is the interaction of the silver with the oxygen atoms in the monomer building the polymer network of the PMMA.

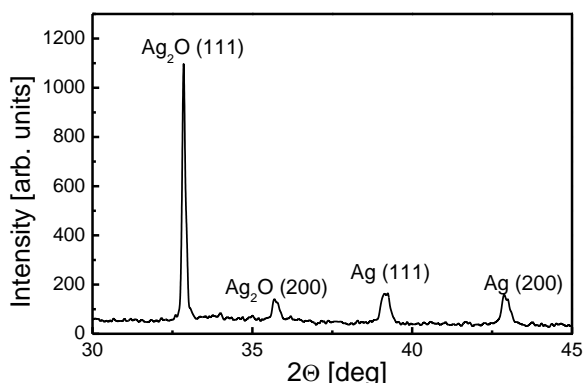


Fig. 2. X-ray diffraction pattern of thin Ag-PMMA film.

The Debye-Scherrer formula was applied for calculation of the average crystallite size:

$$d_p = \frac{0.94\lambda}{\beta \cdot \cos\theta} \quad (1)$$

where β is the peak width, λ is wavelength of the X-rays (in the present study Cu_α line was used and λ = 1.54056Å). Applying equation (1) for the diffraction peaks of the silver we found that the size of the crystallites is 25.9 nm.

In the next step we calculated the optical constants (refractive index, n and extinction coefficient, k) of the thin films. The calculation procedure is described in our previous papers [10,11]. It is seen that the refractive index of the thin films in the infrared spectral range (800-2000 nm) is 1.45-1.35. Abnormal dispersion is observed for wavelengths shorter than 550 nm.

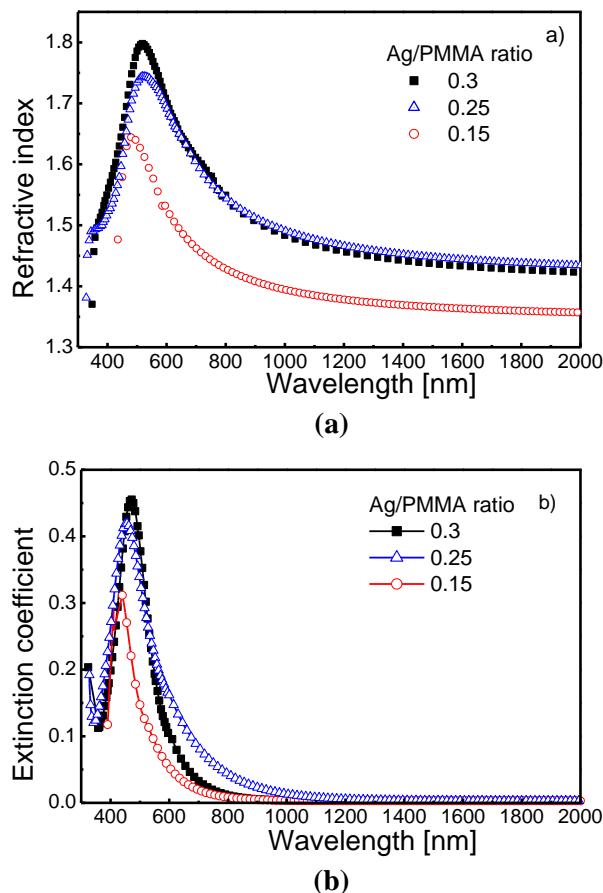


Fig. 3. Dispersion of the refractive indices (a) and extinction coefficients (b) of Ag-PMMA films.

The real and imaginary parts of the complex permittivity, $\epsilon = \epsilon' + i\epsilon''$ can be calculated from the refractive index and extinction coefficient by the following equations:

$$\epsilon' = n^2 - k^2 \quad \text{and} \quad \epsilon'' = 2nk \quad (2)$$

We applied the Burgezman effective media theory to analyze the dispersion of the composite coatings. According to [12] the effective complex permittivity, ϵ is given by the equation 3, where ϵ_m and ϵ_d are the complex permittivity of the metal and dielectric material respectively, while f_1 and f_2 are their fractions, which satisfy the following condition - $\sum f_i = 1$.

The relation between the fractions f_1 and f_2 of the thin films in the multilayered coatings and their thickness is given in [13]. The period of the structure is $a = d_1 + d_2$, where d_1 and d_2 are the thicknesses of the metal and polymer thin films, respectively. The volume filling fractions f_1 and f_2 for the metal and polymer films are given by the following equations: $f_1 = d_1/a$ and $f_2 = d_2/a$.

$$\varepsilon = 1/4\{(3f_1 - 1)\varepsilon_m + (3f_2 - 1)\varepsilon_d \pm \sqrt{[(3f_1 - 1)\varepsilon_m + (3f_2 - 1)\varepsilon_d]^2 + 8\varepsilon_m\varepsilon_d}\} \quad (3)$$

$$\varepsilon_m(\omega) = \varepsilon'(\omega) + i\varepsilon''(\omega) = \varepsilon_\infty - \frac{\omega_p^2}{\omega^2 + i\Gamma\omega} = \varepsilon_\infty - \frac{\omega_p^2}{\omega^2 + \Gamma^2} + i\frac{\omega_p^2\Gamma}{\omega(\omega^2 + \Gamma^2)} \quad (4)$$

To describe the complex permittivity, $\varepsilon(\omega)$, of the silver as a function of the angular frequency we used the Drude-Sumerfield model, given by the equation 4, where ε_∞ is the relative dielectric constant (for the silver $\varepsilon_\infty = 9$ [12]).

$\omega_p = \sqrt{n_e e^2 / \varepsilon_0 m}$ is the metal plasma frequency, where n_e is the number of free electrons, e and m are the electron's charge and mass, respectively. Γ is a damping parameter and is related with the electron mean free path, $l = 4.375 \times 10^{-8} \text{ m}^{-1}$ and the Fermi velocity $v_F = 1.4 \times 10^6 \text{ m/s}$ by:

$$\Gamma = \frac{v_F}{l} \quad (5)$$

For the description of the dispersion of the PMMA we used the data for the Sellmeier's coefficients published in [14]. In Fig. 4 a comparison is given of the real and imaginary parts of the complex permittivity calculated by Eqs. 2 and simulated from Eq. 3. Good coincidence between both is seen. Deviation close to the resonance frequency suggests the use of the Drude-Sumerfield model along with a critical point model [15].

It is well known that the pure PMMA films transmits up to 92% of visible light and gives a reflection of about 4% from each of its surfaces [14]. It filters ultraviolet (UV) light at wavelengths below about 300 nm (similar to ordinary window glass). Some additives to PMMA can be used to improve absorption in the 300-400 nm range. In Fig. 5 the simulated transmittance and reflectance are presented for a coating consisting of 10 alternate films from PMMA and Ag-PMMA. It is seen that the transmission drops drastically in the UV spectral range for wavelengths shorter than 400 nm and such coatings can be used for protection from the UV beams in the spectral range 300-380 nm. The coating possesses good transmittance in the visible spectral range. The value of T increase from 25-70% in the spectral range 400-550 and the coating possesses higher than 70 % transmittance for the wavelengths longer than 550 nm. It is known that the PMMA transmits infrared light up

to 2.8 μm and blocks longer wavelengths up to 25 μm [14] which would insure good heat-insulation performance.

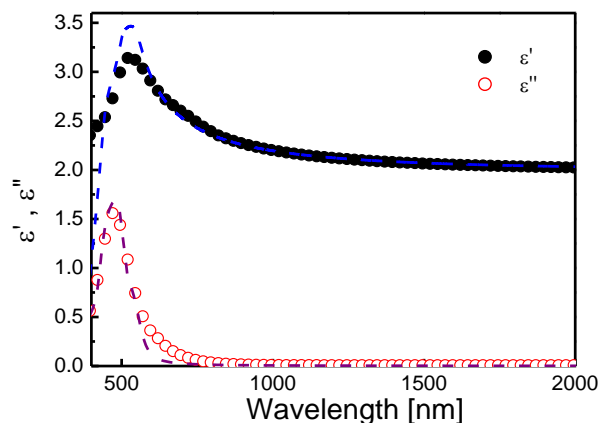


Fig. 4. Calculated (symbols) and simulated (dash lines) spectra of the complex permittivity, $\varepsilon = \varepsilon' + i\varepsilon''$ for a coating with Ag/PMMA ratio 0.15 (or $f_1 = 0.055$).

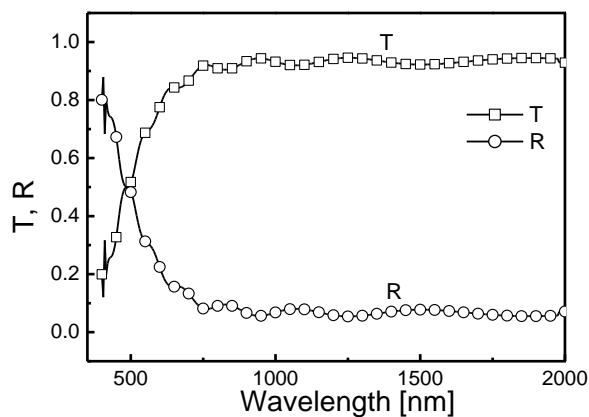


Fig. 5. Simulated transmittance and reflectance spectra of coating consisting from 10 alternated films from PMMA and Ag-PMMA with ratio 0.15.

CONCLUSION

The present paper reports the optical properties of nanocomposite materials from Ag and poly-

methyl methacrylate (PMMA) deposited through layer-by layer technique. The single Ag-PMMA coating demonstrates an absorption band in 350-550 nm range due to surface plasmon resonance in silver nanoparticles. The complex permittivity, ϵ was analyzed by the Bruggeman's model for the effective media. The optical properties of each individual layer were studied in order to consider the possibilities for optimization of the heat-insulation performance and the visible-light transmittance of the heat-insulating multilayers.

REFERENCES

1. R. Pacheco, J. Ordóñez, G. Martínez, *Renewable Sustainable Energy Rev.*, **16**, 3559 (2012).
2. M. Kamalisarvestani, R. Saidur, S. Mekhilef, F. S. Javadi, *Renewable Sustainable Energy Rev.*, **26**, 353 (2013).
3. R. Baetens, B. Petter Jelle, A. Gustavsen, *Sol. Energ. Mat. Sol. C.*, **94**, 87 (2010).
4. D. K. Avasthi, Y. K. Mishra, D. Kabiraj, N. P. Lalla, J. C. Pivin, *Nanotechnology*, **18**, 125604 (2007).
5. Y-W. Chang, S. W. Kim, *Surf. Coat. Tech.*, **232**, 182, (2013).
6. M. J. Bloemer, M. Scalora, *Appl. Phys. Lett.*, **72**, 1676 (1998).
7. A. Biswas, Z. Marton, J. Kanzow, J. Kurse, V. Zaporojtchenko, T. Strunskus, F. Faupel, *Nano Lett.*, **3**, 69 (2003).
8. H. Takele, H. Greve, C. Pochstein, V. Zaporojtchenko, F. Faupel, *Nanotechnology*, **17**, 3499 (2006).
9. C. A. Foss Jr., G. L. Hornyak, J. A. Stockert, C. R. Martin, *J. Phys. Chem.*, **98**, 2963 (1994).
10. R. Todorov, A. Lalova, K. Petkov, J. Tasseva, *Semicond. Sci. Tech.*, **27**, 115014 (2012).
11. V. Lozanova, J. Tasseva, R. Todorov, *Bulg. Chem. Commun.*, **45(B)**, 43 (2013).
12. W. Cai, V. Shalaev, *Optical Metamaterials, Fundamentals and Applications*, Chapters 1 and 2, Springer New York, Dordrecht Heidelberg, London, 2010, pp. 1-36.
13. M. Tschikin, S-A. Biehs, R. Messina, P. Ben-Abdallah, *J. Opt.*, **15**, 105101 (2013).
14. I. D. Nikolov, C. D. Ivanov, *Appl. Opt.*, **39**, 2067 (2000).
15. A. Vial, T. Laroche, *J. Phys. D: Appl. Phys.*, **40**, 7152, (2007).

ОПТИЧНИ СВОЙСТВА НА СРЕБРО-ОРГАНИЧНИ ПОЛИМЕРНИ ТЪНКИ СЛОЕВЕ КАТО СЛЪНЦЕЗАЩИТНИ ПОКРИТИЯ ЗА СЪВРЕМЕННИ ПРИЛОЖЕНИЯ В АРХИТЕКТУРАТА

Р. Тодоров^{1*}, Ю. Илиева², В. Лозанова¹, А. Лалова¹

¹Институт по оптични материали и технологии "Акад. Й. Малиновски", Българска Академия на Науките, ул. Акад. Г. Бончев, бл. 109, 1113 София, България

²Архитектурен факултет, Висше Строително Училище "Л. Каравелов", ул. Суходолска река 175, 1373 София, България

Постъпила на 01 май 2014 г.; Коригирана на 02 юли 2014 г.

(Резюме)

В настоящата статия е представено изследване на оптичните свойства на нанокomпозит от слой от сребро и полиметилметакрилат (PMMA) получен чрез техника на послойно отлагане. Чрез рентгенова дифракция е потвърдено присъствието на сребърни частици в тънки слоеве. Средният размер на сребърни частици се изчислява чрез формулата на Дебай-Шерер. Абсорбционната ивица в спектралния диапазон 350-550 nm в спектрите на пропускане се дължи на повърхностен плазмонен резонанс на сребърни наночастици. Позицията на ивицата е анализирана чрез прилагане на модела на Бругеман за ефективната среда. На основата на получените резултати за оптичните свойства на полимерни-неорганични хибридни слоеве са направени изводи за приложение, като слънцезащитни покрития.

Holographic investigation of the corona discharge effect on the photo-doping of Ag, Au and Cr into nano-sized As₂S₃ films

I. Bodurov^{1*}, R. Todorov², T. Yovcheva¹, S. Sainov³

¹Plovdiv University "Paisii Hilendarski", Department of Experimental Physics, 24 Tsar Asen str., 4000 Plovdiv, Bulgaria

²Institute of Optical Materials and Technologies "Acad. Jordan Malinowski", Bulgarian Academy of Sciences, Acad. G. Bonchev str., bl. 109, 1113 Sofia, Bulgaria

³HOLOBUL Ltd, Acad. G. Bonchev str., bl. 109, 1113 Sofia, Bulgaria

Received June 30, 2014; Revised August 13, 2014

Dedicated to Acad. Dimiter Ivanov on the occasion of his 120th birth anniversary

The paper presents the results of holographically investigated photo-diffusion of Ag, Au and Cr ions into nano-sized As₂S₃ films. Evanescent wave's holographic recordings with spatial resolution 2 500 nm⁻¹ in chalcogenide/metal sandwich like structures with 50 nm thick As₂S₃ layer, were performed. When the exposure was switched off at the maximum point of the diffraction efficiency during the holographic recording, 5 kV corona discharge was applied. During the holographic recording 5 kV corona discharge was applied. The maximum measured value of the diffraction efficiency was greater than 8%. The metal ions (Ag, Au and Cr) mobility in thin chalcogenide films was investigated. The mobility of the metal ions, μ , at temperature 17°C was calculated by the Nernst-Einstein equation. The diffusion coefficient D is obtained using the method of holographic grating spectroscopy (Forced Rayleigh Scattering). The values of the mobility and the diffusion coefficients for Ag, Au and Cr ions were discussed.

Key words: chalcogenide glasses, Forced Rayleigh Scattering, metal electromigration, diffusion coefficient, metal ions mobility

INTRODUCTION

The diffusion of silver into thin semiconductor layers is reported for the first time by Kostyshin and co-authors [1] in 1966. In this study the photographic properties of thin semiconductor layers of lead (II) iodide and As₂S₃, deposited on silver substrates were investigated. The authors observed that the layers become photosensitive in the red region of the visible light (the region that usually the layers are non-sensitive) and the hidden image turns visible without feature processing. They assumed that this phenomenon is caused by diffusion of the metal ions from substrate into layers, thus causing a chemical reaction leading to the occurrence of new chemical compounds. Subsequent studies revealed that the same effect is observed in different kind of photosensitive layers deposited on substrates made from Cu, Zn, Pb, Cd, Al, Fe, Ni and others.

Despite of the numerous models which have been proposed, the mechanism of metal photo-doping in chalcogenide glasses is still not clear. To solve this problem it is necessary exact knowledge

of the diffusion coefficients of the metal atoms in the glassy network. This is reason to apply different methods for their determination. Investigations on a diffusion of Au and Ag into As₂S₃ chalcogenide glasses are carried out by Suptitz and Willert [2]. They use radioactive tracers Ag¹¹⁰ and Au¹⁹⁸ to make evaluation of the diffusion coefficient of these metals into bulk As₂S₃ and its temperature dependence.

In [3] for investigation of photo-induced diffusion of Ag in As₂S₃ the method of direct weighting is used. The authors have been using the fact that the compounds which are a product of the reaction of Ag with As₂S₃ are resistant to alkalis and it can be dissolved only in HF at 180°C. They have etched removed the non-reacted silver by etching in acid (HCl) after illumination. By measuring the mass of As₂S₃ layer and the mass of silver layers before the illumination, the authors determined the amount of silver that had penetrated into the chalcogenide layer. They have found that the amount of silver increases with exposure increasing.

In [4,5] a technique for measuring the metal diffusion kinetics in As₂S₃ by changes in the electric conductivity of the layer is proposed. The

* To whom all correspondence should be sent:
E-mail: bodurov@uni-plovdiv.net

results show a connection between the exposition energy, the wavelength used for illumination, the thickness of metal layer, the thickness of chalcogenide glass and the conductivity.

Terakado and Tanaka [6] demonstrated that the photo-doping rate can be controlled by applying bias voltage of ~ 0.1 V. This rate modulation can be attributed to modulation of an effective internal electric field in the photo-doped layer.

Despite of the studies made, there is not enough systematic, reliable and modern data on these photo-induced processes. This article is continuation of our previous researches [7,8] related to the diffusion of metal ions in the amorphous layers. The aim of this paper is to investigate the electro-stimulated diffusion of Ag, Au and Cr ions into As_2S_3 films and to provide new exact data for diffusion and mobility coefficients.

EXPERIMENTAL

Sample preparation

We performed holographic recording in an As_2S_3 /Metal/Cr multilayer system. Firstly, a thin transparent chromium electrode with 10 nm thickness was deposited on a glass substrate by radio-frequency sputtering in argon plasma. A thin metal layer ($d \sim 20$ nm) was sputtered over the chromium film in the same vacuum cycle. Thin As_2S_3 films with thicknesses 50 nm were deposited on the metal coating by high vacuum thermal evaporation in a Leybold Heraeus A 720 Q deposition system. The chalcogenide films were

prepared in a vacuum of 10^{-3} Pa, at a deposition rate of 0.1 nm/s. The constant thickness of the obtained layers was guaranteed by the planetary rotation of the substrate holders.

Optical arrangement

The general optical arrangement for holographic recording is given in Fig. 1.

In the optical system a crown K-8 glass 45-90-45 prism for the holographic recording is used. The refractive index of the prism at wavelength $\lambda = 442$ nm was $n = 1.526$ and the calculated critical angle was $\varphi_{cr} = 40.9^\circ$. Therefore the incidence angle $\varphi = 41.5^\circ$ was selected for the experiments. The total light intensity of the recording He-Cd laser was $10 \mu W/cm^2$. For real-time diffraction efficiency monitoring a He-Ne laser with $23 \mu W/cm^2$ intensity was used. The reconstructed red light beam was measured with "ThorLabs" PM 130 powermeter. Signal to noise ratio was higher than 100:1. Microscope oil with refractive index 1.53 was used as a matching liquid between the substrate and the prism's reflecting wall. When the exposure was switched off at the maximum point of the diffraction efficiency (DE), high voltage with different polarity (± 5 kV) was applied to the corona electrode (needle), situated at a distance of 10 mm from the As_2S_3 film. The Cr sub layer was used with a spring contact as a second electrode and to improve the adhesion of the other metals to the glass substrate. The corona discharge occurred between the needle and the grounded electrode (Cr sub-layer).

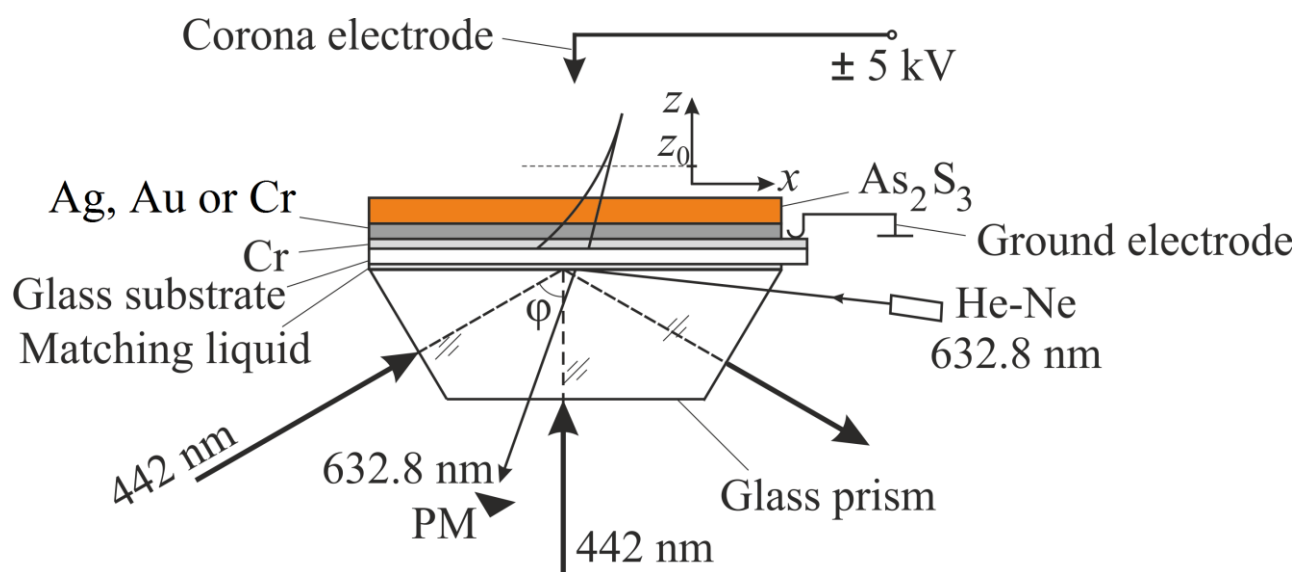


Fig. 1. Optical set-up for evanescent-wave holographic recording.

RESULTS AND DISCUSSION

The time dependences of the diffraction efficiency during the holographic recording at the presence of positive or negative corona discharge of $As_2S_3/Ag/Cr$ multilayer system are shown in Fig. 2.

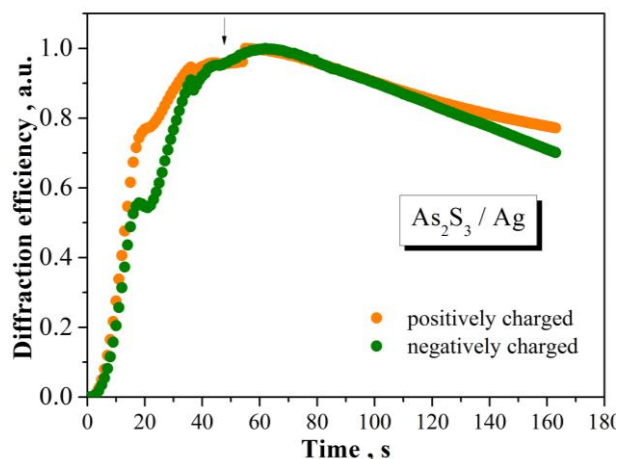


Fig. 2. Normalized diffraction efficiency of holographic recording in As_2S_3/Ag films the presence of a corona discharge.

The experimental results show that the diffraction efficiency time dependences are not influenced by the corona polarity. That is why the subsequent experiments are carried out with applying only negative voltage to the corona electrode. The time dependences of the diffraction efficiency during the holographic recording at the presence of negative corona discharge for $As_2S_3/Au/Cr$ and $As_2S_3/Cr/Cr$ multilayer system are shown in Fig. 3 and Fig. 4.

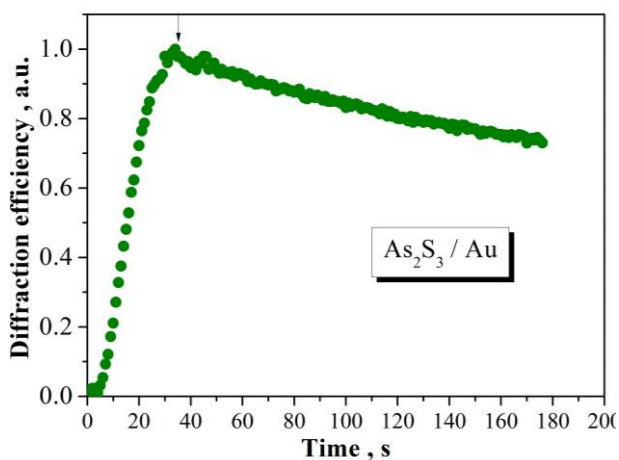


Fig. 3. Normalized diffraction efficiency of holographic recording in As_2S_3/Au the presence of a negative corona discharge.

The results observed show that the diffraction efficiency changes more drastically in the first 30 s of the holographic recording process. The time-dependent decay of the diffraction efficiency is proportional to the interference term and its time constant τ can be obtained by fitting of the experimental data with time dependent expression described in [9].

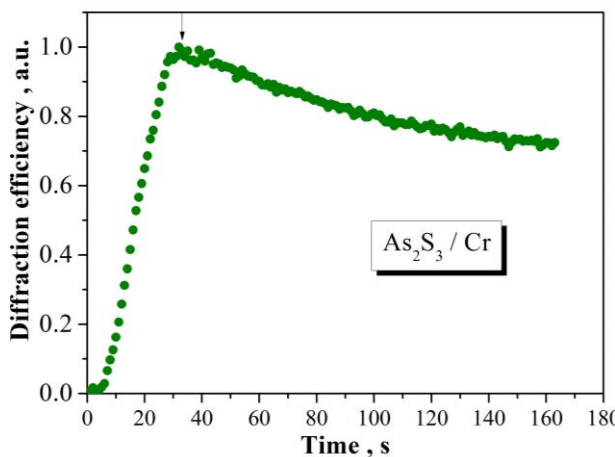


Fig. 4. Normalized diffraction efficiency of holographic recording in As_2S_3/Cr in the presence of a negative corona discharge.

The diffusion coefficient D are calculated by the method of the holographic grating relaxation spectroscopy (Forced Rayleigh Scattering) [7] by the following relation using already obtained values of the time constant τ :

$$D = \frac{4.84}{\tau} 10^{-11} \text{ cm}^2/\text{s}, \quad \text{for } \lambda = 442 \text{ nm} \quad (1)$$

With the obtained values of the diffusion coefficient, the mobility of metal ions are calculated using the modified Nernst-Einstein relation:

$$\mu = D \frac{q}{kT} = D \frac{e}{kT} (1 + \Delta) \quad (2)$$

where:

- e is the elementary charge of the electron;
- q is the metal ions charge;
- k is the Boltzmann constant;
- T is the absolute temperature;

Δ is the correlation coefficient [10] and in our case it is defined as:

$$\Delta = \frac{(\epsilon_0 - 1)}{2(2\epsilon_0 + 1)} \quad (3)$$

For As₂S₃ the constant ϵ_0 is 7.8 [11,12] and the correction coefficient was calculated from eqn. (3) to be $\Delta = 0.205$. This result is in very good agreement with the experimentally obtained value of the silver ion charge

$$q = (1.2 \pm 0.2)e.$$

The results obtained by eqn. (1) and eqn. (2) are presented in Table 1.

Table 1. Calculated values of the coefficients of diffusion and mobility.

Metal	Atomic number	Ion charge	$D, \times 10^{-13}$ cm ² /s	$\mu, \times 10^{-11}$ cm ² /V.s
Ag	47	+1	3.43	1.65
Au	79	+1	2.02	1.01
Cr	24	+2, +3	2.49	1.19

The results for the coefficients of diffusion and mobility indicate that they decrease with increasing of the atomic number as well as increase of the charge of the ions. To explain this result, we applied the Born-Mayer potential, which can be written as follows:

$$U = \frac{-\alpha q_c q_a}{r} + Z\lambda \exp\left(-\frac{r}{\rho}\right) \quad (4)$$

where α is the pseudo-Madelung constant, r is the internuclear distance, Z is the coordination number of metal cations in glassy network, ρ is the repulsion parameter and λ is the empirical parameter, q_c and q_a are the charges of metals cations and anions from the glassy network of the chalcogenide films, respectively.

The second term in eqn. (4) takes into account the bonding interactions as the electronic delocalization of the metal atoms, overlap of the valence electron and bond stretch. And it explains the lower values of the diffusion coefficient of the gold in comparison to that of the silver ions. The ion charge of silver and gold is equal and does not influence on the diffusion coefficient value. The gold atomic number is 1.68 times bigger than the silver atomic number which is in very good agreement with the diffusion coefficient ration of silver and gold that is 1.70.

This first term in the eqn. (4) describes the electrostatic interactions between charged ions and

glassy network. It is seen that the increase of the charge of the ions leads to increasing of the electrostatic forces of interaction of ions with anions from the chalcogenide network which the ion's jumps more difficult.

The ratio of the diffusion coefficients of chromium and silver is 0.73 while the atomic number of the silver is 1.96 times higher than the chromium atomic number. The difference between the diffusion coefficients cannot be explained only with the radius of the atoms of both metals. In this case the value of the diffusion coefficient for chromium could be explained if we take into account two terms of the eqn. (4). On the base of the second term the silver atomic number is 1.96 times higher than the chromium atomic number which is not in agreement with diffusion coefficient ration of chromium and silver that is 0.73. On the base of the first term if we take into account that the average chromium ion charge is 2.5 times higher than the silver ion charge and multiplied by it the ratio 0.73 we get 1.83 that is close to 1.96.

Analogically, we could compare the diffusion coefficient of chromium and gold. The gold/chromium atomic number ratio is 3.29 and the chromium/gold diffusion coefficient ratio is 1.23. If we multiply the second ratio by 2.5, we get 3.08 that is close to 3.29.

For more clear understanding and explanation of this phenomenon the good knowledge of the coordination numbers of silver, gold and chromium is necessity.

CONCLUSION

The combination between the holographic grating spectroscopy (Forced Rayleigh Scattering and corona charging seems to be a useful experimental method for electromigration study of metal diffusion coefficient and ion mobility in nanometer-thick amorphous chalcogenide layers. Two coefficient values for three metal ions – silver, gold and chromium were experimentally calculated and analyzed by the Born-Mayer potential equation. It was obtained that the diffusion coefficient and the ion mobility of silver are the highest and of gold are the lowest.

Acknowledgements: The financial support by the EU projects BG161PO003-1.1.005-0085-C0001, is gratefully acknowledged.

REFERENCES

1. M. Kostyshin, E. Mikhaylovskaya, P. Romanenko, *Sov. Phys. Solid State*, **8**, 451 (1966).
2. P. Suptitz, J. Teltow, E. Lebedev, I. Willert, *Phys. Stat. Sol. A*, **31**, 31 (1975).
3. V. V. Petrov, A. A. Kryuchin, *Proc. USSR Acad. Sci.*, **230**, 326 (1976)..
4. D. Goldschmidt, P. S. Rudman, *J. Non-Cryst. Solids*, **22**, 229 (1976).
5. D. Goldschmidt, T. Bernstein, P. S. Rudman, *Phys. Stat. Sol. A*, **41**, 283 (1977).
6. N. Terakado, K. Tanaka, *Thin Solid Films*, **519**, 3773 (2011).
7. S. Sainov, R. Todorov, I. Bodurov, T. Yovcheva, *J. Opt.*, **15**, 105705 (2013).
8. I. Bodurov, R. Todorov, T. Yovcheva, G. Spassov, S. Sainov, *Bul. Chem. Commun.*, **45 B**, 86 (2013).
9. S. Sainov, *J. Chem. Phys.*, **104**, 6901 (1996).
10. E. Katz, *Phys. Rev.*, **99**, 1334 (1955).
11. N. Goyal, A. Zolanvari, S. K. Tripathi, *JOAM*, **3**, 741 (2001).
12. Z. Borisova, *Semiconductors*, Plenum Press, New York, 1981.

ХОЛОГРАФСКО ИЗСЛЕДВАНЕ НА ВЛИЯНИЕТО НА КОРОННИЯ РАЗРЯД ПРИ ФОТОДОПИНГ НА СРЕБРО, ЗЛАТО И ХРОМ В НАНОРАЗМЕРНИ ФИЛМИ ОТ As_2S_3

И. Бодуров^{1*}, Р. Тодоров², Т. Йовчева¹, С. Съинов³

¹Пловдивски университет „Паисий Хилендарски“, Катедра Експериментална физика, ул. Цар Асен 24, 4000 Пловдив, България

²Институт по оптически материали и технологии „Акад. Йордан Малиновски“, Българска Академия на Науките, ул. Акад. Г. Бончев, бл. 109, 1113 София, България

³“ХОЛОБУЛ“ ООД, ул. Акад. Г. Бончев, бл. 109, 1113 София, България

Постъпила на 30 юни 2014 г.; Коригирана на 13 август 2014 г.

(Резюме)

В настоящата работа са изследвани подвижността и фото-дифузията на йоните на Ag, Au и Cr в наноразмерни слоеве от системата As_2S_3 при прилагане на коронен разряд. Холографските записи в структура тип сандвич от слой As_2S_3 с дебелина 50 nm и метален слой са направени с помощта на нормално падаща и на затихваща вълна, създадена при пълно вътрешно отражение при пространствена честота $2\ 500\ \text{mm}^{-1}$. При достигане на максималната дифракционна ефективност, записващият лазерен лъч се изключва и се прилага електричното поле на 5 kV коронен разряд. Измеренаат максимална дифракционна ефективност е по-голяма от 8%. Изследвана е подвижността на металните йони (Ag, Au and Cr) в тънки халкогенидни филми. Подвижността на металните йони, при температура 17°C е изчислена с уравнението на Нернст-Айнщайн. Коефициентът на дифузия D е получен по метода на холографската релаксационна спектроскопия (Форсирано разсейване на Релей). Обсъдени са получените стойности за подвижността и коефициента на дифузия за йоните на Ag, Au и Cr.

Inter- and intra-molecular interactions in anionic polymerization of polar vinyl monomers

Ch. P. Novakov, Ch. B. Tsvetanov*

Institute of Polymers, Bulgarian Academy of Sciences, Acad. G. Bonchev str., bl. 103, 1113 Sofia, Bulgaria

Received July 19, 2014; Revised August 18, 2014

Dedicated to Acad. Dimiter Ivanov on the occasion of his 120th birth anniversary

This review article presents the results on the nature of the active centers of propagation (AC) in anionic polymerization of polar vinyl monomers such as acrylates, methacrylates, vinyl nitriles and vinyl ketones and especially their interactions with donor-acceptor ligands, carried out in the Laboratory of Polymerization Processes of the Institute of Polymers, Bulgarian Academy of Sciences. Particular attention to the interactions involving AC with lithium and magnesium counter-ions was paid due to their strong tendency of interacting with a variety of ligands, as well as in reactions of self-association resulting in numerous possibilities of controlling the structure of the polymers as well as the composition of copolymers. The model compounds or “living” oligomers of polar vinyl monomers were studied intensively by using IR spectroscopy and conductometry. Their physicochemical characteristics in solution, before and after adding of ligands, were investigated. A typical feature is the use of lithium picrate as a model in studying the interactions with monomers, compounds with polar groups, and most typical additives: alkoxide, LiCl, tetraalkylammonium salts and trialkylaluminum compounds.

Key words: anionic polymerization, polar vinyl monomers, “living” oligomers, propagation active centers, polymer tacticity, ambifunctional nucleophilic species, ligands

INTRODUCTION

The chemistry of carbanions is a traditional subject for research in Bulgaria. The first studies in the field of the chemistry of organometallic compounds are placed by acad. D. Ivanov and his world-known school. Carbanions are the centers for the growth of the polymer chain in the anionic polymerization. By means of anionic polymerization can be obtained the so-called “living” polymers in which the growing centers or propagation active centers (AC) retain their reactivity after full consumption of the monomer. Indeed, living anionic polymerization is the first successful method for the synthesis of polymers with very narrow molecular weight distribution (MWD), for the synthesis of macromers and active polycondensation oligomers, as well as for the preparation of well defined block copolymers. Until now “living” polymerization is the best method for achieving good control over the molecular weight and the polymer tacticity. It is apparent that the anionic polymerization is far more complex process as compared to the radical polymerization. To study the mechanism of anionic polymerization researcher must be familiar with the chemistry of carb-

anions, all modern spectral methods, kinetic methods for fast reactions in solution, non-aqueous solutions electrochemistry, etc.

There are several reviews (cited below) describing anionic polymerization of (meth)acrylates: mainly kinetic results and MWD of the polymers obtained. The present review article presents the results on the nature of the active centers of propagation in anionic polymerization of polar vinyl monomers (PVM) such as acrylates, methacrylates, acrylonitriles, and vinyl ketones and especially their interactions with donor-acceptor ligands, carried out in the Laboratory of Polymerization Processes of the Institute of Polymers, Bulgarian Academy of Sciences. Mostly works of our own are presented, since our approach is not so much popular as the kinetic investigations.

Anionic polymerization of PVM is by far more complex than that of styrene and dienes. In contradiction with the simplicity of polymerization of nonpolar monomers, the polymerization of PVM is rather complicated due to the presence of polar groups. Indeed, PVMs are bidentate species, and each polar group competes with the double >C=C< bond for the initiator or the propagating centers. A problem arises from: a) the side reactions by nucleophilic attack of the AC onto the monomer or polymer unit due to the reactive side group (e.g.

* To whom all correspondence should be sent:

E-mail: chtsvet@polymer.bas.bg

© 2014 Bulgarian Academy of Sciences, Union of Chemists in Bulgaria

ester, nitrile, amide, or keto groups); b) different, sometimes competitive, available forms of aggregation of AC, as in contrast to polystyrene active chain, the AC aggregation in the case of PVM occurs also in polar solvents like ethers; c) ambident nature of the AC, which refers to active species containing two centers susceptible to monomer attack, in other words, two nucleophilic sites. Table 1 represents the most important ambident nucleophilic species, typical for the anionic polymerization of PVM.

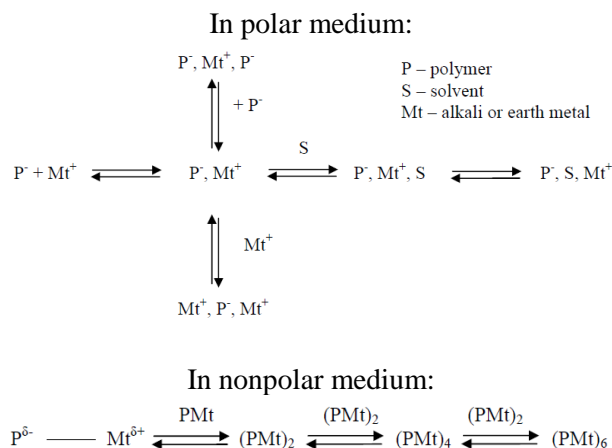
Characteristic of our investigations is the wide use of IR spectroscopy of carbanions having a cyano- or a carbonyl group adjacent to the anion. From the pioneering works of Juchnovski [7,8] on nitriles and Lochmann on ester enolates [5,9], it is well known that in such cases the IR $C\equiv N$ and $C=O$ stretching frequencies decrease by 20 to 200 cm^{-1} .

On account that the AC of the anionic polymerization of PVMs are ambident nucleophiles, different forms of active species coexist such as free ions, contact or solvent-separated ion-pairs, triple ions, dimers, and higher associates (see Scheme 1) depending on the solvent medium nature (polar or non-polar), size of counter ion, concentration and temperature. The above mentioned ionic forms are in dynamic equilibrium and most of them are capable of initiating the polymerization, but with different rates and mode of addition.

Each active site for a certain time can exist in any of the ionic forms shown in Scheme 1 involved in the propagation reaction in a manner consistent with the current state. A slow equilibrium between ionic species results in broadening and even multimodality of the MWD. Obviously, aggregation and ion dissociation of anionic AC direct the course of the anionic polymerization. Hence, the propagation rate, the MWD and the polymer stereoregularity strongly depend on the reaction conditions.

The mechanism of living anionic polymerization is associated primarily with the nature of the active

centers of growth and donor-acceptor interactions in which they participate.



Scheme 1. Different forms of active species in anionic polymerization of PVM.

There are five main interactions involving the active site of growth:

1. AC – solvent molecules or other cation-binding ligands (e.g. ethers, glymes, crown-ethers, cryptands)
2. AC – polar groups from polar vinyl monomer or monomer unit
AC – additives:
3. AC – μ -type ligands (e.g. LiCl, LiClO₄, *tert*-BuOLi)
4. AC – Lewis acid agents (e.g. AlR₃, BR₃, ZnR₂)
5. AC – quaternary ammonium salts

Another characteristic feature of our research is that for the purpose of estimating the interactions of the AC with different ligands, the approach of studying a reference system was adopted, i.e. lithium picrate (LiPi) in dioxane (DO). We look upon the picrate as a model of ambident organolithium compound imitating the AC. The interaction LiPi/ligands were studied in DO, a solvent of comparatively low solvation capacity and low polarity. This avoids the formation of solvent separated ion pairs and free ions and, hence,

Table 1. Ambifunctional nucleophilic growing centers in anionic polymerization of PVM.

No	Nucleophilic site	Anion structure	ν_{CN} or ν_{CO} IR absorption (cm^{-1})	Polymer
1	Alkyl cyanide anions	$\overline{>C(R)CN}$	2000 – 2050 alkali cations [1,2] 2050 – 2080 Mg ⁺² [3]	Polyacrylonitrile (R = H) Polymethacrylonitrile (R = CH ₃)
2	Ketoenolate anions	$\overline{>C(R)CO}$	1560-1610 [4]	Polyvinylketone
3	Esterenolate anions	$\overline{>C(OR)CO}$	1620 – 1680 [5,6]	Polyacrylate Polymethacrylate

reduces the number of possible structural types of AC when small amounts of ligands are introduced. The method was firstly applied to investigate weak interactions of organic compounds with polar groups and LiPi [10].

These AC/ligand interactions have a decisive influence on the overall mechanism of the polymerization process and the polymer properties. A striking example of the importance of the additives is the influence of LiCl on the MWD of *tert*-butyl acrylate as shown in Fig. 1 [11].

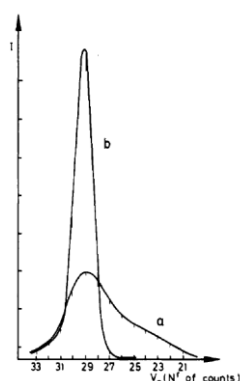
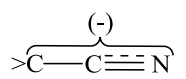


Fig. 1. Influence of LiCl as additive in anionic polymerization of *tert*-butyl acrylate: no salt (a); LiCl/AC = 5 (b) [11].

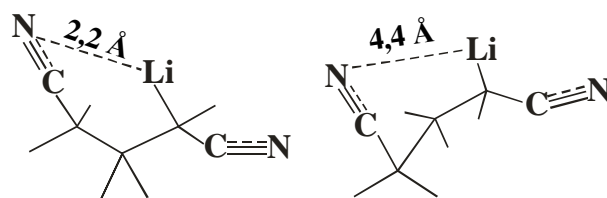
Clarification of the nature of AC/polar group and AC/additive interactions contributes to finding the most suitable conditions under which polymerization process takes place with minimal involvement of side reactions, preparation of polymer with defined molecular mass and narrow MWD, as well as stereocontrol of the propagation step. In this review, we will pay particular attention to the interactions involving AC with lithium or in some cases magnesium counter-ions. As opposed to the other alkali ions, they show strong tendency of interacting with a variety of ligands, as well as in reactions of self-association. This results in numerous possibilities of controlling the structure of the polymers as well as the composition of copolymers.

TYPES OF INTERACTIONS INVOLVING AC OF ANIONIC POLYMERIZATION OF VINYL NITRILES

The AC in the anionic polymerization of AN or MAN are ambident anions. Therefore, the negative charge is distributed on the group



the nitrogen atom being partially charged. This might result in increased electrostatic interaction between the counterions, which hampers the formation of loose or solvent separated ion-pairs. In order for a clearer distinction of the interactions, typical for the closest to the AC cyano-groups, the following model compounds were used: α -lithiated isobutyronitrile ($P_{1(\text{CN})}\text{Li}$) and 1,3,3-trimethylglutaronitrile ($P_{2(\text{CN})}\text{Li}$). The quantum-chemical calculations indicate the existence of different conformers of $P_{2(\text{CN})}\text{Li}$ in non-polar media [12]. The distance between Li^+ and the penultimate CN group is 2.2 to 4.4 Å (see Scheme 2). Obviously, the structure in which the distance is smallest, i.e. 2.2 Å, is characterized by the strongest interaction between Li^+ and the penultimate CN group in $P_{2(\text{CN})}\text{Li}$:



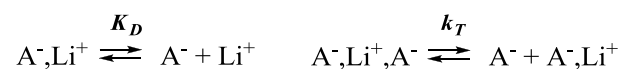
Scheme 2. Conformers of $P_{2(\text{CN})}\text{Li}$, according to [12].

The results on measurements of the dissociation constant in THF are consistent with the calculations: they show very low values for K_D of order 10^{-11}M and close to the theoretical values of counterion distance [13] (see Table 2).

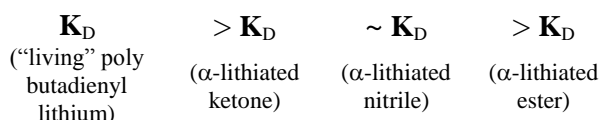
Table 2. Dissociation constants of ion pairs (K_D) and ion triples (k_T) of lithium salts of ambident anions ($P_{n(\text{X})}\text{Li}$) as model living oligomers of PVM in THF at -30°C [13,14].

"Living" oligomer	$K_D \times 10^{12} \text{ M}$	$k_T \times 10^4 \text{ M}$	[ABA]/[A ⁻]
$P_{1(\text{X})}\text{Li}$			
$P_{1(\text{CN})}\text{Li}$	69	7.0	7
$P_{1(\text{COC}(\text{CH}_3)_3)}\text{Li}$	75	6.5	8
$P_{1(\text{COOR})}\text{Li}$	0.4	0.2	250
$P_{2(\text{X})}\text{Li}$			
$P_{2(\text{CN})}\text{Li}$	6.0	1.0	50
$P_{2(\text{COOR})}\text{Li}$	1.5	3.0	16

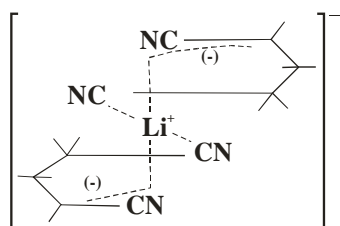
It should be noted that the calculations of the dissociation constants were made by using Woosters equation [15]. The anion triple $\text{A}^{\ominus}, \text{Li}^+, \text{A}^{\ominus}$ is energetically more stable than the triple $\text{Li}^+, \text{A}^{\ominus}, \text{Li}^+$ [16], so we suppose the existence mainly of negative ion triple. The ionic equilibrium can be described by the following equations:



K_D values are in agreement with data for the dissociation constants of other anions, containing a heteroatom, e.g. 2-ethylpyridine salts [17], and “living”MMA oligomers [14]. Mainly tight ion pairs are formed with the interionic distance of about 2.5 Å. Importantly, the dissociation constants of the studied salts are smaller than these of polybutadienyl lithium and polyisoprenyl lithium [18], and diminish in the following order:



In the case of lithium derivatives of nitriles, the dissociation constant of the dimer $P_{2(CN)}Li$ is one order of magnitude less than that of $P_{1(CN)}Li$, which is indicative of chelate complex formation [19]. Both $P_{1(CN)}Li$ and $P_{2(CN)}Li$ tend to form ion triples, the concentration of ion triples in $P_{2(CN)}Li$ solutions being much higher than in solutions of $P_{1(CN)}Li$. We consider the most probable structure of the ion triple to be as shown:



Obviously, the $-CN$ group competes with THF molecules for the lithium coordinating sites. The formation of ion triple is consistent with the results on measurements of binding constants (K_L) between lithium picrate, used as model of ambident AC, and some nitriles and THF as presented in Table 3 [20,21]. It is widely assumed that interactions of alkali metal cations with oxygen donor atoms are stronger than with the softer nitrogen atoms, contrary to the data for aliphatic nitriles shown in Table 3. In our opinion, the rod-like structure of the most nitriles suggests that in complex formation with Li^+ steric hindrance is less important than for the cyclic ethers. This could be the reason why $K_L(THF) < K_L(CH_3CN)$ in spite of the higher DN for THF. In addition to a favorable steric factor, interaction of Li^+ with the π system of the nitrile group may contribute to the binding energy.

IR spectroscopy is especially convenient for studying the character and changes of the AC during the polymerization process. It should be

noted that the study of mechanism of chain propagation of AN/MAN polymerization by IR assisted measurements is complicated because of insolubility of the polymers. In order to prepare soluble species, polybutadiene and polystyrene “living” chains were used as initiators. Thus, a technique of “capped” polymers was successfully used by addition of small number ($n = 1-6$) of AN/MAN monomer units to the quite soluble polybutadiene or polystyrene active ends [22,1]. Thus, polymerization does not lead to precipitation and made it possible to study the solution properties of AC in the anionic propagation of AN/MAN directly in the range of AC concentrations $1 \cdot 10^{-1} - 1 \cdot 10^{-3}$ M.

Table 3. Complex formation constants K_L of lithium picrate with THF and some nitriles, ketones and esters in dioxane at 25°C [20,21].

Ligand	K_L, M^{-1}	DN	ϵ
THF	0.95	20	7.6
Acetonitrile	1.22	14.0	36.2
Acetone	1.16	17.0	20.7
Ethylacetate	0.75	17.1	6.0
iso-Butyronitrile	1.80	15.4	20.8
Propionitrile	2.80	16.1	27.7
Methacrylonitrile	0.55		
Acrylonitrile	0.46		38
Methylmethacrylate	0.16		

The carbanion next to the cyano group reduces the absorption frequency of the latter by 20 - 200 cm^{-1} [23]. It should be noted that the wave length of the nitrile absorption bands at the AC are strongly dependent on the nature of the counterion and solvent as well on the presence of donor or acceptor additives, but remain unchanged within the whole temperature range between 20°C and -60°C in THF [24,2].

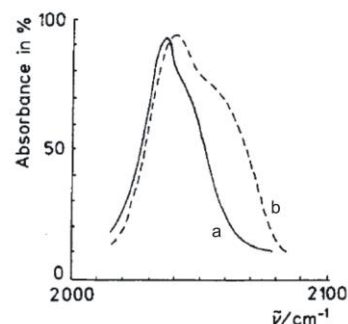


Fig. 2. IR spectra of $P_{1(CN)}Li$ (a) and $P_{2(CN)}Li$ (b) in THF [25].

$P_{2(CN)}Li$ resembles to a greater extent the real AC in comparison to $P_{1(CN)}Li$, because it possesses one more monomer unit. As in the case of conductivity measurements, the characteristics of IR band

have to be greatly influenced by the second nitrile group being in interaction with lithium counterion. Indeed, as seen from Fig. 2, the ν_{CN} band of the active site for $\text{P}_{2(\text{CN})}\text{Li}$ is significantly wider and shifted to higher wave numbers ($2037\text{ cm}^{-1} \rightarrow 2042\text{ cm}^{-1}$).

The result is in full agreement with the data obtained in the synthesis of "living" oligomers of MAN at different initial ratio M/In [1] as shown in Fig.3.

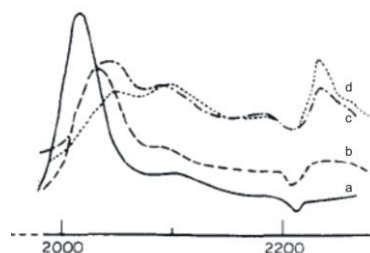


Fig. 3. IR spectra of MAN active species in the reaction of oligostyryllithium with different M/In ratio: MAN/ In =1 (a); MAN/ In =2.2 (b); MAN/ In =3.6 (c); MAN/ In = 5.5 (d); THF, ambient temperature [2]

The shift of the band at $2020\text{--}2060\text{ cm}^{-1}$ towards higher frequencies, as the number of adjacent monomer units is increased (Fig. 3) is explained by interaction of the AC with the nitrile groups of the polymer chain next to the growing end. The dependence of the shift of the maxima in the IR spectra on the number of the groups attached is shown in Fig. 4.

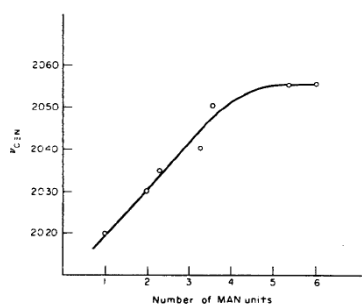


Fig. 4. Dependence of the band (ν_{CN}) shift of MAN AC on the number of MAN units attached to the polymer chain [2].

The addition of about 3-4 monomer units changes the position of the IR spectral bands. At higher ratios ν_{CN} levels off. The results are direct evidence of the intramolecular interaction of active centers with neighboring monomer units (penultimate effect), which was hinted at in conductivity studies.

With the aid of IR spectroscopy it is possible to follow the interaction of AC's with the cyano group of the monomer. The intermolecular interaction $\text{Li}^+ \dots \text{CN}$ characterized by the appearance of a band at $2255\text{--}2285\text{ cm}^{-1}$ is of special importance and it is quite similar to that between LiI and a nitrile [26,27]. Indeed, in non-polar solvents the AC's of oligomethacrylonitrile with lithium and magnesium counterions form complexes with nitriles having characteristic bands in the range $2250\text{--}2280\text{ cm}^{-1}$ [2,3]. In case of organomagnesium compounds, used as initiators, the AC or the initiator itself form complexes even with the monomer without addition reaction. This observation is especially worth noting, since it permits a more detailed investigation of the initial act of complex formation between the initiator and the monomer or between the AC and the monomer before the propagating step:



The organomagnesium compounds are very suitable for such studies because of their lower reactivity: thus in hydrocarbon media, they do not initiate AN, or MAN polymerization at temperatures below -60°C . No polymer formation takes place on mixing the ether-free organomagnesium halide $[(\text{C}_{12}\text{H}_{35})_3\text{Mg}_2\text{Br}]_n$ in toluene with MAN [25]. The IR spectrum of the mixture at room temperature exhibits an absorption band at 2225 cm^{-1} (free monomer), and at 2263 cm^{-1} (initiator/monomer complex) as shown in Fig. 5.

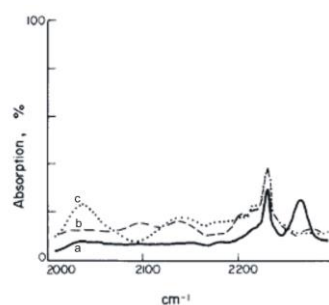
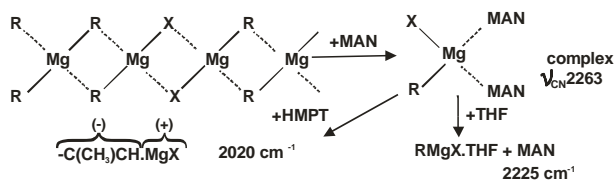


Fig. 5. IR spectra of the reaction mixture MAN/ $[\text{R}_3\text{Mg}_2\text{Br}]_n$ in toluene (a); after adding THF (b); after adding hexamethylphosphortriamide (HMPT) (c) [3]

Addition of equivalent amount of THF, causes increasing of intensity of the band for free monomer and disappearance of band at 2263 cm^{-1} . This is due to the greater binding constant of THF as compared to that of MAN (Table 3). When the additive is HMPT, the new band for AC appears.

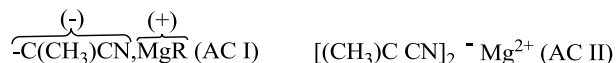
The observed interactions can be represented schematically (Scheme 3) thus:



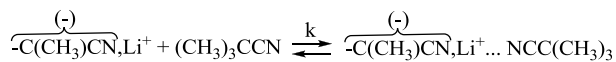
Scheme 3. Complex formation between MAN and $[R_3Mg_2Br]_n$ in toluene [3].

Dielectric susceptibility and electric conductivity measurements carried out on the $[R_3Mg_2Br]_n$ solution during “titration” with MAN reveal that the MAN/Mg complex is 2:1.

The investigations have shown also that two types of AC (AC I and AC II) are formed during polymerization of MAN initiated by organo-magnesium compounds. Growth of the polymer chain in ether solvents proceeds through AC I. AC II are found by polymerization in toluene, initiated with R_2Mg . This is in agreement with studies of Joch *et al.* [28], who suggested, on the basis of MWD, the existence of two types of AC in the polymerization of MAN in toluene initiated with diethylmagnesium:



$Li^+ \dots RCN$ complex was formed also when trimethylacetonitrile (TMAN) is added to the benzene solution of “living” MAN oligomers [2]. The complex formation is characterized by a new IR band at 2260 cm^{-1} . As in the case of $[R_3Mg_2Br]_n$ and MAN, the complex is in equilibrium with the free nitrile and AC:



Scheme 4. Equilibrium between AC and complex of AC with TMAN in benzene. Equilibrium constant at 20°C , $K = 0.25 \pm 0.05\text{ M}$ [2].

The result reveals the possibility for intermolecular interaction with the participation of $-CN$ groups attached to the monomer units. This is clearly shown in the case of $P_{2(CN)}Li$. In the IR spectrum of a mixture of $P_{2(CN)}Li$ and non-metallated dimer $P_{2(CN)}H$ in benzene along with the band of the unperturbed CN-group a band at 2265 cm^{-1} is again observed (Fig. 6).

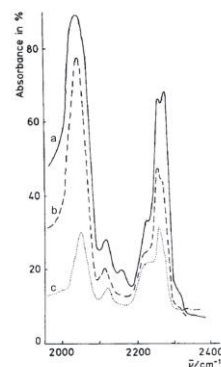


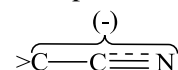
Fig. 6. IR spectra of a mixture of lithiated and non-metallated dimer in benzene, $P_{2(CN)}H/P_{2(CN)}Li=50$. $[P_{2(CN)}Li]=0.071\text{ M}$ (a); $[P_{2(CN)}Li]=0.06\text{ M}$ (b); $[P_{2(CN)}Li]=0.33\text{ M}$ [25]

Evidences for the interaction of AC with *tert*-BuOLi

The serious drawback of the anionic polymerization of AN and MAN is that it is accompanied by several side reactions. The reason for the formation of these byproducts is the high capacity of the nitrile group to react with strong bases, as well as to take part in donor-acceptor interactions. It is well known that *t*-BuOLi is able to interact with the AC of acrylates and methacrylates [29,30] and is successfully used to improve the mode of polymerization. Therefore, it is of great interest to study the interactions of polyAN and polyMAN AC with lithium alkoxide in order to use it as additive in more efficient polymerization process.

The interaction between $P_{n(CN)}Li$ and *t*-BuOLi is very different from $P_nLi \dots NC-$ complex formation. *t*-BuOLi affects the association equilibria of the AC of PVM transforming them into mixed associates and on these ground this kind of interaction can be formulated as associative.

The interaction of AC and *t*-BuOLi causes a shift of the band of the ν_{CCN^-} toward higher wave numbers. The IR spectrum of the system $P_{1(CN)}Li/t$ -BuOLi shows changes that indicate a specific interaction between AC and *t*-BuOLi (Fig. 7) [25]. The intensity of the absorption of the group



decreases in the presence of additive depending on the mole ratio of the two compounds. At the same time, there is an increase in intensity of a new band at 2047 cm^{-1} . The assumption for complex formation is confirmed by the conductometric measurements of $P_{1(CN)}Li$ solutions with different $[t\text{-BuOLi}]/P_{1(CN)}Li$ ratios, which indicates the existence of adduct with 1:1 stoichiometry. It should be noted, that both $P_{1(CN)}Li$ and *t*-BuOLi and

their adducts are aggregates in THF, which hampers more detailed study.

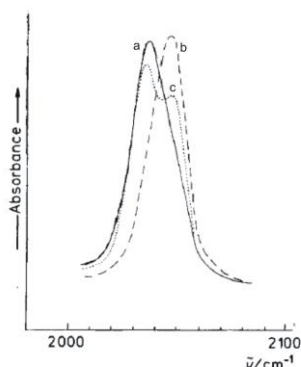


Fig. 7. IR spectra of $P_{1(\text{CN})}\text{Li}$ without and in the presence of $t\text{-BuOLi}$ in THF: $[P_{1(\text{CN})}\text{Li}] = 0.06 \text{ M}$ (a); $[t\text{-BuOLi}]/[P_{1(\text{CN})}\text{Li}] = 3$ (b); $[t\text{-BuOLi}]/[P_{1(\text{CN})}\text{Li}] = 1$ (c) [25]

The interaction of $P_{2(\text{CN})}\text{Li}$ and $t\text{-BuOLi}$ has a more complicated character. At the ratio $[t\text{-BuOLi}]/[P_{2(\text{CN})}\text{Li}] = 2$, however, unlike $P_{1(\text{CN})}\text{Li}$, the larger part still exists in a form of free AC. Most probably, the explanation is in the possibility $t\text{-BuOLi}$ to interact both with AC and the second nitrile group of $P_{2(\text{CN})}\text{Li}$.

INTERACTIONS INVOLVING AC OF ANIONIC POLYMERIZATION OF VINYL KETONE

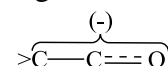
The ACs of vinyl ketones resemble enolates, the most characteristic representatives of ambient anions. The negative charge in an enolate is delocalized between a carbon atom and an oxygen atom, and their site may act as a nucleophile depending on the reaction conditions. Thus, enolate are capable of forming covalent bonds with both carbon and oxygen atoms, when interacting with electrophilic compounds [31,32]. The effects of solvent, counterion, and temperature as well as the structure of the nucleophile and the electrophile on this C/O competition, have been studied extensively. It should be noted that the data of dissociation constants K_D and k_T of α -lithiated ketones and nitriles are very close (see Table 2).

As it is the case in the anionic polymerization of vinyl nitriles, the AC of vinyl ketones are able to

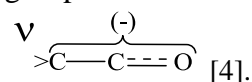
interact with the adjacent monomeric units, thus forming intramolecular complexes. The keto groups of the last one unit and the next to it are situated near the cation as shown (Scheme 5) for the trimer conformations.

The intramolecular interactions, shown in Scheme 5 are in agreement with the results of Lyons and Catterall [33] who proposed the formation of cyclic products with the growing AC as a result of interaction between the Li^+ counterion and the carbonyl group of the next to the last but one monomeric unit. Indeed, for some conformers, shown in Scheme 5, the distance between the lithium and the carbonyl group does not exceed 3.5 \AA , which proves the formation of coordinative bonds.

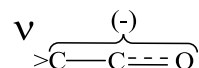
The negative charge distributed on 3 atoms



causes decreased adsorption of the carbonyl group, characterized by a band at $1560\text{--}1610 \text{ cm}^{-1}$, attributed to the stretching vibrations of the delocalized group

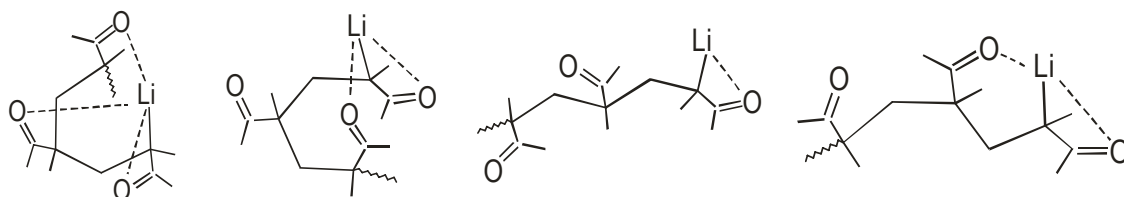


Alkali derivatives of acetone (ADA) are simplest model compounds of AC. In contrast to nitriles, the position of the



band strongly depends on the counterion dimensions (Fig. 8).

The most probable explanation for this dependence is the decreased electrostatic interaction between the counterions from Li^+ to Cs^+ , due to the increased average contact ion pair interionic distance. The band at 1688 cm^{-1} in the spectrum of acetone-lithium can be observed only in the presence of unreacted acetone in solution. If acetone is fully metalated only one band at 1602 cm^{-1} is observed. The addition of acetone results in the appearance of maxima at 1688 and 1712 cm^{-1} (free acetone) as well as decrease of the band intensity at 1602 cm^{-1} (Fig. 9).



Scheme 5. Different conformations of $P_{3(\text{COCH}_3)}\text{Li}$.

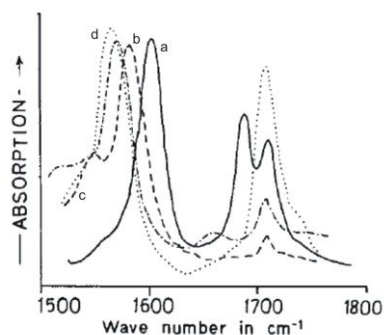


Fig. 8. IR spectra of ADA in THF with different counterions at 25°C, Li⁺ (a); Na⁺ (b); K⁺ (c); Cs⁺ (d) [4].

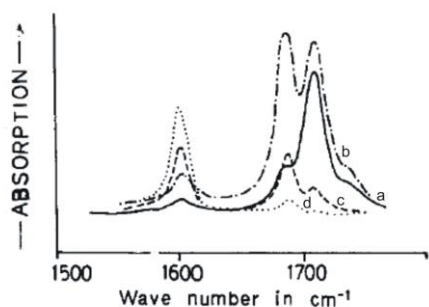


Fig. 9. IR spectra of ADA (Li⁺) in THF at different [acetone]/[ADA] ratios: r = 13.3 (a); r = 3.8 (b); r = 1.2 (c); r = 0.27 (d) [4].

Temperature dependence between these three bands was established as well. At low temperature the peak at 1688 cm⁻¹ increases in intensity, thus compensating the maxima at 1602 and 1712 cm⁻¹. Obviously, this is due to the formation of 1:1 complex, proved also by electroconductivity measurements:



The coordination of AC with the next carbonyl group (self-association) resembles the interaction between ADA and acetone. The IR spectra of solutions of “living” oligoisopropenylmethyl ketone exhibit nearly the same bands. They easily form intramolecular complex characterized by bands at 1685-1700 cm⁻¹. The equilibrium process in “living” oligomers is rather complicated since the AC of the trimer can form complexes with different monomeric units, each of them being characterized by a definite equilibrium constant. The strength of interaction decreases in the order Li⁺ > Na⁺ > K⁺ > Cs⁺. It is established that the MWD of the polymer narrows by diminishing the intramolecular

Mt⁺...C=O interaction: e.g. by using Cs counterion the most narrow MWD is obtained (Fig. 10) [34].

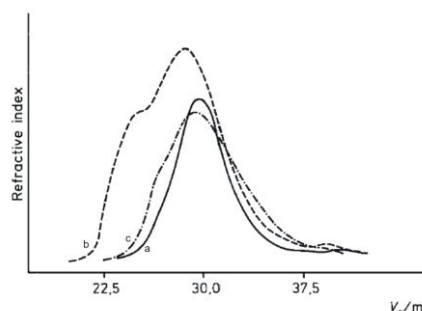


Fig. 10. GPC curves for poly(isopropenyl methyl) ketone by polymerization in THF at -70°C with counterions: Cs⁺(a); Li⁺(b); K⁺(c) [34].

It should be noted that the intramolecular interaction Li... C=O is much stronger than the interaction Li...CN: IR spectra of α-lithiated oligomers of methyl isopropenyl ketone give evidence for intramolecular complex formation between the lithium counterion and the carbonyl groups of the neighboring monomer units even in THF at temperature as high as 20°C [4], whereas the IR spectra of the α-lithiated dimer of MAN indicates strong chelate formation only in benzene and toluene [2].

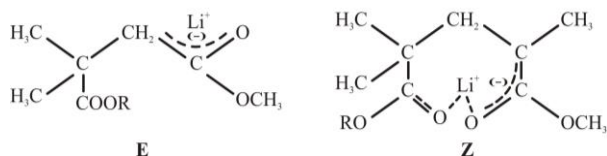
STRUCTURE OF LITHIUM ESTER ENOLATES IN THF

The dissociation constants of α-lithiated esters are smaller by about two orders of magnitude in comparison with lithium derivatives of nitriles and ketones (Table 2). This can be explained by the possibility for existence of mesomeric structures of ester anion:



The partial charge distribution on -OR group leads to lower electron density of the ester enolate group in contrast to the same group in lithium keto-enolates, which may be judged by the different shifts of ν_{CCO} bands in the IR spectra of α-lithiated esters [5] and lithium keto-enolates [4] (Table 1). The resonance structure is supported also by ¹³C-NMR measurements of Vancea and Bywater [35], who reported reduced freedom of motion of the alkoxy groups in THF solutions of α-lithiated methylisobutyrate at low temperatures.

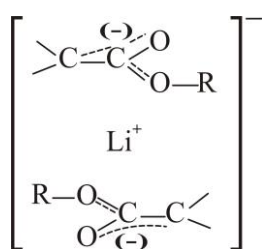
In contrast to lithium derivatives of nitriles, the difference between the dissociation constants of $P_{1(\text{COOR})}\text{Li}$ and $P_{2(\text{COOR})}\text{Li}$ is insignificant, the constants of the dimer being slightly higher (see Table 2). The values of K_D are of the order 10^{-12}M . It can be assumed that the AC of MMA exists in THF mainly as the nonchelated E form contact ion-pair:



^{13}C -NMR spectra of the lithiated dimer in THF are also not in accordance with the formation of chelate Z structures [36], neither are the IR spectra of the same model at different concentrations indicative for intramolecular complexation.

The strong $-\text{O}-\text{Li}$ bond in ester enolates tends to form aggregated species. The tendency of lithium ester enolates ($P_{1\text{COOR}}\text{Li}$ and $P_{2\text{COOR}}\text{Li}$) to aggregate in THF was observed for the first time by Halaska and Lochmann [37] by using vapor pressure osmometry as presented in Table 4.

In contrast to the cyano derivatives, the concentration of ion triples in solution of $P_{1(\text{COOR})}\text{Li}$ is several times higher than that of $P_{2(\text{COOR})}\text{Li}$ solutions, which is in agreement with decreased aggregation tendency for $P_{2(\text{COOR})}\text{Li}$ shown in Table 2. In case the lithium cation lays over the plane of a nearly planar CCOOR group as postulated by Eizner *et al.* [38], the ion triples (ABA)⁻ should possess a sandwich structure which is energetically more favorable for $P_{1(\text{COOR})}\text{Li}$ than for $P_{2(\text{COOR})}\text{Li}$:



Obviously, the principal difference in the structure of ion triples of lithiated dimers of MMA and MAN consists in the assumption that the cyano group of the second monomer unit in the lithiated dimer of MAN has a share in the ion triple construction by formation of a coordinate bond, whereas complexation of counterion with the

second ester group is not likely in the case of the α -lithiated dimer of MMA. This assumption is in agreement with the complexation order of nitriles and esters towards lithium picrate in dioxane: nitrile > esters [20] (Table 3). It should be mentioned, however, that lithium counterion in $P_{3(\text{COOR})}\text{Li}$ is able to coordinate intramolecular with the carbonyl group of the third monomer unit (γ -carbonyl) [39].

Ligated growing centers

In the last 20 years of 20th century efficient ligands have been discovered able to control the livingness and stereospecificity of anionic polymerization of (meth)acrylic ester monomers. The most important function of ligand additives is steric hindrance (steric shielding or electronic protecting of the functional groups of the polar vinyl monomers) providing space area around the AC contact ion pair. It appears to be determining factor for the controlled living polymerization. At least, steric hindrance leads to stabilization of the linear $P_{3\text{COOR}}\text{Li}$ as rotational isomerization of $P_{3\text{COOR}}\text{Li}$ is found to be the bottleneck in the intramolecular cyclization reaction. The efficient ligands, discovered to date are classified into the following main groups:

- Lithium alkoxides [40] and enolates [21].
- Inorganic salts:
- Lithium and magnesium halide i.e. LiCl , and MgBr_2 [41,42].
- Salts with bulky groups i.e. LiClO_4 or R_4NX [43,44].
- Aluminium and boron alkyls [45- 47].

Lithium alkoxide and enolate as additives

The role of lithium alkoxides as additives, studied in considerable detail by Trekoval, Lochmann, and Müller, turned out to be significant in both reaction kinetics and tacticity of the resulting polymers [29,48]. Cross-associates such as $\text{AC}/t\text{-BuOLi}$ are acting as propagating centers. The AC's are "enveloped" by alkoxide molecules and the inner voids of the contact ion pair loses most of the solvent molecules. This makes the access to the AC more difficult. As a result, the polymerization process is practically insensitive to the solvent nature because of the strong shielding effect of $t\text{-BuOLi}$. Obviously, the mixed associate $P_{1(\text{COOR})}\text{Li}/t\text{-BuOLi}$

Table 4. Average degree of aggregation for model ester enolates in THF [37].

Ester enolate	Degree of aggregation
$(\text{CH}_3)_2\text{CLi COOCH}_3$	3.5
$(\text{CH}_3)_2\text{CHCO}_2\text{C}(\text{CH}_3)_2\text{CH}_2\text{C}(\text{CH}_3)\text{LiCO}_2\text{C}(\text{CH}_3)_3$	1.7

is strong enough to withstand competitive solvation by solvent or monomer molecules, thus, preventing the influence of σ -ligands such as glymes or crown ethers on the mode of polymerization process. $P_{1(\text{COOR})}\text{Li}/t\text{-BuOLi}$ lowers the basicity of the AC but for steric reasons considerably restricts side reactions like intramolecular cyclization.

In $P_{1(\text{COOR})}\text{Li}$ and $P_{2(\text{COOR})}\text{Li}$ the cation is close to the O atom of the ester enolate group resembling the lithium alkoxide structure. Indeed, alkoxide, keto-enolates and ester enolates tend to form aggregates such as dimers, trimers or tetramers with a slow exchange rate [49]. Because, in the most cases, the initiator is not fully consumed during the polymerization process, the unreacted $P_{1(\text{COOR})}\text{Li}$ plays the role of additive in the same manner as the ligation by $t\text{-BuOLi}$. This means that additive like $t\text{-BuOLi}$ should compete with the unreacted lithium enolate in case of low initiator efficiency. This raises the question, which of both compounds has a higher binding capacity.

Table 5. Association constants, K_{ass} of LiPi complexes with different μ -ligands and AlEt_3 in dioxane [21].

Additive	$K_{\text{ass}}, \text{M}^{-1}$	$\lambda_{\text{max}}, \text{nm}$
LiCl	75	337
$t\text{-BuOLi}$	120	400
Pin-Li	150	390
$P_{1(\text{COOR})}\text{Li}$	600	404
AlEt_3	350	325

Pin-Li = α -Lithiopinacolone

The problem was solved with the aid of LiPi, which services as a model compound for AC. According to measurements of the interaction LiPi-additive, shown in Table 5 the association ability of Li-alkoxide and Li-enolate ranges as follows:

K_{ass} Li-esterenolate $>$ K_{ass} Li-ketoenolate $>$ K_{ass} Li-alkoxide

The data, presented in the Table 5, indicate that the $t\text{-BuOLi}$ associates several times less than lithium ester enolate. It is evident that in order to have an effect as an additive on the polymerization kinetics as well as on the stereochemistry on the polyaddition reaction, the ratio alkoxide/initiator should be much greater than the equimolar ratio. Indeed, Lochman and Müller [30] found that in order to decrease the propagation rate constant by one order of magnitude, addition of $t\text{-BuOLi}$ at alkoxide/enolate ratio of 3/1 is needed. Wang *et al.* [50] also studied the effects of $t\text{-BuOLi}$ on the stereochemistry of methyl methacrylate anionic polymerization upon addition of 10 equiv. $t\text{-BuOLi}$.

Lithium chloride as additive

It has been shown by the Teyssie group that LiCl-modified organolithium compounds initiate living anionic polymerization of methyl methacrylate, t -butyl methacrylate and t -butyl acrylate at low temperatures in THF [41]. This enables synthesis of (meth)acrylate based block copolymers with high efficiency and low polydispersity [51]. The explanation of the complexation behavior of LiCl with the lithium oligomers of $t\text{-BuMA}$ was presented in [52]. The interaction between lithium ester enolate and LiCl is regarded as strong electrostatic interaction. The most pronounced effect of LiCl as an additive is the lowering of polydispersity index of PMMA and PBuA. Addition of LiCl leads to only one type of complex growing center species with equimolar ratio. Our studies on the interaction between LiCl and lithium picrate in dioxane as reference system is in agreement with the equimolar complex ratio. The association constant K_{ass} 75 M^{-1} (Table 5) is several times less than K_{ass} for alkoxide and enolate derivatives. This gives us grounds to believe that by simultaneous presence of lithium alkoxide/lithium enolate and LiCl, the R-OLi additive will be favored by the interactions with ACs.

Organometallic Lewis acids as additives

Tsvetanov *et al.* [45] first employed AlEt_3 , $\text{Al}(i\text{-Bu})_3$, $\text{Al}(n\text{-Bu})_3$, BEt_3 , and ZnEt_2 as additives and $s\text{-BuLi}$ as initiator in the polymerization of MMA in THF and toluene at -70°C . The AC of oligo-MMA form 1:1 complexes with trialkylaluminum and triethylboron. Addition of acceptors leads to decrease in the rate of MMA polymerization. The presence of such kind of additives increases substantially the syndiotactic sequences. Later on, Hatada *et al.*, studied anionic polymerization of MMA in toluene at -78°C by using $t\text{-BuLi}$ as initiator and aluminum alkyls as additives [42,53]. Syndiotactic polymers with controlled molecular weight and narrow MWD were obtained. The steric hindrance due to the bulkiness of the aluminum alkyls plays important role. Ballard *et al.* [47] were able to polymerize alkyl methacrylates at elevated temperatures ($0 - 40^\circ\text{C}$) in toluene by using bulky diaryloxyalkyl-aluminum as additives. The AC in the form of "ate" complexes is very stable.

Another improvement was the use of tetraalkylammonium halides as co-additives forming a complex with trialkylaluminium, e.g., $\text{NBu}_4[\text{Al}_2\text{Et}_6\text{Br}]$ [54]. The rate of polymerization is two orders of

the incoming monomer. The idea of industrial researchers is to prepare AC with high-volume complex counter ion, thus, it will “screen” the growing species from side reactions [47]. Thus, for example, the intramolecular cyclization reaction requires a metal ion like lithium for the activation of ester group and the expulsion of alkoxide ions. In order to avoid the influence of the metal counterion, Reetz [56] was the first, who used non-metallic tetrabutyl ammonium counterion in anionic polymerization of (meth)acrylic monomers.

We set ourselves the task to expand the research by examining the interaction of $P_{1(\text{COOR})}\text{Li}$ with quaternary ammonium salts (QAS) with quite different structure and size [45,57]. Once again, LiPi was considered as a model of an AC of chain propagation as it is well known that the optical spectrum of the picrate anion is very sensitive towards changes in the interionic distance [58].

In contact with LiPi , the QAS can intervene in two ways. On one hand, counter ion exchange reactions are possible:



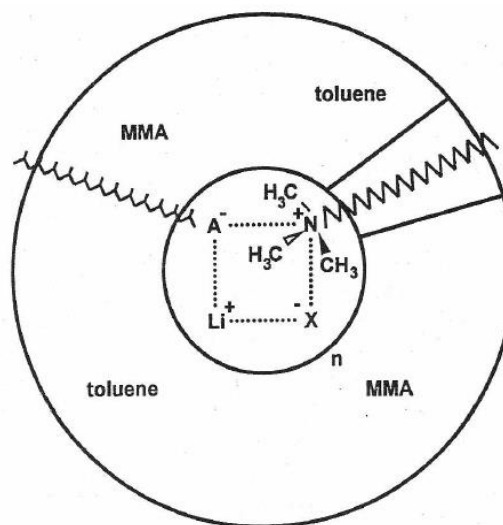
where R = alkyl substituent, X = Cl, Br

The exchange reaction leads to a definite change in the behavior of the picrate anion. The quaternary ammonium cation (Q^+) makes the organophobic picrate anion soluble, while LiX is insoluble in toluene. In case of $P_{n(\text{COOR})}\text{Li}/\text{QAS}$ system the exchange reaction leads to formation of AC with bulky Q^+ .

The second possible reaction is the formation of mixed associates $(\text{Q}^+, \text{Pi}^-, \text{Li}^+\text{X}^-)_n$. In this case Li^+ remained in the solution. As already mentioned, the two cases are distinguished by the ability of lithium to be dissolved in toluene. Indeed, Table 7 reveals that depending on QAS salts structure, these two quite different types of interactions can be recognized. In the case of symmetrical $\text{R}_4\text{N}^+\text{X}^-$, almost quantitative counter ion exchange occurs, whereas the presence of QAS with very long chain alkyl groups namely $\text{C}_{17}\text{C}_{12}\text{Me}_2\text{NBr}$ or $(\text{C}_{12})_2\text{Me}_2\text{NBr}$, leads to increase in Li^+ solubility more than two orders of magnitude, i.e. to the formation of mixed associates. In order to diminish the steric hindrance, the Q^+ is oriented to the growing anion from the side of the smaller size groups, e.g. methyl groups (Scheme 6).

The longer fatty alkyl chains participate in the formation of the first solvation shell. This way the microenvironment is highly hydrophobic, shifting

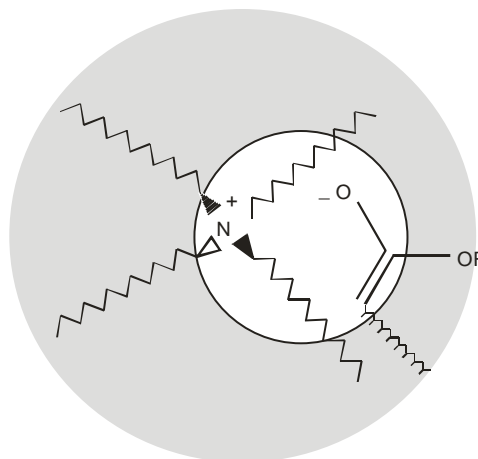
the mode of monomer addition to $P_{n(\text{COOR})}\text{Li}$ towards isotactic structure.



Scheme 6. Sketch of the mixed associate $(\text{Q}^+, \text{Pi}^-, \text{Li}^+\text{X}^-)_n$ [44].

Completely different, when the QAS additive causes ion exchange, the syndiotactic addition is much more pronounced, the size of Q^+ being very important: $rr \text{ Hex}_4\text{N}^+ \gg rr \text{ Bu}_4\text{N}^+$.

Results, presented in Table 7 show that in both cases the ester enolate species are not “naked” as it is traditionally termed in the phase transfer catalysis reactions. Obviously, the growing species penetrate also into the void spaces of R_4N^+ :



Due to the steric hindrance, the anion penetration suppresses the attack of the ester enolate anion to the carbonyl group of the third (γ) unit. This type of propagating species favors syndiotactic placement. The same trends were observed when using *t*-BuOK [59] and Bu_2Mg [60] initiators.

Table 7. Comparison between the solubility of LiPi in toluene in the presence of QAS and PMMA stereochemistry when $P_{1(\text{COOR})}\text{Li}$ is used as initiator.

QAS	LiPi		$P_{1(\text{COOR})}\text{Li}/\text{QAS}$, PMMA triad placements		
	λ_{max} , nm	$[\text{Li}^+]/[\text{PiQ}] \times 10^3$	<i>mm</i>	<i>mr</i>	<i>rr</i>
-	337	-	80	17	3
Bu ₄ NBr	364	< 1	65	18	17
Hex ₄ NCl	361	< 1	16	28	56
(C ₁₂) ₂ Me ₂ NBr	360.5	214	77	16	7
C ₁₇ C ₁₂ Me ₂ NBr	360.5	299	95	4	1

CONCLUSION

The fine control of the anionic polymerization of polar vinyl monomers and especially of (meth)acrylates has been successfully realized in the 1980s and 1990s. One of the strategies that received a special attention is the ligated anionic polymerization. The interest in this field has produced a large number of excellent comprehensive reviews [39,61,62]. The attention of researchers has been focused mainly on the study of the polymerization kinetics and preparation of well defined poly(meth) acrylates or their blockcopolymers with narrow molecular weight distribution.

This review paper summarizes the research on the penultimate effects in anionic polymerization and the influence of ligands performed in the Institute of Polymers, BAS during 1980s and 1990s. The approach in our studies is slightly different. The main subjects of our study are model compounds or "living" oligomers of polar vinyl monomers, such as nitrile, esters, and ketons. Their physico-chemical characteristics in solution, before and after adding of ligands, were investigated with the aid of IR spectra and conductometry. In almost all cases the interactions involve lithium counter ion. A typical feature is the use of LiPi as a model in studying the interactions with monomers, compounds with polar groups, and most typical additives: alkoxide, LiCl, tetraalkylammonium salts and trialkylaluminum compounds.

We will mention some of the most important conclusions of the study:

1. The propagating species comprise contact ion pairs and ion triples in THF.

2. In THF the interaction growing center-penultimate monomer unit is not typical for PMMA, but it was demonstrated in living oligomers of AN, MAN, and vinyl ketone.

3. In the case of anionic polymerization in toluene of AN and MAN, initiated by lithium or magnesium compounds, interactions AC-monomer and AC-polar group of monomer unit are registered.

4. The approach by using reference system LiPi in dioxane distinguishes four types of interactions: LiPi-electron pair donors (polar groups of monomer or monomer unit); LiPi – μ ligands (LiCl, RO₂Li, Li-ketoenolate, and Li-esterenolate); LiPi – Lewis acids (R₃Al); and LiPi – quaternary ammonium salts.

REFERENCES

- Ch. Tsvetanov, I. Panayotov, B. Erussalimsky, *Eur. Polym. J.*, **10**, 557 (1974).
- Ch. B. Tsvetanov, I. M. Panayotov, *Eur. Polym. J.*, **11**, 209 (1975).
- Ch. B. Tsvetanov, *Eur. Polym. J.*, **15**, 503 (1979).
- Ch. B. Tsvetanov, D. T. Petrova, I. M. Panayotov, *Makromol. Chem.*, **183**, 517 (1982).
- L. Lochmann, J. Trekoval, *Makromol. Chem.*, **182**, 1361 (1982).
- I. M. Panayotov, Ch. B. Tsvetanov, A. C. Alexandrov, *Eur. Polym. J.*, **11**, 875 (1975).
- I. N. Juchnovski, *Theor. Eksp. Khim.*, **3**, 410 (1967); *Chem. Abstr.* **68**, 100, 135.
- I. N. Juchnovski, Ch. Tsvetanov, I. Panayotov, *Monatsh. Chem.*, **100**, 1980 (1969).
- L. Lochmann, D. Lim, *J. Organomet. Chem.*, **50**, 9 (1973).
- D. K. Dimov, E. B. Petrova, I. M. Panayotov, Ch. B. Tsvetanov, *Macromolecules*, **21**, 2733 (1988).
- R. Fayt, R. Forte, C. Jacobs, R. Jerome, T. Oukadi, P. Teyssie, S. K. Varshney, *Macromolecules*, **20**, 1442 (1987).
- Ch. B. Tsvetanov, Y. Y. Eizner, B. L. Erussalimsky, *Eur. Polym. J.*, **16**, 219 (1980).
- Ch. B. Tsvetanov, D. T. Dotcheva, *J. Polym. Sci.: Part A: Polym. Chem.*, **24**, 2253 (1986).
- D. Dotcheva, Ch. B. Tsvetanov, L. Lochmann, *J. Polym. Sci., Polym. Chem. Ed.*, **25**, 3005 (1987).
- C. B. Wooster, *J. Am. Chem. Soc.*, **59**, 377 (1937).
- D. Hounore, J. C. Kavier, P. Sigwalt, M. Fontanille, *Europ. Polym. J.*, **10**, 425 (1974).
- T. E. Hogen-Esch, W. L. Jenkins, *J. Am. Chem. Soc.*, **103**, 3666 (1981).
- L. V. Vinogradova, V. N. Zgonnik, N. I. Nikolaev, Ch. B. Tsvetanov, *Eur. Polym. J.*, **15**, 545 (1979).
- M. Tardi, D. Rouge, P. Sigwalt, *Eur. Polym. J.*, **3**, 85 (1967).

20. Ch. B. Tsvetanov, E. B. Petrova, D. K. Dimov, I. M. Panayotov, J. Smid, *J. Solution Chem.*, **19**, 425 (1990).
21. Ch. B. Tsvetanov, D. K. Dimov, E. B. Petrova, D. T. Dotcheva, *Macromol. Chem., Makromol. Symp.*, **60**, 297 (1992).
22. Ch. Tsvetanov, V. Sgonnik, I. Panayotov, B. Erussalimsky, *Justus Liebigs Ann. Chem.*, **763**, 53 (1972).
23. I. N. Juchnovski, I. G. Binev in: *The Chemistry of Functional Groups*, Suppl. C, Part 1, S. Patai and Z. Rappoport, Eds., p. 107, John Wiley & Sons, 1983.
24. Ch. B. Tsvetanov, D. T. Dotcheva, D. K. Dimov, E. B. Petrova, I. M. Panayotov in: *Recent Advances in Anionic Polymerization*, T.E. Hogen-Esch, J. Smid, Eds., Elsevier 1987.
25. H.-J. Adler, L. Lochmann, D. T. Dotcheva, Ch. B. Tsvetanov, *Makromol. Chem.*, **187**, 1253 (1986).
26. I. S. Pominov, A. Z. Gadjiev, *Izv. Vuzov SSSR Phys.*, **19** (1965).
27. Y.-S. Kim, T.-H. Kim, A. Lee, H.-K. Song, *Energy Environm. Sci.*, **4**, 4038 (2011).
28. Y. Joch, S. Kurihara, T. Tomita, *J. Polym. Sci.*, **B9**, 1463 (1971).
29. J. Trekoval, *Coll. Czech. Chem. Commun.*, **42**, 1259 (1977).
30. L. Lochmann, A.H.E. Müller, *Makromol. Chem.*, **191**, 1657 (1990).
31. O. A. Reutov, A. L. Kurts, *Russ. Chem. Rev. (Engl. Transl.)*, **46**, 1040 (1977).
32. O. A. Reutov, I. P. Beletskaya, A. L. Kurts, *Ambident Anions*, Plenum Publishing Corp. New York 1983.
33. A. R. Lyons, E. Catterall, *Eur. Polym. J.*, **7**, 839 (1971).
34. D. Dotcheva, Ch. B. Tsvetanov, *Macromol. Chem.*, **186**, 2103 (1985).
35. L. Vancea, S. Bywater, *Macromolecules*, **14**, 1321 (1981).
36. L. Vancea, S. Bywater, *Macromolecules*, **14**, 1776 (1981).
37. V. Halaska, L. Lochmann, *Coll. Czech. Chem. Commun.*, **38**, 1780 (1973).
38. Y. Y. Eizner, B. L. Erussalimsky, *Eur. Polym. J.*, **12**, 59 (1976).
39. C. Zune, R. Jerome, *Prog. Polym. Sci.*, **24**, 631 (1999).
40. L. Lochmann, M. Rodova, J. Trekoval, *J. Polym. Sci., Polym. Chem. Ed.*, **12**, 2091 (1974).
41. S. K. Varshney, J. P. Hautekeer, R. Fayt, R. Jerome, P. Teyssie, *Macromolecules*, **23**, 2618 (1990).
42. T. Kitayama, T. Shinozaki, T. Sakamoto, M. Yamamoto, K. Hatada, *Makromol. Chem., Suppl.*, **15**, 167 (1989).
43. D. Baskaran, S. Sivaram, *Macromolecules*, **30**, 1550 (1997).
44. Ch. B. Tsvetanov, Ch. P. Novakov, *Macromolecular Symposia*, **107**, 265 (1996).
45. Ch. B. Tsvetanov, D. T. Petrova, P. H. Li, I. M. Panayotov, *Eur. Polym. J.*, **14**, 25 (1978); Erratum: *Eur. Polym. J.*, **14**, 391 (1978).
46. K. Hatada, K. Ute, Y. Okamoto, T. Kitayama, *Polym. Bull.*, **18**, 1037 (1986).
47. D. G. H. Ballard, R. J. Bowles, D. M. Haddleton, S. N. Richards, R. Sellens, D. L. Twose, *Macromolecules*, **25**, 5907 (1992).
48. M. Janata, L. Lochmann, A. H. E. Müller, *Makromol. Chem.*, **191**, 2253 (1990).
49. J. Kriz, J. Dybal, L. Lochmann, M. Janata, *Macromol Chem. Phys.*, **195**, 3039 (1994).
50. J.-S. Wang, R. Jerome, R. Warin, P. Teyssie, *Macromolecules*, **26**, 5984 (1993).
51. S. K. Varshney, C. Jacobs, J. P. Hautekeer, P. Bayard, R. Jerome, R. Fayt, P. Teyssie, *Macromolecules*, **24**, 4997 (1991).
52. C. Zune, P. Dubois, R. Jerome, J. Kriz, J. Dybal, L. Lochmann, M. Janata, P. Vlcek, T. M. Werkhoven, J. Lugtenburg, *Macromolecules*, **31**, 2744 (1998).
53. T. Kitayama, T. Shinizaki, E. Masuda, M. Yamamoto, K. Hatada, *Polym. Bull.*, **20**, 505 (1988).
54. H. Schlaad, B. Schmitt, A. H. E. Müller, *Angew. Chem. Int. Ed.*, **37**, 1389 (1998).
55. Ch. Tsvetanov, V. N. Sgonnik, *C. r. Acad. bulg. Sci.*, **32**, 55 (1979).
56. M. T. Reetz, *Angew. Chem.*, **100**, 1026 (1988).
57. Ch. P. Novakov, Ch. B. Tsvetanov, *Macromol. Rapid Commun.*, **16**, 741 (1995).
58. K. H. Wong, K. Yagi, J. Smid, *J. Membr. Biol.*, **18**, 379 (1974).
59. Ch. P. Novakov, Ch. B. Tsvetanov, *Macromol. Rapid Commun.*, **17**, 181 (1996).
60. Ch. P. Novakov, Ch. B. Tsvetanov, *Macromol. Symp.*, **132**, 273 (1998).
61. J.-S. Wang, R. Jerome, P. Teyssie, *J. Phys. Org. Chem.*, **3**, 208 (1995).
62. D. Baskaran, A. H. E. Müller, *Prog. Polym. Sci.*, **32**, 173 (2007).

МЕЖДУ- И ВЪТРЕШНО МОЛЕКУЛНИ ВЗАИМОДЕЙСТВИЯ ПРИ АНИОННАТА ПОЛИМЕРИЗАЦИЯ НА ПОЛЯРНИ ВИНИЛОВИ МОНОМЕРИ

Хр. П. Новаков и Хр. Б. Цветанов*

Институт по Полимери, Българска Академия на Науките, ул. Акад. Г. Бончев, бл. 103, 1113 София, България

Постъпила на 19 юли 2014 г.; Коригирана на 18 август 2014 г.

(Резюме)

Настоящата обзорна работа представя резултатите от изследванията, проведени в лаборатория „Полимеризационни процеси” на Института по полимери – БАН, върху природата на активните центрове на нарастване (АЦ) в процеса на анионна полимеризация на полярни винилови мономерни (ПВМ) – акрилати, метакрилати, винилови нитрили и винилови кетони, като е обърнато внимание на взаимодействията на АЦ с донорно-акцепторни лиганди. Обект на особен интерес са взаимодействията на АЦ с различни лиганди съдържащи литиев и магнезиев противойон, поради протичащите процеси на взаимодействие и самоасоцииране, които осигуряват възможност за осъществяване на контрол на структурата и състава на получаваните (съ)полимери. Използвани са и моделни съединения или „живи” олигомери на ПВМ, като чрез ИЧ спектроскопия и кондуктометрично са изследвани физикохимичните им характеристики в разтвор, преди и след добавяне на лиганд. Литиевият пикрат е използван като моделно съединение за изучаване на взаимодействието с мономерни, съединения с полярни групи и най-типичните добавки: алкоксиди, литиев хлорид, кватернерни амониеви соли и триалкилалуминиеви съединения.

BULGARIAN CHEMICAL COMMUNICATIONS

Instructions about Preparation of Manuscripts

General remarks: Manuscripts are submitted in English by e-mail or by mail (in duplicate). The text must be typed double-spaced, on A4 format paper using Times New Roman font size 12, normal character spacing. The manuscript should not exceed 15 pages (about 3500 words), including photographs, tables, drawings, formulae, etc. Authors are requested to use margins of 3 cm on all sides. For mail submission hard copies, made by a clearly legible duplication process, are requested. Manuscripts should be subdivided into labelled sections, e.g. **Introduction, Experimental, Results and Discussion**, etc.

The title page comprises headline, author's names and affiliations, abstract and key words.

Attention is drawn to the following:

a) **The title** of the manuscript should reflect concisely the purpose and findings of the work. Abbreviations, symbols, chemical formulas, references and footnotes should be avoided. If indispensable, abbreviations and formulas should be given in parentheses immediately after the respective full form.

b) **The author's** first and middle name initials, and family name in full should be given, followed by the address (or addresses) of the contributing laboratory (laboratories). **The affiliation** of the author(s) should be listed in detail (no abbreviations!). The author to whom correspondence and/or inquiries should be sent should be indicated by asterisk (*).

The abstract should be self-explanatory and intelligible without any references to the text and containing not more than 250 words. It should be followed by key words (not more than six).

References should be numbered sequentially in the order, in which they are cited in the text. The numbers in the text should be enclosed in brackets [2], [5, 6], [9–12], etc., set on the text line. References, typed with double spacing, are to be listed in numerical order on a separate sheet. All references are to be given in Latin letters. The names of the authors are given without inversion. Titles of journals must be abbreviated according to Chemical Abstracts and given in italics, the volume is typed in bold, the initial page is given and the year in parentheses. Attention is drawn to the following conventions:

a) The names of all authors of a certain publications should be given. The use of “*et al.*” in

the list of references is not acceptable.

b) Only the initials of the first and middle names should be given.

In the manuscripts, the reference to author(s) of cited works should be made without giving initials, e.g. “Bush and Smith [7] pioneered...”. If the reference carries the names of three or more authors it should be quoted as “Bush *et al.* [7]”, if Bush is the first author, or as “Bush and co-workers [7]”, if Bush is the senior author.

Footnotes should be reduced to a minimum. Each footnote should be typed double-spaced at the bottom of the page, on which its subject is first mentioned.

Tables are numbered with Arabic numerals on the left-hand top. Each table should be referred to in the text. Column headings should be as short as possible but they must define units unambiguously. The units are to be separated from the preceding symbols by a comma or brackets.

Note: The following format should be used when figures, equations, etc. are referred to the text (followed by the respective numbers): Fig., Eqns., Table, Scheme.

Schemes and figures. Each manuscript (hard copy) should contain or be accompanied by the respective illustrative material as well as by the respective figure captions in a separate file (sheet). As far as presentation of units is concerned, SI units are to be used. However, some non-SI units are also acceptable, such as °C, ml, l, etc.

The author(s) name(s), the title of the manuscript, the number of drawings, photographs, diagrams, etc., should be written in black pencil on the back of the illustrative material (hard copies) in accordance with the list enclosed. Avoid using more than 6 (12 for reviews, respectively) figures in the manuscript. Since most of the illustrative materials are to be presented as 8-cm wide pictures, attention should be paid that all axis titles, numerals, legend(s) and texts are legible.

The authors are asked to submit **the final text** (after the manuscript has been accepted for publication) in electronic form either by e-mail or mail on a 3.5” diskette (CD) using a PC Word-processor. The main text, list of references, tables and figure captions should be saved in separate files (as *.rtf or *.doc) with clearly identifiable file names. It is essential that the name and version of

the word-processing program and the format of the text files is clearly indicated. It is recommended that the pictures are presented in *.tif, *.jpg, *.cdr or *.bmp format, the equations are written using "Equation Editor" and chemical reaction schemes are written using ISIS Draw or ChemDraw programme.

The authors are required to submit the final text with a list of three individuals and their e-mail addresses that can be considered by the Editors as potential reviewers. Please, note that the reviewers should be outside the authors' own institution or organization. The Editorial Board of the journal is not obliged to accept these proposals.

EXAMPLES FOR PRESENTATION OF REFERENCES

REFERENCES

1. D. S. Newsome, *Catal. Rev.–Sci. Eng.*, **21**, 275 (1980).
2. C.-H. Lin, C.-Y. Hsu, *J. Chem. Soc. Chem. Commun.*, 1479 (1992).
3. R. G. Parr, W. Yang, *Density Functional Theory of Atoms and Molecules*, Oxford Univ. Press, New York, 1989.
4. V. Ponec, G. C. Bond, *Catalysis by Metals and Alloys (Stud. Surf. Sci. Catal., vol. 95)*, Elsevier, Amsterdam, 1995.
5. G. Kadinov, S. Todorova, A. Palazov, in: *New Frontiers in Catalysis (Proc. 10th Int. Congr. Catal., Budapest, 1992)*, L. Guzzi, F. Solymosi, P. Tetenyi (eds.), Akademiai Kiado, Budapest, 1993, Part C, p. 2817.
6. G. L. C. Maire, F. Garin, in: *Catalysis. Science and Technology*, J. R. Anderson, M. Boudart (eds), vol. 6, Springer-Verlag, Berlin, 1984, p. 161.
7. D. Pocknell, *GB Patent 2 207 355* (1949).
8. G. Angelov, PhD Thesis, UCTM, Sofia, 2001.
9. JCPDS International Center for Diffraction Data, *Power Diffraction File*, Swarthmore, PA, 1991.
10. *CA* **127**, 184 762q (1998).
11. P. Hou, H. Wise, *J. Catal.*, in press.
12. M. Sinev, private communication.
13. <http://www.chemweb.com/alchem/articles/1051611477211.html>.

CONTENTS

<i>B. Blagoev</i> , ACADEMICIAN DIMITER IVANOV 120 Years of His Birth	5
<i>P. M. Ivanov, I. G. Pojarlieff, S. D. Simova, G. D. Velinov</i> , Interaction between charged groups. pK-values and conformations of the diastereomers of 3-amino-2,3-diphenylpropanoic acids and their ester and N-acetyl derivatives	9
<i>V. Dimitrov</i> , Catalytic method for synthesis of Grignard compounds with magnesium attached to tertiary bridge head C-atom	16
<i>I. Philipova, G. Stavrov, V. Dimitrov</i> , Phosphino-carboxamide hybrid ligands with a camphane scaffold for Pd-catalyzed asymmetric allylic alkylation	21
<i>G. Stavrov, I. Philipova, V. Valcheva, G. Momekov</i> , Synthesis and antimycobacterial activity of bornylamine derived amido-alcohols	27
<i>K. Dikova, M. Kamenova-Nacheva, K. Kostova, V. Dimitrov</i> , Enantioselective addition of diethylzinc to ferrocene carbaldehyde - reaction outcome by using natural compound based catalysts	33
<i>I. E. Ismailov, I. K. Ivanov, V. C. Christov</i> , Bifunctionalized allenes. Part XIV. A convenient and efficient regioselective synthesis of phosphorylated β -hydroxyallenes with protected and unprotected hydroxy group	39
<i>V. B. Kurteva, L. A. Lubenov, S. D. Simova</i> , 2,3-Disubstituted imidazo[1,2-a]pyridines from 2-aminopyridines and acetophenones. Catalyst's efficiency and solid state NMR study.	47
<i>V. T. Angelova, W. Frey, I. C. Ivanov, N. Vassilev, T. N. Glasnov</i> , One-pot synthesis of a chromeno[4,3,2- <i>de</i>]-1,6-naphthyridine derivative from 4-chlorocoumarin-3-carbaldehyde	53
<i>M. G. Kratchanova, P. N. Denev², C. G. Kratchanov</i> , Rose hip extract synergistically increase antioxidant activity of fruit and herb extracts	59
<i>A. H. Atanasova, P. N. Denev, I. I. Tringovska, S. Y. Grozeva, D. G. Ganeva, M. G. Kratchanova, I. N. Panchev</i> , Optimization of the key parameters for extraction of polyphenol compounds from tomato fruits (<i>Solanum lycopersicum</i> L.). Kinetics of the process.	65
<i>M. Nikolova, M. G. Kratchanova, E. V. Pavlova, I. Ianakieva, V. Kussovski</i> , Purification and biological activity of pectic polysaccharides from leek	71
<i>M. H. Ognyanov, Y. N. Georgiev, I. Z. Yanakieva, V. K. Kussovski, M. G. Kratchanova</i> , Chemical composition and anti-complementary activity of enzyme-modified citrus pectins	79
<i>M. Popova, A. Stoyanova, N. Valyovska-Popova, V. Bankova, D. Peev</i> , A new coumarin and total phenolic and flavonoids content of Bulgarian celeriac	88
<i>D. V. Nedeltcheva-Antonova, K. S. Tsandeva, R. D. Dimitrova</i> , Determination of Benzethonium Chloride in Grapefruit Seed Extracts - a GC/MS alternative	94
<i>Z. Y. Petkova, G. A. Antova</i> , Phospholipid composition of <i>Cucurbitaceae</i> seed oils	100
<i>T. N. Ovcharova, M. D. Zlatanov, A. S. Ivanov</i> , Sterol and fatty acid composition of grape seed oils	106
<i>Y. Raynova, S. Todinova, D. Yordanov, K. Idakieva</i> , SDS-induced phenoloxidase activity of <i>Helix aspersa</i> maxima hemocyanin	111
<i>M. Popova, K. Yoncheva, A. Szegedi, Y. Kalvachev, N. Benbassat, V. Mavrodinova</i> , Resveratrol loading on mesoporous silica and zeolite carriers by solid state method	117
<i>M. Stefanova, L. Gonsalvesh, S. P. Marinov, J. Czech, R. Carleer, J. Yperman</i> , Reductive pyrolysis of leonardite humic acids	123
<i>I. G. Racheva, B. G. Tsyntsarski, B. N. Petrova, T. K. Budinova, N. V. Petrov, B. Nagel, S. Pusz, U. Szeluga</i> , Conversion of polyolefin wax to carbon adsorbents by thermooxidation treatment	129
<i>I. Genova, B. Tsyntsarski, M. Dimitrov, D. Paneva, D. Kovacheva, T. Budinova, R. Ivanova, I. Mitov, N. Petrov, T. Tsoncheva</i> , Cobalt and iron modified activated carbons from renewable sources as catalysts in methanol decomposition: Effect of the precursor	134
<i>V. V. Ivanova, M. K. Stoyanova, S. G. Christoskova</i> , Study on the catalytic activity of nanosized NiOx for oxidative degradation of 2,4-dichlorophenol in aqueous solutions	141
<i>A. Popova, B. Stamboliyska, E. Velcheva</i> , Experimental and DFT studies on the IR spectral and structural changes arising from the conversion of 4-amino-N-[amino(imino)methyl] benzenesulfonamide (sulfaguanidine) into azanion	149
<i>A. D. Popova, E. A. Velcheva</i> , IR spectral and structural changes, caused by the conversion of 4-cyanobenzenesulfonamide into azanion	157
<i>Z. I. Glavcheva, D. Y. Yancheva, Y. K. Kancheva, E. A. Velcheva, B. A. Stamboliyska</i> , Development of FTIR spectra database of reference art and archaeological materials	164
<i>S. S. Stoyanov, J. A. Tsenov</i> , IR spectra and structure of 1,1,3,3-tetracyanopropane and its carbanions: experimental and quantum chemical study	170
<i>D. Yancheva, S. Stoyanov, B. Stamboliyska, L. Daskalova, E. Cherneva, A. Smelcerovic</i> , Influence of the environment on the antioxidant action of two 6-(propan-2-yl)-4-methyl-morpholine-2,5-diones	179

<i>S. E. Angelova, A. K. Slavova-Kazakova, L. Saso, S. V. Malhotra, A. K. Prasad, M. E. Bracke, V. S. Parmar, V. D. Kancheva</i> , DFT/B3LYP calculated bond-dissociation enthalpies, radical-scavenging and antioxidant activities of natural-like coumarins	187
<i>I. Georgieva, N. Trendafilova</i> , Metal-ligand interactions in transition metal complexes of glyoxilic acid oxime	196
<i>V. B. Delchev</i> , Xanthine and hypoxanthine: in a search for conical intersections S_0/S_1 connected with deformations of pyrimidine residue of the purine ring	203
<i>B. P. Stoyanov, P. R. Kostadinov, M. V. Kolev, Z. A. Mustafa, M. N. Moskovkina, R. S. Milina, I. P. Bangov</i> , Use of the descriptor fingerprints to clustering of chemical datasets	209
<i>B. P. Stoyanov, E. P. Petrov, N. T. Kochev, I. P. Bangov</i> , A novel program for computer-aided generation of 2D chemical structures	215
<i>A. Z. Patleeva, D. D. Enchev, G. D. Neykov</i> , Stereoselectivity in intramolecular Diels-Alder reactions of 2,4-pentadienyl butadienamides in the “Remote Stereocontrol Group” approach	220
<i>S. Kawauchi, L. Antonov, Y. Okuno</i> , Prediction of the color of dyes by using time-dependent density functional theory (TD-DFT)	228
<i>P. Ivanov</i> , Further studies on the conformations of large-ring cyclodextrins	238
<i>G. S. Spasov</i> , Application of Isohypes method for AES quantification of semiconductor solid solutions	246
<i>R. Todorov, Y. Ilieva, V. Lozanova, A. Lalova</i> , Optical properties of silver-doped organic polymer films as solar control coating materials for advanced architectural glazing application	251
<i>I. Bodurov, R. Todorov, T. Yovcheva, S. Sainov</i> , Holographic investigation of the corona discharge effect on the photo-doping of Ag, Au and Cr into nano-sized As_2S_3 films	256
<i>Ch. P. Novakov, Ch. B. Tsvetanov</i> , Inter- and intra-molecular interactions in anionic polymerization of polar vinyl monomers	261
INSTRUCTIONS TO THE AUTHORS	276

СЪДЪРЖАНИЕ

Б. Благоев, Академик Димитър Иванов 120 години от рождението му	5
П. М. Иванов, И. Г. Пожарлиев, С. Д. Симова, Г. Д. Велинов, Взаимодействие на заредени групи. рК и конформации на диастереомерите на 3-амино-2,3-дифенилпропановата киселина, метиловите и етиловите й естери и п-ацетилни производни	9
В. Димитров, Каталитичен метод за синтез на Гринярови съединения с магнезий свързан с третичен мостови въглероден атом	16
И. Филипова, Г. Ставраков, В. Димитров, Фосфин-карбоксамиди с камфанов скелет като лиганди за Pd-катализирано асиметрично алкилиране	21
Г. Ставраков, И. Филипова, В. Вълчева, Г. Момаков, Синтез и антимикубактериална активност на амидоалкохоли производни на борниламин	27
К. Дикова, М. Каменова-Начева, К. Костова, В. Димитров, Енантиселективно присъединяване на диетилцинк към фероценкарбалдехид – резултати от използване на природни съединения като катализатори	33
И. Е. Исмаилов, И. К. Иванов, В. Х. Христов, Бифункционализирани алени. Част XIV. Удобен и ефикасен региоселективен синтез на фосфорилирани β-хидроксиалени със защитена и незащитена хидрокси група	39
В. Б. Куртева, Л. А. Любенов, С. Д. Симова, 2,3-Дизаместени имидазо[1,2-а]пиридини от 2-аминопиридини и ацетофенони. Ефективни катализатори и ЯМР изследване в твърдо състояние.	47
В. Т. Ангелова, В. Фрай, И. Х. Иванов, Н. Василев, Т. Н. Гласнов, Едностъпков синтез на хромено[4,3,2-d,e]-1,6-нафтиридиново производно от 4-хлорокумарин-3-карбалдехид	53
М. Г. Крачанова, П. Н. Денев, Х. Г. Крачанов, Екстракт от шипка синергично повишава антиоксидантната активност на плодови и билкови екстракти	59
А. Х. Атанасова, П. Н. Денев, И. И. Тринговска, С. Й. Грозева, Д. Г. Ганева, М. Г. Крачанова, И. Н. Панчев, Оптимизация на ключови параметри на екстракция на фенолни компоненти от домати плодове (<i>Solanum lycopersicum</i> L.). Кинетика на процеса.	65
М. Николова, М. Крачанова, Е. Павлова, И. Янакиева, В. Късовски, Пречистване и биологична активност на пектинови полизахариди от праз	71
М. Х. Огнянов, Й. Н. Георгиев, И. Ж. Янакиева, В. К. Късовски, М. Г. Крачанова, Химичен състав и антикомплементарна активност на ензимно-модифицирани цитрусови пектини	79
М. Попова, А. Стоянова, Н. Вальовска-Попова, В. Банкова, Д. Пеев, Нов кумарин и съдържание на тотални флавоноиди и тотални феноли в българска целина	88
Д. В. Неделчева-Антонова, К. С. Цандева, Р. Д. Димитрова, Определяне на бензетониев хлорид в екстракти от семена на грейпфрут – алтернативен подход чрез използване на газова хроматография с масспектрална детекция	94
Ж. Ю. Петкова, Г. А. Антова, Фосфолипиден състав на масла от сем. <i>Cucurbitaceae</i>	100
Т. Овчарова, М. Златанов, А. Иванов, Стероли и мастно-киселинен състав на масло от гроздови семки	106
Ю. Райнова, С. Тодинова, Д. Йорданов, К. Идакиева, SDS-индуцирана фенолоксидазна активност на хемоцианин от <i>Helix aspersa maxima</i>	111
М. Попова, К. Йончева, А. Сегеди, Ю. Кълачев, Н. Бенбасат, В. Мавродинова, Натоварване на ресвератрол върху мезопорести силикатни и зеолитни носители чрез твърдофазен метод	117
М. Стефанова, Л. Гонсалвеш, С. П. Маринов, Я. Чех, Р. Карлие, Я. Иперман, Редукционен пиролиз на хуминови киселини от леонардит	123
И. Г. Рачева, Б. Г. Цинцарски, Б. Н. Петрова, Т. К. Будинова, Н. В. Петров, Б. Нагел, С. Пуш, У. Шелуга, Термоокислителна конверсия на полиолефинов восък до въглеродни адсорбенти	129
И. Генова, Б. Цинцарски, М. Димитров, Д. Панева, Д. Ковачева, Т. Будинова, Р. Иванова, И. Митов, Н. Петров, Т. Цончева, Катализатори за разлагане на метанол на основата на кобалт и желязо модифициран активен въглен от възобновяеми източници: влияние на прекурсора	134
В. В. Иванова, М. К. Стоянова, С. Г. Христоскова, Изследване на каталитичната активност на наноразмерен NiOx за окислителна деструкция на 2,4-дихлорфенол във водни разтвори	141
А. Попова, Б. Стамболийска, Е. Велчева, Експериментално и теоретично изследване на ИЧ спектрални и структурни промени, произтичащи от превръщането на 4-амино-N-[амино(имино)метил] бензенсулфонамид (сулфагуанидин) в азанион	149
А. Попова, Е. Велчева, ИЧ-спектрални и структурни промени, породени от превръщането на 4-цианобензенсулфонамид в азанион	157

З. И. Главчева, Д. Я. Янчева, Й. К. Кънчева, Е. А. Велчева, Б. А. Стамболийска, Създаване на спектрална база данни от референтни художествени и археологически материали	164
Д. Янчева, С. Стоянов, Б. Стамболийска, Л. Даскалова, Е. Чернева, А. Шмелцерович, Влияние на обкръжаващата среда върху антиоксидантното действие на два 6-(пропан-2-ил)-4-метил-морфолин-2,5-диона	179
С. Е. Ангелова, А. К. Славова-Казакова, Л. Сасо, Ш. В. Малхотра, А. К. Прасад, М. Е. Браке, В. С. Пармар, В. Д. Кънчева, DFT/B3LYP изчислителни енталпии на дисоциация на връзка, радикалово-уловителна и антиоксидантна активност на синтетични аналози на природни кумарини	187
И. Георгиева, Н. Трендафилова, Метал-лиганд взаимодействия в комплекси на преходни метали с оксима на глиоксилната киселина	196
В. Б. Делчев, Ксантин и хипоксантин: в търсене на конични сечения S_0/S_1 , свързани с деформация на пиримидиновия фрагмент на пуриновия пръстен	203
Б. П. Стоянов, П. Р. Костадинов, М. В. Колев, З. А. Мустафа, М. Н. Московкина, Р. С. Милина, И. П. Бангов, Използване на дескрипторните отпечатъци на пръстите за клъстериране на химични множества от данни	209
Б. П. Стоянов, Е. П. Петров, Н. Т. Кочев, И. П. Бангов, Една нова програма за генериране на 2D химични структури с помощта на компютри	215
А. Ж. Патлеева, Д. Д. Енчев, Г. Д. Нейков, Теоретично изследване на стереоселективността на вътрешномолекулна реакция на Дилс-Алдер на 2,4-пентадиенил бутадиенамиди с участието на контролиращи стереоселективността групи	220
С. Каваучи, Л. Антонов, И. Окуно, Предсказване на цвета на багрила посредством зависеща от времето теория на функционала на плътността (TD-DFT)	228
П. Иванов, Изследване върху конформациите на големи циклодекстрини	238
Г. С. Спасов, Приложение на метода на изохипсите за електронен Оже спектроскопски количествен анализ на полупроводникови твърди разтвори	246
Р. Тодоров, Ю. Илиева, В. Лозанова, А. Лалова, Оптични свойства на сребро-органични полимерни тънки слоеве като слънцезащитни покрития за съвременни приложения в архитектурата	251
И. Бодуров, Р. Тодоров, Т. Йовчева, С. Съйнов, Холографско изследване на влиянието на коронния разряд при фотодопинг на сребро, злато и хром в наноразмерни филми от As_2S_3	256
Хр. П. Новаков и Хр. Б. Цветанов, Между- и вътрешно молекулни взаимодействия при анионната полимеризация на полярни винилови мономери	261
ИНСТРУКЦИЯ ЗА АВТОРИТЕ	276